

3.3.2 Number of research papers per teachers in the Journals notified on UGC website during the year

Title of paper	Name of the author/s	Department of the teacher	Name of journal	Year of publication	ISSN number	Link to the recognition in UGC enlistment of the Journal
Investigation on photocatalytic activity of ZnS/NiFe ₂ O ₄ NCs under sunlight irradiation via a novel two-step synthesis approach	Dr.I.J.Isaac Premkumar	Mechanical Engineering	Inorganic Chemistry Communications	2021	1387-7003	UGC Journal No. 21219
UV - and visible - light - driven TiO ₂ / La ₂ O ₃ and TiO ₂ / Al ₂ O ₃ nanocatalysts: synthesis and enhanced photocatalytic activity	Dr.I.J.Isaac Premkumar	Mechanical Engineering	Applied Physics A: Material Science and Processing	2022	9478396	UGC Journal No. 8053
Evaluation of Boiler Performance with using of Bio- Ethanol Absorbed Wood Pellets	Dr.I.J.Isaac Premkumar	Mechanical Engineering	Thermal Science	2022	3549836	UGC Journal No. 1192
Design and Material Characteristics of Hybrid Electric Vehicle	Dr.I.J.Isaac Premkumar	Mechanical Engineering	Materials Today: Proceedings	2021	10.1016	UGC Journal No. 49021
Performance enhancement of selective layer coated on solar absorber panel with reflector for water heater by response surface method: A case study	Dr.M.Vijayakumar	Mechanical Engineering	Case Studies in Thermal Engineering	2022	102093	UGC Journal No. 5145
Effect of Silicon Carbide on the Mechanical and Thermal Properties of Snake Grass/Sisal Fiber Reinforced Hybrid Epoxy Composites	Dr.M.Vijayakumar	Mechanical Engineering	Journal of New Materials for Electrochemical Systems	2021	10.14447	UGC Journal No. 24863
Development of AL ₆ O ₆ 1-Si ₃ N ₄ Graphite using Stir casting for wear Application	D.Ananda Kumar	Mechanical Engineering	Adalya Journal of Science	2022	1301-2746	UGC Journal No. 11561
Non-destructive Evaluation for Composite Aluminium Composites	Dr.I.J.Isaac Premkumar	Mechanical Engineering	Advances in Industrial Automation and Smart	2021	9.78981E+12	No
Transesterification Studies on Avocado Seed Oil Using Carbon Supported CuO Nano Catalyst: Rate Kinetics and Thermodynamic Aspects	J. B. Veeramalini Bashyam Sasikumar , Prabakar Jeevanandam, Venkatesh Babu Samikkannu	Petroleum Engineering	Journal of Nano Materials	2022	1687-4129	UGC Journal No. 24752
Characterization and performance enhancement of electrical submersible pump (ESP) using artificial intelligence (AI)	A. Balasubramanian M. Panbarasan , Subhashini Sankar, S. Venkateshbabu	Petroleum Engineering	Materials Today: Proceedings	2022	2214-7853	UGC Journal No. 49021
An analytical study of the technological & managerial advancements in the sedimentary basins of Brazil with special emphasis on Campos basin over a period of 5 decades	J. Sudharsan, M. Panbarasan, S. Venkateshbabu, R. Karthikeswaran	Petroleum Engineering	Journal of Petroleum Engineering & Technology	2022	2231-1785	No
Application of a polymer-magnetic-algae based nano-composite for the removal of methylene blue – Characterization, parametric and kinetic studies	Arivalagan Pugazhendhie, G. Sarojini, S. Venkatesh Babub, N. Rajamohan, M. Rajasimman	Petroleum Engineering	Environmental Pollution	2022	0269-7491	UGC Journal No. 19815
Adsorptive potential of iron oxide based nanocomposite for the sequestration of Congo red from aqueous solution	M. Rajasimman, G. Sarojini , S. Venkatesh Babu	Petroleum Engineering	Chemosphere	2022	0045-6535	UGC Journal No.5539




Performance evaluation of polymer-marine biomass based bionanocomposite for the adsorptive removal of malachite green from synthetic wastewater	Rajasimman d, G. Sarojini, S. Venkatesh Babu, N. Rajamohan	Petroleum Engineering	Environmental research	2021	0013-9351	UGC Journal No.19815
Surface modified polymer-magnetic-algae nanocomposite for the removal of chromium- equilibrium and mechanism studies	M. Rajasimman, G. Sarojini, S. Venkatesh Babu, N. Rajamohan, P. Senthil Kumar	Petroleum Engineering	Environmental Research	2021	0013-9351	UGC Journal No.19815
Facile synthesis and characterization of polypyrrole - iron oxide - seaweed (PPy-Fe ₃ O ₄ -SW) nanocomposite and its exploration for adsorptive removal of Pb(II) from heavy metal bearing water	Manivasagan Rajasimman, Samikannu Venkateshbabu, Gopalakrishnan Sarojini	Petroleum Engineering	Chemosphere	2021	0045-6535	UGC Journal No.5539
Text Based Graphical Password System to Enhance Security	Dr.G.Rajivsureshkumar	Computer Science and Engineering	Journal of Telecommunication, Switching Systems and Networks	2022	2231-0401	No
	M. Rupa, S. Athira					No
Enhanced Graphical Password System with Intelligent User Identification Model	Dr.S.Dhanabal,	Computer Science and Engineering	Journal of Telecommunication, Switching Systems and Networks	2022	2231-0401	No
	S. Athira, M. Ravikumar					No
Intelligent Transportation System Avoids Collision by Disseminate the Warning Messages in Vehicular Adhoc Network	Dr.G.Rajivsureshkumar	Computer Science and Engineering	Journal of Telecommunication, Switching Systems and Networks	2022	2454-6372	No
	Dr.S.Karthikeyini, R. Divya					No
Refinement Model based on deep Learning Technique for Prediction of Temperature using Missing Data(Scopus)	Dr. S. Karthikeyini	Computer Science and Engineering	Mathematics Theory and its Contribution in Robotics and Computer Engineering	2022	2094-0343	No
Detection and Prediction of HMS from drinking water by analysing the absorbents from residuals using deep learning	Mrs.Chandragandhi	Computer Science and Engineering	Hindawi Adsorption Science and T	2022	3265366	UGC Journal No.11614
Data Poison Detection using Associative Support-Vector Machine(ASVM) Algorithm (Scopus)	Mrs.D. Divya	Computer Science and Engineering	Journal of Positive School Psychology	2022	3378-3385	No
An Energy Efficient Architecture for Furnace Monitor and Control in Foundry Based on Industry 4.0 Using IoT	Mrs.Chandragandhi	Computer Science and Engineering	Hindawi Scientific Programming	2022	1128717	UGC Journal No.35610
Resume Screening using TF-IDF	Chandragandi S	Computer Science and Engineering	International Journal of Advanced Research in Computer and Communication Engineering	2022	2278-1021	No
Location Based Alarm System using Android Development	Dr. G. RajivSureshkumar	Computer Science and Engineering	International Journal of Advanced Research in Computer and Communication Engineering	2022	2278-1021	No
Diabetes disease Prediction using Machine Learning Techniques	Dr. G. RajivSureshkumar	Computer Science and Engineering	International Journal of Advanced Research in Computer and Communication Engineering	2022	2278-1021	No
Real Time Pedestrian Detection	Dr. S. Karthikeyini	Computer Science and Engineering	International Journal of Advanced Research in Computer and Communication Engineering	2022	2319-5940	No
Detection of Cyber bullying on Social media using Machine Learning	Athira S	Computer Science and Engineering	International Journal of Advanced Research in Computer and Communication Engineering	2022	2278-1021	No

PRINCIPAL
JCT College of Engineering and Technology
PICHANUR, COIMBATORE - 641 105.



Integrates Parking System for Real-time Parking	K. Greeshma	Computer Science and Engineering	International Journal of Advanced Research in Computer and Communication Engineering	2022	2278-1021	No
Android Game Development using VCROSS- Platform Application in Unity Game Engine with C# Language ZOMBIE SHOOTER	M. Ravikumar	Computer Science and Engineering	International Journal of Advanced Research in Computer and Communication Engineering	2022	2278-1021	No
Human Computer Interaction (HCI) through EYE-GAZE Technologies based on Image Processing	M. Rupa	Computer Science and Engineering	International Journal of Advanced Research in Computer and Communication Engineering	2022	2278-1021	No
Online Bus pass Issue and Renewal using Selenium	R. Divya	Computer Science and Engineering	International Journal of Advanced Research in Computer and Communication Engineering	2022	2278-1021	No
Machine Learning Empowered accurate CSI prediction for large scale 5G networks	Mrs.Chandragandhi	Computer Science and Engineering	Wireless Communication and mobi	2022	7085731	No
Public Auditing Scheme for Integrity Verification in Distributed Cloud Storage System	Mrs.Chandragandhi	Computer Science and Engineering	Hindawi Scientific Programming	2022	10589244	UGC Journal No.35610


PRINCIPAL
 JCT College of Engineering and Technology
 PICHANUR, COIMBATORE - 641 105.





Short communication

Investigation on photocatalytic activity of ZnS/NiFe₂O₄ NCs under sunlight irradiation via a novel two-step synthesis approach

C. Dharmaraja ^a  , P. Emmanuel Nicholas ^b, P. Ramya ^c, I.J. Isaac Premkumar ^d, V. Vijayan ^e, N. Senthilkumar ^f[Show more](#) 

Outline



Share



Cite

<https://doi.org/10.1016/j.inoche.2021.108481>[Get rights and content](#)

Highlights

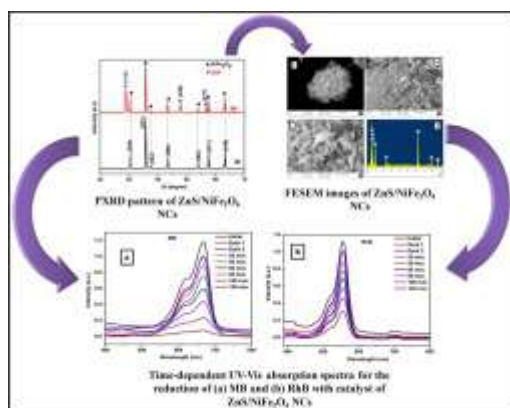
- A simple two-step process, ZnS/NiFe₂O₄ NCs were fabricated for photocatalytic activity.
- The band-gap values are 1.50 eV and 1.89 eV respectively for pure and ZnS/NiFe₂O₄ NCs.
- The seed like morphologies were achieved from the prepared ZnS/NiFe₂O₄ NCs.
- The degradation efficiency of ZnS/NiFe₂O₄ NCs were found 93% for MB and 72% for RhB.

Abstract

This work focuses on the facile two-step approach of Zinc Sulphide (ZnS)/ Nickel Ferrite (NiFe₂O₄) nanocomposites (NCs) were developed for the first time. The PXRD pattern reveals that the survival of spinel cubic and cubic symmetry phases were obtained by synthesized ZnS/NiFe₂O₄ NCs. The optical band-gap values of synthesized NCs were achieved to be 1.50 eV

and 1.89 eV respectively for NiFe₂O₄ and ZnS/NiFe₂O₄ NCs which were established by UV–Visible absorption spectrum via Tauc's relation. From the BET analysis, the surface area of the prepared ZnS/NiFe₂O₄ NCs was achieved to be 44.72 m²/g. The as-prepared ZnS/NiFe₂O₄ NCs exhibit superior photocatalytic performance than that of pure NiFe₂O₄ for degradation of methylene blue (MB) and rhodamine B (RhB) dyes under direct sunlight illumination. The photocatalytic efficiency of ZnS/NiFe₂O₄ NCs was estimated to be 93% and 72% for MB and RhB within 120 min illumination. Thus the result shows, developed nanocomposites demonstrated a proficient photodegradation process with a high reaction kinetic rate due to their separation as well as the transfer of photogenerated charge carriers.

Graphical abstract



[Download : Download high-res image \(137KB\)](#)

[Download : Download full-size image](#)

[<](#) Previous

Next [>](#)

Keywords

ZnS/NiFe₂O₄ NCs; Two-step approach; Structural; Optical; Photocatalytic activity

[Recommended articles](#)

Cited by (7)

Construction of delaminated

Ti₃C₂MXene/NiFe₂O₄/V₂O₅ ternary composites for expeditious pollutant degradation and bactericidal property

2022, Journal of Environmental Chemical Engineering

[Show abstract](#) ✓

Preparation and photocatalytic activity of HC/BiOBr/Bi₂WO₆ microspheres

2022, Inorganic Chemistry Communications

[Show abstract](#) ✓

Synthesis of nano-ZnS by lyotropic liquid crystal template method for enhanced photodegradation of methylene blue

2022, Inorganic Chemistry Communications

[Show abstract](#) ✓

S-scheme heterojunction based on ZnS/CoMoO₄ ball-and-rod composite photocatalyst to promote photocatalytic hydrogen production

2021, Applied Surface Science

[Show abstract](#) ✓

Two Supra Molecular Co(II) Coordination Polymers Based on 2, 5-Dimethoxyterephthalic Acid and Imidazole Derivatives: Crystal Structures and Photo-Catalytic Reactions

2022, Rengong Jingti Xuebao/Journal of Synthetic Crystals

Tracking the changes in the structural, optical and photoluminescent properties of CuCo₂O₄/MnS nanocomposites with different composition ratios

2022, Zeitschrift fur Naturforschung - Section A Journal of Physical Sciences



[View all citing articles on Scopus](#)

[View full text](#)



Copyright © 2022 Elsevier B.V. or its licensors or contributors.
ScienceDirect® is a registered trademark of Elsevier B.V.



[Home](#) > [Catalyst](#) > [Catalysis](#) > [Chemistry](#) > [Nanocatalysts](#)Article [Publisher preview available](#)UV- and visible-light-driven TiO₂/La₂O₃ and TiO₂/Al₂O₃ nanocatalysts: synthesis and enhanced photocatalytic activity SpringerMarch 2022 · [Applied Physics A](#) 128(4)DOI:[10.1007/s00339-022-05293-7](https://doi.org/10.1007/s00339-022-05293-7)

Authors:

**S. Sudhagar****S. Satheeskumar**

CMR Institute of Technology Hyderabad

**I. J. Isaac Premkumar****Venkatraman Vijayan**

K.Ramakrishnan College of Technology

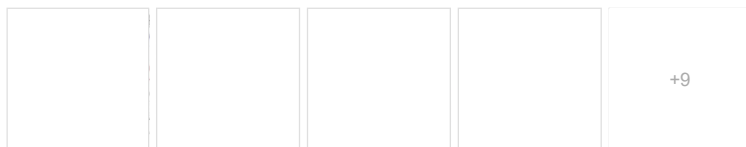
[Show all 7 authors](#)[Read publisher preview](#)[Request full-text](#)[Download citation](#)[Copy link](#)

To read the full-text of this research, you can request a copy directly from the authors.

[Citations \(8\)](#)[References \(62\)](#)[Figures \(14\)](#)

Abstract and Figures

The hydrothermal method was used to make the anatase phase of TiO₂ nanoparticles, TiO₂/La₂O₃ and TiO₂/Al₂O₃ composites. FTIR spectroscopy, X-ray diffraction (XRD), UV–Vis absorption spectroscopy and scanning electron microscopy (SEM) were used to investigate the crystal structure, shape, and optical characteristics of TiO₂, TiO₂/La₂O₃ and TiO₂/Al₂O₃ nanomaterials. The photocatalytic studies were comparatively analyzed by degrading the textile dyes methylene blue (MB) and crystal violet (CV). The degradation process was carried out in both UV light and visible light irradiation. The efficiency achieved by TiO₂, TiO₂/La₂O₃ and TiO₂/Al₂O₃ was 87, 95, 45% and 80, 92, 29%, respectively, for MB and CV dye under UV light while under visible light it is 34, 27, 84%, and 29, 24, 81%, respectively, for MB and CV dye.



The XRD patterns of a TiO₂, b... The FT-IR patterns of TiO... a UV-DRS absorbance... SEM images of a, a–d EDS color mapping image...

Figures - available from: [Applied Physics A](#)This content is subject to copyright. [Terms and conditions](#) apply.

Discover the world's research

- 20+ million members
 - 135+ million publications
 - 700k+ research projects
- [Join for free](#)

 Publisher Preview 1 SpringerA preview of this full-text is provided by Springer Nature. · [Learn more](#)
[Preview content only](#)Content available from [Applied Physics A](#)This content is subject to copyright. [Terms and conditions](#) apply.

UV- and visible-light-driven TiO₂/La₂O₃ and TiO₂/Al₂O₃ nanocatalysts: synthesis and enhanced photocatalytic activity

S. Sudhagar¹ · S. Sathees Kumar² · I. J. Isaac Premkumar³ · V. Vijayan⁴ · R. Venkatesh⁵ · S. Rajkumar⁶ · Mandeep Singh⁷

Received: 4 October 2021 / Accepted: 13 January 2022 / Published online: 12 March 2022

© The Author(s), under exclusive licence to Springer-Verlag GmbH, DE part of Springer Nature 2022

Abstract

The hydrothermal method was used to make the anatase phase of TiO₂ nanoparticles, TiO₂/La₂O₃ and TiO₂/Al₂O₃ composites. FTIR spectroscopy, X-ray diffraction (XRD), UV–Vis absorption spectroscopy and scanning electron microscope (SEM) were used to investigate the crystal structure, shape, and optical characteristics of TiO₂, TiO₂/La₂O₃ and TiO₂/Al₂O₃ nanomaterials. The photocatalytic studies were comparatively analyzed by degrading the textile dyes methylene blue (MB) and crystal violet (CV). The degradation process was carried out in both UV light and visible light irradiation. The efficiency achieved by TiO₂, TiO₂/La₂O₃ and TiO₂/Al₂O₃ was 87, 95, 45% and 80, 92, 29%, respectively, for MB and CV dye under UV light while under visible light it is 34, 27, 84%, and 29, 24, 81%, respectively, for MB and CV dye.

Keywords Hydrothermal method · Photocatalyst · Nanocomposites · Textile dyes

1 Introduction

Usable water is a basic necessity, yet industrial contamination and textile dyes in water bodies can be dangerous to one's health. Organic dyes have caused water contamination,

which has become a serious environmental issue [1]. The current requirement is for a simple decontamination procedure that may be used even in remote areas of developing countries. Solar water disinfection, as recommended by the World Health Organization, is a viable option, although it takes 6 h of direct sunlight. For the point of use of water purification, semiconductor photocatalysis would be a viable option. Nanostructures were frequently used for dye removal because of its distinct physicochemical features [2]. Due to its outstanding optical and electronic characteristics, biocompatibility, chemical sustainability, and inexpensive, semiconductor photocatalysis is gaining attention [3–5]. Photocatalysts are materials that can accelerate processes without being reacted in the influence of light [6]. In a variety of ways, TiO₂ is an excellent photocatalyst. It is quite inexpensive, chemically extremely stable, and abundant in nature. Furthermore, the light-generated electrons are sufficiently reducing to make superoxide from oxygen and the holes are strongly oxidizing. Without the use of any chemical additions, it enhances the oxidation of the primary categories of industrial pollutants at atmospheric temperatures [7–9]. Rutile TiO₂ is photocatalytically less effective despite its apparent absorption is in the visible region, while anatase is better, which is stimulated by UV-A radiation [10, 11]. On the other side, TiO₂'s photocatalytic ability is insufficient for massive industrial use. Low interactions among TiO₂ and

✉ S. Sudhagar
ssudhagar6@gmail.com

¹ Department of Mechanical Engineering, University College of Engineering Dindigul, Dindigul, Tamil Nadu, India

² Department of Mechanical Engineering, Institute of Aeronautical Engineering, Dundigal, Hyderabad, India

³ Department of Mechanical Engineering, JCT College of Engineering and Technology, Coimbatore 641 105, Tamil Nadu, India

⁴ Department of Mechanical Engineering, K. Ramakrishnan College of Technology, Samayapuram, Trichy, Tamil Nadu, India

⁵ Institute of Mechanical Engineering, Saveetha School of Engineering, SIMATS, Chennai, Tamil Nadu, India

⁶ Department of Mechanical Engineering, Faculty of Manufacturing, Hawassa Institute of Technology, Hawassa University, Hawassa, Ethiopia

⁷ School of Mechanical and Mechatronic Engineering, University of Technology Sydney, Sydney, NSW 2007, Australia

Vol.:(2022) Springer

Content courtesy of Springer Nature, terms of use apply. Rights reserved.

Citations (8)

References (62)

... As a result, the contact reactions considerably impact the mechanical properties of MMCs. The microstructural design of lightweight MMCs is mainly utilized in creep-resistant usages [33]. It requires the homogenous scattering of the thermally stable state of nano-scale ceramic particles during the grain refinement structure [34][35] [36] [37][38]. Ceramics are the most commonly used reinforcing materials in aluminium composites [39]. ...

Influence of nano titanium oxide reinforced Al-7075 matrix composites in stir casting method[Article](#)

Sep 2022

K.P. Dhanabalakrishnan · N. Mathan Kumar ·  Mothilal Thulasiraman · S. Socrates[View](#) [Show abstract](#)

... Dharbai fibres are lignocellulosic fibres containing OH chemicals that absorb water quickly and compromise the performance of natural composites [34], particularly their high dimension stability [35,36]. Natural fibres have varying potential due to the chemical ingredients cellulose, hemicellulose, and lignin [32, 33]. ...

Mechanical performance of aloe vera/dharbai-based hybrid epoxy composites with enhanced NaHCO₃ treatment[Article](#)

Sep 2022

P. Yogesh · S. Paul Singarayar · M.D. Rajkamal ·  Yatika Gori[View](#) [Show abstract](#)

... According to current projections, the global trend in the NFPC industry will continue to accelerate [4]. Natural fibrebased polymer composites have grown in popularity in consumer items and emerging industrial sectors [5]. According to projections, the NFPC industry will grow by 12 % globally during the next five years (2021-2025) [6]. ...

Effect of Roselle and biochar reinforced natural fiber composites for construction applications in cryogenic environment[Conference Paper](#)

Sep 2022

Tamil Mannan ·  Sivaprakash Vetrivel ·  Raja S. · S. Socrates[View](#) [Show abstract](#)

... Mudar is a moderate dimension shrub having 26 cm of stem diameter and a height of two to three metres [11]. The plant may flourish in arid environments with about 150 to 1000 mm of rainfall and poorly drained sandy regions with up to 2000 mm of seasonal rainfall [12]. With a serious lack of forest products in Iran, scientific study and industrial growth are exploring alternate cellulosic fibre resources [13]. ...

Significance of Si 3 N 4 /Lime powder addition on the mechanical properties of natural calotropis gigantea composites[Article](#)

Sep 2022

K Tamil Mannan ·  Sivaprakash Vetrivel ·  Raja S. ·  Kaliappan Seeniappan[View](#) [Show abstract](#)

... This operation needs microfiltration which consumes energy and time. To overcome this problem, many studies report the TiO₂ immobilization on an inert support like activated carbon [11,25,28], alumina [26], silica [27], zeolite [28], clays [23,24,[29][30][31][32] and porous ceramic [33]. In this work, commercial clay "K10-montmorillonite" as acid-activated clay [34] has been chosen as a support for TiO₂ particles. ...

Calcined or Microwaved TiO₂-K10 as Catalysts for p-Nitrophenol Photodegradation: Optimization Study Using Response Surface Methodology[Article](#)[Full-text available](#)

Aug 2022

 Manel Baizig ·  Latifa Bergaoui ·  Bassem Jamoussi ·  Narjes Batis[View](#) [Show abstract](#)**Tribological and Viscoelastic Behaviour of Jute, Prosopis Juliflora Bark, and Kenaf Fibers Reinforced Polyester Hybrid Composites for Engineering Applications**[Article](#)[Full-text available](#)

Nov 2022

R. Muthalagu ·  Srinivasan Vijayaraghavan ·  s. Satheeskumar · V. Murali Krishna[View](#)**Effect of walnut powder reinforcement on the mechanical properties of biodegradable natural flax/hemp fibre-based composites**[Article](#)

Sep 2022

L. Rathan Kumar · S. Madhu · T. Mothilal · M.D. Raj Kamal

[View](#) [Show abstract](#)

Activated Carbon-Loaded Titanium Dioxide Nanoparticles and Their Photocatalytic and Antibacterial Investigations

[Article](#) [Full-text available](#)

Jul 2022

C. Parvathiraja · Snehlata Katheria · Masoom Raza Siddiqui ·  Wen-Cheng Lai

[View](#) [Show abstract](#)

Recommendations Discover more about: [Nanocatalysts](#)

Project

Investigation on Mechanical and Tribological Behaviors of PA6 and Graphite-Reinforced PA6 Polymer Composites

 s. Satheeskumar

[View project](#)

Project

An implementation of mechanical and tribological properties of polymer matrix Composites

 s. Satheeskumar

[View project](#)

Project

Evaluation of mechanical properties and characterization of silicon carbide–reinforced polyamide 6 polymer composites and their engineering applications

 s. Satheeskumar

[View project](#)

Project

Investigation of Characterization and Mechanical Performances of Al₂O₃ and SiC Reinforced PA6 Hybrid Composites

 s. Satheeskumar

[View project](#)

Article

The Effects of Sintering on the Photocatalytic Activity of N-Doped TiO₂ Nanoparticles

March 2008 · Chemistry of Materials

 Yixin Zhao ·  Xiaofeng Qiu ·  Clemens Burda

N-Doped titanium oxide nanoparticles (NPs) were synthesized through the hydrolysis of N-substituted titanium isopropoxide precursors and postsynthesis treated by sintering at different temperatures in a nitrogen atmosphere and in air. X-ray diffraction (XRD) results revealed that the presence of oxygen during the sintering also affects the crystallization of the N-doped TiO₂ NPs. The air and N₂ ... [\[Show full abstract\]](#)

[Read more](#)

Article

Characterization of Porous SiO₂-TiO₂ Photocatalyst and the Effect of PEG1000 Concentration

January 2014 · Asian Journal of Chemistry

Wenjie Zhang · Hongbo He · Li Li · Tingting Hu

A porous SiO₂-TiO₂ photocatalyst was prepared through co-sol-gel method for photocatalytic degradation of methyl orange. PEG1000 was used as a template to induce porous structure in the material. Photocatalytic degradation was conducted after adsorption equilibrium to identify the contribution of both adsorption and photocatalytic degradation. The prepared material was composed of anatase TiO₂ ... [\[Show full abstract\]](#)

[Read more](#)

Article

Characterization of SiO₂-TiO₂ and Photocatalytic Degradation of Methyl Orange

July 2014 · Asian Journal of Chemistry

Wenjie Zhang · Lina Zhou · Xiaofang Han · H. Hongbo

A SiO₂-TiO₂ composite photocatalyst was prepared through sol-gel method for photocatalytic degradation of methyl orange. The material is composed of anatase TiO₂ and most probably amorphous SiO₂. The crystallite size of the TiO₂ (101) plane is 14.39 nm. The surface of the sample is fairly rough. Some particles in the size smaller than 1000 nm scatter on the surface. The pore size of the material ... [\[Show full abstract\]](#)

[Read more](#)

Article

Porous TiO₂-Al₂O₃ Composite Photocatalyst Prepared by Sol-gel Method: the Role of Calcination Temper...

June 2012 · Nanoscience and Nanotechnology - Asia

Wenjie Zhang · Ruyuan Li · Bo Yang

Porous TiO₂-Al₂O₃ composites were prepared by sol-gel method using tetrabutyl titanate and aluminum isopropoxide as the sol precursors. PEG1000 was used as the pore forming template. The materials were composed of anatase TiO₂ and amorphous Al₂O₃. Long grooves distributed on the rough surfaces of the materials. FT-IR and XPS spectra indicated that the samples were composed of TiO₂ and Al₂O₃. The ... [\[Show full abstract\]](#)

[Read more](#)

Article

Synthesis of Mesoporous TiO₂ - Al₂O₃ Binary Oxides Photocatalyst by Sol-Gel Method Using PEG1000...

June 2012 · International Journal of Photoenergy

Wenjie Zhang · Ruyuan Li · Hongbo He

The mesoporous TiO₂-Al₂O₃ binary oxides were prepared by sol-gel method using PEG1000 as template. The effects of PEG1000 concentration on the properties and photocatalytic activity of the materials were investigated. The binary oxides were composed of nanocrystallite anatase TiO₂ and amorphous Al₂O₃. The surfaces of the samples prepared with PEG1000 were rough and had many long grooves on the ... [\[Show full abstract\]](#)

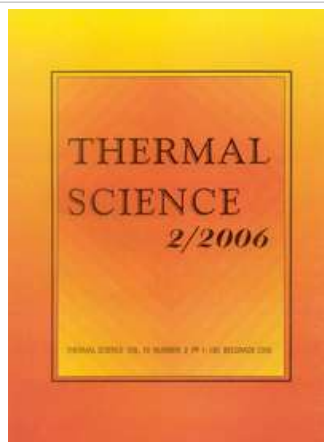
[Read more](#)

Last Updated: 13 Nov 2022



Company	Support	Business solutions
About us	Help Center	Advertising
News		Recruiting
Careers		

National library of Serbia



About the journal

Editorial policy

Instructions for authors

Cobiss

All issues

2022 OnLine-First

2022

Volume 26 Issue 5 Part B

Volume 26 Issue 5 Part A

Volume 26 Issue 4 Part B

Volume 26 Issue 4 Part A

Volume 26 Issue 3 Part B

Volume 26 Issue 3 Part A

Volume 26 Issue 2 Part C

Volume 26 Issue 2 Part B

Volume 26 Issue 2 Part A

Volume 26 Issue 1 Part B

Volume 26 Issue 1 Part A

2021

2020

2019

2018

2017

2016

2015

2014

2013

2012

2011

2010

2009

2008

2007

2006

2005



Thermal Science 2022 Volume 26, Issue 2 Part A, Pages: 931-936

<https://doi.org/10.2298/TSCI200906216J>[Full text](#) (525 KB)

Evaluation of boiler performance with using of bio-ethanol absorbed wood pellets

Joswa Lazaras Issac Premkumar (Department of Mechanical Engineering, JCT College of Engineering and Technology, Coimbatore, Tamilnadu, India), issacprkumar007@gmail.com

Kandhasamy Raja (Department of Mechanical Engineering, University College of Engineering, Dindigul, Tamilnadu, India)

Vijayaraj Vijay Prabha (Kalasalingam School of Agriculture and Horticulture, Kalasalingam Academy of Research and Education, Krishnakoil, Tamilnadu, India)

Tekelemariam Akilu (Department of Mechanical Engineering, Faculty of Manufacturing, Insititute of Technology, Hawassa University, Hawassa, Ethiopia)

Tufa Mebra (Department of Mechanical Engineering, Faculty of Manufacturing, Insititute of Technology, Hawassa University, Hawassa, Ethiopia)

Venkatraman Vijayan (Department of Mechanical Engineering, K.Ramakrishnan College of Technology (Autonomous), Samayapuram, Tiruchirappali, Tamilnadu, India)

Ramalingam Kamalakannan (Department of Mechanical Engineering, M. Kumarasamy College of Engineering (Autonomous), Karur, Tamilnadu, India)

In current trends the wood pellets are very significance role in the replacing of boiler fuel, it is a surrogate and renewable fuel. For this study comparative analysis of the fuel performance in the boiler is carried out effectively. Two categorize of fuel like as raw wood pellets and wood pellets are immersed in the bio-ethanol are taken to this experimental work. The thermal characteristics and thermal efficiency of the boiler with influence of two types of fuels are conducted efficiently. Normally the wood pellets having small pores it is used to absorb the bio ethanol while in immersion. Wood pellets immersed in the bio ethanol are provided and increase the thermal properties as well as thermal efficiency com-pared to raw pellets, due to amid in the two fuels. The flue gas constituent's percentage such as CO₂, O₂, CO, and NO_x are analyzed, additionally the high temperature of flue gas also measured in the outlet of the chimney. No alteration is made in the boiler set-up which is comfortable to both fuels.

Keywords: Wood pellets, Bio ethanol, Flue gas, Boiler, Thermal efficiency, CO₂

[Show references](#)

- Citation export
- Email this article

2004
2003
2002

Developed and maintained by National Library of Serbia 2005-2022

[ISSN - 2683-3867](#)

[COBISS.SR-ID - 278404108](#)



Materials Today: Proceedings

Volume 37, Part 2, 2021, Pages 351-353

Design and material characteristics of hybrid electric vehicle

S. Baskar ^a , V. Vijayan ^b, I.J. Isaac Premkumar ^c, D. Arunkumar ^d, Dowhi Thamaran ^a[Show more](#)  Outline |  Share  Cite<https://doi.org/10.1016/j.matpr.2020.05.352>[Get rights and content](#)

Abstract

The environmental pollution has turn into a serious problem in the country, especially in countries where urbanization lead to crowded atmosphere with stuck traffic in the road. Very big amount of pollutants are emitted from the vehicles day by day. Engineers initiated to monitor various technologies to deal with the pollution issues. The electric vehicles (EV) are enable full consumption of energy and produce almost zero emission. Hybrid power system is conceived to give back for underperformance in the battery. A HEV consists of I.C engine vehicle with battery and electric motor. The benefits of HEVs comprise good fuel economy and less emission. The natural flexibility of HEVs will permit them to be utilized in wide range of applications. A HEV provides increased fuel efficiency and emissions are decreased. HEVs can minimize dependence on fossil fuels. Global automobile giant are research and developing the concept HEVs.

 PreviousNext 

Keywords

EV; Electric motor; Zero emissions; Battery; HEV

[Special issue articles](#)[Recommended articles](#)

Cited by (22)

[Experimentation and optimization of cutting parameters of abrasive jet cutting on AA6082 through response surface methodology](#)

2021, Materials Today: Proceedings

[Show abstract](#) ✓

[Synthesis of silver nanoparticle using marine red seaweed Gelidiella acerosa -A complete study on its biological activity and its characterisation](#)

2020, Materials Today: Proceedings

[Show abstract](#) ✓

[DMLS - An insight for unproblematic production](#)

2020, Materials Today: Proceedings

[Show abstract](#) ✓

[A review on mechanical and wear properties of ASTM a 494 M grade nickel-based alloy metal matrix composites](#)

2020, Materials Today: Proceedings

[Show abstract](#) ✓

[Optimization of environmental parameters by Plackett-Burman design and response surface methodology for the adsorption of Malachite green onto Gracilaria edulis](#)

2020, Materials Today: Proceedings

[Show abstract](#) ✓

[Comparison of chassis frame design of Go-Kart vehicle powered by internal combustion engine and electric motor](#)

2020, Materials Today: Proceedings

[Show abstract](#) ✓



View all citing articles on Scopus

© 2020 Elsevier Ltd. All rights reserved. Selection and peer-review under responsibility of the scientific committee of the International Conference on Newer Trends and Innovation in Mechanical Engineering: Materials Science.



Copyright © 2022 Elsevier B.V. or its licensors or contributors.
ScienceDirect® is a registered trademark of Elsevier B.V.





Case Studies in Thermal Engineering

Volume 36, August 2022, 102093

Performance enhancement of selective layer coated on solar absorber panel with reflector for water heater by response surface method: A case study

C. Ramesh ^a, M. Vijayakumar ^b, Saad Alshahrani ^c , G. Navaneethakrishnan ^d, R. Palanisamy ^e, Natrayan L ^f, C Ahamed Saleel ^c, Asif Afzal ^{g, j, k} , Saboor Shaik ^h, Hitesh Panchal ⁱ

[Show more](#)

Outline | Share Cite

<https://doi.org/10.1016/j.csite.2022.102093>[Get rights and content](#)Under a Creative Commons [license](#)[Open access](#)

Abstract

In solar thermal applications, the performance of a solar absorber panel with a reflector is critical. In sense, different absorbers are used to enhance thermal efficiency. In addition to this, various coatings on solar absorber panels are introduced, and the performance of the same coated panels are examined with experimental study by design of experiment concept. For the reason, this work utilized the black-chrome coating (BC) and nickel-cobalt-coating (Ni-Co) on copper solar absorber panel. The reflectors were also used to maximize the incident solar radiation on the absorber. In this experiment the process variables are flow rate, collector angle, and reflector angle and the thermal efficiency of solar panel is the response. The response surface methodology with Box Behnken design is used to collect the experimental data from experimental setup. The collected data from designed experiment are analyzed by using Analysis of Variance Table (ANOVA). From this the coating on the absorber panel and reflectors are improved the thermal efficiency up to 89.3% of the Black – Chrome solar flat plate collector than Ni-Co panel.

Keywords

Solar absorber panel; Black-chrome coating; Box-behnken; Nickel-cobalt coating; Reflectors; Response surface methodology

1. Introduction

According to the green environment, pollution free atmosphere requirements the government introduces various policies for dwindling fossil fuel with the incorporation of renewable energies such as solar energy. From various methods to collect solar energies the simplest method is the solar water heater. Generally, the solar water heater uses a flat plate collector, which converts the solar radiation into heat, and the same heat energy is absorbed by the fluid medium as in normal cases water as the medium. In low temperature conditions the Solar Flat Plate Collector (SFPC) is used to convert the solar energy to thermal energy. However it has a low relative efficiency [1].

Recent research focusing on enhancing thermal efficiency of the solar water heater by various methods of utilizing hybrid nano-fluids [2], phase change materials, reflectors, coating the absorber, altering the designs and materials. One of the major research subjects is to reduce the heat losses on the upper side of the collector to increase the heat utilization by proper design of the collector. The general evaluation analysis employed the heat loss coefficient and efficiency factor. The examination of the effect of various process variables on thermal efficiency concluded that the absorber's optical properties are highly influenced by the coefficient of total heat loss. The collector was redesigned with a corrugated absorber and recorded an efficiency of 67% with 0.013 kg/s [3]. The thermal efficiency of corrugated plate absorber is observed 14% more as compare to the smooth duct for solar air heater with jet impingement [4]. The triangle-shaped prototype SFPC has a high heat transfer area and showed 55% efficiency with 800 W/m² and 900 W/m² solar fluxes [5]. Research on the SFPC designed to take the water at the circumference of a spiral tube and leaves at the center reported that water's solar radiation and flow rate highly influence the thermal efficiency of flat plate collectors (FPC) [6]. The flat reflectors enhanced the intensity of incident solar energy on the absorber area [7]. The analysis of direct solar radiation and the combination of direct and reflected solar radiation was done by considering the variable reflector and collector angle [8]. A researcher used reflectors at both longer sides of the SFPC to reflect the direct radiation to increase the intensity of radiation on the collector. They found that the efficiency was increased by 10% due to the reflectors [9].

The researchers also analyzed selective layer coating on the absorber. The solar paints and black chrome coating were compared with the standard one. The results showed enhanced thermal performance. Further, higher emittance coating reduced the risk of overheating during the stagnation period. Research on thermochromic layer on absorber reported the

higher thermal efficiency up to 4.5% compared to conventional collector [10]. The optimization of black Nickel-Cobalt coating on solar absorber panel reported the improved optical properties which are required for improving the thermal efficiency of a collector [11]. A pure aluminum sheet with electroless Ni coating and Ni-pigmented anodized coating showed a lower emission coefficient and higher absorption coefficient [12,13]. The absorber with TiAlC, TiAlCN, TiAlSiCN layers with anti-reflecting (TiAlSiO), and semi-transparent (TiAlSiCO) layers were unstable when operating at higher temperatures [14].

The evolutionary algorithms such as response surface methodology have been receiving attention in the last two decades in various fields [15]. Taguchi and the grey relational method optimized the process variables to improve the efficiency of SFPC [16]. Box-Behnken method of experiment design and response surface method of optimization are the best suited for optimizing three process variables [17]. The various researchers are concentrated about different coated absorbers in SFPC. Moreover, their research works are not concentrated to identify the best variables to operate the SFPC with maximum thermal efficiency. So, this work concentrated about modelling of SFPC thermal performance enhancement with reflectors and selective layer coated absorber. This work utilized the black-chrome coating (BC) and nickel-cobalt-coating (Ni-Co) on copper solar absorber panel for improving the performance of solar water heater.

2. Experimental setup, methods and measurement

2.1. Fabrication of experimental test setup

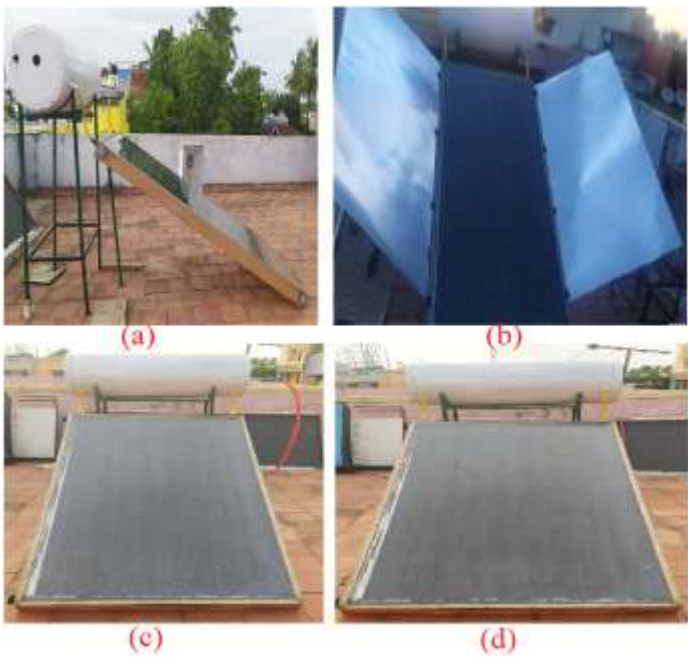
One copper plate of 100 mm × 100 mm was electroplated with black-chrome, and another copper plate was electro-plated with Ni-Co. These coatings were checked for solar absorptivity and emissivity. The electro-plating was detailed in [Table 1](#).

Table 1. Technical data for electroplating.

S.No.	Description	Black-Chrome plating	Nickel-Cobalt plating
1	Solution	CrCl ₃ CoCl ₂ -	NiSo ₄ - (300 g/l)
		(14.1 g/l)	NiCl- (25 g/l)
		H ₂ SiF ₆ - (7.50 g/l)	H ₃ BO ₃ - (30 g/l)
		NaH ₂ PO ₄ -(3.80 g/l)	Saccharin - (1 g/l)
		Naf- (19.7 g/l)	MnSo ₄ - (5 g/l)
		H ₂ O - (940 ml)	H ₂ O - (639 g/l)
2	PH value of the solution	5.4	4

S.No.	Description	Black-Chrome plating	Nickel-Cobalt plating
3	Temperature	20 °C	24 °C
4	Voltage (Tension)	4 V	5 V
5	Current Density	2.5 A	4 A
6	Duration	150 Sec	120 Sec

The solar absorber panel used in this study was fabricated using 12.5 mm copper tubes of 2 m as risers and 25 mm tubes as headers. Copper strips of 50 mm × 1 mm were used as the fins. The collector (size 1500 mm × 500 mm x 150 mm) is a GI sheet. The solar absorber panel was placed over the glass wool-filled box and was closed by the glass of 1500 mm × 500 mm x 4 mm. This setup was built with hinges at both long sides to fix the glass reflector of size 1500 mm × 500 mm x 3 mm at any angle concerning the collector as presented in Fig. 1. The water inlet and outlet line has temperature sensors to measure the temperature and a Rota meter to measure the flow rate. The setup was installed at Coimbatore, Tamilnadu, India. It is geographically at latitude 11.0168°N, 76.9558°E.



[Download : Download high-res image \(701KB\)](#)

[Download : Download full-size image](#)

Fig. 1. Experimental Setup (a) flat plate collector - with 45° inclination, (b) flat plate collector with reflectors, (c) flat plate collector with Black Chrome coating, (d) flat plate collector with nickel cobalt coating.

2.2. Experiment design and measurements

The process variables volume flow rate of water (v°), Collector inclination (θ) and Reflector inclination (α), and the response thermal efficiency (η) were chosen with 3 levels. The levels and ranges are selected based on solar panel manufacturer recommendations the same is presented in Table 2. The Box-Behnken experimental plan is used to conduct the solar panel experiments. Normally, this design is required 3 levels of variables and 15 experimental run and the observed data is tabulated in Table 3. The design eliminates the experiments with all the three parameters at the extreme condition as the optimum set of parameters would not be at the extreme points. The position of design points at the center of the edges of the cuboid is shown in Fig. 2.

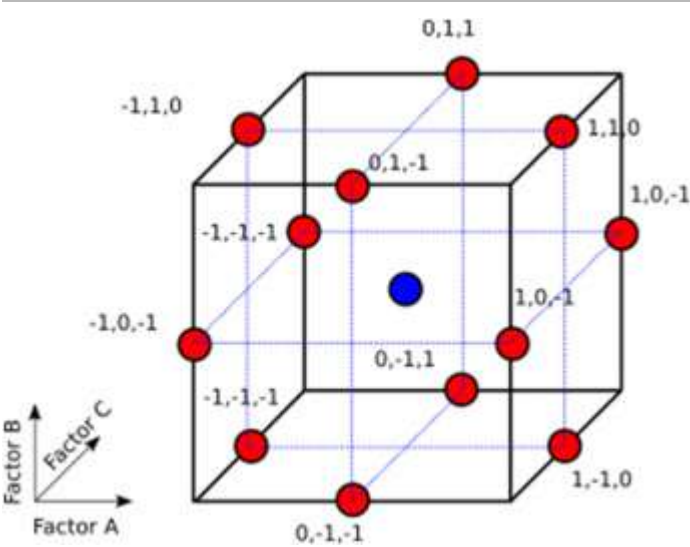
Table 2. Control variables and their levels.

S.No.	Variables	Units	Levels		
			Low (-1)	Medium (0)	High (+1)
1	Volume flow rate of water (v°)	l/min	0.5	1.5	2.5
2	Collector inclination (θ)	Degree	30	45	60
3	Reflector inclination (α)	Degree	30	45	60

Table 3. Experiments design and observations.

Std. Order	Run Order	The volume flow rate of water (v°)	Collector inclination (θ)	Reflector inclination (α)
		l/min	Degree	Degree
1	1	0.5	30	45
13	2	1.5	45	45
3	3	0.5	60	45
10	4	1.5	60	30
11	5	1.5	30	60
2	6	2.5	30	45
8	7	2.5	45	60
4	8	2.5	60	45

Std. Order	Run Order	The volume flow rate of water (v°)	Collector inclination (θ)	Reflector inclination (α)
		l/min	Degree	Degree
6	9	2.5	45	30
5	10	0.5	45	30
15	11	1.5	45	45
9	12	1.5	30	30
12	13	1.5	60	60
14	14	1.5	45	45
7	15	0.5	45	60



[Download : Download high-res image \(225KB\)](#)

[Download : Download full-size image](#)

Fig. 2. Box-Behnken design points.

The experiments were conducted per run order, and the responses were noted. The responses observed were analyzed for their fitness by type I sum of squares of sequential model and lack of fit test. The suitable polynomial to build the model was chosen to give the accuracy above 95% confident level. Then, ANOVA (Type III – Partial sum of squares) was carried out to find the fitness of the model and the significant of the terms. The model developed represents the curve design space. The curves of various levels of different parameters built a design surface in which the optimum point was found.

The uncertainty analysis was also done to find the reliability of the observed data and was expressed by standard deviation as depicted in equation (1). The acceptable uncertainty was

determined by dividing the difference between the maximum and minimum thermal efficiency by four. The following relationship calculated the standard uncertainty of type A by observing the experiments three times.

$$\text{Standard Deviation, SD } (\eta_k) = \frac{1}{(n-1)} \sum_{k=1}^n (\eta_i - \bar{\eta}) \quad (1)$$

where, n - No. of observations.

k - Individual observations

$\bar{\eta}$ - Average of the observations

SD - Standard deviation

η_i - Repeated observations.

The highest uncertainty was found to be +9.7 for a permitted uncertainty of ± 15 . As a result, it was clear that the observed data fell well within the permissible ranges of $\pm 3\sigma$.

3. Results and discussion

3.1. A. optical properties of the electroplated absorber

The solar absorptance and emittance were checked before and after electroplating. Copper has an absorptance of 0.68 and an emissivity of 0.09 before electroplating. The black chrome coating had chromium oxides (Cr_2O_3) and crystalline structured chromium. But, their composition may vary across the area. The absorptance was increased to 0.91 in black chrome coating and was 33.8% higher when compared to the non-coated copper.

Similarly, the emissivity also doubled to 0.16. On the other side, Ni-Co coating has Ni (86.73%) and Co (3.27%) and has 0.92 absorptances and 0.37 emittance. It was noted that the absorptance was increased by about 34%. The emittance of Ni-Co coating was significantly high and enhanced the heat loss.

3.2. Design surface of variables – black-chrome coated panel

The optimization was carried out using Design Expert 7.0 software. The behavior pattern of the responses in both black-chrome and Ni-Co panels was almost the same. The maximum and minimum thermal efficiency ratios were less than 3, which means no transformation of the response data needed to develop the model that fits the data. The approximate quadratic model was selected based on the fitness level by the sequential sum of square type I. The deviations of the actual, predicted R-squared, and Ra-squared values were presented. These were ($R = 0.9944$, and $R_a = 0.9872$) closer to 1 ([Table 4](#)), and the difference between them was negligible. The ANOVA ([Table 5](#)) also ensures the model's fitness for the confidence level above 95%. The normal plot of residuals (3. a) and the predicted and actual responses (3. b) as the deviation less than 5% and were evenly distributed on either side of the line ensures the

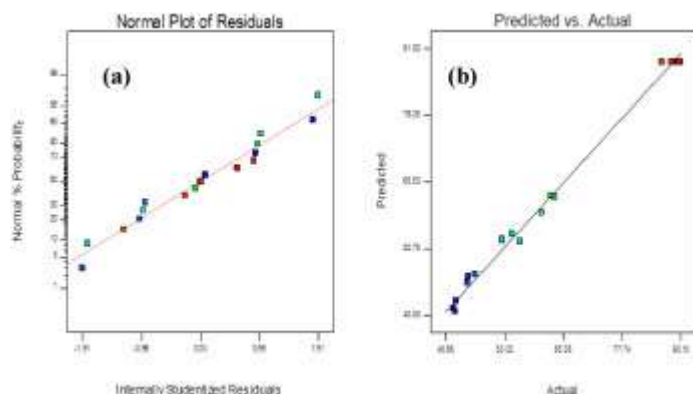
fitness. The normal plot of residuals and the responses (predicted and actual) are shown in Fig. 3.

Table 4. Fitness statistics.

Std. Dev.	0.0013	R-Squared	0.9944
Mean	0.0121	Adj R-Squared	0.9872
C.V. %	5.2785	Pred R-Squared	0.9468
PRESS	0.0001	Adeq Precision	54.97

Table 5. ANOVA statistics - BC panel.

Source	Sum of squares	df	Mean Square	F Value	p-value Prob > F	
Model	0.002929854	9	0.000326	239.1987597	<0.0001	significant
v° -Volume flow rate of water	0.001707325	1	0.001707	1254.502486	<0.0001	
θ -Collector inclination	0.000797582	1	0.000798	586.0446114	<0.0001	
α -Reflector inclination	7.91974E-05	1	7.92E-05	58.19241457	0.0001	
$v^\circ\theta$	0.000119356	1	0.000119	87.69974218	<0.0001	
$v^\circ\alpha$	0.00003364	1	3.36E-05	24.71789098	0.0016	
$\theta\alpha$	8.82566E-05	1	8.83E-05	64.84892286	<0.0001	
v°^2	7.06538E-05	1	7.07E-05	51.9148048	0.0002	
θ^2	1.09022E-05	1	1.09E-05	8.010716751	0.0254	
α^2	2.58625E-05	1	2.59E-05	19.00316112	0.0033	
Residual	9.5267E-06	7	1.36E-06			not significant
Lack of Fit	7.84822E-06	3	2.62E-06	6.234388852	0.0547	
Pure Error	1.67848E-06	4	4.2E-07			
Cor Total	0.002939381	16				

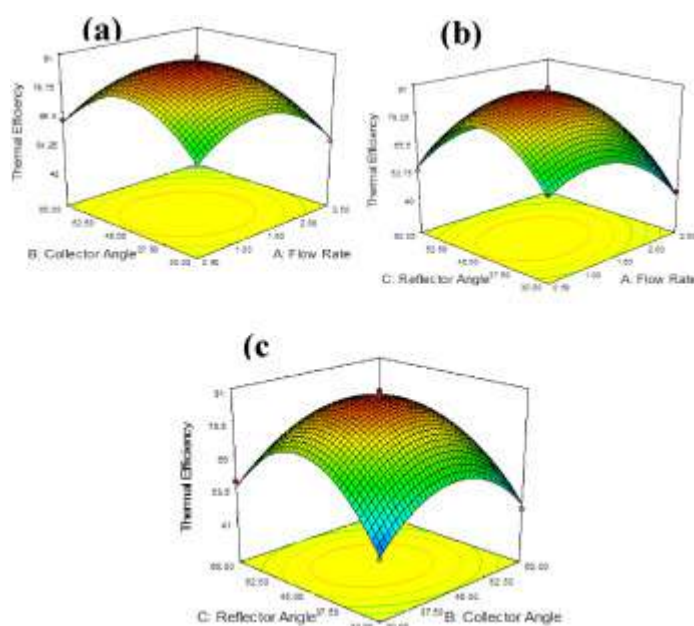


[Download : Download high-res image \(182KB\)](#)

[Download : Download full-size image](#)

Fig. 3. (a) Normal probability vs. internally studentized residuals, (b) Predicted vs. actual responses for Black-Chrome coated panel.

The response surface designed based on the derived regression model for black chrome coating was shown in Fig. 4(a), (b) and (c). Fig. 4(a) shows the interaction between the flow rate and the collector angle. At a lower flow rate, the collector angle records lower efficiency. The increase in these responses caused a rise in the efficiency to the maximum, and further increases in these responses reduced the thermal efficiency. Similarly, Fig. 4(b) shows the effect of interactions of flow rate and the reflector angle. Fig. 4(c) shows the influence of collector angle and reflector angle interaction.



[Download : Download high-res image \(619KB\)](#)

[Download : Download full-size image](#)

Fig. 4. Response surfaces of interactions for Black-Chrome coated panel (a) Flow rate vs. Collector angle, (b) Flow rate vs. Reflector angle, (c) Collector angle vs. Reflector angle.

When the flow rate was low, the water could not absorb more heat as the temperature between water and panel was low. As the flow rate increases, more heat is absorbed, and thus thermal efficiency increases. Further increase in flow rate reduced the time of heat absorption and resulted in lower thermal efficiency. The collector position should be such that to receive more incident solar rays perpendicular to its surface. If the angle of the collector deviates from that particular angle, the amount of energy received by the panel is reduced and results in reduced thermal efficiency.

Similarly, the reflector is to reflect the maximum rays felt on it to the panel, which happens at a certain angle. If the angle changes, the amount of reflected rays and the energy focused on the pane are reduced. It is evident from the discussion, all the there process variables in both the absorbers behave in the same manner. The lower value of the response shows the lower efficiency. Then, the efficiency was increased to a maximum with the process variable, and a further increase in the process variable reduced the efficiency. According to [Fig. 4](#), the flowrate and collector angle don't play individually but both are having interaction effects on thermal efficiency.

3.3. Design surface of variables – nickel-cobalt coated panel

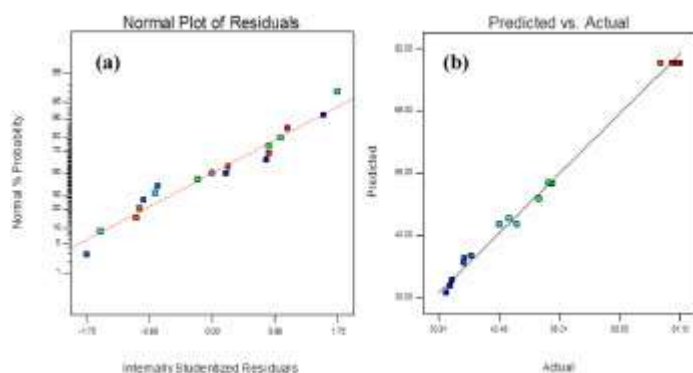
The Ni-Co panels observed data did not require any transformation as the maximum, and the minimum response ratio was less than 3. The sequential sum of the square of type I suggested the quadratic polynomial to develop the regression model. The values of R and Ra were 0.9864 and 0.9439 (presented in [Table 6](#)), which ensures the fitness of the model and data with the model. The ANOVA results (shown in [Table 7](#)) have also assured the accuracy above 95% confidence level. [Fig. 5](#) (a) shows the plot of residuals, and the predicted and actual responses are shown in [Fig. 5](#) (b). These plots are represented the prediction ability of proposed models.

Table 6. Fitness statistics.

Std. Dev.	0.0109	R-Squared	0.9896
Mean	0.0155	Adj R-Squared	0.9439
C.V. %	9.2801	Pred R-Squared	0.8854
PRESS	0	Adeq Precision	31.627

Table 7. ANOVA statistics.

Source	Sum of squares	df	Mean Square	F Value	p-value Prob > F	
Model	0.000639843	9	7.11E-05	74.24223809	<0.0001	significant
v° -Volume flow rate of water	0.000366392	1	0.000366	382.619336	<0.0001	
θ -Collector inclination	0.000194439	1	0.000194	203.0505749	<0.0001	
α -Reflector inclination	1.19561E-05	1	1.2E-05	12.48556271	0.0096	
$v^\circ\theta$	2.6061E-05	1	2.61E-05	27.21522259	0.0012	
$v^\circ\alpha$	4.55625E-07	1	4.56E-07	0.475803841	0.5125	
$\theta\alpha$	2.12982E-05	1	2.13E-05	22.24148644	0.0022	
$v^\circ\alpha^2$	6.4715E-06	1	6.47E-06	6.758106288	0.0354	
$\theta\alpha^2$	3.44662E-06	1	3.45E-06	3.599266195	0.0996	
α^2	1.025E-05	1	1.03E-05	10.70397698	0.0136	
Residual	6.70313E-06	7	9.58E-07			
Lack of Fit	4.89225E-06	3	1.63E-06	3.602116098	0.1238	not significant
Pure Error	1.81088E-06	4	4.53E-07			
Cor Total	0.000646546	16				

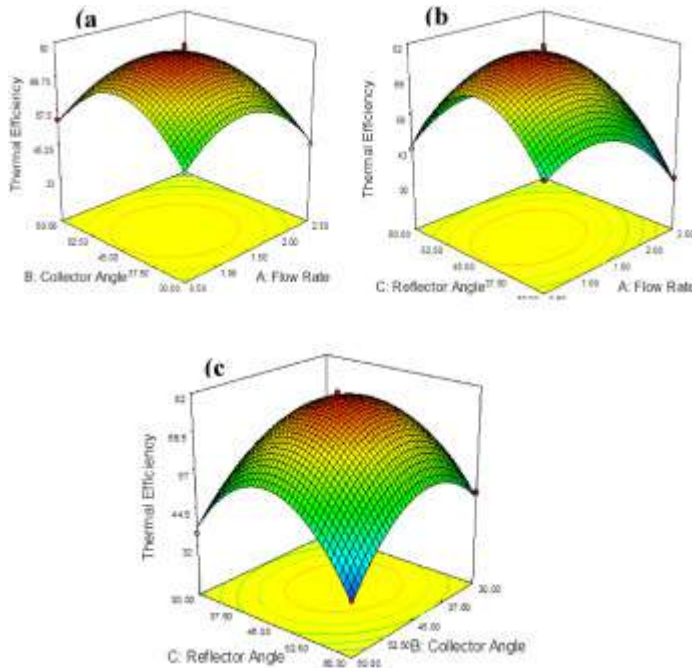


[Download : Download high-res image \(183KB\)](#)

[Download : Download full-size image](#)

Fig. 5. (a) Normal probability vs. internally studentized residuals, (b) Predicted vs. actual responses for Nickel-Cobalt coated panel.

The response surface designed based on the derived regression model is shown in Fig. 6. Fig. 6 (a) shows the interaction between the flow rate and the collector angle. At a lower flow rate, the collector angle records lower efficiency. The increase in these responses increases the efficiency to the maximum, and further increases in these responses reduce the thermal efficiency. The reason for this was already discussed in the previous section. Similarly, Fig. 6 (b) shows the effect of interactions of flow rate and the reflector angle.



[Download : Download high-res image \(699KB\)](#)

[Download : Download full-size image](#)

Fig. 6. Response surfaces of interactions for Nickel-Cobalt coated panel (a) Flow rate vs. Collector angle, (b) Flow rate vs. Reflector angle, (c) Collector angle vs. Reflector angle.

Fig. 6(c) shows the influence of collector angle and reflector angle interaction. It is evident from the discussion, all the three process variables in both the absorbers behave in the same manner. The lower value of the response shows the lower efficiency. Then, the efficiency was increased to a maximum with the process variable, and a further increase in the process variable reduced the efficiency. Fig. 6 also propose the effects of collector angle, reflector angle and flow rate on thermal efficiency on Nickel cobalt coated solar absorber panel.

In general, the thermal efficiency of the SEPC was influenced by flow rate, collector angle, and reflector angle. The Thermal Efficiency (TE) of the BC panel at all combinations of parameters were higher than the thermal efficiencies of the Ni-Co panel. Even though both BC and Ni-Co panels have almost identical solar absorptance, the Ni-Co panel has a higher emittance of 0.34, which is double that of the emittance of the BC panel. So, the energy emitted by the Ni-Co panel was more. The maximum difference in TEs was 10.3% which was observed in 1.5 L/min and 45°. The average efficiency found experimentally for BC panel was 58.67%, and for the Ni-

Co panel, 50.2% as comparatively higher than Flat Plate Collector (FPC). The efficiency of the FPC only increased from 41.5% to 48.9% by using Phase Change Materials [18].

3.4. Regression models

The independent variables of flow rate, collector angle and relector angle on dependent variables are predicted with developed regression models. The model developed based on significant factors identification from ANOVA Table. From this model terms are selected. The regression model developed for the response thermal efficiency of the SFPC with BC coated solar absorber panel and Ni-Co coated panels were presented in equations (2) and (3) below.

$$TE_{(BC)} = -322.632 + 39.458 * \text{flow rate} + 7.73783 * \text{collector angle} + (9.65783 * \text{reflector angle} - 0.210 * \text{flow rate} * \text{collector angle} - 0.188 * \text{flow rate} * \text{reflector angle} - 0.01388 * \text{collector angle} * \text{reflector angle} - 14.96758 * \text{flow rate}^2 + 0.07796 * \text{collector angle}^2 - 0.10330 * \text{reflector angle}^2 \quad (2)$$

$$TE_{(Ni-Co)} = -327.325 + 38.352 * \text{flow rate} + 7.60783 * \text{collector angle} + (9.61117 * \text{reflector angle} - 0.21000 * \text{flow rate} * \text{collector angle} - 0.1967 * \text{flow rate} * \text{reflector angle} - 0.01389 * \text{collector angle} * \text{reflector angle} - 14.8925 * \text{flow rate}^2 + 0.076522 * \text{collector angle}^2 - 0.10330 * \text{reflector angle}^2$$

$$TE_{(Ni-Co)} = -327.325 + (38.352 * \text{Flow rate}) + (7.60783 * \text{Collector angle}) + (9.61117 * \text{Reflector angle}) - (0.21000 * \text{Flow rate} * \text{Collector angle})$$

$$+ (0.1967 * \text{Flow rate} * \text{Reflector angle}) - (0.01389 * \text{Collector angle} * \text{Reflector angle}) - (14.8925 * \text{Flow rate}^2) - (0.076522 * \text{Collector angle}^2) - (0.103 * \text{Reflector angle}^2)$$

$$\text{Reflector angle}) - (14.8925 * \text{Flow rate}^2) - (0.076522 * \text{Collector angle}^2) - (0.103 * \text{Reflector angle}^2)$$

3.5. Optimization

The desirability approach is used to identify the best value. Generally the desirability approach is performed based on the target levels. So the desirability value is fixed around 0.984 and 0.974 for black chrome and Ni-Co coated solar absorber panel respectively. The objective of this optimization was to maximize the thermal efficiency in equation (4) subjected to the constraints as follows.

Objective function.

Thermal Efficiency = maximize $f(x)$,

$$f(x) = \frac{mC_p(T_2 - T_1)}{AG} \quad (4)$$

where.

$$f(x) = \frac{mC_p(T_2 - T_1)}{AG}$$

Subjected to.

0.5 l/min <= Flow rate >= 1.5 l/min.

30°<= Collector angle >= 60° and.

30°<= Reflector angle >= 60°

All the process variables were given equal importance and weightage. The software found about 30 solutions. Based on the desirability, the best combination of process variables was chosen. The corresponding response was noted, as shown in [Table 8](#).

Table 8. Optimized values of process variables and corresponding responses.

Panel	Flow Rate	Collector Angle	Reflector Angle	Thermal Efficiency	Desirability	
Black-Chrome	1.28	43.89	44.92	89.3283	0.984	Selected
Ni-Co	1.32	46.91	42.34	79.246	0.974	Selected

4. Conclusions

- The absorptance and emittance of the BC panel were 0.91 and 0.16, and for the Ni-Co panel, 0.92 and 0.34.
- Due to the high emittance of the Ni-Co panel, the energy emitted was more and always registered lower TE than BC panel.
- The average efficiency of BC panel was 58.67%, and the Ni-Co panel was 50.19%
- The maximum thermal efficiency of 89.3% can be obtained at 1.28 l/min, 43.89° of collector angle, and 44.92° of reflector angle for Black Chrome panel and Nickel-Cobalt panel, the maximum thermal efficiency is 79.2% at 1.32 l/min of flow rate, 46.91° of collector angle, and 42.34° of reflector angle.
- The maximum efficiency of the Black Chrome panel is 10.01% higher than the maximum efficiency of the Nickel-Cobalt panel.

All authors have no conflict of interest

C. Ramesh, M. Vijayakumar, Saad Alshahrani 3, G. Navaneethakrishnan, R. Palanisamy, – conceptualization, Methodology.

Natrayan L - Validation.

Asif Afzal, Saboor Shaik, Hitesh Panchal – supervision.

C Ahamed Saleel - Funding acquisition, Project administration.

Declaration of competing interest




The authors declare that they have no known competing financial interests or personal relationships that could have appeared to influence the work reported in this paper.

Acknowledgement

The authors extend their appreciation to the Deanship of Scientific Research at King Khalid University, Saudi Arabia for funding this work through Large Groups under Grant No: [RGP 2/32/43](#).

[Recommended articles](#)

References

- [1] Seyed Ali Sakhaei, Mohammad Sadegh Valipour
Performance enhancement analysis of the flat plate collectors. A comprehensive review
Renew. Sustain. Energy Rev., 102 (2019), pp. 186-204, [10.1016/j.rser.2018.11.014](#)
[Google Scholar](#)
- [2] Shady M. Henein, Ahmed A. Abdel-Rehim
The performance response of a heat pipe evacuated tube solar collector using MgO/MWCNT hybrid nanofluid as a working fluid
Case Stud. Therm. Eng., 33 (2022), Article 101957, [10.1016/j.csite.2022.101957](#)
[Article](#)  [Download PDF](#) [View Record in Scopus](#) [Google Scholar](#)
- [3] Tadahmun A. Yassen, Nassir D. Mokhlif, Muhammad Asmail Eleiwi
Performance investigation of an integrated solar water heater with corrugated absorber surface for domestic use
Renew. Energy, 138 (2019), pp. 852-860, [10.1016/j.renene.2019.01.114](#)
[Article](#)  [Download PDF](#) [View Record in Scopus](#) [Google Scholar](#)
- [4] Alsanossi M. Aboghrara, B.T.H.T. Baharudin, M.A. Alghoul, Nor Mariah Adam, A.A. Hairuddin, Husam A. Hasan
Performance analysis of solar air heater with jet impingement on corrugated absorber plate
Case Stud. Therm. Eng., 10 (2017), pp. 111-120, [10.1016/j.csite.2017.04.002](#)
[Article](#)  [Download PDF](#) [View Record in Scopus](#) [Google Scholar](#)
- [5] IonVisa, Macedon Moldovan, Anca Duta
Novel triangle flat plate solar thermal collector for facades integration

Renew. Energy, 143 (2019), pp. 252-262, [10.1016/j.renene.2019.05.021](https://doi.org/10.1016/j.renene.2019.05.021)

[Google Scholar](#)

- [6] Sebastian Müller, Federico Giovannetti, Rolf Reineke-Koch, Oliver Kastner, Bernd Hafner
Simulation study on the efficiency of thermochromic absorber coatings for solar thermal flat-plate collectors
Sol. Energy, 188 (2019), pp. 865-874, [10.1016/j.solener.2019.06.064](https://doi.org/10.1016/j.solener.2019.06.064)
[Article](#)  [Download PDF](#) [View Record in Scopus](#) [Google Scholar](#)
- [7] Ljiljana T. Kostic, Zoran T. Pavlovic
Optimal position of flat plate reflectors of solar thermal collector
Energy Build., 45 (2012), pp. 161-168, [10.1016/j.enbuild.2011.10.059](https://doi.org/10.1016/j.enbuild.2011.10.059)
[Article](#)  [Download PDF](#) [View Record in Scopus](#) [Google Scholar](#)
- [8] D.K. McDaniels, D.H. Lowndes, H. Mathew, J. Reynolds, R. Gray
Enhanced solar energy collection using reflector-solar thermal collector combinations
Sol. Energy, 17 (5) (1975), pp. 277-283, [10.1016/0038092X\(75\)90044-4](https://doi.org/10.1016/0038092X(75)90044-4)
[Article](#)  [Download PDF](#) [View Record in Scopus](#) [Google Scholar](#)
- [9] Mojtaba Moravej, Mohammad Reza Saffarian, Larry K. B. Li, Mohammad Hossien Doranehgard and Qingang Xiong. (2020). Experimental investigation of circular flat-panel collector performance with spiral pipes. Journal of Thermal Analysis and Calorimetry, 140:1229-1236. <https://doi.org/10.1007/s10973-019-08879-1>.
[Google Scholar](#)
- [10] N. Karuppiah, S. John
Characterization of electrodeposited nickel-cobalt based selective coatings for solar thermal energy conversion
Bull. Electrochem., 16 (2) (2000), pp. 71-74
[View Record in Scopus](#) [Google Scholar](#)
- [11] M. Bagheri, F. Ashrafizadeh, M. Hosseini Najafabadi
Black nickel coating and color anodized layers for solar absorber
Trans. Indian Inst. Met., 67 (2014), pp. 927-934, [10.1007/s12666-014-0418-3](https://doi.org/10.1007/s12666-014-0418-3)
[View Record in Scopus](#) [Google Scholar](#)
- [12] Himangshu Bhowmik, Ruhul Amin
Efficiency improvement of flat plate solar collector using reflector
Energy Rep., 3 (2017), pp. 119-123, [10.1016/j.egyr.2017.08.002](https://doi.org/10.1016/j.egyr.2017.08.002)
[Article](#)  [Download PDF](#) [View Record in Scopus](#) [Google Scholar](#)
- [13] Sebastian Foste, Alexandra Pazidis, Rolf Reineke-Koch, Bernd Hafner, David Mercks, Christine Delord
flat plate collectors with thermochromic absorber coatings to reduce loads during stagnation

Energy Proc., 91 (2016), pp. 42-48, [10.1016/j.egypro.2016.06.169](https://doi.org/10.1016/j.egypro.2016.06.169)

[Article](#)  [Download PDF](#) [View Record in Scopus](#) [Google Scholar](#)

- [14] J. Jyothi, Harsh Chaliyawala, G. Srinivas, H.S. Nagaraja, Harish C. Barshilia
**Design and fabrication of spectrally selective
TiAlC/TiAlCN/TiAlSiCN/TiAlSiCO/TiAlSiO tandem absorber for high temperature
solar thermal power applications**

Sol. Energy Mater. Sol. Cell., 140 (2015), pp. 209-216, [10.1016/j.solmat.2015.04.018](https://doi.org/10.1016/j.solmat.2015.04.018)

[Article](#)  [Download PDF](#) [View Record in Scopus](#) [Google Scholar](#)

- [15] Reyhaneh Loni, Alibakhsh Kasaeian, Kazem Shahverdi, Ezzatollah Askari Asli-Ardeh, Barat Ghobadian, H. Mohammad, Ahmadi
**ANN model to predict the performance of parabolic dish collector with tubular cavity
receiver**

Mechan. Ind., 18 (4) (2017), p. 408, [10.1051/meca/2017016](https://doi.org/10.1051/meca/2017016)

[View Record in Scopus](#) [Google Scholar](#)

- [16] Chung-Feng Jeffrey Kuo, Te-Li Su, Po-Ruei Jhang, Chao-Yang Huang, Chin-Hsun Chiu
**Using the Taguchi method and grey relational analysis to optimize the flat-plate
collector process with multiple quality characteristics in solar energy collector
manufacturing**

Energy, 36 (5) (2011), pp. 3554-3562, [10.1016/j.energy.2011.03.065](https://doi.org/10.1016/j.energy.2011.03.065)

[Google Scholar](#)

- [17] Rogério Antônio Xavier Nunes, Vilma Conceição Costa, Sade Wagner, Frederico Resende Araújo, Guilherme Marconi Silva

Selective surfaces of black chromium for use in solar absorbers

Mater. Res., 21 (1) (2018), pp. 1-5, [10.1590/1980-5373-MR-2017-0556](https://doi.org/10.1590/1980-5373-MR-2017-0556)

[Google Scholar](#)

- [18] Seyed Ali Sakhaei, Mohammad Sadegh Valipour
**Thermal behavior of a flat plate solar collector with simultaneous use of helically heat
collecting tubes and phase change materials**

Sustain. Energy Technol. Assessments, 46 (2021), Article 101279,

[10.1016/j.seta.2021.101279](https://doi.org/10.1016/j.seta.2021.101279)

[Google Scholar](#)

Cited by (10)

[Inedible oil feedstocks for biodiesel production: A review of production
technologies and physicochemical properties](#)

2022, Sustainable Chemistry and Pharmacy

[Show abstract](#) ✓

Biofuel from leather waste fat to lower diesel engine emissions: Valuable solution for lowering fossil fuel usage and perception on waste management

2022, Process Safety and Environmental Protection

[Show abstract](#) ✓

Recent developments in utilizing hydrous ethanol for diverse engine technologies

2022, Chemical Engineering and Processing - Process Intensification

[Show abstract](#) ✓

Influence of nano titanium oxide reinforced Al-7075 matrix composites in stir casting method

2022, Materials Today: Proceedings

[Show abstract](#) ✓

Effect of walnut powder reinforcement on the mechanical properties of biodegradable natural flax/hemp fibre-based composites

2022, Materials Today: Proceedings

[Show abstract](#) ✓

Mechanical performance of aloe vera/dharbai-based hybrid epoxy composites with enhanced NaHCO_3 treatment

2022, Materials Today: Proceedings

[Show abstract](#) ✓

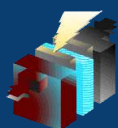
View all citing articles on Scopus

© 2022 The Authors. Published by Elsevier Ltd.



Copyright © 2022 Elsevier B.V. or its licensors or contributors.
ScienceDirect® is a registered trademark of Elsevier B.V.





Effect of Silicon Carbide on the Mechanical and Thermal Properties of Snake Grass/Sisal Fiber Reinforced Hybrid Epoxy Composites

Vijayakumar M^{1*}, Kumaresan K², Gopal R³, Vetrivel S D⁴ and Vijayan V⁵

¹ Department of Mechanical Engineering, JCT college of Engineering and Technology, Coimbatore, Tamilnadu, India

² Department of Mechanical Engineering, Park College of Engineering and Technology, Coimbatore, Tamilnadu, India

³ Department of Mechanical Engineering, Trichy Engineering College, Trichy, Tamilnadu, India

⁴ Department of Robotics and Automation Engineering, PSG College of Technology, Coimbatore 641004, Tamil Nadu, India

⁵ Department of Mechanical Engineering, K.Ramakrishnan College of Technology, Trichy, Tamil Nadu, India

Corresponding Author Email: mechmvijay@gmail.com

ABSTRACT

In this study, an attempt was made to develop and characterize Snake Grass Fiber (SGF)/Silicon Carbide (SiC)/epoxy and Snake Grass Fiber/Sisal Fiber (SF)/Silicon Carbide/epoxy hybrid composites using a compression moulding technique. Mechanical characteristics of the produced hybrid composites such as tensile, flexural, and hardness tests were analyzed. Also experiments have been carried out to predict the thermal stability of the fabricated composite samples. The interface between fiber and matrix was examined by using Scanning Electron Microscopy (SEM). Among SGF/SiC/epoxy and SGF/SF/SiC/epoxy composites, it has been observed that hybrid composite SGF/SF/SiC/epoxy exhibits the higher hardness of 82 Shore-D, tensile strength of 51 MPa and flexural strength of 73 MPa. In contrast to the mechanical properties, the percentage of water absorption was lower in the SGF/SiC/epoxy hybrid composite. It is proven from the results that the SGF/SF/SiC/epoxy hybrid composites will enhance the strength of the composites. This composite material is also a potential candidate for the hardware of energy devices including electrochemical energy along with Fuel Cell systems.

Keywords: hybrid composite, snake grass fiber, sisal fiber, SiC, mechanical properties, water absorption, thermal properties

Received: January-25-2021, Accepted: April-15-2021, <https://doi.org/10.14447/jnmes.v24i2.a09>

1. INTRODUCTION

Natural fiber reinforced polymer composites have attracted considerable interests especially in automotive, energy, including electrochemical energy hardware devices construction and furniture applications. The Natural fibers are low density, high strength, biodegradability and lightweight fibers which are extracted from plants, suitable for fabricating low cost, non-toxicity, high strength to weight ratio and good wear resistance polymer Composites [1].

Sathiskumar et al. [2] extracted the snake grass fiber, tested its properties like density, diameter, tensile strength and % elongation. Also prepared the composites with snake fiber reinforcement and isophthalic unsaturated polyester resin for different volume fractions. They reported that the 25 % volume fraction composite exhibited the highest tensile strength and flexural strength. Ganeshan et al. [3] investigated the effect of fiber length and fiber content on the mechanical properties in the madar fiber reinforced polyster composites. It is found that Mechanical properties increase with the increase in fiber length (5 mm to 10 mm) and fiber wt% (20 to 25). Likewise Higher madar fiberwt % composites strength decreased with the increased in fiber length (15 mm and 20 mm). de Andrade Silva et al. [4] studied the tensile strength of the sisal fiber reinforced FRP composite with different fiber length and concluded that short length of the fiber imparts notable tensile strength in the composite. Sathish et al. [5] prepared the hybrid composites of different volume fractions using flax and bamboo fibers and epoxy resin by compression molding technique. They reported that the tensile and flexural

strength was high for the sample contains 30% bamboo fiber.

However, proper fiber surface treatment is required to improve the interface between the fibers and matrix. Various methods used are Acetylation treatment, alkaline treatment, Benzoylation, furfuryl alcohol (FA) treatment, Peroxide treatment and Permanganate treatment. Alkaline, heat and coupling agent treatments are necessary to overcome the poor interfacial bonding between sisal fiber and the matrix [6]. Bakare et al. [7] analyzed the water treated and untreated sisal fiber reinforced polyurethane composite for its mechanical behavior. Li et al. [8] investigated the adhesion behavior between sisal fiber and the matrix by using Silane and KMnO₄ treated sisal fiber reinforced to high density polyethylene (HDPE) composites. Because of the hydrophilic nature of cellulose and the hydrophobic properties of HDPE the interaction between sisal fibers and the HDPE matrix was poor. But KMnO₄ surface treatment method is more helpful in adhesion bonding between fibers and the HDPE resin. Proper selection of fibers, epoxy resin and surface treatments of the natural fibers plays an important role in fiber reinforced polymer based composites. Rong et al. [9] studied the effect of various chemically treated sisal fibers in the epoxy composites to predict the relationship between mechanical properties and adhesion property. It is found that achieved higher fiber stiffness and the adhesion between fiber bundles. Also the matrix has increased flexural strength. Sathiskumar et al. [10] studied the influences of two different combinations natural fibers in the hybrid polymer matrix.

Hybrid composites are reinforced with snake grass/banana fibers and snake grass/coir fibers fabricated to compare its

DEVELOPMENT OF Al6061-Si₃N₄- GRAPHITE USING STIR CASTING FOR WEAR APPLICATION

¹Ananda Kumar.D, ²Krishnakumar.R

¹Department Of Mechanical Engineering, JCT College Of Engineering And Technology, Coimbatore.

²Department Of Mechanical Engineering, JCT College Of Engineering And Technology, Coimbatore.

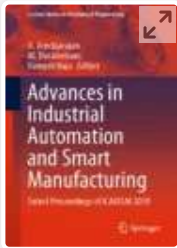
Abstract

Composite have been significantly improved with the introduction of ceramic particles .They show high hardness and they lead to intensive abrasive wear in cutting tool. Composites are wonder material with light weight ,high strength to weight ratio and stiffness property have come along a long way in replacing the conventional materials like metals, wood etc. Metal Matrix Composites (MMC's) have evoked a keen interest in recent times for potential applications. Metal Matrix Composites have very light weight, high strength, and stiffness and exhibit greater resistance to corrosion, oxidation and wear. Fatigue resistance is an especially important property of Al-MMC, which is essential for automotive application. Because their superior properties such as light weight, low density, high strength to weight ratio, high hardness, high temperature and thermal shock resistance, superior wear and corrosive resistance, high specific modulus, high fatigue strength has been improved. In this study metal-matrix composites (MMCs) are fabricated by melt-stirring technique. This new edition has been greatly enlarged and updated to provide both scientists and engineers with a clear and comprehensive understanding of composite materials. In describing both theoretical and practical aspects of their production, properties and usage, the book crosses the borders of many disciplines. Topics covered include: fibbers, matrices, laminates and interfaces; elastic deformation, stress and strain, strength, fatigue crack propagation and creep resistance; toughness and thermal properties; fatigue and deterioration under environmental conditions; fabrication and applications. Coverage has been increased to include polymeric, metallic and ceramic matrices and reinforcement in the form of long fibres, short fibres and particles. Designed primarily as a teaching text for final year undergraduates in materials science and engineering, this book will also interest undergraduates and postgraduates in chemistry, physics, and mechanical engineering. In addition, it will be an excellent source book for academic and technological researchers on materials.

Keywords: Metal Matrix Composites, Al 6061 , Si₃N₄-Gr, STIR Casting, EDM.

1. Introduction

Composites consist of one or more discontinuous phases embedded in a continuous phase. The discontinuous phase is usually harder and stronger than the continuous phase and is called the 'reinforcement' or 'reinforcing material', whereas the continuous phase is termed as the 'matrix'. Properties of composites are strongly dependent on the properties of their constituent materials, their distribution and the interaction among them. The composite properties may be the volume fraction sum of the properties of the constituents or the constituents may interact in a synergistic way resulting in improved or better properties. Apart from the nature of the constituent materials, the geometry of the reinforcement (shape, size and size distribution) influences the properties of the composite to a great extent. The concentration distribution and orientation of the reinforcement also affect the properties. Metal Matrix Composites are composed of a metallic matrix (Al,Mg,Fe,Cu etc) and dispersed ceramic (oxide, carbides) or metallic phase(Pb,Mo,W etc). Ceramic reinforcement may be silicon carbide, boron, alumina, silicon nitride, boron carbide, boron nitride etc. whereas Metallic Reinforcement may be tungsten, beryllium etc. MMCs are used for Space Shuttle, commercial airliners, electronic substrates, bicycles, automobiles, golf clubs and a variety of other applications. From a material point of view, when compared to polymer matrix composites, the advantages of MMCs lie in their retention of strength and stiffness at



Advances in Industrial Automation and Smart Manufacturing pp 711–716

Non-destructive Evaluation for Composite Aluminium Composites

[I. J. Isaac Premkumar](#) , [V. Vijayan](#), [K. Rajaguru](#) & [B. Suresh Kumar](#)

Conference paper | [First Online: 21 October 2020](#)

888 Accesses

Part of the [Lecture Notes in Mechanical Engineering](#) book series (LNME)

Abstract

Aluminium can be used to make parts of aircrafts, and it is less in strength. The combination of aluminium with titanium carbide will increase the strength of the material. By varying the

Your Privacy

We use cookies to make sure that our website works properly, as well as some 'optional' cookies to personalise content and advertising, provide social media features and analyse how people use our site. By accepting some or all optional cookies you give consent to the processing of your personal data, including transfer to third parties, some in countries outside of the European Economic Area that do not offer the same data protection standards as the country where you live. You can decide which optional cookies to accept by clicking on 'Manage Settings', where you can also find more information about how your personal data is processed. Further information can be found in our privacy policy.

**Accept all
cookies**

Manage preferences

sub surface of the material; Different types of aluminium alloys are mixed with different composition of titanium carbide to increase the strength.

Keywords

Aluminium **Titanium carbide strength**

Non-destructive testing **Penetrant test**

This is a preview of subscription content, [access via your institution](#).

▼ Chapter

EUR 29.95

Price includes VAT (India)

- DOI: 10.1007/978-981-15-4739-3_62
- Chapter length: 6 pages
- Instant PDF download
- Readable on all devices
- Own it forever
- Exclusive offer for individuals only
- Tax calculation will be finalised during checkout

Buy Chapter

> eBook

EUR 181.89

> Softcover Book

EUR 219.99

Your Privacy

We use cookies to make sure that our website works properly, as well as some ‘optional’ cookies to personalise content and advertising, provide social media features and analyse how people use our site. By accepting some or all optional cookies you give consent to the processing of your personal data, including transfer to third parties, some in countries outside of the European Economic Area that do not offer the same data protection standards as the country where you live. You can decide which optional cookies to accept by clicking on ‘Manage Settings’, where you can also find more information about how your personal data is processed. Further information can be found in our privacy policy.

2. Hellier C (2003) Handbook of nondestructive evaluation. McGraw-Hill. p 1.1. ISBN 0-07-028121-1

3. Introduction to nondestructive testing. asnt.org

4. Bridges, A (2013) High speed cameras for non-destructive testing, NASA TechBriefs

5. Radiography (RT) Reference Standards, PH Tool. customers.phtool.com

6. Singh S, Goyal A (2007) The origin of echocardiography: a tribute to Inge Edler. Tex Heart Inst J 34:431–435. PMC 2170493. PMID 18172524

7. Ahi, K (2018) A method and system for enhancing the resolution of Terahertz imaging. Measurement

8. Hellier C (2003) Handbook of nondestructive

Your Privacy

We use cookies to make sure that our website works properly, as well as some 'optional' cookies to personalise content and advertising, provide social media features and analyse how people use our site. By accepting some or all optional cookies you give consent to the processing of your personal data, including transfer to third parties, some in countries outside of the European Economic Area that do not offer the same data protection standards as the country where you live. You can decide which optional cookies to accept by clicking on 'Manage Settings', where you can also find more information about how your personal data is processed. Further information can be found in our privacy policy.

nondestructive testing in detecting surface cracks of welded components. *Nondestruct Tes Eval* 33(3):290–300

11. Tamizharasan T, Senthil Kumar N, Selvkumar V, Dinesh S (2019) Taguchi's methodology of optimizing turning parameters over chip thickness ratio in machining PM AMMC. *SN Appl Sci* 1:160
 12. Raju R, Sivalingam V, Sun J, Natarajan M, Zhao Y (2019) Experimental and Taguchi-based grey approach of laser metal deposition technique on nickel-based superalloy. *Trans Indian Inst Met* 72(1):205–214
 13. Dinesh S, Rajkumar T, Muthukumarasamy S, Satheesh Kumar G, Kajendrakumar SV, Suresh Kumar B (2019) Analysis and optimization of machining parameters in through feed centerless grinding of high carbon steel. *J Mech Eng Technol* 9(13):431–441
-

Your Privacy

We use cookies to make sure that our website works properly, as well as some 'optional' cookies to personalise content and advertising, provide social media features and analyse how people use our site. By accepting some or all optional cookies you give consent to the processing of your personal data, including transfer to third parties, some in countries outside of the European Economic Area that do not offer the same data protection standards as the country where you live. You can decide which optional cookies to accept by clicking on 'Manage Settings', where you can also find more information about how your personal data is processed. Further information can be found in our privacy policy.

15. Parameswaran P, Godwin Antony A, Dinesh S, Radhakrishnan K (2018) Experimental study on mechanical and corrosion characteristics NAB alloy with the addition of chromium. Mater Today Proc 5:8089–8094

16. Jeyaprakash N, Duraiselvam M, Raju R (2018) Modelling of Cr_3C_2 -25% NiCr laser alloyed cast iron in high temperature sliding wear condition using response surface methodology. Arch Metall Mater 63(3):1303–1315

17. Dinesh S, Godwin Antony A, Rajaguru K, Vijayan V (2017) Experimental investigation and optimization of material removal rate and surface roughness in centerless grinding of magnesium alloy using grey relational analysis. Mech Mech Eng 21(1):17–28

18. Thirugnanasambantham KG, Raju R, Sankaramoorthy T, Velmurugan P, Kannagi A, Reddy MCK, Chandra VR (2018) Degradation

Your Privacy

We use cookies to make sure that our website works properly, as well as some 'optional' cookies to personalise content and advertising, provide social media features and analyse how people use our site. By accepting some or all optional cookies you give consent to the processing of your personal data, including transfer to third parties, some in countries outside of the European Economic Area that do not offer the same data protection standards as the country where you live. You can decide which optional cookies to accept by clicking on 'Manage Settings', where you can also find more information about how your personal data is processed. Further information can be found in our privacy policy.

aeronautical turbine applications. Lasers Eng
37(4–6):247–260

20. Venkatesh R, Vijayan V (2016) Performance evaluation of multipurpose solar heating system. Mech Mech Eng 20(4):359–370

21. Sivalingam V, Sun J, Yang B, Liu K, Raju R (2018) Machining performance and tool wear analysis on cryogenic treated insert during end milling of Ti–6Al–4V alloy. J Manuf Process 36:188–196

22. Dinesh S, Godwin Antony A, Rajaguru K, Vijayan V (2016) Experimental investigation and optimization of material removal rate and surface roughness in CNC turning of EN24 alloy steel. Mech Mech Eng 20(4):451–466

23. Raju R, Manikandan N, Palanisamy D, Arulkirubakaran D, Sambathkumar S, Bhanu Prakash P (2018) Optimization of process

.

Your Privacy

We use cookies to make sure that our website works properly, as well as some 'optional' cookies to personalise content and advertising, provide social media features and analyse how people use our site. By accepting some or all optional cookies you give consent to the processing of your personal data, including transfer to third parties, some in countries outside of the European Economic Area that do not offer the same data protection standards as the country where you live. You can decide which optional cookies to accept by clicking on 'Manage Settings', where you can also find more information about how your personal data is processed. Further information can be found in our privacy policy.

I. J. Isaac Premkumar

**Department of Mechanical Engineering,
K.Ramakrishnan College of Technology,
Samaypuram, Tiruchirappalli, Tamil Nadu,
621112, India**

V. Vijayan, K. Rajaguru & B. Suresh Kumar

Corresponding author

Correspondence to [I. J. Isaac Premkumar](#).

Editor information

Editors and Affiliations

**Indian Institute of Technology Madras, Chennai,
India**

Dr. A. Arockiarajan

**National Institute of Technology Tiruchirappalli,
Tiruchirappalli, India**

Dr. M. Duraiselvam

Santhiram Engineering College, Nandyal, India

Dr. Ramesh Raju

Rights and permissions

— . — . .

Your Privacy

We use cookies to make sure that our website works properly, as well as some 'optional' cookies to personalise content and advertising, provide social media features and analyse how people use our site. By accepting some or all optional cookies you give consent to the processing of your personal data, including transfer to third parties, some in countries outside of the European Economic Area that do not offer the same data protection standards as the country where you live. You can decide which optional cookies to accept by clicking on 'Manage Settings', where you can also find more information about how your personal data is processed. Further information can be found in our privacy policy.

Isaac Premkumar, I.J., Vijayan, V., Rajaguru, K., Suresh Kumar, B. (2021). Non-destructive Evaluation for Composite Aluminium Composites. In: Arockiarajan, A., Duraiselvam, M., Raju, R. (eds) Advances in Industrial Automation and Smart Manufacturing. Lecture Notes in Mechanical Engineering. Springer, Singapore.
https://doi.org/10.1007/978-981-15-4739-3_62

[.RIS](#)  [.ENW](#)  [.BIB](#) 

DOI

https://doi.org/10.1007/978-981-15-4739-3_62

Published	Publisher Name	Print ISBN
21 October 2020	Springer, Singapore	978-981-15- 4738-6
Online ISBN	eBook Packages	
978-981-15- 4739-3	Engineering , Engineering (R0)	

Not logged in - 182.76.193.198

AICTE Electrical & Electronics & Computer Science Engineering (3000684219) - JCT College of Engineering and Technology (3000987508) - AICTE Mechanical Engineering e-Jour (3000684257)

SPRINGER NATURE

© 2022 Springer Nature Switzerland AG. Part of [Springer Nature](#).

Your Privacy

We use cookies to make sure that our website works properly, as well as some 'optional' cookies to personalise content and advertising, provide social media features and analyse how people use our site. By accepting some or all optional cookies you give consent to the processing of your personal data, including transfer to third parties, some in countries outside of the European Economic Area that do not offer the same data protection standards as the country where you live. You can decide which optional cookies to accept by clicking on 'Manage Settings', where you can also find more information about how your personal data is processed. Further information can be found in our privacy policy.

Your Privacy

We use cookies to make sure that our website works properly, as well as some 'optional' cookies to personalise content and advertising, provide social media features and analyse how people use our site. By accepting some or all optional cookies you give consent to the processing of your personal data, including transfer to third parties, some in countries outside of the European Economic Area that do not offer the same data protection standards as the country where you live. You can decide which optional cookies to accept by clicking on 'Manage Settings', where you can also find more information about how your personal data is processed. Further information can be found in our privacy policy.

Research Article

Transesterification Studies on Avocado Seed Oil Using Carbon Supported CuO Nano Catalyst: Rate Kinetics and Thermodynamic Aspects

Bashyam Sasikumar¹, **Prabahar Jeevanandam**,² **Venkatesh Babu Samikkannu**,³
and **J. B. Veeramalini**⁴

¹Faculty of Mechanical Engineering, Arba Minch University, Arba Minch, Ethiopia

²Mechanical Engineering, JCT College of Engineering and Technology, Pichanur, Coimbatore 641105, India

³Department of Petroleum Engineering, JCT College of Engineering and Technology, Pichanur, Coimbatore 641105, India

⁴Vel Tech High Tech Dr Rangarajan Dr Sakunthala Engineering College, Chennai, India

Correspondence should be addressed to Bashyam Sasikumar; bashyam.sasikumar@amu.edu.et

Received 25 May 2022; Revised 26 June 2022; Accepted 4 July 2022; Published 25 July 2022

Academic Editor: Samson Jerold Samuel Chelladurai

Copyright © 2022 Bashyam Sasikumar et al. This is an open access article distributed under the Creative Commons Attribution License, which permits unrestricted use, distribution, and reproduction in any medium, provided the original work is properly cited.

This study focused on the production of biodiesel using avocado seed oil (ASO) through esterification of free fatty acids (FFA) in the presence of carbon supported CuO nanoparticles (CuO/C). ASO was obtained using hexane as a solvent by Soxhlet extraction. Further characterization of ASO revealed that the oil had 8.2-10.2% ($\pm 0.2\%$) of FFA content. Using a two-step technique, the FFA content was decreased below 1% through esterification using a catalyst prepared from carbon supported nanoparticles of CuO. Additionally, CuO/C catalyst was characterized by different techniques, such as XRD and BET. From the investigations, the optimal time for the esterification process was found to be 6 h at 673 K. The use of carbon supported CuO nanoparticle for the transesterification process of ASO has not been attempted in earlier. Also, the studies on FFA present in the avocado seed oil had a significant outcome in this investigation. Further, the data observed from the reactions conducted at different temperatures were subjected for kinetic analysis to determine the reaction rate and thermodynamic study for activation energy.

1. Introduction

At present, global energy requirement is accelerating daily. Undeniably, fossil fuels are depleting, which result in a serious look for alternative renewable fuels [1]. Alternative renewable fuels can be obtained from biogenic wastes and residues through chemical, biochemical, and thermochemical processing. In this view, a numerous researches are showing interest towards the synthesis biodiesel which refers to any diesel fuel substitute. Biodiesel is classified as a combustion fuel which derived from renewable resources that can be used in diesel engines. It is an environmentally

friendly fuel equivalent to petroleum diesel [2–7]. As an alternative to fuel, biodiesel has many benefits over petroleum diesel. It is derived from a sustainable, domestic resource that relieves the dependence on imports of petroleum fuel. Biodiesel exhibits a more comfortable emission profile relative to petroleum fuel, such as low carbon monoxide emissions and particulate matter. Yet, another salient advantage of biodiesel are biodegradable, nontoxic, and unburned hydrocarbons. Furthermore, the CO₂ expelled by the combustion process can be reused using photosynthesis technique. Hence, the greenhouse effect is reduced considerably [8]. However, the feedstock required for the production

of biodiesel needs approximately 75% of the overall cost. The biodiesel feedstocks are selected based on some notable properties of the oil such as low price, good free fatty acid content and high content of oil, low cost for cultivation, controllable growth and effective harvesting, rate of maturity of the seeds, and comparable better market for byproducts [9, 10].

Biodiesel holds many advantages because of its significant molecular similarities between biodiesel and paraffinic diesel fuel compounds, which makes a suitable alternative fuel that likely to meet the diesel engine's fuel requirements. Basically, there is no need for engine modifications to replace biodiesel with diesel fuel that can improve the performance of the IC engine. Further, the biodiesel has superior lubricating property, but no nonparticulate matter pollutants, aromatic content, and sulfur content which produce lesser toxic emissions.

Still now, biodiesel produced from different edible oils was not yet attained successfully worldwide since the cost of production is very high due to the elevated budget of raw materials and food security; consequently, a look for cutting-edge low price nonedible feedstock goods for biodiesel production still continues. In this regard, avocado seed oil (ASO) can be a promising feedstock for biodiesel production due to its low price. It comprises with 80% of unsaturated fatty acids. Hence, a significant content of the fatty acid can aid to increase the value of cloud point and cetane number for the biodiesel [11].

Generally, an ASO extracted by cold press method contains a significant content of free fatty acids that provides better appropriateness for esterification. However, with the excess of poly unsaturation, cloud point, cetane number, and stability of the biodiesel may be decreased. Hence, a suitable alkali or acid is used as a catalyst during the transesterification process to yield biodiesel. Due to their lower catalyst cost and shorter reaction time, alkali route is more preferable than the acid route. Commonly, palm oil, soybean oil, and rapeseed oil are the widely used as biodiesel feedstock. The alkali route shows high sensitivity to both water and FFA [12–14]. The performance of catalytic activity for the nanoparticles has been observed better than the solid catalysts due to its special characteristic of high surface to volume ration. Also, the nanoparticles have shown relatively high rate of the reaction. However, the immobilization of the nanoparticles in the reaction mixture is found to be difficult task. Hence, several researches have been undertaken to immobilization of nanoparticles to carry out the reaction. In such a way, this study focused to immobilize the CuO nanoparticles using carbon support.

So far, no detailed studies using avocado seed oil have not been conducted towards the biodiesel production. Moreover, the investigations on the CuO/C catalyst have not been studied on the ASO. In addition, the attempt on the kinetics of the reactions also needs further scale-up process. Keeping this novel view, the present study aimed to use the carbon supported CuO nanoparticles (CuO/C) as a catalyst for esterification of the FFA present in the ASO. Additionally, the rate kinetic studies and thermodynamic studies were performed for the esterification reaction.

2. Materials and Methods

2.1. Raw Materials, Apparatus, Chemicals, and Reagents. Avocado seeds were collected at a local plantation and gently washed with pure double distilled water to remove all unwanted impurities and dust. Rota evaporator, grinding mill, heater, water bath, and coffee miller were used wherever it needs. Mass spectroscopy gas chromatography, digital balance, vibro-viscometer, condenser, Soxhlet apparatus, hot air oven, and pH monitors were also used. Methanol, *n*-hexane, NaOH, copper (II) nitrate (CN), NaBH₄, and CuCl₂·2H₂O were purchased from Merck (Addis Ababa, Ethiopia) and HiMedia Laboratories Private Ltd. (Addis Ababa, Ethiopia). They were of analytical reagent. Double distilled water was used without further purification.

2.2. Preparation of ASO. Avocado seeds were collected and subjected to dry for a day. Then, skins on the seeds were carefully expelled from the kernel. The known weight of seed sample was investigated for the moisture content. The moisture content was ascertained using an oven drying method at 100 °C for 2 h to allow the mass loss by evaporation. Then, the seeds were crushed by using laboratory blender. To increase the volume to surface ratio, crushed seeds subjected to make until the particle size reached to desired point. The obtained powder was sieved using a laboratory sieves (ASTM) for segregate different particle size. Accordingly, the plant materials were ranged from 0.15 to 1.5 mm. Resulted seed sample powder was kept at 4 °C for the experiments [15, 16]. In this present study, mechanical pressing method was used to extract the ASO. In this method, oil was forced out from the avocado seeds by applying pressure. For this purpose, an oil extracting machine was used (GT-OT-T600, Gorek Tech). The pressure was linearly increased up to 60–70 kgf/m² within 10–15 min. Using a screw press, it obtained a better yield of ASO. It was found that ASO extraction by this mechanical pressing removed only 45% of the oil. The remaining oil was extracted by Soxhlet method; ASO was extracted from the seeds. About 20 g of crushed seed sample was fed to Soxhlet extractor setup with a 250-ml round bottom flask. Further, 200 ml of *n*-hexane (food grade solvent) was added into the distillation set-up. Extraction process was carried out at 344.15 K for 360 min. After extracting, the flask allowed to cool to room temperature. In order to evaporate the additional solvent, water bath was used and excess solvent (*n*-hexane) was removed at 70 °C. Because of the oil has less volatility, they can retain in the experimental flask [17]. The extracted oil was observed to be golden yellowish color. This mixture was kept to settle for 4 h, and the resulted oil as extract was collected. This essential oil was kept in a refrigerator at 4 °C for purification and characterization [18]. Figure 1 depicts the avocado seed and extracted ASO.

2.3. Catalyst Preparation. Initially, the prepared copper nanoparticles were well-dissolved in polyvinyl alcohol (1%), further, deionized water was added to get the appropriate solution. Next, ascorbic acid was added to the PVA solution for maintaining the pH of the solution. After that,



FIGURE 1: Image of the avocado seed and the extracted ASO.

TABLE 1: Physicochemical properties of ASO.

Properties	Experimental value for ASO
AV (mg KOH/g)	82.654
PV (mg/g)	3.5625
FFA (wt. %)	40.9284
IV (mg/I ₂ /g oil)	119.685
ν (mm ² /s)	42.147
SG	0.910
HHV (MJ/kg)	38.98

AV: acid value; PV: peroxide value; FFA: free fatty acids; IV: iodine value; ν : viscosity; SG: specific gravity; and HHV: high heating value.

copper chloride dihydrate salt and $\text{CuCl}_2 \cdot 2\text{H}_2\text{O}$ (0.732 mmol in 2 ml deionized water) were added to the 50 ml PVA solution. It was dissolved into the aqueous solution of PVA by vigorously stirring to maintain 0.0148 M $\text{CuCl}_2 \cdot 2\text{H}_2\text{O}$ solution. At this stage, the solution color changed from blue to light yellow. Further, a NaBH_4 solution (8.796 mmol) was added drop by drop with the previously prepared precursor solution under gentle stirring. At this stage, color of aqueous phase changed from light yellow to wine red. The occurrence of such a darkness revealed that the reduction reaction had taken place. Further, the mixture was then quickly stirred for about 15–17 min in the ambient atmosphere to complete the reaction and dried in a vacuum oven at 75 °C. The CuO/C catalysts were prepared by carrying out the reaction of activated carbon with CuO NP. CuO/C was prepared by mixing activated carbon with 10% Cu NP solution at 60 °C for 2 h to remove the water. The gel type mixture was placed inside furnace at 400 °C for 6 h. The dry crystalline catalyst was obtained after furnace process.

2.4. Characterization of Catalyst. To evaluate the BET surface and pore volume, the nitrogen isotherms of adsorption/stripping were obtained using a porometer (US Micrometrics ASAP 2010, American Micrometrics). Prepared catalyst was subjected in to XRD analysis and the

observed patterns were recorded. Using a “DiffracPlus” program, the collected data were analyzed. Further, the power diffraction database was examined for the stages.

2.5. Esterification of ASO. Esterification was carried out in 500-ml round bottom flasks. The reaction temperature was maintained at 80 °C using a water bath. The mole ratio of RSO to methanol was taken as 1:10 with oil to catalyst ratio 1:10 (in terms of weight).

3. Results and Discussion

Table 1 displays the physicochemical properties of the ASO used in the present study, and the properties of ASO reported elsewhere in the literature [16]. Many reports were documented on the appropriateness and suitability of ASO to prepare biodiesel using different catalysts. However, the physicochemical properties of ASO observed from this study have well supported with the results reported by Kaur et al. [17]. Thus, the reliability and viability of obtained ASO were ensured for the further esterification process.

The esterification reaction using free fatty acids (FFA) and methanol is represented in Eq. (1)[18].

4. Characterization of Prepared Catalyst

4.1. BET Analysis. Brunauer-Emmett-Teller method was employed to determine the porosity and precise surface area of the prepared catalysts. In order to conduct textural analysis, a surface area and porosity analyzer were used (BEL-SORP, MAX G Model). The BET surface area graph is shown in Figure 2. The physicochemical assessments of the catalyst are presented in Table 2.

4.2. XRD Analysis. Figure 3 illustrates the X-ray diffraction pattern of the CuO/C nanoparticles. Copper oxide and the sharp peaks of XRD were compatible with the XRD peak positions indicating the crystalline character. The peaks observed in $2\theta = 35.043^\circ$, 38.521° , 48.467° , 53.81° , 57.97° , and 61.14° correspond to (002,111), (111,200), (202), (020),

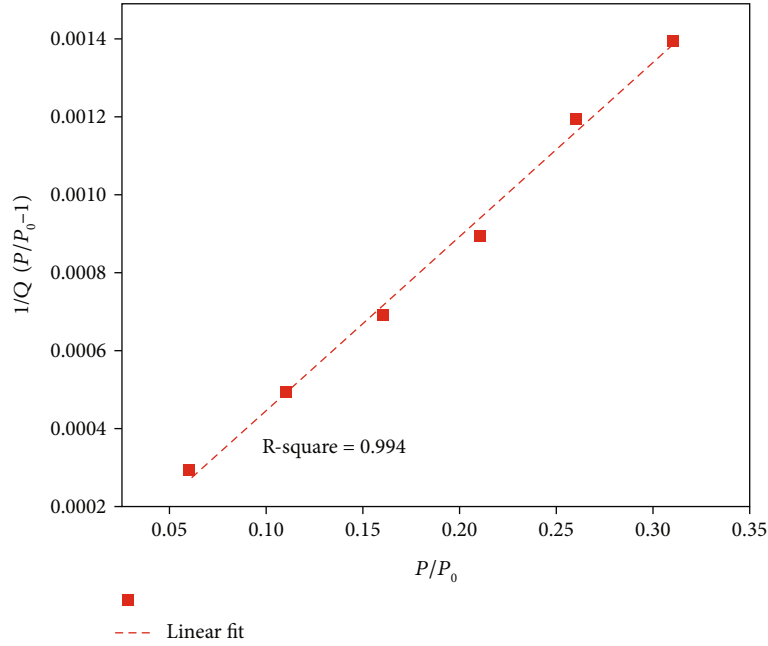


FIGURE 2: BET graph for carbon-supported copper oxide catalyst (CuO/C).

TABLE 2: Typical physicochemical characteristics of the prepared samples.

Sample	External area (m^2g^{-1})	Extreme opening diameter (m)	Volume of pore (cm^3g^{-1})
CuO/C	985.7411	21.3309	0.5257

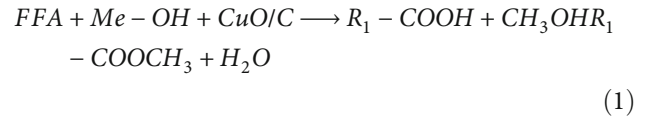
(202), and (113) Bragg's representations of CuO's monoclinic structure, respectively.

4.3. Influence of Time on FF Conversion with and without Catalyst. The FFA conversion based on the presence of catalyst was examined. As revealed in Figure 4, the esterification reaction did not occur in absence of a catalyst which was consistent with the results recorded. On other hand, a significant conversion of FFA by esterification was observed when the reaction was conducted with catalyst CuO/C. During the reaction, it was found that the maximum FFA of 91.446% was converted at 210 min. Hence, the optimal time needed for the ASO esterification reaction was observed to be 210 min. Beyond this, reaction time there was no significant conversion was not found.

4.4. Influence of Temperature on FFA Conversion. The reaction temperature is one of the important factors which can influence the rate of esterification. In order to examine the influence of temperature on the esterification, reactions at different temperatures (30 to 75 °C) were carried out. Catalyst concentration also plays an important role on conversion of FFA to methyl ester. Hence, the catalyst to oil weight ratio (1:10) was kept constant. Figure 5 shows the results of FFA conversion on different temperatures which were carried out among the temperature range 30-75 °C. In

this esterification, reaction time has significant effect on conversion. Figure 5 demonstrated that certain time interval increases the reaction conversion, but the catalyst activity was observed to be higher at 75 °C compared to other reactions. The response degree (conversion) can remain increased rapidly by increasing the temperature. It clearly showed that the catalyst activity was found to be increased while increasing the reaction temperature. From the results, the maximum conversion was improved significantly from 58.56% to 91.446%, while the reaction temperature increases from 35 °C to 75 °C at 210 min. Further increase in time, the conversion was found to be constant and did not get any change. It is clear that the optimum reaction time for the esterification reaction was 210 min to complete the esterification reaction which results a maximized yield.

4.5. Kinetic Studies. The standard esterification reaction (Eq. (1)) based on the Langmuir-Hinshelwood (LH) mechanism is well known:



From Arrhenius equation, we get Equation (2):

$$k_1 t = \frac{1}{a(\alpha - \beta)} \ln \left(\frac{X - \alpha}{X - \beta} \right) \dots \dots \quad (2)$$

By using Eq. (2), we get the value of the equilibrium constant K . At the start of reaction, $t = t_0$, $C_{\text{FFAt}} = C_{\text{FFA0}} = 0.2636 \text{ mol/dm}^3$, $C_{\text{FAMEt}} = C_{\text{FAME0}} = 0$, $C_{\text{Wt}} = C_{\text{W0}} = 0$, and $C_{\text{MeOH0}} = 7.554 \text{ mol/dm}^3$; and at $t = t_{\infty}$, $C_{\text{FFAt}} = C_{\text{FFAe}} = 0.0180 \text{ mol/dm}^3$, $C_{\text{FAMEt}} = C_{\text{FAMEe}} = C_{\text{FFA0}} - C_{\text{FFAt}} = 0.2456 \text{ mol/dm}^3$,

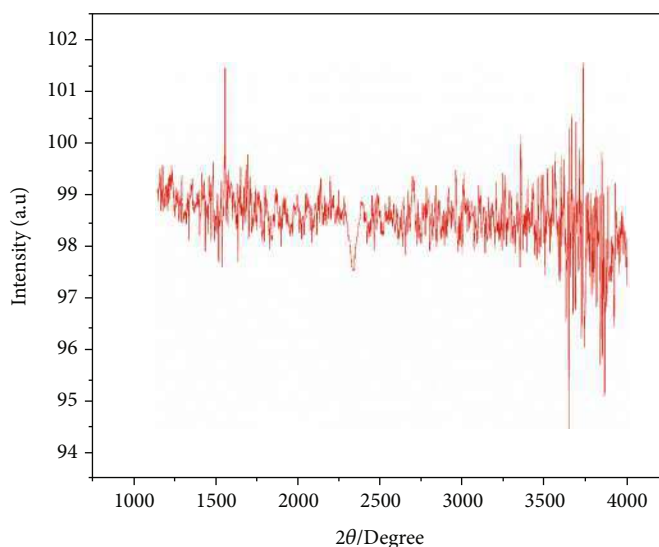


FIGURE 3: XRD pattern of CuO/C catalyst.

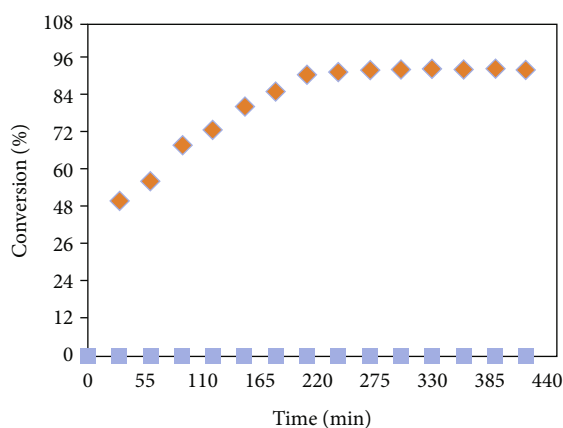


FIGURE 4: Conversion of FFA with catalyst and without catalyst (catalyst: CuO/C; reaction temperature: -75°C ; mass quantity: 10% catalyst; and methanol to FFA ratio: $-10:1$). Black diamond indicates with catalyst, and black box indicates without catalyst.

$$C_{\text{Wt}} = C_{\text{We}} = 0.2456 \text{ mol/dm}^3, \quad \text{and} \quad C_{\text{MeOHe}} = C_{\text{MeOH0}} - C_{\text{FAMEe}} = 7.3084 \text{ mol/dm}^3.$$

From the above equilibrium data substitution in Eq. (2), the obtained K value is 0.4585. A scheme of t versus $1/(a(\alpha - \beta)) \ln((X - \alpha)/(X - \beta))$ remains a straight forward route, and slope of curve gives a rate of the straight reaction constant k_1 (Figure 6). The rate of constant for the particular temperature and catalyst concentration is given in Table 3. The reaction was carried out at methanol to FFA molar proportion of 10:1.

Graphical representation of Eq. (1) gives a curve which represents conversion with respect to time (the dense line represents theoretical conversion, and the points represent experimental conversion). The curves for different reaction conditions are given in Figure 7 for different temperatures and different catalyst types, respectively. Thermodynamics

explains the relationship work, heat, and energy. In the present study, temperature and heat play a key role for the esterification reaction. Hence, thermodynamic study is a must to deal for the determination of energy requirement and to define the amount of mechanical work. The influence of temperature can be assessed by evaluating the activation energy required for the reaction. In order to calculate the activation energy, Arrhenius equation was used which is given in Eq. (2).

$$K = Ae^{-E_{act}/RT} \dots \dots \dots (3)$$

By solving this equation, we get

$$\ln K = \left(-\frac{E_{act}}{R}\right) \frac{1}{T} + \ln A \dots \dots \dots (4)$$

where K is reaction rate constant, A is constant, E_{act} is activation energy, T is the temperature, and R is the gas constant. The plot of $\ln K$ vs T^{-1} (Figure 6) was generated, and the values for A and E_{act} were determined from intercept and slope, respectively. From the results, slope was found to be 0.2622 and the activation energy is calculated to be -2.180 J/mol K .

5. Conclusions

In this study, biodiesel was synthesized using avocado seed oil. The use of carbon supported CuO nanoparticle for the transesterification process of ASO has not been attempted in earlier. Also, the studies on FFA present in the avocado seed oil had a significant outcome in this investigation. In this present study, mechanical pressing method was used to extract the ASO. The oil was extracted using a machine by applying a pressure up to $60\text{--}70 \text{ kgf/m}^2$. Such a mechanical press method resulted in 45% of oil yield. The carbon supported nano CuO (CuO/C) was prepared and used as catalyst. CuO/C catalyst was prepared using activated

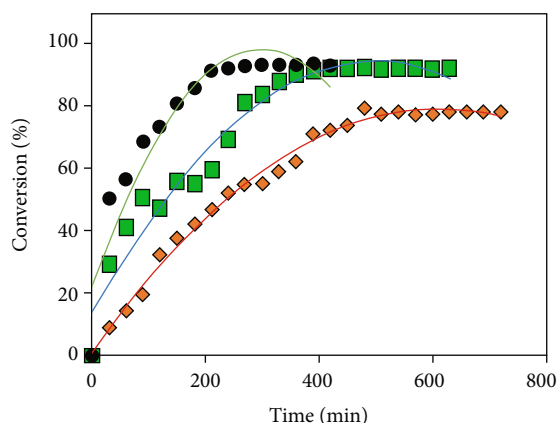


FIGURE 5: Impact of temperature on FFA conversion (reaction time, 420 to 720 min; mass catalyst concentration, 10%; methanol/FFA, 10:1). Black diamond: 30 °C; black box, 50 °C; black circle 75 °C.

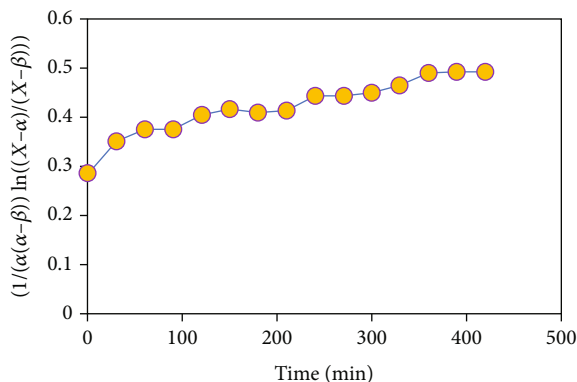


FIGURE 6: A graph of t versus $1/(a(\alpha - \beta)) \ln((X - \alpha)/(X - \beta))$ (75 °C, CuO/C).

TABLE 3: Reaction rate constant for the particular temperature and catalyst.

Reaction condition	k_1 (min ⁻¹)
75 °C (Cu NP as catalyst)	0.9369

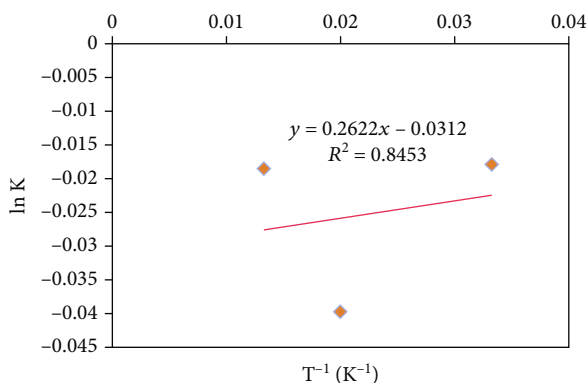


FIGURE 7: The Arrhenius plot for activation energy determination.

carbon and with 10% of CuO nanoparticles. Further, the catalyst was characterized using XRD and BET techniques. The esterification was carried out using methanol at 1:10 oil to catalyst weight ratio. The investigation on different temperatures explicated that the catalyst activity was observed to be more at 75 °C. From the findings, it was cleared that avocado kernel oil can be used potential feedstock for biodiesel production.

Data Availability

The underlying data supporting the results of this study were included with in the paper.

Conflicts of Interest

The authors declare that they have no conflicts of interest.

References

- [1] J. Mani and N. Karmegam, "Heterogeneous base catalysts: synthesis and application for biodiesel production - a review," *Bioresource Technology*, vol. 331, article 125054, 2021.
- [2] V. P. Sundramurthy, T. G. Nithya, C. Masi, C. Gomadurai, and E. M. Abda, "Recent advances and prospects for industrial waste management and product recovery for environmental appliances," *Physical Sciences Reviews*, 2021.
- [3] N. Geng and Y. Sun, "Multiobjective optimization of sustainable WCO for biodiesel supply chain network design," *Discrete Dynamics in Nature and Society*, vol. 2021, Article ID 6640358, 16 pages, 2021.
- [4] V. P. Sundramurthy, B. Rajoo, N. R. Srinivasan, and R. Kavitha, "Bioleaching of Zn from sphalerite using *Leptospirillum ferriphilum* isolate: effect of temperature and kinetic aspects," *Applied Biological Chemistry*, vol. 63, no. 1, pp. 1–13, 2020.
- [5] Z. Zaidi, N. Maiti, M. I. Ali et al., "Fabrication, characteristics, and therapeutic applications of carbon-based nanodots," *Journal of Nanomaterials*, vol. 2022, Article ID 8031495, 12 pages, 2022.
- [6] M. Jayakumar, K. B. Gebeyehu, K. V. Selvakumar, S. Parvathy, W. Kim, and N. Karmegam, "Waste Ox bone based heterogeneous catalyst synthesis, characterization, utilization and reaction kinetics of biodiesel generation from *Jatropha curcas* oil," *Chemosphere*, vol. 288, article 132534, 2022.
- [7] C. Sivasankaran, P. K. Ramanujam, B. Balasubramanian, and J. Mani, "Recent progress on transforming crude glycerol into high value chemicals: a critical review," *Biofuels*, vol. 10, no. 3, pp. 309–314, 2019.
- [8] A. Sharma, A. Saxena, S. K. Dinkar, R. Kumar, and A. S. Al-Sumaiti, "Process optimization of biodiesel production using the Laplacian Harris Hawk Optimization (LHHO) algorithm," *Modelling and Simulation in Engineering*, vol. 2022, Article ID 6766045, 13 pages, 2022.
- [9] S. M. Beyan, S. V. Prabhu, T. T. Sissay, and A. A. Getahun, "Sugarcane bagasse based activated carbon preparation and its adsorption efficacy on removal of BOD and COD from textile effluents: RSM based modeling, optimization and kinetic aspects," *Bioresource Technology Reports*, vol. 14, article 100664, 2021.

- [10] A. Regalado-Méndez, S. Skogestad, R. Natividad, and R. Romero, "Biodiesel production by reactive flash: a numerical simulation," *International Journal of Chemical Engineering*, vol. 2016, Article ID 7843081, 8 pages, 2016.
- [11] P. M. Ejikeme, I. D. Anyaogu, C. L. Ejikeme et al., "Catalysis in biodiesel production by transesterification processes-an insight," *E-Journal of Chemistry*, vol. 7, article 689051, pp. 1120–1132, 2010.
- [12] N. Kolesárová, M. Hutňan, I. Bodík, and V. Špalková, "Utilization of biodiesel by-products for biogas production," *BioMed Research International*, vol. 2011, Article ID 126798, 15 pages, 2011.
- [13] E. Johansson, G. M. Spencer, E. Bettini et al., "Biobased materials production from biodiesel residuals of rapeseed," *International Scholarly Research Notices*, vol. 2012, Article ID 193541, 6 pages, 2012.
- [14] A. Wang, W. Quan, and H. Zhang, "Efficient synthesis of biodiesel catalyzed by chitosan-based catalysts," *International Journal of Chemical Engineering*, vol. 2021, Article ID 8971613, 11 pages, 2021.
- [15] B. Wang and I. Alrueyemi, "Comprehensive modeling in predicting biodiesel density using Gaussian process regression approach," *BioMed Research International*, vol. 2021, Article ID 6069010, 13 pages, 2021.
- [16] Y. Xing, Z. Zheng, Y. Sun, and M. Agha Alikhani, "A review on machine learning application in biodiesel production studies," *International Journal of Chemical Engineering*, vol. 2021, Article ID 2154258, 12 pages, 2021.
- [17] T. A. Zughaibi, A. A. Mirza, M. Suhail et al., "Evaluation of anticancer potential of biogenic copper oxide nanoparticles (CuO NPs) against breast cancer," *Journal of Nanomaterials*, vol. 2022, Article ID 5326355, 7 pages, 2022.
- [18] S. V. Prabhu and R. Baskar, "Detoxification of Electroplating Sludge by Bioleaching: Process and Kinetic Aspects," *Polish Journal of Environmental Studies*, vol. 24, no. 3, pp. 1249–1257, 2015.



Characterization and performance enhancement of electrical submersible pump (ESP) using artificial intelligence (AI)

M. Panbarasan^{a,*}, Subhashini Sankar^b, S. Venkateshbabu^c, A. Balasubramanian^d

^a Department of Petroleum Engineering, AMET University, Chennai 603112, India

^b Department of Petroleum Engineering, VELS Institute of Science, Technology & Advanced Studies (VISTAS), Chennai 600117, India

^c Professor & Head, Department of Petroleum Engineering, JCTCET, Coimbatore 641105, India

^d Department of Chemical Engineering, Saveetha Engineering College, Chennai 602105, India

ARTICLE INFO

Article history:

Available online 18 May 2022

Keywords:

Airborne survey
Annulus pressure
Gas-Oil ratio
Lube match
Machine Learning
Naive Bayes

ABSTRACT

Electrical submersible pump (ESP) technology is the first choice of artificial lift for the operators both in offshore and onshore to increase the rate of production in all types of reservoirs. Even though, the ESP was designed, engineered and fabricated to withstand in harsh subsurface natural and man-made environment such as corrosion, high temperature and extreme pressure but it fails under these circumstances without any prerequisite signal. Even the monitoring systems in place failed to notify the failure of ESP. These ESP failures cut off the production and revenue circulation in the firm. The cost required for the repair and replacement of the ESP is also high and is time consuming. The prevention of ESP failures using machine learning technique is discussed.

Copyright © 2022 Elsevier Ltd. All rights reserved.

Selection and peer-review under responsibility of the scientific committee of the International Conference on Materials, Mechanics, Mechatronics and Manufacturing.

1. Introduction

1.1. Artificial lift

When the primary energy of the reservoir declines over a period of time and it don't have enough pressure to moves the oil from producing zone to the wellhead, artificial lift is employed to increase the production.[1] In United States, 96% of the wells deploy artificial lift since the beginning of the production to increase the rate of production.

Generally, there are two types of artificial lift systems and are:

- a) Pumping system
- b) Gas lifts

1.1.1. Gas lift

It uses the gases produced from wellbore, recompresses it and sent it to the formation through side mandrels and valves to build-up the pressure. The injected gas reduces the viscosity of the oil and increases the volume, which makes the oil to move upwards along the surface. It is of two types:

- i. Continuous gas lift
- ii. Intermittent gas lift

1.1.2. Pumping system

This system is similar to the household hand bore well system and is employed in larger size & scale for getting higher rate of output. The types of pumping system are.

- i. Sucker rod pump
- ii. Hydraulic pump
- iii. Electrical submersible pump

Abbreviations: ESP, Electrical Submersible Pump; H₂S, Hydrogen Sulphide; IIoT, Industrial Internet of Things; BOP, Blowout Preventer; NPT, Non-Productive Time; UAV, Unmanned Aerial Vehicle; TB, TeraBytes; SKU, Stock-Keeping Unit; NASA, National Aeronautics and Space Administration; IBM, International Business Machine; LIDAR, Light Detection And Ranging; 3D, Three Dimensional; ANN, Artificial Neural Network; MIT, Massachusetts Institute of Technology; ROV, Remote Operated Vehicles; VA, Virtual Assistants; B2B, Business to Business; SME, Subject Matter Expert; SRP, Sucker Rod Pump; GL, Gas Lift; PCP, Progressive Cavity Pump; IPR, Inflow Performance Relationship; PI, Productivity Index; BHP, Bottom Hole Pressure; GOR, Gas-Oil Ratio; IIoT, Internet of Things; DCS, Distributed Control System; SCADA, Supervisory Control And Data Acquisition; KPI, Key Performance Indicators; AL, Artificial Lift; ML, Machine Learning.

* Corresponding author.

<https://doi.org/10.1016/j.matpr.2022.05.101>

2214-7853/Copyright © 2022 Elsevier Ltd. All rights reserved.

Selection and peer-review under responsibility of the scientific committee of the International Conference on Materials, Mechanics, Mechatronics and Manufacturing.

In an average, 82% of wells uses sucker rod pump, 10% uses gas lift, 4% uses electrical submersible pump and 2% uses hydraulic pumps for artificial lift in a well.

1.2. Electrical submersible pump

1.2.1. Construction

ESP is nothing but a centrifugal pump consists of numerous impellers and blades connected with a long electric motor.

1.2.2. Positioning

The centrifugal pump is kept at the lower margin of the reservoir fluids and is connected with the motor which is located at the bottom of the production casing.

1.2.3. Operation

Once the motor gets the electrical power through the electric cable runs along the length of the well it starts the pump. The rotating action of impeller creates a centrifugal force and pushes the reservoir fluid towards the surface. ESP is the highly efficient in all types of artificial lift; it can lift and deliver more than 1000 bbl/hr.

1.3. Artificial intelligence

Artificial intelligence is the duplication of Homo sapiens intelligence processes by man-made machines especially computer software and systems. [6] AI includes learning, reasoning and self-correction. [2].

It is of two types:

- a) **Weak AI** – It is an AI system which is designed and trained for a specific task
- b) **Strong AI** – It is an AI system generalized with the human psychological knowledge of perception, learning and reasoning. When presented with an unknown activity, a strong AI system has the capability of finding a solution without human interference.

The following are some of the common application of AI in various fields such as healthcare, business, education, finance, law and manufacturing.

1.4. Machine learning

It is the practical application of AI which allows the systems to learn on its own and out of experience without any external program languages and human intervention. It majorly concentrates on the development of computer programs that can analyze the data for self-learning. [3].

Some of the machine learning methods is supervised machine learning algorithms, unsupervised machine learning algorithms, semi-supervised machine learning algorithms and reinforcement machine learning algorithms. [24] Major applications of machine learning are personalized marketing - where the website offers product to the individuals based on their interest by collecting the details of them from their browsing history, fraud detection, spam filtering, network security threat detection, predictive maintenance and building news feeds. [4].

1.5. Deep learning

Deep learning is a subdivision of machine learning and artificial intelligence which was found in 1943 by Walter Pitts and Warren McCulloch whom created a computer model by imitation of the neural networks of the human brain. They used a process called

threshold logic which is a combination of algorithms and mathematics for the duplication process.

The deep learning will be successful when it has large number of labelled data and significant computing power. Some examples of deep learning are automated driving, aerospace and defence operations, medical research, industrial automation and electronics.

2. Selection criterion for artificial lift

The following are the major factors in the selection of artificial lift for a well and are.

- i. Well conditions and well geometry
- ii. Production characteristics
- iii. Location of the field
- iv. Cost and performance of the system
- (i). well conditions and well geometry
 - a. Well depth – Shallow, Deep, Ultradeep
 - b. Type of well – Horizontal or Vertical
 - c. Presence of aquifer
 - d. Size of casing – Production
 - e. Type of completion – Open, cased hole completion
- (ii). production characteristics
 - a. Rate of production – High, Low
 - b. Bottom hole pressure – High, Medium, Low
 - c. Gas liquid ratio – High, Low
 - d. Viscosity of fluid – High, Low
 - e. Presence of hydrogen sulfide (H₂S)
 - f. Intermittent flow
 - g. Problems encountered during production
 - h. Intrusion of solids
 - i. Corrosion in tubing
 - j. Deposition of wax/ paraffin in production casing
 - k. Scale deposition in tubing
- (iii). location of the field
 - a. Developed region
 - b. Remote location
- (iv). cost and performance of the system
 - a. Reliability of the artificial lift
 - b. Installation cost
 - c. Cost of operation

The above 17 parameters are considered and a suitable artificial lift method is employed.

3. Artificial intelligence in oil & gas industry

Since 2006, AI helped in increasing the business of online retail sellers to 1600 folds. [19] Now AI entering into the Oil & gas industry and is the promising technology which has enough potential to unlatch productivity in oil & gas industry. E&P operators started adopting manufacturing models accompanied by huge electrification, automatization and digitalization. The AI in oil & gas industry is expected to reach the growth of Rs.20,500 crore at the end of 2022 and then it will progress at a growth rate of 12.66% per annum. [1].

AI in oil & gas industry has its prominent centers in North America where the world class software companies namely Google, IBM, Microsoft and Oracle doing their research and pilot project.

A sum of Rs.3.6 Lakh crore can be saved by the predictive analysis of big data using AI & ML. This could be economically viable when there is a relationship between gigantic machines and advanced computer intelligence is established. [5].

AI technology is employed in the following sections of the oil & gas industry.

- I. Asset maintenance
 - II. Improving life of BOP
 - III. Inspection of wellsite
 - IV. Financial planning of an oil & gas project
 - V. Safe routing of oil transportation
 - VI. Efficient reservoir management
 - VII. Easy detection of problems
 - VIII. Increasing lifespan of equipment
 - IX. Detection of oil seepage
 - X. Virtual Assistants
- Asset maintenance

Unplanned shutdown is the primary reason for loss of oil & gas companies. A day unplanned closure in offshore leads to a loss of Rs.10 crore approximately. In an average life of an offshore well, 27 days of unplanned shutdown per year occurs which results in the loss of Rs.270 crore roughly. To extenuate the probability of the failure of equipment, predictive maintenance is the key to success for all the three segments of the petroleum industry viz., upstream, midstream and downstream. [6].

Predictive maintenance is currently the largest application of AI in oil & gas industry. It offers the companies to improve safety during operation and maintenance. This predictive maintenance tool prognosticates the failure of equipment thereby reducing the risk of major accidents, minimize unplanned shutdown and improves abidance to safety standards.

In United States, 40 lakh Kilometre of pipelines distribute the oil & gas across the country which is connected with Industrial Internet of Things (IIoT) sensors which measures both the external environmental factors and internal pipeline parameters such as soil movement, climate, pressure, flowrate and corrosion. [7] These sensors produces terabytes of streaming data daily, that can be collected and analysed by AI tools to respond immediately.

During fracking operation more number of failures occurs. A company named Liquid Frameworks developed an AI tool which is installed in the fracking equipment will predict the next probable event where the failure can occur. Thus prevents and regulates the workflow of the process and increases the safety.

Improving life of BOP

Blowout Preventers (BOPs) are the equipment which is used to control the kick during drilling operation. The performance & operation of BOP has to be in good condition at all times to assure its capacity to seal and control high pressure to prevent sudden influx into the wellbore. Failure of BOPs leads to extremely harmful damages to the environment and drastically affects the financial stability of the operator eg. Deepwater horizon. The monitoring of BOP is difficult because of its remote location, unprecedented nature of the subsurface formation and lack of experienced workers in handling blowout condition.

Current digital companies start entering into the area of the maintenance of bigger equipment. A private digital entity named Deepwater Subsea which currently commingles the power of AI and ML to infer the condition of BOPs in real time and cut down rig non-productive time (NPT). The currently available rig's data obtained from previous errors in Blowout Preventer is altogether stored in a cloud platform through pattern recognition.

The BOP pressure testing is done for various pressure ranges are gathered from leading companies such as Chevron, Pacific drilling & TransOcean and the values are analyzed by comparison of the data obtained & stored and is termed as golden fingerprint. During

operation cycle, a BOP equipment starts degrading, the data will be transferred to the database in real time and is history matched with the golden fingerprint and the discrepancy is notified to the maintenance team simultaneously. The notification comes along with the datum of previous encounters of BOP degradation and its reason for sudden change of pressure and remedies carried out.

Inspection of wellsite

Operating companies must undergo routine examination of their equipment and installations namely wells, storage tanks and pipeline to ascertain its complete management and its maintenance. The data generated and transferred by the sensors installed in that equipment won't be sufficient enough for analysis of the integrity of them. Conventional way of inspection is time-consuming, costlier and also be a hazard to the personnel involved in it. [8] The pipeline route and the well location is a huge mass of land; sending an official to look into that manually through truck is of higher risk. For example, the official has to inspect in remote location and in some terrorist countries there is a probability of kidnap by the local peoples. In such cases, the company has to pay a huge ransom and also it will damage the reputation of the company.

Airborne survey is a good alternative solution but cost associated with deployment of aircraft is huge. Mostly the oil fields are located in the remote regions of the country, survey through helicopter is alone possible but weather conditions and safety compliance cannot permit aircraft engines in the oilfield.

To overcome this, AI comes out with a solution of cost-effective and intelligent unmanned aerial vehicle (UAV) called drones to perform the inspections. The drones are fitted with high precision photo image capturing techniques and send the visuals in real time to the processing center. The AI technology combines the photos with aerial mapping and modelling software thus gives the physical examination information of the oilfield. Numerous terabytes (TB) of aerial images are analysed with high degree of accuracy through machine learning. [9].

Financial planning of an oil & gas project

A correct estimation of demand in market allows the oil & gas companies to produce and transport hydrocarbons in an efficient manner. The availability of the product in right place in right time is the key to increase the profitability and credibility of the company. Several companies based on Silicon Valley offers the ML solutions to furnish the accurate forecasting of product demand with high speed.

AI forebode the demand for a specific product upto stock-keeping unit (SKU) level for a region which aids the companies to keep up stocks in advance before customers order for it.

For example, Gas consumption is very high during the winter season in Middle East countries. This AI & ML based software will gives the solution of the current year anticipated demand by comparison of the previous year consumption and weather conditions of the current year & recent past year. If the temperature of the ensuing year is lower than that of previous year, then the rate of gas consumption increases and vice-versa. This ML based model gives the consumption range of each region which advocates the companies to increase/decrease production in advance. Thereby the company can reduce working capital and manpower during off time which results in profit of the company.

Safe routing of oil transportation

Oil is transported in containers through roadways, railways, pipelines and cargo ships. Out of these, cargo ships are the major

source of transportation. The weather condition in the sea is unpredictable and dynamic in nature.

Gulf of Mexico is listed as the most active regions for oil & gas operation in world. Gulf of Mexico is located between United States and Cuba in the Atlantic Ocean. The Atlantic Ocean is always prone to vulnerable hurricanes which pose threat to the oil & gas operation in that region. The regular hurricane season for the Atlantic Ocean is from June to November and is high at the mid of the August to end of October. During this time the deadly storms causes the oil tanker to collapse and sink which adversely affects the environment as well as cut off the oil supply.

Dataminr is an AI tool which collectively gathers the data from the open source network and social media regarding natural disasters in the ocean environment then verifies with the Meteorological research center and alerts the ongoing sailing ships in that region in real time.

Beyond Limits is a software company which uses cognitive AI to provide solutions for the space programs of National Aeronautics and Space Administration (NASA). The same cognitive AI starts tracking till its reaches the offloading terminal at destination port. The AI tool proposes the route and travel itinerary for the ship crew.

Efficient reservoir management

Identification of drilling location is one of the major challenges encountered by oil & gas companies most often. The success rate of stuck with oil in a drilled well is approximately in the range of 1:5. Drilling a single well in deepwater offshore shelf costs upto Rs.10,000 crore approximately. Once the drilling hits oil bearing zone, it has to be developed to extract the resources by delineation of subsurface geological structures and type of fluid encompassing in it. It has been done by analogy method (or) history matching which comprises of data gathered for several decades about the lithology and oil properties in an unorganized manner.

Lucid Works and Beyond Works are the software developing companies which use AI to figure out the foresaid problems. ML can give vital information such as pressure regime, temperature variation, alteration of permeability, induced seismic activity and so on. [3] Once the required subsurface parameter information is given to ML tool, it synchronizes and differentiates huge set of data then transforms it into a precise summary. This aids in better spotting of drilling location with minimal environmental impact. [10].

Easy detection of problems

The experienced professionals in the oil & gas companies easy detect the problems in producing wells and they know what remedial operations have to be carried out to regularize its working performance. This knowledge is gained out of experience by trial and error & knowhow procedures. Once this workforce retires, the new & younger professionals found difficult to deal with the situation and they depends mainly on the documented information which was kept in isolated condition over a certain period of time. [11].

International Business Machine (IBM) used an AI technology named Watson created a digital assistant that help all younger employees during their routine operations. This tool has technical answers for all the common problems encountered during drilling and production operations which consist of more than 6 lakh pages of daily reports and documents. This technology reduces 3/4th of the time required for identification of problems in a well and its remedial measures. [12] The AI tool is updating on its own, it carries over the problem encountered and solution taken by younger engineers to its database. This will results in increase in rate of production and also acts as a bridge between older and future generations.

Increasing lifespan of equipment

Offshore structures are always prone to degradation and corrosion as it is in saline water where the density is higher and the ionic action on the metal is also faster. Current problem faced by offshore industry is that the structures have exceeded their original life time. The decreased stability of the offshore structure is not good for the working crew as well as to the environment. There are two alternatives at this stage.

- a. To decommission the offshore facility and left out oil & gas in place
- b. To upgrade (or) strengthen the existing structure by new investments.

Digital twin means the digital replica of physical things. It is now used in oil & gas industry to oversee the integrity of the physical assets such as rigs, pipelines, separators, BOP, valves and other equipment. Using Light Detection And Ranging (LIDAR) technology, three dimensional (3D) point clouds are designed. Model plant is constructed using analytics model. By correlation of LIDAR & analytics, technicians can forecast the deformation of structure and evaluate their maintenance requirement which extends the durability of the structure substantially.

The models made by digital twins and analytics are purely static not dynamic which does not considers the factual, on field physical conditions of an offshore structure which affects its performance. A new model named Ramboll evolved by combination of machine learning, pattern recognition, Industrial Internet of Things and Digital mining which considers the real time environmental loads acting on the structure and helps in the monitoring. [9] Through this Ramboll AI model the complete structural set up can be tested, estimated and altered to meet out the on-field conditions thus reduces the cost of manual testing in real operating conditions. [13].

Detection of oil seepage

The crude oil or gas escapes to the surface of earth through the pores or fractures present in the subsurface is called oil seepage (or) petroleum seep. It happens both in offshore and onshore. Around 60% of oil found in North America region enters the surface through seeps and ranging 1.6 lakh ton approximately. In Gulf of Mexico alone more than 600 natural oil seeps occur which seeps 1 lakh ton of oil to the environment. [14].

Oil seeps can damage the environment where the lighter hydrocarbons such as methane, ethane can mixes in atmosphere and crude oil gets deposited in the shore and affects the flora and fauna of the ocean environment.

Exploration of oil seeps will help the investors to extent oil & gas with minimum investment. A well renowned oil field giant ExxonMobil join hands with Massachusetts Institute of Technology (MIT) to contrive an AI equipped underwater robots & remote operated vehicles (ROV) for ocean exploration which is similar to that of NASA's Mars curiosity Rover. These AI enabled equipment will monitor the ocean floor, took samples and relay the subsurface images to data processing center. These robots can detect the seepages and flow pathway of hydrocarbons in the oceanic environment.

Virtual Assistants

For the last few years oil & gas industry introduced virtual assistants to give their customers more satisfaction in service they are offered. A leading oil & gas veteran Royal Dutch Shell introduced its virtual assistants (VA) named Lube Chat powered with AI tech-

nology for its Business to Business (B2B) lubricants customers and suppliers in May 2018. This VA will enable the customers to select lubricants to their engineers & machineries based on the specifications provided by them.

Another major oil & gas player named Shell introduced its VA in United States, China and India. In August 2019, Shell introduced its B2B VA services with full AI for lubricants in India and are tabulated below: [15]. (See Table 1.).

3.1. Advantages

- The younger workforce can easily adopt with the operational platform and internet of things
- Large amount of various E&P data can be handled simultaneously viz., Exploration, Drilling, Production & Reservoir data

3.2. Disadvantages

- The aging workforce has to be trained with latest AI technologies
- The initial implementation of AI costs high

4. Why artificial intelligence is needed in selection of artificial lift?

Artificial lift selection by humans is based on consideration of the various parameters and by analogy. The accuracy of the selected artificial lift method is liable to the experience of the engineer and the quality & quantity of the available well data. The engineers look out only to the previously failed artificial lift methods and successfully installed methods. But they don't see the operational expenditure and performance analysis of the artificial lift system.

After collecting data from the mature fields and delineated wells, the algorithm for the selection can be written as.

$$y = f(x).$$

Artificial lift selection = Algorithm (Field data).

The mature field and delineated well having the full set of data of production, temperature & pressure profile, sand intrusion, water cut which enables the subject matter expert (SME) to analyse the suitable artificial lift method [21]. The SME can discuss with the artificial intelligence experts for creation of an algorithm and program for the selection of artificial lift methods.

The algorithm is to be prepared in such a way that it can select the exact artificial lift method with considering the minimum operational and investment cost. Once the input values are fed into the algorithm, the algorithm will give the output value by manipulating, cleaning & arranging the dataset to provide low cost per barrel of oil production.

The natural flow well data and artificial lift methods of various types such as sucker rod pump (SRP), gas lift (GL), electrical submersible pump (ESP) and progressive cavity pump (PCP) data were

collected from various operating companies. These values were grouped and put together in a dataset.

If we feed our current data of a well, it will analyse with the pre-existing dataset of a well and matches with will which exactly and similarly resembles the current well. The artificial lift method is also selected based on the history matching.

The following models are used for analysis of the better performance of artificial lift selection and are.

- Naive Bayes algorithm
- Decision tree
- Artificial Neural network

(i) Naive Bayes algorithm

Naïve Bayes algorithm is based on Bayes' theorem. This theorem is based on the assumptions that all parameters of a data under consideration are not dependent on each other. Naïve Bayes' algorithm is not a single algorithm; it is a set of machine learning algorithms that makes uses of existing statistical data. [9] It is widely used in oil & gas industry for the detection of net payzone thickness. [16].

(ii) Decision tree

Decision trees are simply the graphical representation which has alternate choices which enables the decision maker to figure out the most appropriate option for a particular project. In oil and gas, it is used to find the inflow performance relationship (IPR) and productivity index (PI) of a well for selection of artificial lift. Decision tree algorithm is same as that of the human thinking process in decision making process.

4.1. Advantages

- Aid to make the best decision with the available data
- Easy and simple to understand and interpret

4.2. Disadvantages

- Lack of accuracy
 - Data may be taken from the past doesn't matches with current situation
 - Reliability of the estimation
- (iii) artificial Neural networks

Neural networks are mathematical (or) computational models that are similar to that of the neural scheme of the human brain. Petroleum Engineering is always accepting the recent developments & technologies from other disciplines to improve its efficiency. ANN was first used in petroleum engineering by Juniardi and Ershaghi in 1993. Over the 25 years it gains its attention and used in characterization of reservoir, field development, multiphase flow in pipelines, interpretation of well test data, analysis of completion jobs, prediction of formation damage, identification of fractured reservoirs and estimation of permeability. [17] The major application is the prediction of oil flow rate from the subsurface to the surface through well head.

4.3. Advantages

- Store information on the network
- Once trained, it can work even with incomplete data
- Continuous to work even in case of corruption of one or more cells of ANN
- Memory capacity is high
- Performs multitask parallel

Table 1
B2B Virtual Assistances & its uses.

S. No	Virtual Assistants	Purpose
1	Lube Analyst	Health check-up of oil & engine condition
2	Lube Advisor	Improves lubrication and maintenance of equipment & engines
3	Lube Chat	Solution for real time problems
4	Lube Coach	Increasing lubrication performance
5	Lube Match	Proper selection of engine oil
6	Lube Expert	Periodic maintenance of equipment

4.4. Disadvantages

- Highly depends on processors and hardware
- No specific rule for structure of neural network
- Translation of data into numerical value is time consuming

The performance and accuracy of the ML algorithms are tabulated as follows: (See Table 2.).

4.5. C program for AL selection

The Artificial Lift Selection requires the following parameters such as:

- i. Pressure
- ii. Temperature
- iii. Speed of the Motor
- iv. Energy Required
- v. Depth of the well
- vi. Geology of the well
- vii. Size of the tubing

From the producing well the above parameters i-iv are recorded simultaneously and saved in cloud server. The parameter v-vi is standard, parameter vii remains same unless or otherwise any maintenance or reconstruction work is carried out. The data from the producing well is transferred to the offshore data processing center and store in cloud server. If there is any data mismatching or discrepancy in the operation of the motor it is verified using analogous method from the existing data and brought out to notice of the operator with the help of AI model.

The following C program is written on the basis of the inputs obtained from the above figures:

Fig. 1 Well parameters such as pressure, temperature and operational parameters such as energy required and speed of the motor which is used for selection of artificial lift method.

Fig. 2 Existing well and operational data stored in cloud server matching with the real data of producing well for the performance evaluation of artificial lift.

Fig. 3 Giving the remedial suggestions to overcome the problems encountered during production by history matching with the big data analysis.

The C Program for the selection of artificial lift can be written as follows: [23].

```
#include <stdio.h>
#include <conio.h>
void main()
{
    int j,k,l,m,n;
    printf("data from new well\n");
    for(i = 0;i < 3;i++)
    {
        printf("suggested artificial lift method\n");
        for(j = 0;j < 3;j++)
        {
            printf("installation of AL\n");
            for(k = 0;k < 3;k++)
            {
```

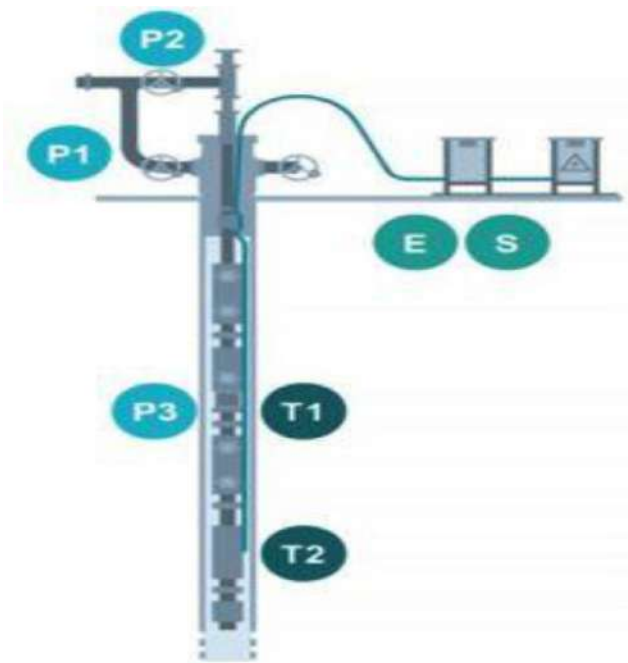


Fig. 1. Process Variables monitored in ESP.

```
}.
printf("performance evaluation (data set fair wells\n");
for(m = 0;m < 3;m++)
{
    printf("available data set fair wells\n");
    for(n = 0;n < 3;n++)
    {
        printf("\n");
        getch();
    }
}
```

5. Electrical submersible pump (ESP) in oil field

Electrical Submersible Pump system is one of the best artificial lift methods to lift oil from the subsurface [20]. Currently 10 lakh wells in the world have artificial lift production, out of which one-fifth of wells uses ESP technology because of high volume handling capacity and operational performance at greater depths. [18] It can be used in wells having. (See Table 3.).

- Low bottom hole pressure (BHP)
- Low gas-oil ratio (GOR)
- Low Bubble point
- High water cut

5.1. Advantages

- Low maintenance
- Cost effective

Table 2
ML algorithms and its parameters.

S.No	ML Algorithms	Duration of Algorithm process	Accuracy	Performance
1	Decision tree	Faster	94%	High
2	Naive Bayes	Moderate	72%	Low
3	Artificial Neural Network	Slower	86%	Moderate

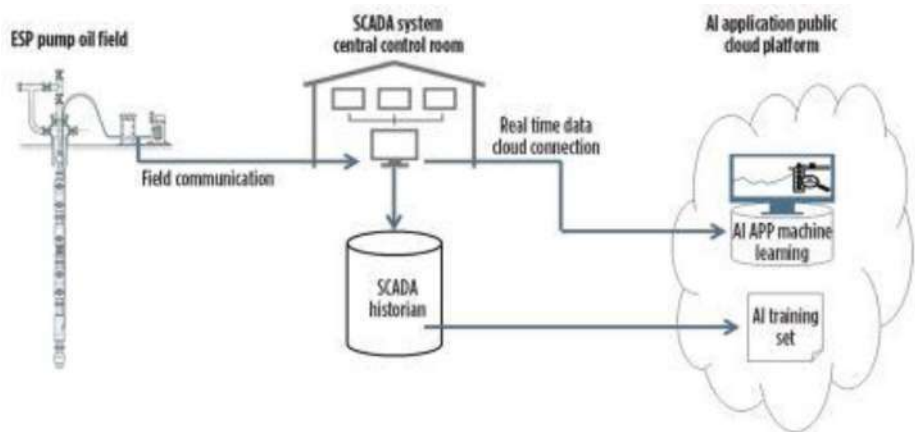


Fig. 2. Components and data flow within the AI enabled maintenance model.



Fig. 3. Automation Control Loop with Machine Learning.

Table 3
Operational parameters and range.

S.No	Parameters	Operating Range
1	Flow rate	70 to 64,000 bpd
2	Depth	0 – 15,000 ft
3	rpm	4000

- Withstands in high downhole temperature conditions
- Deployed in vertical, horizontal & deviated wells
- Can be effective in corrosive environments such as H₂S & CO₂
- Nullifies sand intrusion

5.2. Design specifications of ESP

- Impeller is made of Nickel (Ni) which resists corrosion and abrasion
- Motor works even at 500°F and a pressure of 500 psi

6. Artificial intelligence in ESP

AI was introduced in the ESP operation with an aim of reduction of production costs less than \$10 per barrel. Siemens conducted a pilot test in a mature onshore field employing 30 ESP upgraded with AI technology. [19] The result shows the reduced maintenance, increase in performance and low disruptions during production. It fails at sometimes which disrupts production and cash flow of industry. It can be overcome by right mixture of newer technologies namely AI, Internet of Things (IoT) and Cloud computing and

automatic surveillance mechanism. [17] This will alerts the operators in case of degradation in the performance of ESP.

6.1. Overseeing of ESP performance

Before deploying ESP into the reservoirs, numerous numbers of sensors at regular intervals is placed in the well at regular intervals is placed in the well to monitor the subsurface and physical parameters continuously. [7] It measures both the surface & subsurface variables such as.

7. Surface variables

- P₁ – Annular pressure
- P₂ – Production oil pressure
- E – Motor current
- S – Speed of motor

8. Subsurface variables

- P₃ – Inlet oil pressure at pump
- T₁ – Inlet temperature of oil at pump
- T₂ – Temperature of motor pump

The variables are mentioned in Fig. 1. Fig. 2. Fig 3. Once the ESP is deployed for operation, the distributed control system (DCS) & supervisory control and data acquisition (SCADA) system transmits the data in 5 to 10 sec interval to the recording unit. The data is stored in a mother board and can be used in the future for the error detection. This have a limitation that it cannot simultaneously figure out the problem whilst operation. [17].

8.1. AI based pattern recognition

Pattern recognition is a model with AI which can predict and monitor the operation of ESP. This AI model can easily identify the anomalies with its root causes using machine learning. [16].

With the available information, the on-field engineer can prepare an action report to increase the ESP's performance. The AI tool alone rectifies and modifies the production control to certain extent where the limit is fixed earlier. These will save the time and man power needed in supervision of the production installation.

8.2. Machine learning in ESP

Machine learning is employed along with ANN to create an ESP monitoring model by using the historical data set. The ANN codes all the dynamic data and its relational variables to figure out the key performance indicators (KPI) for the smooth production of well. [22].

Once the ML model is architecture it correlates normal operational relations with various parameters of ESP. Then it can fix its own baseline data set and equates with the incoming real time data through pattern recognition algorithm to detect any deviations in that. If so, it can provide the possible solutions to overcome the deviations simultaneously. This can be efficient only for ESP pumps ranging from 200 to 500 kW power motors. [9].

8.3. On-field test of AI enabled ESP

A set of 30 ESP enabled with AI is put into operation and is run continuously for a period of 12 days and a single ESP motor reports its failure. [6] The failure report is sent to the field engineer for further follow up and the data is analyzed & history matched with the past failure records. The pilot test shows the high degree of accuracy obtained using AI/ML based tool. [22] This test detects the numerous anomalies simultaneously during the operation and some of which were not detected earlier.

9. Recent advancements in ESP

ESP is widely used in the production of oil due to its higher efficiency and reliability. Depending upon the wellbore parameters such as payzone thickness and volume of oil present in the reservoir condition the operating parameters vary accordingly and simultaneously the power required by the ESP also changes accordingly. If there is any failure in the operation of ESP that leads to increase of NPT, loss of production and high cost for replacement. The operational failure is due to the formation of unwanted gas, water intrusion and accumulation of emulsions and identifying this problems at earlier stage is quite difficult and it also requires continuous monitoring of physical and chemical properties of wellbore fluid by SMEs. [25].

In order to overcome the above, AI and ML are used for the invariant analysis of the borehole data and fluid parameters. This can reduce the replacement costs, repair and other constraints associated with logistics. A study shows that AI induced ESP is having less pull-out in comparison with conventional ESP. AI clearly captures the signals from ESP and alerts the crew members about the failure of ESP much earlier. This enables AI & ML is the better technique for the proper functioning of ESP for a long run.

10. Conclusion

This AI enabled ESP will deliver production for a long range of time without any malfunction. The advantages of this system are as follows:

- Less maintenance
- No loss of production days
- Minimum damage to the equipment
- No need of SCADA and DCS monitoring system
- Automatic problem identification and rectification

AI technology is safer to environment and is compliance with the HSE policy. It automatically plans the shutdown procedure of a well for a certain period of time because each unplanned shutdown will be a huge loss to the company and its stakeholders and it also affects the supply chain management of the entire well. This will increase the overall efficiency of an ESP and leads to the increased profitability of the operator. This also found economical and trust worthy in the pilot test run conducted by Siemens and AI enabled ESP will deliver production for longer run without any intermittence.

CRediT authorship contribution statement

M. Panbarasan: Conceptualization, Methodology, Writing – original draft. **Subhashini Sankar:** Visualization, Investigation. **S. Venkateshbabu:** Validation, Supervision. **A. Balasubramanian:** .

Declaration of Competing Interest

The authors declare that they have no known competing financial interests or personal relationships that could have appeared to influence the work reported in this paper.

References

- [1] Pragale, R. and Shipp, D.D., "Investigation of Premature ESP Failures and Oil Field Harmonic Analysis", Petroleum and Chemical Industry Conference, New Orleans, 24–26 September 2012.
- [2] Gupta, S., Saputelli, L. and Nikolaou, M., "Applying Big Data Analytics to Detect, Diagnose, and Prevent Impending Failures in Electric Submersible Pumps", Society of Petroleum Engineers Annual Technical Conference and Exhibition, Dubai, 26–28 September 2016, SPE-181510-MS.
- [3] S.T. Pham, P.S. Vo, D.N. Nguyen, *Effective electrical submersible pump management using machine learning*, OJCE 11 (01) (2021) 70–80.
- [4] Nico Jansen Van Rensburg, "AI4ESP- Autonomous Well Surveillance for ESP Pumps Using Artificial Intelligence", Presented at SPE Oil and Gas India Conference and Exhibition, Mumbai, 9–11 April, 2019. Paper Number: SPE-194587-MS.
- [5] Popaleny, P., Duyar, A., Ozel, C. and Erdogan, Y., "Electrical Submersible Pumps Condition Monitoring Using Motor Current Signature Analysis", Abu Dhabi International Petroleum Exhibition & Conference, Abu Dhabi, 12–15 November 2018.
- [6] S. Sherif, O. Adenike, E. Obehi, A. Funso, B. Eyiutoyo, *Predictive Data Analytics for Effective Electric Submersible Pump Management*, SPE Nigeria Annual International Conference and Exhibition, Lagos, August 2019.
- [7] Liu, Y., Yao, K., Liu, S., Raghavendra, C. S., Lenz, T. L., Olabinjo, L., B.Seren., S. Seddighard, Dinesh Babu, C. G., "Failure Prediction for Rod Pump Artificial Lift Systems", Paper presented at SPE Western Regional Meeting, Anaheim, California, USA. 27–29 May, 2010, SPE-133545-MS.
- [8] Mohammad Rasheed Khan, et.al., "Machine Learning Application for Oil Rate Prediction in Artificial Gas Lift Wells", SPE Middle East Oil and Gas Show and Conference, Bahrain, 18–21 March 2019.
- [9] Mike Pennel, Jeffrey Hsiung, and V. B. Putcha., "Detecting Failures and Optimizing Performance in Artificial Lift Using Machine Learning Models", SPE Western Regional Meeting, California, USA, 22–27 April 2018.
- [10] Guo, D., Raghavendra, C.S., Yao, K.-T., Harding, M., Anvar, A. and Patel, A., "Data Driven Approach to Failure Prediction for Electric Submersible Pump Systems", SPE Western Regional Meeting, Garden Grove, 27–30 April 2015.
- [11] S. Gupta, M. Nikolaou, L. Saputelli, C. Bravo, *ESP health monitoring KPI: a real time predictive analytics application*, SPE Intelligent Energy International Conference and Exhibition, Aberdeen, September 2016.

- [12] A. Mirzaei-Paiaman, S. Salavati, The application of artificial neural networks for the prediction of oil production flow rate, *Energy Sources, Part A: Recovery, Utilization, and Environ. Effects* 34 (19) (2012) 1834–1843.
- [13] Amey Ambade, Saniya Karnik, Praput Songchitruksa., Rajeev Ranjan Sinha., Supriya Gupta., “Electrical Submersible Pump Prognostics and Health Monitoring Using Machine Learning and Natural Language Processing”, Paper presented at the SPE Symposium: Artificial Intelligence - Towards a Resilient and Efficient Energy Industry, Virtual, 18 October 2021. Paper Number: SPE-208649-MS. <https://doi.org/10.2118/208649-MS>.
- [14] L. Muradkhanli, *Neural Networks for Prediction of Oil Production*, Science Direct, Elsevier 51–30 (2018) 415–417.
- [15] “Shell Lubricants India showcases B2B capabilities”, NBM & CW Infra Construction and Equipment Magazine, August 2019. Link: <https://www.nbmcw.com/equipment-machinery/others/lubricants/shell-lubricants-india-showcases-b2b-service-capabilities.html>.
- [16] Abdelaziz, M., Lastra, R. and Xiao, J.J., “ESP Data Analytics: Predicting Failures for Improved Production Performance”, Abu Dhabi International Petroleum Exhibition & Conference, Abu Dhabi, 13–16 November 2017.
- [17] Sneed, J., “Predicting ESP Lifespan with Machine Learning”, SPE/AAPG/SEG Unconventional Resources Technology Conference, Austin, 24–26 July, 2017.
- [18] X. Zhu, A.B. Goldberg, “Introduction to Semi-supervised Learning”, *Synthesis Lectures on Artificial Intelligence and Machine Learning*, Morgan & Claypool Publishers 3 (1) (2009) 1–130.
- [19] AL-Qutami, Tareq Aziz, Rosdiazli Ibrahim, Idris Is, and Mohd Azmin Ishak., “Development of Soft Sensor To Estimate Multiphase Flow Rates Using Neural Networks”, *International Journal on Smart Sensing and Intelligent Systems*, Volume 10, Issue 1, 2017:199 - 222
- [20] Steve Breit., Neil Ferrier., “Using ESP systems for artificial lift”, *Electrical Submersible Pumps in the Oil and Gas Industry*., Pumps & Systems, April 2008. Link: <https://www.pumpsandsystems.com/electric-submersible-pumps-oil-and-gas-industry>.
- [21] Duru, Ugochukwu Ilozurike., “Evaluating Lift Systems for Oil Wells Using Integrated Production Modeling: A Case Study of A Niger Delta Field”, *Journal of Petroleum Engineering & Technology*, Volume 11, Issue 3, 20Link: <https://engineeringjournals.stmjournals.in/index.php/JoPET/article/view/6057>.
- [22] D. Koroteev, Z. Tekic, Artificial intelligence in oil and gas upstream: Trends, challenges, and scenarios for the future, *Energy and AI* 3 (2021) March.
- [23] Matthew Chinn, Mirkowut Kewicz., “Artificial intelligence drives early-warning alerts to prevent ESP disruptions”, *World Oil*, January 2019. Page Number: 51-54. Link: <https://assets.siemens-energy.com/siemens/assets/api/uuid:8809bea3-f169-4d2e-89ad-8a6e20235e1e/worldoil-ai-jan2019.pdf>.
- [24] P. Panja, R. Velasco, M. Pathak, M. Deo, Application of artificial intelligence to forecast hydrocarbon production from shales, *Petroleum* 4 (1) (2018) 75–89.
- [25] Al Maghlouth, A., Cumings, M., Al Awajy, M. and Amer, A., “ESP Surveillance and Optimization Solutions: Ensuring Best Performance and Optimum Value”, SPE Middle East Oil and Gas Show and Conference, Manama, 10–13 March 2013, SPE-164382-MS.

An analytical study of the technological & managerial advancements in the sedimentary basins of Brazil with special emphasis on Campos basin over a period of 5 decades

*M.Panbarasan¹, Dr.J.Venkateshbabu², R.Karthikeswaran³, J.Sudharsan⁴

¹Assistant Professor & SPE Ambassador Lecturer, AMET University, Chennai

²Professor & Head, Department of Petroleum Engineering, JCTCET, Coimbatore

³Assistant Professor, VELS Institute of Science, Technology & Advanced Studies (VISTAS), Chennai

⁴Doctoral Research Fellow, UPES, Dehradun

Abstract: Once a basin is found to be economically viable after the G&G studies and various reserve estimation methods it has to be exploited for the extraction of hydrocarbon. The basin consists of numerous wells drilled at different depths depending upon the stratigraphical variations in it. For the purpose of drilling a well and installation of production facilities over the life of well and basin, the technology deployed initially will have to be upgraded in a sequential manner. In this study, we will discuss about the technological advancements made in the span of 50 years with 80 production systems engaged in more than 30 oil & gas wells in detail.

Keywords: Actuator Manifold, Bore screen, Drilling riser, Frac pack, Prototype, Slender well, Umbilical

1. Introduction

1.1. Brazil – Geography & Location

Brazil is the largest country in South American continent and 5th largest in the world which almost covers half the landmass of entire South America with an area encompassing of 8,514,215 Sq.Km bordering Atlantic Ocean. [1]

1.2. History of Brazilian Oil era

The historical record of oil exploration of Brazil started in the mid of 19th century. In 1864, Thomas Denys got permission to extract oil for a period of 90 years in Bahia province. The first well was drilled in 1892 upto a depth of 488m where two barrels of oil were produced.

At the beginning of 20th century the government of Brazil started its initiatives to explore hydrocarbon through its entity named Geological and Mineralogical Service of Brazil (GMSB) in 1907. GMSB drilled more than 60 wells in various regions of Brazil and all found to be dry.

National Department of Mineral Production (DNMP) was established in 1934 to carry out mineral production in the country. DNMP outsourced US oil specialists to identify the hydrocarbon prospects in Brazilian soil.

Again in 1938, a separate entity named National Petroleum Council (CNP) was created exclusively to look after the activities related to exploration of oil resources. In 1953, DNPM drilled a well at Lobato it was stuck with oil and found to be economically unviable. [2]

In 1953, Petrobras – a semi-public Brazilian MNC controls the entire E&P operation in Brazil with the Brazilian government holds 54% share of it. [3]

2. Sedimentary basins of Brazil

Brazil is the 10th largest producer of oil & gas in world with a production (as on 2017) rate of 2.7MMbpd of oil & 105 MMscf/d of gas. It has a proven resources of 12.7 billion bbl of oil & gas resource of 378 billion m³. [7]

Total sedimentary basin is 3,200,000 sq.km. which is 37.8% of the total land mass of Brazil [5]. Out of 3,200,000 sq.km of sedimentary basin, offshore accounts for 1,550,000 sq.km. and onshore prospects of 1,650,000 sq.km. [6]

The major geology of the basin is turbidite sandstones and pre-salt carbonates which are high quality reservoirs with API value of 27° and having high success rate of 46%. [7]

The sedimentary basins in Brazil consists of 20 onshore & 14 offshore basins and are listed as follows:

Table 1: Sedimentary basins of Brazil

Onshore/ Offshore	Province	No. of basins	Name of the basin
Onshore	Amazon	6	Acre, Madre de Deus, Solimoes, Tacutu, Amazon, Marajo
	Central	6	Alto do Tapajos, Bananal, Parecis-Alto Xingu, Parnaiba, Sao Luis-Grajau, Sao Francisco
	North-eastern	4	Araripe, Jatoba, Reconcavo, Tucano
	Southern	4	Itaborai, Pantanal, Parana (Bauru), Taubate
Offshore	Offshore	14	Foz do Amazonas, Para-Maranhao, Barreirinhas, Ceara, Potiguar, Pernambuco-Paraiba, Sergipe-Alagoas, Camamu-Almada, Jequitinhonha, Cumuruxatiba, Espirito Santo, Campos, Santos, Pelotas

3. Campos basin

Campos basin consists of both Onland and offshore reservoirs. It has a total area of 115,000 s.km offshore basin in South Atlantic and 500 sq.km Onland portion near Rio de Janeiro. This basin named after a military revolutionist Antonio de Siqueira Campos.[9]

The fossils belongs to early cretaceous period and the principal structures are synthetic faults, strike-slip faults formed by divergent boundaries [10].

Campos basin consists of 30 fields that have potential to produce hydrocarbons and they are Garoupa, Enchova, Enchova East, Enchova West, Linguado, Carapeba, Vermelho, Marimba, Albacora, Albacora East, Marlim, Marlim East, Marlim South, Barracuda, Caratinga, Espadarte, Roncador, Jubarte, Cachalote, Badejo, Bonito, Bicudo, Pampo, Corvina, Bijupira, Voador, Polvo, Congro, Baleia Franca, Papa-Terra, Frade, Tartaruga Verde [9]; [14]. Out of which, Marlim field is the biggest field in Campos basin with water depth of 650 to 1050m having a capacity of 1.5 billion barrels of total oil reserves. [11].

4. Technologies implemented

Petrobras Deep and Ultra deep water technology program named PROCAP was designed to reach the identified payzone. It spans over 28 years with 4 versions which brought 2 OTC awards in 1992 & 2001 respectively which fosters Petrobras as a major player in offshore operations worldwide.

Other notable technologies implemented in the Campos basin are

- (i) Life extension methodologies
- (ii) Heavy crude processing
- (iii) Oil & Gas impurities treatment
- (iv) Subsea boosting mechanism
- (v) Phase separation methodology
- (vi) Uniform distribution and transmission of power

5. Hierarchy of operations

More number of operations related to subsea exploration & production were carried out in the Campos basin for the first time in Brazil and World. The following table enlists the various type of operations carried out in Campos basin over a span of last 50 years commences from 1971.

Table 2: Year-wise Operations carried out in Campos basin

Year	Name of the field	Type of Operation	Equipment used
1968	Campos basin	Exploration	Gravity & Magnetic tools
1971	Campos basin	Exploration	Jack-up rig, 1-RJS-1
1972	Campos basin	Exploration	Jack-up rig, 1-RJS-1
1973	Campos basin	Exploration	Jack-up rig, 1-RJS-1
1974	Campos basin	Exploration	Petrobras Drillship-II, 1-RJS-9
Dec, 1974	Garoupa	Exploration	Petrobras Drillship-II, 1-RJS-9A
1975	Enchova	Production	Dry X-mas tree
July 1976-1978	Enchova, Enchova East, Bonito, Bicudo, Pampo, Linguado & Corvina	Directional Drilling	Bent-sub, BOP
1977	Enchova	Production	EPS & Semi-submersible drilling platform
1977-1978	Garoupa, Namorado	Transportation	Flexible flowlines

1979	Garoupa, Namorado	Production Installation	Surface wellhead cellars & Manifolds
	Bonito	Production	Subsea X-mas tree
1981	Bicudo	Production	EPS, Sedco-135D
1982	Bonito	Production	Satellite X-mas tree & Manifold
1983	Pirauna	Well completion	Drilling rig
1984	Garoupa, Namorado	Production	Dry X-mas tree
1985	Marimba	Subsea Well completion	Production string, GL & DHSV
		Production Installation	X-mas tree
1986	Campos basin	Deepwater Production	Production equipment
1987	Marimba	Production Installation	X-mas tree, Flexible line, Umbilical
1988	Marimba	Subsea completion	X-mas tree
1989	Vermelho, Pargo & Carapeba	Production Installation	ESP, DHSV, X-mas tree
1991	Marlim	Well completion	Gravel pack
	Bonito	Horizontal drilling	MWP, BHA, GLM, DHSV
1992	Marlim	Well completion	Gravel packing, TCP
	Bijupira	Vertical connections	Prototype
	Marlim East	Temporary abandonment	X-mas tree, Flowline man drill
	Campos basin	UDWT, PROCAP2000	Drilling & Completion tools
1993	Campos basin	Standardization of X-mas tree	GL, Connector, DHSV, ROV
1994	Marlim	Subsea well completion	Production tools
	Carapeba	Artificial Lift	ESP
1995	Albacora	Manifold Installation	Crane barge, Valves, Chokes
	Marlim	Horizontal well completion	Sandscreen, Liner
1996	Albacora	Vertical connection	Pipe lay vessel, Flowline
	Marlim East	Well stimulation	Frac Pack, TSR Mandrel, TSR String, Ceramic flapper valve
1997	Marlim South	Well completion	Gravel pack
1998	Albacora East	ESP Installation	Horizontal X-mas tree
	Marlim	Slender well technology	Well heads, Tubing hanger, Production Column, Drilling riser
	Marlim	Open hole completion	Screens, Gravel packing
	Voador	Injection wells	Directional drilling tools, Sandscreen
1999	Roncador	Production	DPR & DP
		Well Completion	Frac pack, Stimulation materials
2000	Marlim, Roncador, Albacora	UDWT, PROCAP 3000	Drilling, Subsea boosting equipment
	Marlim	Well completion	Sandscreen
		Production	Production string

	Marlim South	Openhole completion	Gravel pack, Frac pack
	Roncador	Subsea well completion	Triple frac pack
		Production	Triple selective frac pack
2001	Marlim East	Manifold Installation	DP & DPR
	Marimba	Phase separation	VASPS
	Roncador	Well Completion	Horizontal subsea tree
	Enchova west	Well completion	Actuator manifold
	Marlim south	Horizontal drilling	Directional drilling tools
2002	Roncador	Production	Pulley manifold
	Marlim	Well Completion	HOHGP, Bore screen
2003	Jubarte	Production	DP, DPR, ESP
	Marlim South	Horizontal drilling	Electric prototype completion
2004	Albacora	Anchoring FPSO	Torpedo pile
2005	Albacora East	Wellhead	Torpedo wellhead
2006	Jubarte	Offshore platform	Flexible risers
	Roncador	Offshore Installation	Manifold, Crane, Cable
	Enchova	Well Completion	Liner, Perforator, Acids
2007	Roncador	Production Installation	FSHR
	Jubarte	Production	ESP, PAB
2008	Jubarte	Production	LTPT
2009	Marlim	Production Installation	SBM
2010	Jubarte	Subsea Installation	SESV, Suspended Cable, X-mas tree
	Congro	BSR Installation	SCR, BSR, FPU, Flexible jumpers
	Baleia Franca	Production testing	LTPT
	Caratinga	Production testing	LTPT
2011	Campos basin	PROCAP	Exploration & Production
	Marlim	Phase separation	SSAO, Injection pump
	Espadarte	Mudline ESP Installation	ESP, Flowbase, Pump
	Marlim East	Production testing	LTPT
	Marlim	Production testing	LTPT
2012	Albacora	Water Injection	SRWI
	Barracuda	Subsea boosting	Multiphase pump
2015	Papa-Terra	Offshore Platform	TLWP, Production riser, Production string, Dry X-mas tree
	Marlim East	Drilling	FMCD
2016	Marlim East, Marlim South	Subsea Drilling	MPD, FMCD
2017	Roncador	Casing Running, Cementing	Surface & Conductor casing
2018	Tartaruga Verde	Offshore platform	MV29
2019	Tartaruga Verde, Espadarte	Data Acquisition	Exploration tools
2020	Polvo	Production	Floating Production Storage and Offloading vessel

Numerous results were obtained during the operations which may be tried for the first time in the Brazil as well as in the Universe. The results are tabulated below:

Table 3: Year-wise Major Operational results in Campos basin

Year	Name of the basin	Result
1971	Campos basin	A well was drilled upto a WD of 49m and found to be dry.
1972	Campos basin	A well was drilled upto a WD of 60m and no indication of hydrocarbon shows.
1973	Campos basin	5 wells were drilled and all found to be dry.
1974	Campos basin	8 th exploratory well was drilled upto 110m WD encountered with calcareous formation enriched with hydrocarbons but is not commercially viable.
Dec, 1974	Garoupa	9 th well was drilled at 124m WD with the target depth of 3750m but oil show was found at 3500m depth in a calcareous rock with reservoir thickness of 100m.
1975	Enchova	X-mas tree was covered with wellhead cellar in atmosphere but production was postponed.
July 1976-1978	Enchova, Enchova East, Bonito, Bicudo, Pampo, Linguado & Corvina	Four directional wells were drilled at an inclination of 35°C and water depth of 120m & 160m.
1977	Enchova	1 st LPLT in Brazilian offshore with a production of 10,000 bbl/day, the largest at that time in Brazil.
1977-1978	Garoupa, Namorado	Flexible flowlines was installed at a water depth of 160m for connecting wellhead cellars to the surface manifold and transports crude to processing and loading towers. This flowlines converts the drilling lines to production lines.
1979	Garoupa, Namorado	The wellhead and manifold systems were controlled by a ship called Stad Troll which was especially dedicated for it.
	Bonito	The well named 1-RJS-38 at Bonito was the first satellite well which was completed at a water depth of 189m and was the deepest at that time. The speciality of the well was that the oil was produced through production string using STT inside the BOP.
1981	Bicudo	3 satellite wells named 4-RJS-134, 7-BI-1D-RJS & 7-RJS-158D were drilled & completed with gravel pack for sand control and connected with another well named 7-BI-2D-RJS to the platform Sedco-135D at a water depth of 130m for processing of crude oil upto 30,000 bpd.
1982	Bonito	Production manifold was built was using 30" O.D & 5/8" ID and the dimensions are 20m length, 10m width & 4m height. It minimizes the costly subsea connections between x-mas tree and manifolds.
1983	Pirauna	The well named 4-RJS-232 was drilled & completed at a water depth of 293m and was the deepest subsea completion at that time.
1984	Campos basin	Due to high maintenance cost & operational complications the dry x-mas tree was dismantled.

1985	Marimba	The well named 1-RJS-284 was drilled, completed and production begins at a WD of 383m using 4½” production string, 8 GLM & DHSV. This was the deepest subsea well completion during that period.
		In 1-RJS-284 well at a WD of 383m, first diverless X-mas tree was installed.
1986	Campos basin	A program named PROCAP1000 was devised to develop production infrastructure for more than 400m WD and equipment such as wet X-mas tree, Manifold for 1000m, ESP, ROV were manufactured. This process starts on 1986 and ends at 1991.
1987	Marimba	At a water depth of 411m, the X-mas tree was installed and coupled with flexible line & umbilical using a special vessel and was the first diverless guideline subsea tree installed using the lay-away method.
1988	Marimba	A well named 1-RJS-376D was drilled, completed and produced at a WD of 492m and was the deepest subsea completion at that time.
1989	Vermelho, Pargo & Carapeba	Seven fixed platforms were installed at a WD between 80m & 101m. From that 120 wells were drilled and completed using 7” perforated liner, 3½” production string with ESP, DHSV & X-mas tree.
1991	Marlim	A vertical well named 3-MRL-3-RJS was drilled and completed using gravel pack to mitigate sand production from unconsolidated sandstone formation and started its production at a WD of 721m and was the world’s deepest subsea completion during that time period.
	Bonito	A well named 7-BO-13H-RJS was drilled horizontally and completed with hydraulic packer and 4½” production string with 4 GLM’s & DHSV. It was the 1 st horizontal subsea well in Brazil.
1992	Marlim	A well named 7-MRL-9-RJS was drilled and completed using gravel packing, 5½” production string, DHSV & TCP which started its production at a WD of 781m. It was the world’s deepest subsea completion at that period of time.
	Bijupira	The 1 st version of Petrobras standard vertical connections with prototype was tested at a WD of 550m.
	Marlim East	At a WD of 600m, new X-mas tree installation method was developed as a replacement for existing lay-way method.
		PROCAP2000 was aimed to develop new technologies for a WD of 2000m. It was intended for minimum CAPEX & OPEX using advanced and cost-effective technologies such as VASPS, SCR, Flexible risers, Torpedo anchor & Vertical connection system.
1993	Campos basin	Standardization of subsea X-mas tree involves the addition of equipment namely connectors, GL, wireless equipment, DHSV, flowline connection & ROV interfaces in the existing X-mas tree thus allows the movement of equipment from one place to another.

1994	Marlim	The oil production commenced at a WD of 1024m and was the deepest subsea completion at that period.
	Carapeba	In October 1994, the ESP with a power range of 100hp was installed in a subsea well at a WD of 86m which is 500m away from FPU and was the world's first ESP in subsea.
1995	Albacora	Diverless manifold were installed at a WD of 620m. Each manifold weighs 450 ton was designed for 2 wells which consists of all valves and choke installed in four retrievable modules. It is mounted & installed using crane barge.
	Marlim	An injector well named 8-MRL-38H-RJS was drilled in an unconsolidated sandstone reservoir and completed with 7" liner and 226m of horizontal section using sand screens.
1996	Albacora	The flowline was directly connected to the subsea equipment by the pipelay vessel at a WD of 610m.
	Marlim East	A well named 7-MRL-29D-RJS was completed using frac pack technique which was the 1 st well to use this technique.
1997	Marlim South	A vertical well named 6-MLS-3B-RJS was drilled and completed using gravel pack in unconsolidated sandstone formation at a WD of 1709m was the deepest subsea completion in the world at that time.
1998	Albacora East	The ESP was installed inside the well through the horizontal X-mas tree at a WD of 1107m and 6.5km from FPU.
	Marlim	It was an integrated project involving drilling, completion & well intervention in deepwater and Ultradeep water reservoirs. It reduces 15% of total cost of a well. The 1 st well was drilled in 1998 at a WD of 692m.
		The first OHGP technology was implemented in 7-MRL-88H-RJS well using 5½" premium screens and it results in high PI.
	Voador	2 multilateral wells named 8-VD-6HP-RJS & 8-VD-7HP-RJS were drilled and completed with inverted standalone premium screens. It was the 1 st level 5 multilateral well drilled from a floating platform.
1999	Roncador	DSR system was devised to decrease the installation time of X-mas tree and tubing hanger. DSR is a combination of drillpipe, control pod, surface control system, umbilical control and it provides access to annular space. It was first deployed from the FPSO Seillean in the well 1-RJS-436 where the DPR produces at a WD of 1853m and was the world record at that time. DP was used for installation of DPR.
		The vertical well 1-RJS-436A was completed with dual zone frac pack and started its production at a WD of 1803m. It was the deepest subsea completion at that period.
2000	Marlim, Roncador, Albacora	To drill upto a water depth of 3000m new technologies such as SURF, subsea boosting systems were employed.
	Marlim	An injector well named 8-MRL-132D-RJS was completed using expandable screens to sand control for the 1 st time in Campos basin.

		Due to higher PI in a well 7-MRL-112H-RJS, a 7" production string was installed instead of 5½" for the first time in Campos basin.
	Marlim South	For the 1 st time in Campos basin, A well named 7-MLS-37H-RJS was completed with OGHP on horizontal section and frac pack on the incline section above the OGHP.
	Roncador	The 1 st well to be completed with triple frac pack was 7-RO-8-RJS and was produced at a WD of 1,877m. It was the deepest subsea completion between 1977-2000.
		A well named 7-RO-9-RJS was completed with triple selective frac pack for 3 production zones which was the first well to employ this technique in Campos basin.
2001	Marlim East	Instead of cable installation method, DPR was installed at a WD of 983m as manifold using DP for exact co-ordinates & azimuth.
	Marimba	It is a two-phase subsea separation and pumping system installed at a WD of 430m has the capacity of 1500 m ³ /d liquid flowrate, 190000 Nm ³ /d gas flowrate, 70°C separation temperature, separation pressure of 175psi and design pressure of 3000psi.
	Roncador	For high flowrate wells, the dual bore horizontal subsea trees are used. It can be used upto 2500m of WD and is employed in this field.
	Enchova west	MAC manifold replaces the existing hydraulic valve into manual valves and is first employed at a WD of 100m.
	Marlim south	A well named 7-MLS-42HA-RJS was drilled to a horizontal departure of 3250m and completed with 7" production string made up of Cr13.
2002	Roncador	Pulley method was used for the installation of gas lift manifold at a WD of 1900m for the 1 st time in Campos basin.
	Marlim	A horizontal well named 7-MRL-156HP-RJS was drilled with 9½" along the reservoir and completed with 6 5/8" of large bore screens made up of Cr13.
2003	Jubarte	This reservoir is having high viscous oil. So the well was completed with X-mas tree at a WD of 1325m using 900hp ESP to produce 2500 bpd of crude.
	Marlim South	The first horizontal injector well named 8-MLS-67H-RJS was drilled and completed entirely with the electric intelligent completion for the first time in world.
2004	Albacora	Torpedo piles was used for fixing the FPSOs. It is an alternative for mooring and was first applied in P-50 FPSO.
2005	Albacora East	Torpedo wellhead was installed and consists of LPWHH which was coupled with the conductor casing before the drilling process. This reduces one rig day and minimizes the CAPEX, OPEX and risks associated with drilling. It was first installed at a WD of 1500m.
2006	Jubarte	An FPSO named P-34 operated at a WD of 840m which consists of 34 number of flexible risers, diverless bell mouth connectors, provisions for pigging and de-waxing, three

		phase cyclone & gravity separators, high power ESPs. It is the only FPSO in the world which consists of 34 flexible risers.
	Roncador	Pendulum motion is used for manifold installation in offshore. Two boats were used for this operation. One has crane and another connected with the manifold through installation cable. The first manifold installation by pendulum method was at a WD of 1900m.
	Enchova	A horizontal well named 7-EN-52H-RJS was drilled and completed at a WD of 1423m with 7" liner and perforated at 7 zones with an interval of 2m using hydraulic acid fracturing technique.
2007	Roncador	FSHR is a long vertical stud pipe tensioned by a buoyancy can near the surface. The FSHR is connected to the seabed through riser and installed in a very large size range of 18" at a WD of 1800m.
	Jubarte	MOBO is an alternative of PAB and a pump is installed 200m away from the production well. MOBO works when the pump fails. MOBO has an advantage of installing higher capacity ESP without increasing the diameter of the well and it also aids in pigging operation. The first MOBO was installed with an ESP of 1200hp at a WD of 1000m.
2008	Jubarte	A well named 1-ESS-103A was comprises of a pre-salt layer and completed, then started its LTPT. It was the 1 st pre-salt layer well to commence production at that period.
2009	Marlim	SBMS was installed at a WD of 641m which has a flow capacity of 500m ³ /h, pressure gain of 60 bar, gas volume fraction of 0.95 driven by an electric canned motor & is controlled by VFD.
2010	Jubarte	The SESV technique replaces the existing use of drilling ships and reduces the CAPEX, OPEX & operational time period. It involves the installation of X-mas tree into the subsurface using a suspended cable for positioning of it by a subsea equipment guidance system.
	Congro	To reduce the formation damage in sea floor, BSR disconnects the FPU from SCR. BSR acts as an intermediary between FPU & SCR. It stands in the midway path where flexible jumpers & FPU are above it and SCR below it with the flowlines till sea floor. Generally the installation was carried out using lift barges but this BSR installation process uses AHTS boats which is cost effective & less time consuming. It is highly applicable in pre-salt reservoirs.
	Baleia Franca	A pre-salt layer well named 6-BFR-1-ES was completed and put into long term production test.
	Caratinga	A pre-salt layer well from Carimbe prospect named 6-CRT-43-RJS was completed and put into production for a long time with an initial production of around 24,000 bpd.
2011	Campos basin	It is designed for pre-salt reservoir. It majorly aims in the separation of compact oil-water, gas-liquid system and gas

		compression sing multiphase pump with high differential pressure.
	Marlim	A well named MRL-141 was the world's first well to employ SSAO 3-Phase subsea separation at a WD of 900m for the separation of heavy oil & water, then uses the same produced water for injection. This SSAO is designed for separation of liquid ranging 3300m ³ /d with water cut of > 65% with an efficiency of 70%.
	Espadarte	The mudline ESP consists of two modules. i.e. pump module and flowbase. The pump module consists of two ESP connected in series at an inclination angle of 5° from the horizontal axis and the flowbase is attached below it. This arrangement facilitates the increase in number of pumps in parallel connection without any extra addition of pump. It was first installed at a WD of 1300m.
	Marlim East	A well named 6-MLL-70-RJS was the 4 th pre-salt layer well to be completed and put into LTPT with an initial production of 23,300 bpd.
	Marlim	The 5 th pre-salt layer well to put into LTPT is 6-MRL-199D-RJS with a production rate of 6000 bpd initially.
2012	Albacora	The SRWI was installed to increase the reservoir pressure. To equip these we need many number of smaller & larger equipment which occupies a larger space in production installation which was not feasible. To overcome this, 3 SRWI systems were installed between 400 to 600m WD and the water intake point was located at a WD of 100m above the seabed.
	Barracuda	The subsea high boost multiphase pump was devised to handle high differential pressure with the specifications of 60 bar differential pressure, 820 kW shaft power and 70% GVF installed at a WD of 1040m.
2015	Papa-Terra	A well named 7-PPT-16H-RJS was the 1 st well put into operation with TLWP in Brazil at a WD of 1181m. Because of the heavy oil characteristics of the reservoir, artificial lift was employed at the earlier stage of production using 7" production string with ESP, 14" production riser and dry X-mas tree.
	Marlim East	A well named 7-MLL-60D-RJS was the 1 st well in the world to use the FMCD technique at a WD of 1422m. It is mainly used in reservoirs having natural fractures. i.e., Carbonates. MCD involves the injection of cuttings into the natural fractures present in the formation. To prevent the influx of wellbore fluids, we circulate sacrificial fluid through string and annulus.
2016	Marlim East, Marlim South	Two wells named 7-MLL-59DB-RJS & 7-MLS-225D-RJS was completed using FMCD at a WD of 1313m & 1819m respectively. This technique reduces the NPT, fluid loss, stuck pipe events which is most common in conventional drilling.

2017	Roncador	Two wells named 7-RO-167 & 7-RO-168 were drilled at different locations upto a WD of 1800m at same time. The lowering of surface and conductor casing was assembled and the cementing operation were done at same stage for both casings thus reduces the operational time and cost.
2018	Tartaruga Verde	An FPSO named Cidade de Campos dos Goytacazes MV29 has a crude processing capacity of 1,50,000 bpd, gas compression of 176 MMscf/d and storage capacity of 1.6MMbbl of oil. [17]
2019	Tartaruga Verde, Espadarte	Exploration process acquired the subsurface geological structure and the field will commence its production on 2021. [12]; [18]
2020	Polvo	FPSO operation from BM-C-8 block will be extended for a period of one year. [13]

6. Campos Basin – A front-runner in Brazil Petroleum Era

For the first time in the history of Brazil, the following operations were carried out in Campos basin and are tabulated below.

Table 4: Operations carried out for the first time in history of Brazil

Year	Name of the field	Type of Operation
1977	Enchova	LTPT achieved 10000 bpd of oil production, the greatest production ever by a single well at that time.
1991	Bonito	A well named 7-BO-13H-RJS was the 1 st subsea horizontal well in Brazil which was drilled using MWD & completed with hydraulic packer.
2015	Papa-Terra	A well named 7-PPT-16H-RJS was completed at a WD of 1181m and produced from TLWP.

6.1. Campos Basin – An exemplar in World's Subsea Operations

The operations carried out in Campos basin was innovative & cost-effective which holds world record and got award many times. This basin was the pacesetter in subsea completion. The following operations were the evidence for that and are tabulated below.

Table 5: Operations carried out for the first time in World's history

Year	Name of the field	Type of Operation
1979	Bonito	A well named 1-RJS-38 was completed with a subsea X-mas tree at a WD of 189m by PETROBRAS was the world's deepest subsea completion at that time.
1983	Pirauna	A well named 4-RJS-232 was drilled and completed at a WD of 293m was the world's deepest subsea completion at that period.
1985	Marimba	A well named 1-RJS-284 was drilled and completed at a WD of 383m earns the world's record of the deepest subsea completion.

1988	Marimba	A well named 1-RJS-376D was drilled, completed and produced at a WD of 492m and obtained the deepest subsea completion world record.
1991	Marlim	A well named 3-MRL-3-RJS was drilled and completed using gravel pack at a WD of 721m receives the world record of the deepest subsea completion.
1992	Marlim	A well named 7-MRL-9-RJS was drilled and completed with conventional gravel packing at a WD of 781m got the award of world's deepest subsea completion at that time period.
1994	Marlim	Marlim field was the first to produce in subsea at a depth of greater than 1000m. A well named 3-MRL-4-RJS was completed at a WD of 1024m earns the deepest subsea completion world record for third time.
	Carapeba	The world's first ESP was installed at a WD of 86m with a capacity of 100hp.
1997	Marlim South	A well named 6-MLS-3B-RJS was completed with gravel pack at a WD of 1709m earns the world's deepest subsea completion record.
1998	Marlim	A semi-submersible platform named P-18 installed steel catenary riser at a WD of 910m for the 1 st time in universe.
	Voador	Two multilateral level 5 wells named 8-VD-6HP-RJS & 8-VD-7HP-RJS were drilled from a floating vessel for the first time in world's history.
1999	Roncador	A well named 1-RJS-436 was produced through a drill pipe riser at a WD of 1853m was the world record at that time.
	Roncador	A well named 1-RJS-436A was completed using dual zone frac pack at a WD of 1803m was the world's deepest subsea well completion at that period.
2000	Roncador	A well named 7-RO-8-RJS was completed with triple frac pack at 1877m WD earns the world's record of deepest subsea well completion.
2003	Marlim South	A well named 8-MLS-67H-RJS was the 1 st horizontal injector well drilled and completed entirely using electric intelligent completion in the world.
2006	Jubarte	An FPSO named P-34 was the platform with 34 number of flexible risers and holds the record of having maximum number of risers.
2011	Marlim	A producer well named MRL-141 uses SSAO 3-phase subsea separation at a WD of 900m was the 1 st well to use this equipment in the world for the separation of heavy oil & water.

2015	Marlim East	A well named 7-MLL-60D-RJS employed FMCP at a WD of 1422m in a carbonate reservoir which was the 1 st well to use FMCP technique.
------	-------------	--

7. Campos Basin – Calendar full of Engagement

Various operations were carried out in Campos basin throughout the year and are tabulated below.

Table 5: Operations carried out year-wise

S.No	Year	No. of Operations carried out
1	1971	1
2	1972	Nil
3	1973	1
4	1974	1
5	1975	1
6	1976	Nil
7	1977	2
8	1978	Nil
9	1979	2
10	1980	Nil
11	1981	1
12	1982	1
13	1983	1
14	1984	1
15	1985	2
16	1986	1
17	1987	1
18	1988	1
19	1989	1
20	1990	Nil
21	1991	2
22	1992	4
23	1993	1
24	1994	2
25	1995	2
26	1996	2
27	1997	1
28	1998	5
29	1999	2
30	2000	6
31	2001	5
32	2002	2
33	2003	2

34	2004	1
35	2005	1
36	2006	3
37	2007	2
38	2008	1
39	2009	1
40	2010	4
41	2011	5
42	2012	2
43	2013	Nil
44	2014	Nil
45	2015	2
46	2016	1
47	2017	1
48	2018	1
49	2019	1
50	2020	1

8. Why GLM is mostly used during completion of subsea well in Brazil?

All the wells drilled in the Brazilian subsea was completed with packers and production strings with GLM's. The reason for installing GLM is that the gas obtained from the well is neither be flared nor be processed because the quantity of gas obtained is higher than the cut-off value for flaring and lower than the value for further processing. It is temporarily stored in the storage tank and is sent to the reservoir for reducing the viscosity of crude oil using gas lift technology. Depending upon the type of formation, reservoir thickness, drainage area, the GL may either be continuous gas lift or intermittent gas lift.

9. Campos Basin – A golden duck

For more than half century the basin is producing hydrocarbon and more number of well locations were identified which turns out to achieve production later 2020s. Even now Petrobras open its application for carrying out E&P operations in Campos basin. This itself fosters Campos basin a major asset and everlasting economy driver for the Brazilian economy.

9.1. Management advancements in Campos Basin

Over the period of past 50 years, various technological advancements were made. Campos basin composed of several fields which has to be managed and accounted correctly for both hydrocarbon resources and financial resources. CIOP controls all the offshore operations in Campos basin since 2015 which is responsible for controlling, monitoring and supporting of subsea vessels also it aids in the logistics & supply-chain demand and contingency process to smoothen the E&P operation. Personnel from various sectors such as Finance, Human Resource Management, and Subject Matter Expert & Engineers works altogether to make the complicated management process into simpler. Various technologies were implemented for an effective reservoir management [16]:

- i. Data acquisition during drilling & production phase to neglect uncertainties
- ii. Continuous improvement in designing and modelling using dynamic data
- iii. Using 4D seismic data for monitoring of oil & gas production and prediction of oil in secondary gaps.
- iv. Production logs to find out the remaining oil in reservoir.

9.2. Future Operations in Campos Basin

To ensure continuous & sustainable development of the Campos basin, the equipment used in the operation are designed in such a way that it has to be withstand for a longer period of time and the atmospheric conditions has to be taken into account. Newer technologies are needed in controlling, supporting and monitoring of subsea equipment for its integrity in operation. This can be met out by tie-up with external R&D organizations and own. Technological advancements is needed in the recently discovered heavy oil prospects for its economical extraction.

10. Conclusion

Campos basin already proven its potential for the past 5 decades and it has to continue its operation for furthermore 50 years in the Brazilian petroleum era to fulfil the requirement of nation's and world's energy sector. To enable this the Campos basin O&G operators has to closely associate with R&D section, Educational institutions and global consultants to deploy the feasible technology in the offshore for subsea operations at a reasonable cost. More liberalisation and transparency is needed in the award of blocks which in turn increases the number of players for the healthy participation in bidding process.

11. Abbreviations & Acronyms

AHTS – Anchor Handling Tug and Supply

BOP – Blow Out Preventer

bbl - barrel

bpd – barrels per day

BSR – Buoy Support Riser

CAPEX – CAPital Expenditure

CIOP – Integrated Operation Control center

CNP – National Petroleum Council

DHSV – DownHole Safety Valve

DNMP – National Department of Mineral Production

DP – Dynamic Positioning

DPR – Drill Pipe Riser

E&P – Exploration and Production

EPS – Early Production System

ESP – Electrical Submersible Pump

FMCD – Floating Mud Cap Drilling

FPSO – Floating Production Storage Offloading

FPU – Floating Production Unit

GL – Gas Lift

GLM – Gas Lift Mandrels

GMSB – Geological and Mineralogical Service of Brazil
GVF – Gas Volume Factor
HOHGP – Horizontal Open Hole Gravel Packing
hp – horse power
ID – Inner Diameter
LPWHH – Low-Pressure WellHead Housing
LTPT – Long Term Production Test
MCD – Mud Cap Drilling
MOBO – Pumping Module installed on the seabed in a dummy well
MMbpd – Million barrels per day
MMscf – Million standard cubic feet
MNC – Multi National Company
MPD – Managed Pressure Drilling
NPT – Non-Productive Time
O.D – Outer Diameter
OHGP- Open Hole Gravel Packing
OPEX – Operational Expenditure
PAB – Production Adaptive Base
PI – Production Index
PLSV – Pipe Laying Support Vessel
PROCAP – Deep Water Technology Program
R&D – Research and Development
ROV – Remotely Operated Vehicles
SBMS – SuBsea Multiphase Pump
SCR – Steel Catenary Riser
SESV – Subsea Equipment Support Vessel
SIT - System Integration Test
SOT – Subsea Operational Technology
SRWI – Subsea Raw Water Injection system
SS – Semi-Submersible platform
STT – Subsea Test Tree

STU – Steel Tubing Umbilical
 TCA – Technical Cooperation Agreement
 TCP – Tubing-Conveyed Perforating
 TLWP – Tension Leg Wellhead Platform
 TSR – Tubing Seal Receptacle
 UDWT – Ultra Deep Water Technology
 UTM – Umbilical Termination Module
 VASPS – Vertical Annular Separation and Pumping System
 VFD – Variable Frequency Driver
 WD – Water Depth
 X-mas Tree – Subsea Christmas Tree

Acknowledgement

We would like to thank the management of AMET, VISTAS for providing us with enough resources for the timely publication of this article.

References

1. https://en.wikipedia.org/wiki/Geography_of_Brazil dated 02/02/2020
2. Braga Luciana, "OIL IN BRAZIL: EVOLUTION OF EXPLORATION AND PRODUCTION", Accueil - Sources fossiles, 29 November 2018.
3. <https://en.wikipedia.org/wiki/Petrobras> dated 02/02/2020
4. https://en.wikipedia.org/wiki/Template:Sedimentary_basins_of_Brazil dated 02/02/2020
5. Drielli Peyer, Silvia Fernanda De Mendonca Figueiroa, Elvio Pinto Bosetti., "The North American Geologist Walter Karl Link and Oil Exploratory Research at Petrobras (1954–1960)", Earth sciences history: journal of the History of the Earth Sciences Society, Volume 35, Issue 2, October 2016: 387-398.
6. <https://www.offshoremag.com/geosciences/article/16757635/brazil-expands-exploration-on-its-20-offshore-sedimentary-basins> dated 03/02/2020
7. http://www.anp.gov.br/images/Palestras/15_cisbgf/DG_ABERTURA_SBGf_Publicacao.pdf dated 03-02-2020
8. C.H.L. Bruhn, J.A.T. Gomes, C. Del Luchese, P.R.S. Johann., "Campos Basin: reservoir characterization and management: historical overview and future challenges", 35th Offshore Technology Conference, Richardson, Texas, 2003:1406-1419
9. https://en.wikipedia.org/wiki/Campos_Basin dated 04/02/2020
10. E.J. Milani, A.Thomaz Filho., "Sedimentary basins of South America", Tectonic evolution of South American 31st International Geological Congress, Rio de Janeiro, 2000: 389-449
11. <https://en.wikipedia.org/wiki/Marlim> dated 04/02/2020
12. Business Guide, OFFSHOREENERGYTODAY.COM, "Petronas closes acquisition of two Petrobras Campos Basin assets", December, 2019.
13. Offshore, Rigs/Vessels, "Polvo field FPSO secures seventh extension offshore Brazil", January, 2020.

14. M.Roberto, A.B.Countinho, A.R.Dos Santos., “Campos Basin Technologies Yard:40 years of Lessons Learned”, Offshore Technology Conference, Houston, Texas, USA, 2018 – OTC-28716-MS.
15. <https://www.offshore-mag.com/production/article/14035410/petrobras-pursuing-offers-for-campos-basin-fields> dated 05-02-2020
16. Guilherme.E.S.Dumas, Ednilson.B.Freire, Paulo.R.S.Johann, Luciana.S.Silva, Roberto.A.B.Vieira, Carlos H.L.Bruhn, Antonio.C.C., “Reservoir Management of the Campos Basin Brown Fields”, Offshore Technology Conference, Houston, Texas, USA, 2018 – OTC-28657-MS.
17. <https://www.offshore-mag.com/field-development/article/16803365/tartaruga-verde-fpso-starts-operations-offshore-brazil/> dated 31/01/2020
18. <https://www.nsenergybusiness.com/news/petrobras-c-m-477-campos-basin/> dated 31/01/2020



Application of a polymer-magnetic-algae based nano-composite for the removal of methylene blue – Characterization, parametric and kinetic studies[☆]

G. Sarojini^a, S. Venkatesh Babu^b, N. Rajamohan^c, M. Rajasimman^d, Arivalagan Pugazhendhi^{e,*}

^a Department of Petrochemical Engineering, SVS College of Engineering, Coimbatore, India

^b Department of Petroleum Engineering, JCT College of Engineering & Technology, Coimbatore, India

^c Faculty of Engineering, Sohar University, Sohar, P O: 311, Oman

^d Department of Chemical Engineering, Annamalai University, Annamalai Nagar, India

^e Innovative Green Product Synthesis and Renewable Environment Development Research Group, Faculty of Environment and Labour Safety, Ton Duc Thang University, Ho Chi Minh City, Viet Nam

ARTICLE INFO

Keywords:

Methylene blue
Dye
Nano-composite
Adsorption
Kinetics

ABSTRACT

The potential ability of synthesized PPy-Fe₃O₄-SW nano-composite to remove Methylene Blue (MB) from synthetic textile dye solution was investigated under batch conditions. Through parametric studies, the influence of process parameters namely solution pH, on the effective performance of nano-composite was studied. PPy - Fe₃O₄- SW nano-composite removed 99.14% of MB at the optimized conditions of pH-10, temperature - 25 °C, initial MB concentration - 50 mg/L, nano-composite dosage - 20 mg and contact time - 20 min. PPy - Fe₃O₄- SW nano-composite has a maximum sorption capacity of 666.66 mg/g. The kinetics and isotherm study revealed that the chromium adsorption obeys pseudo second order (PSO) model ($R^2 = 0.9941$) and Freundlich isotherm ($R^2 = 0.9910$) respectively. The PSO kinetic constant (K_2) was found to be 0.000442 (g/mg) min. The thermodynamic feasibility was confirmed through negative values of standard free energy at all tested conditions. The characteristics of adsorption study were analyzed and the results of FTIR, SEM and EDS confirmed the uptake of MB by PPy-Fe₃O₄-SW nano-composite.

1. Introduction

Nanotechnology applications in engineering and environmental science has increased significantly during the current decade due to the availability of nanomaterials with enhanced properties and modified molecular structure (Sajid and Plotka-Wasylika, 2020). Dyeing industry has expanded its operations in various production lines such as leather, cosmetic, textile, plastic, pharmaceutical, food, rubber, paper and printing industries (Aluigi et al., 2014; Tkaczyk et al., 2020). Dyeing operations are highly water sensitive with extensive requirements during various processing stages and the effluent from these industries are the contaminated with dye due to the process inefficiency. The global discharge of dyes in industrial waste water is reported to be 280,000 tons and accounts to 10–60% of the dyes used in industrial processes (Berradi et al., 2019). The release of dyes could be due to inefficient attachment, excess use, and release during downstream operations.

Dyes, classified based on their molecular structure, do possess varied solubility and resistivity to chemical changes. The discharge of dyes into natural ecosystem results in several deleterious effects, namely reduced dissolve oxygen levels, lack of penetration of sunlight inhibiting the aquatic photosynthesis, tendency to bioaccumulate affecting mineral proliferation in aquatic systems and deposition in soil layers (Hynes et al., 2020; Kishor et al., 2021; Zafar et al., 2021). Dyes, owing to their reactive properties, do have short term health effects like skin disorders, allergic reactions and related ill effects on limited exposure. The serious threat is related to the combination of the dye molecules with intermediates resulting in products with carcinogenic and mutagenic properties (Rajeshkannan et al., 2011). Removal of dyes have been investigated using a variety of techniques which are physical, chemical and biological methods (Bhatti et al., 2020; Rajasimman et al., 2017; Rajeshkannan et al., 2011; Sathian et al., 2014). The suitability of chemical methods is very restricted due to the limited reactivity or inert

[☆] This paper has been recommended for acceptance by Rinklebe “CRJJO”

* Corresponding author. Faculty of Environment and Labour Safety, Ton Duc Thang University, Ho Chi Minh City, Viet Nam.

E-mail address: arivalagan.pugazhendhi@tdtu.edu.vn (A. Pugazhendhi).

nature of the dyes. Among the physical methods, adsorption remains as an effective technique in removal of dyes owing to its physical nature, ease of operation, wide application, simplicity and low cost (Pandian et al., 2021a).

Conventional adsorbents are found to be less attractive based on their limited life cycle, expensive regeneration and high replacement cost (Pandian et al., 2021b). Nanomaterials-based composite have emerged as a potential candidate for the removal of various pollutants including heavy metals, dyes, pharmaceuticals and pesticide products (Sarojini et al., 2021). Several nano-composites such as cellulose/ Fe_3O_4 /activated carbon (Yang et al., 2008), magnetic activated carbon nano-composites (Zhao et al., 2015). Graphene/ Fe_3O_4 composite (Xie et al., 2012), magnetic-multi-wall carbon nanotube nano-composite have been utilized in removal of dyes from aqueous solution. To enhance the adsorption capacity, many researchers incorporated polymers to increase the functional groups which complements the pre-existing groups. Polymer based composites have higher dispersion ability in aqueous medium and face difficulties during recovery. Therefore combination of Fe_3O_4 nanoparticles enables easier separation after adsorption and enhanced surface attachment. In addition, Fe_3O_4 acts as a stabilizer and prevents the spheres of polypyrrole from agglomeration. Recently polypyrrole based composites have been employed in removal of various contaminants and attainment of higher removal efficiencies are reported. Magnetic nano-composite was prepared by coating PPy on Fe_3O_4 . Gholivand et al. (2015) synthesized polypyrrole-coated Fe_3O_4 nanoparticles and investigated its sorptive behavior towards anionic alizarin red-S and alizarin yellow GG dye. Shانهsaz et al. (2015) synthesized polypyrrole-coated Fe_3O_4 nanoparticles to remove RB19 synthetic textile dye. Nevertheless Fe_3O_4 -PPy composite faces major difficulty in adsorption as they tends to agglomerate. Nano-composites could overcome the problem of aggregation by providing increased surface area. Therefore, many researchers investigated modification of PPy based composite into nano-composite by incorporating with suitable biomaterial. Wang et al. synthesized PPy- Fe_3O_4 /RGO magnetic composite and applied it in removal of Cr (VI) (Wang et al., 2015). But the synthesized composite showed lower adsorption capacity due to poor dispersion capacity. There is no research is done on the modification of magnetic PPy-based materials with seaweed for the removal of aqueous dyes. As a result, the PPy- Fe_3O_4 -SW nano-composite was fabricated with integrated adsorption properties. PPy- Fe_3O_4 -SW nano-composite was synthesized using in-situ polymerization technique. Intercalation of polypyrrole provides specific functionalities for environmental remediation. Fe_3O_4 makes the separation easier and seaweed improves the adsorption capacity. There was no report on the use of PPy- Fe_3O_4 -SW nano-composite in removal of methylene blue from aqueous medium. The novelty in this study is the application of PPy- Fe_3O_4 -SW nano-composite for the removal of methylene blue from aqueous solution. Effects of vital operating variables, namely initial pH, nano-composite dosage, dye concentration, contact time and temperature on adsorption are assessed. Isotherms are applied to model the equilibrium data. The kinetic and thermodynamic studies have been performed to determine the mechanism and verify the feasibility, respectively.

2. Materials and methods

2.1. Synthesis of PPy- Fe_3O_4 -SW

The nano-composite used in this study was synthesized and characterized as reported (Sarojini et al., 2021). The first stage of Fe_3O_4 nanoparticles synthesis involves co-precipitation technique. In the second stage, 0.5 g Fe_3O_4 was added to pre-determined volume of distilled water followed by ultrasonication. Then six grams of ferric chloride were added as oxidant followed by magnetic stirring. To the entire solution, 0.8 mL of pyrrole was poured to initiate polymerization reaction and sonicated for 30 min. At the appearance of black color, acetone was

added to stop the polymerization reaction. Then Fe_3O_4 -seaweed composite was added and sonicated for 30 min. The obtained precipitate was filtered, washed many times with distilled water and acetone. The washed product was dried in oven and stored in an air-tight container.

2.2. Batch experiments

The stock solution of methylene blue (1000 mg/L) was prepared, and the working solution was synthesized by diluting the stock solution. The sorption trials were conducted in an environmental shaker (REMI, India). Tests were conducted in a conical flask (250 mL) holding 50 mL MB solution. Effect of initial dye solution pH (2–12), nano-composite dosage (5–20 mg/L), initial MB concentration (10–150 mg/L), contact time (10–60 min) and temperature (298–323 K) were investigated. The initial solution pH was varied using 1 M HCl or 1 M NaCl. Methylene blue concentrations were measured using double beam UV–vis spectrophotometer (Shimadzu, Japan) at maximum adsorptive wavelength of 618 nm. The amount of MB adsorbed per unit mass of nano-composite under equilibrium q_t (mg/g) and MB removal efficiency (% RE) were obtained from equations given below:

$$q_t = \frac{(C_0 - C_t) * V}{m} \quad (1)$$

$$\text{Removal efficiency (RE) of MB, \%} = \frac{C_0 - C_t}{C_0} * 100 \quad (2)$$

where C_0 and C_t – initial MB concentration and equilibrium MB concentration (mg/L) respectively, V is sample volume (L) and m is mass of nano-composite (g).

2.3. Desorption experiments

To verify the reusability of the nano-composite, desorption studies were conducted. MB sorbed nano-composites were washed with 25 mL of ethanol-water solvent mixture under room temperature and dispersed for 12 h. The regenerated nano-composite sorbent was again washed using distilled water and dried. Then it was reused in next cycle.

3. Results and discussion

3.1. Characterization of PPy- Fe_3O_4 -SW

The surface functional group identification was carried out by FTIR analysis. Fig. 1(a–c) shows the FTIR of seaweed, PPy- Fe_3O_4 -SW nano-composite and PPy- Fe_3O_4 -SW nano-composite after adsorption. The characteristic band at 665.06 cm^{-1} is attributed to the vibration of Fe–O confirming the presence of Fe_3O_4 (Wang et al., 2012). The peak at 1560 cm^{-1} is due to C=C stretching vibrations of pyrrole ring and the characteristic band at 1202 cm^{-1} is attributed to C–N stretching vibrations (Qian et al., 2013). The band at 1196 cm^{-1} corresponds to C–H in plane bending mode. The peaks at 3333.02 and 1702 cm^{-1} correspond to OH stretching vibration of seaweed polysaccharide and water molecules respectively. The presence of these functionalities proves that pyrrole and Fe_3O_4 nanoparticles are effectively coated on the surface of the nano-composite. After adsorption of MB, the change in intensity of peak was observed due to the surface attachment of the nano-composite by dye molecules.

SEM result was used to analyse the micro-structure and morphology of seaweed, synthesized PPy- Fe_3O_4 -SW nano-composite and PPy- Fe_3O_4 -SW nano-composite after adsorption. Fig. 2a represents the SEM image of raw seaweed having thread like structure with high pores and cavities. However, after fabrication with Fe_3O_4 and PPy, formation of spherical particles is observed which confirms the coating of Fe_3O_4 and PPy. The spherical particles are responsible for enhanced sorption and pores for adsorbing contaminants (Fig. 2b). Fig. 2c shows the image of nano-composite after adsorption. It is observed that no regular spherical

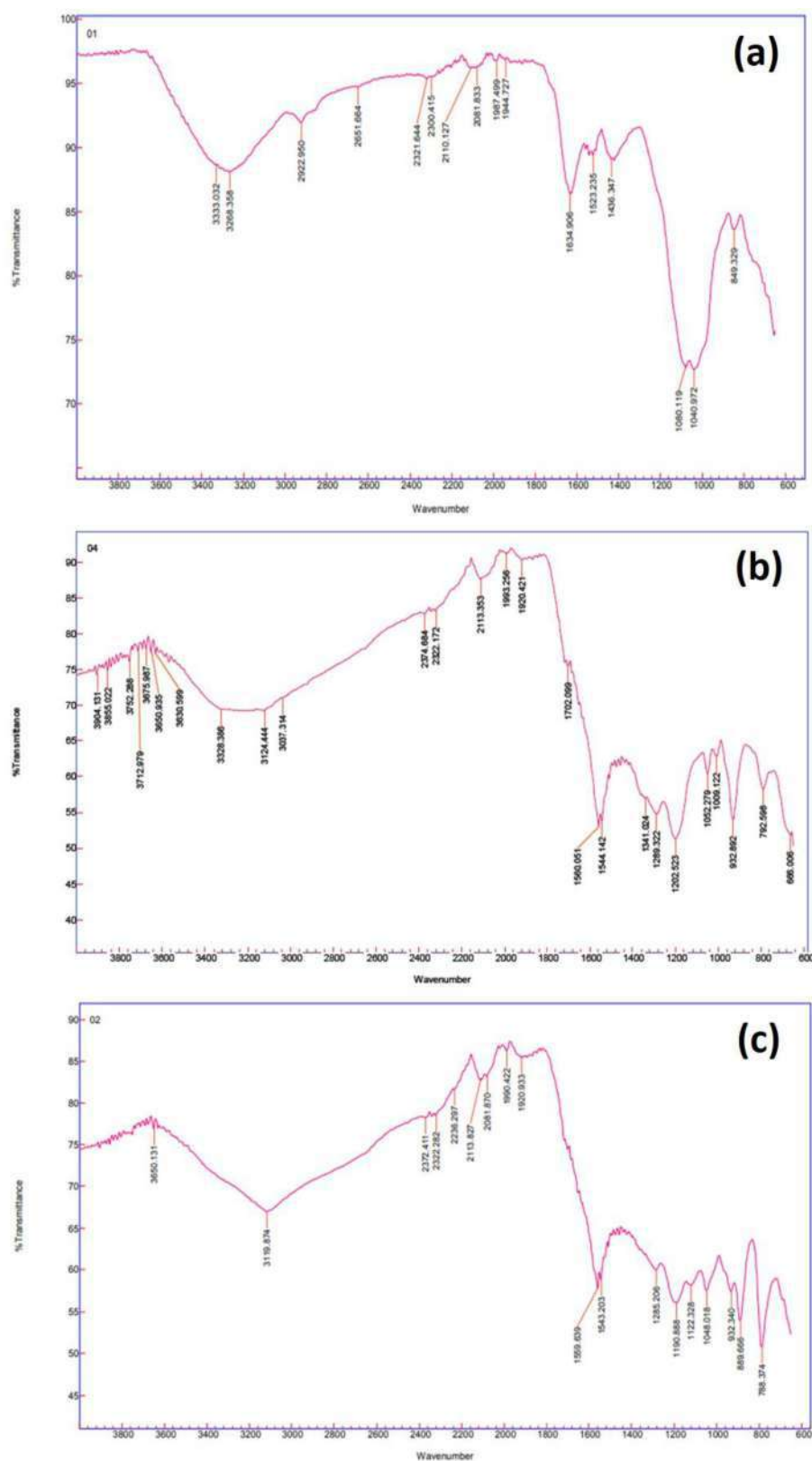


Fig. 1. (a) FTIR of Seaweed; (b) FTIR of PPy - Fe_3O_4 -SW before adsorption; (c) FTIR of MB loaded PPy - Fe_3O_4 -SW.

particles are found indicating that surface of the nano-composite is covered by the dye. The agglomerated state of the particles is noticed in SEM image (Fig. 2c) and indicates the binding of MB on nano-composite surface. The energy dispersive X-ray spectroscopy (EDS) spectra of the MB adsorbed PPy- Fe_3O_4 -SW nano-composite is shown in Fig. 3.

Existence of C, O, N and Fe represents the origins of three components namely polypyrrole, iron oxide and seaweed. The main elemental content of MB encompasses Cl, S and C. Cl arises from FeCl_3 added as an oxidant during polymerization and also by adsorption of MB. The presence of S point out the adsorption of MB ($\text{C}_{16}\text{H}_{18}\text{N}_3\text{SCL}$).

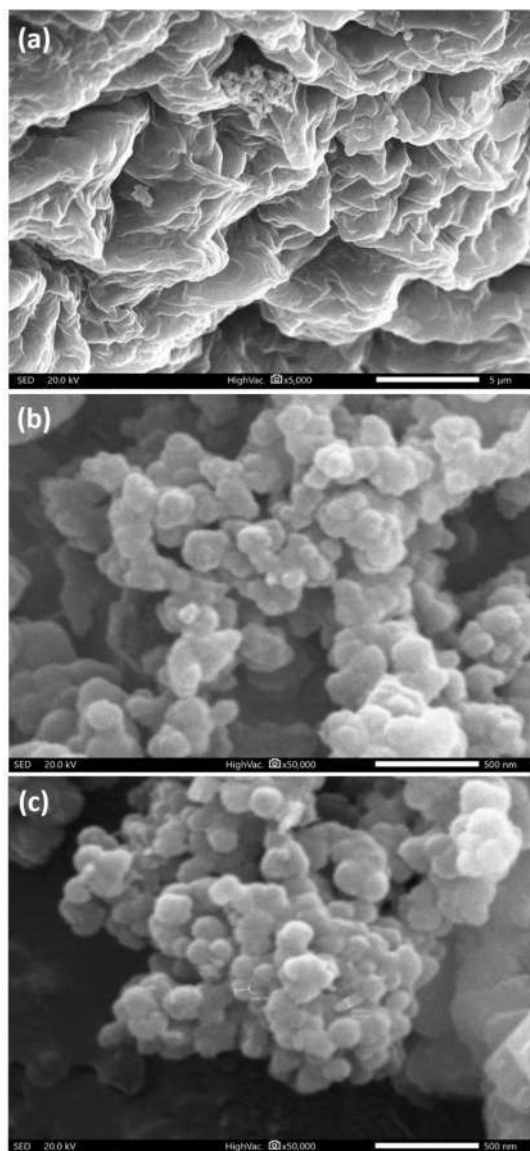


Fig. 2. (a) SEM image of seaweed; (b) SEM image of PPy - Fe₃O₄- SW before adsorption; (c) SEM image of MB loaded PPy - Fe₃O₄- SW after adsorption.

3.2. Influence of solution pH

The influence of pH on dye removal performance of the nano-composite was studied in the range of 2–12 and the results are given in Fig. 4a. From the figure, it was observed that lower pH was unfavorable for adsorption of MB due to the fact that at acidic conditions the excess protons available in solution competing with cations of MB for adsorption. Also, under acidic conditions availability of negatively charged adsorbent sites gets reduced thereby the surface of the composite becomes unsuitable for adsorption of MB cations (Gusmao et al., 2012; Rajeshkannan et al., 2010). The removal rate gradually increases as pH increases and maximum removal is obtained at higher pH. The positive charges of MB molecules encouraging electrostatic attraction between nano-composite and cationic MB dye. These results showed that pH is a vital parameter in sorption process as it greatly influences the interaction force between sorbate and sorbent. The maximum removal is obtained at pH of 10 and this value was selected in the succeeding experiments.

3.3. Influence of nano-composite dosage

The quantity of nanocomposite decides the operational cost of process and removal efficiency of pollutant. The influence of addition of varied quantities of nano-composite on the MB dye removal efficiency is depicted in Fig. 4b. It was noted that the increase in dosage from 5 to 20 mg enhances the removal efficiency from 56.85% to 97.65%. The attainment of higher removal efficiency of MB at higher dosage is related to the higher ratio of vacant sites to sorbate ions. From the results, 20 mg of adsorbent dosage was chosen as an optimum value and used in the other experimental trials. Previous literatures on the application of nanocomposites (Pandian et al., 2021a; Pandian et al., 2021b) and algal biomass (Jayakumar et al., 2021) reported similar results for the decontamination of pollutant by sorption process.

3.4. Influence of initial dye concentration

The concentration of the MB is one of the prime factor which influence the rate of adsorption. Fig. 4c represents the influence of MB dye concentration on removal efficiency. It was seen that a highest removal of 98.86% was achieved at an initial MB concentration of 10 ppm and a lowest removal of 15.26% was attained at an initial MB dye concentration of 200 ppm. With fixed number of available active sites on nano-composite surface, increase of MB dye concentration increases competition between the ions for the same active sites. Based on the results, the optimum initial concentration was chosen as 50 mg/L. As active sites are not enough to accommodate all contaminants, lower removal efficiency was observed at higher concentration (Afzal et al., 2018). Studies on removal of dye using plant based adsorbent reported similar effect of concentration on dye removal efficiency (Rajeshkannan et al., 2011).

3.5. Influence of contact time

The results of contact time versus removal efficiency of MB onto PPy-Fe₃O₄-SW nano-composite are shown in Fig. 4d. From the plot, it was observed that MB adsorption is very fast within the first 20 min and then gradually reduced. Fast adsorption at initial stages was due to the availability of abundant active sites on the surface of the nano-composite. With increase in contact time, active sites get occupied and the rate of adsorption of MB reduces. Studies on sorption confirmed the need for more active sites (Rajeshkannan et al., 2011). The equilibrium time of 20 min was used in all other experiments.

3.6. Influence of temperature

The effect of temperature on RE of MB onto PPy-Fe₃O₄-SW nano-composite was explored in the range of 298–323 K. From Fig. S1 (a) it is seen that removal efficiency increases as temperature increases from 298 to 313 K and then remains constant. Highest removal efficiency of 99.14% is obtained at 313 K. This observation is related to the fact that the higher temperature provides sufficient energy required for the interaction of dye molecules with the available active sites on the nano-composite surface. At 323 K, the removal efficiency decreased due to the desorption of dye molecules. Forced molecular motion of dye molecules at higher temperature increased resistance to adsorption of MB molecules on the surface of the nano-composite (Jia et al., 2015).

3.7. Adsorption thermodynamics

To examine the feasibility, spontaneity and nature of sorption interaction, thermodynamic parameters namely ΔH° , ΔS° and ΔG° are determined. The thermodynamic properties are determined by the equations given below:

$$\Delta G^\circ = -RT \ln k \quad (3)$$

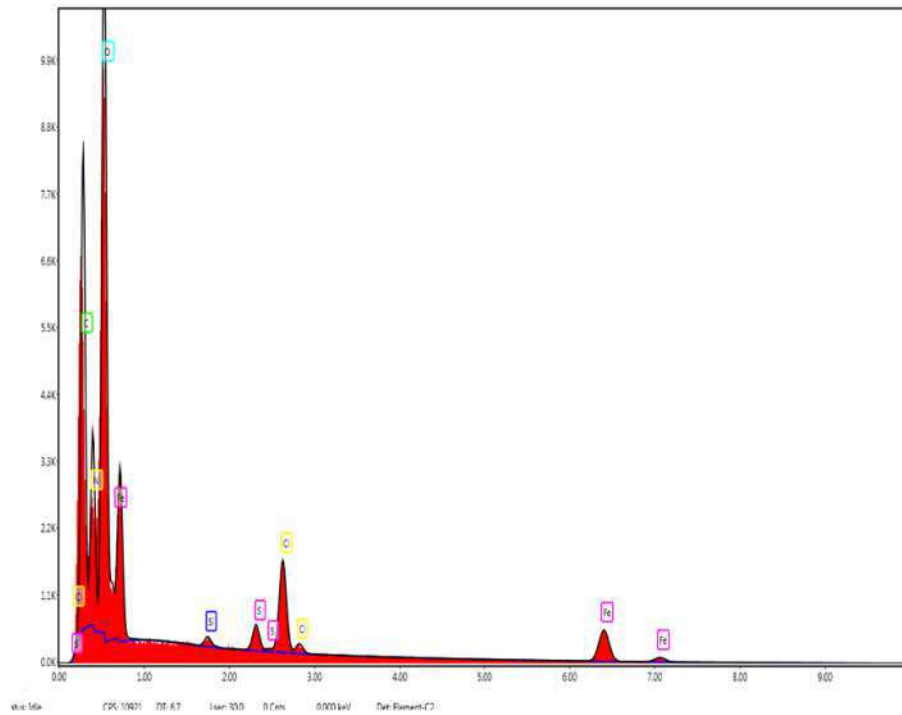


Fig. 3. EDS spectrum image of MB loaded on PPy - Fe₃O₄- SW.

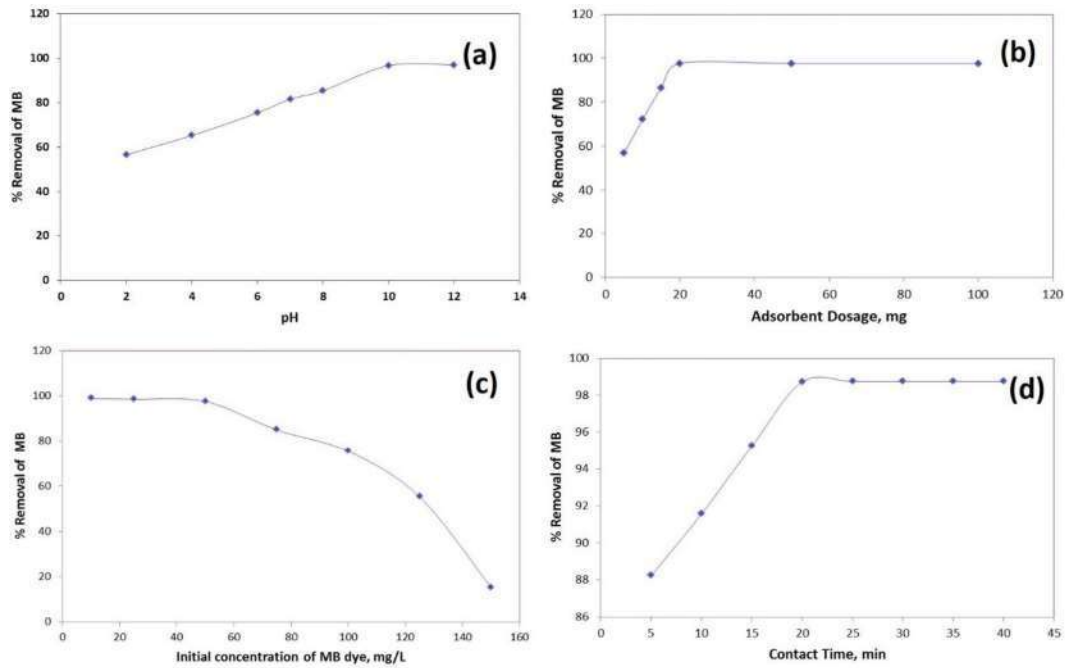


Fig. 4. (a) Influence of pH on MB removal; (b) Influence of sorbent dosage on MB removal; (c) Influence of initial MG concentration on MB removal; (d) Influence of contact time on MB removal.

$$\Delta G^0 = \Delta H^0 - T\Delta S^0 \quad (4)$$

k - equilibrium constant ($k = q_e/C_e$).

R - Universal gas constant (8.314 J/mol K).

T - temperature (K).

ΔH^0 - enthalpy change (kJ/mol).

ΔG^0 - Gibbs free energy (kJ/mol).

ΔS - entropy change (kJ/mol K).

The values of ΔH and ΔS were found from the plot of ΔG versus T

(Fig. S1(b)) and the thermodynamic parameters values are provided in Table 1. The positive values of ΔS^0 proved the feasibility of the sorption and increase in randomness at solid/liquid solution interface. The higher values of ΔH further specify that the sorption process is chemical in nature. The endothermic nature of sorption was confirmed through ΔH (>0) values. The negative values of ΔG^0 conveyed the feasibility of process and nature of sorption was found to be spontaneous. From Fig. S1 (b) it was observed ΔG^0 values decrease as temperature increases representing that sorption process was highly favorable at increased

Table 1
Thermodynamic parameters and their values.

Temp (K)	ΔG° (kJ/mol)	ΔS° (kJ/mol k)	ΔH° (kJ/mol)
298	-9.6879	0.1991	49.315
303	-10.778		
308	-12.0868		
313	-12.4933		
318	-13.7384		
323	-14.9738		

temperature. The thermodynamic parameters proved the feasibility and favorable nature of the sorption process under the experimental conditions tested.

3.8. Equilibrium sorption isotherm studies

Isotherm studies were performed to realize the interaction between adsorbed molecule and sorbent surface. Interaction between sorbate and sorbent is analyzed using Langmuir isotherm, Freundlich isotherm, Temkin isotherm, Dubinin-Radushkevich (D-R) isotherm.

3.8.1. Langmuir isotherm

The Langmuir equation (Langmuir, 1918) applies for monolayer sorption processes and is characterized by the resulting equation:

$$\frac{1}{q_e} = \frac{1}{q_m b C_e} + \frac{1}{q_m} \quad (5)$$

C_e – equilibrium MB concentration (mg/l); q_m – Langmuir maximum adsorbing capacity (mg/g); b – Langmuir sorption constant representing the attraction of binding sites (L/mg).

3.8.2. Freundlich isotherm

Freundlich isotherm (Freundlich, 1906) designates to multilayer process and the linear form of Freundlich model is given below:

$$\log_{10} q_e = \log_{10} K_f + \frac{1}{n} \log_{10} C_e \quad (6)$$

K_f (mg/g) represents Freundlich constant; n – adsorption intensity. Slope K_f and intercept $1/n$ were calculated from the graph of $\log_{10} q_e$ vs $\log_{10} C_e$. For enhanced adsorption studies the value of $1/n$ should be between 0 & 1. In the adsorption of MG, the value of $\frac{1}{n}$ was found to be 0.5731. This confirms that the adsorption of MB dye onto the bio-nanocomposite was favorable. Also, based on the R^2 values, as shown in Table 2, the Freundlich isotherm has a high value of 0.9910.

3.8.3. Temkin isotherm

The linear form of Temkin equation (Temkin, 1940) is specified by:

$$q_e = B \ln K_T + B \ln C_e \quad (7)$$

B (J/mol) denotes Temkin constants and K_T (L/g) represents binding

Table 2
Equilibrium isotherm parameters and their values for MB sorption.

Isotherm model	Parameters	Methylene Blue sorption
Langmuir	q_m (mg/g)	666.66
	b (L/mg)	0.2027
	R^2	0.9901
Freundlich	K_f (L/mg)	62.618
	$1/n$	0.5731
	R^2	0.9910
Dubinin- Redushkevich	q_m (mg/g)	419.51
	β (mol ² /kJ ²)	0.5318
	E (kJ/mol)	0.9696
	R^2	0.8462
Temkin	B	168.39
	K_T (L/mg)	1.5144
	R^2	0.9458

energy. Slope B and intercept $B \ln K_T$ were obtained from the graph of q_e vs $\ln C_e$.

3.8.4. D-R isotherm

The linear form of D-R equation (Dubinin, 1960) helps to calculate apparent energy (E) and is represented as follows:

$$\ln q_e = \ln q_m + \beta \epsilon^2 \quad (8)$$

where ϵ -Polanyi potential

$$\epsilon = RT \ln(1 + 1/C_e)$$

B - D-R isotherm constants (mol²/kJ²). The slope and intercepts are calculated from the plot of q_e versus ϵ^2 .

Apparent energy (E) is characterized by the following equation given below:

$$E = \frac{1}{\sqrt{-2\beta}}$$

The isotherm constants were calculated from the graph of the isotherm models (Figs. S2 a-d) and were given in Table 2. Among all the isotherms tested, the correlation coefficient value is higher ($R^2 > 0.9910$) for Freundlich isotherm, and the adsorption process was confirmed as multi-layered. The calculated apparent energy (E) is very small ($E = 0.9696 \text{ kJ mol}^{-1} < 8 \text{ kJ mol}^{-1}$) suggesting that the type of sorption is physical. For a chemisorption the E value should be more than 8 kJ mol^{-1} .

3.9. Kinetics studies

Kinetics of MG removal was studied in order to predict the total reaction time along with rate controlling step and reaction pathways. The adsorption kinetics of MG was verified by the pseudo first order (PFO), pseudo second order (PSO), power function equation, Elovich and Intra-particle diffusion (IPD) models.

PFO equation (Yuh-Shan, 2004) is given by Eq. (9):

$$\log(q_e - q_t) = \log(q_e) - \frac{k_1 t}{2.303} \quad (9)$$

k_1 - PFO kinetics rate constant (min⁻¹). Slope (k_1) and intercept (q_e) is calculated from the graph of $\log(q_e - q_t)$ and t .

PSO model (Ho and McKay, 1999) is given by Eq. (10):

$$\frac{t}{q_t} = \frac{1}{h} + \frac{1}{q_e} t \quad (10)$$

$$h = \frac{1}{k_2 q_e^2}$$

k_2 – PSO rate constant (g/mg min) and t -time in minute.

The values of k_2 and q_e were estimated from the slope and intercept, respectively of the plot $\frac{t}{q_t}$ versus t . The values of q_e , k_2 , and the correlation coefficient (R^2) are given in Table 3.

IPD equation (Weber Jr and Morris, 1963) is stated as Eq. (11):

$$q_t = k_{id} \sqrt{t} + c \quad (11)$$

k_{id} - rate constant of IPD (mg g⁻¹ min^{-0.5}).

C - constant.

Elovich model (Juang and Chen, 1997) is indicated by Eq. (12):

$$q_t = \frac{1}{\beta} \ln(\alpha\beta) + \frac{1}{\beta} \ln t \quad (12)$$

where α - constant of Elovich model (mg g⁻¹ min⁻¹) and β - exponent in Elovich model (g mg⁻¹).

Fractional power kinetic equation (Pandian et al., 2017) is indicated by the equation given below:

Table 3

Kinetic model parameters and their values.

Kinetic model	Parameters	Methylene Blue sorption
Pseudo first order	K_1 (min^{-1})	0.0284
	R^2	0.9698
Pseudo second order	K_2 ((g/mg)min)	0.000442
	R^2	0.9941
Intra particle diffusion	qe, cal (mg/g)	147.0588
	K_{id} ((mg/g)min ^{-0.5})	11.181
Elovich	R^2	0.9477
	α	0.0299
	β	57.3965
	R^2	0.9759
Power function	k	16.0097
	v	0.4209
	R^2	0.9384

$$\log q_t = \log k + v \log t \quad (13)$$

where v and k were calculated from graph of $\log q_t$ versus $\log t$.

The linearized plots of Eqs. (10)–(14) are presented in Fig. S3 (a–e) respectively. The values of rate constants and kinetic parameters are reported in Table 2. From the results, it is observed that the higher correlation coefficient (R^2) of the PSO model describes the kinetics of adsorption of MB on nano-composite. The results indicated that adsorption obeys chemisorption mechanism via electrostatic interaction. The values of the PSO model constants will be useful in scaling up of the process.

3.10. Adsorption mechanism

To predict the probable mechanism accompanied with the adsorption of MB onto PPy-Fe₃O₄-SW nano-composite, the physiochemical properties of MB and features of PPy-Fe₃O₄-SW nano-composite are to be clearly understood. MB is a cationic dye and presence of nitrogen and sulphur groups in MB are responsible for acquiring positive charge in aqueous solution. Point of zero charge (pH_{PZC}) of PPy-Fe₃O₄-SW nano-composite is 3.14 which is less than 7 (Sarojini et al., 2021) and it represents that acidic functional clusters are major components on the surface of the nano-composite. The nano-composite contains several surface active groups namely carboxyl and hydroxyl groups from seaweed. These combined functional groups of three components remains as adsorption active sites and are responsible for binding of MB molecules. Under alkaline condition, carboxyl groups of seaweed get deprotonated, and the anionic nature of nano-composite gets increased thereby facilitating the interaction between PPy-Fe₃O₄-SW and MB molecules. The carboxyl group present on the nano-composite, confirmed by the FTIR, interacts with sulphur molecule of MB via electrostatic interaction. The hydroxyl groups of the nano-composite could bind with nitrogen lone pair of MB through hydrogen bonding. Additionally, π - π interaction also occurs between MB and nano-composite. In addition, strong electrostatic force of attraction was found to exist between carboxylate groups of seaweed and cationic dyes. Coordination bonding was involved between lone pair hydroxyl group or amine groups and the dye. van der Waals forces of attraction was identified to exist between dye and cell wall of seaweed.

3.11. Comparison with other sorbents

The applicability of nano-composite employed for the sorptive removal of Methylene Blue was compared with the other adsorbents and were given in Table 4. The results convey that this novel nano-composite synthesized in this research has better adsorption capacity of 666.66 mg/g when compared to other adsorbents. The synthesized PPy-Fe₃O₄-SW nanocomposite has higher removal efficiency and MB dye uptake. The reason may be due to the addition of the algal functional groups to the polymer's outer surface through binding. Hence, it could be

Table 4

Comparison of adsorption capacity of MG with different adsorbents.

Adsorbent	Adsorption capacity, mg/g	References
PPy/TiO ₂	273	Li et al. (2013)
PANI hydrogel	71.2	Yan et al. (2015)
Fe ₃ O ₄ @PPy/RGO	270.3	Bai et al. (2015)
γ -Fe ₂ O ₃ /SiO ₂ (M- γ FS) nanocomposite	116.09	Chen et al. (2016)
AGDPA@AC	219.9	Naushad et al. (2019)
DA/PDA composite	88.2	Cheng et al. (2020)
PANI/GO	14.2	El-Sharkaway et al. (2020)
PANI/RGO	19.2	Gopal et al. (2020)
Fe ₂ O ₃ -PPy	464	Kara et al. (2021)
(NaIO ₄ -NC)	90.91	Bayantong et al. (2021)
CuFe ₂ O ₄ @GO	25.81	
CoFe ₂ O ₄ @GO	50.15	
NiFe ₂ O ₄ @GO	76.34	
Cu(OH) ₂ -NWs-PVA-AC	139.9	Lakkaboyana et al. (2021)
PPy-Fe ₃ O ₄ -SW	666.66	This work

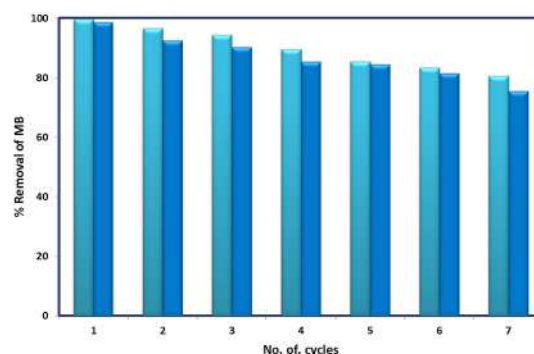
suggested that the use of this polymers based nanocomposite for the sorptive removal of dyes as an economical alternative to the other sorbents.

3.12. Adsorbent regeneration

To estimate its economic significance, the reusability of composite was investigated for five consecutive cycles. The desorption of MB was performed by washing the sorbed nano-composites using 25 mL of ethanol-water solvent mixture under room temperature with a contact time of 12 h. The results were represented in Fig. 5 and it can be seen that the maximum desorption percentage occurs in the first cycle. With an increase in the number of cycles, the percentage of sorption decreased. This decrease in sorption might be a direct result of the measure of sorbent lost during the sorption-desorption process (Jaya-kumar et al., 2021). It was also found that RE remains 90% even after four cycles which predicts good stability and activity of the composite inherited from combination of PPy and seaweed. The magnetic property of the composite promotes easier separation and reuse.

4. Conclusions

The potential of PPy-Fe₃O₄-SW as an effective adsorbent to remove MB was examined and the results were confirmed by analytical techniques like FTIR, SEM and EDS. The adsorption process was found to be endothermic in nature with chemisorption mechanism. The maximum MB removal efficiency achieved under the optimal conditions is 99.14% with a nano-composite dosage of 20 mg/L. The equilibrium experimental data are well explained by Freundlich isotherm and the isotherm constant is found to be 62.618 L/mg. MB removal by means of PPy-

**Fig. 5.** Effect of regeneration of adsorbent on removal efficiency.

Fe₃O₄-SW was governed by PSO kinetics model. The mechanism of adsorption was explored and electrostatic interaction played a major role in removal of MB molecules. Cost effectiveness, nontoxicity, higher removal efficiency and easy availability are the important features of PPy-Fe₃O₄-SW. PPy-Fe₃O₄-SW could be employed in removal of pharmaceutical pollutants in future works. The use of seaweed as one of the chief biomaterials proved to be very effective and offers a potential solution to treat dye polluted wastewater.

Declaration of competing interest

The authors declare that they have no known competing financial interests or personal relationships that could have appeared to influence the work reported in this paper.

Appendix A. Supplementary data

Supplementary data to this article can be found online at <https://doi.org/10.1016/j.envpol.2021.118376>.

Author statement

G. Sarojini: Conceptualization, Methodology, Writing – original draft preparation. **S. Venkatesh Babu:** Investigation, Writing – original draft preparation. **N. Rajamohan:** Writing-Reviewing and Editing. **M. Rajasimman:** Reviewing and Editing. **Arivalagan Pugazhendhi:** Supervision, Project administration.

References

- Afzal, M.Z., Sun, X.-F., Liu, J., Song, C., Wang, S.-G., Javed, A., 2018. Enhancement of ciprofloxacin sorption on chitosan/biochar hydrogel beads. *Sci. Total Environ.* 639, 560–569.
- Aluigi, A., Rombaldoni, F., Tonetti, C., Jannoke, L., 2014. Study of Methylene Blue adsorption on keratin nanofibrous membranes. *J. Hazard Mater.* 268, 156–165.
- Bai, L., Li, Z., Zhang, Y., Wang, T., Lu, R., Zhou, W., Gao, H., Zhang, S., 2015. Synthesis of water-dispersible graphene-modified magnetic polypyrrole nanocomposite and its ability to efficiently adsorb methylene blue from aqueous solution. *Chem. Eng. J.* 279, 757–766.
- Bayantong, A.R.B., Shih, Y.J., Ong, D.C., Abarca, R.R.M., Dong, C.D., Luna, M.D.G., 2021. Adsorptive removal of dye in wastewater by metal ferrite-enabled graphene oxide nanocomposites. *Chemosphere* 274, 129518.
- Berradi, M., Hissou, R., Khudhair, M., Assouag, M., Cherkaoui, O., El Bachiri, A., El Harfi, A., 2019. Textile finishing dyes and their impact on aquatic environs. *Heliyon* 5 e02711.
- Bhatti, H.N., Safa, Y., Yakout, S.M., Shair, O.H., Iqbal, M., Nazir, A., 2020. Efficient removal of dyes using carboxymethyl cellulose/alginate/polyvinyl alcohol/rice husk composite: adsorption/desorption, kinetics and recycling studies. *Int. J. Biol. Macromol.* 150, 861–870.
- Chen, D., Zeng, Z., Zeng, Y., Zhang, F., Wang, M., 2016. Removal of methylene blue and mechanism on magnetic γ -Fe₂O₃/SiO₂ nanocomposite from aqueous solution. *Water Resour. Ind.* 15, 1–13.
- Cheng, J., Zhan, C., Wu, J., Cui, Z., Si, J., Wang, Q., Peng, X., Turng, L.S., 2020. Highly efficient removal of methylene blue dye from an aqueous solution using cellulose acetate nanofibrous membranes modified by polydopamine. *ACS Omega* 5 (10), 5389–5400.
- Dubin, M., 1960. The potential theory of adsorption of gases and vapors for adsorbents with energetically nonuniform surfaces. *Chem. Rev.* 60, 235–241.
- El-Sharkawy, E.A., Kamel, R.M., El-Sherbiny, I.M., Gharib, S.S., 2020. Removal of methylene blue from aqueous solutions using polyaniline/graphene oxide or polyaniline/reduced graphene oxide composites. *Environ. Technol.* 41 (22), 2854–2862.
- Freundlich, H., 1906. Over the adsorption in solution. *J. Phys. Chem.* 57, 1100–1107.
- Gholivand, M.B., Yamini, Y., Dayeni, M., Seidi, S., Tahmasebi, E., 2015. Adsorptive removal of alizarin red-S and alizarin yellow GG from aqueous solutions using polypyrrole-coated magnetic nanoparticles. *J. Environ. Chem. Eng.* 3, 529–540.
- Gopal, R.A., Song, M., Yang, D., Lkhagva, T., Chandrasekaran, S., Choi, D., 2020. Synthesis of hierarchically structured γ -Fe₂O₃-PPy nanocomposite as effective adsorbent for cationic dye removal from wastewater. *Environ. Pollut.* 267, 115498.
- Gusmão, K.A.G., Gurgel, L.V.A., Melo, T.M.S., Gil, L.F., 2012. Application of succinylated sugarcane bagasse as adsorbent to remove methylene blue and gentian violet from aqueous solutions—kinetic and equilibrium studies. *Dyes Pigments* 92, 967–974.
- Ho, Y.-S., McKay, G., 1999. Pseudo-second order model for sorption processes. *Process Biochem.* 34, 451–465.
- Hynes, N.R.J., Kumar, J.S., Kamyab, H., Sujana, J.A.J., Al-Khashman, O.A., Kuslu, Y., Ene, A., Suresh, B., 2020. Modern enabling techniques and adsorbents based dye removal with sustainability concerns in textile industrial sector-A comprehensive review. *J. Clean. Prod.* 272, 122636.
- Jayakumar, V., Govindaradjane, S., Rajamohan, N., Rajasimman, M., 2021. Sustainable removal of cadmium from contaminated water using green alga – optimization, characterization and modeling studies. *Environ. Res.* 199, 111364.
- Jia, Y.-Y., Zhang, Y.-H., Xu, J., Feng, R., Zhang, M.-S., Bu, X.-H., 2015. A high-performance “sweeper” for toxic cationic herbicides: an anionic metal–organic framework with a tetrapodal cage. *Chem. Commun.* 51, 17439–17442.
- Juang, R.-S., Chen, M.-L., 1997. Application of the Elovich equation to the kinetics of metal sorption with solvent-impregnated resins. *Ind. Eng. Chem. Res.* 36, 813–820.
- Kara, H.T., Anshebo, S.T., Sabir, F.K., Workineh, G.A., 2021. Removal of methylene blue dye from wastewater using periodiated modified nanocellulose. *Int. J. Chem. Eng.* 2021, 9965452.
- Kishor, R., Purchase, D., Saratale, G.D., Saratale, R.G., Ferreira, L.F.R., Bilal, M., Chandra, R., Bhargava, R.N., 2021. Ecotoxicological and health concerns of persistent coloring pollutants of textile industry wastewater and treatment approaches for environmental safety. *J. Environ. Chem. Eng.* 9 (2), 105012.
- Lakkaboyana, S.K., Soontarapa, K., Asmel, N.K., Kumar, V., Marella, R.K., Yuzir, A., Yaacob, W.Z.W., 2021. Synthesis and characterization of Cu(OH)₂-NWs-PVA-AC Nano-composite and its use as an efficient adsorbent for removal of methylene blue. *Sci. Rep.* 11, 5686.
- Langmuir, I., 1918. The adsorption of gases on plane surfaces of glass, mica and platinum. *J. Am. Chem. Soc.* 40, 1361–1403.
- Li, J., Feng, J., Yan, W., 2013. Excellent adsorption and desorption characteristics of polypyrrole/TiO₂ composite for Methylene Blue. *Appl. Surf. Sci.* 279, 400–408.
- Naushad, M., Alqadami, A.A., Othman, Z.A.A., Alsohaimi, I.H., Algami, M.S., Aldawsari, A.M., 2019. Adsorption kinetics, isotherm and reusability studies for the removal of cationic dye from aqueous medium using arginine modified activated carbon. *J. Mol. Liq.* 293, 111442.
- Pandian, A.M.K., Gopalakrishnan, B., Rajasimman, M., Rajamohan, N., Karthikeyan, C., 2021a. Green synthesis of bio-functionalized nano-particles for the application of copper removal—characterization and modeling studies. *Environ. Res.* 197, 111140.
- Pandian, A.M.K., Karthikeyan, C., Rajasimman, M., 2017. Isotherm and kinetic studies on adsorption of malachite green using chemically synthesized silver nanoparticles. *Nanotechnol. Env. Eng.* 2, 2.
- Pandian, A.M.K., Rajasimman, M., Rajamohan, N., Varjani, S., Karthikeyan, C., 2021b. Anaerobic mixed consortium (AMC) mediated enhanced biosynthesis of silver nano particles (AgNPs) and its application for the removal of phenol. *J. Hazard Mater.* 416, 125717.
- Qian, T., Yu, C., Wu, S., Shen, J., 2013. A facile prepared polypyrrole-reduced graphene oxide composite with a crumpled surface for high performance supercapacitor electrodes. *J. Mater. Chem. A* 1, 6539–6542.
- Rajasimman, M., Babu, S.V., Rajamohan, N., 2017. Biodegradation of textile dyeing industry wastewater using modified anaerobic sequential batch reactor—Start-up, parameter optimization and performance analysis. *J. Taiwan Inst. Chem. Eng.* 72, 171–181.
- Rajeshkannan, R., Rajasimman, M., Rajamohan, N., 2010. Optimization, equilibrium and kinetics studies on sorption of Acid Blue 9 using brown marine algae *Turbinaria conoides*. *Biodegradation* 21, 713–727.
- Rajeshkannan, R., Rajasimman, M., Rajamohan, N., 2011. Sorption of acid blue 9 using *Hydrilla verticillata* biomass—optimization, equilibrium, and kinetics studies. *Bioremediat. J.* 15, 57–67.
- Sajid, M., Plotka-Wasyłka, J., 2020. Nanoparticles: synthesis, characteristics, and applications in analytical and other sciences. *Microchem. J.* 154, 104623.
- Sarojini, G., Venkateshbabu, S., Rajasimman, M., 2021. Facile synthesis and characterization of polypyrrole-iron oxide–seaweed (PPy-Fe₃O₄-SW) nanocomposite and its exploration for adsorptive removal of Pb (II) from heavy metal bearing water. *Chemosphere* 278, 130400.
- Sathian, S., Rajasimman, M., Rathnasabapathy, C., Karthikeyan, C., 2014. Performance evaluation of SBR for the treatment of dyeing wastewater by simultaneous biological and adsorption processes. *J. Water Process Eng.* 4, 82–90.
- Shanehsaz, M., Seidi, S., Ghorbani, Y., Shoja, S.M.R., Rouhani, S., 2015. Polypyrrole-coated magnetic nanoparticles as an efficient adsorbent for RB19 synthetic textile dye: removal and kinetic study. *Spectrochim. Acta A. Mol. Biomol. Spectrosc.* 149, 481–486.
- Temkin, M., 1940. Kinetics of ammonia synthesis on promoted iron catalysts. *Acta physiochim. URSS* 12, 327–356.
- Tkaczyk, A., Mitrowska, K., Posyniak, A., 2020. Synthetic organic dyes as contaminants of the aquatic environment and their implications for ecosystems: a review. *Sci. Total Environ.* 717, 137222.
- Wang, H., Yuan, X., Wu, Y., Chen, X., Leng, L., Wang, H., Li, H., Zeng, G., 2015. Facile synthesis of polypyrrole decorated reduced graphene oxide-Fe₃O₄ magnetic composites and its application for the Cr (VI) removal. *Chem. Eng. J.* 262, 597–606.
- Wang, Y., Zou, B., Gao, T., Wu, X., Lou, S., Zhou, S., 2012. Synthesis of orange-like Fe₃O₄/PPy composite microspheres and their excellent Cr (VI) ion removal properties. *J. Mater. Chem.* 22, 9034–9040.
- Weber Jr., W.J., Morris, J.C., 1963. Kinetics of adsorption on carbon from solution. *J. Sanit. Eng. Div.* 89, 31–59.
- Xie, G., Xi, P., Liu, H., Chen, F., Huang, L., Shi, Y., Hou, F., Zeng, Z., Shao, C., Wang, J., 2012. A facile chemical method to produce superparamagnetic graphene oxide-Fe₃O₄ hybrid composite and its application in the removal of dyes from aqueous solution. *J. Mater. Chem.* 22, 1033–1039.
- Yan, B., Chen, Z., Cai, L., Chen, Z., Fu, J., Xu, Q., 2015. Fabrication of polyaniline hydrogel: synthesis, characterization and adsorption of methylene blue. *Appl. Surf. Sci.* 356, 39–47.

- Yang, N., Zhu, S., Zhang, D., Xu, S., 2008. Synthesis and properties of magnetic Fe₃O₄-activated carbon nanocomposite particles for dye removal. *Mater. Lett.* 62, 645–647.
- Yuh-Shan, H., 2004. Citation review of Lagergren kinetic rate equation on adsorption reactions. *Scientometrics* 59, 171–177.
- Zafar, Z., Fatima, R., Kim, J.-O., 2021. Experimental studies on water matrix and influence of textile effluents on photocatalytic degradation of organic wastewater using Fe–TiO₂ nanotubes: towards commercial application. *Environ. Res.* 197, 111120.
- Zhao, L., Gao, M., Yue, W., Jiang, Y., Wang, Y., Ren, Y., Hu, F., 2015. Sandwich-structured graphene-Fe₃O₄@ carbon nanocomposites for high-performance lithium-ion batteries. *ACS Appl. Mater. Interfaces* 7, 9709–9715.



Adsorptive potential of iron oxide based nanocomposite for the sequestration of Congo red from aqueous solution

Gopalakrishnan Sarojini^{a,*}, Samikannu Venkatesh Babu^b, Manivasagan Rajasimman^c

^a Department of Petrochemical Engineering, SVS College of Engineering, Coimbatore, India

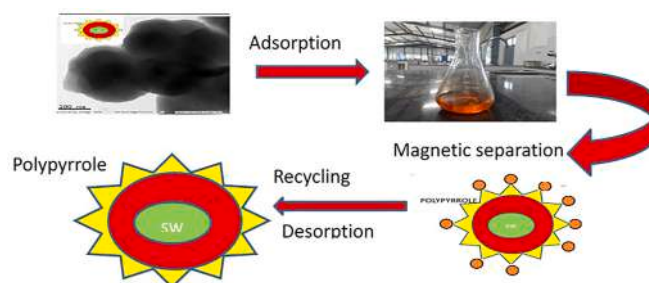
^b Department of Petroleum Engineering, JCT College of Engineering & Technology, Coimbatore, India

^c Department of Chemical Engineering, Annamalai University, Annamalai Nagar, India

HIGHLIGHTS

- Polypyrrole-Iron oxide-seaweed nanocomposite was employed for CR dye removal.
- The removal of CR by PPy-Fe₃O₄-SW was characterized using SEM - EDX, FTIR.
- A maximum dye uptake of 500 mg/g was obtained.
- Mechanism of congo red dye sorption was also proposed.
- The congo red adsorption process is a spontaneous, endothermic process.

GRAPHICAL ABSTRACT



ARTICLE INFO

Handling Editor: Derek Muir

Keywords:

Adsorption
Iron-oxide
Nanocomposite
Polypyrrole
Seaweed
Isotherm kinetics

ABSTRACT

The ability of polypyrrole-Iron oxide-seaweed nanocomposite has been tested for the removal of congo red from aqueous solution. The characteristics of nanocomposite after adsorption of Congo red (CR) have been analyzed. FTIR results authorized the involvement of various functional groups in the adsorption of CR. The change in morphology of nanocomposite was analyzed using scanning electron microscope (SEM). TEM and BET analysis were performed to characterize the nanocomposite. The effect of various parameters namely pH, adsorbent dosage, initial dye concentration, adsorption time and temperature are studied. The optimum condition for the effective removal of CR are: pH-3, initial CR concentration- 40 mg/L, nanocomposite dosage- 20 mg, contact time-40 min and temperature-40°C. Adsorption isotherm studies and kinetic studies were done. Langmuir isotherm fits with the experimental data very well with high coefficient of determination ($R^2 = 0.98$) and maximum dye uptake of 500 mg/g is reported. In kinetic studies, pseudo second order model was obeyed ($R^2 = 0.994$). Thermodynamic properties were determined and found that the nature of process is spontaneous, endothermic and increased in randomness. The mechanism of sorption was proposed. Desorption studies were carried out and showed that the nanocomposite could be effectively reused up to five cycles. Thus the outcomes proved that the polypyrrole-iron oxide-seaweed nanocomposite to be an operative, recyclable and low-cost adsorbent for the treatment of dye bearing water.

* Corresponding author.

E-mail address: grsarojini@gmail.com (G. Sarojini).

<https://doi.org/10.1016/j.chemosphere.2021.132371>

Received 21 April 2021; Received in revised form 8 September 2021; Accepted 24 September 2021

Available online 28 September 2021

0045-6535/© 2021 Elsevier Ltd. All rights reserved.

1. Introduction

Dyes are coloured organic compounds widely used in plastics, paper, ink, cosmetics, food industry and textile industries for coloring. These industries releases coloured discharge to the environment and creates water pollution. Presence of chromophore and auxochromes in dye are in authority for coloring. Functional groups and molecular structure arrangement of dyes imparts high stability and so degradability is difficult (Kishor et al., 2021). Moreover dyes present in discharge reduce the photosynthetic activity thereby affecting the aquatic planktons (Nekouei et al., 2015). Few dyes at very low concentration (<1 ppm) cause a serious threat on water bodies (Dogan et al., 2007). Inhalation of some dyes causes mutation, lung, skin disorder and cancer. Therefore removal of dyes in water bodies is essential and effluent from various industries must undergo treatment prior to their discharge to the aquatic environment.

Congo red is an anionic dye. The solubility of CR in aqueous media is high. This dye is mostly applied in paper, textile and leather industries. CR is highly harmful and causes skin and eyes irritation, gastrointestinal irritation and induces clotting of blood. During metabolism it gets converted into a carcinogen named benzidine. This dye was selected for the present dye owing to its harmfulness, high persistence in the aquatic environment and the amputation is very essential.

Numerous techniques namely adsorption, flocculation, filtration, coagulation and photo-oxidation are followed by researchers to remove dyes (Bhatti et al., 2020; Guo et al., 2019; Yun et al., 2020; Do Vale-Júnior et al., 2018; Mais et al., 2020). But all these methods are expensive. Recent research was concentrated on the elimination of dyes by means of photocatalysis involving UV- radiation and quantum dots (Rajabi et al., 2013; Shamsipur and Rajabi, 2014). But those methods require huge investment and operating cost is also high. Amongst all adsorption is found to simple, flexible, economical and high efficient process and can be effectively applied in large scale industrial treatment for high concentration of dyes (Pandian et al., 2021a). Activated carbon remains as a best sorbent in removal of dyes in adsorption process. But activated carbon faces suffers several limitations such as low sorption capacity, difficult to regenerate, high capital investment and less reactivity (Pandian et al., 2021b; Sarojini et al., 2021b). Sorbent with excellent adsorption ability and regeneration capacity has to be developed. Therefore choosing a suitable sorbent is a main task in adsorption process.

Polypyrrole (PPy), an emerging sorbent has gained high interest in adsorption because of its remarkable characteristics of redox properties, biocompatibility, good stability, easy synthesis and excellent electrical conductivity. Nevertheless PPy can also be easily prepared through chemical oxidation method using FeCl_3 as oxidizing agent. PPy is preferred mainly in the removable of different heavy metals namely Cu (II) (Lin et al., 2012), Pb(II) (Choi and Jang, 2008), Cr(VI) (Tian and Yang, 2007), Hg(II) (Chandra and Kim, 2011). The excellent sorption property is accompanied by nitrogen atoms in the PPy molecular chain (Rodriguez et al., 2000). However the amputation tendency of PPy towards heavy metals depends on the diffusion of dopant anions from the polypyrrole and removal mechanism usually occurs through ion exchange of doped anions. Nevertheless the diffusion and exchange of doped anions from the surface of PPy is difficult. Also pure PPy show low adsorption capacity (Zhang et al., 2006; Pei and Qian, 1991; Zhang and Bai, 2003; Karthikeyan et al., 2009). To provide proper solution to this difficulty and to increase the sorption capacity, exploration has been performed by combining PPy components with additional materials such as cellulose (Lei et al., 2012), carbon nanotubes (Maity and Ray, 2010), graphene oxide (Gu et al., 2010), magnetic iron oxide (Bhaumik et al., 2011), etc to prepare polypyrrole based composites. Fe_3O_4 nanoparticles are green sorbents and find its application in the removal of variety of dyes (Saha et al., 2011). As pure Fe_3O_4 nanoparticles tends to agglomerate in aqueous solution and it is recommended to combine with other conducting materials (Li et al., 2011). Further combination of

PPy with magnetic Fe_3O_4 nanoparticles eliminate the steps of purification such as centrifugation/filtration.

Apart from removing heavy metals, polypyrrole based composite has the potential to remove organic dyes also. But only few researches have been made in the removal of dyes using polypyrrole based sorbents. Ma et al. (2018) synthesized Polydopamine-assisted deposition of polypyrrole on electrospun poly(vinylidene fluoride) nanofibres and explored the removal efficacy towards methylene dye and congo red. Li et al. (2013) synthesized polypyrrole/ TiO_2 composite and examined its adsorptive behavior towards methylene blue. Feng et al. (2014) synthesized PPy with a hierarchical structure and studied its sorptive ability using acid red G. Xin et al. (2015) prepared and also studied the adsorptive behavior of PPy nanofibres towards methylene orange. Ghoviland et al. (2015) synthesized polypyrrole-coated Fe_3O_4 nanoparticles and studied its sportive behavior towards anionic alizarin red-S and alizarin yellow GG dye.

Chafai et al. (2017) carried out the research on comparing the adsorptive capabilities of Polyaniline (PANI) and PPy towards CR dye. Li et al. (2017) synthesized PPy/CNTs- CoFe_2O_4 composite and investigated its sorption ability towards Acid Fuchsin, methyl orange and methylene blue. Currently research has been focused on the coating of polymers on bioadsorbent to improve its selectivity towards contaminant because limited functional groups are present in polypyrrole and hence to enhance its adsorptive ability, additional functional group of amine, hydroxyl and sulphonic groups should be introduced to form polypyrrole based composites (Zhou et al., 2017).

Polypyrrole (PPy) - Iron oxide (Fe_3O_4) - seaweed (SW) nanocomposite has been synthesized by combining polypyrrole along with magnetic Fe_3O_4 and seaweed. Seaweed, a marine algae contains large number of active functional groups namely carboxyl, bioactive amines, hydroxyl and sulfates groups (Donmez et al., 1999). Combination of PPy, Fe_3O_4 and seaweed can extensively increase the adsorptive capacity. PPy- Fe_3O_4 -SW nanocomposite was prepared through in-situ polymerization process. Here seaweed along with iron-oxide acts as stabilizers. Therefore the combination of polymer along with carbon-based and mineral ingredients would definitely boost the adsorptive features of the sorbent. Also Fe_3O_4 provides easier separation of CR from aqueous medium. In this work, a novel PPy- Fe_3O_4 -SW nanocomposite was formulated using polypyrrole, Fe_3O_4 and seaweed in order to have the advantages of all the three components in the removal of pollutants. Until now no study has been done in the usage of PPy- Fe_3O_4 -SW as a sorbent for the removal of CR dye. Here in this report attempt was made to investigate the adsorptive tendency of PPy- Fe_3O_4 -SW towards the removal of CR from aqueous solution. The effect of several effective factors namely pH, sorbent dosage, initial CR concentration, adsorption time and temperature were studied. Equilibrium isotherm studies and uptake of CR kinetic were performed to explore the adsorptive capacity of the composite.

2. Experimental

2.1. Chemicals required

Ferric chloride, Ferrous sulphate, Sodium Hydroxide (NaOH), Iron chloride, acetone, HCl and $\text{C}_{32}\text{H}_{22}\text{N}_6\text{Na}_2\text{O}_6\text{S}_2$ obtained from Fisher Scientific. Pyrrole ($\text{C}_4\text{H}_5\text{N}$) was obtained from Sigma – Aldrich. Thermogravimetric analyzer (TGA) and differential scanning calorimetry (DSC) (SDT Q600 model TA Instruments, USA) is used to evaluate the thermal strength of nanocomposite. The surface area, average pore diameter and pore volume are found using Brunauer Emmett and Teller (BET) method (Micromeritics ASAP 2020, USA). The characterization studies on CR loaded Polypyrrole-iron oxide-seaweed nanocomposite have been made using FTIR, SEM. FTIR (SHIMADZU) spectrum is performed to categorize the functionalities of the adsorbent. The surface organization of nanocomposite (before and post sorption) was examined by means of SEM (HITACHI SU 6600 Japan). UV–Vis spectra of the

materials were obtained using UV–Vis spectrometer (SYSTRONICS, India).

2.2. Synthesis of PPy-Fe₃O₄-SW

The nanocomposite used in this study was synthesized and characterized in our earlier study (Sarojini et al., 2021a, 2021b). Nanocomposite was synthesized by adding 0.5 g Fe₃O₄ to 80 mL distilled water following ultrasonication. Then six grams of ferric chloride were added as oxidant following magnetic stirring. To the entire solution, 0.8 mL of pyrrole was poured to initiate polymerization reaction and sonicated for 30 min. When the look of black colour was found acetone was added to stop the polymerization reaction. Then Fe₃O₄-seaweed composite was added and sonicated for 30 min. The obtained precipitate was filtered, washed many times with distilled water and acetone followed by drying in oven. The schematic route for the synthesis of PPy-Fe₃O₄-SW followed by its congo red dye adsorption in reaction scheme (Fig. 1).

2.3. Preparation of Congo red stock solution

About 1 g of analytic grade C₃₂H₂₂N₆Na₂O₆S₂ was dissolved in distilled water to produce 1000 ppm of stock solution. The required concentration working solution was prepared by diluting the stock solution (Wanyonyi et al., 2014).

2.4. Batch experiments

The sorption trials were accomplished in batch method. Tests were conducted in a conical flask (250 mL) holding 50 mL CR solution. Effect of pH (2–11), adsorbent dosage (20–100 mg), initial CR concentration (10–100 mg/L), contact time (10–120 min) and temperature (298–318 K) were analyzed. The initial solution pH was varied using 1 M HCl or 1

M NaCl. CR concentrations were measured using UV–vis spectrophotometer at maximum adsorptive wavelength of 497 nm.

The amount of CR adsorbed per mass under equilibrium q_t (mg/g) and CR removal efficiency (% RE) were obtained from equations given below:

$$q_t = \frac{C_o - C_t}{m} * v \quad (1)$$

$$\text{Percentage removal, \%} = \frac{C_o - C_t}{C_o} * 100 \quad (2)$$

where C_o and C_t – initial CR concentration and equilibrium CR concentration (mg/L), v is volume (L) and m is mass of nanocomposite (sorbent) in grams.

2.5. Desorption experiments

CR sorbed nanocomposites was washed with 25 mL of 0.1 mol/L of sodium hydroxide solution under room temperature and allowed to stay for 12 h. Then the rectified sorbent was again washed away using distilled water and dried. Then it was reused in next cycle.

Desorption efficiencies were calculated as:

$$\text{Desorption efficiency} = \frac{\text{Amount of CR dye desorbed}}{\text{Amount of CR dye adsorbed}} * 100 \quad (3)$$

3. Results and discussion

3.1. Influence of solution pH

pH remains as a significant factor in CR removal as it has a tendency to alter the surface charge of the composite, interaction between sorbate and sorbent, adsorbed surface features and degree of ionization. The consequence of solution pH was examined and results are presented in

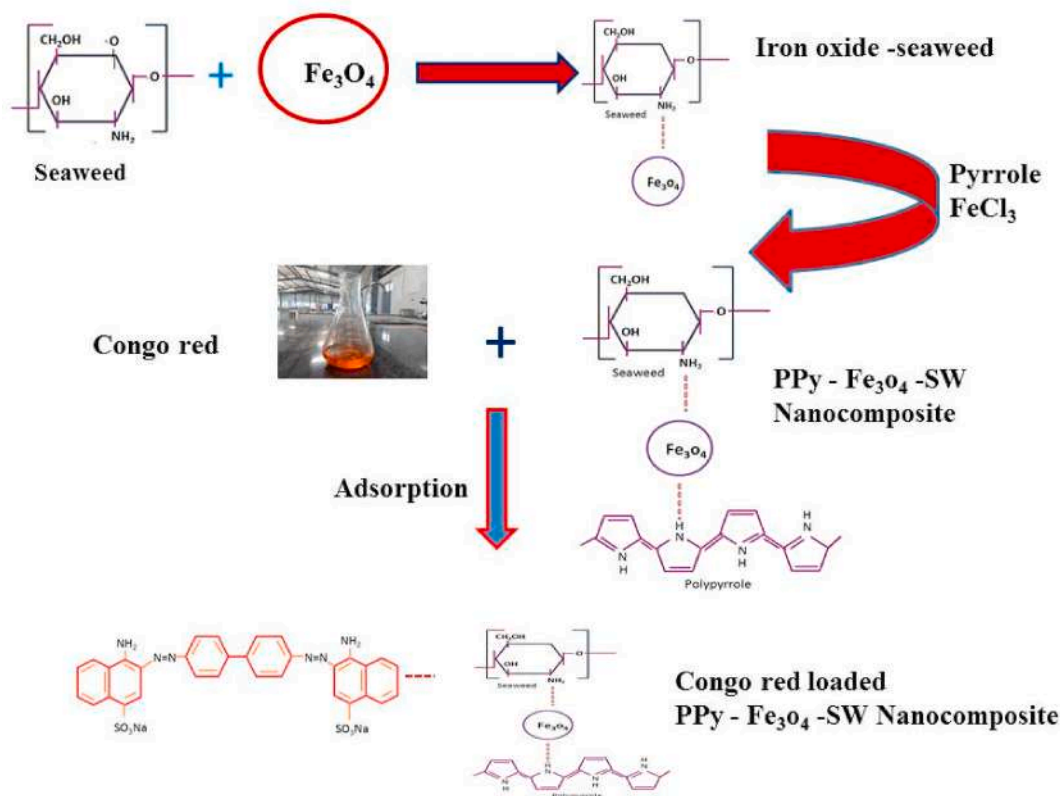


Fig. 1. Scheme of adsorption of CR on PPy - Fe₃O₄- SW.

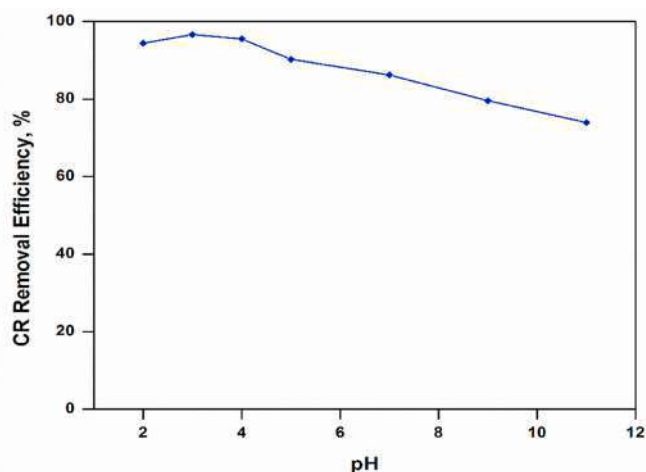


Fig. 2. Influence of pH on CR removal.

Fig. 2. The pH of the solution was varied in the series of 2–11 and the highest RE was achieved at pH 3. At lower pH, surface of the composite turn into positively charged surface due to the presence of excess of H^+ ions. Meanwhile at lower pH the sulphonated group present in CR dissociates in aqueous solution and produces anions. So there is higher affinity between positively charged nanocomposite and negatively charged CR dye. Further it was observed that RE decreases as solution pH increases because of the competition of OH^- ions with SO_3^- ions of CR and availability of less protonated ions composite surface. Moreover under alkaline conditions there was an electrostatic repulsion between nanocomposite and CR, as the composite surface turned to negatively charged surface because of deprotonation and therefore decrease in % RE was found. The adsorption behavior of dye could be easily accessed by means of point of zero charge (pH_{ZPC}). pH_{ZPC} was an important parameter that designates the kinetic characteristics of surface. Usually $pH > pH_{ZPC}$ promotes for sorption of cations and $pH < pH_{ZPC}$ promotes for anions (Zhou et al., 2019). pH_{ZPC} of the composite was found to be 3.14. Below pH_{ZPC} the composite surface becomes positively charged because of protonation of functional groups and above pH_{ZPC} the surface turned to negatively charged. Therefore maximum dye sorption was found to occur at pH 3 ($pH < pH_{ZPC}$). Similar result was obtained for the removal of CR using poly (acrylamide)-grafted-guar gum/silica nanocomposite (Pal et al., 2015).

3.2. Influence of sorbent dosage

The amount of sorbent dosage is an essential parameter to be decided in adsorption process as adsorption depends on surface area and availability of active sites on the sorbent surface. The effect of PPy- Fe_3O_4 -SW on % RE of CR is shown in Fig. 3. It was found that initially % RE increases as dosage amount increases owing to ready availability of large binding sites. In this study, maximum removal was achieved at low dosage. This result confirms the availability of sites at low dosage itself. Further increase in dosage does not produce any change in % RE. Similar behavior was found for adsorption of anionic dyes on wet terrified microalgal biochar (Yu et al., 2021). This effect is due to the availability of excess active sites at higher sorbent dosage than saturated limit. However available CR particles were inadequate to accommodate the entire sites available on composite surface.

3.3. Influence of initial dye concentration

The influence of initial dye concentration on % RE was determined by changing CR concentration from 20 mg/L to 100 mg/L. From the Fig. 4 it was observed that % RE rises gradually as CR concentration

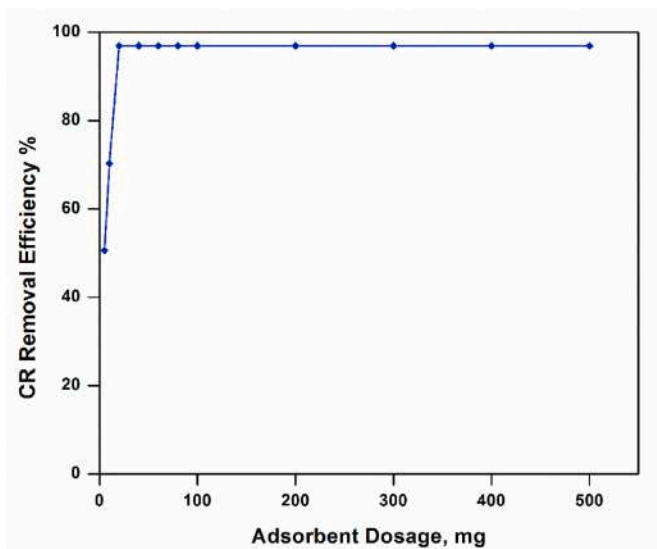


Fig. 3. Influence of sorbent dosage on Pb removal.

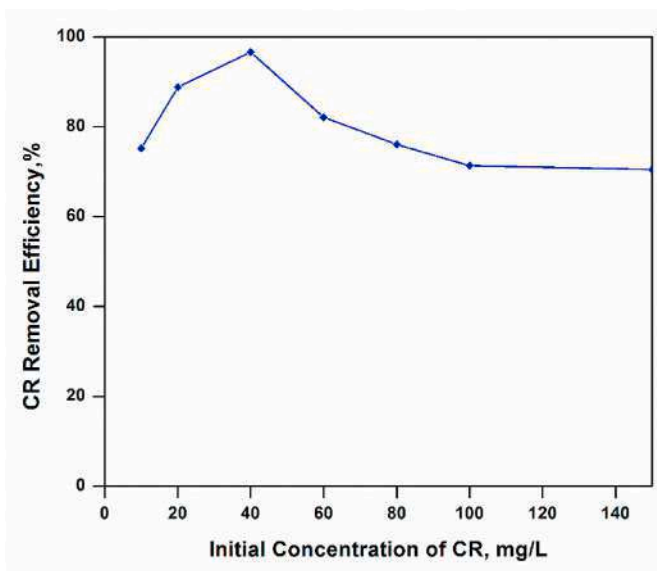


Fig. 4. Influence of initial CR concentration on CR removal.

increases thereby reaching a maximum due to the entrapment of more dye molecule as more active sites are available. Low concentration provides less diffusion resistance which facilitates easy migration of dye molecules from the solution. The optimum initial concentration was chosen as 40 mg/L. On further increase in dye concentration the decrease trend was found because at higher concentration the active sites gets saturated and repulsion occurs between adsorbed dye molecule and unadsorbed dye (Zhou et al., 2019).

3.4. Influence of contact time

Contact time is a central factor that determines the time requirement for attainment of equilibrium. From Fig. 5, it was observed that the CR intake remains fast during the beginning stage owing to the availability of sufficient amount of vacant stages at beginning. The equilibrium contact time was fixed for 40 min. In next stage there was no change in % RE because amount of dye adsorbed remains unchanged due to the saturation of active sites on the composite surface.

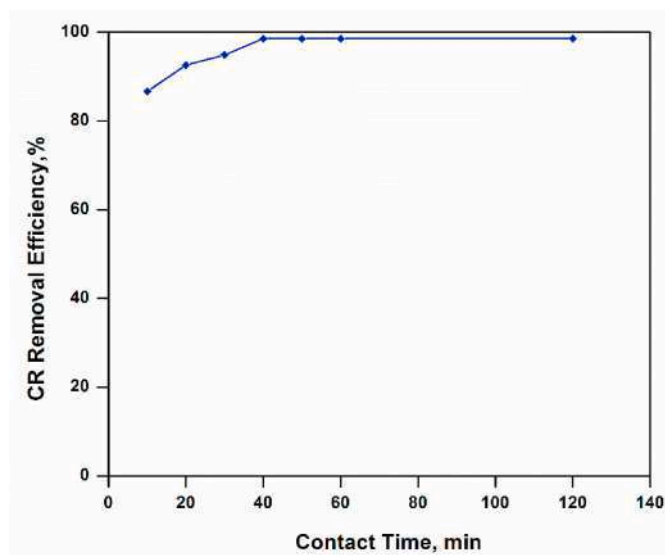


Fig. 5. Influence of contact time on CR removal.

3.5. Influence of temperature

The influence of temperature on RE of CR onto PPy-Fe₃O₄-SW nanocomposite was investigated in the range of 298–323 K. From the Fig. 6 it was witnessed that RE increases with rise in temperature. This might have occurred as a result of decrease in viscosity of sorbate solution and increased diffusion rate of CR molecules. The results suggest that process is endothermic and high temperature is favourable for adsorption of CR.

3.6. Adsorption thermodynamics

To examine the feasibility, spontaneity and nature of interaction, thermodynamic parameters namely ΔH° , ΔS° and ΔG° are to be determined. The thermodynamic properties are determined by the equations given below:

$$\Delta G^\circ = -RT \ln k \quad (4)$$

$$\Delta G^\circ = \Delta H^\circ - T\Delta S^\circ \quad (5)$$

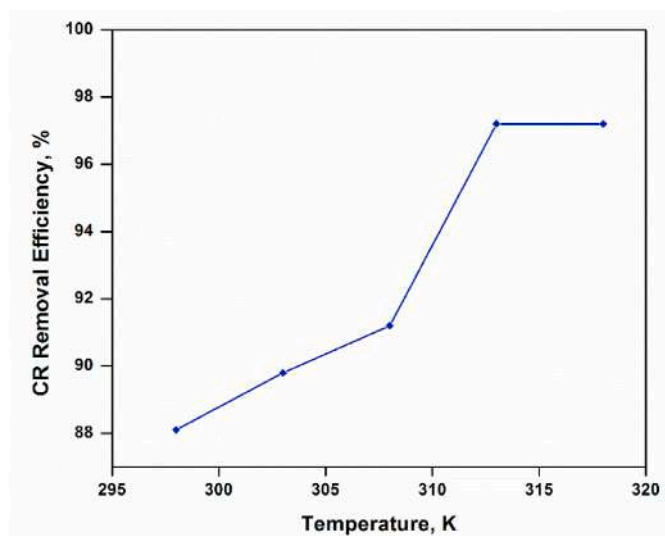


Fig. 6. Influence of temperature on CR removal efficiency.

k - equilibrium constant ($k = q_e/C_e$).

R - Universal gas constant (8.314 J/mol K).

T - temperature (K).

ΔH° - enthalpy change (kJ/mol).

ΔS° - entropy change (kJ/mol K).

ΔG° - Gibbs free energy (kJ/mol).

The values of ΔH° and ΔS° were found from the graph of ΔG° versus T (Supplementary file: Fig. S1) and the thermodynamic parameters values are provided in Table 1. The positive values of ΔS° shown the disorder and increase in randomness at solid/liquid solution interface (Gupta and Rastogi, 2008; Jayakumar et al., 2015, 2019). The positive value of ΔH° suggests that the adsorption is an endothermic process. The higher values of ΔH° further specify that the sorption process is chemical. The negative values of ΔG° conveyed the feasibility of process and nature to be spontaneous. From the Fig. S1, it was observed ΔG° values decreases as temperature increases representing that sorption process was highly favourable at increased temperature.

3.7. Characterization

The N₂ isothermal adsorption-desorption method was employed to study the textural properties. The surface area of the nanocomposite was measured using BET analysis and found to be 70.56 m²/g. The pore volume and pore size are found to be 19.66 cm³/g (STP) and 8.36 nm respectively. The isotherm profile displayed a Type II isotherm (Fig. 7) indicating a complete monolayer coverage. The *in-situ* polymerization of pyrrole has enhanced the surface area. The higher surface area of nanocomposite could enhance adsorption ability and also favours for removal of dyes in waste water.

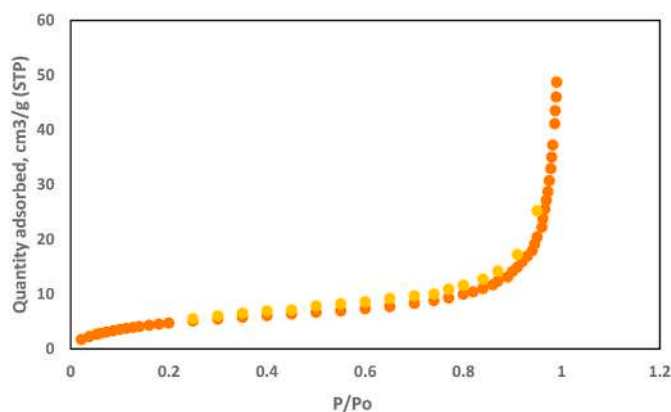
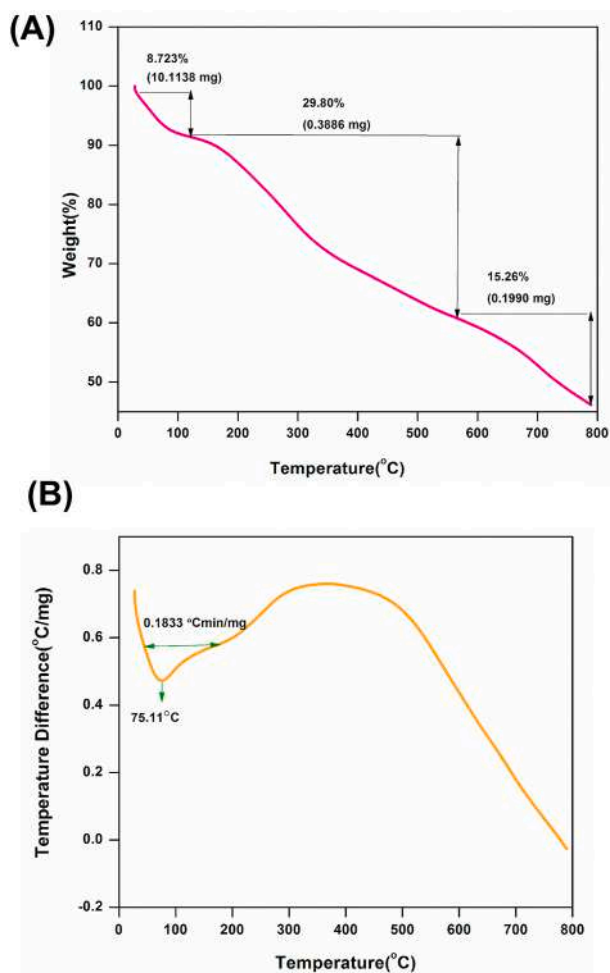
The nanocomposite thermal stability behaviour was represented using TGA plots (Fig. 8(a)). TGA plots shows that with increase in temperature the weight loss occur in three different stages. The results of the thermal plots showed that the primary weight losses occurred owing to loss of water molecules attached to nanocomposite surface (Karimzadeh et al., 2017). The primary weight loss (8.732%) had occurred up to 150°C (Ballav et al., 2014). The second weight loss of 29.80% has happened in the range of 150–500°C. This loss has occurred because of degradation of polymeric ingredients present in nanocomposite (Das et al., 2016). Degradation of polymers was due to the breakage of bond affinity between PPy and doped chlorine ions in the polymers (Saleh et al., 2016). Above 500°C third stage of weight loss occurred due to decomposition of organic matter. The total weight loss is 53.86% was found and could be concluded that the nanocomposite had a higher thermal stability (Shahnaz et al., 2020). Therefore thermal results suggests that nanocomposite could be used effectively for real field of water purification in an air atmosphere up to temperature of 200°C.

DSC analysis of nanocomposite (Fig. 8(b)) was carried out under N₂ atmosphere (30 - 800°C) with heating rate of 20° C min⁻¹. The endothermic peak was observed at 75.11° C which corresponds to the glass transition temperature of FeCl₃ used as dopant during synthesis of nanocomposite.

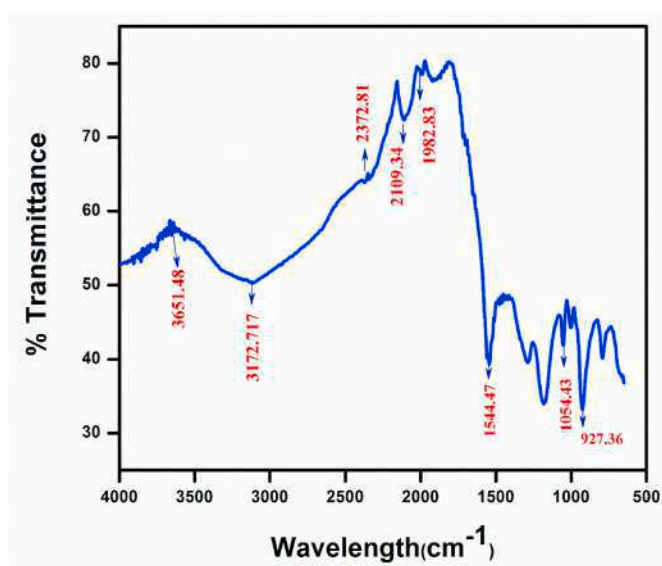
FTIR is a vital instrument used to pinpoint the functional groups present. FTIR results of Congo red loaded PPy-Fe₃O₄-SW nanocomposite was shown in Fig. 9. The characteristic peak at 3328.386 cm⁻¹ corresponds to hydroxyl group. Characteristic peaks observed in raw

Table 1
Thermodynamic parameters and their values.

Temp(K)	ΔG° (kJ/mol)	ΔS° (kJ/mol k)	ΔH° (kJ/mol)
303	-7.2301	0.1863	48.394
308	-7.7879		
313	-8.934		
318	-9.6151		
323	-11.801		
328	-11.986		
333	-12.172		

Fig. 7. N₂ sorption – desorption of Nanocomposite.Fig. 8. a TGA plot of PPY - Fe₃O₄-SW, b DSC thermogram of PPY - Fe₃O₄- SW.

nanocomposite were also present in CR loaded composite with some shift. A shift in band from 3328.386 cm⁻¹ to 3314.641 cm⁻¹ was observed which indicates that adsorption has occurred. This shift indicates that the involvement of hydroxyl group on the nanocomposite in adsorption and this hydroxyl group is derived from seaweed. These groups are capable of providing active sorption sites and also reacts with CR. Fig. 9 also shows the presence of characteristic peaks of polypyrrole at 1544 cm⁻¹, 1054 cm⁻¹ and 927 cm⁻¹ which attributes to polypyrrole stretching, conjugated C–N stretching, C–H stretching vibration and C–H deformation (Bhaumik et al., 2013). The shift of peaks (1544.474 cm⁻¹

Fig. 9. FTIR of CR loaded PPY - Fe₃O₄-SW.

to 1544.142 cm⁻¹, 1052.279 cm⁻¹ to 1054.279 cm⁻¹, 932.882 cm⁻¹ to 927.363 cm⁻¹) also indicated the participation of groups in binding of dyes. Thus the result confirmed the involvement of various functional groups on the sorption process and shows that the sorption was mainly by means of chemisorption.

Fig. 10(a) represents the SEM image of PPY-Fe₃O₄-SW before adsorption of CR having particles of spherical shape with smooth and uniform surface (Mollahosseini et al., 2019). This may occurred as a result of dense coating of PPY. Fig. 10(b) represents the nanocomposite morphology after the adsorption of CR. There was change in morphology which indicates the adsorption of dye on the nanocomposite surface. Shinning sites suggests that the CR adsorption has occurred. Also it is noticeable the particles are more agglomerated which indicates the binding of CR on nanocomposite surface.

TEM images shown in Fig. 10(c) and (d) represents inner morphology of nanocomposite. It was observed that PPY particles are light and located in the outer shell while iron oxide-seaweed being darker in colour is present in central part of the nanocomposite forming a core-shell structure. The results are same in accordance with the results obtained for TEM image of PPY-Fe₃O₄ composite (Sarojini et al., 2021a). These results confirm the encapsulation of PPY onto Fe₃O₄. Also it was noticed that there was no aggregation of Fe₃O₄ as PPY inhibits the formation of aggregate.

The energy dispersive X-ray spectroscopy (EDS) spectra of the bare nanocomposite and CR loaded composite is shown in Fig. 10 (e) and 10 (f) respectively. Existence of C, O, N and Fe represents the origins of three components namely polypyrrole, iron oxide and seaweed. Cl arises from FeCl₃ added as an oxidant during polymerization. The presence of Na and S point out the adsorption of CR (C₃₂H₂₂N₆Na₂O₆S₂). Thus the EDS spectra established the CR sorption.

Fig. 11 represents UV-Vis spectra of individual materials and nano-composite. UV-Vis spectra of PPY exhibits two absorption peaks at 290 nm and 470 nm. The peak at 290 nm is associated to the π-π* transition of aromatic benzene rings and other peak at 470 nm is correlated to polar ionic transition (Choudhary et al., 2014). The absorption peaks changes according with change in availability of delocalized electrons which highly depends on the chain length of polypyrrole. UV-Vis spectra of Fe₃O₄ shows the absorption band at 350 nm representative for Fe₃O₄ (Dash et al., 2018). PPY-Fe₃O₄-SW nanocomposite shows a peak around 390 nm which is in between the characteristic absorption peak of both Fe₃O₄ and PPY. This peak is assigned to the interaction between Fe₃O₄ and quinoid ring of PPY (Zhang et al., 2016). Also it is clearly

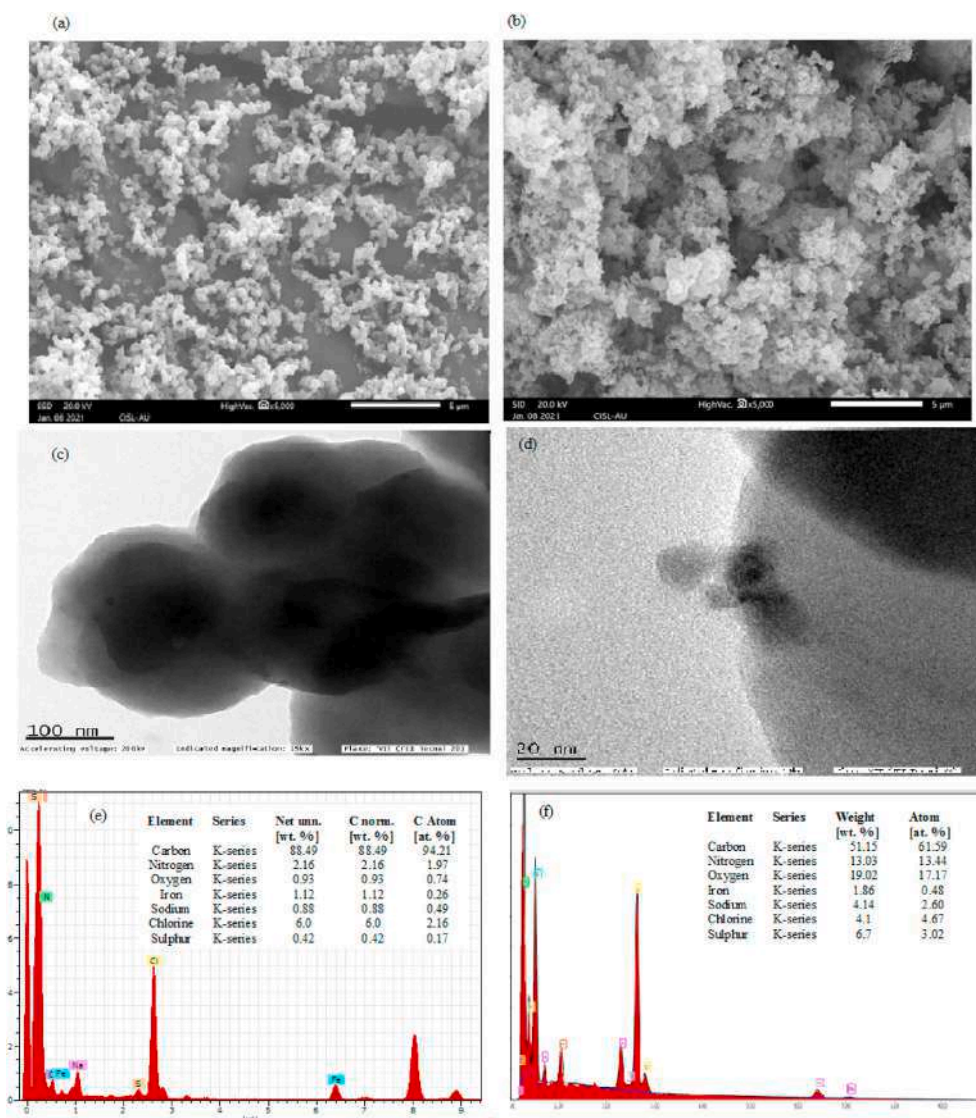


Fig. 10. SEM images of PPY - Fe₃O₄- SW (a) before adsorption, (b) after adsorption, (c) TEM image of PPY - Fe₃O₄- SW (d) HR- TEM image of PPY - Fe₃O₄- SW. EDS elemental pattern of PPY - Fe₃O₄- SW (e) before adsorption, (f) after adsorption.

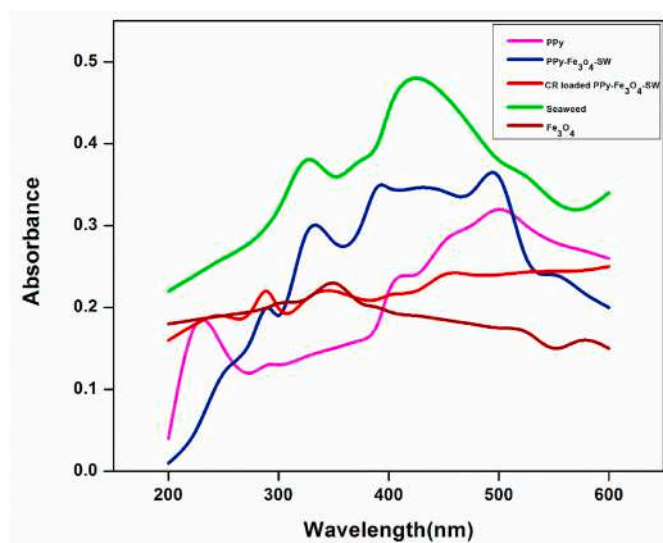


Fig. 11. UV-Vis absorption spectrum.

understood that presence of Fe₃O₄ and coating of PPY causes a shift in absorption band. UV-Vis spectra of CR loaded nanocomposite shows two weak absorption peak at 336 and 498 nm indicating the presence of CR on the nanocomposite which confirms the adsorption.

3.8. Equilibrium sorption isotherm studies

Isotherm studies were performed to realize the interaction between adsorbed molecule and sorbent surface. Interaction between sorbate and sorbent is analyzed using Langmuir isotherm, Freundlich isotherm, Temkin isotherm, Dubinin-Radushkevich (D-R) isotherm.

3.8.1. Langmuir isotherm

The Langmuir equation (Langmuir, 1918) applies for monolayer sorption processes and is characterized by the resulting equation:

$$\frac{1}{q_e} = \frac{1}{q_m b C_e} + \frac{1}{q_m} \quad (6)$$

C_e – equilibrium dye concentration (mg/l); q_m – Langmuir maximum adsorbing capacity (mg/g); b – Langmuir sorption constant representing the attraction of binding sites (L/mg). The constants were evaluated from the Fig.S2a (Supplementary file).

3.8.2. Freundlich isotherm

Freundlich isotherm (Freundlich, 1906) designates to multilayer process and the linear form of Freundlich model is given below:

$$\log_{10} q_e = \log_{10} K_f + \frac{1}{n} \log_{10} C_e \quad (7)$$

K_f (mg/g) represents Freundlich constant; n - adsorption intensity. Slope K_f and intercept $1/n$ were calculated from the graph of $\log_{10} q_e$ vs $\log_{10} C_e$ (Fig. S2b). For enhanced adsorption studies the value of $1/n$ should be between 0 & 1.

3.8.3. Temkin isotherm

The linear form of Temkin equation (Temkin and Pyzhev, 1940) is specified by:

$$q_e = B \ln K_T + B \ln C_e \quad (8)$$

B (J/mol) denotes Temkin constant and K_T (L/g) represent binding energy. Slope B and intercept $B \ln K_T$ were obtained from the graph of q_e vs $\ln C_e$ (Fig. S2c).

3.8.4. D-R isotherm

The linear form of D-R equation (Dubinin, 1960) helps to calculate apparent energy (E) and is represented as follows:

$$\ln q_e = \ln q_m - \beta \varepsilon^2 \quad (9)$$

where ε - Polanyi potential

$$\varepsilon = RT \ln(1 + 1/C_e)$$

B - D-R isotherm constants (mol^2/kJ^2). The slope and intercepts are calculated from the plot of q_e versus ε^2 (Fig. S2d).

Apparent energy (E) is characterized by the following equation given below:

$$E = \frac{1}{\sqrt{-2\beta}}$$

The isotherm constants were calculated from the graph of the isotherm models (Figs. S2 a-d) and were given in Table 2. Correlation coefficient value is higher for Langmuir isotherm proposing the adsorption process was single layer. The calculated apparent energy E is very small ($E = 0.853 \text{ kJ mol}^{-1} < 8 \text{ kJ mol}^{-1}$) suggests that the type of sorption is physical. As value of R^2 of D-R model is less, it does not fit the experimental values. Comparatively speaking, Langmuir isotherm fits the CR adsorption well when compared to all other isotherms based on R^2 (see Table 3).

3.9. Kinetics studies

Kinetic of CR were performed in order to predict the total reaction time along with rate controlling step and reaction pathways. The

Table 2
Equilibrium isotherm parameters and their values.

Isotherm model	Parameters	Value
Langmuir	q_m (mg/g)	500
	K_L (L/mg)	0.0465
	R^2	0.98
Freundlich	K_f (L/mg)	4.22
	$1/n$	0.633
	R^2	0.906
Dubinin- Redushkevich	q_m (mg/g)	133
	β (mol^2/kJ^2)	0.687
	E (kJ/mol)	0.853
	R^2	0.85
Temkin	B	116.2
	K_T (L/mg)	1.151
	R^2	0.956

Table 3

Kinetic model parameters and their values.

Kinetic model	Parameters	Values
Pseudo first order	$K_1(\text{min}^{-1})$	0.026
	R^2	0.963
Pseudo second order	$K_2((\text{g/mg})\text{min})$	0.000275
	R^2	0.994
Intra particle diffusion	$q_{e,\text{cal}}$ (mg/g)	142.86
	$K_{id}((\text{mg/g})\text{min}^{-0.5})$	12.560
	R^2	0.961
Elovich	α	0.034
	β	74.845
	R^2	0.992
Power function	k	10.339
	v	0.559
	R^2	0.962

adsorption kinetics of CR was explored by the pseudo first order (PFO), pseudo second order (PSO), power function equation, Elovich and Intra-particle diffusion (IPD).

PFO equation (Ho, 2004) is given by:

$$\log(q_e - q_t) = \log(q_e) - \frac{k_1 t}{2.303} \quad (10)$$

k_1 - PFO kinetics rate constant (min^{-1}). Slope (k_1) and intercept (q_e) is calculated from the graph of $\log(q_e - q_t)$ and t (Fig. S3a).

PSO model (Ho and McKay, 1999) was indicated as given below:

$$\frac{t}{q_t} = \frac{1}{h} + \frac{1}{q_e} t \quad (11)$$

$$h = \frac{1}{k_2 q_e^2}$$

k_2 - PSO rate constant (g/mg min) and
t-time in minute.

IPD equation (Weber and Morris, 1963) is stated as follows:

$$q_t = k_{id} \sqrt{t} + C \quad (12)$$

k_{id} - rate constant of IPD ($\text{mg g}^{-1} \text{min}^{-0.5}$).
C - constant.

Elovich model (Juang and Chen, 1997) is indicated by the equation below:

$$q_t = \frac{1}{\beta} \ln(\alpha\beta) + \frac{1}{\beta} \ln t \quad (13)$$

where α - constant of Elovich model ($\text{mg g}^{-1} \text{min}^{-1}$) and β - exponent in Elovich model (g mg^{-1}).

Fractional power kinetic equation (Pandian et al., 2017) is indicated by the equation given below:

$$\log q_t = \log k + v \log t \quad (14)$$

where v and k were calculated from graph of $\log q_t$ versus $\log t$.

The linearized plots of Eqs. (10)–(14) are offered in Figs. S3(a-e) respectively. The values of rate constants and kinetic parameters are reported in Table 2. From the results, it is observed that the higher correlation coefficient (R^2) of the PSO model describes the kinetics of adsorption of CR on nanocomposite. The results indication that adsorption obeys chemisorption mechanism via electrostatic interaction.

3.10. Role of Fe_3O_4 in adsorption process

Fig. 12 represents the comparison of adsorption efficiency of nanocomposite with its pure components. It was observed that CR adsorption efficiency of polypyrrole was 3 times lower than that of nanocomposite whereas seaweed provided only 29.56% removal efficiency. These

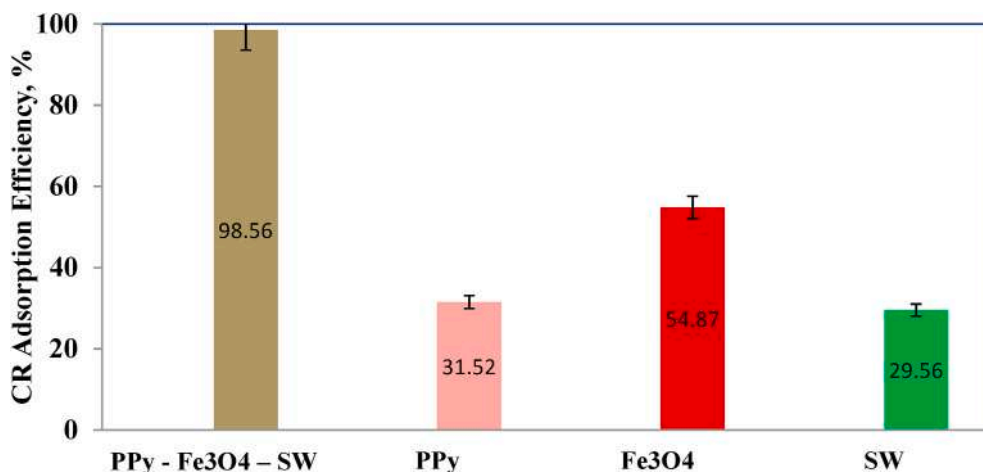


Fig. 12. Comparison of CR adsorption efficiency.

efficiencies are much lower than composite. The results validated that the presence of Fe₃O₄ in nanocomposite played a major role in CR removal. Fe₃O₄ induces the generation of adsorption active sites for CR which in turn increases adsorption efficiency. Fe2p XPS spectra information (Fig. 13) of nanocomposite, before and after CR adsorption, was

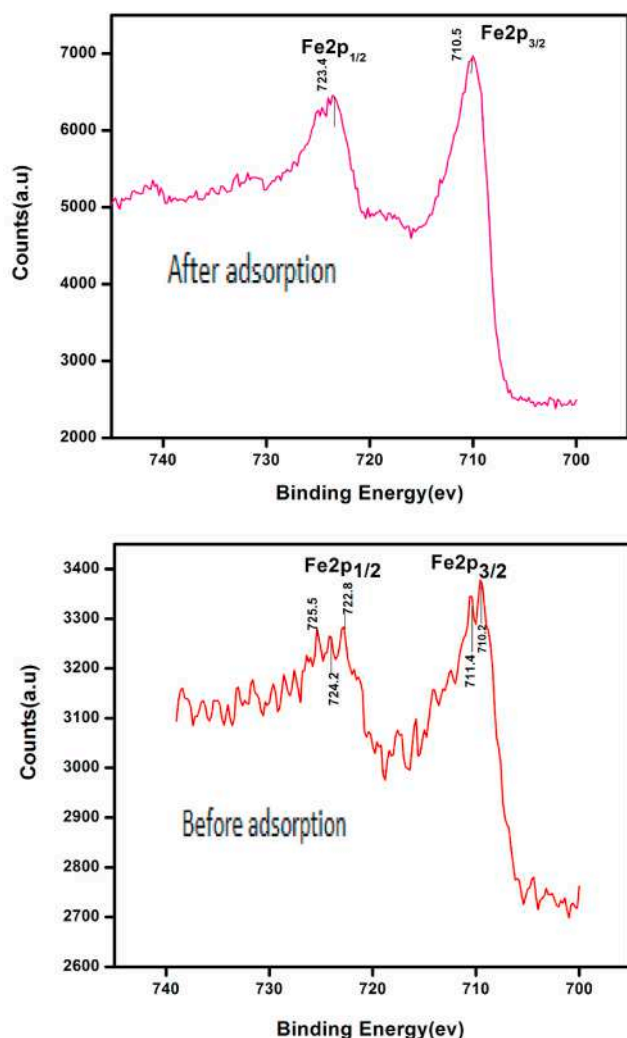


Fig. 13. Fe2p XPS spectrum of nanocomposite before and after adsorption of CR.

examined to propose the role of Fe₃O₄ in adsorption process. Appearance of two main peaks at 710.5 eV and 724.4 eV assigned to Fe2p_{1/2} and Fe2p_{3/2} states was observed in Fe2p XPS spectra of nanocomposite after CR adsorption. Corresponding peaks at 710.2 eV, 711.4 eV and 722.8 eV, 724.2 eV, 725.5 eV assigned to Fe2p_{1/2} and Fe2p_{3/2} states respectively was observed in Fe2p XPS spectra of nanocomposite before CR adsorption. Peak at 710.2, 710.5 and 711.4 eV represents only for the fully oxidized form of iron on the surface (Cornell and Schwertmann, 2003). Remaining peaks were assigned to Fe(II) of Fe2p_{3/2} state. The binding energy of Fe2p_{1/2} and Fe2p_{3/2} after CR adsorption is higher than that of before CR adsorption. The increase in binding energy of Fe2p_{1/2} was indication of Fe₃O₄ involvement in adsorption process (Manjanna and Venkateswaran, 2002). Meanwhile Fe₃O₄ have the ability to form complex by means of electrostatic attraction between carboxyl and hydroxyl group of the nanocomposite and surface complexation property. Thus CR forms complex with the nanocomposite with the help of Fe₃O₄ (Sirajudheena et al., 2020). Moreover magnetic surface on exposure to oxygen environment gets converted to maghemite. As a result, Fe(II) gets oxidized to Fe(III) leading to a creation of cation vacancies at the sites. In order to maintain electroneutrality, Fe(II) must from diffuse from inner surface of iron oxide to the oxidized surface of nanocomposite (Zhong et al., 2018). Presence of Fe(II) makes the surface of nanocomposite to remain positively charged favoring CR bonding with Fe²⁺ (Kim and Choi, 2017). Thus Fe₃O₄ aids in the generation of chemisorption sites for adsorption of CR and enhances the adsorption of CR. Table 4 provides the comparison of adsorption capacities of Fe₃O₄ based nano-adsorbents. It was noticed that maximum adsorption capacity was achieved with Fe₃O₄ based adsorbents. Higher adsorption performance was due to large specific surface area and mesoporous structure of Fe₃O₄ which in turn increases adsorption efficiency. Also Fe₃O₄ adsorbents separated from aqueous media by applying external magnetic field separation.

3.11. Adsorption mechanism

Sorption of CR onto PPy-Fe₃O₄-SW nanocomposite occurred through

Table 4

Comparison of adsorption capacity of Congo red with Iron oxide based adsorbents.

Adsorbent	Adsorption capacity, mg/g	References
Fe ₃ O ₄ @ carbon composites	247.5248	Ren et al. (2019)
Fe ₃ O ₄ /Bi ₂ S ₃ microspheres	92.24	Zhu et al. (2017)
Fe ₃ O ₄ @NiO	128	Li et al. (2015)
Chitosan coated Fe ₃ O ₄	56.66	Zhu et al. (2012)
Fe ₃ O ₄ @TiO ₂ @GO	89.65	Li et al. (2014)

electrostatic interaction, π - π interaction and ion exchange process. At acidic condition there exists an electrostatic attraction between protonated ($-\text{NH}^+$) of nanocomposite and CR. pH study clearly depicts the dependence of sorption mainly on the surface charge of the nanocomposite. Under the conditions of lower pH, available of excess positive hydrogen ions induces the protonation of nitrogen atoms of polymer present in the nanocomposite thereby making the surface of the nanocomposite to remain positively charged. In case of anionic CR, at lower pH, H^+ stimulates the dissociation of $-\text{SO}_3\text{Na}$ to Na^+ and $-\text{SO}_3^-$. Hence there exists an electrostatic attraction between $-\text{NH}^+$ and SO_3^- groups. Also anionic CR replaces doped Cl^- ion by means of ion exchange mechanism. CR exhibits aromatic structure and thereby π - π interaction occurs between $\text{C}=\text{C}$ of polypyrrole and aromatic ring of CR (Fig. 14). So the combined interaction increases the uptake of CR dye from aqueous solution at acidic conditions.

3.12. Comparison with other sorbents

The adsorptive capacity of the nanocomposite depends on surface, process operating conditions and the active functional groups. Comparison of the sorption ability with other sorbents is given in Table 5 and found that the nanocomposite contributed better performance. This outcome is due to the interacting properties of polypyrrole, surface properties and functional groups of seaweed. Fe_3O_4 makes the separation much easier. This obviously confirmed that this nanocomposite was an effective applicant for the treatment of dye bearing waste water.

3.13. Adsorbent regeneration

In economical point of view it is highly recommended to regenerate the sorbent. To assess the recovery, several adsorption/desorption experiments were carried out. The desorption experiments were performed using different solvents. Ionic affinity between positively charged nanocomposite and negatively charged CR molecules remains as a main mechanism in adsorption of CR on the surface of nanocomposite. Nevertheless NaOH solution has a tendency to reduce the electrostatic attraction and stability of polypyrrole chains. However during desorption the negative hydroxyl ions of NaOH solution easily replaces the absorbed anionic CR dye species present on the surface of the nanocomposite. Therefore a maximum desorption efficiency of 96.56% was obtained using NaOH solution. Hence NaOH solution was

Table 5

Comparison of adsorption capacity of CR with different adsorbents.

Adsorbent	Adsorption capacity, mg/g	References
Activated carbon	6.7	Namasivayam and Kavitha (2002)
Chitosan/montmorillonite nanocomposite	54.52	Wang and Wang (2007)
Palm Kernel seed coat	66.23	Oladoja and Akinlabi (2009)
Zn- Fe_2O_4	16.58	Rahimi et al. (2011)
Bamboo hydrochars	33.70	Ibrahim (2019)
Ca-bentonite	23.25–85.29	Lian et al. (2009)
Wet-torrefied microalgal biochar	164.32 mg/g	Yu et al. (2021)
$\text{Fe}_{3-x}\text{La}_x\text{O}_4$ Ferrite	37.4–79.1	Wang et al. (2011)
CuO-ZnO	126.4	Malwal and Gopinath (2017)
Xanthangum-graft poly (acrylamide)/ SiO_2 Nanocomposite	209.205	Ghorai et al. (2013)
$\gamma\text{-Fe}_2\text{O}_3$	208.2	Afkhami and Moosavi (2010)
GO/CS/ETCH	294.1	Du et al. (2014)
NCPYP	298.8	Shahnaz et al. (2020)
CAC	300	Purikait et al. (2007)
g-GG/ SiO_2 nanocomposite	233.24	Pal et al. (2015)
PANi/ Bi_2WO_6	142.92	Laabd et al. (2016)
PPy	66.7	Dall Acqua et al. (2004)
CS/CNTS	402	Chatterjee et al. (2010)
PPy-PANI	222.22	Bhaumik et al. (2013)
PVDF/PDA/PPy	384.6	Ma et al. (2018)
PPy- Fe_3O_4 -SW	500	This work

chosen as an effective-low cost solvent compared with other solvent used for regeneration. Meanwhile under alkaline conditions as the composite surface charge is negative, it is much easier to desorb anionic CR dye using NaOH solution (Ghoviland et al., 2015). Also under alkaline condition an electrostatic repulsion occurs between nanocomposite and CR. As a result more amount of binding sites remains unoccupied and hence decrease in desorption efficiency was found after third cycle (Fig. 15). Thus the findings specifies the reusability of nanocomposite for several cycles.

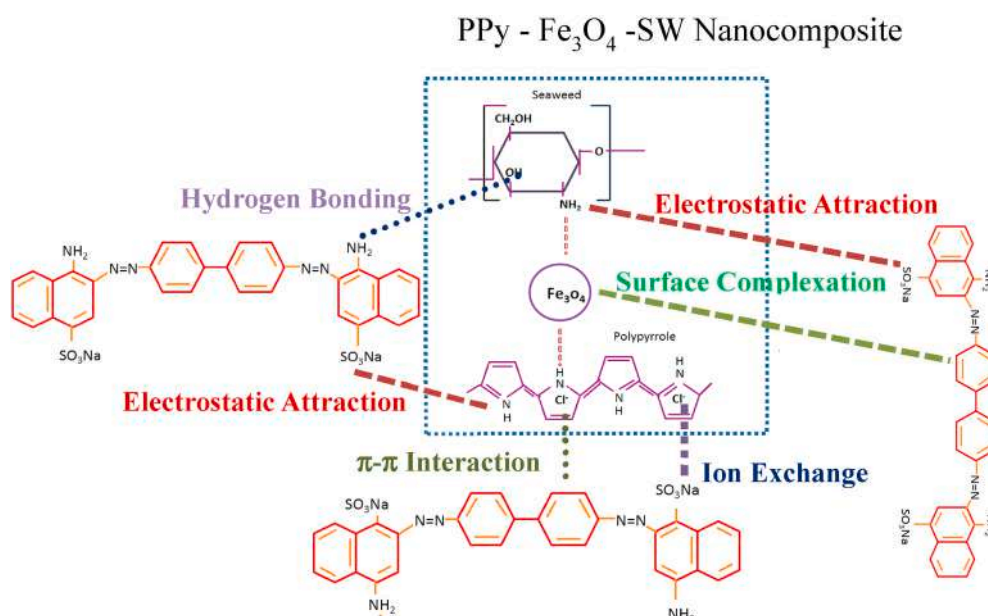


Fig. 14. Schematic representation of plausible mechanism of CR by PPy- Fe_3O_4 -SW composite.

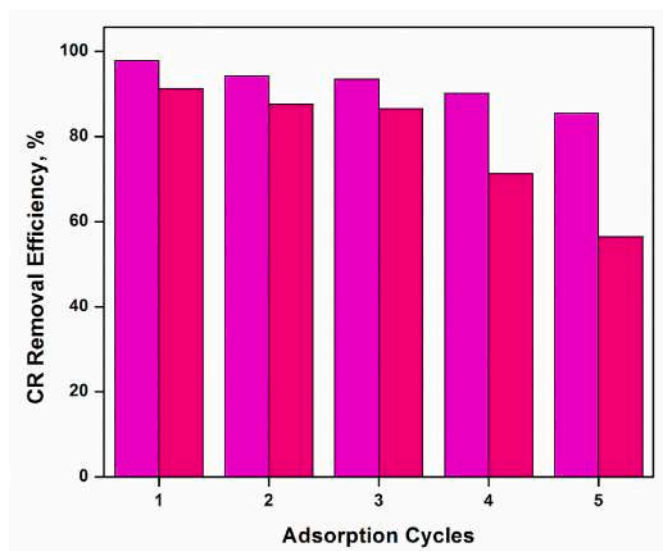


Fig. 15. Effect of regeneration of adsorbent on removal efficiency.

4. Conclusion

Present work explored the adsorptive capability of PPy-Fe₃O₄-SW nanocomposite towards CR. The categorized characterization results confirmed the sorption of CR. The experimental data showed that the RE depends on operating parameters mainly pH, mass of sorbent and initial CR concentration. The optimum condition for effective removal of CR were:- pH-3, initial CR concentration- 40 mg/L, nanocomposite dosage- 20 mg, contact time-40 min and temperature-40°C. The experimental results of CR onto nanocomposite well fits with Langmuir isotherm model ($R^2 = 0.98$) confirms monolayer CR adsorption. capacity and values of maximum Q_{max} was about 500 mg/g. The kinetics studies showed the adsorption of CR on PPy-Fe₃O₄-SW follows PSO model kinetics ($R^2 = 0.994$). The desorption results signifies that PPy-Fe₃O₄-SW could be reused up to 5 cycles. The adsorption mechanism of CR on PPy-Fe₃O₄-SW is mainly governed by electrostatic attraction. Finally PPy-Fe₃O₄-SW can be used as effective adsorbent in the removal of synthetic dyes from the aqueous solution. Outcome of the results points out that the nanocomposite can be utilized as ecofriendly sorbent in dye removal from waste water. The collective inputs of each constituent in PPy-Fe₃O₄-SW nanocomposite played an important role in removal of CR. Thus PPy-Fe₃O₄-SW can be used as low cost sorbent for removal of anionic dye with excellent regeneration, reusability and easier separation from aqueous system by means of external magnet.

Declaration of competing interest

The authors declare that they have no known competing financial interests or personal relationships that could have appeared to influence the work reported in this paper.

Appendix A. Supplementary data

Supplementary data to this article can be found online at <https://doi.org/10.1016/j.chemosphere.2021.132371>.

Author contributions

G.Sarojini – Conceptualization, Resources, Methodology, Investigation, Validation, Writing – original draft, Writing – review & editing, **S.Venkatesh Babu**: Writing – review & editing, Supervision. **M. Rajasimman**: Characterization, Methodology, Formal analysis, Writing – review & editing, Supervision.

References

- Afkhami, A., Moosavi, R., 2010. Adsorptive removal of Congo red, a carcinogenic textile dye, from aqueous solutions by maghemite nanoparticles. *J. Hazard Mater.* 174, 398–403.
- Ballav, N., Choi, H.J., Mishra, S.B., Maity, A., 2014. Polypyrrole-coated halloysite nanotube clay nanocomposite: synthesis, characterization and Cr(VI) adsorption behavior. *Appl. Clay Sci.* 102, 60–70.
- Bhatti, H.N., Safa, Y., Yakout, S.M., Shair, O.H., Iqbal, M., Nazir, A., 2020. Efficient removal of dyes using carboxymethyl cellulose/alginate/polyvinyl alcohol/rice husk composite: adsorption/desorption, kinetics and recycling studies. *Int. J. Biol. Macromol.* 150, 861–870.
- Bhaumik, M., Maity, A., Srinivasu, V.V., Onyango, M.S., 2011. Enhanced removal of Cr (VI) from aqueous solution using polypyrrole/Fe₃O₄ magnetic nanocomposite. *J. Hazard Mater.* 190, 381–390.
- Bhaumik, M., Mccrindle, R., Maity, A., 2013. Efficient removal of Congo red from aqueous solutions by adsorption onto interconnected polypyrrole–polyaniline nanofibres. *Chem. Eng. J.* 228, 506–515.
- Cornell, R.M., Schwertmann, U., 2003. *The Iron Oxides: Structure, Properties, Reactions, Occurrences and Uses*. Wiley-VCH, Weinheim.
- Chafai, H., Laabd, M., Elbariji, S., Bazzou, M., Albourine, A., 2017. Study of Congo red adsorption on the polyaniline and polypyrrole. *J. Dispersion Sci. Technol.* 38, 832–836.
- Chandra, V., Kim, K.S., 2011. Highly selective adsorption of Hg²⁺ by a polypyrrole–reduced graphene oxide composite. *Chem. Commun.* 47, 3942–3944.
- Chatterjee, S., Lee, M.W., Woo, S.H., 2010. Adsorption of Congo red by chitosan hydrogel beads impregnated with carbon nanotubes. *Bioresour. Technol.* 101, 1800–1806.
- Choi, M., Jang, J., 2008. Heavy metal ion adsorption onto polypyrrole-impregnated porous carbon. *J. Colloid Interface Sci.* 325, 287–289.
- Choudhary, M., Islam, M., Witcomb, M., Mallick, K., 2014. In situ generation of a high-performance Pd-polypyrrole composite with multi-functional catalytic properties. *Dalton Trans.* 43, 6396–6405.
- Dall Acqua, L., Tonin, C., Peila, R., Ferrero, F., Catellani, M., 2004. Performances and properties of intrinsic conductive cellulose–polypyrrole textiles. *Synth. Met.* 146, 213–221.
- Das, D., Borthakur, L.J., Nath, B.C., Saikia, B.J., Mohan, K.J., Dolui, S.K., 2016. Designing hierarchical NiO/PANI-MWCNT core–shell nanocomposites for high performance super capacitor electrodes. *RSC Adv.* 6, 44878–44887.
- Dash, A., Ahmed, M.T., Selvaraj, R., 2018. Mesoporous magnetite nanoparticles synthesis using the Peltophorum pterocarpum pod extract, their antibacterial efficacy against pathogens and ability to remove a pollutant dye. *J. Mol. Struct.* 1178, 268–273.
- Do Vale-Júnior, E., da Silva, D.R., Fajardo, A.S., Martínez-Huitle, C.A., 2018. Treatment of an azo dye effluent by peroxi-coagulation and its comparison to traditional electrochemical advanced processes. *Chemosphere* 204, 548–555.
- Dogan, M., Ozdemir, Y., Alkan, M., 2007. Adsorption kinetics and mechanism of cationic methyl violet and methylene blue dyes onto sepiolite. *Dyes Pigments* 75 (3), 701–713.
- Dommez, G., Aksu, Z., Ozturk, A., Kutsal, T.A., 1999. Comparative study on heavy metal biosorption characteristics of some algae. *Process Biochem.* 34, 885–892.
- Du, Q., Sun, J., Li, Y., Yang, X., Wang, X., Wang, Z., Xia, L., 2014. Highly enhanced adsorption of Congo red onto graphene oxide/chitosan fibers by wet-chemical etching off silica nanoparticles. *Chem. Eng. J.* 245, 99–106.
- Dubinin, M.M., 1960. The potential theory of adsorption of gases and vapors for adsorbents with energetically non-uniform surface. *Chem. Rev.* 60, 235–266.
- Feng, J., Li, J., Lv, W., Xu, H., Yang, H., Yan, W., 2014. Synthesis of polypyrrole nanofibers with hierarchical structure and its adsorption property of Acid Red G from aqueous solution. *Synth. Met.* 191, 66–73.
- Freundlich, H.M.F., 1906. Over the adsorption in solution. *J. Phys. Chem.* 57, 385–471.
- Ghorai, S., Sarkar, A.K., Panda, A.B., Pal, S., 2013. Effective removal of Congo red dye from aqueous solution using modified xanthan gum/silica hybrid nanocomposite as adsorbent. *Bioresour. Technol.* 144, 485–491.
- Ghoviland, M.B., Yamini, Y., Dayeni, M., Seidi, S., Tahmasebi, E., 2015. Adsorptive removal of alizarin red-S and alizarin yellow GG from aqueous solutions using polypyrrole-coated magnetic nanoparticles. *J. Environ. Chem. Eng.* 3 (1), 529–540.
- Gu, Z., Li, C., Wang, G., Zhang, L., Li, X., Wang, W., Jin, S., 2010. Synthesis and characterization of polypyrrole/graphite oxide composite by in situ emulsion polymerization. *J. Polym. Sci., Part B: Polym. Phys.* 48, 1329–1335.
- Guo, K., Gao, B., Tian, X., Yue, Q., Zhang, P., Shen, X., Xu, X., 2019. Synthesis of polyaluminum chloride/papermaking sludge-based organic polymer composites for removal of disperse yellow and reactive blue by flocculation. *Chemosphere* 231, 337–348.
- Gupta, V.K., Rastogi, A., 2008. Equilibrium and kinetic modelling of cadmium(II) biosorption by nonliving algal biomass *Oedogonium* sp. from aqueous phase. *J. Hazard Mater.* 153, 759–766.
- Ho, Y.S., 2004. Citation review of Lagergren kinetic rate equation on adsorption reactions. *Scientometrics* 59, 171–177.
- Ho, Y.S., McKay, G., 1999. Pseudo-second order model for sorption processes. *Process Biochem.* 34, 451–465.
- Ibrahim, M.M., 2019. Cr₂O₃/Al₂O₃ as adsorbent: physicochemical properties and adsorption behaviors towards removal of Congo red dye from water. *J. Environ. Chem. Eng.* 7 (1), 102848.
- Jayakumar, R., Rajasimman, M., Karthikeyan, C., 2015. Sorption and desorption of hexavalent chromium using a novel brown marine algae *Sargassum myricostum*. *Kor. J. Chem. Eng.* 32, 2031–2046.

- Jayakumar, V., Govindaradjane, S., Rajasimman, M., 2019. Isotherm and kinetic modeling of sorption of Cadmium onto a novel red algal sorbent, *Hypnea musciformis*. *Model Earth Syst Environ* 5, 793–803.
- Juang, R.S., Chen, M.L., 1997. Application of the Elovich equation to the kinetics of metal sorption with solvent-impregnated resins. *Ind. Eng. Chem. Res.* 36, 813–820.
- Karimzadeh, I., Aghazadeh, M., Ganzali, M.R., Doroudi, T., Kolivand, P.H., 2017. Surface modification of magnetic iron oxide nanoparticles. *J. Magn. Mater.* 433, 148–154.
- Karthikeyan, M., Satheshkumar, K.K., Elango, K., 2009. Removal of fluoride ions from aqueous solution by conducting polypyrrole. *J. Hazard Mater.* 167, 300–305.
- Kim, S.-H., Choi, P.-Pa, 2017. Enhanced Congo red dye removal from aqueous solutions using iron nanoparticles: adsorption, kinetics, and equilibrium studies. *Dalton Trans.* 46, 15470–15479.
- Kishor, R., Purchase, D., Saratale, G.D., Saratale, R.G., Ferreira, L.F.R., Bilal, M., Chandra, R., Bharagava, R.N., 2021. Ecotoxicological and health concerns of persistent coloring pollutants of textile industry wastewater and treatment approaches for environmental safety. *J. Environ. Chem. Eng.* 9 (2), 105012.
- Laabd, M., Ahsaine, H.A., Jaouhari, A.E., Bakiz, B., Bazzou, M., Ezahri, M., Albourine, A., Benhachemi, A., 2016. Congo red removal by PANI/Bi₂WO₆ nanocomposites: kinetic, equilibrium and thermodynamic studies. *J. Environ. Chem. Eng.* 4, 3096–3105.
- Langmuir, I., 1918. The adsorption of gases on plane surface of glass, mica and platinum. *J. Am. Chem. Soc.* 40, 1361–1368.
- Lei, Y., Qian, X., Shen, J., An, X., 2012. Integrated reductive/adsorptive detoxification of Cr (VI)-contaminated water by polypyrrole/cellulose fiber composite. *Ind. Eng. Chem. Res.* 51, 10408–10415.
- Lian, L., Guo, L., Guo, C., 2009. Adsorption of Congo red from aqueous solutions onto Ca bentonite. *J. Hazard Mater.* 161, 126–131.
- Li, G., Zhao, Z., Liu, J., Jiang, G., 2011. Effective heavy metal removal from aqueous systems by thiol functionalized magnetic mesoporous silica. *J. Hazard Mater.* 192, 277–283.
- Li, J., Feng, J., Yan, W., 2013. Excellent adsorption and desorption characteristics of polypyrrole/TiO₂ composite for Methylene Blue. *Appl. Surf. Sci.* 279, 400–408.
- Li, L., Li, X., Duan, H., Wang, X., Luo, C., 2014. Removal of Congo Red by magnetic mesoporous titanium dioxide-graphene oxide core-shell microspheres for water purification. *Dalton Trans.* 43, 8431–8438.
- Lin, M., Hu, X., Ma, Z., Chen, L., 2012. Functionalized polypyrrole nanotube arrays as electrochemical biosensor for the determination of copper ions. *Anal. Chim. Acta* 746, 63–69.
- Li, T., Yang, C., Rao, X., Xiao, F., Wang, J., Su, X., 2015. Synthesis of magnetically recyclable Fe₃O₄@NiO nanostructures for styrene epoxidation and adsorption application. *Ceram. Int.* 41, 2214–2220.
- Li, X., Lu, H., Zhang, Y., He, F., 2017. Efficient removal of organic pollutants from aqueous media using newly synthesized polypyrrole/CNTs-CoFe₂O₄ magnetic nanocomposites. *Chem. Eng. J.* 316, 893–902.
- Ma, F.F., Zhang, D., Zhang, N., Huang, T., Wang, Y., 2018. Polydopamine-assisted deposition of polypyrrole on electrospun poly(vinylidene fluoride) nanofibers for bidirectional removal of cation and anion dyes. *Chem. Eng. J.* 354, 432–444.
- Maity, A., Ray, S., 2010. Highly conductive core-shell nanocomposite of poly(N-vinylcarbazole) polypyrrole with multiwalled carbon nanotubes. *Macromol. Rapid Commun.* 29, 1582–1587.
- Malwal, D., Gopinath, P., 2017. Efficient adsorption and antibacterial properties of electrospun CuO-ZnO composite nanofibers for water remediation. *J. Hazard Mater.* 321, 611–621.
- Manjanna, J., Venkateswaran, G., 2002. Effect of oxidative pretreatment for the dissolution of Cr-substituted hematites/magnetites. *Ind. Eng. Chem. Res.* 41, 3053–3063.
- Mais, L., Vacca, A., Mascia, M., Maria Usai, E., Tronci, S., Palmas, S., 2020. Experimental study on the optimisation of azo-dyes removal by photo-electrochemical oxidation with TiO₂ nanotubes. *Chemosphere* 248, 125938.
- Mollahosseini, A., Khadir, A., Saeidian, J., 2019. Core shell polypyrrole/Fe₃O₄ nanocomposite as sorbent for magnetic dispersive solid-phase extraction of Al³⁺ ions from solutions: investigation of the operational parameters. *J. Water Process. Eng.* 29, 100795.
- Namasivayam, C., Kavitha, D., 2002. Removal of Congo Red from water by adsorption onto activated carbon prepared from coir pith, an agricultural solid waste. *Dyes Pigments* 54, 47–58.
- Nekouei, F., Nekouei, S., Tyagi, I., Gupta, V.K., 2015. Kinetic, thermodynamic and isotherm studies for acid blue 129 removal from liquids using copper oxide nanoparticle-modified activated carbon as a novel adsorbent. *J. Mol. Liquids* 201, 124–133.
- Oladoja, N.A., Akinlabi, A.K., 2009. Congo red biosorption on palm kernel seed coat. *Ind. Eng. Chem. Res.* 48, 6188–6196.
- Pal, S., Patra, A.S., Ghorai, S., Sarkar, A.K., Mahato, V., Sarkar, S., Singh, R.P., 2015. Efficient and rapid adsorption characteristics of templating modified guar gum and silica nanocomposite towards removal of toxic reactive blue and Congo red dyes. *Bioresour. Technol.* 191, 291–299.
- Pandian, A.M.K., Gopalakrishnan, B., Rajasimman, M., Rajamohan, N., Karthikeyan, C., 2021a. Green synthesis of bio-functionalized nano-particles for the application of copper removal-characterization and modeling studies. *Environ. Res.* 197, 111140.
- Pandian, A.M.K., Karthikeyan, C., Rajasimman, M., 2017. Isotherm and kinetic studies on adsorption of malachite green using chemically synthesized silver nanoparticles. *Nanotechnol. Env. Eng.* 2, 2.
- Pandian, A.M.K., Rajasimman, M., Rajamohan, N., Varjani, S., Karthikeyan, C., 2021b. Anaerobic mixed consortium (AMC) mediated enhanced biosynthesis of silver nano particles (AgNPs) and its application for the removal of phenol. *J. Hazard Mater.* 416, 125717.
- Pei, Q.B., Qian, R.Y., 1991. Protonation and deprotonation of polypyrrole chain in aqueous solutions. *Synth. Met.* 45, 35–48.
- Purikait, M.K., Maiti, A., Dasgupta, S., De, S., 2007. Removal of Congo red using activated carbon and its regeneration. *J. Hazard Mater.* 145, 287–295.
- Rahimi, R., Kerdari, H., Rabbani, M., Shafiee, M., 2011. Synthesis, characterization and adsorbing properties of hollow Zn-Fe₂O₄ nanospheres on removal of Congo red from aqueous solution. *Desalination* 280, 412–418.
- Rajabi, H.R., Khani, O., Shamsipur, M., Vatanpour, V., 2013. High-performance pure and Fe³⁺-ion doped ZnS quantum dots as green nanophotocatalysts for the removal of malachite green under UV-light irradiation. *J. Hazard Mater.* 250–251, 370–378.
- Ren, L., Lin, H., Meng, F., Zhang, F., 2019. One-step solvothermal synthesis of Fe₃O₄@Carbon composites and their application in removing of Cr (VI) and Congo red. *Ceramics* 43 (7), 9646–9652.
- Rodriguez, F.J., Gutiérrez, S., Ibanez, J.G., Bravo, J.L., Batina, N., 2000. The efficiency of toxic chromate reduction by a conducting polymer (polypyrrole): influence of electropolymerization conditions. *Environ. Sci. Technol.* 34, 2018–2023.
- Saha, B., Das, S., Saikia, J., Das, G., 2011. Preferential and enhanced adsorption of different dyes on iron oxide nanoparticles: a comparative study. *J. Phys. Chem. C* 115 (16), 8024–8033.
- Saleh, T.A., Naemullah, M., Tuzen, A., Sari, A., 2016. Polyethylenimine modified activated carbon as novel magnetic adsorbent for the removal of uranium from aqueous solution. *Chem. Eng. Res. Des.* 117, 218–227.
- Sarojini, G., Venkateshbabu, S., Rajasimman, M., 2021a. Facile synthesis and characterization of polypyrrole-iron oxide-seaweed (PPy-Fe₃O₄-SW) nanocomposite and its exploration for adsorptive removal of Pb(II) from heavy metal bearing water. *Chemosphere* 278, 130400.
- Sarojini, G., Venkateshbabu, S., Rajamohan, N., Senthilkumar, P., Rajasimman, M., 2021b. Surface modified polymer-magnetic-algae nanocomposite for the removal of chromium-equilibrium and mechanism studies. *Environ. Res.* 201, 111626.
- Shahnaz, T., Fazil, S.M.M., Padmanaban, V.C., Narayanasamy, S., 2020. Surface modification of nanocellulose using polypyrrole for the adsorptive removal of Congo red dye and chromium in binary mixture. *Int. J. Biol. Macromol.* 151, 322–332.
- Shamsipur, M., Rajabi, H.R., 2014. Study of photocatalytic activity of ZnS quantum dots as efficient nanoparticles for removal of methyl violet: effect of ferric ion doping. *Spectrochim. Acta Mol. Biomol. Spectrosc.* 122, 260–267.
- Sirajudheena, P., Nikitha, M.R., Karthikeyana, P., Meenaksh, S., 2020. Perceptive removal of toxic azo dyes from water using magnetic Fe₃O₄ reinforced graphene oxide-carboxymethyl cellulose recyclable composite: adsorption investigation of parametric studies and their mechanisms. *Surfaces and Interfaces* 21, 10648.
- Temkin, M.J., Pyzhev, V., 1940. Kinetics of ammonia synthesis on promoted iron catalysts. *Acta Phys. Chem. URSS.* 12, 217–256.
- Tian, Y., Yang, F., 2007. Reduction of hexavalent chromium by polypyrrole-modified steel mesh electrode. *J. Clean. Prod.* 15, 1415–1418.
- Wang, L., Li, J., Wang, Y., Zhao, L., 2011. Preparation of nanocrystalline Fe₃-xLa₂O₄ ferrite and their adsorption capability for Congo red. *J. Hazard Mater.* 196, 342–349.
- Wang, L., Wang, A., 2007. Adsorption characteristics of Congo red onto the chitosan/montmorillonite nanocomposite. *J. Hazard Mater.* 147, 979–985.
- Wanyonyi, W.C., Onyari, J.M., Shiundu, P.C., 2014. Adsorption of Congo Red dye from aqueous solutions using roots of *Eichhornia Crassipes*: kinetic and equilibrium studies. *Energy Procedia* 50, 862–869.
- Weber, W.J., Morris, J., 1963. Kinetics of adsorption on carbon from solution. *J. Sanit. Eng. Div.* 89, 31–60.
- Xin, Q., Fu, J., Chen, Z., Liu, S., Yan, Y., Zhang, J., 2015. Polypyrrole nanofibers as a high efficient adsorbent for the removal of methyl orange from aqueous solution. *J. Environ. Chem. Eng.* 3, 1637–1647.
- Yu, K.L., Lee, X.J., Ong, H.C., Chen, W.H., Chang, J.S., Lin, C.S., Show, P.L., Ling, T.C., 2021. Adsorption removal of cationic methylene blue and anionic Congo red dyes using wettorrefied torrefied microalgal biochar: equilibrium, kinetic and mechanism modeling. *Environ. Pollut.* 272, 115986.
- Yun, J., Wang, Y., Liu, Z., Li, Y., Yang, H., Xu, Z., 2020. High efficient dye removal with hydrolyzed ethanalamine Polycrylonitrile UF membrane: rejection of anionic dye and selective adsorption of cationic dye. *Chemosphere* 259, 127390.
- Zhang, X., Bai, R.B., 2003. Surface electric properties of polypyrrole in aqueous solutions. *Langmuir* 19, 10703–10709.
- Zhang, X., Bai, R.B., Tong, Y.W., 2006. Selective adsorption behaviors of proteins on polypyrrole-based adsorbents. *Separ. Purif. Technol.* 52, 161–169.
- Zhang, W., Chen, J., Wang, W., Hao, L., Ni, Y., Lu, C., Xu, Z., 2016. Super-paramagnetic core-shell material with tunable magnetic behavior by regulating electron transfer efficiency and structure stability of the shell. *Results Phys.* 6, 606–613.
- Zhong, D., Zhang, Y., Wang, L., Chen, J., Jiang, Y., Tsang, D.C.W., Zhao, Z., Ren, S., Liu, Z., Crittenden, J.C., 2018. Mechanistic insights into adsorption and reduction of hexavalent chromium from water using magnetic biochar composites: key roles of Fe₃O₄ and persistent free radicals. *Environ. Pollut.* 243 (b), 1302–1309.
- Zhou, J., Lu, Q.F., Luo, J.J., 2017. Efficient removal of organic dyes from aqueous solution by rapid adsorption onto polypyrrole-based composites. *J. Clean. Prod.* 167, 739–748.
- Zhou, Y., Lu, J., Zhou, Y., Liu, Y., 2019. Recent advances for dyes removal using novel adsorbents: a review. *Environ. Pollut.* 252, 352–365.
- Zhu, H., Zhang, M., Liu, Y., Zhang, L., Han, R., 2012. Study of Congo red adsorption onto chitosan coated magnetic iron oxide in batch mode. *Des. Water Treat* 37, 46–54.
- Zhu, H., Jiang, R., Li, J., Fu, Y., Jiang, S., Yao, J., 2017. Magnetically recyclable Fe₃O₄/Bi₂S₃ microspheres for effective removal of Congo red dye by simultaneous adsorption and photocatalytic regeneration. *Separ. Purif. Technol.* 179, 184–193.



Performance evaluation of polymer-marine biomass based bionanocomposite for the adsorptive removal of malachite green from synthetic wastewater

G. Sarojini^{a,*}, S. Venkatesh Babu^b, N. Rajamohan^c, M. Rajasimman^d

^a Department of Petrochemical Engineering, SVS College of Engineering, Coimbatore, India

^b Department of Petroleum Engineering, JCT College of Engineering & Technology, Coimbatore, India

^c Faculty of Engineering, Sohar University, Sohar, P O;311, Oman

^d Department of Chemical Engineering, Annamalai University, Annamalai Nagar, India

ARTICLE INFO

Keywords:

Nanocomposite
Malachite green
Adsorption
Mechanism
Isotherm

ABSTRACT

In this experimental investigation, feasibility and performance of a polymer hybrid bio-nano composite were evaluated to remove malachite green (MG) under controlled environment conditions. The polymer hybrid bionanocomposite was characterized using FTIR, SEM and EDS. The influence of operating variables, namely effect of pH (2–11), nanocomposite dosage (20–100 mg), initial MG concentration (10–200 mg/L), contact time (10–120 min) and temperature (298–318 K) were explored. The maximum removal efficiency (RE) of 99.79% was achieved at neutral pH at the dosage level of 50 mg with the initial MG concentration of 150 mg/L in 40 min. The equilibrium results revealed that the adsorption of MG data fitted to Langmuir isotherm ($R^2 > 0.970$) indicating monolayer adsorption. The maximum adsorption capacity of polymer hybrid nanocomposite was found to be 384.615 mg/g. Kinetic studies were performed using five kinetic models and results showed the pseudo second order model fitted very well with the MG adsorption data ($R^2 > 0.990$). The thermodynamic results confirmed that MG adsorption onto polymer hybrid nanocomposite is feasible and ($\Delta S = 0.2893$ kJ/mol K), spontaneous ($\Delta H = 81.103$ kJ/mol K) and exothermic ($\Delta G < 0$). A mechanism is also proposed for the removal of MG using the polymer nanocomposite and identified that electrostatic attraction and hydrogen bonding as the major mechanism for removal of MG. FTIR results confirmed the presence of carboxyl (-COO) and hydroxyl (-OH) groups which helped in effective binding of cationic dye. The overall results revealed that polymer nanocomposite could be used as a potential adsorbent for removing MG from aqueous solution.

1. Introduction

Most of the industries namely textile, rubber, paper, cosmetic and printing use dye as a raw material and additive to manufacture their products (Kushwaha et al., 2014). All these industries discharge large amount of dye into environment along with their effluent due to inefficient use of dye, poor attachment properties and other production related process factors (Adeyi et al., 2019). These effluents are potential threat to the environment because dyes are mutagens and produces carcinogenic effect (Sallam et al., 2018). Approximately 10,000 tonnes of dyes are being used by textile industries every year with the quantity released accounting to 10–15% of dyes (Dawood and Sen, 2014). Malachite green (MG), a cationic dye finds application in many extensive areas such as a dyeing material for leather, silk and wool products,

parasiticides in fishing industry (Santhi et al., 2015). Nevertheless, MG is identified as a carcinogenic agent and even very low concentration (1 mg/L) causes severe health disorders (Rajeshkannan et al., 2009, 2013). Development of new systems for the removal of dyes has gained significant importance due to the drawbacks associated with the conventional methods. Several techniques including adsorption, coagulation, oxidation, ozonation, biological degradation and photocatalysis are commonly employed for the removal of dyes from waste streams. Coagulation creates secondary pollution as it produces colloids, while ozonation and photocatalysis are expensive. Chemical oxidation requires use of reactive chemicals and is time consuming one. As dyes are highly bio-resistant, biological methods are not suitable. Adsorption is the most suitable conventional technique for the removal of dye due to high efficiency, simple operation and minimum sludge formation.

* Corresponding author.

E-mail address: grsarojini@gmail.com (G. Sarojini).

<https://doi.org/10.1016/j.envres.2021.112132>

Received 11 August 2021; Received in revised form 14 September 2021; Accepted 22 September 2021

Available online 25 September 2021

0013-9351/© 2021 Elsevier Inc. All rights reserved.

Selection of adsorption is a vital problem in adsorption process. The selected adsorbent should be low cost, stable and reusable (Rajeshkannan et al., 2010a, b). Most of the low cost adsorbent employed for dye removal possesses poor adsorption capacity. Nowadays, research is focused on the use of nano-sized magnetic nanomaterial as effective sorbent in removal of dyes (Sadeghi et al., 2014). They are preferred due to their large surface area and high sorption capacity. Magnetic properties help in easier separation within short time so that sorbent could be regenerated quickly and reused effectively. Magnetic iron oxide (Fe_3O_4) gained special interest as it inhibits toxicity, promotes good stability and biocompatibility (Hong et al., 2017). Hence it is highly recommended to tailor with some stable components. In most of the studies, surface of Fe_3O_4 is modified by coating of conducting polymers (Muliwa et al., 2016). In environmental applications, polypyrrole coated Fe_3O_4 nanoparticles are employed for the removal of RB19 (Shanehsaz et al., 2015). Polypyrrole- Fe_3O_4 magnetic nanocomposites have been used in the removal of 2, 4-dichlorophenoxyacetic acid (Goswami and Mahanta, 2020). In recent year, research has been focused on the development of adsorbent from naturally occurring resources containing natural biopolymers. Seaweed, marine algae is one of the promising natural polymers and effectively used as a sorbent in many studies. Seaweed inherits several advantages of high uptake capacity, easy availability, economical, selectivity and chemical structure with presence of many function groups.

In this study, polymer based bio-nanocomposite was synthesized and utilized for the MG dye removal from synthetic wastewater. The novelty of this research work is related to the application of PPy- Fe_3O_4 -SW nanocomposite for the removal of malachite green from aqueous solution. No detailed research has been conducted on sorption of MG on polymer hybrid. The factors affecting the adsorption process, namely initial pH of dye solution, polymer hybrid nano composite dosage, dye concentration and solution temperature, were investigated. The kinetic, isotherm and thermodynamic studies are performed. The reusability of the composite was explored through regeneration experiments.

2. Materials and methods

2.1. Chemicals used

Ferric chloride, ferrous sulphate, iron chloride, acetone, HCl, ethanol and MG ($\text{C}_{23}\text{H}_{25}\text{ClN}_2$) were obtained from Fisher Scientific and are used as received. Pyrrole ($\text{C}_4\text{H}_5\text{N}$) was obtained from Sigma – Aldrich and further purified by vacuum distillation. Seaweed were collected from coastal area of Kanniyakumari district, Tamilnadu, India.

2.2. Synthesis of polymer hybrid

The nanocomposite used in this study was synthesized and characterized as reported earlier (Sarojini et al., 2021a). The first stage of Fe_3O_4 nanoparticles synthesis involves co-precipitation mechanism. In the second stage, 0.5 g Fe_3O_4 was added to predetermined volume of distilled water following ultrasonication. Then six grams of ferric chloride were added as oxidant following magnetic stirring. To the entire solution, 0.8 mL of pyrrole was added to initiate polymerization reaction and sonicated for 30 min. After the appearance of black colour, acetone was added to stop the polymerization reaction. Then, Fe_3O_4 -seaweed composite was added and sonicated for 30 min. The obtained precipitate was filtered, washed many times with distilled H_2O and acetone. The washed material was dried in oven and stored.

2.3. Malachite green dye solution

About 1 g of analytic grade malachite green was dissolved in distilled H_2O to produce 1000 ppm solution. The required concentration of working solution was prepared from this stock solution by serial dilution.

2.4. Parametric studies

The sorption trials were accomplished in batch method. Tests were conducted in a conical flask (250 mL) holding 50 mL MG solution. Effect of pH (2–11), adsorbent dosage (20–100 mg), initial MG concentration (10–200 mg/L), contact time (10–120 min) and temperature (298–318 K) were analyzed. The initial pH of MG dye solution was varied using 1 M HCl or 1 M NaCl. MG concentrations were measured using UV–vis spectrophotometer (Shimadzu, Japan) at maximum adsorptive wavelength of 616 nm.

The amount of MG sorbed per unit nano composite mass under equilibrium q_t (mg/g) and MG removal efficiency (% RE) were obtained from Eqs (1) and (2):

$$q_t = \frac{C_0 - C_t}{m} * v \quad (1)$$

$$\% \text{ RE} = \frac{C_0 - C_t}{C_0} * 100 \quad (2)$$

where C_0 and C_t - MG concentration at initial and equilibrium conditions (mg/L); V is volume (L) and m is mass of nanocomposite (sorbent) in grams.

2.5. Regeneration experiments

Batch mode desorption experiments were performed to test the regenerability of the polymer composite. To regenerate the used adsorbent, MG loaded nanocomposite was treated with 25 mL of ethanol-water solvent mixture under room temperature and allowed to stay for 12 h. It was further washed with distilled water and dried. Consecutive adsorption-desorption cycles were performed using the same nanocomposite to examine the reusability of the nanocomposite. Desorption efficiency was calculated using Eq (3):

$$\text{Desorption efficiency} = \frac{\text{MG dye quantity desorbed}}{\text{MG dye quantity adsorbed}} * 100 \quad (3)$$

3. Results and discussion

3.1. Surface characterisation

FTIR Spectrum (FTIR- Shimadzu, Japan) was used for the identification of functional groups in the bio-nanocomposite. Fig. 1 represents the FTIR spectra of synthesized Polymer hybrid bio-nanocomposite and MG sorbed bio-nanocomposite. The characteristic band at 3630 cm^{-1} is attributed to hydroxyl groups. The vibrational peak at 2374 cm^{-1} is assigned to stretching of C–H raised from aromatic groups. The vibrational peak at 2322 cm^{-1} is assigned to N–H stretching vibrations. The characteristic band at 2311 cm^{-1} correspond to NH_2 bending, C=O and C=N stretching (amide I and amide II). The characteristic peaks in the range of 1100 cm^{-1} corresponds to polysaccharides. These results convey the incorporation of seaweed in the nanocomposite. The vibrational band at 3328 cm^{-1} is attributed to the stretching vibrations of NH groups of polypyrrole. The vibrational bands at 1541 and 1702 cm^{-1} is attributed to the asymmetrical and symmetrical stretching vibration bands of pyrrole rings (Sarojini et al., 2021b). The results proved the presence of polypyrrole in the composite. The peak at 665 cm^{-1} corresponds to stretching vibration of Fe–O provide the evidence for existence of iron oxide particles. The FTIR spectrum of nanocomposite after adsorption of MG Fig. 1(b) showed a peak at 1587 cm^{-1} assigned for C=C stretching of benzene rings of MG. The band at 1560 cm^{-1} attributed for C–N stretching vibrations of aromatic compounds of MG dye (Ramezani et al., 2013). Fig. 2(a) & (b) represents the SEM image (HITACHI SU 6600, Japan) of pure PPy at different magnifications. It was observed that polymerized PPy homopolymer contains aggregated spherical particles (Maponya et al., 2020). Fig. 2(c) represents the SEM

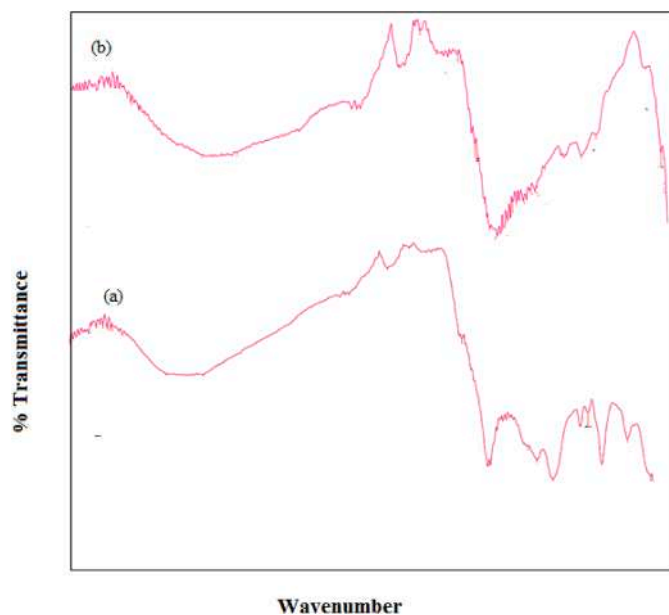


Fig. 1. FTIR of PPy - Fe_3O_4 - SW composite (a) before adsorption (b) after adsorption.

image of raw Polymer hybrid nano composite indicating the surface with heterogeneous pores produced due to the incorporation of surface functional groups. Pores of Fe_3O_4 were occupied by polypyrrole molecules and the active site was increased for MG adsorption. It was observed that the size of the spherical particles becomes reduced for Polymer hybrid nanocomposite (Bhaumik et al., 2016). This is due to the formation of nanocomposite through in-situ polymerization process greatly decreases the size and produced small sized agglomerates. Nevertheless, the polymerization will not alter the surface morphology of the nanocomposite. Seaweed acts as a stabilizer and prevents the growth of polypyrrole particles. It was observed that surface of nanocomposite become rough with more active absorption sites. These results proved that addition of polypyrrole and Fe_3O_4 can enhance the adsorption capacity. Fig. 2(d) represents the SEM image of polymer

hybrid after MG dye adsorption. Change in morphology was observed and accumulation of MG species on the surface of the composite conveys that adsorption has occurred. Furthermore, the SEM-EDS image (Fig. 3) displays the presence of chief constituents such as C, O, Fe, Cl and N.

3.2. Effect of hydrogen ion concentration

The effect of hydrogen ion concentration of the dye solution was examined in the range of 2–11 and it is depicted in Fig. 4. With a rise in solution pH, the removal capacity of nanocomposite increases and found to be maximum at neutral pH 7. To understand the effect of pH on RE, it is essential to have better knowledge about the surface nature of the composite. Zero point charge (pH_{ZPC}) provides clear knowledge regarding the surface charge of the nanocomposite. The pH_{ZPC} of nanocomposite was found to be 3.14 (Sarojini et al., 2021a) indicating that surface is positively charged at $\text{pH} > 3.14$ and negatively charged at $\text{pH} < 3.14$. MG is a cationic dye containing large number of positively charged alkyl amine groups. Highest % RE is obtained at neutral pH 7 due to the electrostatic attraction between positively charged groups of MG and negatively charged groups of nanocomposite. Under acidic conditions the presence of excess of hydrogen ions turns the surface of the composite into positive. The concentration of hydrogen ions in the solution protonates ($-\text{N}$ into $-\text{N}^+$) PPy and OH groups of seaweed (to produce OH^+). Therefore, electrostatic repulsion occurs between positively charged surface of composite and cationic dyes, thereby RE decreases. A rise in pH, the negative active sites of composite increases and the negative surface is most favorable for the sorption of MG dye via electrostatic attraction. Also, pK_a of MG is 4.52 and retains strongest basicity. At lesser pH, a low RE was observed, due to the strong basicity of MG. When solution $\text{pH} = \text{pK}_a$ of MG, it turns into half cationic and half non-ionic form. As the pH of the solution increased from 5 to 7, the cationic characteristics gets inhibited. The physical surface forces and hydrogen bonding with nanocomposite contributed to better removal (Baek et al., 2010). Moreover the colour of MG remains unaffected under acidic and neutral pH. Meanwhile, most of the adsorbents seemed to be highly effective in adsorbing MG under alkaline conditions. However, high alkaline conditions might change the stability and structure of MG due to hydrolysis. At very high pH, MG solution tend to remain as colorless solution and no change is observed in adsorption of MG. Therefore to avoid hydrolysis of MG under high alkaline conditions

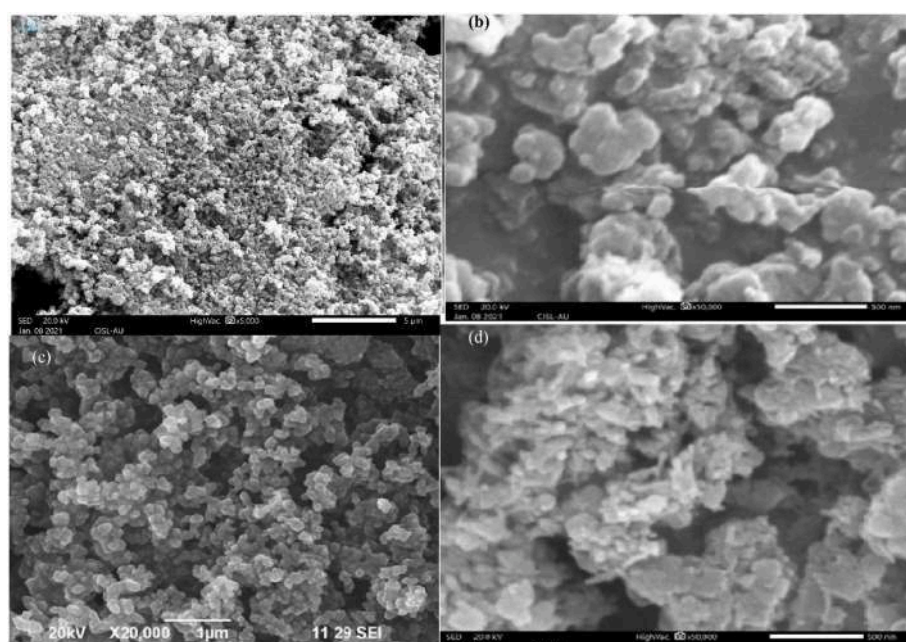


Fig. 2. SEM images of (a) & (b) Pure polypyrrole at different magnification (c) PPy - Fe_3O_4 - SW before adsorption (d) MG loaded PPy - Fe_3O_4 - SW after adsorption.

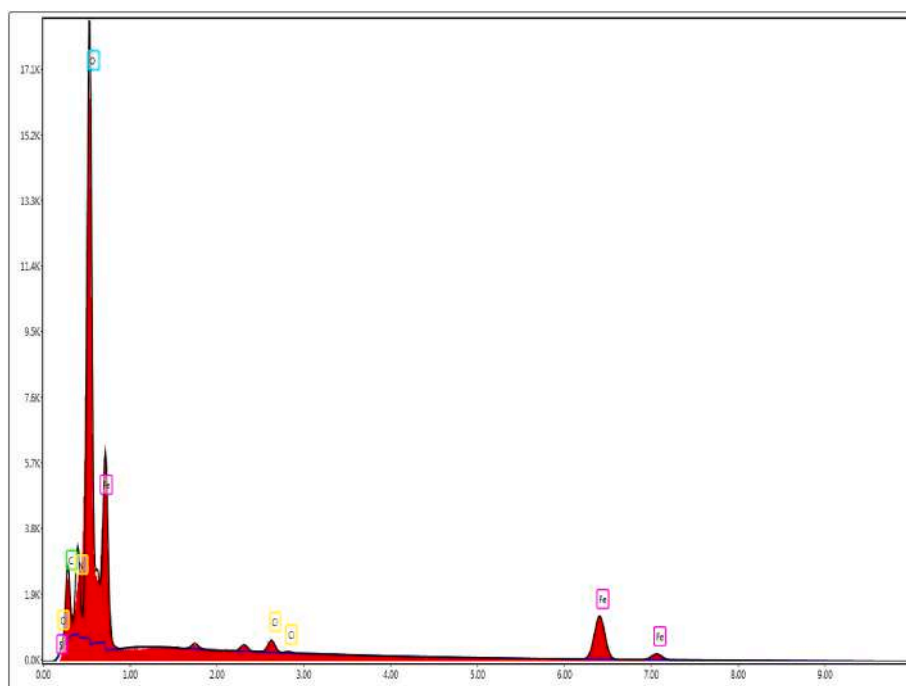


Fig. 3. EDS spectrum image of MG loaded on PPy - Fe_3O_4 -SW.

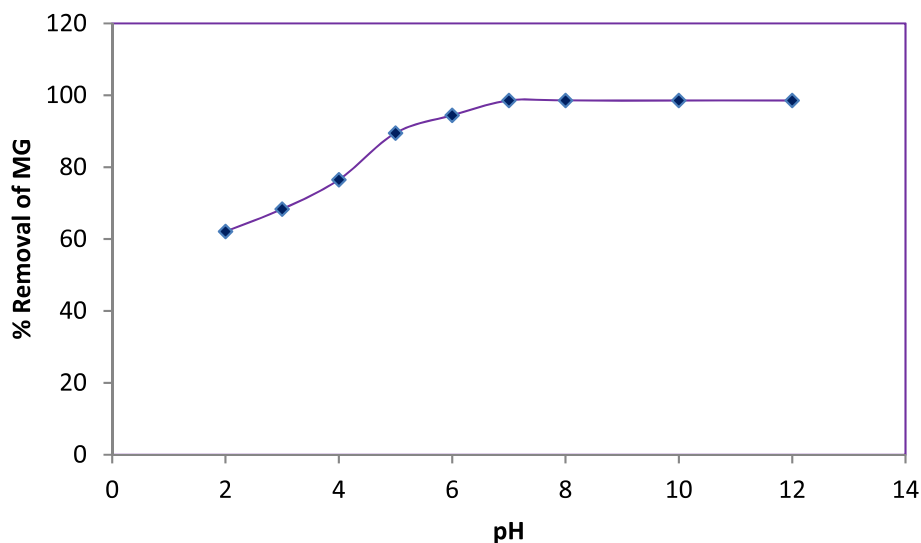


Fig. 4. Influence of pH on MG removal.

neutral pH was chosen an optimum value for this study. Similar effect was observed for MG dye RE using Graphene oxide decorated with cellulose and copper nanoparticle as sorbent (Khawaja et al., 2021).

3.3. Influence of sorbent dosage

Fig. 5 shows the influence of composite dosage on RE of dye. The MG dye removal were executed in the composite dosage range of 10 mg–100 mg. MG RE increases rapidly from 68.52 to 99.14% as the dosage gets increased from 10 mg to 50 mg and after that remains plateau. This result was pronounced due to the availability of large number of active sites and contact surface area at the composite surface. Therefore, 50 mg of adsorbent dosage was chosen as an optimum value. Studies on application of nanocomposites (Pandian et al., 2021a, 2021b) and algal biosorbent (Jayakumar et al., 2021) reported similar results

for the sorptive removal of solute.

3.4. Influence of initial MG dye concentration

The influence of initial MG dye concentration on % RE was determined by varying MG concentration from 10 to 200 mg/L. From the Fig. 6 it was observed that % RE rises gradually as MB concentration increases and reached a maximum due to the entrapment of more dye molecule as more active sites are available. Low concentration provides less diffusion resistance which facilitates easy movement of MG dye molecules from the synthetic wastewater. The optimum initial concentration was chosen as 150 mg/L. On further increase in dye concentration the decrease trend was found because at higher concentration the active sites get saturated, and repulsion occurs between adsorbed dye molecule and unreacted dye. Studies on removal of manganese

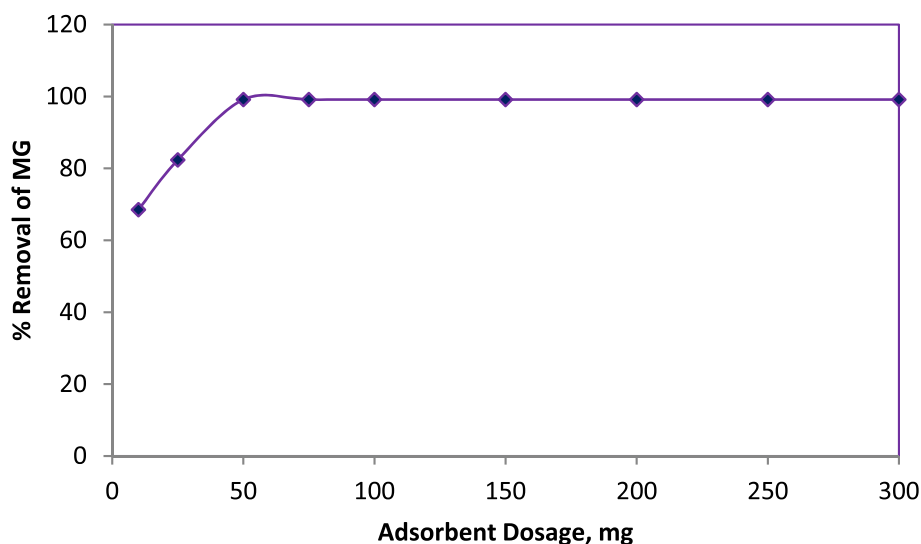


Fig. 5. Influence of sorbent dosage on MG removal.

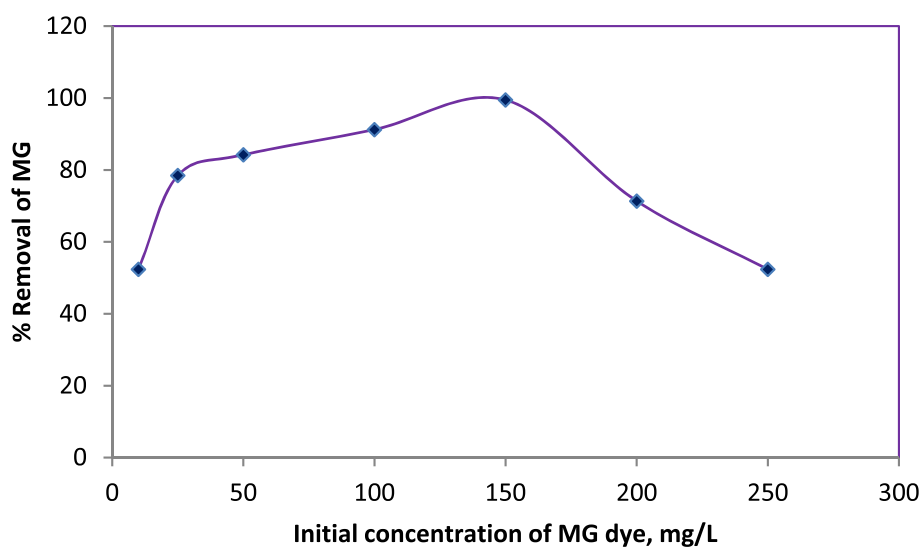


Fig. 6. Influence of initial MG concentration on MG removal.

(Rajamohan et al., 2020) and naphthol green-B (Gunasundari et al., 2020) by adsorption reported similar effects of initial pollutant concentration.

3.5. Influence of batch time

Batch contact time influences the duration and probability of solute-sorbent interaction. The effect of batch time is shown in Fig. 7 and it was noticed that the MG sorption was fast in the initial stage (0–15 min) and then it remains constant in later stage up to 40 min. This effect is probably due to the presence of multiple active sites at the beginning stage which favors electrostatic attraction. However as time proceeds, most of the active sites get filled with dye molecules and availability of functional group also gets reduced. At the equilibrium point a constant rate was obtained owing to the saturation of active sites of nanocomposite. Similar results for obtained for effect of time on removal of MG using mesoporous magnetic biochar composite (Eltaweil et al., 2020) and for removal of organic dyes onto polypyrrole based composites (Zhou et al., 2017). Therefore a contact time of 40 min was employed for all the experiments.

3.6. Influence of temperature

The influence of temperature on RE of MG onto Polymer hybrid nanocomposite was investigated in the range of 298–323 K. From the Fig. 8(a) it was noticed that RE of MB increased with increase in temperature. Rise in temperature alters the surface activity of the composite which tends to increase the RE. Higher temperature enhances activation energy of the nanocomposite which in turn promotes the adsorption capacity. Also increased temperature might have altered the physical forces of attraction between MG and composite. Further higher temperature provides more active sites on the surface of the nanocomposite for adsorption of MG molecules. This is in accordance with the literature (Gautam et al., 2018). The result indicated that the process of adsorption was endothermic.

3.7. Adsorption thermodynamics

To examine the nature of interaction and degree of spontaneity, thermodynamic parameters, namely ΔH° , ΔS° and ΔG° are required to be determined. The thermodynamic properties are determined by using Eqs (4) and (5):

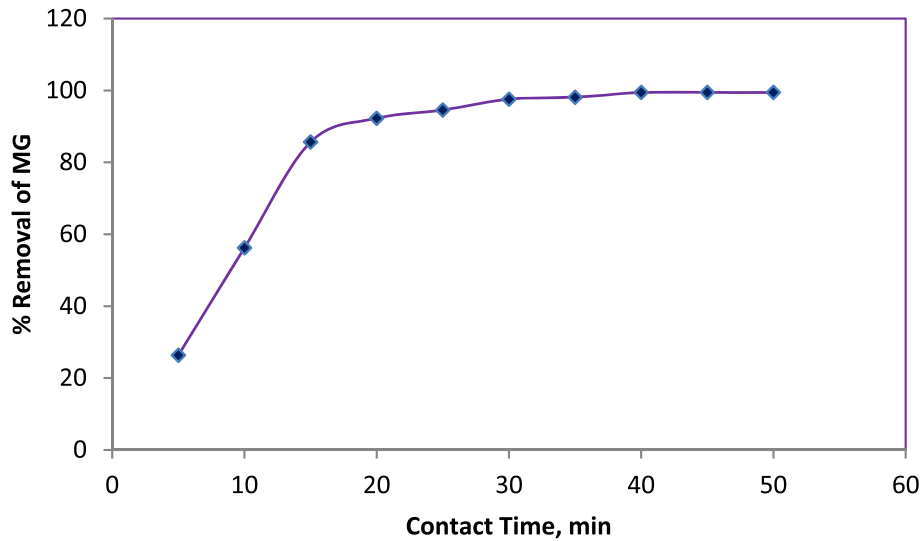


Fig. 7. Influence of contact time on MG removal.

$$\Delta G^0 = -RT \ln k \quad (4)$$

$$\Delta G^0 = \Delta H^0 - T\Delta S^0 \quad (5)$$

k - Equilibrium constant ($k = q_e/C_e$)

R - Universal gas constant (8.314 J/mol K)

T - temperature (K)

ΔH^0 - change in enthalpy (kJ/mol)

ΔG^0 - change in Gibbs free energy (kJ/mol)

ΔS^0 - change in entropy change (kJ/mol K).

The values of ΔH and ΔS were found from the plot, ΔG^0 versus T (Fig. 8(b)) and the estimated parameters are provided in Table 1. Negative ΔG showed that the process was feasible under the conditions tested and spontaneous in nature. The positive value of ΔS indicated the increase in randomness in treatment process of MG. The higher values of ΔH further specified that the sorption process was chemisorption which is > 20 kJ/mol and proved that the nature of process was endothermic. The thermodynamic parameters proved the favorable nature of the sorption process under the experimental conditions tested. From the Fig. 8 (b) it was observed ΔG^0 values decreases as temperature increases representing that sorption process was highly favorable at increased temperature.

3.8. Equilibrium sorption isotherm studies

An isotherm study was performed to have a detailed knowledge on relationship between pollutants concentration with the adsorbent surfaces and helps to optimize the usage of adsorbents in removal of pollutants from aqueous solution. The interaction between adsorbed molecule and sorbent surface was evaluated through equilibrium isotherm experiments. To perform equilibrium studies, Langmuir, Freundlich, Temkin and Dubinin-Radushkevich (D-R) isotherms were examined and fitted to the experimental data.

Langmuir isotherm.

The Langmuir equation (Langmuir, 1918) applies for monolayer sorption processes and is characterized by the Eq (6):

$$\frac{1}{q_e} = \frac{1}{q_m b C_e} + \frac{1}{q_m} \quad (6)$$

C_e - MG concentration at equilibrium (mg/l); q_m -MG dye uptake (mg/g); b - Sorption constant (L/mg).

Freundlich isotherm.

Freundlich isotherm (Freundlich, 1906) designates to multilayer process and the linear form is given by Eq (7):

$$\log_{10} q_e = \log_{10} K_f + \frac{1}{n} \log_{10} C_e \quad (7)$$

K_f (mg/g) represents Freundlich constant; n - adsorption intensity. Slope K_f and intercept $1/n$ were calculated from the graph of $\log_{10} q_e$ vs $\log_{10} C_e$.

Temkin isotherm.

The linear form of Temkin equation (Temkin and Pyzhev, 1940) is specified by Eq (8):

$$q_e = B \ln K_T + B \ln C_e \quad (8)$$

B (J/mol) denotes Temkin constants and K_T (L/g) represents binding energy.

D-R isotherm.

Linear form of D-R equation (Dubinin, 1960) helps to calculate apparent energy (E) and is represented as follows in the Eq (9):

$$\ln q_e = \ln q_m - \beta \varepsilon^2 \quad (9)$$

where ε -Polanyi potential

$$\varepsilon = RT \ln(1 + 1/C_e)$$

B - D-R isotherm constants (mol^2/kJ^2). The slope and intercepts are calculated from the plot of q_e versus ε^2 .

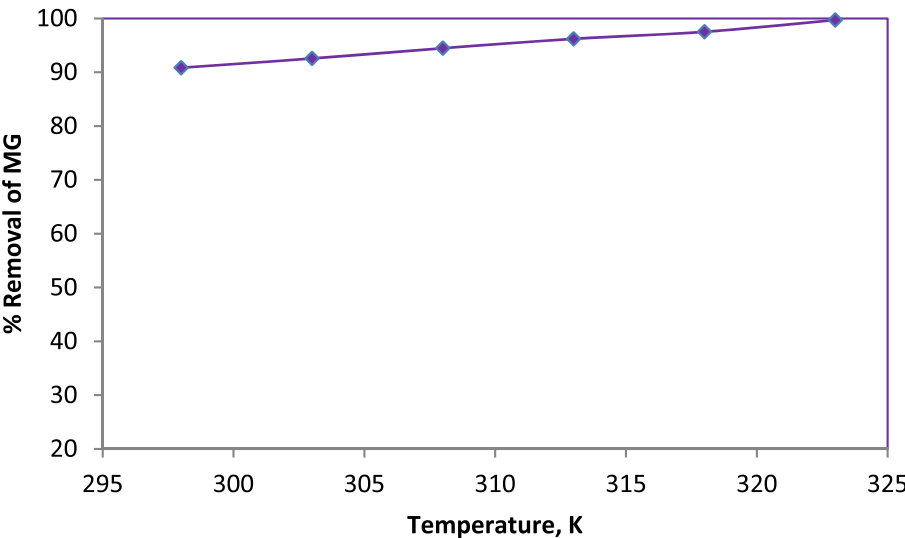
Apparent energy (E) is calculated by the Eq (10):

$$E = \frac{1}{\sqrt{-2\beta}} \quad (10)$$

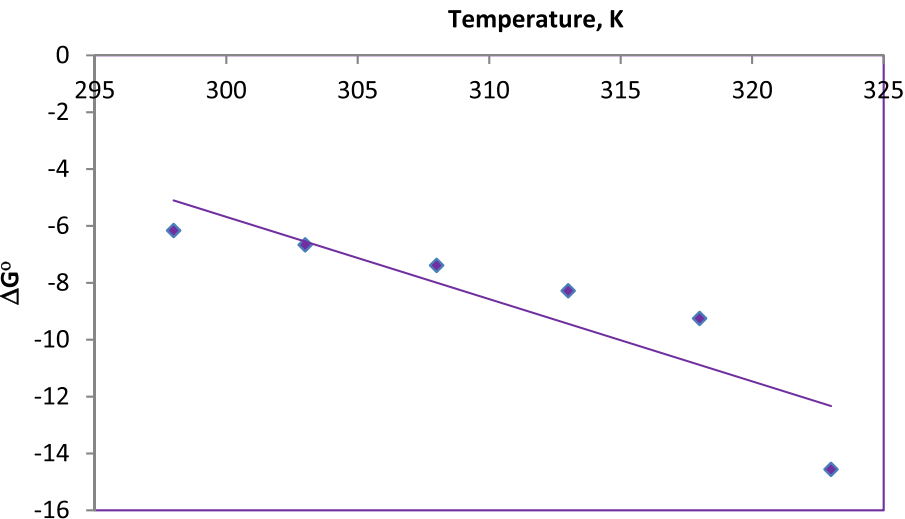
The isotherm constants were calculated from the graph of the isotherm models (Fig. 9). The selection was made on the basis of R^2 and adsorption capacity (q_{\max}) obtained by every model. The value of R^2 and the calculated experimental parameters are given in Table 2. The results showed that value of R^2 (0.996) was higher for Langmuir than other models suggesting that the MG adsorption equilibrium was demonstrated by monolayer coverage and is mainly due to the chemical reactions involved in the surface of adsorbent. Thus Langmuir model describes the chemisorption process.

3.9. Kinetics studies

Kinetics of MG removal was studied to predict the total reaction time along with rate controlling step and reaction pathways. The kinetics of MG adsorption was evaluated using the pseudo first order (PFO), pseudo second order (PSO), power function equation, Elovich and Intra-particle



(a) Influence of temperature on MG Removal



(b) Thermodynamics plot for the sorption of MG

Fig. 8. (a) Influence of temperature on MG Removal. (b) Thermodynamics plot for the sorption of MG.

Table 1
Thermodynamic parameters.

Temp(K)	ΔG° (kJ/mol)	ΔS° (kJ/mol k)	ΔH° (kJ/mol)
298	-6.161	0.2893	81.103
303	-6.665		
308	-7.385		
313	-8.281		
318	-9.249		
323	-14.556		

diffusion (IPD) models.

PFO equation (Ho, 2004) is given by Eq (11):

$$\log(q_e - q_t) = \log(q_e) - \frac{k_1 t}{2.303} \quad (11)$$

k_1 - PFO kinetics rate constant (min^{-1}). Slope (k_1) and intercept (q_e) is calculated from the graph of $\log(q_e - q_t)$ and t .

PSO model (Ho and McKay, 1999) is specified by Eq (12):

$$\frac{t}{q_t} = \frac{1}{h} + \frac{1}{q_e} t \quad (12)$$

$$h = \frac{1}{k_2 q_e^2}$$

k_2 - PSO rate constant (g/mg min) and t -time in minute

IPD equation (Weber and Morris, 1963) is represented by Eq (13):

$$q_t = k_{id} \sqrt{t} + c \quad (13)$$

k_{id} - rate constant of IPD ($\text{mg g}^{-1} \text{min}^{-0.5}$)

C - constant.

Elovich model (Juang and Chen, 1997) is represented by the Eq (14):

$$q_t = \frac{1}{\beta} \ln(\alpha\beta) + \frac{1}{\beta} \ln t \quad (14)$$

where α - constant of Elovich model ($\text{mg g}^{-1} \text{min}^{-1}$) and β - exponent in Elovich model (g mg^{-1}).

Fractional power kinetic equation (Muthu Kumara Pandian et al.,

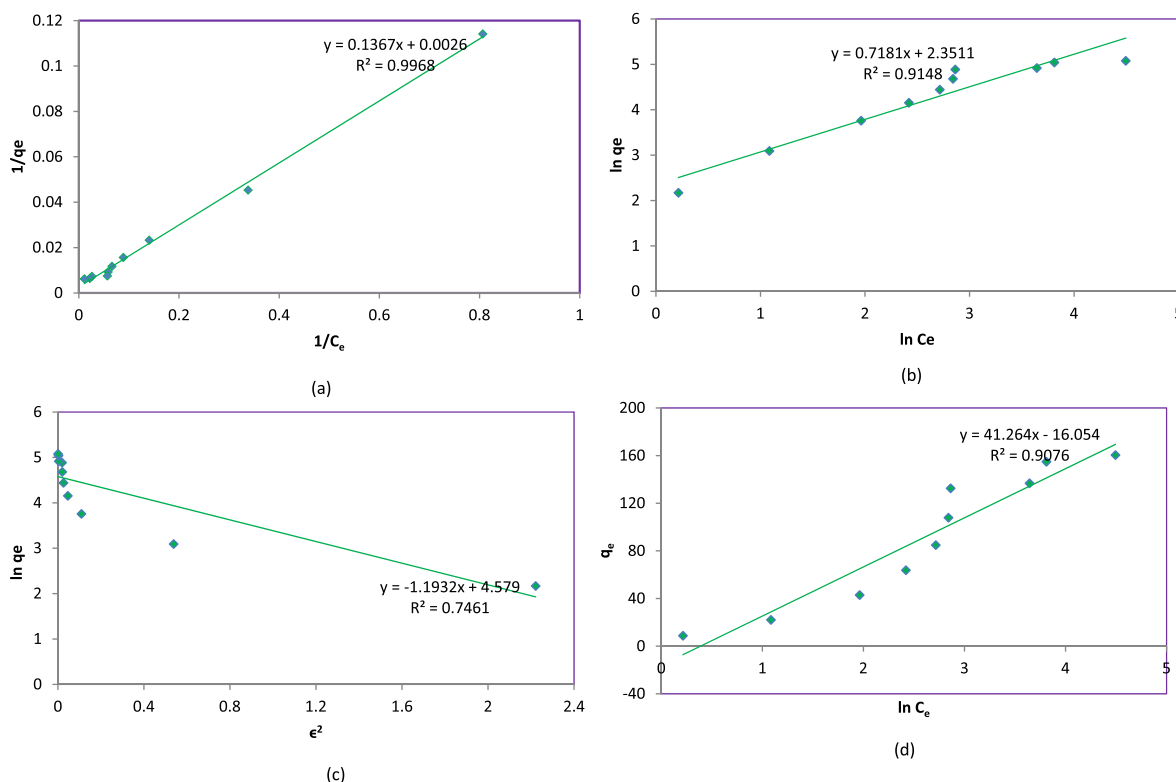


Fig. 9. Equilibrium modeling (a) Langmuir (b) Freundlich (c) Dubinin–Radushkevich, and (d) Temkin isotherm.

Table 2

Adsorption Isotherm data for removal of MG.

Isotherm model	Parameters	Value
Langmuir	q_m (mg/g)	384.61
	b (L/mg)	0.01902
	R^2	0.9968
Freundlich	K_f (L/mg)	10.50
	$1/n$	0.7181
	R^2	0.9148
Dubinin–Redushkevich	q_m (mg/g)	97.42
	β (mol ² /kJ ²)	1.1932
	E (kJ/mol)	0.647
	R^2	0.7461
Temkin	B (J/mol)	41.26
	K_T (L/mg)	1.475
	R^2	0.9076

2017) is indicated by the Eq (15):

$$\log q_t = \log k + v \log t \quad (15)$$

Where v and k were calculated from graph of $\log q_t$ versus $\log t$.

The linearized plots of Eqs. (11)–(15) are presented in Fig. 10a, b, 10c, 10d and 10e respectively. The values of rate constants and kinetic parameters are reported in Table 3. PSO model fitted well to the experimental data and lower value of k_2 suggests that adsorption of MG is governed by chemical reaction. The regression coefficient of PFO model is slightly lower than PSO model. Therefore PSO model describes the kinetics of adsorption of MB on nanocomposite follows chemisorption mechanism via electrostatic interaction and hydrogen bonding.

3.10. Adsorption mechanism

The mechanism of adsorption of MG by Polymer hybrid nanocomposite is influenced by various factors including surface charge density of the interacting species, structure, electrostatic interactions,

hydrogen bonding, etc. The pH_{zpc} of seaweed was found to be 6.8 (Fig. 11). The surface of seaweed remains positively charged when $pH < pH_{zpc}$ due to the protonation of OH and NH_2 functional groups. For $pH > pH_{zpc}$ the surface becomes negatively charged due to the deprotonation of hydroxyl, carbonyl, carboxyl, and phosphate groups (Moham-madi et al., 2017). Therefore, uptake of cationic dyes is electrostatically possible at $pH > pH_{zpc}$. The pH_{zpc} of Fe_3O_4 particles are found to be 6.2 (Fig. 11) which is well supported by related studies (Gautam et al., 2015). In this case, pH_{zpc} of nanocomposite (3.2) was less than that of pH_{zpc} of seaweed and Fe_3O_4 particles. From this result it was clearly understood that the surface of nanocomposite was highly modified with more negative functional groups. Addition of seaweed in Polymer hybrid nanocomposite makes the adsorbent to enclose large number of carboxyl (-COO) and hydroxyl (-OH) groups which helps to bind cationic dye easily (Zwane et al., 2019). Also polypyrrole provides more nitrogen containing functional groups and decreased the agglomeration of Fe_3O_4 particles (Ghoviland et al., 2015). This developed negative charged surface aids in the attraction of positively charged dye molecules and higher RE was obtained (Zhou et al., 2017).

The chemical transformation of composite before and after MG adsorption analyzed using FTIR spectrum (Fig. 1) was taken for consideration to analyze the MG sorption mechanism. The presence of characteristic peaks of polypyrrole at 1541 cm^{-1} , 1052 cm^{-1} and 932 cm^{-1} attributes to polypyrrole stretching, conjugated C–N stretching, C–H stretching vibration and C–H deformation (Bhaumik et al., 2013). Characteristic peaks observed in raw nanocomposite were also present in MG loaded composite with some shift. A shift in band from 1650 cm^{-1} to 1421 cm^{-1} was observed which indicates that adsorption has occurred. This shift indicates that the involvement of polypyrrole in adsorption. Shift in the peaks were also observed in the range of $3000\text{--}3500\text{ cm}^{-1}$. This observation proves the involvement of hydroxyl group derived from seaweed provides active sorption sites and also reacts with MG. However, the peak at 1421 cm^{-1} corresponds to C=C stretching vibrations of benzene ring of MG. The peak at 1458 cm^{-1} attributes to C–C aromatic stretching of MG molecules (Haounati et al.,

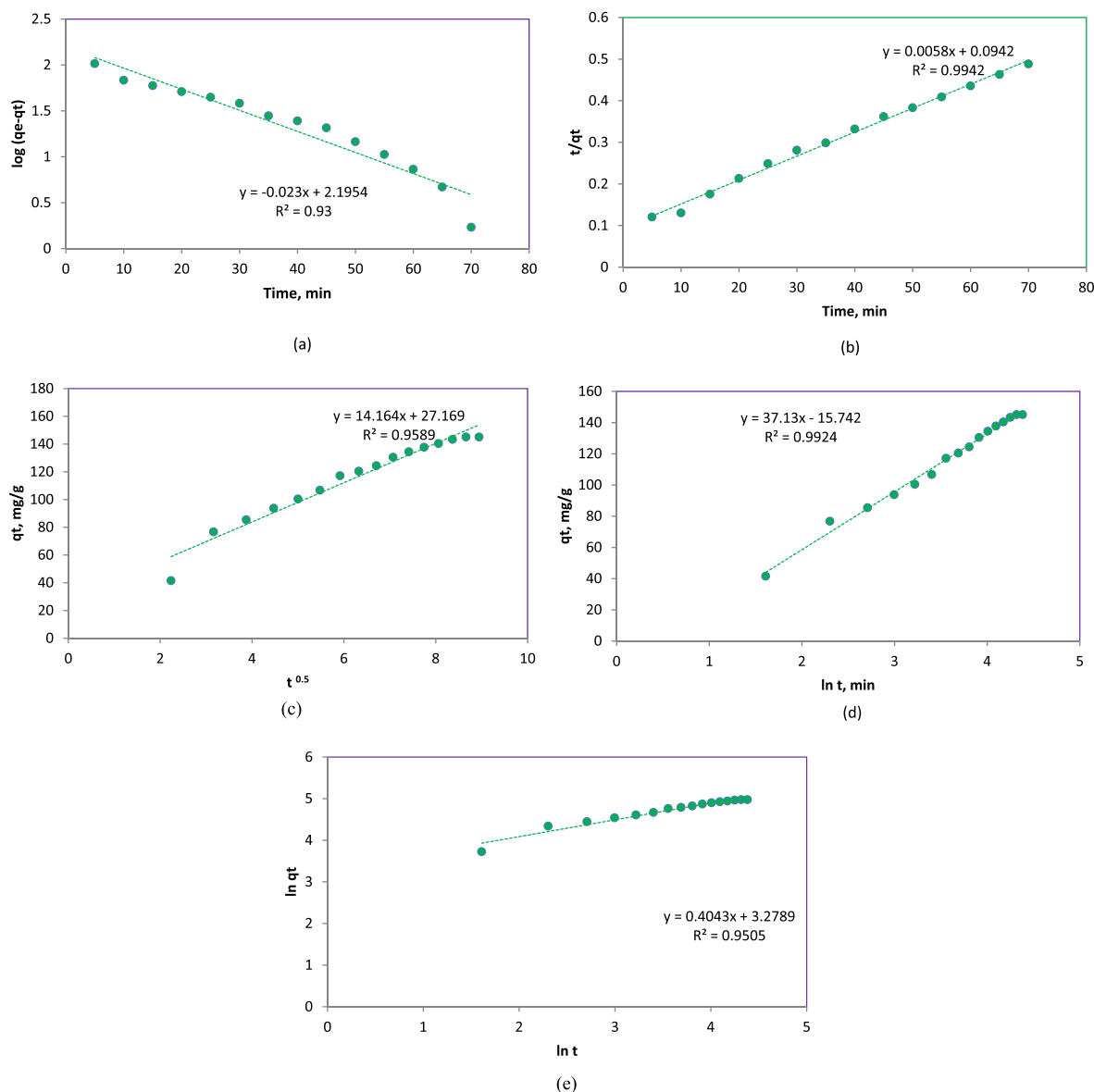


Fig. 10. Kinetic models (a) PFO (b) PSO (c) IPD (d) Elovich (e) Power function.

Table 3

Kinetic model parameter for MG removal.

Model	Parameters	Value
PFO	K_1 (min^{-1})	0.026
	R^2	0.963
PSO	K_2 ((g/mg.min)	0.000357
	R^2	0.9942
	q_e , cal (mg/g)	172.4138
IPD	K_{id} ((mg/g min ^{0.5}))	14.14
	R^2	0.9589
Elovich	α (mg/g min)	0.0269
	β (g/mg)	100.8085
	R^2	0.9924
Power function	K	26.5469
	V	0.404
	R^2	0.9509

2020). Thus, the result confirmed the sorption of MG on nanocomposite and sorption is due to the interaction occurring between nanocomposite and dye.

To further examine the removal mechanism, SEM images of bio-

nanocomposite after MG dye adsorption (Fig. 2(d)) were investigated. It was observed that there are large flocs instead of spherical particles due to MG adsorption. As the surfaces of the pores are occupied by MG molecules, the nanocomposite gets cohesive after adsorption and confirms the bonding of MG molecules with nanocomposite (Mokhtar et al., 2017).

The attainment of appreciable RE of MB is due to the incorporation of PPy with seaweed and Fe_3O_4 , as they provide a large number of active sites. Presence of hydrophilic groups on the surface of the composite namely hydroxyl and carboxylic groups increases the dispersion ability of nanocomposite in water. Additionally positive charges in MG were positioned onto nitrogen and hydrogen atoms whereas negative charges were fixed on carbon atoms. Also, MG possess three edge sites with high positive charges such as alkyl amine groups $-\text{N}(\text{CH}_3)_2$ and $=\text{N}(\text{CH}_3)_2^+$ and low positive charged benzene ring. These groups make MG to remain cationic (Tian et al., 2016). The negatively charged hydroxyl group and carboxylic group available on the surface of the nanocomposite interact with positively charged alkyl amine groups of MG via electrostatic attraction (Fig. 12). Apart from electrostatic interaction, chemical bonding also occurs between positively alkyl amine groups and oxides. Furthermore, hydrogen bonding occurs between hydroxyl

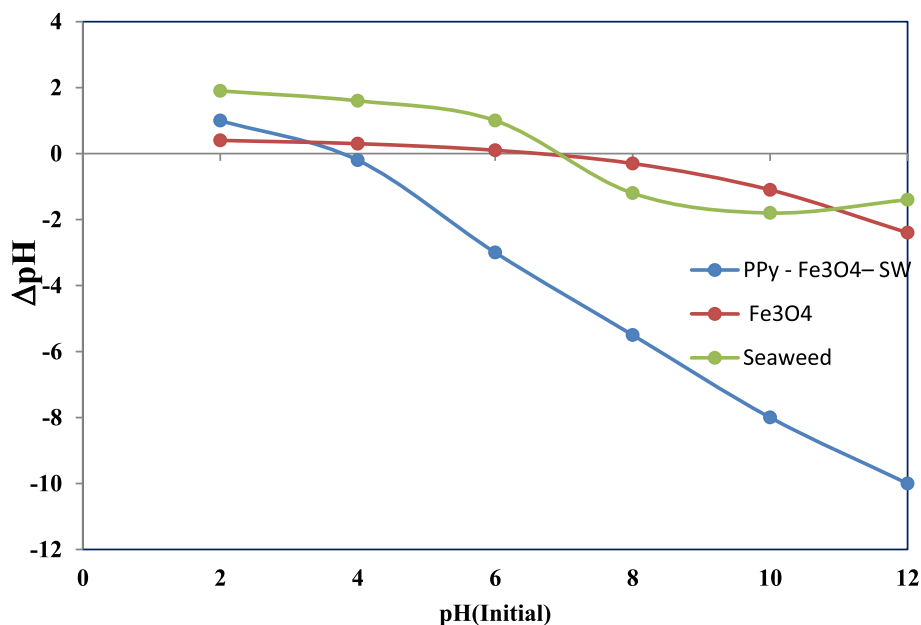


Fig. 11. Point of zero charge (pH_{ZPC}) estimation.

groups of nanocomposite and hydrogen atoms of positively charged alkyl amine groups. Also, hydrogen bonding was formed between ($-\text{N}^+$) species of polypyrrole and hydrogen species of benzene ring. π - π interaction was expected to occur between aromatic rings of MG and aromatic rings of polymer chain. Also van der Waals forces of attraction exists between dye and cell wall of seaweed. The combined efforts of electrostatic attraction, hydrogen bonding, chemical bonding, π - π interaction and van der Waals forces of attraction might have increased the adsorption ability. The electrostatic attraction and hydrogen bonding were the primary mechanisms involved in the adsorption of MG. Fig. 13 represents the possible interactions between polymer coated adsorbent surface and MG cationic species.

3.11. Comparison with other sorbents

Iron oxide supported polymer composite is stable, natural and safe metal oxide composite. The combinations with PPy increased the MG RE. Moreover, iron oxide is not subjected to oxidation and simplified the separation of composite from the solution. Furthermore, the cost estimation suggests that synthesis of composite was cheap. Comparison of the sorption ability with other sorbents is given in Table 4 and found that the nanocomposite contributes better performance. To achieve better sustainability and large scale production nanocomposite should be prepared from low cost and easily available raw materials by eco-friendly method. The synthesis method followed for the preparation of

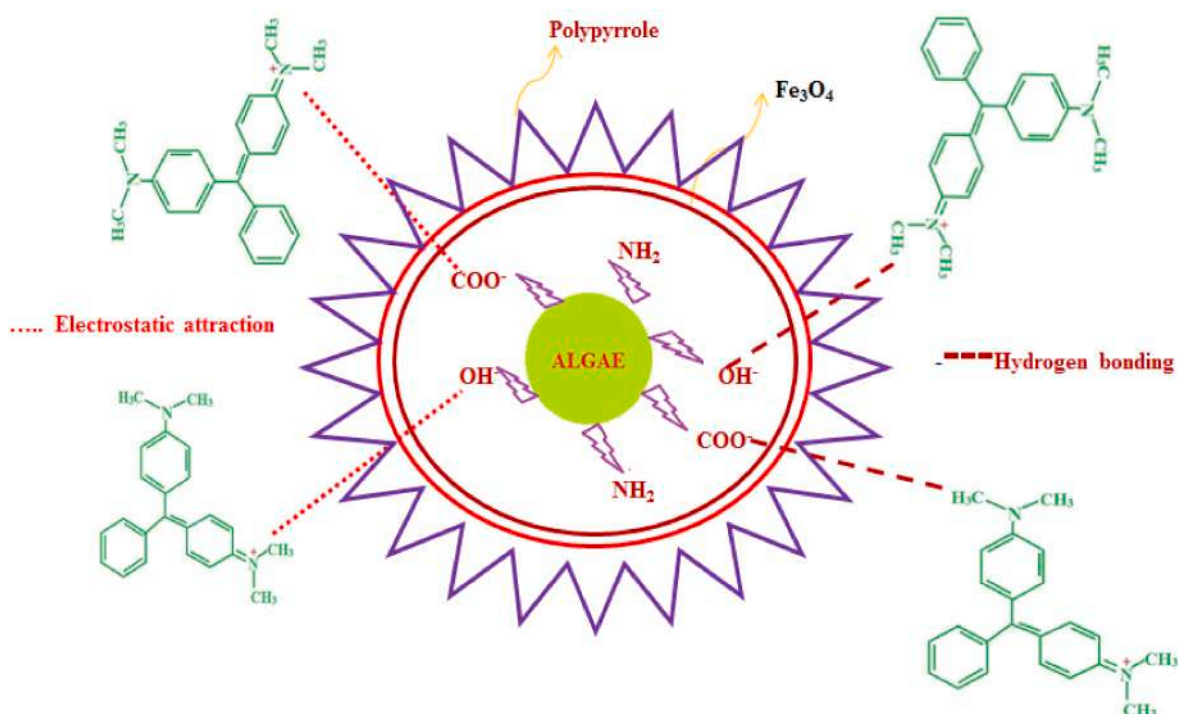


Fig. 12. Possible mechanism between MG dye molecule and functional groups associated with algae present in the nanocomposite.

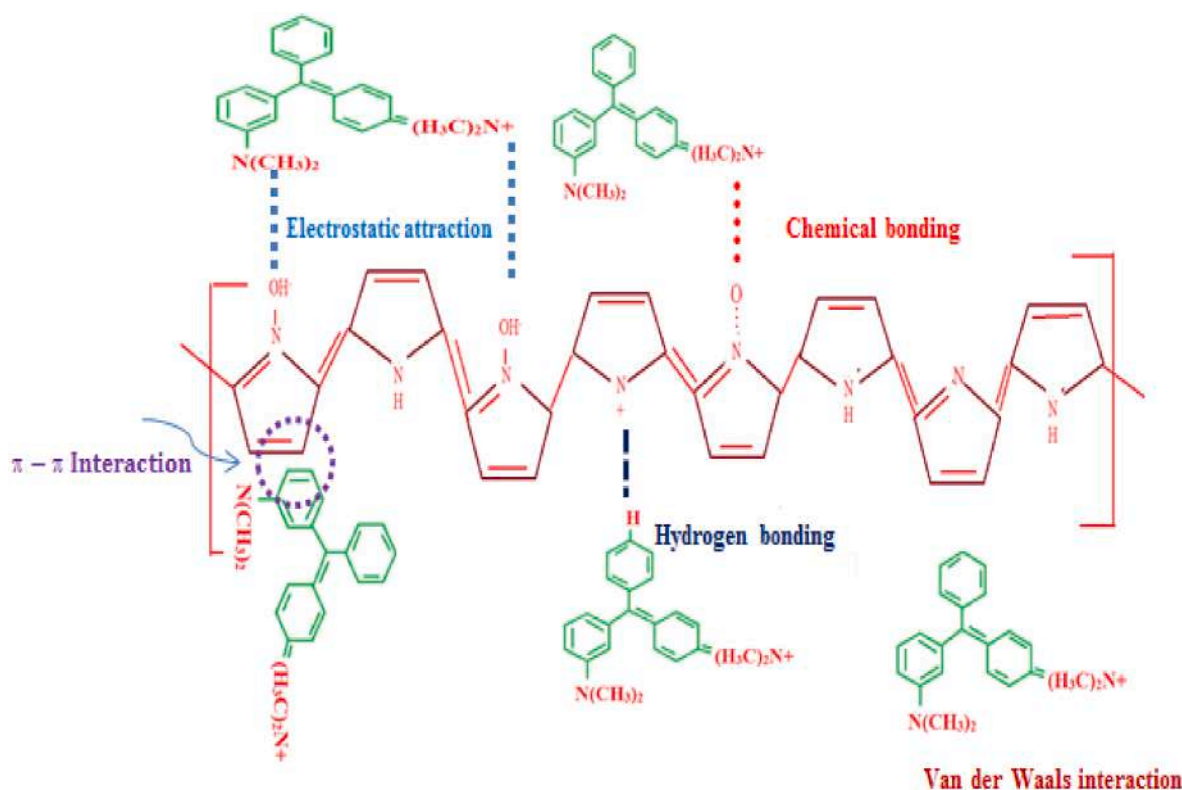


Fig. 13. Possible mechanism between polymer coated adsorbent surface and MG cationic species.

synthesized Polymer hybrid nanocomposite used in this study is simple, less time consuming inexpensive and processed at moderate conditions. Seaweed is selected as the starting material because of its easy availability, abundance and low cost. The production of Fe_3O_4 is also simple and cost-effective. The maximum removal of 99.79% of MG was achieved in the present study.

3.12. Adsorbent regeneration

To estimate its economic significance, the reusability of composite was investigated for five consecutive cycles. The results were

Table 4
Malachite green uptake capacity reported in various studies.

Adsorbent	Adsorption capacity, mg/g	Reference
Lemon peel	51.7	Kumar (2007)
Rice straw derived char	148.7	Hameed et al. (2008)
Chitosan bead	93.5	Bekci et al. (2009)
Rice husk-AC	63.85	Sharma et al. (2009)
Turbinaria conoides	66.66	Rajeshkannan et al. (2010a)
Hydrilla Verticillata	69.88	Rajeshkannan et al. (2010b)
Tamarind seed	54.95	Rajeshkannan et al. (2011)
Wheat bran	59.52	Rajeshkannan et al. (2012)
Magnetic chitosan/GO	76.9	Fan et al. (2013)
Walnut shell	90.8	Dahri et al. (2014)
Silver nanoparticles - (<i>Allium sativum</i>)	54.05	Muthu Kumara Pandian et al. (2016a)
Silver nanoparticles - (<i>Aspergillus flavus</i>)	60.24	Muthu Kumara Pandian et al. (2016b)
Silver nano particles - (Chemical)	64.52	Muthu Kumara Pandian et al. (2017)
Almond gum	172.41	Bouaziz et al. (2017)
Chitosan composite	4.8	Arumugam et al. (2019)
nZVI/BC composite	515.77	Eltaweil et al. (2020)
CO-CEL-Cu nanocomposite	208.80	Khawaja et al. (2021)
Polymer hybrid	384.615	This work

represented in Fig. 14 and found that RE remains 90% even after four cycles which predicts good stability and activity of the composite inherited from combination of PPy and seaweed. The magnetic property of the composite promotes easier separation and reuse.

4. Conclusion

The hybrid polymer bio-nanocomposite was synthesized and utilized as adsorbent for the effective removal of MG from synthetic wastewater. The process of adsorption depends on pH, sorbent dosage, contact time and temperature. The maximum removal of 99.79% was achieved at optimized conditions. The surface analysis tests confirmed the sorption of MB onto polymer hybrid composite. The monolayer sorption was described by Langmuir isotherm and the maximum uptake capacity of bio-nanocomposite was estimated as 384.61 mg/g. The dye removal kinetics was represented by PSO model and the mechanism involved in adsorption was described. The thermodynamic data showed that the MG adsorption was through chemisorption. Negative values of ΔG , positive values of ΔS and ΔH revealed that treatment of MG process is spontaneous, random and endothermic process. This study concludes that Polymer hybrid nanocomposite is a promising adsorbent for the removal of cationic dyes from wastewater.

Author contributions

G.Sarojini: Conceptualization, Methodology, Investigation, Validation, Writing – original draft. **S.Venkatesh Babu:** Writing – review & editing Supervision. **N. Rajamohan:** Conceptualization, Resources, Writing – review & editing. **M. Rajasimman:** Characterization, Methodology, Formal analysis, Supervision, Writing – review & editing

Declaration of competing interest

The authors declare that they have no known competing financial interests or personal relationships that could have appeared to influence

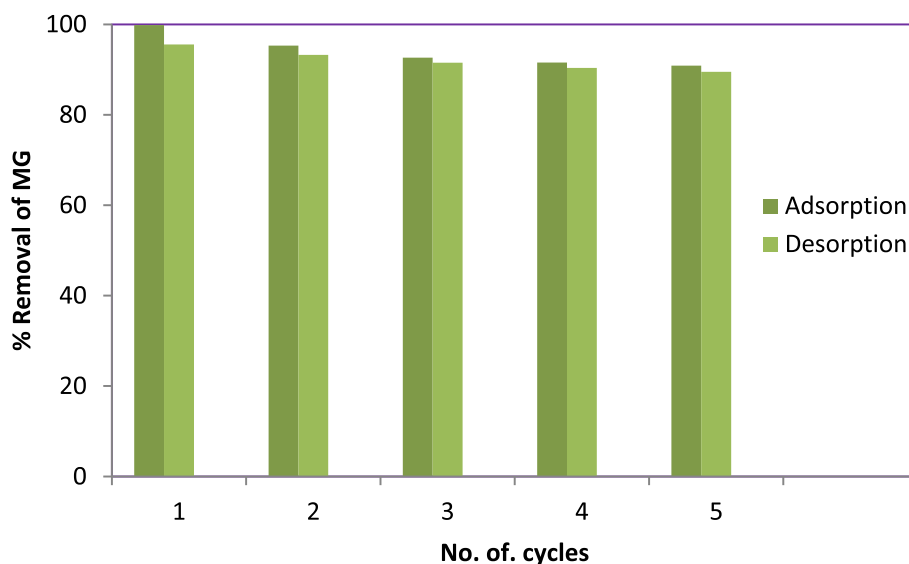


Fig. 14. Regeneration and reuse of nanocomposite for MG dye sorption.

the work reported in this paper.

References

- Adeyi, A.A., Jamil, S.N.A.M., Abdullah, L.C., Choong, T.S.Y., 2019. Adsorption of malachite green dye from liquid phase using hydrophilic thiourea-modified poly (acrylonitrile-co-acrylic acid): kinetic and isotherm studies. *J. Chem.*, 4321475, 2019.
- Arumugam, T.K., Krishnamoorthy, P., Rajagopalan, N.R., Nanthini, S., Vasudevan, D., 2019. Removal of malachite green from aqueous solutions using a modified chitosan composite. *Int. J. Biol. Macromol.* 128, 655–664.
- Baek, M.H., Ijagbemi, C.O., Se-Jin, O., Kim, D.S., 2010. Removal of malachite green from aqueous solution using degraded coffee bean. *J. Hazard Mater.* 176 (1–3), 820–828.
- Bekki, Z., Seki, Y., Cavas, L., 2009. Removal of malachite green by using an invasive marine alga *Caulerpa racemosa* var. *cyllindracea*. *J. Hazard Mater.* 161 (2–3), 1454–1460.
- Bhaumik, M., Agarwal, S., Gupta, V.K., Maity, A., 2016. Enhanced removal of Cr (VI) from aqueous solutions using polypyrrole wrapped oxidized MWCNTs nanocomposites adsorbent. *J. Colloid Interface Sci.* 470, 257–267.
- Bhaumik, M., McCrindle, R., Maity, A., 2013. Efficient removal of Congo red from aqueous solutions by adsorption onto interconnected polypyrrole-polyaniline nanofibres. *Chem. Eng. J.* 228, 506–515.
- Bouaziz, F., Koubaa, M., Kallel, F., Ghorbel, R.E., Chaabouni, S.E., 2017. Adsorptive removal of malachite green from aqueous solutions by almond gum: kinetic study and equilibrium isotherms. *Int. J. Biol. Macromol.* 105, 56–65.
- Dahri, M.K., Kooh, M.R.R., Lim, L.B., 2014. Water remediation using low cost adsorbent walnut shell for removal of malachite green: equilibrium, kinetics, thermodynamic and regeneration studies. *J. Environ. Chem. Eng.* 2 (3), 1434–1444.
- Dawood, S., Sen, T., 2014. Review on dye removal from its aqueous solution into alternative cost effective and non-conventional adsorbents. *J. Chem. Process Eng.* 1, 1–11.
- Dubinin, M.M., 1960. The potential theory of adsorption of gases and vapors for adsorbents with energetically non-uniform surface. *Chem. Rev.* 60, 235–266.
- Eltaweil, A.S., Ali Mohamed Eman, H., Abd El-Monaem, M., El-Subriti, G.M., 2020. Mesoporous magnetic biochar composite for enhanced adsorption of malachite green dye: characterization, adsorption kinetics, thermodynamics and isotherms. *Adv. Powder Technol.* 31, 1253–1263.
- Fan, L., Luo, C., Sun, M., Qiu, H., Li, X., 2013. Synthesis of magnetic β -cyclodextrin-chitosan/graphene oxide as nano-adsorbent and its application in dye adsorption and removal. *Colloids Surf. B Biointerfaces* 103, 601–607.
- Freundlich, H.M.F., 1906. Over the adsorption in solution. *J. Phys. Chem.* 57, 385–471.
- Gautam, D., Kumari, S., Ram, B., Chauhan, G.S., Chauhan, K., 2018. A new hemi-cellulose-based adsorbent form malachite green. *J. Environ. Chem Eng.* 6 (4), 3889–3897.
- Gautam, R.K., Gautam, P.K., Banerjee, S., Soni, S., Singh, S.K., Chattopadhyaya, M.C., 2015. Removal of Ni(II) by magnetic nanoparticles. *J. Mol. Liq.* 204, 60–69.
- Ghovilani, H., Yamini, Y., Dayeni, M., Seidi, S., Tahmasebi, E., 2015. Adsorptive removal of alizarin red-S and alizarin yellow GG from aqueous solutions using polypyrrole-coated magnetic nanoparticles. *J. Environ. Chem. Eng.* 3 (1), 529–540.
- Goswami, B., Mahanta, D., 2020. Polyaniline-Fe₃O₄ and polypyrrole-Fe₃O₄ magnetic nanocomposites for removal of 2, 4-dichlorophenoxyacetic acid from aqueous medium. *J. Environ. Chem. Eng.* 8, 103919.
- Gunasundari, E., Kumar, P.S., Rajamohan, N., Vellaichamy, P., 2020. Feasibility of naphthol green-B dye adsorption using microalgae: thermodynamic and kinetic analysis. *Desalin. Water Treat.* 192, 358–370.
- Hameed, B., El-Khaiary, M., 2008. Kinetics and equilibrium studies of malachite green adsorption on rice straw-derived char. *J. Hazard Mater.* 153 (1–2), 701–708.
- Haounati, R., Quachtak, H., El Haouti, R., Akhouairi, S., Largo, F., Akbal, F., Benlhachemi, A., Jada, A., Ait Addi, A., 2020. Elaboration and properties of a new SDS/CTAB@Montmorillonite organoclay composites a superb adsorbent for the removal of malachite green from aqueous solution. *Separ. Purif. Technol.* 255, 117335.
- Ho, Y.S., 2004. Citation review of Lagergren kinetic rate equation on adsorption reactions. *Scientometrics* 59, 171–177.
- Ho, Y.S., McKay, G., 1999. Pseudo-second order model for sorption processes. *Process Biochem.* 34, 451–465.
- Hong, Y., Shi, H., Shu, X., Zheng, Y., Zhang, Y., Wu, Y., 2017. Controlled synthesis of hollow magnetic Fe₃O₄ nanospheres: effect of the cooling rate. *Particuology* 33, 24–28.
- Jayakumar, V., Govindaradjane, S., Rajamohan, N., Rajasimman, M., 2021. Biosorption potential of brown algae, *Sargassum polycystum*, for the removal of toxic metals, cadmium and zinc. *Environ. Sci. Pollut. Res.* (in press).
- Juang, R.S., Chen, M.L., 1997. Application of the Elovich equation to the kinetics of metal sorption with solvent-impregnated resins. *Ind. Eng. Chem. Res.* 36, 813–820.
- Khawaja, H., Zahir, E., Asghar, M.A., 2021. Graphene oxide decorated with cellulose and copper nanoparticle as an efficient adsorbent for the removal of malachite green. *Int. J. Biol. Macromol.* 167, 23–34.
- Kumar, K.V., 2007. Optimum sorption isotherm by linear and non-linear methods for malachite green onto lemon peel. *Dyes Pigments* 74 (3), 595–597.
- Kushwaha, A.K., Gupta, N., Chattopadhyaya, M.C., 2014. Removal of cationic methylene blue and malachite green dyes from aqueous solution by waste materials of *Daucus carota*. *J. Saudi Chem. Soc.* 18, 200–207.
- Langmuir, I., 1918. The adsorption of gases on plane surface of glass, mica and platinum. *J. Am. Chem. Soc.* 40, 1361–1368.
- Maponya, T.C., Ramohlola, K.E., Kera, N.H., Modibane, K.D., Maity, A., Katata-Seru, L. M., Hato, M.J., 2020. Influence of magnetic nanoparticles on modified polypyrrole/m-phenylenediamine for adsorption of Cr(VI) from aqueous solution. *Polymers* 12, 679.
- Mohammadi, M., Izadbakhsh, E., Ehsandoost, E., 2017. Biosorption of cadmium as toxic metal from aqueous solutions by marine green algae *Ulva compressa* (Linnaeus). *Res. J. Environ. Toxicol.* 11, 28–34.
- Mokhtar, N., Aziz, E.A., Aris, A., Ishak, W.F.W., Mohd Ali, N.S., 2017. Biosorption of azo-dye using marine macro-alga *Eucheima spinosum*. *J. Environ. Chem. Eng.* 5, 5721–5731.
- Muliwa, A.M., Leswif, T.Y., Onyango, M.S., Maity, A., 2016. Magnetic adsorption separation (MAS) process: an alternative method of extracting Cr(VI) from aqueous solution using polypyrrole coated Fe₃O₄ nanocomposites. *Separ. Purif. Technol.* 158, 250–258.
- Muthu Kumara Pandian, A., Rajasimman, M., Karthikeyan, C., 2017. Isotherm and kinetic studies on adsorption of malachite green using chemically synthesized silver nanoparticles. *Nanotechnol. Environ. Eng.* 2, 2.
- Muthu Kumara Pandian, A., Karthikeyan, C., Rajasimman, M., 2016a. Isotherm and kinetic studies on nano-sorption of Malachite Green onto *Allium sativum* mediated synthesis of silver nano particles. *Biocatal. Agric. Biotechnol.* 8, 171–181.
- Muthu Kumara Pandian, A., Karthikeyan, C., Rajasimman, M., 2016b. Isotherm and kinetic studies on nano-sorption of malachite green onto *Aspergillus flavus* mediated synthesis of silver nano particles. *Environ. Nanotechnol. Monit. Manage.* 6, 139–151.
- Pandian, A.M.K., Rajasimman, M., Rajamohan, N., Varjani, S., Karthikeyan, C., 2021a. Anaerobic mixed consortium (AMC) mediated enhanced biosynthesis of silver nano particles (AgNPs) and its application for the removal of phenol. *J. Hazard Mater.* 416, 125717.

- Pandian, A.M.K., Gopalakrishnan, B., Rajasimman, M., Rajamohan, N., Karthikeyan, C., 2021b. Green synthesis of bio-functionalized nano-particles for the application of copper removal-characterization and modeling studies. *Environ. Res.* 197, 111140.
- Rajamohan, N., Kumar, P.S., Al Qasbi, F., Rajasimman, M., 2020. Separation of manganese from water using hybrid nanocomposite to control water pollution: kinetic and equilibrium modelling. *Int. J. Environ. Anal. Chem.* (in press).
- Rajeshkannan, R., Rajamohan, N., Rajasimman, M., 2009. Removal of malachite green from aqueous solution by sorption on hydrilla verticillata biomass using response surface methodology. *Front. Chem. Eng. China* 3 (2), 146–154.
- Rajeshkannan, R., Rajamohan, N., Rajasimman, M., 2010a. Removal of malachite green from aqueous solution by sorption on turbinaria conoids using response surface methodology. *Front. Environ. Sci. Eng. China* 4 (1), 116–122.
- Rajeshkannan, R., Rajamohan, N., Rajasimman, M., Sivaprakash, B., 2010b. Equilibrium and kinetic studies on sorption of malachite green using hydrilla verticillata biomass. *Int. J. Environ. Res.* 4 (4), 817–824.
- Rajeshkannan, R., Rajamohan, N., Rajasimman, M., 2011. Decolourization of malachite green using tamarind seed: optimization, isotherm and kinetic studies. *Chem. Ind. Chem. Eng. Q.* 17 (1), 67–79.
- Rajeshkannan, R., Rajamohan, N., Rajasimman, M., 2012. Removal of malachite green from aqueous solutions using wheat bran: optimization, equilibrium and kinetic studies. *Int. J. Environ. Eng.* 4 (1/2), 1–23.
- Rajeshkannan, R., Rajasimman, M., Rajamohan, N., 2013. Packed bed column studies for the removal of dyes using novel sorbent. *Chem. Ind. Chem. Eng. Q.* 19, 461–470.
- Ramezani, S., Pourbabaee, A., Daneshmand, J.H., 2013. Biodegradation of malachite green by *Klebsiella Terrigenaptcc* 1650: the critical parameters were optimized using Taguchi optimization method. *J. Bioremediat. Biodegradation* 4, 175.
- Sadeghi, S., Rad, F.A., Moghaddam, A.Z., 2014. A highly selective sorbent for removal of Cr(VI) from aqueous solutions based on Fe₃O₄/poly(methyl methacrylate) grafted Tragacanth gum nanocomposite: optimization by experimental design. *Mater. Sci. Eng. C* 45, 136–145.
- Sallam, S., El-Subruiti, G., Eltaweil, A., 2018. Facile synthesis of Ag-c-Fe₂O₃ superior nanocomposite for catalytic reduction of nitroaromatic compounds and catalytic degradation of methyl orange. *Catal. Lett.* 148, 3701–3714.
- Santhi, M., Kumar, P., Muralidharan, B., 2015. Removal of malachite green dyes by adsorption onto activated carbon-MnO₂-nanocomposite-kinetic study and equilibrium isotherm analyses. *IOSR J. Appl. Chem.* 8, 33–41.
- Sarojini, G., Venkateshbabu, S., Rajasimman, M., 2021a. Facile synthesis and characterization of polypyrrole - iron oxide -seaweed (PPy-Fe₃O₄-SW) nanocomposite and its exploration for adsorptive removal of Pb(II) from heavy metal bearing water. *Chemosphere* 278, 130400.
- Sarojini, G., Venkateshbabu, S., Rajamohan, N., Senthilkumar, P., Rajasimman, M., 2021b. Surface modified polymer-magnetic-algae nanocomposite for the removal of chromium- equilibrium and mechanism studies. *Environ. Res.* 201, 111626.
- Shanehsaz, M., Seidi, S., Ghorbani, Y., Shoja, S.M.R., Rouhani, R., 2015. Polypyrrole-coated magnetic nanoparticles as an efficient adsorbent for RB19 synthetic textile dye: removal and kinetic study. *Spectrochim. Acta A. Mol. Biomol. Spectrosc.* 149, 481–486.
- Sharma, Y., Singh, B., Uma, 2009. Fast removal of malachite green by adsorption on rice husk activated carbon. *Open Environ. Pollut. Toxicol. J.* 1, 74–78.
- Tian, L., Zhang, J., Shi, H., Li, N., Ping, Q., 2016. Adsorption of malachite green by diatomite:equilibrium isotherms and kinetic studies. *J. Dispersion Sci. Technol.* 37, 1059–1066.
- Temkin, M.J., Pyzhev, V., 1940. Kinetics of ammonia synthesis on promoted iron catalysts. *Acta Phy. Chem. URSS* 12, 217–256.
- Weber, W.J., Morris, J., 1963. Kinetics of adsorption on carbon from solution. *J. Sanit. Eng. Div.* 89, 31–60.
- Zwane, S., Masheane, M.L., Kuvarega, A.T., Vilakati, G.D., Mamba, B.B., Nyoni, H., Mhlanga, S.D., Dlamini, D.S., 2019. Polyethersulfone/Chromolaena odorata (PES/CO) adsorptive membranes for removal of Congo red from water. *J. Water Process Eng* 30, 100498.
- Zhou, J., Lu, Q.F., Luo, J.J., 2017. Efficient removal of organic dyes from aqueous solution by rapid adsorption onto polypyrrole-based composites. *J. Clean. Prod.* 167, 739–748.



Surface modified polymer-magnetic-algae nanocomposite for the removal of chromium- equilibrium and mechanism studies

G. Sarojini^{a,*}, S. Venkatesh Babu^b, N. Rajamohan^c, P. Senthil Kumar^d, M. Rajasimman^e

^a Department of Petrochemical Engineering, SVS College of Engineering, Coimbatore, India

^b Department of Petroleum Engineering, JCT College of Engineering & Technology, Coimbatore, India

^c Chemical Engineering Section, Sohar University, Oman

^d Department of Chemical Engineering, Sri Sivasubramaniya Nadar College of Engineering, Kalavakkam, Chennai, 603110, India

^e Department of Chemical Engineering, Annamalai University, Annamalai Nagar, India

ARTICLE INFO

Keywords:

Nanocomposite

Chromium

Polypyrrole

Mechanism

Isotherm

ABSTRACT

The present work explains the sorption ability of a novel nano-composite, Polypyrrole-iron oxide-seaweed (PPy-Fe₃O₄-SW), for Cr(VI) removal. The influence of operating parameters, namely pH, contact time, nano-composite dosage, initial Chromium concentration and operating temperature, on the hexavalent chromium removal was studied. The novel nano-composite was analyzed using FTIR, SEM and EDS to confirm the sorption of Cr(VI) and to understand the mechanism of sorption. PPy-Fe₃O₄-SW nano-composite removed 96.36% of Cr(VI) at the optimized conditions of pH = 2, temperature = 30 °C, initial Cr(VI) concentration = 50 mg/L, nanocomposite dosage = 100 mg and contact time = 30min. PPy-Fe₃O₄-SW nanocomposite has a maximum sorption capacity of 144.93 mg/g. The kinetic studies revealed that the metal adsorption obeys pseudo second order (PSO) model and the sorption was found to be monolayer in nature as confirmed by Langmuir isotherm ($R^2 > 0.9985$). Electrostatic interaction and ion-exchange are identified as the fundamental mechanisms for Cr(VI) sorption on PPy-Fe₃O₄-SW composite.

1. Introduction

Industrial development and expansion in production have contributed to the depletion of water resources and resulted in hazardous contamination. Water remains an important requirement both for human consumption and industrial production. Fast exploitation of underground water and increased release of toxic loads into the ecosystem has contributed to searching alternatives to reuse and recycle of wastewater. Wastewater from various industries containing hazardous metals like chromium(Cr), cadmium(Cd), copper(Cu), lead(Pb), nickel(Ni) and zinc(Zn) are discharged directly into fresh water thereby contaminating the fresh water. Heavy metals are non-biodegradable contaminants which create major problem to the environment due to their tendency to resist decomposition and ability to accumulate. Among various heavy metals, Cr is an anthropogenic hazardous metal released from various industries like plating, alloying, ceramic glasses, pressure treated lumber, pigments, tannery, dyes and refractory bricks (Losi et al., 1994; Barnhart, 1997; Durai and Rajasimman, 2011). Hexavalent chromium is highly toxic compared with trivalent form and its ingestion

causes epigastric pain, hemorrhage, dermatitis, ulcer and tissue necrosis (Yahya et al., 2020a). The environmental legislation of WHO require the concentration of Cr(VI) should not exceed 0.05 mgL⁻¹ (Levankumar et al., 2009). Various technologies namely reverse osmosis, chemical precipitation, photocatalytic degradation, flocculation, filtration, membrane separation, ion exchange and adsorption are employed to removal Cr(VI) (Cai et al., 2014; Rajasimman et al., 2009; Jayakumar et al., 2014, 2015; Selvi et al., 2019; Malathi et al., 2021). The physical separation method is better alternative for metal removal as they are less reactive (Rajamohan et al., 2014; Theerthagiri et al., 2018). Among those various conventional technologies, adsorption is recognized as a promising and potential process in the elimination of Cr(VI) as it owns great efficacy, simplicity in operation and reduced energy requirements (Yu et al., 2019). The efficiency of adsorption process depends on the nature of adsorbent used. Huge surface area, great porosity and high pore volume are the desirable properties of adsorbent. The adsorbents which are of synthetic origin are less preferred due to their non-biodegradability. Therefore it is recommended to synthesize adsorbent from naturally available low cost biomaterials

* Corresponding author.

E-mail address: grsarojini@gmail.com (G. Sarojini).

(Vijayaraghavan et al., 2005).

Heavy metal removal using biomaterials as adsorbent reduces the investment cost by 20%, operation cost by 36% and entire treatment cost by 28% when matched with several conventional technologies. Furthermore, usage of biomaterials makes the process an eco-friendly, economically feasible, rapid and reversible one with no sludge formation (Dwivedi, 2012). Agricultural wastes, industrial wastes, micro-organisms and macro-organisms are most widely used biomaterial adsorbents (Zahmatkesh et al., 2018). Recently seaweed are preferred as a promising sorbent owing to its low cost, abundance, low sensitivity to environment, high metals uptake and high retention capacity (Al-Homaidan et al., 2018). Seaweed possesses several active functionalities namely carboxyl, amine, amide, hydroxyl phosphate in the polysaccharides of cell wall (Davis et al., 2003). These functional groups promote selective uptake of metal ions through mechanisms like ion exchange, electrostatic interaction, complexation, adsorption and micro precipitation (Murphy et al., 2009). *Ulva lactuca* is a type of aquatic green seaweed algae present in large quantities in many coastal area and helpful in bioremediation of toxic heavy metals owing to its structure, large surface area and homogeneous distribution of active binding sites (Turner et al., 2007; Sari and Tuzen, 2008).

Nowadays magnetic nanomaterial has gained interest due to its superior magnetic properties, non-toxicity and surface area which promotes high removal efficiency, ease of separation and quicker operation (Dave and Chopda, 2014). However, usage of magnetic nanoparticles in wastewater treatment tends to form agglomerates and this difficulty could be overcome by encapsulating magnetic nanoparticles on supporting materials (Ilankoon, 2014). Seaweeds are chosen as a supporting material as they possess bioactive amines, sulfates, carboxyl and hydroxyl compounds which plays a major role in adsorption process.

Conducting polymers has proved as versatile adsorbents and are reported to possess high affinity towards various contaminants due to its higher surface contact area, sufficient high energy active sites, short mass diffusion length, thermal stability, insolubility in water and ease of synthesis with low cost (Bhaumik et al., 2013). Polypyrrole (PPy) is considered as important emerging conducting polymer due to its facile synthesis, adjustable conductivity, distinct transport properties and good environmental stability (Karmakar et al., 2017; Khan and Malook, 2017). A novel nanocomposite, polypyrrole - iron oxide - *Ulva Lactuca* nanocomposite, was synthesized to have the combined advantages of algae, magnetic nano particle and conducting polymers. The synthesized composite was applied to remove Cr(VI) from aqueous solution. There was no report for the removal of Cr(VI) using polypyrrole - iron oxide - *Ulva Lactuca* nanocomposite. Hence, the intention of the current work is to explore the adsorptive efficiency of synthesized polypyrrole - iron oxide - *Ulva Lactuca* nanocomposite in removal of Cr(VI). Characterization, kinetics studies and equilibrium studies are performed to explore the performance and mechanism of sorption.

2. Materials and methods

2.1. Chemicals used

Ferric chloride, Ferrous sulphate, Sodium Hydroxide, potassium dichromate and acetone were procured (Fisher Scientific, India). Pyrrole (C_4H_5N) (99.9% pure) was procured as analytical reagent (Sigma Aldrich, India). Pyrrole was further purified by vacuum distillation and stored at below 0°C in dark. The chemicals employed in the experiments were of analytical grade. The synthesized PPy - Fe_3O_4 - SW nanocomposite (Sarojini et al., 2021) was used as adsorbent in this work.

2.2. Preparation of standard stock solution

About 2.835 g of analytical grade potassium dichromate was dissolved in deionized water to prepare 1000 mg/L solution of Cr(VI) and serial dilution was practiced to prepare other concentrations.

2.3. Characterization of nanocomposite

The Fourier transform infrared analysis (Shimadzu, Japan) is performed under the spectrum array of 4000–400 cm^{-1} to categorize the functionalities of the adsorbent. The surface organization of nanocomposite (prior and post adsorption) was investigated by means of scanning electron microscopy (Hitachi SU 6600, Japan). The composition analysis of nanocomposite was performed with an energy dispersive spectrometer (EDS) attached to a SEM instrument. X-ray diffraction (XRD) analysis was performed using XPert PRO-Diffractometer (Shimadzu XRD 6000, Japan) having Cu K α radiation ($\lambda = 0.154$ nm) with variable slits at 45kV/40 Ma.

2.4. Point of zero charge

Point of zero charge (pH_{PZC}) method was performed to identify the point where the nanocomposite surface charge remains neutral (Farahani et al., 2011). When pH equals pH_{PZC} , the surface has no charge (Mestre et al., 2014). In sorption studies, it is very essential to have detailed understanding regarding surface properties of any sorbent. The surface charge was calculated by pH drift method using 0.01 N NaCl. About 5.0 mg of nanocomposite was added to a series of solutions containing NaCl and pH of the solution was varied from 2 to 12 with addition of 0.01 N HCl and 0.01 N NaCl. The initial pH of all solutions were noted and the solutions were shaken for 12 h to attain equilibrium. The point at which initial pH equals final pH was termed as point of zero charge (pH_{PZC}).

2.5. Sorption equilibrium experiments

The sorption experiments were accomplished to investigate the influence of solution pH, nanocomposite dosage, initial concentration of Cr(VI) and temperature. To examine the influence of several parameters, the sorption studies were performed in conical flask and agitated at 500 rpm and 40 °C. The Cr(VI) concentration was modified to required concentration from $K_2Cr_2O_7$ standard stock solution. About 50 mg of nanocomposite was introduced to 50 mL of 100 mg/L of Cr(VI) ion solution and the sorption experiment was performed at 40 °C for 30 min. At fixed time interval, the samples were taken to measure the residual concentration using UV-Vis absorption spectroscopy. The solution pH was varied from 2 to 8 to investigate the pH influence. The effect of contact time (10–50 min) was investigated by carrying out the experiment at the optimized pH. In order to optimize the variables and to study the effect of parameters, sorption experiments were performed by changing initial Cr(VI) concentration (50–250 mg/L), nanocomposite dosage (50–140 mg), and temperature (303–333 K).

The amount adsorbed at equilibrium, q_e , and Cr(VI) percentage removal efficiency (RE) were calculated as given below in Eqs. (1) and (2):

$$q_e = \frac{(C_0 - C_e)V}{m} \quad (1)$$

$$\text{Removal Efficiency of Cr (\%)} = \frac{C_0 - C_e}{C_0} * 100 \quad (2)$$

q_e (mg/g) - sorption capacity under equilibrium condition; C_0 & C_e - Cr (VI) concentration at initial and equilibrium conditions (mg/L); V (L) - volume and m (g) - mass of nanocomposite (sorbent).

2.6. Desorption

The desorption experiments were performed with various concentrations of NaOH and HCl. The composite was washed with excess alkali/acid and deionized water with respect to reuse the composite. The desorption efficiency was calculated using Eq. (3):

$$\text{Desorption efficiency} = \frac{\text{Amount of metal ions desorbed}}{\text{Amount of metal ion adsorbed}} \times 100 \quad (3)$$

3. Results and discussion

3.1. Characterization studies

The FTIR band of the Cr(VI) sorbed composite was given in Fig. 1 and small peaks in the category of 689.942 cm^{-1} are representative peaks of iron oxide and distinct wide band peak in the array of $3400\text{--}3250 \text{ cm}^{-1}$ correspond to N–H enlarging peak of PPy (Bhaumik et al., 2011a,b). These outcomes point out the existence of iron oxide and PPy in the composite. Distinctive peaks of 1541 and 1341 cm^{-1} are consigned to the symmetric and anti-symmetric ring stretching modes of PPy. The characteristic peak at 1052 cm^{-1} accredits to C–H deformation vibration of PPy (Ma et al., 2009). The sharp peak at 934 cm^{-1} is attributed to C–H in-plane vibration and out of plane vibration of PPy (Zhang et al., 2008). The distinguishing peak observed in the range of $3000\text{--}3500 \text{ cm}^{-1}$ are considerably sharper due to the involvement of NH group of PPy in the sorption process of Cr(VI). The intensity of amine stretching band declined after Cr(VI) sorption (Bayramoglu and Arica, 2011).

3.2. SEM analysis

SEM analysis was performed to investigate the surface modification of composite after sorption. SEM analysis of composite before and after sorption is given in Fig. 2(a) & (b) respectively. SEM result of Fig. 2 (a) showed the synthesized composite has nearly regular and uniform particles resembling spherical structure. The presence of small globules and porous surface which aids for the diffusion of sorbate can be observed. Iron oxide particles are completely covered by spherical particles of pyrrole and form multiple agglomerated particles with voids due to weak inter-particle interactions. After adsorption it turned to smooth as sorbent apertures and active surface have been completely entrapped by Cr(VI) ions. A reduction in particle size was noticed. This might be due to the dissolution of the reactive materials from the nanocomposite and chromium ions might have deposited into the nanocomposite surface. Further, it suggests that the chromium ions not only gets adsorbed on the surface of the composite but also reacted with the reactive species present inside the core of the nanocomposite thus producing a change in morphology.

Fig. 3 displays the spectrum and the elements of PPy- Fe_3O_4 -SW from EDS analysis. The spectrum of PPy- Fe_3O_4 -SW reveals that C, N, Fe, N and

O are the major components in the synthesized composite. The presence of Cr peak along with prime elements established the sorption of Cr(VI) onto synthesized composite.

3.3. XRD analysis

Fig. 4 (a) & 4(b) depicts the XRD patterns of the nanocomposite before and after adsorption of Cr(VI). The presence of broad peak at $2\theta = 25^\circ$ is the characteristic peak of PPy. The main peaks at $2\theta = 30.093^\circ$, 35.421° and 43.050° are characteristic peak of Fe_3O_4 . The peak at $2\theta = 21.50^\circ$ is the characteristic peak of seaweed (Sarojini et al., 2021). Thus, the results proved the presence of seaweed, Fe_3O_4 and polypyrrole in the nanocomposite. It is visualized from Fig. 4(b) there is no change in the XRD pattern of nanocomposite after adsorption. This might be described by the fact that Cr(VI) were removed by the nanocomposite through ion exchange mechanism.

3.4. Point of zero charge (pH_{PZC})

The pH_{PZC} of PPy- Fe_3O_4 -SW was calculated as 3.8 (where initial pH equals final pH) from Fig. 5, and at this pH, net surface charge of composite is neutral. The composite surface below this value is positively charged and therefore anionic adsorption is more effective. For pH above pH_{PZC} , the surface of PPy- Fe_3O_4 -SW remains negatively charged favoring for cationic sorption. At $\text{pH} < \text{pH}_{\text{PZC}}$, the sorption of Cr(VI) was more because of strong electrostatic attraction between positively charged PPy- Fe_3O_4 -SW composite and HCrO_4^- . At $\text{pH} > \text{pH}_{\text{PZC}}$, the sorption was lesser due to repulsion between negatively charged PPy- Fe_3O_4 -SW composite and CrO_4^{2-} .

3.5. Effect of pH

In sorption process, pH is a significant factor that controls the sorption of Cr(VI) ions and determines the sorption capacity. Solubility, degree of ionization of the sorbate, active functional groups and sorbent surface properties are seriously affected by pH of the solution. Influence of pH was examined in the range varying from 2 to 8. From the Fig. 6, it was inferred that the maximum removal efficiency (RE) of Cr(VI) occurs at lower pH. The removal efficiency was maximum at acidic pH of 2 because of the strong electrostatic force of attraction between H^+ ions on the surface of the sorbent and HCrO_4^- . At lower pH, presence of excess hydrogen ions promotes easier coordination with the functional groups of amino and carboxyl groups of sorbent. Also lower pH promotes the

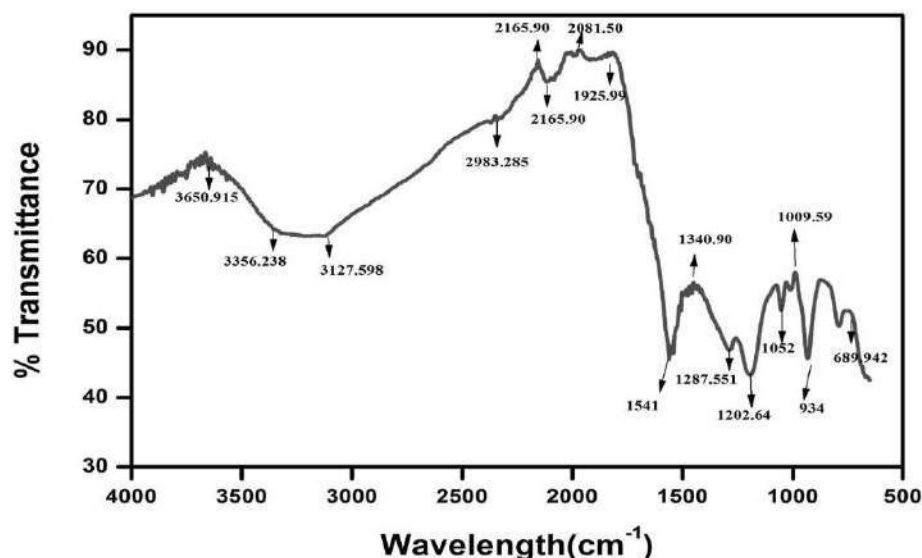


Fig. 1. FTIR of Cr(VI) loaded on raw PPy - Fe_3O_4 - SW.

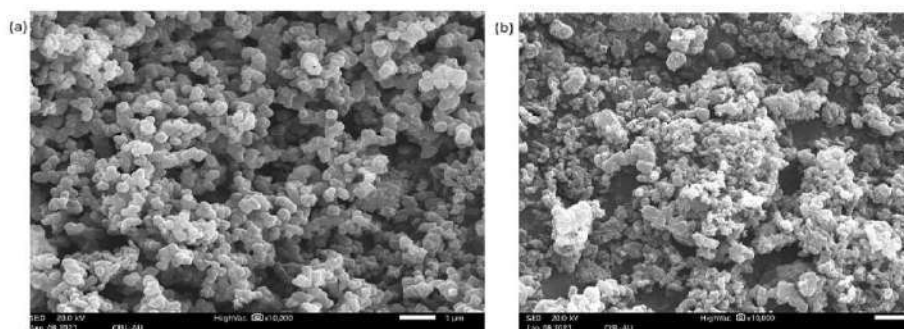


Fig. 2. SEM images of (a) raw PPY - Fe_3O_4 - SW nanocomposite (b) PPY - Fe_3O_4 - SW: after sorption.

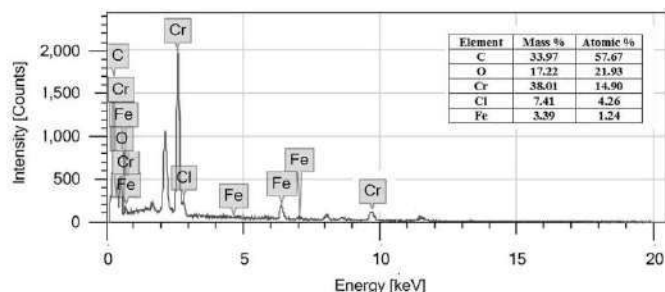


Fig. 3. EDS spectrum of PPY - Fe_3O_4 - SW after adsorption.

sorbent surface with more positively charged groups whereby binding of anionic Cr(VI) ions to positively charged groups is enriched leading to higher removal. At acidic conditions, up to pH 6, the Cr(VI) species is present in the form of HCrO_4^- and $\text{Cr}_2\text{O}_7^{2-}$ oxyanions which become CrO_4^{2-} at higher pH (Garg et al., 2017). At higher pH there was a decrease in proton ion prompted by the generation of negative hydroxyl ions which causes repulsion between Cr(VI) and sorbent. At higher pH, deprotonation of the nitrogen atoms of the polypyrrole matrix might occur and hence removal efficiency decreases (Rapti et al., 2016).

3.6. Effect of contact time

The influence of contact time on metal removal efficiency was examined between 10 min and 50 min. From Fig. 7, it was witnessed that during initial stage the removal efficiency increases gradually. During initial stage, the sorbent embraces extremely large active pores for metals uptake (Bakhtiari and Azizian, 2015). The sorption was faster during first 20 min and reaches equilibrium at 50 min with a removal efficiency of 92.45%. With increase in time, concentration difference between sorbent and metal ions decreases and results in attainment of adsorption equilibrium. Further, it was observed that increase of time did not create any substantial impact on removal efficiency as sorbent surface gets saturated.

3.7. Effect of nanocomposite dosage

Nanocomposite dosage is an essential controlling factor which determines the economy of the process and surface area available for contact. A set of experiment was carried out to evaluate the minimum dosage of sorbent needed to eliminate entire chromium ions. The consequence of nanocomposite dosage on Cr(VI) removal was performed in the range of 50–140 mg/L. The removal efficiency was 70.22% at 50 mg/L and increased to 92.45% at 100 mg/L. From Fig. 8, it was noticed that removal efficiency increases with sorbent dosage as availability of active pores and more surface area on the sorbent surface that promotes the sorption process are high. Meanwhile it was noticed that the increase in sorbent dosage (above 100 mg/L) did not produce

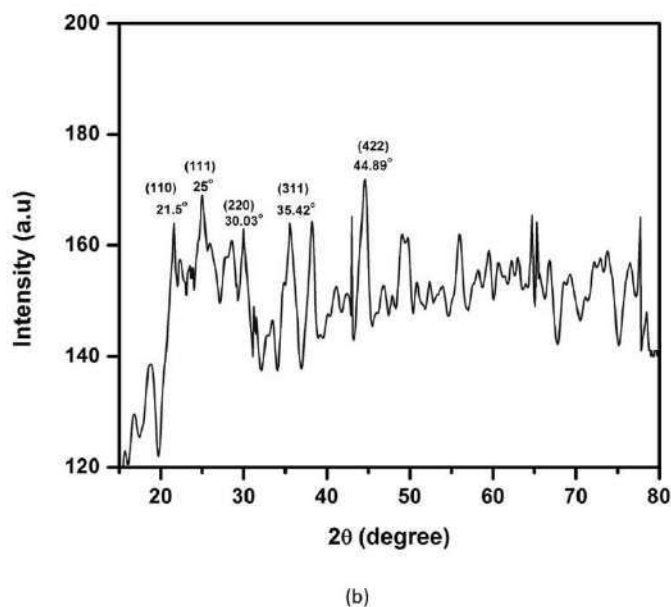
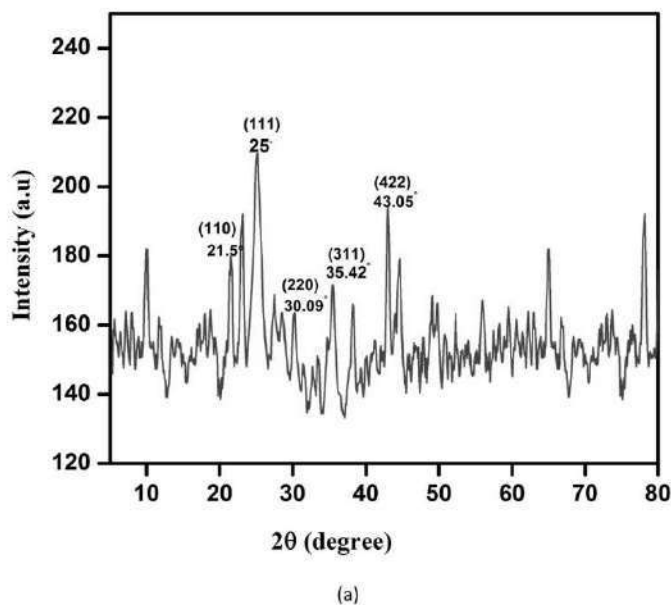


Fig. 4. XRD of PPY - Fe_3O_4 - SW (a) before adsorption (b) after adsorption.

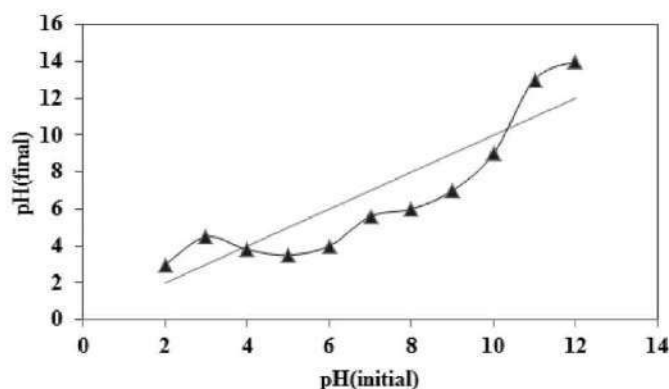
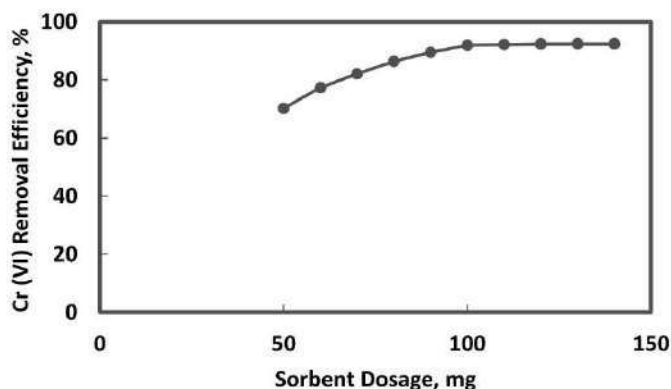
Fig. 5. Plot for pH_{ZPC} determination of PPy- Fe_3O_4 -SW before adsorption.

Fig. 8. Effect of Nanocomposite dosage on Cr(VI) removal.

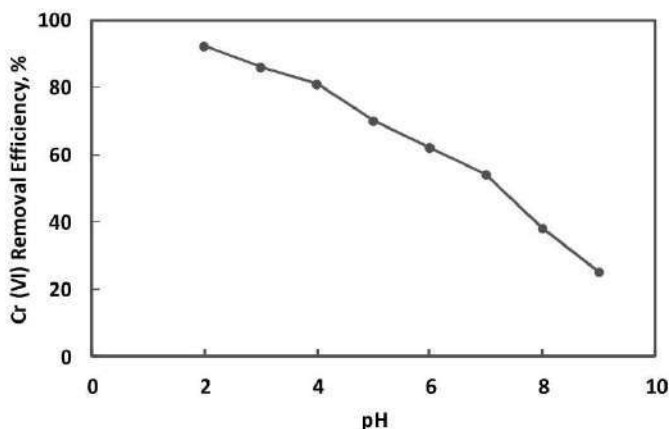


Fig. 6. Effect of initial pH on Cr(VI) removal.

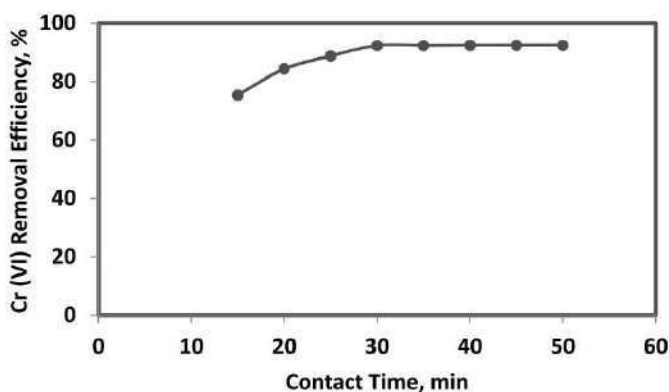


Fig. 7. Effect of contact time on Cr(VI) removal.

any change in removal efficiency.

3.8. Effect of initial chromium concentration

The removal efficiency of Cr(VI) decreases with increase in Cr(VI) metal ion concentration. Sufficient active sites are present at low concentration which enhanced the sorption efficiency. Further increase in initial concentration causes increased number of adsorbed molecules which reduces removal efficiency. From Fig. 9, it was inferred that, as the initial Cr(VI) concentration was increased from 50 to 250 mg/L, the RE of Cr(VI) decreased from 96.44% to 63.04%.

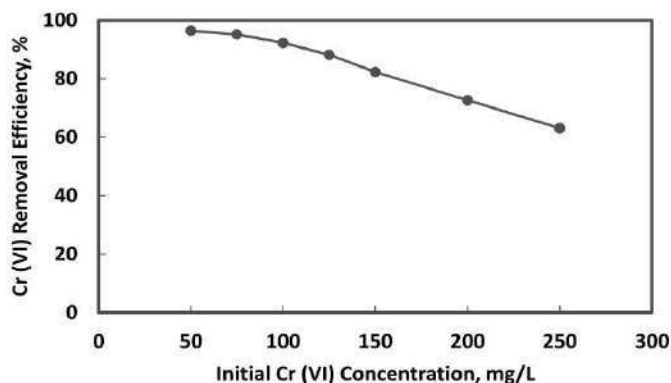


Fig. 9. Effect of initial Chromium concentration on Cr(VI) removal.

3.9. Effect of temperature

The influence of temperature was explored by changing the process temperature from 303 K to 333 K. It is noticed from Fig. 10, that the removal efficiency increased as temperature increases which might be attributed to higher thermal energy of chromium ions. The increased removal efficiency at high temperature shows the endothermic nature of the Cr(VI) sorption. Higher temperature accelerates the ions mobility as a result the interaction between metal ion and composite surface increases. The optimum conditions were: pH-2, temperature - 30 °C, initial Cr(VI) - 50 mg/L, nanocomposite dosage - 100 mg and contact time - 30 min.

3.10. Equilibrium adsorption study

To perform equilibrium study, the following isotherm models were examined for relating the sorption equilibrium data:

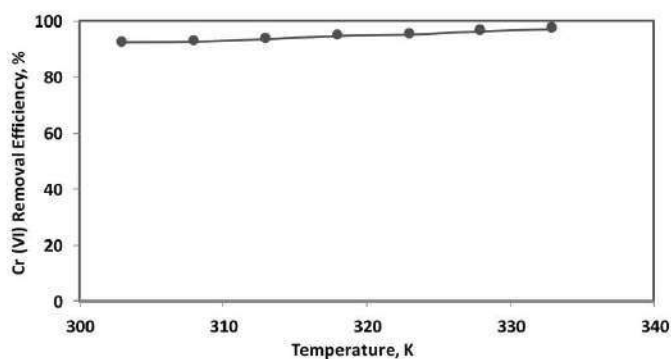


Fig. 10. Effect of temperature on Cr(VI) removal.

The Langmuir isotherm (Langmuir, 1918) is characterized by the resulting Eq (4):

$$\frac{1}{q_e} = \frac{1}{q_m b C_e} + \frac{1}{q_m} \quad (4)$$

C_e - equilibrium concentration (mg/L); q_m - maximum monolayer adsorbing capacity (mg/g); b - Langmuir constant representing the attraction of binding sites (L/mg).

The linearized equation of Freundlich isotherm (Freundlich, 1906) is given below as Eq (5):

$$\log q_e = \log K_f + \frac{1}{n} \log C_e \quad (5)$$

where K_f represents Freundlich isotherm capacity (mg/g); $1/n$ - adsorption intensity. Linear plot of $\log q_e$ vs $\log C_e$ produces a straight line with slope K_f and intercept $1/n$ and presented in Table 2. For enhanced adsorption studies the value of $1/n$ should be between 0 & 1. The $1/n$ value of 0.3101 confirms the sorption of chromium.

The Temkin isotherm (Temkin and Pyzhev, 1940) is specified by Eq. (6):

$$q_e = B \ln K_T + B \ln C_e \quad (6)$$

where B and K_T denotes Temkin constants (J/mol) and binding energy (L/g) respectively. The plot of q_e vs $\ln C_e$ produces a straight line with slope B and intercept $B \ln K_T$ and are given in Table 1. The correlation coefficient for Temkin isotherm is 0.997 indicating that the isotherm fits the model well.

Dubinin-Radushkevich (D-R) (Dubinin, 1960) isotherm is represented in Eq. (7):

$$\ln q_e = \ln q_m - \beta \epsilon^2 \quad (7)$$

where ϵ^2 and β (mol^2/kJ^2) are D-R isotherm constants. ϵ is $RT \ln(1 + 1/C_e)$. The D-R constants β and q_m were calculated from the slope and intercept of $\ln C_e$ versus ϵ^2 . The plot of the isotherm models are given in Fig. 11 and the isotherm constants and correlation coefficients (R^2) were presented in Table 1. Langmuir isotherm fits the Cr(VI) adsorption well when compared to all other isotherms based on R^2 .

3.11. Adsorption kinetics

The adsorption kinetics of Cr(VI) was explored by the Pseudo-first order (PFO), Pseudo-second order (PSO), Elovich and Intra-particle diffusion (IPD) models.

PSO kinetic model is derived based on weak interaction between sorbate and sorbent predominantly prevailing with physisorption. The linear form of PSO kinetics (Ho, 2004) is given by Eq. (8).

$$\ln(q_e - q_t) = \ln(q_e) - k_1 t \quad (8)$$

Table 1
Equilibrium isotherm parameters and their values for Cr(VI) sorption.

Isotherm model	Parameters	Values
Langmuir	q_m (mg/g)	144.93
	K_L (L/mg)	0.275
	R^2	0.9985
Freundlich	K_f (L/mg)	45.18
	$1/n$	0.3101
	R^2	0.9608
Dubinin- Radushkevich	q_m (mg/g)	115.51
	β (mol^2/kJ^2)	0.7474
	E (kJ/mol)	0.817
	R^2	0.845
Temkin	B (J/mol)	27.77
	K_T (L/mg)	3.434
	R^2	0.997

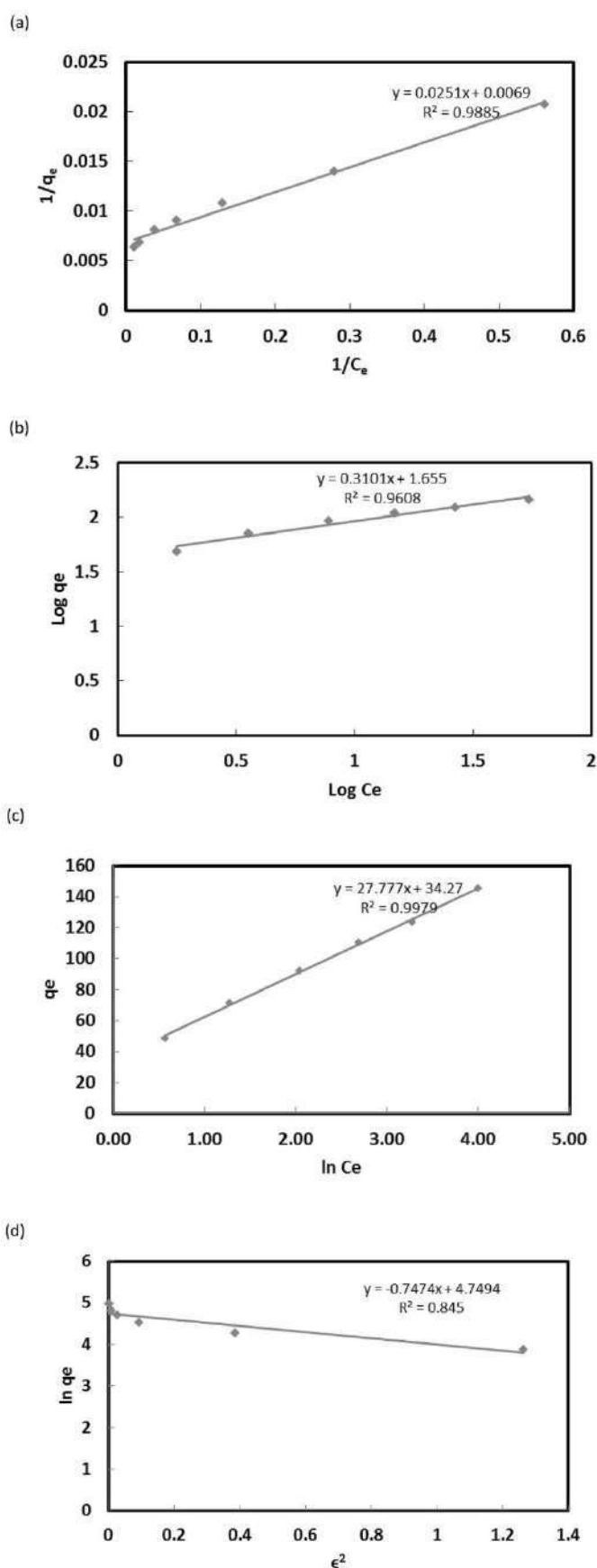


Fig. 11. Isotherm plot for Cr(VI) removal using Nanocomposite (a) Langmuir (b) Freundlich (c) Temkin (d) D-R isotherm.

k_1 - rate constant for PSO kinetic model (1/min). The rate constant and correlation coefficient were evaluated from the slope and intercept of the plot between $\log(q_e - q_t)$ and t .

PSO kinetic model (Ho and McKay, 1999) is based on chemisorption. Linear form of Pseudo – second order kinetics was represented by Eq. (9).

$$\frac{t}{q_t} = \frac{1}{k_2 q_e^2} + \frac{t}{q_e} \quad (9)$$

where k_2 - rate constant of PSO (g/mg min).

t -time (min).

IPD model (Weber and Morris, 1963) is given by Eq. (10).

$$q_t = k_{id} t^{0.5} + C \quad (10)$$

where k_{id} - IPD rate constant (mg/(g min^{-0.5})) and C - intercept.

Elovich model (Juang and Chen, 1997) is specified by Eq. (11).

$$q_t = \frac{1}{\beta} \ln(\alpha\beta) + \frac{1}{\beta} \ln t \quad (11)$$

where α - Elovich constant (mg/g min), β - Elovich exponent (g/mg).

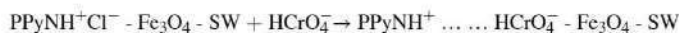
The linearized plots of Eqs. (8)–(11) are presented in Fig. 12a, 12b, 12c and 12d respectively. The rate constants, kinetic parameters and correlation coefficients obtained through these plots are listed in Table 2. From the results, it is observed that the correlation coefficient (R^2) of the PSO model was found to be much higher than those of other models indicating that the adsorption mechanism was well suited with PSO model. Comparison of the sorption ability of the synthesized nanocomposite for Cr was made with other sorbents and it was given in Table 3. From the table, it can be seen that the nanocomposite has comparable sorption capacity.

3.12. Desorption and regeneration studies

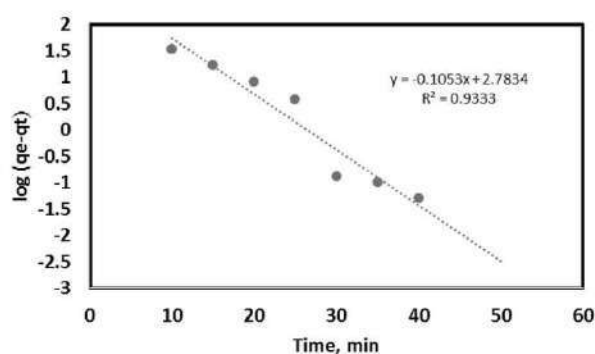
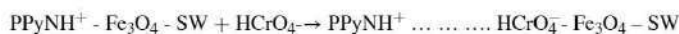
Regeneration assists in the recovery and reuse of the sorbent, and it is a vital parameter for achieving improved cost-effective removal process. The desorption was performed with various concentrations of NaOH and the desorption efficiency was observed. Cr(VI) gets reduced to Cr(III) species and desorption could not be achieved using NaOH solution. Therefore, desorption was carried out by treating the sorbent with 2 M HCl solution and the sorption could be regenerated by the doped Cl^- ions. Fig. 13 shows that removal efficiency was 78% and 72% for the first and second cycles, respectively. The removal efficiency was reduced in second and third cycles which might be due to reduction in available active sites. The repeated oxidation reaction with highly oxidizing Cr(VI) species ruptures the polymer chain and thereby the available active sites gets reduced. The sorbent can be reused for two cycles effectively.

3.13. Adsorption mechanism

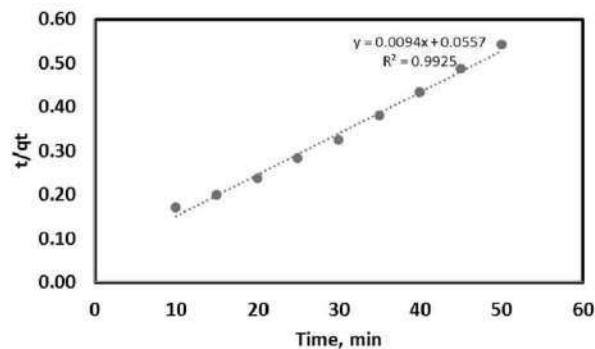
The mechanism of Cr(VI) removal by the nanocomposite follows the mechanism viz. electrostatic attraction, ion-exchange and reduction. Amino and carboxyl group have strong electrostatic attractions towards Cr(VI). The Fe^{3+} has rigorous synchronized interactions with Cr(VI) and the Cr(VI) is reduced to Cr(III) by means of hydroxyl radicals present in solution which aids in the removal of Cr(VI). Ultimately electrostatic interaction and ion-exchange are fundamental mechanisms of Cr^{6+} sorption on PPy- Fe_3O_4 -SW composite and represented in Fig. 14. Ion exchange between doped Cl^- of PPy moiety and negatively charged $HCrO_4^-$ ion in aqueous solution can be explained as follows:



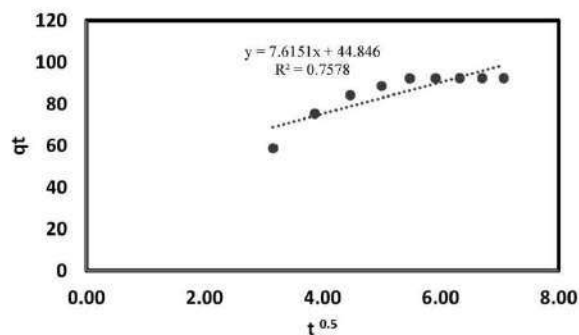
Electrostatic attraction between positively charged nitrogen of PPy and $HCrO_4^-$ can be explained as follows:



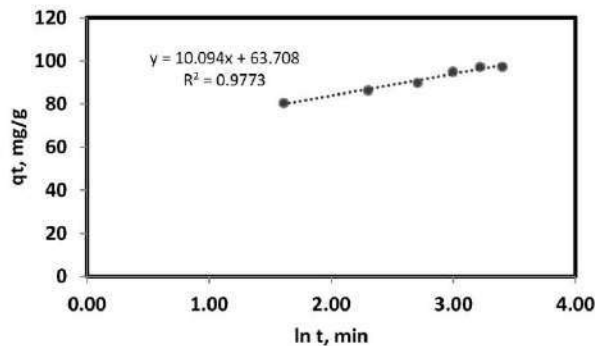
(a)



(b)



(c)



(d)

Fig. 12. Adsorption kinetics of PPy- Fe_3O_4 -SW composite. (a) PFO (b) PSO (c) IPD and (d) Elovich models.

Table 2
Kinetic model parameters.

Kinetic model	Parameters	Values
PFO	$K_1(\text{min}^{-1})$	0.053
	R^2	0.915
PSO	$K_2(\text{g/mg} \cdot \text{min})$	0.002
	R^2	0.992
IPD	$K_{\text{id}}(\text{mg/g} \cdot \text{min}^{0.5})$	3.130
	R^2	0.758
Elovich model	$\alpha(\text{mg/g} \cdot \text{min})$	10.074
	$\beta(\text{g/mg})$	0.0990
	R^2	0.9773

Table 3
Comparison of sorption capacities of different sorbents towards Cr(VI) removal.

Adsorbent	Sorption capacity, mg/g	Reference
Dolochar	1.90	Panda et al. (2011)
Ppy/OMWCNTS	294.00	Bhaumik et al. (2016)
Soy hull	7.29	Blanes et al. (2016)
Magnetite particle	0.015	Padmavathy et al. (2016)
CoFe ₂ O ₄ /NOM	5.99	Cruz et al. (2017)
Ppy/FeO	202.02	Matome et al. (2020)
Raw almond shell	21.92	Yahya et al. (2020b)
Cashew nut shell	10.79	Yahya et al. (2020a)
PPy-Fe ₃ O ₄ -SW	144.93	Present study

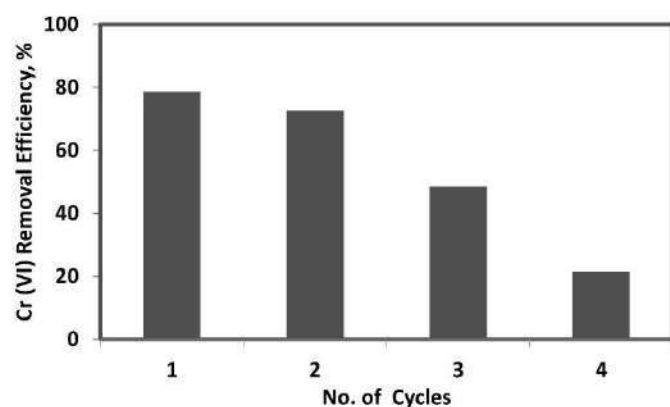


Fig. 13. Desorption study of Cr(VI) using PPy-Fe₃O₄-SW nanocomposite.

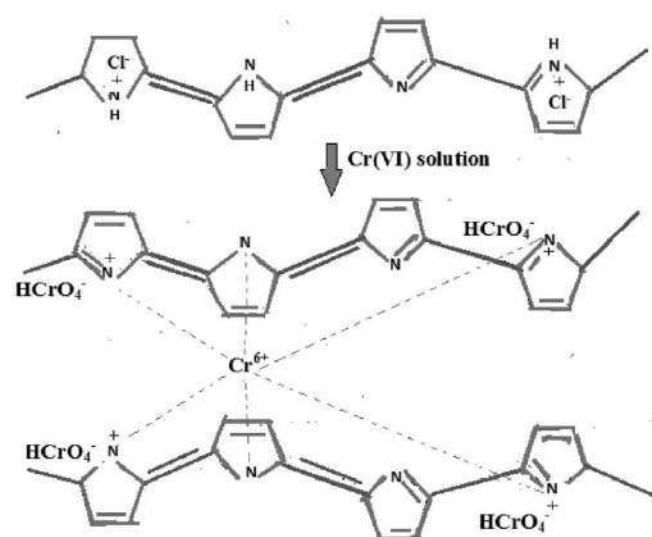


Fig. 14. Schematic representation of adsorption of Cr(VI) on PPy-Fe₃O₄-SW composite.

4. Conclusions

In this present study, a cheap and sustainable PPy-Fe₃O₄-SW sorbent was effectively applied for Cr(VI) sorption. The categorized characterization studies established the sorption of Cr(VI) through active surface area and favorable surface functional groups. The optimum condition for efficient Cr(VI) removal were: pH-2, temperature-30 °C, nano-composite dosage - 100 mg and contact time-30 min. The maximum uptake of Cr(VI) achieved by the nanocomposite was 144.93 mg/g. Desorption studies using acid proved repeatability of the performance up to two cycles. The experimental results fitted well with Langmuir isotherm ($R^2 = 0.9985$) confirming single layer of sorbent-sorbate interaction and correlated with PSO kinetics ($R^2 = 0.992$). The sorption of Cr(VI) occurs through electrostatic interaction and ion-exchange process. The sorption of Cr(VI) using PPy-Fe₃O₄-SW is identified as a potential alternative due to the low cost, renewable source, recyclable and bio-compatibility properties of the synthesized nanocomposite.

Author contributions

G.Sarojini – Conceptualization, Methodology, Investigation, Validation, Writing – original draft. **S.Venkatesh Babu** – Writing – Review & Editing Supervision. **N. Rajamohan** – Conceptualization, Resources, Writing – Review & Editing. **P.Senthil Kumar** – Characterization, Writing – Review & Editing. **M. Rajasimman** – Characterization, Methodology, Formal analysis, Writing – Review & Editing.

Declaration of competing interest

The authors declare that they have no known competing financial interests or personal relationships that could have appeared to influence the work reported in this paper.

References

- Al-Homaidan, A.A., Al-Oahtani, H.S., Al-Ghanayem, A.A., Ameen, F., Mohammed Ibraheem, I.B., 2018. Potential use of green algae as a biosorbent for hexavalent chromium removal from aqueous solutions. *Saudi J. Biol. Sci.* 25, 1733–1738. <https://doi.org/10.1016/j.sjbs.2018.07.011>.
- Bakhtiari, N., Azizian, S., 2015. Adsorption of copper ion from aqueous solution by nanoporous MOF-5: a kinetic and equilibrium study. *J. Mol. Liq.* 206, 114–118. <https://doi.org/10.1016/j.molliq.2015.02.009>.
- Barnhart, J., 1997. Occurrences, uses, and properties of chromium. *Regul. Toxicol. Pharmacol.* 26, S3–S7. <https://doi.org/10.1006/rtp.1997.1132>.
- Bayramoglu, G., Arica, M.Y., 2011. Synthesis of Cr(VI)-imprinted poly(4-vinyl pyridine-co-hydroxyethyl methacrylate) particles: its adsorption propensity to Cr(VI). *J. Hazard Mater.* 187, 213–221. <https://doi.org/10.1016/j.jhazmat.2011.01.022>.
- Bhaumik, M., Agarwal, S., Gupta, V.K., Maity, A., 2016. Enhanced removal of Cr(VI) from aqueous solutions using polypyrrole wrapped oxidized MWCNTs nanocomposites adsorbent. *J. Colloid Interface Sci.* 470, 457–467. <https://doi.org/10.1016/j.jcis.2016.02.054>.
- Bhaumik, M., Maity, A., Srinivasu, V.V., Onyango, M.S., 2011a. Enhanced removal of Cr(VI) from aqueous solution using polypyrrole/Fe₃O₄ magnetic nanocomposite. *J. Hazard Mater.* 190, 381–390. <https://doi.org/10.1016/j.jhazmat.2011.03.062>.
- Bhaumik, M., Leswif, T.Y., Maity, A., Srinivasu, V.V., Onyango, M.S., 2011b. Removal of fluoride from aqueous solution by polypyrrole/Fe₃O₄ magnetic nanocomposite. *J. Hazard Mater.* 186, 150–159. <https://doi.org/10.1016/j.jhazmat.2010.10.098>.
- Bhaumik, M., Setshedi, K., Maity, A., Onyango, M.S., 2013. Chromium(VI) removal from water using fixed bed column of polypyrrole/Fe₃O₄ nanocomposite. *Separ. Purif. Technol.* 110, 11–19. <https://doi.org/10.1016/j.seppur.2013.02.037>.
- Blanes, P.S., Bordoni, M.E., González, J.C., García, S.I., Atriac, A.M., Sala, L.F., Belló, S. E., 2016. Application of soyhull biomass in removal of Cr(VI) from contaminated waters. Kinetic, thermodynamic and continuous sorption studies. *J. Environ. Chem. Eng.* 4 (1), 516–526. <https://doi.org/10.1016/j.jece.2015.12.008>.
- Cai, W., Tan, L., Yu, J., 2014. Synthesis of amino-functionalized mesoporous alumina with enhanced affinity towards Cr(VI) and CO₂. *Chem. Eng. J.* 239, 207–215. <https://doi.org/10.1016/j.ccej.2013.11.011>.
- Cruz, D.R.S., Santos, B.T.J., Cunha, G.C., Romão, L.P.C., 2017. Green synthesis of a magnetic hybrid adsorbent (CoFe₂O₄/NOM): removal of chromium from industrial effluent and evaluation of the catalytic potential of recovered chromium ions. *J. Hazard Mater.* 334, 76–85. <https://doi.org/10.1016/j.jhazmat.2017.03.062>.
- Dave, P.N., Chopda, L.V., 2014. Application of iron oxide nanomaterials for the removal of heavy metals. *J. Nanotechnol.* 4, 1–14. <https://doi.org/10.1155/2014/398569>.

- Davis, T.A., Volesky, B., Mucci, A., 2003. A review of the biochemistry of heavy metal biosorption by brown algae. *Water Res.* 37, 4311–4330. [https://doi.org/10.1016/S0043-1354\(03\)00293-8](https://doi.org/10.1016/S0043-1354(03)00293-8).
- Dubinin, M.M., 1960. The potential theory of adsorption of gases and vapors for adsorbents with energetically non-uniform surface. *Chem. Rev.* 60, 235–266. <https://doi.org/10.1021/cr60204a006>.
- Durai, G., Rajasimman, M., 2011. Biological treatment of tannery wastewater – a review. *J. Environ. Sci. Technol.* 4, 1–17. <https://doi.org/10.3923/jest.2011.1.17>.
- Dwivedi, S., 2012. Bioremediation of heavy metal by algae: current and future perspective. *J. Adv. Lab. Res. Biol.* 3, 195–199.
- Farahani, M., Abdullah, S.R.S., Hosseini, S., Shojaeipour, S., Kashisaz, M., 2011. Adsorption-based cationic dyes using the carbon active sugarcane bagasse. *Proc. Environ. Sci.* 10 (Part A), 203–208. <https://doi.org/10.1016/j.proenv.2011.09.035>.
- Freundlich, H.M.F., 1906. Over the adsorption in solution. *J. Phys. Chem.* 57, 385–471.
- Garg, U.K., Kaur, M.P., Garg, V.K., Suda, D., 2017. Adsorption of hexavalent chromium onto sisal pulp/polypyrrole composites. *Mater. Sci. Eng.* 170 <https://doi.org/10.1088/1757-899X/170/1/012007>.
- Ho, Y.S., McKay, G., 1999. Pseudo-second order model for sorption processes. *Process Biochem.* 34, 451–465. [https://doi.org/10.1016/S0032-9592\(98\)00112-5](https://doi.org/10.1016/S0032-9592(98)00112-5).
- Ho, Y.S., 2004. Citation review of Lagergren kinetic rate equation on adsorption reactions. *Scientometrics* 59, 171–177. <https://doi.org/10.1023/B:SCIE.0000013305.99473.cf>.
- Ilankoon, N., 2014. Use of iron oxide magnetic nanosorbents for Cr(VI) removal from aqueous solutions: a review. *J. En. Res. Appl.* 4, 55–63.
- Jayakumar, R., Rajasimman, M., Karthikeyan, C., 2014. Sorption of hexavalent chromium from aqueous solution using marine green algae *Halimeda gracilis*: optimization, equilibrium, kinetic, thermodynamic and desorption studies. *J. Environ. Chem. Eng.* 2, 1261–1274. <https://doi.org/10.1016/j.jece.2014.05.007>.
- Jayakumar, R., Rajasimman, M., Karthikeyan, C., 2015. Sorption and desorption of hexavalent chromium using a novel brown marine algae *Sargassum myricostatum*. *Kor. J. Chem. Eng.* 32, 2031–2046. <https://doi.org/10.1007/s11814-015-0036-8>.
- Juang, R.S., Chen, M.L., 1997. Application of the Elovich equation to the kinetics of metal sorption with solvent-impregnated resins. *Ind. Eng. Chem. Res.* 36, 813–820. <https://doi.org/10.1021/ie960351f>.
- Karmakar, N., Jain, S.P., Patil, U.V., Shimpi, N.G., Bhat, N.V., Kothari, D.C., 2017. Room temperature NO₂ gas sensing properties of p-toluenesulfonic acid doped silver-polypyrrole nanocomposite. *Sens. Actuators, B* 242, 118–126. <https://doi.org/10.1016/j.snb.2016.11.039>.
- Khan, H., Malook, K., 2017. Highly selective and sensitive ammonia sensor using polypyrrole/V₂O₅ composites. *J. Mater. Sci. Mater. Electron.* 28, 13873–13879. <https://doi.org/10.1007/s10854-017-7235-5>.
- Langmuir, I., 1918. The adsorption of gases on plane surface of glass, mica and platinum. *J. Am. Chem. Soc.* 40, 1361–1368. <https://doi.org/10.1021/ja02242a004>.
- Levakumar, L., Muthukumar, V., Gobinath, M.B., 2009. Batch adsorption and kinetics of chromium (VI) removal from aqueous solutions by *Ocimum americanum* L. seed pods. *J. Hazard Mater.* 161, 709–713. <https://doi.org/10.1016/j.jhazmat.2008.04.031>.
- Losi, M.E., Amrhein, C., Frankenberger Jr., W.T., 1994. Environmental biochemistry of chromium. In: *Reviews of Environmental Contamination and Toxicology*. Springer, New York, pp. 91–121.
- Ma, Y., Jiang, S., Jian, G., Tao, H., Yu, L., Wang, X., Wang, X., Zhu, J., Hu, Z., Chen, Y., 2009. CNx nanofibers converted from polypyrrole nanowires as platinum support for methanol oxidation. *Energy Environ. Sci.* 2, 224–229. <https://doi.org/10.1039/B807213M>.
- Malathi, A., Yu, Y., Jung, H.J., Yeon, S., Lee, H., Theerthagiri, J., Lee, S.J., Choi, M.Y., 2021. Solvent-mediated synthesis of BiOI with a tunable surface structure for effective visible light active photocatalytic removal of Cr(VI) from wastewater. *Environ. Res.* 197, 111080. <https://doi.org/10.1016/j.envres.2021.111080>.
- Matome, S.M., Makhadob, E., Katata-Serua, L.M., Maponyab, T.C., Modibane, K.D., Hatob, M.J., Bahadura, I., 2020. Green synthesis of polypyrrole/nanoscale zero valent iron nanocomposite and use as an adsorbent for hexavalent chromium from aqueous solution S. Afr. J. Chem. Eng. 34, 1–10. <https://doi.org/10.1016/j.sajce.2020.05.004>.
- Mestre, A.S., Pires, R.A., Aroso, I., Fernandes, E.M., Pinto, M.L., Reis, R.L., Andrade, M. A., Pires, J., Silva, S.P., Carvalho, A.P., 2014. Activated carbons prepared from industrial pretreated cork: sustainable adsorbents for pharmaceutical compounds removal. *Chem. Eng. J.* 253, 408–417. <https://doi.org/10.1016/j.cej.2014.05.051>.
- Murphy, V., Tofail, S.A.M., Hughes, H., McLoughlin, P., 2009. A novel study of hexavalent chromium detoxification by selected seaweed species using SEM-EDX and XPS analysis. *Chem. Eng. J.* 148, 425–433. <https://doi.org/10.1016/j.cej.2008.09.029>.
- Padmavathy, K.S., Madhub, G., Haseena, P.V., 2016. A study on effects of pH, adsorbent dosage, time, initial concentration and adsorption isotherm study for the removal of hexavalent chromium Cr(VI) from wastewater by magnetite nanoparticles. *Proc. Technol.* 24, 585–594. <https://doi.org/10.1016/j.protec.2016.05.127>.
- Panda, L., Das, B., Rao, D.S., Mishra, B.K., 2011. Application of Dolochar in the removal of cadmium and hexavalent chromium ions from aqueous solutions. *J. Hazard Mater.* 192 (2), 822–831. <https://doi.org/10.1016/j.jhazmat.2011.05.098>.
- Rajamohan, N., Rajasimman, M., Rajeshkannan, R., Saravanan, V., 2014. Equilibrium, kinetic and thermodynamic studies on the removal of Aluminum by modified *Eucalyptus camaldulensis* barks. *Alex. Eng. J.* 53, 409–415. <https://doi.org/10.1016/j.aej.2014.01.007>.
- Rajasimman, M., Sangeetha, R., Karthic, P., 2009. Statistical optimization of process parameters for the extraction of chromium (VI) from pharmaceutical wastewater by emulsion liquid membrane. *Chem. Eng. J.* 150, 275–279. <https://doi.org/10.1016/j.cej.2008.12.026>.
- Rapri, S., Pournara, A., Sarma, D., Papadakis, I.T., Armatas, G.S., Tsipis, A.C., Lazarides, T., Kanatzidis, M.G., Manos, M.J., 2016. Selective capture of hexavalent chromium from an anion-exchange column of metal organic resin-alginate acid composite. *Chem. Sci.* 7, 2427–2436. <https://doi.org/10.1039/C5SC03732H>.
- Sari, A., Tuzen, M., 2008. Biosorption of Pb(II) and Cd(II) from aqueous solution using green alga (*Ulva lactuca*) biomass. *J. Hazard Mater.* 152, 302–308. <https://doi.org/10.1016/j.jhazmat.2007.06.097>.
- Sarajini, G., Venkateshbabu, S., Rajasimman, M., 2021. Facile synthesis and characterization of polypyrrole - iron oxide - seaweed (PPy-Fe₃O₄-SW) nanocomposite and its exploration for adsorptive removal of Pb(II) from heavy metal bearing water. *Chemosphere* 278, 130400. <https://doi.org/10.1016/j.chemosphere.2021.130400>.
- Selvi, A., Rajasekar, A., Theerthagiri, J., Ananthaselvam, A., Sathishkumar, K., Madhavan, J., Rahman, P.K.S.M., 2019. Integrated remediation processes toward heavy metal removal/recovery from various environments-a review. *Front. Environ. Sci.* 7, 66. <https://doi.org/10.3389/fenvs.2019.00066>.
- Temkin, M.J., Pyzhev, V., 1940. Kinetics of ammonia synthesis on promoted iron catalysts. *Acta Phy. Chem. URSS.* 12, 217–256.
- Theerthagiri, J., Murthy, A., Elakkiya, V., Chandrasekaran, S., Nithyadharseni, P., Khan, Z., Senthil, R.A., RaviShanker Raghavender, M., Kuppusami, P., Jagannathan, M., Ashokkumar, M., 2018. Recent development on carbon based heterostructures for their applications in energy and environment: a review. *J. Ind. Eng. Chem.* 64, 16–59. <https://doi.org/10.1016/j.jiec.2018.02.029>.
- Turner, A., Lewis, M.S., Shams, L., Brown, M.T., 2007. Uptake of platinum group elements by the marine macroalga, *Ulva lactuca*. *Mar. Chem.* 105, 271–280. <https://doi.org/10.1016/j.marchem.2007.02.009>.
- Vijayaraghavan, K., Josephraj, J., Kandhasamy, P., 2005. Biosorption of copper, cobalt and nickel by marine green alga *Ulva reticulata* in a packed column. *Chemosphere* 60 (3), 419–426. <https://doi.org/10.1016/j.chemosphere.2004.12.016>.
- Weber, W.J., Morris, J., 1963. Kinetics of adsorption on carbon from solution. *J. Sanit. Eng. Div.* 89, 31–60.
- Yahya, M.D., Abubakar, H., Obayomi, K.S., Iyaka, Y.A., Suleiman, B., 2020a. Simultaneous and continuous biosorption of Cr and Cu(II) ions from industry tannery effluent using almond shell in a fixed bed column. *Results Eng.* 6, 100–113. <https://doi.org/10.1016/j.rineng.2020.100113>.
- Yahya, M.D., Aliyu, A.S., Obayomi, K.S., Olugbenga, A.G., Abdullahi, U.B., 2020b. Column adsorption study for the removal of chromium and manganese ions from electroplating water using cashew nutshell adsorbent. *Cogent. Eng.* 7 (1), 1748470. <https://doi.org/10.1080/23311916.2020.1748470>.
- Yu, Q., Li, M., Ning, P., 2019. Characterization of metal oxide-modified Walnut shell activated carbon and its application for phosphine adsorption: equilibrium, regeneration, and mechanism studies. *J. Wuhan Univ. Technol.* 34 (2), 487–495. <https://doi.org/10.1007/s11595-019-2078-y>.
- Zahmatkesh, M., Spanjers, H., Van Lier, J.B., 2018. A novel approach for application of white rot fungi in wastewater treatment under non-sterile conditions: immobilization of fungi on sorghum. *Environ. Technol.* 39 (16), 2030–2040. <https://doi.org/10.1080/09593330.2017.1347718>.
- Zhang, H., Zhong, X., Xu, J.J., Chen, H.Y., 2008. Fe₃O₄/polypyrrole/Au nanocomposites with core/shell structure: synthesis, characterization and their electrochemical properties. *Langmuir* 24, 13742–13752. <https://doi.org/10.1021/la802893s>.



ScienceDirect



View PDF

Access through **your institution**

Purchase PDF

Chemosphere

Volume 278, September 2021, 130400

Facile synthesis and characterization of polypyrrole - iron oxide – seaweed (PPy-Fe₃O₄-SW) nanocomposite and its exploration for adsorptive removal of Pb(II) from heavy metal bearing water

Gopalakrishnan Sarojini ^a  , Samikannu Venkateshbabu ^b, Manivasagan Rajasimman ^cShow more 

Outline



Share



Cite

<https://doi.org/10.1016/j.chemosphere.2021.130400>

Get rights and content

Highlights

- A new method is adopted for the synthesis of PPy-Fe₃O₄-SW nanocomposite.
- Synthesized nanocomposite was characterized by SEM, TEM, XPS, EDS, FTIR and XRD.
- The nanocomposite was employed for the removal of lead ions and the uptake was 333.33 mg/g.
- Sorption mechanism, isotherm, kinetics, and thermodynamic studies were carried out.

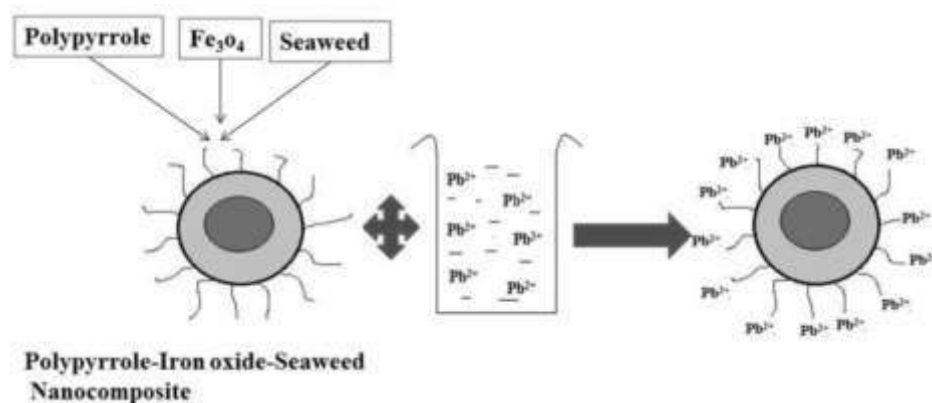
FEEDBACK 

- Desorption and regeneration studies were also performed.

Abstract

Lead is a widely used heavy metal which is highly toxic to kidney, nervous system and reproductive system. A special featured polypyrrole based adsorbent, with admirable salinity confrontation, environmental stability and reusability, was engaged to remove lead ions from aqueous solution. The advantages of using polypyrrole based adsorbent for heavy metal removal are: ease of synthesis, biocompatibility and high metal selectivity. In this study, polypyrrole - iron oxide - seaweed nanocomposite was proposed to remove lead ions from aqueous solution. A new method was adopted for the synthesis of polypyrrole - iron oxide - seaweed nanocomposite. The nanocomposite was prepared within a short time using ultra-assisted polymerization technique. The synthesized nanocomposite adsorbent was characterized using FTIR, SEM, TEM, EDS, XRD, XPS and zeta potential analysis. The adsorption capability of polypyrrole - iron oxide - seaweed nanocomposite towards lead was explored. The influence of pH, contact time, adsorbent dosage, metal ion concentration and recyclability were investigated. The optimum condition of these parameters was found to be: pH- 5, temperature - 40 °C, initial concentration – 100 mg/L and contact time - 20 min and the results showed that the hybrid composite adsorbed 97.25% Pb (II). Different isotherms such as Langmuir, Freundlich, Temkin and D-R models were also studied for the adsorption of Pb ions. The kinetics of the adsorption process was examined by I order, II order and intra particle diffusion kinetic models. The mechanism of lead adsorption onto the nanocomposite was also explored.

Graphical abstract



Download : [Download high-res image \(218KB\)](#)

Download : [Download full-size image](#)

[Previous](#)[Next](#)

Keywords

Heavy metals; Iron oxide; Isotherms; Kinetics; Lead; Polypyrrole; Seaweed

[Special issue articles](#)[Recommended articles](#)[Citing articles \(4\)](#)[View full text](#)

© 2021 Elsevier Ltd. All rights reserved.

[About ScienceDirect](#)[Remote access](#)[Shopping cart](#)[Advertise](#)[Contact and support](#)[Terms and conditions](#)[Privacy policy](#)

We use cookies to help provide and enhance our service and tailor content and ads. By continuing you agree to the **use of cookies**.

Copyright © 2021 Elsevier B.V. or its licensors or contributors. ScienceDirect® is a registered trademark of Elsevier B.V.

ScienceDirect® is a registered trademark of Elsevier B.V.

[FEEDBACK](#)

Text-based Graphical Password System to Enhance Security

Athira S.^{1,*}, G. Rajiv Suresh Kumar², M. Rupa³

Abstract

A graphical password is a type of authentication that requires the user to choose from a set of images in a certain order. For most people, remembering a graphical password is easier than remembering a text-based password. Passwords with graphics may be more difficult to remember. offer better security than text-based passwords. Humans can remember pictures much better than the text. To create passwords more memorable and less vulnerable to security attacks. A text-based movable frame graphical password system is proposed. The system includes both the Graphical and Text- based images interface for identification. It displays a grid which is either graphical images, or alphabets or multiple/mixed alphabets. Traditional text- based password schemes are subjected to dictionary attacks. Graphic password systems, which use graphics instead of words as a password, are a promising alternative to text-based recognition schemes. These are again affected due to shoulder surfing and less effective due to large dictionary space. providing a solution based on text-based graphical password techniques. Our research has a main objective: To enhance the security. The graphical password system with multiple alphabet images is more recognizable. It has less cognitive load on user as compared to image based graphical password schemes.

Keywords: Authorization security, Secured logging, Intruders, Hackers, Unauthorized user.

INTRODUCTION

Password systems are usually simple text-based; graphical image based which are more vulnerable to different kinds of attacks. Password systems should less predictable and strong passwords with more memorability and security. Traditional password systems vulnerable attacks, including shoulder surfing, dictionary attacks, man in the middle attack and eavesdropping etc. The passwords might be easily guessed by the attacker. If a password is hard to guess by an attacker or outsider, then it is also

hard to remember by the user. One can remember pictures easily than a text. This fact has been proposed graphical password schemes as a feasible method to text-based schemes. Which may also have disadvantages over some attacks. Here we propose a system with graphical password scheme which we choose a random image as a password and, we can upload an image as a permanent password which would be easy to remember to the user [1–5].

*Author for Correspondence

Athira S.

E-mail: athirasivadasan35@gmail.com

¹Assistant Professor, Department of Computer Science Engineering, JCT College of Engineering and Technology, Coimbatore, TN, India

²Professor, Department of Computer Science Engineering, JCT College of Engineering and Technology, Coimbatore, TN, India

³Assistant Professor, Department of Computer Science Engineering, JCT College of Engineering and Technology, Coimbatore, TN, India

Received Date: March 16, 2022

Accepted Date: March 24, 2022

Published Date: March 29, 2022

Citation: Athira S., G. Rajiv Suresh Kumar, M. Rupa. Text-based Graphical Password System to Enhance Security. Trends in Opto-electro & Optical Communication. 2021; 11(3): 8–14p.

EXISTING SYSTEM

The existing password security system include text-based, 8-digit codes, pattern lock, fingerprint lock, face recognition locks, graphical password schemes, pass face. All these methods have been

used by decades. Which may induce by hackers. It includes more disadvantages such as color code implemented for some servers only. So that secured server only enjoys the color code. Biometrics devices are used for security purpose, user can't able to carry the devices. In case of hacking admin could not able to track the type of hacker. Thus, the system is more vulnerable to the commonly identified threats [6, 7].

METHODOLOGY

According to SLAS in Online based Application having few main advantages and many disadvantages when it comes to weak single-factor authentication, which many are more familiar with as the single static passwords still employed by most companies. One advantage is that static passwords are easy to remember. When different systems have different passwords, they can be difficult to remember and may have to be written down, raising their vulnerability. One of the numerous drawbacks of single static passwords is how simple they are to crack. They're usually short and focused on topics that are personal to the individual, and they're usually just letters [8].

Static Method

The Internet's impact over the last few years has resulted in significant changes in how we access business systems. While the number of users requesting network access has increased, the network security barrier has disintegrated at all levels. Users' geographical locations have also broadened to the point that they can be anywhere in the world, not only in a different department or company branch office.

While increasing access has substantial productivity benefits, the security concerns have significantly increased. Authentication through the use of passwords was the traditional technique of securing system access. Traditional password security, unfortunately, is completely inadequate for securing the access requirements of today's scattered users. Businesses are still heavily reliant on user IDs and passwords to verify the identity of people attempting to access their systems, according to the DTI Information Security Breaches. Most businesses still utilize weak single factor authentication, which involves the usage of single static passwords. Static passwords have the advantage of being simple to remember. When you have multiple passwords for different systems, it becomes impossible to remember them all and they must be written down, making them susceptible. One of the numerous drawbacks of single static passwords is how easy they are to hack. They are often lettering only and are based on issues close to the user, such as birthdays, partner names, children's names, and so on. They're also subject to social engineering, which involves someone asking for or guessing your password. They are also detectable by spyware. Changing passwords on a regular basis is an alternate way of password management. When used properly, this has the advantage of being more secure than static passwords. Frequent password changes have the disadvantage of being easily forgotten, resulting in very high support expenses and dramatically increased administration expenditures. This is particularly relevant for larger organizations with hundreds of applications [9].

IMPLEMENTATION

In the following paragraphs we will learn more about how secure passwords are made and operated.

Login Authentication

In this project we provide a high security for password at users input level. Here the user while login every time must provide a password, a user defined image and must choose four different images which is given by the system. The user's password security is very much increased by giving various inputs scenarios while login into the system. This will prevent the attackers to view or modify the password and also attackers cannot login into system to misuse the users account. Before login into the system the user should create account by giving his/her details for accessing the account. During signup the user will input the details for their secured password and every time these factors are used for login (Figure 1).

Figure 1. Login Page.

Graphical Password Login

This module describes about how the user defined uploaded image works. The image uploaded by the user during signup is the image that he/she need to upload every time while login into system. The image can be with any format like .jpg, .png, .jpeg. Whenever the user uploads an image while login, the RGB value of the image currently uploaded will be verified with the image that was uploaded by the user during sign up. These two images RGB should match, so that the system accepts the user is an authorized user for login.

Graphical image shuffling: This is the password security where the image will get shuffled every time when the user login, that is the four images which was chosen by the user during sign up will be in any order in display while login. So the user must remember the images which was chosen during sign up but not the order of the image placed. These four images should match every time while the user login into the system. The system throws an exception to the user as unauthorized when even one of the images is chosen wrongly (Figure 2).

Figure 2. After Login.

Graphical Image Shuffling

This is the password security where the image will get shuffled every time when the user login, that is the four images which was chosen by the user during sign up will be in any order in display while login. So, the user must remember the images which was chosen during sign up but not the order of the image placed. These four images should match every time while the user login into the system. The system throws an exception to the user as unauthorized when even one of the images is chosen wrongly.

Graphical password Updates

Here it explains about the changing the password, uploaded image and the chosen images. The system will have an option for updating the current password security level and the user can update the password whenever they need by logging into their corresponding account. When the user updated the security level of password the system will acknowledge the user that the password is updated successfully, and the user can be allowed to use the updated password during login (Figure 3).

Figure 3. Password Update.

MATHEMATICAL CALCULATION

Each new calculation may be created from the past. The method of this type of algorithm, uses a one-way function (call it f). The one-time access system works by starting with an initial seed s , then generating passwords {
 $f(s)$,
 $f(f(s))$,
 $f(f(f(s)))$
 $\}$,
 ... as many times as necessary.

Each password is then dispensed in reverse, with $f(f(...f(s)))$ first, to $f(s)$.

After the set for s has been exhausted, a new seed value can be chosen if an indefinite succession of passwords is desired.

Lamport's method is used in the S/KEY one-time password system and its variant OTP.

An attacker who sees a one-time password may gain access for a limited time or login, but once that time period passes, the password is useless. To calculate the inverse function f^{-1} from the previous passwords, one must first develop a mechanism to calculate the next password in the series. This is incredibly tough to achieve because f was chosen to be one-way. If f is a cryptographic hash function, as is usually the case, the task is computationally infeasible (as far as we know). By supplying only a one-time password, the user can give the server with a static key for use as an encryption key in some mathematical algorithm schemes.

Users must respond to a challenge when using challenge-response one-time passwords. This can be accomplished, for example, by storing the token's created value within the token. To avoid duplicates, an extra counter is frequently used, resulting in separate one-time passwords if the same challenge is received twice. However, instead of applying both procedures, the computation normally does not use the prior one-time password. Instead of using time-synchronization, token-based methods of providing OTPs can employ one of these sorts of algorithms.

UNIT TESTING–MODULE WISE

Unit testing is to segregate each part of field in application and test that the individual parts are working in the given condition, and it test the login form by giving particular username and password of the admin (Figure 4) [10].

TEST CASE-LOGIN PAGE

SNO	TEST CASE-ID	TEST TYPE	STEP	TEST DESCRIPTION	EXPECTED RESULT	ACTUAL RESULT	RESULT
1	TC_01	Unit testing	User enters into application	Enter username & Password	Login accepted	System accepts the Process	Pass
2	TC_02	Unit testing	User enters invalid details	Enter username & Password	Login Not accepted	System not accepts the value	Failed
3	TC_03	Unit testing	If valid login	Displays master page for admin view and data input	Page viewed	Accept input	Pass

Figure 4. Test Case-Login Page.

Functional Testing

Functional testing is used to test the admin whether all the requirements' fields such as respective input format. The main scope is to test the functional requirements; individual process is possible on functional testing on the entire system (Figure 5).

Integration Testing

Integration testing is done after unit testing, that is used to test whether the proper interface is provided (Figure 6).

TEST CASE_Key and User Creation

SNO	TEST CASE_ID	TEST TYPE	STEP	TEST DESCRIPTION	EXPECTED RESULT	ACTUAL RESULT	RESULT
1	TC_01	Functional testing	Create User	Input user details	Data stored in DB	System accepts the data and move to the next field	Pass
2	TC_02	Functional testing	Create Server	Input mail Details	Data stored in DB	System accepts the data and move to the next field	pass
3	TC_03	Functional testing	Generate details	Verify key	Data stored in DB	System accepts the details	pass

Figure 5. Test Case Key and User Creation.

TEST CASE handshake process

SNO	TEST CASE_ID	TEST TYPE	STEP	TEST DESCRIPTION	EXPECTED RESULT	ACTUAL RESULT	RESULT
1	TC_01	Integration testing	Handshake process & data switch over to <u>other</u> server	Check formula and Calculation (For Warning)	Display available space	System accepts and show the available size of the server and current server	Pass

Figure 6. Test Case handshake Process.

CONCLUSION

In the future, safe digital audits research will try to verify the contents of a file system at a precise point in time.

A file system, for example, commits to the current version of its contents by delivering a MAC to a third-party. Using the MAC token, an auditor can check whether the file system still retains the old version at a later date. There has also been work on secure logging. In this work, a trusted machine writes encrypted logs that cannot be read or modified undetectably by an outsider. This work does not consider a large number of users concurrently accessing the data, there is no read and write access control (one key allows both read and write), the log is typically just appended and it is not optimized for writing in the middle, and a malicious outsider manipulating the order in which updates and reads are performed on the logging machine can compromise W and F. Moreover, in all this work,

the owner cannot convince a third party of some security violation. Current implementation of the logging client is loosely coupled with the operating system-based logging.

REFERENCES

1. Basak Bilgi, trBulent Tugrul," A Shoulder-Surfing Resistant Graphical Authentication Method" 2018 IEEE.
2. Bilal Eid Fayyadh, Khalid Mansour, Khaled W. Mahmoud," A New Password Authentication Mechanism Using 2D Shapes" 2018 8th International Conference on Computer Science and Information Technology (CSIT).
3. Chao Shen, Yufei Chen, Yao Liu and Xiaohong Guan," Adaptive Human–Machine Interactive Behavior Analysis With Wrist-Worn Devices for Password Inference"- IEEE Transactions On Neural Networks And Learning Systems.IEEE 2018.
4. Deepika Gupta,Dr. Vishal Goar, Akhand Pratap Singh,Shikha Mathur," Combination Of Textual And Graphical Based Authentication Scheme Through Virtual Environment"- 2017 IEEE.
5. K.Priya T.Venkaiah Naidu R.Vamsi Krishna ," An Advanced Information Security System Using Image Based Graphical Password Scheme"- 2nd International Conference on Trends in Electronics and Informatics (ICOEI 2018).
6. L.Gunaseeli, Dr.R.Aroul Canessane." GRAPHICAL PASSWORDS IMPLIES ON TOLERANCE PASSWORD, IMAGE CHOICE, AND PUZZLE LOGIN SECURITY"- international conference on information,communication & embedded systems (ICICES 2017).
7. Misbah Urrahman Siddiqui,Mohd. Sarosh Umar, Miftah Siddiqui," A Novel Shoulder-Surfing Resistant Graphical Authentication Scheme"- 2018 4th International Conference on Computing Communication and Automation (ICCCA), IEEE 2018.
8. Nida asmath," Conundrum – Pass: A New Graphical Password Approach. "-International conference on communication. IEEE 2019.
9. Noor Ashitah Abu Othman, Anis Shobirin Abdullah Sani, Muhammad Akmal Abdul Rahman, Fakariah Hani Mohd Ali," Directional Based Graphical Authentication Method with Shoulder Surfing Resistant"- 2018 IEEE Conference on Systems, Process and Control (ICSPC 2018), 14–15 December 2018, Melaka, Malaysia.
10. P. A. Sosa-Valles, J. G. Villalobos-Serrano, P. Velarde- Alvarado, V. García, J. R. Parra-Michel, L. Mena, R. Martínez-Peláez," My Personal Images as My Graphical Password"- IEEE Latin America Transactions, VOL. 16, NO. 5, MAY 2018.

Enhanced Graphical Password System with Intelligent User Identification Model

Athira S.^{1,*}, S. Dhanabal², K.M. Ravikumar³

Abstract

Data and authorization security needed everywhere. In case dealing with huge number of data in a cloud server, secured logging is must. This is due to the fact that cloud servers are freely accessible from anywhere at any time. As a result, data should be well-protected against intruders, hackers, and unauthorized users. Furthermore, because log data files frequently contain sensitive information, log records' secrecy and privacy are equally vital. At all times, the integrity of the log files and the logging process must be ensured. The main objective of this project is to develop a secured logging as a service with graphical password authentication method in cloud architecture. So, in the proposed method, privacy and preservation methods are enhanced. Correctness, confidentiality, data logs, privacy, preservation, and virtual private server (VPS) are the six key functions of protected logging (Virtual proxy server). The accuracy is concerned with historical data that is correct. Confidentiality refers to information that isn't displayed during a search. Data logs are used to identify relevant users based on their data history. File linking and data access history are part of the privacy system. The term "preservation" refers to the use of a more advanced color coding. Finally, the proxy server for virtual data access is handled by VPS. In the cloud architecture, there isn't much of a difference between hackers and intruders. Hackers come from different networks, whereas invaders come from the same networks. Intruders cannot be avoided, but hackers may be avoided. This is due to the possibility that intruders are aware of the network. This is because intruders may have prior information of the network into which they intend to break in. As a result, secure logging as a service is critical for all types of cloud server environments in order to ensure correct login for authorized users while preventing unauthorized users from logging in

Keywords: Authorization security, Secured logging, Intruders, Hackers, Unauthorized user.

INTRODUCTION

Traditional password systems are usually text based and vulnerable to many attacks, including shoulder surfing, dictionary attacks, man in the middle attack and eavesdropping and many others. As more users and organizations become familiar with these attacks, the need to address the security of such systems has also grown rapidly. Password authentication systems should encourage less predictable and strong passwords while maintaining memorability and security.

*Author for Correspondence

Athira S.

E-mail: athirasivadasan35@gmail.com

¹Assistant Professor, JCT College of Engineering and Technology, Coimbatore, TN, India

²Professor, JCT College of Engineering and Technology, Coimbatore, TN, India

³Assistant Professor, JCT College of Engineering and Technology, Coimbatore, TN, India

Received Date: December 29, 2021

Accepted Date: January 20, 2022

Published Date: January 29, 2022

Citation: Athira S., S. Dhanabal, K.M. Ravikumar. Enhanced Graphical Password System with Intelligent User Identification Model. Trends in Opto-electro & Optical Communication. 2021; 11(3): 23–29p.

Alphanumeric usernames and passwords are most commonly used for user authentication. One of the drawbacks of choosing such schema is passwords could be simply guessed. It is uncommon to not consider that if a password is hard to guess, then it is often hard to remember. Alphanumeric

passwords are also prone to dictionary attacks. Due to the problem with remembering random strings of characters, most users often settle on an average word or a name without realizing that their chosen passwords can be brute forced extensively in a very less time [1–7].

Humans can remember pictures much better than the text. This fact has been exploited to propose graphical password schemes as a feasible alternative to text-based schemes. In graphical password schemes, images are used instead of alphanumeric characters. User must remember a set of images to correctly login. The obvious drawback of such a scheme is having a large dictionary of such unique images stored in a memory but if the number of possible pictures is sufficiently large, the possible password space of a graphical password presumably offers better resistance to dictionary attacks. Another disadvantage is that these graphical schemes are prone to shoulder surfing attacks. In shoulder surfing, an adversary tries to guess the password by keenly looking at the user login their screens.

EXISTINGSYSTEM

Logging as a service is an outsourcing model for security management. Typically, Security as a Service involves applications such as higher end data security services like Government Information, Military information, Banking Information and etc. These kinds of software delivered over the Internet but the term can also refer to security management provided in-house by an external organization. Storing important data with cloud storage providers comes with serious security risks. The cloud can leak confidential data, modify the data, or return inconsistent data to different users. This may happen due to bugs, crashes, operator errors, or mis configurations. Furthermore, malevolent security breaches are more difficult to discover and more devastating than unintentional ones: foreign enemies may hack the cloud storage provider, or service provider staff may launch an insider attack. Despite its benefits, these worries have kept security-conscious businesses and consumers from utilizing the cloud. These aren't just intellectual concerns [8–10].

Data on Amazon's popular Simple Storage Service (S3) had been corrupted owing to an internal malfunction, and files no longer matched customers' hashes, according to public sources. Amazon verified the incident a day later, blaming a defective load balancer for intermittently corrupting single bytes in S3 responses while under strain. Another example of cloud data security breach happened when Google Docs had an access-control flaw that allowed papers to be shared with unauthorized readers inadvertently. Worse, a cloud storage company went out of business after losing 45 percent of its customers' data due to an administrative error [11–15].

Service Level Agreements from Amazon S3, Google Big Table, HP, Microsoft Azure, Cloud NAS, and others include security guarantees (SLAs). S3's SLA and Azure's SLA, for example, only guarantee availability: if availability falls below 99.9%, clients are refunded a contractual fee. As cloud storage becomes more of a commodity, suppliers will need to differentiate themselves through security. In this work, we look at how to construct a cloud storage system that allows for the detection of security property breaches, resulting in meaningful security SLAs.

The cloud security setting is different from the setting of previous secure storage or file systems research. The first distinction is that clients and cloud providers have entered into a financial agreement: clients pay for services in exchange for specific guarantees, and the cloud is an accountable entity. Previously, the server was usually a collection of untrustworthy remote machines that couldn't guarantee any level of service. The second distinction is that scalability is more significant because it is one of the cloud's major promises. Enterprises are important customers for the cloud; they have many employees requiring highly scalable access control and have large amounts of data [16].

DISADVANTAGES

- No Proxy Server used.
- Color code implemented for Https servers only. So that secured server only enjoys the color code

technology.

- Biometrics devices are used for security purpose, user can't able to carry the devices to allocations
- In case of hacking admin could not able to track the type of hacker.
- No availability of hacker charts and file attacking chart.
- Less security with more complex server handling problems.

SYSTEMDESIGN

SLAS is a record of events occurring within an organization's system or network. Because log data can be used to diagnose problems, fine-tune system performance, uncover policy violations, investigate criminal actions, and even record user activities, logging is essential. In digital forensic investigation of systems, log data are crucial. HIPAA (Health Insurance Portability and Accountability Act), for example, Payment Card Industry Data Security Standard, or Sarbanes-Oxley often require forensically sound preservation of information. To comply with these rules, all evidence presented in court, including log records, must be objective, not tampered with, and complete before they can be used. Since log files contain record of most system events including user activities, they become an important target for malicious attackers. An attacker, breaking into a system, typically would try not to leave traces of his or her activities behind. Consequently, the first thing an attacker often does is to damage log files or interrupt the logging services. Furthermore, the sensitive information contained in log files often directly contributes to confidentiality breaches. An example of this is when logs contain database transaction data. An attacker can frequently use log information to gain unauthorized access to a system. When a user enters her password in the username field while login into a system, this is an example of this. To record the information that a user has failed to log in, logging applications will save the password as the user-id. Last but not least, because the log file maintains a record of all system occurrences, information in the log file can be utilized to cause privacy breaches for system users. Given the foregoing considerations, it is critical that logging be performed in a secure way and that log records be appropriately safeguarded for a defined period of time. In addition, log management requires substantial storage and processing capabilities. The log service must be able to arrange data and provide a quick and useful retrieval mechanism.. Last, but not least, log records may often need to be made available to outside auditors who are not related to the organization.

Deploying a secure logging infrastructure to meet all these challenges entails significant infrastructural support and capital expenses that many organizations may find overwhelming. The emerging paradigm of cloud computing promises a low-cost opportunity for organizations to store and manage log records in a proper manner. Organizations can outsource the long-term storage requirements of log files to the cloud. The challenges of storing and maintaining the log records become a concern of the cloud provider. Since the cloud provider is providing a single service to many organizations that it will benefit from economies of scale. However, keeping and managing log information becomes more difficult when they are pushed to the cloud. The cloud provider may be open and honest, but he or she may also be curious. This means it can try not just to extract secret data from log records directly, but also to link log record-related activities to their sources. There is currently no system in place that covers all of the issues that arise when log storage and management is moved to the cloud [17–20] (Figure 1).

IMPLEMENTATION

CloudFormation

The public cloud environment is the IaaS/PaaS Infrastructure or Platform as a Service that we rent from Linux (IaaS) or Microsoft (PaaS). Both are enabled for web hosting. The SaaS stack will then run in your Internet environment, most likely in a virtualized environment on your own hardware, making it private. We specialize in private cloud technologies in this project. In this case, we're working in the cloud. If severe security requirements are required, choose a public or hybrid cloud environment; otherwise, use a public or community cloud environment. As a result, we're creating a web service for output, and the environment will be displayed in real time while hosting the programme. Finally, SaaS may be fully leveraged as IaaS / PaaS in a cloud context. As a result, we created a cloud environment (Figure 1).

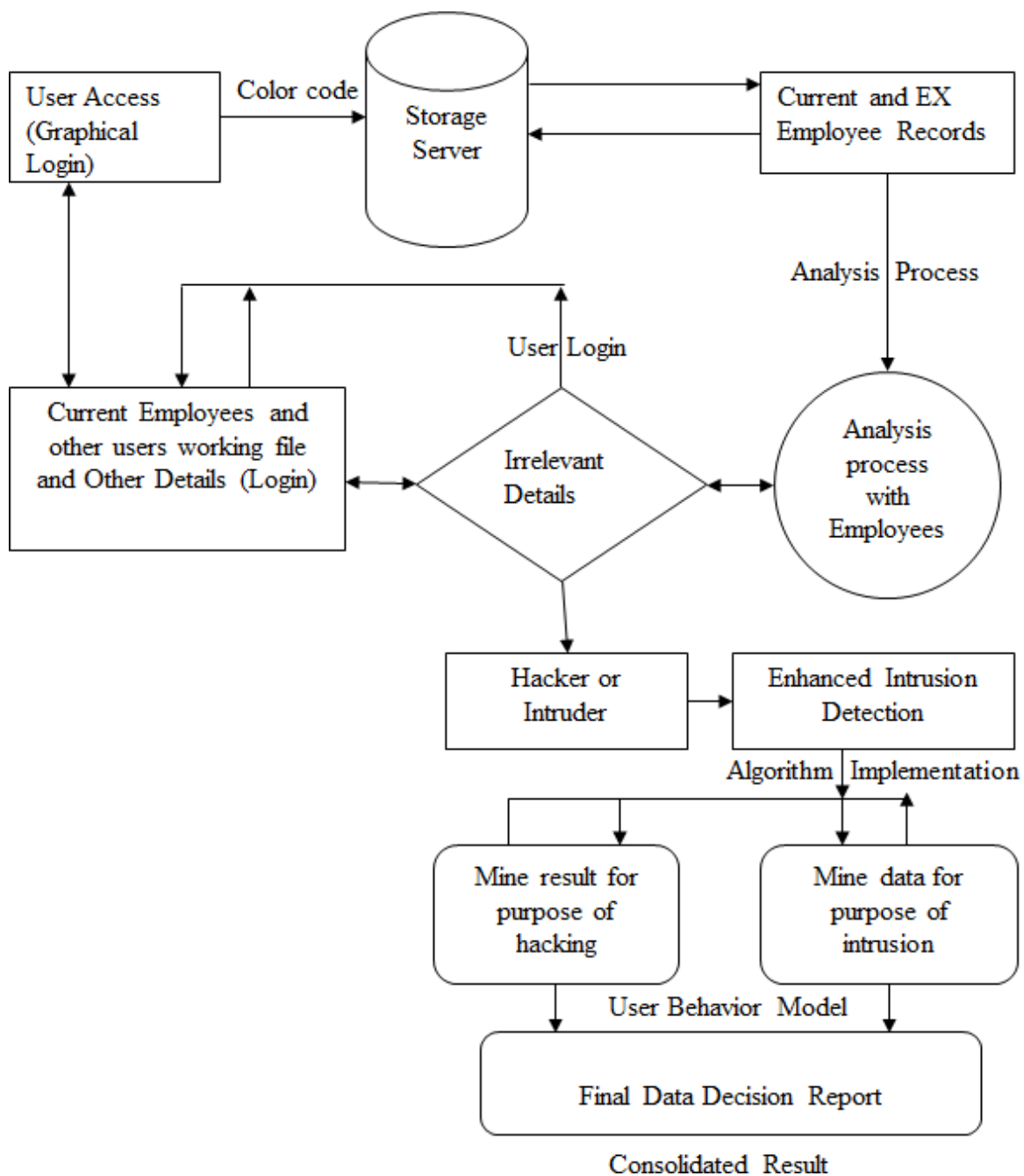


Figure 1. System Architecture.

Data AccessCreation

According to this module, some data or records will be created by the admin or user. The creating data will be the data set to be accessed by anyone. However, the file's security levels would be mentioned while uploading the entries to the server. Sensitive data records, confidential records, private records, and public documents will be divided into four categories for security purposes. The data security levels can be determined from the category itself. The data access strength will be used to classify this security level (Figure 3).

Secure Logging as a service

This module provided log for Cloud computing logging. In recent years, it has become a popular computer paradigm. Computer researches are frequently lacking in today's cloud computing designs..

Analyzing various logs (e.g., process logs, network logs, Performance) plays a vital role in computer forensics. Unfortunately, due to the black-box nature of clouds and multi-tenant cloud models, where numerous users share the same processing and network resources, gathering logs from them is extremely difficult. To overcome the issues of collecting logs from cloud infrastructure, we recommended employing log for cloud administration console. However, no actual work has been done to illustrate how to send cloud logs to investigators while maintaining user privacy and log integrity.

Figure 2. Login Page.

Figure 3. Data Uploading.

Logging of services

We present Secure-Logging-as-a-Service (SecLaaS), a cloud-based service that saves virtual machine logs and enables access to log files while maintaining cloud users' privacy. SecLaaS also saves proofs of previous logs, protecting the logs' integrity against dishonest investigators or cloud providers. Finally, by implementing SecLaaS for network access logs in this module, the scheme's feasibility is assessed. Open Stack, a popular open source cloud platform, by summarizing the desirable properties that we seek from a secure log management service based on the cloud computing paradigm.

LogReports

This is the prime module of this project; here admin will get the clear idea about the User, Intruder or Hacker. In case of attack by an Intruder or Hacker admin will get some notification like IP

monitoring, date and time details and file trying to be accessed. So that admin will provide more security to the current file which is trying to hack. A private data can be converted to a sensitive data zone or to confidential data zone. All the outputs will be shown in chart-based results (Figure 4).

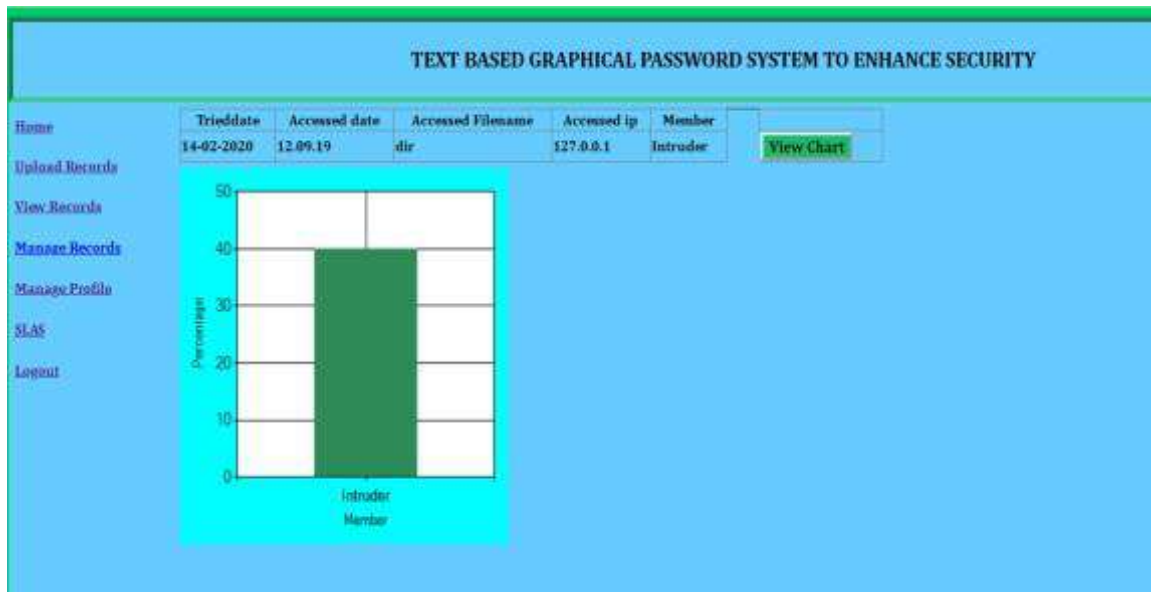


Figure 4. Intruder Identified.

CONCLUSION

We propose proofs of security violations for integrity and freshness as a tool for guaranteeing security in SLAs. We build a secure cloud storage system that detects and proves violations to these properties by combining cryptographic tools in a novel way to obtain an efficient and scalable system. We demonstrate that secured logging as a service in a reasonable overhead to the base cloud service. Logging plays a very important role in the proper operation of an organization's information processing system. Maintaining logs safely for long periods of time, on the other hand, is difficult and costly in terms of resources. In this paper, we proposed a complete system to securely outsource log records to a cloud provider. We reviewed existing solutions and identified problems in the current operating system-based logging services such as syslog and practical difficulties in some of the existing secure logging techniques. We then proposed a comprehensive scheme that addresses security and integrity issues not just during the log generation phase, but also during other stages in the log management process, including log collection, transmission, storage and retrieval. The problem of log privacy that arises when we outsource log management to the cloud is one of the unique challenges. During storage, retrieval, and destruction, log information should not be casually linked or traceable to their sources. Using the Tor network, we provided anonymous upload, retrieve, and delete protocols on log records in the cloud. The protocols we created for this purpose have the potential to be used in a variety of situations, including anonymous publish-subscribe.

REFERENCES

1. Basak Bilgi, trBulentTugrul, "A Shoulder-Surfing Resistant Graphical Authentication Method" 2018 IEEE.
2. Bilal Eid Fayyadh, Khalid Mansour, Khaled W. Mahmoud, "A New Password Authentication Mechanism Using 2D Shapes" 2018 8th International Conference on Computer Science and Information Technology (CSIT).
3. Chao Shen, Yufei Chen, Yao Liu and Xiaohong Guan, "Adaptive Human-Machine Interactive Behavior Analysis With Wrist-Worn Devices for Password Inference"- IEEE Transactions On Neural Networks And Learning Systems. IEEE 2018.
4. Deepika Gupta, Dr. Vishal Goar, Akhand Pratap Singh, Shikha Mathur, "Combination Of Textual

- And Graphical Based Authentication Scheme Through Virtual Environment"- 2017 IEEE.
5. K.PriyaT.Venkaiah Naidu R.VamsiKrishna," An Advanced Information Security System Using Image Based Graphical Password Scheme"- 2nd International Conference on Trends in Electronics and Informatics (ICOEI 2018).
 6. L.Gunaseeli, Dr.R.Aroul Canessane." Graphical Passwords Implies on Tolerance Password, Image Choice, and Puzzle Login Security"- international conference on information, communication& embedded systems (ICICES2017).
 7. Misbah UrrahmanSiddiqui,Mohd. Sarosh Umar, Miftah Siddiqui," A Novel Shoulder-Surfing Resistant Graphical Authentication Scheme"- 2018 4th International Conference on Computing Communication and Automation (ICCCA), IEEE 2018.
 8. Nida asmath," Conundrum – Pass: A New Graphical Password Approach. "-International conference on communication. IEEE 2019.
 9. Noor Ashitah Abu Othman, Anis Shobirin Abdullah Sani, Muhammad Akmal Abdul Rahman, Fakariah Hani Mohd Ali," Directional Based Graphical Authentication Method with Shoulder Surfing Resistant"- 2018 IEEE Conference on Systems, Process and Control (ICSPC 2018), 14– 15 December 2018, Melaka, Malaysia.
 10. P. A. Sosa-Valles, J. G. Villalobos-Serrano, P. Velarde-Alvarado, V. García, J. R. Parra-Michel,L. Mena, R. Martínez-Peláez," My Personal Images as My Graphical Password"- IEEE Latin America Transactions, VOL. 16, NO. 5, MAY 2018.
 11. P. Baskaran, Anurag.EG, Kaviyarasu.S, Eniyavan.AV, Karthikeyan.M," TIME SLOT BASED DATA SHARING WITH TIME SLOT BASED PASSWORD"- 2017 International Conference on Innovations in Information, Embedded and Communication Systems (ICIIECS).IEEE2017.
 12. R. Sudha, M. Shanmugaratnam," An Improved Graphical Authentication System to Resist the Shoulder Surfing Attack". 2019 International Conference on Technical Advancements in Computers and Communications.
 13. Prabhakaran, M.V. Ranjith Kumar," ADVANCED GRAPHICAL PASSWORDS USING CAPTCHA"- International Journal of Pure and Applied Mathematics Volume 118 No. 22 2018, 351-357.
 14. Siva Janaki Raman, Karunya Sri V S, Chathurya Pulluri, Sundararajan Rajagopalan, K Thenmozhi, and Rengarajan Amirtharajan," Numerical Password via Graphical Input – An Authentication System on Embedded Platform"- 2017 International Conference on Computer Communication and Informatics (ICCCI -2017), Jan. 05 – 07, 2017, Coimbatore, India.
 15. Sung-Shiou Shen, Tsai-Hua Kang, Shen-Ho Lin & Wei Chien," Random Graphic User Password Authentication Scheme in Mobile Devices"- International Conference on Applied System Innovation. 2017 IEEE.
 16. Tamajit Bhattacharya, Pushpender Sharma, MS. Sheetal Joshi; Dr. Shilpi Sharma- "Authentication Aura to Secure Graphical Password: The Case of Android Unlock Pattern"- International Journal of Computer Science and Mobile Computing, Vol.8 Issue.3, March-2019,
 17. TowseefAkram, Vakeel Ahmad, IsrarulHaq, Monisa Nazir," Graphical Password Authentication"- International Journal of Computer Science and Mobile Computing, Vol.6 Issue.6, June-2017.
 18. WantongZheng, ChunfuJia,"CombinedPWD: A New Password Authentication Mechanism using Separators betweenKeystrokes"-2017, 13th International Conference on Computational Intelligence and Security.IEEE2017.
 19. Wenjian Luo, Yamin Hu, Hao Jiang, and Junteng Wang," Authentication by Encrypted Negative Password" 2018 IEEE,Transactions on Information Forensics and Security. IEEE2018.
 20. Yeeun Ku, Leo Hyun Park, Sooyeon, And Taekyoung Kwon" Draw It As Shown: Behavioral Pattern Lock for Mobile User Authentication", 2019 IEEE. Volume 7,2019.

Intelligent Transportation System Avoids Collision by Disseminate the Warning Messages in Vehicular Adhoc Network

S. Karthikeyini^{1*}, G. Rajiv Suresh Kumar², R. Divya³

Abstract

Roads overload leftovers a critical issue while they are invariably increased so as to increase their capacity and enhance their effectiveness. This can be likely to cause many troubles specified ecologically, financially and socially. The progress of urban traffic management systems, structure and development of roads are solutions to handle this problem and acquire better the performance of the road transmission, but these solutions are high-priced and also need extra space for the establishment and lasting maintenance. A substitute would be to use the novel technologies within the field of communication for dispatch traffic information like dangerous road conditions and accident sites and also vehicles leaves warning messages to the emergency vehicles. In this paper, we present a VANET framework to avoid traffic congestion and also other vehicles in the network are warned of moving emergency vehicles. The emergency vehicles receive detailed information about the emergency vehicle and additional route information. The driver will take possible right action timely by receiving detailed information. This type of application rescues lives and save precious time.

Keywords: ITS-AC, VANET, Traffic, warning message, maintainance, road congestion

INTRODUCTION

Transportation plays a significant role within financial and social development and might be an influential catalyst for expansion. Nevertheless, the large number of vehicles exceeding the size if the roads cause many problems, especially in terms of road safety, and contamination. One of the foremost

important problems is traffic congestion, and this acts as a critical handicap for the road transport system. Bottleneck on the road is the state in which the power of the infrastructure is inadequate to regulate the flow due to the increased number of users causing a sphere slowdown in road traffic. This spectacle is distinguished by the disintegration of the quality of service, waste of time, stress problems for users, downgraded productivity, extended energy consumption, and increased pollution. Still, land transportation is the most used means of transportation, which demonstrates the exponential development in the number of vehicles each year, particularly in town areas, which makes the road infrastructure and the methods of traffic management out of place. Construction and expansion of roads, traffic, and access organizing roundabouts are answers to deal with this problem of traffic congestion

*Author for Correspondence

S. Karthikeyini
E-mail: karthikeyinicse@gmail.com

¹Assistant Professor, Department of Electrical and Electronics Engineering, JCT College of Engineering and Technology, Coimbatore, Tamil Nadu, India

²Professor, Department of Electrical and Electronics Engineering, JCT College of Engineering and Technology, Coimbatore, Tamil Nadu, India

³Assistant Professor, Department of Electrical and Electronics Engineering, JCT College of Engineering and Technology, Coimbatore, Tamil Nadu, India

Received Date: December 03, 2021

Accepted Date: December 18, 2021

Published Date: December 30, 2021

Citation: S. Karthikeyini, G. Rajiv Suresh Kumar, R. Divya. Intelligent Transportation System Avoids Collision by Disseminate the Warning Messages in Vehicular Adhoc Network. Journal of Telecommunication, Switching Systems and Networks. 2021; 8(3): 28–38p.

and develop the work of the transmission. But these solutions are costly and also need extra space for improved and constant maintenance.

Emergency vehicles such as ambulances, fire-juggernaut and patrol cars are distinctive to react to an emergency condition. In this way, reaching their destination of emergency state as soon as possible is the significant concern. Assume an ambulance arrive at the place of an accident place so ambulance going to the hospital carrying an injured person who requires medical service. When the fire started, fire-juggernaut which arrives at the place on right time. A patrol car which needs to reach the place where a crime has just been announced. In all three scenarios, the right time needed to arrive their destination has create huge difference and also protect human lives and time also. In concern to arrive their destination as possible, the emergency vehicles describeprecedence over the usual vehicles on the road and are frequently allowed by law to break traditional road rules in order to arrive their destinations in the quickly workable time, like driving via a crossing when the traffic signal light is red, or over the speed limit, like in the European countries and America. In a literature survey variousVANET routing protocols connect the mobile userfor disseminating the message along the way for intelligent and safe transportation system. The challenging task of finding and maintaining the route and deliver the information in right time and right destination. In IEEE 802.11p protocol standard support communication vehicle to vehicle and vehicle to a server through the ITS band of 5.9GHz (5.85-5.925 GHz) [1], [2]. IEEE 802.11p MAC covers Carrier Sense Multiple Access/ Collision Avoidance (CSMA/CA), Time Division Multiple Access (TDMA), Frequency Division Multiple Access (FDMA). CSMA/CA which sense the channel is ideal it transmit otherwise it choose the random back-off time slot from Contention Window. The draw of CSMA/CA is anunpredictable delay of channel access and hidden terminal problem occurred without using of packet RTS/CTS, which leads to the high rate of packet collision. The Space Division Multiple Access (SDMA) divides the road into cells and assign the slot for each cell. During the low density it wastes the bandwidth and it reducesthe network utilization [3]. To avoid the issue another IEEE 802.11p MAC TDMA used to allocate the time slot each vehicle to transfer the packet. Assign the slot through the Road Side Unit (RSU) or Cluster Head (CH) which increase the maintenance of centralized unit and can occur the merge collision. In a decentralized way allocate the slot to each vehicle reduce the overhead of maintenance cost, but it increases the access collision [4]. Decentralized ADHOC MAC exchange the frame slot information to one-hop neighborhood. And new entry vehicle acquires the slot from available slot. The draw back of ADHOC MAC not suited for two-way traffic because it doesn't handle the collision avoidance scheme [5]. IEEE 1609.3 covers the topology based routing protocol and position based routing protocol. The position based routing protocol gets the destination position information by GPS or exchange of a beacon message instead of maintain the routing table. In Greedy Perimeter Stateless Routing (GPSR) protocol forward the packet from source to destination. First, it follows the greedy forward to choose the nearest neighbor of destination within the transmission range otherwise it follow the planner graph to forward the packet from source to destination. Dynamic Source Routing (DSR) protocol finds the shortest path bythe Dijkstra algorithm between source to destination and a sequence of junction over the street map. In Greedy Perimeter Coordinator Routing (GPCR) has no need of street map information it need street and junction information and follow the restricted greedy to transfer the packet to node on the junction and not forward the Crossway of junction [6]. Vehicle position, speed, direction needed for the collision avoidance scheme and safety application. United States Department of Transportation (USDOT) supports event driven message which generated when any dangerous condition detected and a periodic message contain vehicle speed, position, direction which is used for safety application and collision prediction application [7, 8].

PROPOSED SYSTEM

Intelligent Transportation System (ITS) examines the information exchange and support Basic Safety Message for V2V various safety applications. It has different system such as Road Side Unit (RSU) may be a traffic signal controller, traffic management center and vehicle. The vehicle may be light vehicle, freight vehicle, transit vehicle and emergency vehicle which are illustrated in Figure 1.

In vehicle communication, initially in our model emergency vehicle transmission the alert message to all nearby vehicles. The broadcast message having the Prevalent State of Emergency Vehicle (PEV), Emergency Vehicle Specification SEV, Partial Route of an Emergency Vehicle (PEV) and length of The length of route varied from time to time. So by using this time1 is the sufficient time to seize a suitable action by the driver. The optimal value for time1 has to be established by field tests and user studies. Relative velocity of Emergency Vehicle (REV) can be calculated maximum speed of vehicle M_s at a time.

$$M_s = \frac{\text{Distance}}{t} \quad (1)$$

A minimum S is defined by mmin to make sure that REV is of effective length, even when the EV is halted or driving slow gradually. Presently we use dmin = 400m. Broadcasting delay is expected to be insignificant in contrast to the additional parameters and is, thus, implicitly and road map material is modeled in every node.

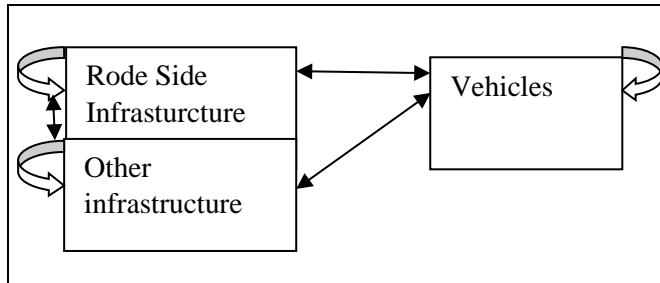


Figure 1. Intelligent Transportation Model for safety application.

Additionally, a 4-digit EV code is included in warning messages that provide information on the organizational type of the EV (e.g., patrol, ambulance, fire-juggernaut), the size of the EV (e.g., car, truck), and special properties (e.g., trailer) that enable other drivers to identify the emergency vehicle easier and react properly. This EV code provides more accurate warnings to identify the processes P for searching the nearest nodes,

$P = \{\text{Set of processes}\} P = \{P1, P2, P3, p4\}$

If (searching)

{

then

$P1 = \{e1, e2, e3, e4, e5\}$

}

Where

{

{e1= find the current position}

{e2= calculate speed}

{e3= find the route}

{e4= find the nearest nodes}

{e5= find the Distance between the nearest nodes}

}

$$EM = \sum_{BFD}^{FFD} \{\text{Broadcast the information}\} \quad (2)$$

FFD = Fix Forward Distance

BFD = Fix Backward Distance

Parameter Distance between two nodes n1, n2

Where to position of $n1 = p1(x1, y1)$ and position of $n2 = p2(x2, y2)$

The distance measurement between two vehicles is denoted in Equation (3).

$$\text{Distance} = \sqrt{(x1 - x2)^2 + (y1 - y2)^2} \quad (3)$$

Nearest neighbor can be calculated as distance < nearest neighbor threshold

Here, the emergency vehicle, sending a warning message between fix forward distance and backward forward distance. So the other vehicle driver took the correct action. By using this technique, emergency vehicle to reach their destination as much early as possible

Skeleton of the Broadcast algorithm on the sender side:

```
# Generate a new message ID if needed
IF (distance (previous_location, current_location) >500)
{
OR (previous_time - current_time> 10)
OR (previous_road≠ current_road)
OR (previous_lane≠ current_lane)
}
THEN message_id← Generate_New_Message_ID()
END
IF
{# Prepare the packet
Packet← New_TC4EV_Packet (message_id, priority, current_location, current_velocity,
current_direction, current_road, current_lane, next_road_1, next_road_2, next_road_3) Send_Packet
(packet) }
```

ALGORITHM FOR EMERGENCY VEHICLE DECISION CONTROL

Begin Algorithm A source broadcasts Emergency message within the VANET.

When receiving Emergency message by a vehicle:

Cardist=dist(*carpath[0])

Ambudist=dist(*ambupath[0])

If (carseg== ambuseg)

```
{
then
```

Broadcast message (“ Ambulance in lane1, Change lane1 to lane2”)

Broadcast speed and distance information

```
}
Else
```

```
{
if (car-dist == ambu-dist) then
```

Broadcast message (“Change your oute, Follow the route 2”)

Broadcast speed and distance information

Broadcast message (“Change your lane Strictly”)

Broadcast speed and metric information vehicle

```
}
End if
End if
```

If(carseg!=ambu-seg && car-dist == ambu-dist)

```
{
then
Broadcast message (“Inform the driver to stay same lane, but slow down to let the ambulance go first”)
}
```

End
if End
Process p2 for forward the alternative path message to avoid the road congestion.
Process p2 = {e1,e2,e3}
{e1 = density of vehicle on the road}
{e2= speed of vehicle on the road}
{e3 = inter distance between the vehicle}

If an accident occurred, work in progress or the road is blocked, traffic congestion can occur. The congestion of road measured by the weighted parameter as speed of vehicle and distance of vehicles. Traffic management predicts the congestion and sends the alternate path message to avoid the congestion.

Number of vehicles on the road segment n_j . Average vehicle speed denoted in Equation (4).

$$V_s = (1/n_j \sum_{i=1}^{n_j} 1/v_i)^{-1} \quad (4)$$

The space between the vehicles V_{space} and S_{speed} is safety speed of vehicles on the road is denoted in Equation (5).

$$V_{space} = \frac{1}{n_j} \left(\sum_{i=1}^{n_j} length(vehic\ le\ i) + \sum_{i=1}^{n_j} \frac{speed(vehic\ lei)}{S_{speed}} \right) \quad (5)$$

The Density K of vehicle on the road segment and where V_{space} is an interspace between vehicles(6)

$$K = 1/V_{space} \quad (6)$$

The density K on the length L on the road segment at given time at t_1 is equal to the inverse of average space of n vehicle (7)

$$K(L, t_1) = \frac{n}{L} = \frac{1}{V_s(t_1)} \quad (7)$$

The number of vehicles Q passing in the road segment (8)

$Q = KV$ where K is the density and V is velocity

$$Q = 1/V_{space} \quad (8)$$

If Flow $Q < \text{Threshold}$ congestion occurred, it broadcasts the alternative path message along the road.

The flow and density relationship illustrated in Figure 2.

If Flow $Q (V_i) < \text{Threshold}$

Prepare the packet

Packet ← New_TC5CC_Packet (message_id, priority, current_location, current_velocity, current_direction, current_road) Send_Packet (packet)

ALGORITHM FOR CONGESTION DECISION CONTROL

Begin Algorithm B source broadcasts Congestion Control within the VANET.

When receiving Congestion Control by a vehicle V1

If Vehicle V1 within RSU range

Broadcast directly

Else

It finds the route from source V1 to destination RSU

RSU broadcast the alternative path decision along the road

P3= Lane changes warning of the microscopic model of the two- way lane traffic (Table 1).

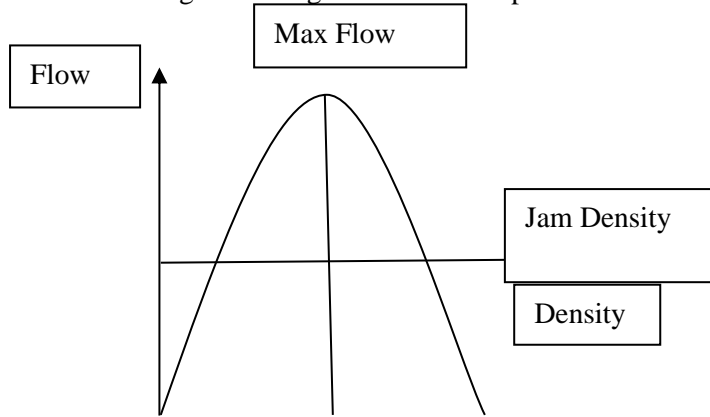


Figure 2. Relationship between Density and Flow of vehicle.

Table 1. Summary of symbols & their definition.

Symbol	Definition
Δt	Time step in [s]
Front distance	Expected inter-distance between I and j+1 after the lane change in [m]
Back distance	Expected inter-distance between I and j-1 After the lane change in [m]
Δx_i^{safe}	Safe distance at highway
$\Delta_{x_{j-1}}^{safe} (v_{j-1})$	Safe inter-distance between I and j-1 vehicle if on the same lane in [m]
$\Delta_{x_{j+1}}^{safe} (v_{j+1})$	Safe inter-distance between I and j+1 vehicle if on the same lane in [m]
V_{max}	Maximum velocity in [m/s]
V_{min}	Minimum velocity in [m/s]
V_{des}	Desired or targeted velocity in [m/s]
V_{safe}	Safe velocity in [m/s]

The combination of Global Navigation Satellite System (GNSS) and wireless communication support the safety application. Aim of safety application mitigates the vehicular collision and increase the traffic flow through the exchange of road condition information [9, 10]. The Lane Change Warning (LCW) application warns the driver who performs lane change when it is unsafe and predict the speed of remote vehicle. Vehicle I want to change the lane, it has to find the maximum movement of following vehicles in the different lane [11, 12]. According to the Pipe's rule safe distance formulated in Equation (9)

$$\Delta x_i^{safe}(v_i) = L + T \cdot v_i + \phi \cdot v_i^2 \quad (9)$$

Where L is a Length of the vehicles, T is reaction time on the highway, ϕ is a adjusting parameter function on deceleration to maintain safe distance, $\phi \cdot v_i^2$ breaking distance.

When $\phi=0$ breaking distance between following and leading vehicle are equal.

It follows the inter-distance with the following vehicle j-1 at maximum speed at the next time stamp. The distance between inter vehicle follows condition which needs the current safe inter-distance with leading vehicle's safety, increased if it would reach the desired speed and the condition (10) and (11) explains inter-distance between vehicle i and j+1, j-1 would not violate safety and avoid the accident on the same lane which is illustrated in Figure (3).

$$v_i^{des} > \Delta x_{i, i+1}$$

$$\Delta x_{i,j+1} \text{ or lead distance} > \Delta_{x_{j+1}}^{safe} (v_{j+1}) \quad (10)$$

$$\Delta x_{i,j-1} \text{ or follow distance} > \Delta_{x_{j-1}}^{safe} (v_{j-1}) \quad (11)$$

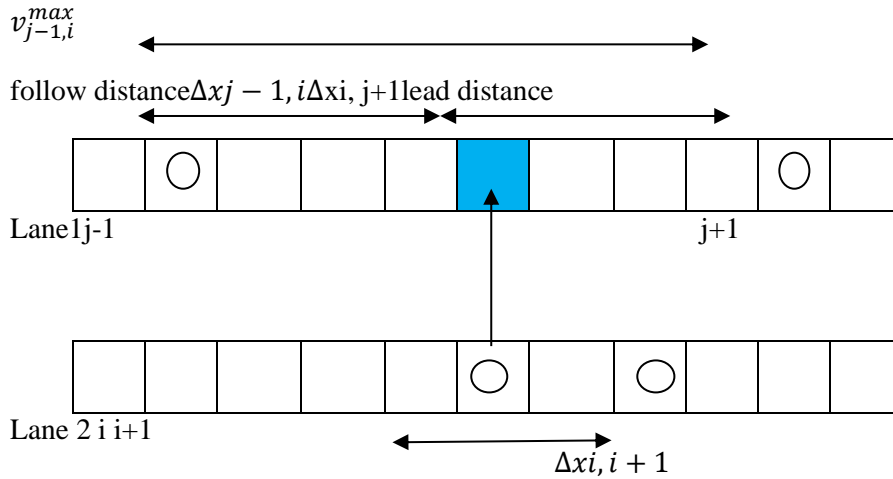


Figure 3. Safe Inter-Distance for Lane-change.

P4 = Broadcast Emergency Break Warning

Each car has a vehicle to vehicle communication devices such as ITRI WAVE/ DSRC(IWCW) is a radio communication system [13]. ITRI has an Advanced Driving Assistant system (ADAS) which integrate Lane Deviation Warning System (LDWS), Front Warning Collision System (FWCS) and Blind Spot Detection System (BSDS) are developed on System on Chip (SoC) [14, 15]. Each car can broadcast the Basic Safety Message (BSM) to warn the neighbor's car which is illustrated in Figure 4(a), (b), & (c).

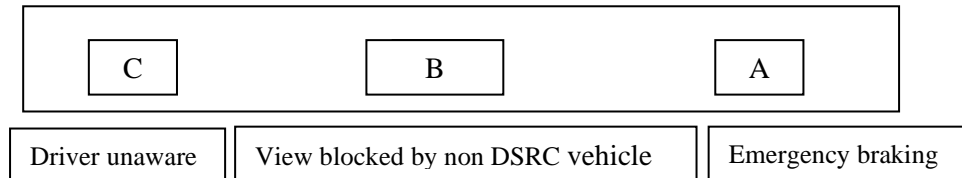


Figure 4. (a) Heavy break

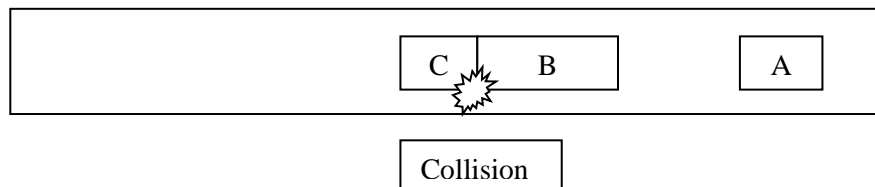


Figure 4. (b) Without EBW.

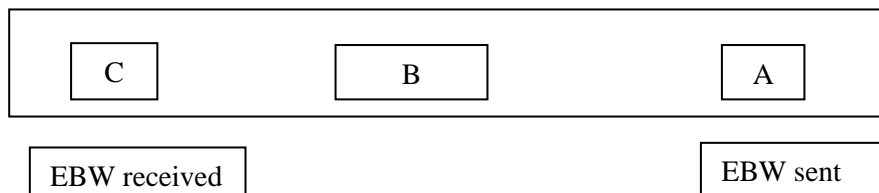


Figure 4. (c) With EBW.

Figure 4(a) brake lights are difficult to see if there is blocking the vehicle in between. (b) Without EBW vehicle C is not informed (c) With EBW, vehicle C is informed about the breaking information of vehicle A before the driver of vehicle B. A vehicle equipped with an IWCW system with consist of image detection, recognition module to collect the vehicle type, color and speed, GPS used to understand the car position information, User Interface (UI) responsible to display warning condition which is connected with IWCW device with Wi-Fi, accelerometer (G-sensor) or On Board Diagnostics -II used for detecting the emergency braking. An IWCW system broadcast vehicle type, color, speed, license plate information, vehicle list, current position and emergency message periodically broadcast nearby vehicle. The License plate comparison technology is to collect information on vehicle type, color and speed from camera to improve the position accuracy. The vehicle's list have the information about lane that are in same or adjacent. The vehicle's list construction module in the IWCW system which adds the license plate information of the front vehicle to BSM. The front vehicle's emergency brake warning information sent back to the car in the same lane not in the different lane which is illustrated in Figure 5.

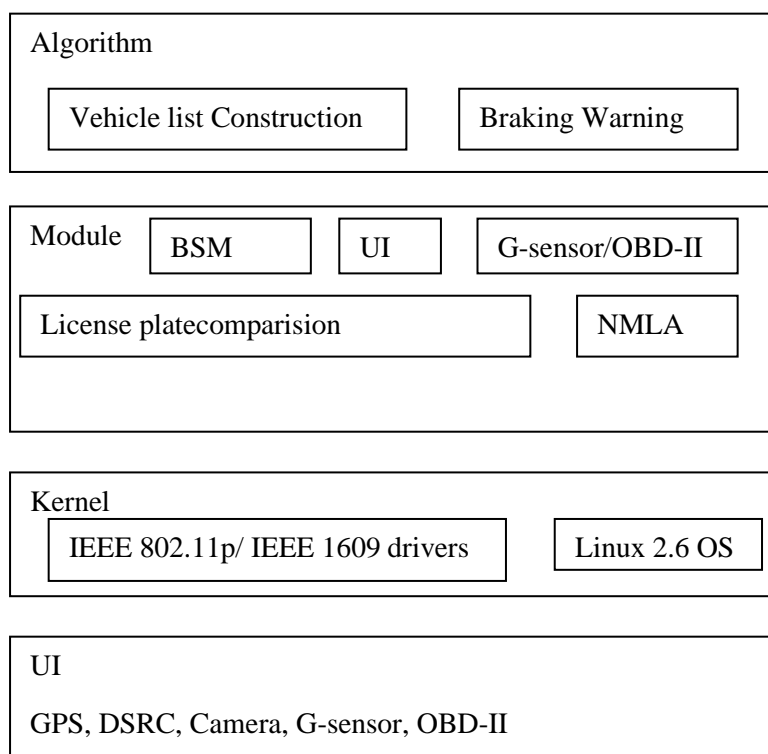


Figure 5. IWCW architecture.

Emergency Brake Warning Display:

1. IWCW broadcast BSM contain license plate of front vehicle, vehicle color, type, speed, current position, vehicle list
2. License plate comparison, continuously collect the information from camera and license plate of the front vehicle
3. Update vehicle list
4. If emergency braking signal arrived the
5. Check signal source in vehicle list
6. If a signal source in the vehicle list
7. Determine the emergency level and display emergency brake warning in UI
8. Continue step 1.

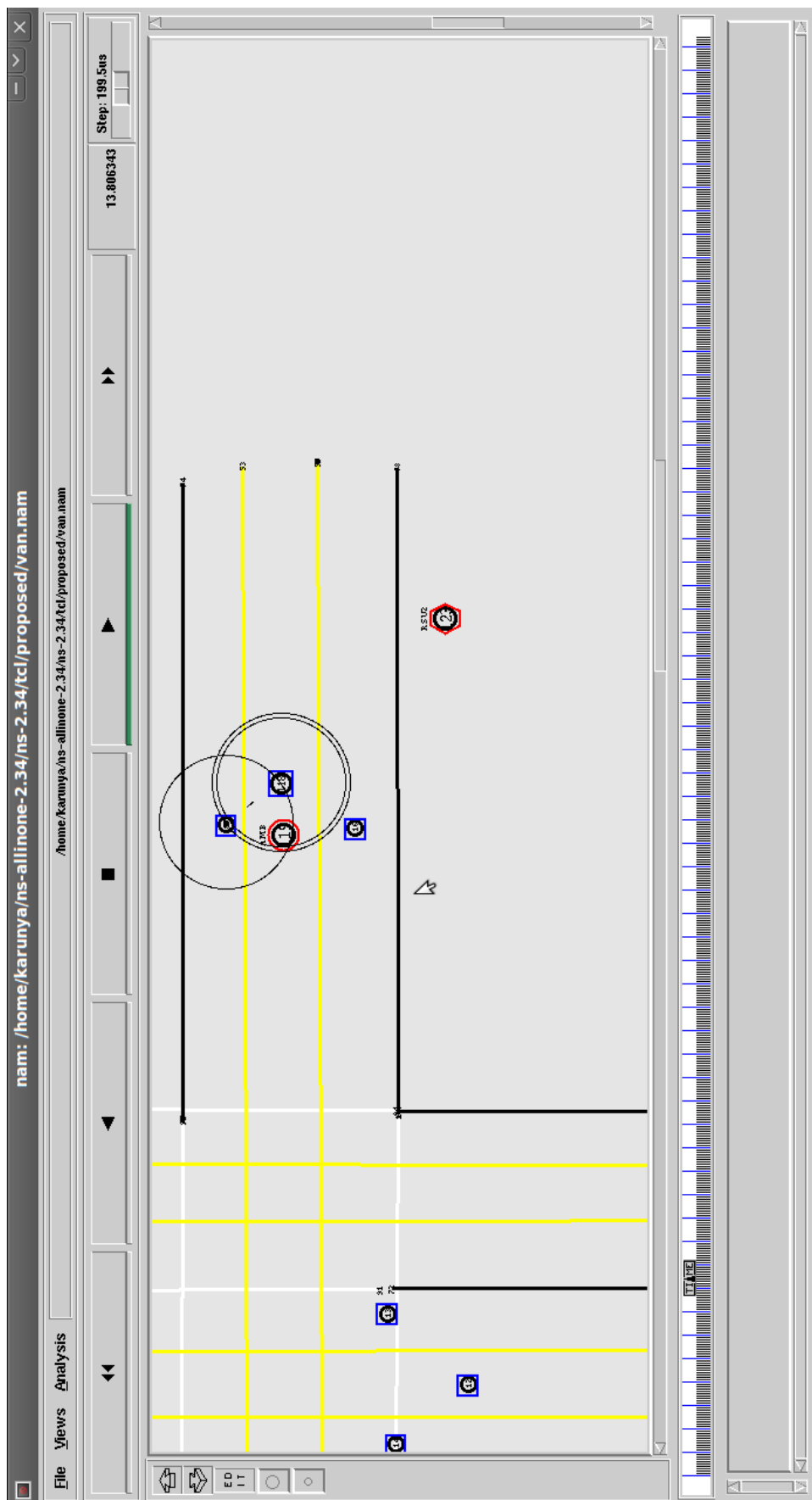


Figure 6. Transmission of Waring Message in Taffic Scenario.

SIMULATION RESULT

The Intelligent Transportation System (ITS) is an advanced application in which information, communication technologies and Artificial Intelligence (AI) are applied in the field of vehicles, drivers and traffic management. To improve road safety and traffic efficiency on the road, it provides traffic information through safety applications such as route information, road curve warning, safe-overtake warning, speed limit warning, accident site information and emergency vehicle warning. Assume that an ambulance has to carry an injured person from the accident site to the hospital for emergency treatment. In such a situation, the ambulance is allowed to break road norms like crossing the road when the traffic light is red or surpassing the speed limits so as to arrive at the destinations at the right time. The ambulance broadcasts this emergency message to its neighbouring vehicle on the road to avoid mishaps and enable it to arrive at the destination at the earliest. Hence, the driver of the neighbouring vehicle will take timely action by receiving emergency information. The simulation of traffic scenario is illustrated in Figure 6.

Table 2 shows the parameters used in the ITS-AC for reliable communication.

Table 2. Simulation parameters for ITS-CA.

Simulation Parameter	Value
Simulator	Ns-allinone-2.34
Topology size	1200 × 1200 m
Speed of vehicles	100m/s
Number of vehicles	100
Transmission range	250 m
Road Side Unit	6
Base Station	1
Packet size	512 bytes
Bandwidth	10MHz
Channel Data Rate	27Mbps
MAC type	802.11p

CONCLUSION

The vehicles in the network are responsible for communicating the warning information from source to destination for which it requires efficient nodes for improving effective communication. For effective communication, it is necessary to build the routing algorithm, which aims to improve the QoS in changing characteristics of the wireless channels over time and space in vehicular communication. The proposed work builds reliable routing protocol and maintains the consistent path when the speed of vehicles increases gradually in the network, resulting in low delay, controlled overhead, less packet loss, low energy consumption and high throughput compared to the existing protocol.

REFERENCES

1. U.S. DOT announces decision to move forward with vehicle-to-vehicle communication technology for light vehicles, <http://www.dot.gov/briefingroom>.
2. Hsieh. T, Chao. Y, Tsai. P, Tsai. M, “Real-time driving safety of dynamic full screen bird view technology and applications”, ICL J. 153(6), 43–50 (2013)
3. M.I. Hassan, H.L. Vu, and T. Sakurai, “Performance analysis of the IEEE 802.11 MAC protocol for dsrc safety applications”, Vehicular Technology, IEEE Transactions on, 60:3882–3896, Oct 2011.
4. Z. Doukha and S. Moussaoui “A sdma-based mechanism for accurate and efficient neighborhood discovery link layer service”, IEEE Transactions on Vehicular Technology, PP(99):1–11, 2015.
5. FlaminioBorgonovo, Antonio Capone, Matteo Cesana, and Luigi Fratta, “Adhoc mac: New mac architecture for ad hoc networks providing efficient and reliable point-to-point and broadcast services”, Wireless Networks, 10:359–366, 2004.
6. Lochert et al., “Geographic Routing in City Scenarios”, Mobile Computing and Communications Review, Volume 9, Number 1, 2005.

7. Y. C. Hu, A. Perrig and D.B. Johnson, "Packet leases: A defense against wormhole attacks in wireless networks", Proceedings of IEEE Infocom'03, 2003.
8. Michael McGurrian, "Vehicle information exchange needs for mobility application", version 3.0. Technical Report FHWA-JPO-13-065, April 2013.
9. Huang. J and Tan H.S , "Vehicle future trajectory prediction with a DGPS/INS- based positioning system", Proceeding of the American Control Conference, pp. 5831-5836, 2006, Minneapolis MN.
10. Robinson. C, Caveney. D, Caminiti. L, Baliga G, laberteaux. K and Kumar. P, "Efficient message composition and coding for a cooperative vehicle safety application", IEEE Transaction on Vehichicular Technology 56(6),3244-3255.
11. Zheng. Q, Hongm. X and Liu. I, " An Agenda -based mobility model", 39th IEEE-Annual Simulation Symposium(ANSS-39-2006), Huntsville, AL, USA.
12. Zhou. B Xu. K and Gerla. M, " Group and Swarm Mobility Models for Ad hoc network Scenarios using virtual Tracks", Proc of the IEEE Military Communication Conference (MILCOM'04)pp. 289-294.
13. Li.M, Wu.T,Lin.W, Lan.K, Chou.C, Hsu.C, " On the Feasiblity of using 802.11p for Communication of Electronic Toll Collecting Systwm(IEEE international Conference on Network-Based Information Syste, Albanic, 2011), pp68-75.
14. Alam.N, Balaai. A.T, Dempster. A.G, " A DSRC Doppler based Cooperation Positioing Enhancement for Vehicular Network with GPS availability", IEEE Trans.Vehicul. Technol.60 (9), 4462-4470(2011).
15. Park. Y, Kim. H, " Collision Control of periodic Safety Message with Strict Messaging frequency Requirement", IEEE Trans.Vehicul.Technol.62(2),843-852(2013).

Refinement Model Based on Deep Learning Technique for Prediction of Temperature Using Missing Data

¹Shifana Begum, ²Dr.Senthil Kumar, ³Dr. Mahaveerakannan R, ⁴S. Karthkeyini,

⁵Dr.Kannadasan R, ⁶Dr. A. S. Anakath,

¹Research Scholar, Department of Computer Science and Engineering, Srinivas University
College of Engineering and Technology, Mangalore

² Professor, Department of Computer Science and Engineering, Srinivas University College
of Engineering and Technology, Mangalore

³Associate Professor, Department of Artificial Intelligence, Saveetha School of Engineering,
Saveetha Institute of Medical and Technical Sciences, Chennai, India.

⁴Assistant professor, Department of CSE, JCT College of Engineering and Technology
Coimbatore.

⁵Assistant Professor (Sr. Grade 1), Department of Software Systems, School of Computer
Science and Engineering, Vellore Institute of Technology (V.I.T.), Vellore, India

⁶Professor, Department of Information Technology, E.G.S. Pillay Engineering College,
Nagapatinam, India

* Corresponding author: mahaveerakannanr.sse@saveetha.com

Article Info

Page Number: 824-835

Publication Issue:

Vol. 71 No. 3s2 (2022)

Abstract

Researchers have recently turned their focus to time sequence predicting of meteorological such as daily heat in an effort to overcome the limitations of standard forecasting methods. Due to the difficulty of the task, it is difficult to create and choose an precise time-series forecast perfect. This is a critical factor in human life and many other areas, including agriculture and manufacturing. People's health will be adversely affected by an increase in temperatures in the highland urban heat, especially in the summer, as a result of this. As a result of this paper's research, a novel temperature prediction model based on deep learning has been developed (i.e., the progressive deep cascade categorization model). In order to achieve this, a large volume of high-quality model training data is required. A drawback to weather data collection is the inability to measure data that has been overlooked. There is a high probability of missing or incorrect data due to the nature of data collection. To make up for the lost weather data, the proposed temperature prediction ideal is being used to fine-tune the existing data. Research also uses a deep learning network for time-series data modelling because the temperature changes throughout the year. Various deep learning techniques are also being examined to verify the model's efficacy. In particular, the suggested model's refinement function can be used to restore lost data. The model is retrained using the refined data after all the missing data is refined. Finally, the proposed model for predicting temperature has the capability of doing so. The suggested model's (RMSE) root-mean-squared error, accuracy, precision, and recall are used to evaluate its performance.

Keywords: Weather Data; Temperature Prediction; Time-Series Prediction; Missing Data; Progressive Deep Cascade Classification; Refining Data.

Article History

Article Received: 28 April 2022

Revised: 15 May 2022

Accepted: 20 June 2022

Publication: 21 July 2022

Introduction

Humans have undergone a variety of weather and climate variations since the beginning of human history, some of which have prompted people to relocate. Dangerous weather phenomena, such as heat waves and torrential deluges, are becoming extra shared and penetrating as a result of climate alteration. Both the environment and human activities are harmed by these changes [1], which are potentially life-threatening. The rate of weather change has accelerated in the last decade, and numerous research have been done to determine the causes of the shift and devise solutions [2]. For example, air quality, wind speed, and electricity consumption can all be predicted using deep learning techniques that have recently gained popularity [3–5].

Throughout the previous few decades, there has been an upsurge in the frequency of thrilling weather events such cold weather, heavy snowfall, torrential rain, and drought, all of which cause harm to people's health and property [6]. People's lives are negatively affected by weather change, in other words. [7] Outdoor workers are particularly vulnerable to unexpectedly high temperatures. Using temperature forecasts, you can decide what to dress and where to work on any given day[8]. At least 10 days' forecast should be provided for each site or region where the temperature forecast is to be used [9].

Numerical weather prediction models (NWP) are commonly used by meteorological institutes to estimate future weather conditions [10]. Over the most part, NWP models are designed to forecast weather for vast geographic areas, such as they are adept at managing weather that is intricately linked to multiple elements that have an impact on the weather the next day. According to [11], the NWP has a tendency to cause temperature anomalies as the elevation and topographical complexity of the area increases. Furthermore, NWP models have difficulty predicting temperature changes in places with complicated topography [12].

A temperature forecast model based on DL is the goal of this project, which uses real-time meteorological data. When it comes to constructing a neural network, a cascade network is used in this approach. Weather data is better suited to a proposed architecture because of its time-series features [13]. When training deep learning models, a lot of training data is required, but it must be free of any errors. The collection of meteorological data, however, has a constraint in that we can't measure data that we have missed. There is a high probability of missing or incorrect data due to the nature of data collection. The projected temperature prediction model therefore adds a missing data function into the PDC framework in order to replace lost meteorological data. The four phases of the suggested model are as follows. The model's initial step is to determine if any input data is missing. Using all of the training data, a PDC-based refinement model is built in the second stage of model training. In the third phase of the projected model, the temperature of the missing vector mechanisms is attempted to be estimated. The final phase is to use the improved data to retrain the temperature prediction model.

According to this structure, the rest of the paper is: Section 2 focuses on existing methods, whereas Section 3 explains the proposed paradigm with PDC description. Section 4 depicts the experimental analysis used to test the proposed model's classification accuracy. Section 5 concludes the investigation with a summary of the findings.

2. Literature Review

When it comes to climate data, Curceac et al. (2019) [14] use both a kernel-based regression model and a SARIMA model. There is an overview of several models, from neural networks to SVM to Markov chains that they provide in a quick but comprehensive literature review. Graf et al. (2019) [15] anticipate river temperature using wavelets and artificial neural networks. Using an ensemble of 12 independent forecasting models, Hassani et al. (2018) [16] emphasis on weather irregularities.

Aladin-HIRLAM was used to estimate air temperatures. Predicting temperature variations in complicated terrain over time and space remains a difficulty for NWP models. According to Frnda et al. [18], the European Centre for Medium-Range Weather Forecasts (ECMWF) could benefit from a neural network-based model to increase its output accuracy and highlight the potential of neural network for weather forecast development. As a result of this, artificial neural networks (ANNs) have become increasingly popular in recent years as a means of forecasting the weather. It was discovered by Fahimi et al. [19] that the most accurate model with the least error and the greatest correlation coefficient used five different neural network models to estimate Tehran's winter maximum temperature. They used this model with three variables: mean temperature, sunshine hours, and difference among extreme temperature and least temperature.

3. Proposed Methodology

With regards to training data collection, as stated in Section 1 (Introduction), the process is very challenging. In other words, the data gathered are likely to be partial, with random or long gaps. The purpose of this section is to present an alternative PDC-based temperature prediction model that joins a role for missing data modification to help fill in the data gaps.

3.1. Investigation of Weather Factors Connected to Temperature

The effects of the weather on temperature are examined in detail in this section. Data from the South Korean Meteorological Office (KMA) is used for this purpose. There are 36 years worth of hourly temperature, wind speed and direction measurements as well as relative humidity and total precipitation accumulation as well as atmospheric pressure and barometric pressure. After that, the correlation coefficients for all 36 years of temperature and other weather variables are calculated (Table 1). Wind speed, direction, and humidity are all closely related to temperature, as you can see in the chart. As a result, this paper's temperature predictions rely on variables including wind speed, direction, and humidity.

Table 1. Coefficients among temperature and other weather issues.

Weather Factors	Wind Direction	Humidity Relative	Wind Speed	Vapor Pressure	Cumulative Precipitation	Barometric Pressure
Correlation	0.71	0.64	0.69	0.25	0.38	0.30

3.2. Proposed Refinement Function Using LSTM

Temperature is linked to three weather variables (wind speed, as discussed in the preceding subsection. This means that if heat data are missing at certain times but other

weather elements are accessible, the missing data can be reconstructed by using the linked features. Using the PDC as a correlator between other meteorological parameters and temperature, a refinement function of the projected model is realised.

In the suggested model, there are four phases of processing. During the first stage, the algorithm checks to see if any of the input vectors are missing, which are 4-D weather data. Each missing component is linearly interpolated using observed data from the past and future if any are lost. All training data is subjected to this procedure. Figure 1 shows the flow of the research work.

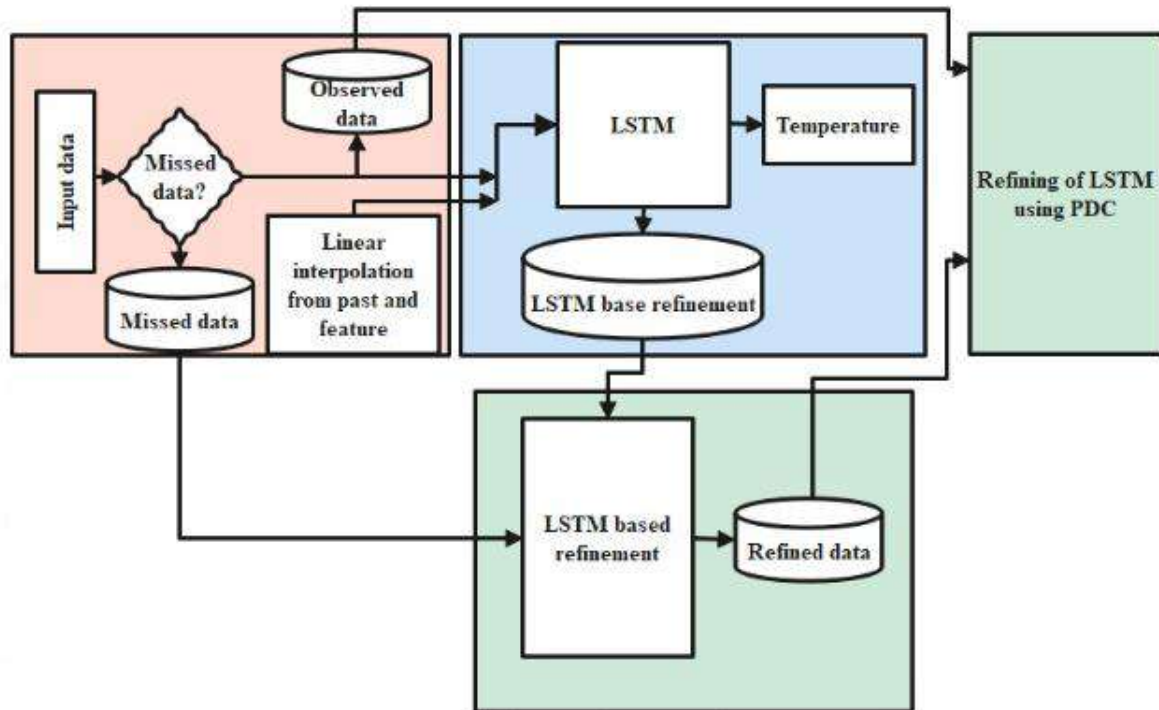


Figure 1: Working flow of the Research Model

Using all of the training data, the second stage creates a PDC refinement model that includes linear interpolation for any missing data. The following is a definition of the PDC-based refining model:

It is usual for researchers to increase the number of traits when they have no prior knowledge. This can lead to feature redundancy as well as an increase in computation complexity and a corresponding increase in computer resources. Consequently, we propose a progressive deep cascade classification model (PDC).

3.2.1. Progressive cascade classification

The class likelihood of a sample is used to classify PDC. Random forest is an collective learning process that employs averaging to increase predictive accuracy and control overfitting to fit a number of decision tree classifiers on numerous sub-samples of the dataset. A dataset with a large number of variables can be effectively processed using random forests. During the forest-building process, they generate an internal, unbiased guess of the generalisation error. Their ability to estimate missing data is also impressive. As a result, we

begin our categorization process with RF (Random Forest). The RF identification results may be influenced by the number of attribute values due to the random nature of the forest construction process. As a result, different RFs are used to categorise the same wavelet energy vector F_l in order to overcome the characteristics' bias. The classification outcomes in each tier of the cascade are then generated by the mean class probability distribution of these RFs. When the classification accuracy of PDC does not improve any more, the cascade classification process comes to an end. It is possible to automatically identify the number of cascade layers by comparing the accuracy of the categorization. By using a progressive cascade classification, an individual sample can be identified.

Suppose there are N data samples $\mathbf{S}_i \in R^{V \times L} (i = 1, 2, \dots, N)$ confidential into K classes by PDC. The feature vector of \mathbf{S}_i in the j th scale is $\mathbf{F}_{il} = [\mathbf{E}_{j1}^i, \dots, \mathbf{E}_{jv}^i, \dots, \mathbf{E}_{jv}^i] (l = J - j + 1)$. Each layer includes a set of M random forests, i. e.

$$RF_S^l = \{RF_1^l, RF_m^l, \dots, RF_M^l\} \quad (1)$$

where $m = 1, 2, \dots, M$. Each RF_m^l yields a classification probability vector p_m^l of \mathbf{S}_i according to F_{ij} , and $p_m^l = [p_{m1}^l, p_{mk}^l, \dots, p_{mk}^l] (k = 1, 2, \dots, K; l = 1, 2, \dots, L)$. p_{mk}^l represents \mathbf{S}_i has a k th-class probability based on the categorization of RF m in the l th layer. It is thus possible to express the probability vector (P_a) of \mathbf{S}_i in the l th layer produced by M random forests as

$$\tilde{P}_i^l = [p_1^l, \dots, p_m^l, \dots, p_M^l] \quad (2)$$

Superimposing results from numerous layers can replicate the progressive recognition procedure of humans if each cascade layer's categorization result is treated as one credit of \mathbf{S}_i . Because of this, the probability distribution (P) of M random forests in the higher level is cascaded with those in all lower layers in the l th layer.

$$p_1^l = [\tilde{P}_i^l, \tilde{P}_i^{l-1}, \dots, \tilde{P}_i^1] \quad (3)$$

Then the l layers can be printed as

$\bar{p}_1^l = [\bar{p}_{i1}^l, \bar{p}_{ik}^l, \dots, \bar{p}_{ik}^l]$, where

$$\bar{p}_{ik}^l = \frac{1}{lM} \sum_{t=1}^l \sum_{m=1}^M p_{mk}^t \quad (4)$$

Sample \mathbf{S}_i 's class label is established by taking the class probability p_{ikl} with the highest value. Classification result fusion of many layers thus realises human coarse-to-fine recognition. The classification accuracy of the present model, M_l , can be determined by comparing the prediction outcomes of all samples. For example, let's say A_l is the prediction accuracy of model M_l in the l th cascade layer. A_l and A_{l-1} will be compared in every layer to see if the l th should be included to the model. As a result, the PDC features a feedback cascade design. A_l is a function of the number of cascade layers, so.

$$H(A_l) = \begin{cases} l & \Delta A_l < 0 \\ l+1 & \Delta A_l \geq 0 \end{cases} \quad (5)$$

where $\Delta A_l = \Delta A_{l+1} - A_l$. Eq. (5) indicates that in the following three scenarios, the categorization cascade comes to an end:

- ❖ Next layer categorization accuracy is lower than the last layer's;
- ❖ There is no increase in categorization error between successive levels;
- ❖ All samples have been accurately categorised.

According to the preceding explanation, the procedure of PDC can be summarised as follows:

Vol. 71 No. 3s2 (2022)

<http://philstat.org.ph>

Step 1. Initialization

1 Input N_1 training samples $S_i(i = 1, 2, \dots, N)$ from all sample dataset. Divide N_1 into sub – training set N_{11} and sub – test set N_{12} .

2 Set initial values of M .

. Classification

1) For every sample $i = 1: N_{11}$

Input F_i^l in the sub – training set to the set of M random forests RF_s^l in the l th layer;
Generates the l th cascade probability distribution \bar{P}_i^l by RF_s^l .
Construct the cascade probability distribution in the l th layer P_i^l and compute the m
Decide the class label of sample according to the largest class probability of \bar{P}_i^l .
End.

2) Output the temporary recognition model M_l .

2. Prediction

i. Input N_{12} samples into M_l .

ii. Predict the class labels of N_{12} samples according to M_l . and compute classification

3. Cascade

If $\Delta A_l < 0 \parallel \Delta A_l = \Delta A_{l-1} = 0 \parallel A_l = 1$, then $L = l$, cascade is stopped and classification model M_L is accomplished, go to Step 4; else $L = l + 1$, go to Step 3-1;

end.

4. Input N_2 test samples into M_L and output the classification result of $S_i(i = 1, 2, \dots, N_2)$.

End.

It is in this third stage of the proposed PDC-based refining model that the temperature data that were already discovered are used to estimate temperatures for times when the data are unavailable. Refinement functions are used to replace the missing temperature data with the expected data. Using the refinement function, the missing data from the proposed model is refined and then mixed with the acquired data that has all of the necessary components to train the PDC.

4. Results and Discussion

4.1. UM Model

Since 2010, the KMA has used the unified model (UM) created by the UK Met Office to forecast the weather. Weather forecasting at KMA is comprised of a trifecta of NWP systems: GDAPS, RDAPS, and the Local Data Assimilation and Prediction System (LDAPS). The RDAPS and LDAPS activities, whose domains are depicted in Figure 2, are bound by the predictions of GDAPS and RDAPS.

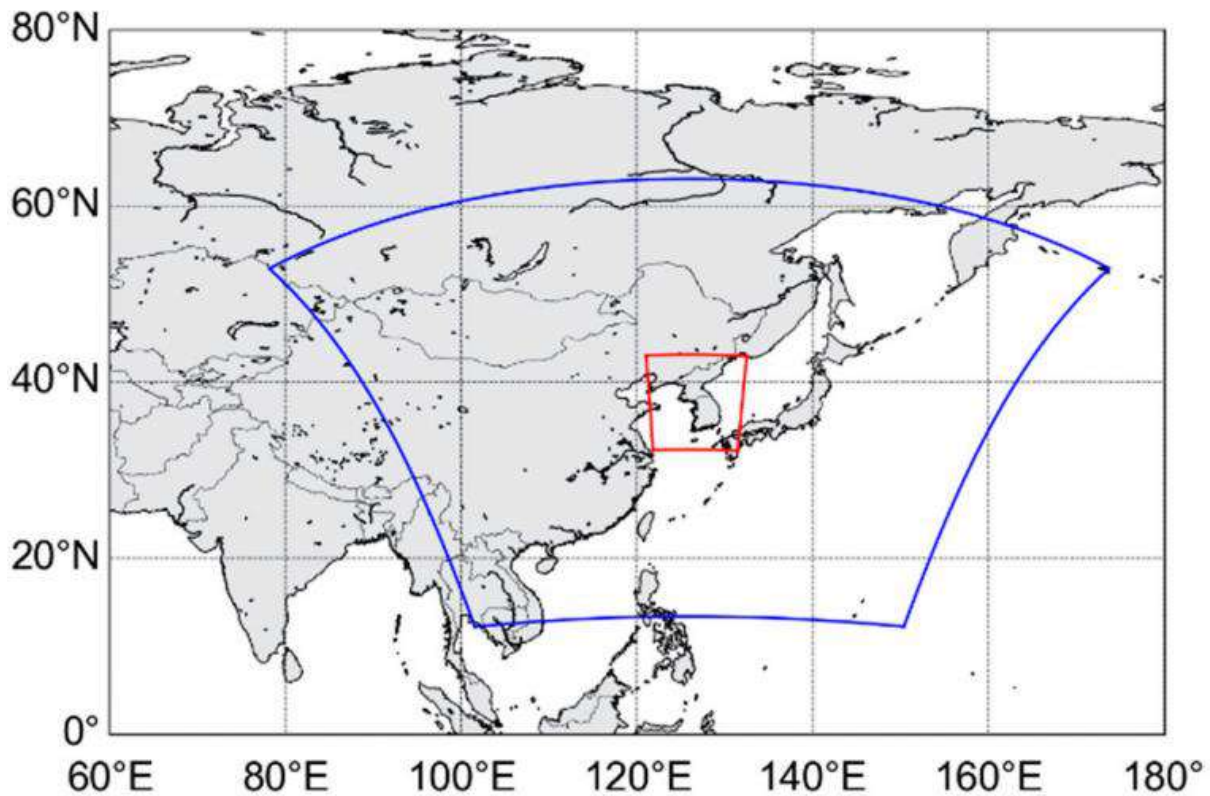


Figure 2. UM system domain, where blue and red lines signify RDAPS and LDAPS (Local Data Assimilation and Prediction System and Regional Data Integration and Prediction System, respectively). [20].

RDPAS and LDAPS, as depicted in the figure, have horizontal resolves of 12 km 12 km and 1.5 km 1.5 km, correspondingly, and cover East Asia and South Korea. The top elevations of the RDAPS and LDAPS are set to 80 and 40 km, respectively, for both systems' 70 sigma vertical layers.

For the KMA UM-based NWP system, Table 2 provides a summary of the physical alternatives that can be used. This model's anticipated temperature was tested against data from the official data archive of the University of Michigan (UM).

Table 2. Physical options of unified model based arithmetical weather prediction (NWP) scheme used in KMA.

Scheme	Physical Options
Mixed-phase precipitation [22]	Microphysics
Mass flux convection with convective available potential energy (CAPE) closure [23]	Cumulus scheme
Met office surface exchange scheme (MOSES)-II land-surface [24]	Land surface model scheme
First-order non-local boundary layer scheme [25]	Planetary boundary layer (PBL) scheme

Edwards-Slingo general 2-stream scheme [26]	Radiation scheme
--	------------------

4.2. Database

Using KMA meteorological data, we compiled hourly readings of temperature, relative humidity, wind speed, and direction for the purposes of this investigation [27]. Over a period of 37 years (from November 1981 to December 2017), weather data was collected across Seoul, Gyeonggi, and Jeolla in South Korea. These data were split into two sets: a training set of 36 years (from November 1981 to December 2016), and a test set of one year (from January to December 2017). The test set was used to determine the accuracy of the model. It should be noted that the training set's period of weather data collection did not coincide with the test set's. If there was no extra explanation for training and testing data, then all prediction models in this study were trained and assessed using the training data and test data, correspondingly. The accuracy of the model's predictions was also averaged across three locations, one for each prediction model.

4.3. Performances Metrics

Here, the proposed model's classification accuracy is tested with various DL classifiers, hence, the parameters are used that are discussed as follows:

- A. Accuracy:** Predicted connection records are estimated by dividing the whole test dataset by the number of predicted records. For DL, the better the model if it has a higher level of precision. Using an experimental dataset with balanced classes, accuracy is a suitable statistic.
- B. Precision:** If the attachment logs are successfully identified, then the estimated ratio of correctly identified attachment logs to total attachment logs is 1. If the precision is higher, the DL model is better than the ML model (Precision [0,1]). Accuracy is listed below.
- C. F1-Score:** F1-Score is also referred to as F1. The harmonic mean is precisely defined and easily recalled.

The results of the three prediction models were summed up to get an average. temperature were all absent from the training set, with 38 percent of the data missing. For the RMSE and MBE, the temperature difference between the actual and anticipated readings was divided by the time interval (t) to find the difference in temperature between Y_{tr} and Y_{tp} .

$$RMSE = \sqrt{\frac{\sum_{t=1}^N (Y_t^r - Y_t^p)^2}{N}} \quad (6)$$

and

$$MBE = \frac{1}{N} \sum_{t=1}^N (Y_t^r - Y_t^p) \quad (7)$$

where N is the total sum of times for the assessment.

4.4. Performance Evaluation of Proposed Model

Here, two different types of validation is carried out, i.e. 60%-40% and 80%-20% of data are used.

Table.3. Comparative analysis of 60% 40% on Proposed with various existing algorithms.

Algorithm	Accuracy	Precision	Recall	F-score
Linear Regression	80.10	87.21	80.15	80.43
Naive Bayes	85.71	84.32	85.93	83.45
KNN	92.10	92.43	92.15	91.68
DT	92.46	93.48	92.44	91.81
SVM	89.52	90.21	89.54	89.03
RNN	94.53	96.61	92.52	92.24
LSTM	94.16	96.17	92.32	92.10
PDC	95.62	98.32	94.62	94.53

Initially, the above Table 3 and Figure 3 shows the comparative analysis of various models for 60%-40% of weather data. In first of Linear Regression algorithm gets an accuracy value of 80.10%. In another LSTM model reaches the accuracy level of 94.16% and finally the proposed model reaches the accuracy of 95.62%, in LSTM model is nearest accuracy percentage of the proposed model.

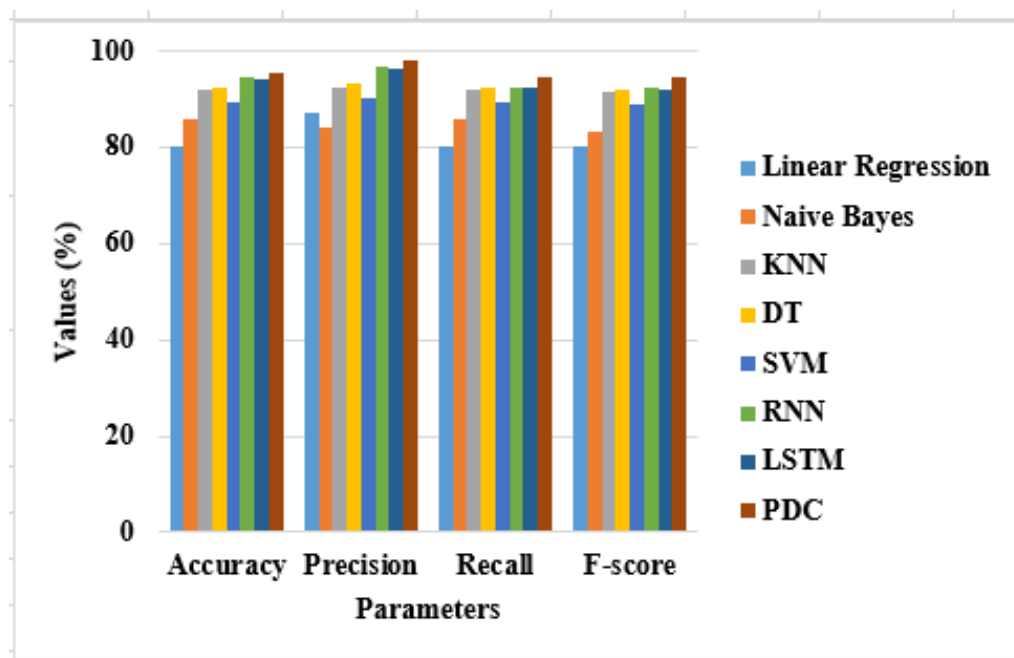


Figure 3: Comparative Analysis of proposed model in terms of various metrics for 60:40

Table.4. Comparative analysis of 80% 20% on Proposed with various existing algorithms.

Algorithm	Accuracy	Precision	Recall	F-score
Linear Regression	81.10	99.41	75.91	86.72
Naive Bayes	87.70	99.41	85.21	91.82
KNN	92.50	99.82	90.98	95.27
DT	92.90	99.78	91.52	95.41

SVM	92.50	99.63	91.38	95.18
RNN	92.70	99.90	91.93	95.32
LSTM	93.27	99.91	92.47	95.63
PDC	94.32	99.95	93.24	96.02

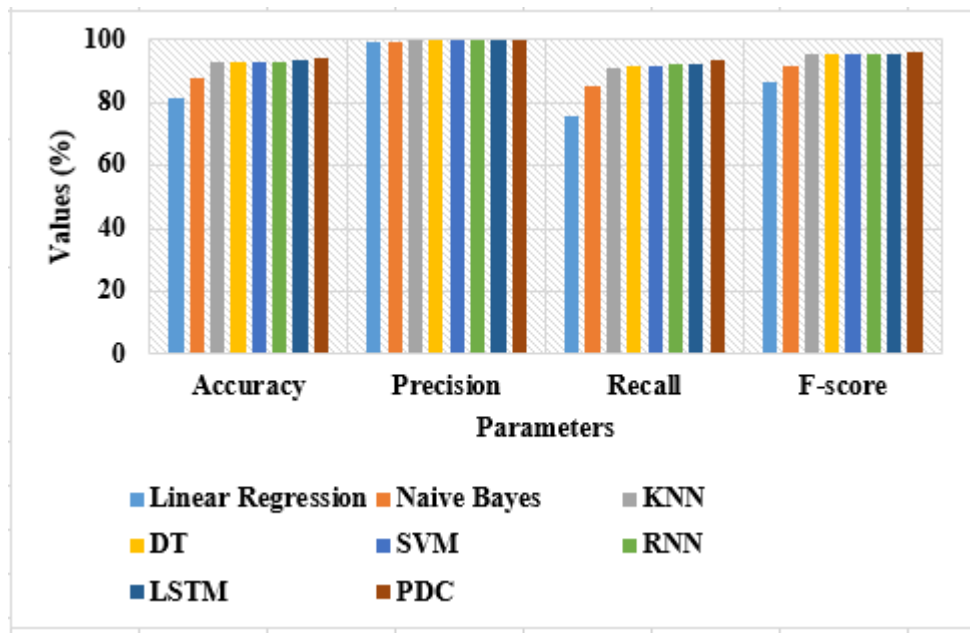


Figure 4: Comparative Analysis of proposed model in terms of various metrics for 80:20

A PDC-based temperature forecast ideal was then expanded to forecast 7 and 14-day future temperatures, and its RMSE was associated to the other models. In Table 4 and Figure 4 mentions the Comparative analysis of 80% 20% on Proposed with various existing algorithms. In this procedure we compare the results of RMSE and MBE values.

Table 5. Compare the RMSE and MBE of the temperature predictions made for 7 and 14 days in advance.

Model/Day	RMSE		MBE	
	7	14	7	14
RNN	3.15	3.61	-2.08	-3.26
LSTM	3.05	3.21	0.93	1.68
PDC	2.81	3.06	0.41	-0.79

Table 5 shows the tendency for this long-period temperature forecast to reduce RMSE and MBE. Refinement of the proposed model resulted in an RMSE of 3.06 for 14-day forecasts, which was lower than the RNN's 14-hour prediction RMSE.

5. Conclusion

DL-based temperature prediction model was suggested in this study to track temperature dissimilarities from 6 h to 14 d time periods by considering the important weather variables. A PDC network was used to fit the time-series data into the model. A PDC

framework comprising temperature, and wind direction was used to refine the missing data, which frequently occurs in the collected weather record. Then an experimental PDC-based temperature forecasting method, such as 7 and 14 days, was used to test the model. Each neural network model's RMSE, or root-mean-square error, between actual and forecast temperatures was also assessed. In addition, the missing data in this research was refined using weather data such as wind direction. It is our goal to develop a temperature prediction model that incorporates additional meteorological variables such as soil temperatures and aerosols in the future. That is to say, a PDC will use all of the available meteorological data as input features and act as a temperature predictor and missing data refiner at the same time.




References

- [1]. World Health Organization. Available online: <https://www.who.int/news-room/fact-sheets/detail/climate-change-and-health> (accessed on 28 August 2019).
- [2]. Salman, A.G.; Kanigoro, B.; Heryadi, Y. Weather forecasting using deep learning techniques. In Proceedings of the International Conference on Advanced Computer Science and Information Systems, Depok, Indonesia, 10–11 October 2015; pp. 281–285.
- [3]. Zhou, Y.; Chang, F.-J.; Chang, L.-C.; Kao, I.-F.; Wang, Y.-S. Explore a deep learning multi-output neural network for regional multi-step-ahead air quality forecasts. *J. Clean. Prod.* 2019, 209, 134–145.
- [4]. Ghaderi, A.; Sanandaji, B.M.; Ghaderi, F. Deep forecast: Deep learning-based spatio-temporal forecasting. In Proceedings of the International Conference on Machine Learning, Time Series Workshop, Sydney, NSW, Australia, 6–11 August 2017; pp. 264–271.
- [5]. Bedi, J.; Toshniwal, D. Deep learning framework to forecast electricity demand. *Appl. Energy* 2019, 238, 1312–1326.
- [6]. Parry, M.; Canziani, O.; Palutikof, J.; van der Linden, P.; Hanson, C. Climate Change 2007: Impacts, Adaptation and Vulnerability. Available online: https://www.ipcc.ch/site/assets/uploads/2018/03/ar4_wg2_full_report.pdf (accessed on 30 October 2019).
- [7]. Schulte, P.A.; Bhattacharya, A.; Butler, C.R.; Chun, H.K.; Jacklitsch, B.; Jacobs, T.; Kiefer, M.; Lincoln, J.; Pendergrass, S.; Shire, J.; et al. Advancing the framework for considering the effects of climate change on worker safety and health. *J. Occup. Environ. Hyg.* 2016, 13, 847–865.
- [8]. Abhishek, K.; Singh, M.P.; Ghosh, S.; Anand, A. Weather forecasting model using artificial neural network. *Procedia Technol.* 2012, 4, 311–318.
- [9]. Campbell, S.D.; Diebold, F.X. Weather forecasting for weather derivatives. *J. Am. Stat. Assoc.* 2005, 100, 6–16.
- [10]. De Giorgi, M.G.; Ficarella, A.; Tarantino, M. Assessment of the benefits of numerical weather predictions in wind power forecasting based on statistical methods. *Energy* 2011, 36, 3968–3978.
- [11]. Zhao, T.; Guo, W.; Hu, C. Calibrating and evaluating reanalysis surface temperature error by topographic correction. *J. Clim.* 2008, 21, 1440–1446.

- [12]. Sekula, P.; Bokwa, A.; Bochenek, B.; Zimnoch, M. Prediction of air temperature in the Polish Western Carpathian Mountains with the ALADIN-HIRLAM numerical weather prediction system. *Atmosphere* 2019, 10, 186.
- [13]. Cao, Q.; Ewing, B.T.; Thompson, M.A. Forecasting wind speed with recurrent neural networks. *Eur. J. Oper. Res.* 2012, 221, 148–154.
- [14] Curceac, S., Ternynck, C., Ouarda, T. B., Chebana, F., & Niang, S. D. (2019). Shortterm air temperature forecasting using nonparametric functional data analysis and SARMA models. *Environmental Modelling & Software*, 111, 394–408.
- [15] Graf, R., Zhu, S., & Sivakumar, B. (2019). Forecasting river water temperature time series using a wavelet–neural network hybrid modelling approach. *Journal of Hydrology*, 578, Article 124115.
- [16] Hassani, H., Silva, E. S., Gupta, R., & Das, S. (2018). Predicting global temperature anomaly: A definitive investigation using an ensemble of twelve competing forecasting models. *Physica A. Statistical Mechanics and its Applications*, 509, 121–139.
- [17] Sekula, P.; Bokwa, A.; Bochenek, B.; Zimnoch, M. Prediction of air temperature in the Polish Western Carpathian Mountains with the ALADIN-HIRLAM numerical weather prediction system. *Atmosphere* 2019, 10, 186.
- [18] Frnda, J.; Durica, M.; Nedoma, J.; Zabka, S.; Martinek, R.; Kostelansky, M. A weather forecast model accuracy analysis and ecmwf enhancement proposal by neural network. *Sensors* 2019, 19, 5144.
- [19] Fahimi Nezhad, E.; Fallah Ghalhari, G.; Bayatani, F. Forecasting Maximum Seasonal Temperature Using Artificial Neural Networks “Tehran Case Study”. *Asia Pac. J. Atmos. Sci.* 2019, 55, 145–153.
- [20]. Korea Meteorological Office of Weather Online Resources. Synoptic Weather Observation Data. Available online: https://web.kma.go.kr/eng/biz/forecast_02.jsp (accessed on 29 October 2019).
- [21]. Met Office Weather Forecasts for the UK. Available online: <https://www.metoffice.gov.uk/research/approach/modelling-systems/unified-model/index> (accessed on 29 October 2019).
- [22]. Wilson, D.R.; Ballard, S.P. A microphysically based precipitation scheme for the UK meteorological office unified model. *Q. J. R. Meteor. Soc.* 1999, 125, 1607–1636. [CrossRef]
- [23]. Gregory, D.; Rowntree, P.R. A mass flux convection scheme with representation of cloud ensemble characteristics and stability-dependent closure. *Mon. Weather Rev.* 1990, 118, 1483–1506. [CrossRef]
- [24]. Essery, R.; Best, M.; Cox, P. MOSES 2.2 Technical Documentation. Available online: http://jules.jchmr.org/sites/default/files/HCTN_30.pdf (accessed on 12 October 2019).
- [25]. Lock, A.P.; Brown, A.R.; Bush, M.R.; Martin, G.M.; Smith, R.N.B. A new boundary layer mixing scheme. Part I: Scheme description and single-column model tests. *Mon. Weather Rev.* 2000, 128, 3187–3199. [CrossRef]
- [26]. Edwards, J.M.; Slingo, A. Studies with a flexible new radiation code: 1. Choosing a configuration for a large-scale model. *Q. J. R. Meteorol. Soc.* 1996, 122, 689–719.
- [27]. Korea Meteorological Administration. Surface Observation. Available online: https://web.kma.go.kr/eng/biz/observation_02.jsp (accessed on 30 October 2019).

Research Article

Detection and Prediction of HMS from Drinking Water by Analysing the Adsorbents from Residuals Using Deep Learning

Sanjay Kumar Suman,¹ N. Arivazhagan ,² L. Bhagyalakshmi,³ Himanshu Shekhar,⁴ P. Shanmuga Priya,⁵ T. Helan Vidhya,⁵ Sushma S. Jagtap,⁵ Gouse Baig Mohammad ,⁶ Shubhangi Digamber Chikte,⁷ S. Chandragandhi,⁸ and Alazar Yeshitla ⁹

¹St. Martin's Engineering College, Hyderabad, Telangana, India

²Department of Computational Intelligence, SRM Institute of Science and Technology, SRM Nagar, Kattankulathur 603203, India

³Department of Electronics and Communication Engineering, Rajalakshmi Engineering College, Chennai, Tamil Nadu, India

⁴Department of Electronics and Communication Engineering, Hindustan Institute of Technology and Science, OMR, Kelambakkam, Chennai 603103, India

⁵Rajalakshmi Engineering College, Chennai, India

⁶Department of Computer Science and Engineering, Vardhaman College of Engineering, Hyderabad, India

⁷Department of Computer Science and Engineering, Visvesvaraya Technological University (VTU), Center for PG Studies, KALABURAGI-585105, Karnataka, India

⁸Department of Computer Science Engineering, JCT College of Engineering and Technology, India

⁹Department of Biotechnology, College of Biological and Chemical Engineering, Addis Ababa Science and Technology University, Ethiopia

Correspondence should be addressed to Alazar Yeshitla; alazar.yeshi@aastu.edu.et

Received 28 December 2021; Revised 9 February 2022; Accepted 18 February 2022; Published 24 March 2022

Academic Editor: Lakshmipathy R

Copyright © 2022 Sanjay Kumar Suman et al. This is an open access article distributed under the Creative Commons Attribution License, which permits unrestricted use, distribution, and reproduction in any medium, provided the original work is properly cited.

Contamination HM is an important issue associated with the environment, and it requires suitable steps for the reduction of HMs in water at an acceptable ratio. With modern technologies, this could be possible by enabling the carbon adsorbents to adsorb the pollutions via deep learning strategies. In this paper, we develop a model on detection and prediction of presence of HMs from drinking water by analysing the adsorbents from residuals using deep learning. The study uses dense neural networks or DenseNets to analyse the microscopic images of the residual adsorbents. The study initially preprocesses and extracts features using standardised procedure. The DenseNets are used finally for detection purpose, and it is trained and tested with standard set of microscopic images. The experimental results are conducted to test the efficacy of the deep learning model on detecting the HM composition. The results of simulation show that the proposed deep learning model achieves 95% higher rate of detecting the HM composition from the adsorption residuals than other methods.

1. Introduction

Humans and animals both need access to clean water. To live a long and healthy life, it is essential to have access to safe drinking water [1]. The problem is that while the global need for water continues to rise each year, pollution from numerous sources has damaged potential water sources [2]. The climate change effects including tempera-

ture increasing and water cycle changes exacerbate the flooding, droughts, and contamination of chemicals in water [3].

For example, if a polluted water supply is used for irrigation, people may be exposed to diseases or poisonous chemicals from the water, or they may eat aquatic species that have been poisoned by the toxins. However, for the vast majority of people in the world poorest

countries, polluted water is the greatest threat to their health [4].

People in underdeveloped nations are particularly vulnerable to the negative effects of rising pollution because they lack the water resources to be treated efficiently or it is considered as its ability on accessing the water system to be safer one [5]. People mostly lack fundamental sanitation, including drinking water, and people tends to spend more on getting water from various sources, including boreholes, piped water, springs, protected wells, packaged water, or rainfall, according to the World Health Organization [6].

Water-related diseases are more likely to occur in impoverished countries if people are unable to consistently obtain an improved drinking water supply. According to the WHO, more than millions die from water borne diseases that include dengue and diarrhoea [7]. The greatest hazard to human health in developing countries is the pollution of drinking water by microbiological pathogens. There is also a rising concern about the increasing of Heavy Metals (HMs) in the drinking water supply [8].

HM contamination has increased as a result of an increase in industrial and urban activity in developing countries in recent years. Many businesses, including coal-fired power stations and mines, release contaminated wastewater, which is combined with solid waste disposal and waste recycling to create a significant amount of pollution, which is further exacerbated by vehicle emissions and other urban activities [9].

More than 80% of municipal and industrial waste is discharged into natural ecosystem without proper treatments. The urban polluted storm water, rainwater transfer, and agricultural runoff transformation into a drinking source is considered as an additional contamination [10].

In light of their well-documented negative impacts on human health, carcinogenicity, and toxicity, HMs are a major source of worry. HM contamination problem occurs as a result of the ineffectiveness of common water treatment methods in developing countries [11].

The presence of HMs in water and the health risks associated with HM contamination have been the subject of numerous review studies when examining their influence on the developing world [12].

A deep learning model is used to analyse adsorbents from residuals to detect and predict the presence of HMs in drinking water. The remaining adsorbed materials are studied using dense neural networks (DenseNets), in this study. After training and testing on a standard collection of microscopic images with the DenseNets, they are used for final detection.

2. Background

The toxicity of HM in water in emerging countries, such as China, India, Bangladesh, Ethiopia, Pakistan, and other developing countries, has been extensively studied by many scholars [13–19]. To make matters worse, because of the well-documented harm that HMs inflict on human health, a great deal of study has been done on ways to remove

HMs from water, such as waste water from municipalities or industry.

Activated carbon adsorption, carbon nanotechnology, and a variety of modified adsorbents are among the treatment methods and technologies that have recently received attention for their HMs removal, and they are investigated as a major sources of research in major developed countries. However, in the context of the developing world, these technologies are not viable or cost-effective. Water treatment systems in most countries tends to be done using purchase, locally built, and cost as little as possible to run [15].

The lack of conventional water treatment procedures for removing HMs is another problem for developing countries. Adsorbents with low cost have been extensively studied to check if the HMs are removed from water [16].

According to research, HMs can be effectively removed from these materials. It appears that agricultural waste and by-products, rather than mineral deposits and natural soil, are the most successful at removing HMs from soil samples in this study. In spite of the fact that chemically modifying the adsorbents boosted the total adsorption capabilities of the materials studied, these technologies are often unavailable to communities [17].

Material properties and quality of water both have an important role in how well these materials remove HMs. The stability and speciation of HMs, as well as the adsorptive properties of the adsorbent, might be affected by these conditions. In addition, ion exchange and the effect of electrostatic forces are the most commonly stated mechanisms for the removal of HMs. When it comes to the efficiency of these systems, water quality plays a huge role [18, 19].

The major contributions of the work involve the following:

- (i) The HPI (Heavy Metal Potential Index) protocols were six quality procedures for groundwater contamination developed using the analysed results of the HM concentrations; these included the HEI, CI, EHC, and HMI, respectively
- (ii) Three groundwater samples had BDL As and Mn concentrations are eliminated from the calculation of several indices
- (iii) The experimental results are conducted to test the efficacy of the deep learning model on detecting the HM composition. The results of simulation show that the proposed deep learning model achieves higher rate of detecting the HM composition from the adsorption residuals than other methods

3. Proposed Method

In the study region, samples were taken from 300 different locations by hand pumping and digging wells. Polyethylene containers were used to collect and filter groundwater samples. In order to prevent metal precipitation and biological growth, the pH from samples is maintained carefully with proper acidification. The atomic absorption

spectrophotometer was used to aspirate water samples at appropriate wavelengths, which were then analysed. As a reductant, potassium iodide and sodium borohydride solution are utilised in the atomic absorption spectrophotometer to evaluate groundwater samples. The proposed method is shown in Figure 1.

For each metal analysis, we used the averages of three independent sets of data. Calibration of the instrument with standards and blanks was performed after every 10 samples to achieve an error of less than 3% in the analytical precession. The latitude/longitude of sampling station using a GPS is recorded during sample collection.

The HPI protocols were the six quality procedures for groundwater contamination developed using the analysed results of the HM concentrations; these included the HEI, CI, EHC, and HMI, respectively. Three groundwater samples had BDL, and As and Mn concentrations are eliminated from the calculation of several indices.

3.1. HPI. Individual HM impacts on the overall water quality state are assessed by HPI. With this method, it is calculated by assigning an appropriate rating to the human factors selected, which are carried out based on quality or by taking into account the maximum acceptable and maximum desired limits for each HM.

3.2. HEI. Heavily contaminated water (HMs) can be assessed using HEI, which is identical to HPI. For the purposes of this approach, the maximum allowable concentration of any given HMI was divided by the measured HMI concentration. Because HEI does not have a critical value, workers must use their own discretion when evaluating pollution levels using this metric. It was so determined that a multiple of mean approach was used to classify the groundwater in the study area into three pollution categories.

3.3. CI. It sums together the combined effects of many quality characteristics that are regarded as detrimental to domestic water in order to provide the degree of contamination. Contamination factors from individual HMs that exceeded the maximum permitted value were used to calculate the current CI values.

3.4. EHCI. Based on information entropy, the EHCI measures water quality. The EHCI drinking water consideration is calculated by first computing the Shannon entropy information weights (w_i) for HMs and then using the weights and subindices (Q_i) to get the EHCI drinking water weights (q_i). The critical value of q_i is 200.

3.5. HMI. An area water quality can be represented using the HMI, i.e. principal component analysis (PCA). Using PCA, factor loadings are calculated by taking into account factors with Eigenvalues greater than 1. To calculate HMI, PCA-based relative eigenvalues and factor loadings are multiplied, and the result is the matching HM weight (π_i).

3.6. PMI. There are no boundaries to the number of variables that can be used in PMI multivariate metal indexing approach. The NSPMI for all derived factors, including

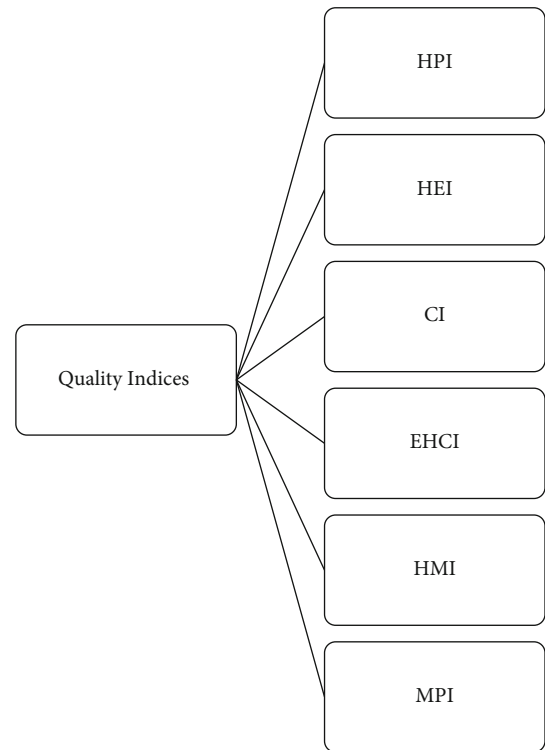


FIGURE 1: Classes of quality procedures in evaluation.

those with both positive and negative values, is added. As a result, a standardised PMI score is computed to simplify the interpretation of the data.

3.7. Classification of Dense Networks

3.7.1. DenseNet Classification. As such, DenseNet can be seen as an extension of this. Let take a short trip to mathematics to figure out how we got here. Taylor expansion of functions is a useful reminder. $x = 0$ is the point at which x equals 0. There are many ways to express this.

$$f(x) = f(0) + f'(0)x + \frac{f''(0)}{2!}x^2 + \frac{f'''(0)}{3!}x^3 + \dots \quad (1)$$

The decomposition of a function into higher and higher-order terms is critical. ResNet, on the other hand, decomposes functions into subfunctions.

$$f(x) = x + g(x). \quad (2)$$

ResNet breaks down the $f(x)$ into a basic linear component and a more sophisticated nonlinear term. DenseNet was one of the options. Mapped values are obtained by progressively more sophisticated functions being applied to an increasing number of variables.

$$\mathbf{x} \longrightarrow [x, f_1(x), f_2([x, f_1(x)]), f_3([x, f_1(x), f_2([x, f_1(x)])]), \dots] \quad (3)$$

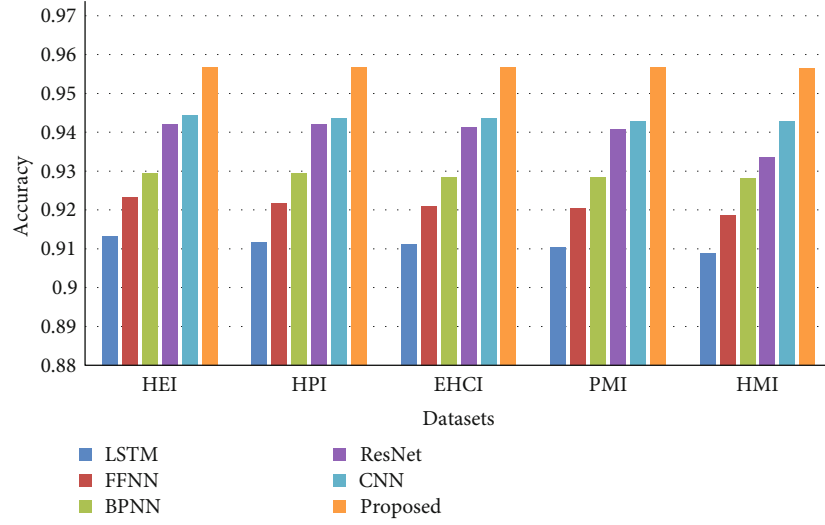


FIGURE 2: Accuracy.

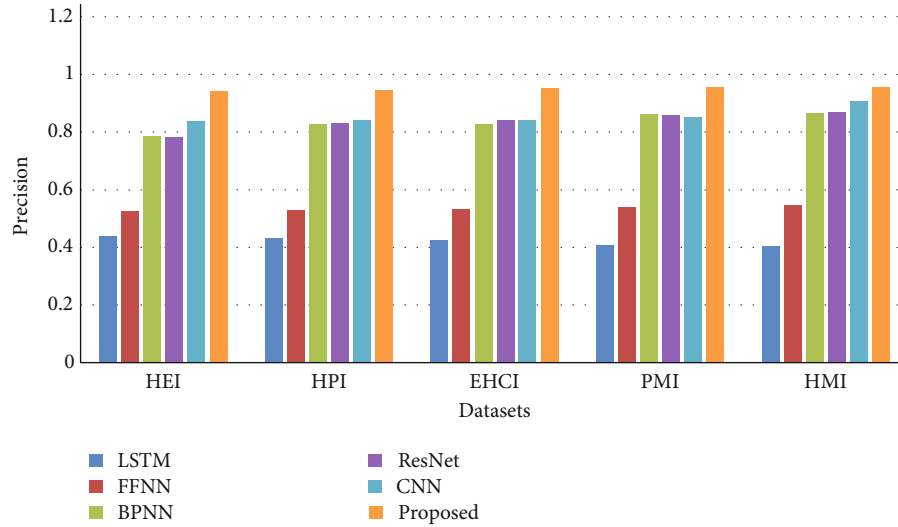


FIGURE 3: Precision.

There are three ways to look at something. As a result, the number of features in MLP is reduced again. In terms of implementation, the study simply concatenates terms rather than adds them. DenseNet gets its name from how dense the graph of interdependencies between variables grows. In a chain like this, the final layer is tightly linked to every layer before it. Dense blocks and transition layers are the primary constituents of a DenseNet. These are the two components that regulate the number of channels and the concatenation of the inputs and outputs.

3.7.2. Dense Blocks. Using the batch normalisation, activation, and convolution structure of ResNet, DenseNet is able to perform better than ResNet. Each convolution block in a dense block uses the same number of output channels, forming a single convolutional block. The input and output of each convolution block are concatenated on the channel dimension in the study forward propagation, however.

3.7.3. Transition Layers. Adding too many dense blocks will result in a model with an excessive number of channels. The model complexity is managed by the use of a transition layer. Convolutional layer $1 \times 11 \times 11 \times 1$ and average pooling layer stride 2 lower the number of channels and the width or height of the pooling layer. The output of the dense block in the preceding example can benefit from the addition of a transition layer with ten channels. There are now only 10 output channels, and the overall size is smaller as well.

3.7.4. DenseNet Model. After that, a DenseNet model will be built. A convolutional and pooling layer are used in DenseNet first stages, just like in ResNet. DenseNet then employs four dense blocks in a manner similar to ResNet four residual block modules. A dense block convolutional layer count can be customised, similar to ResNet. In addition, the study sets the dense block convolutional layer

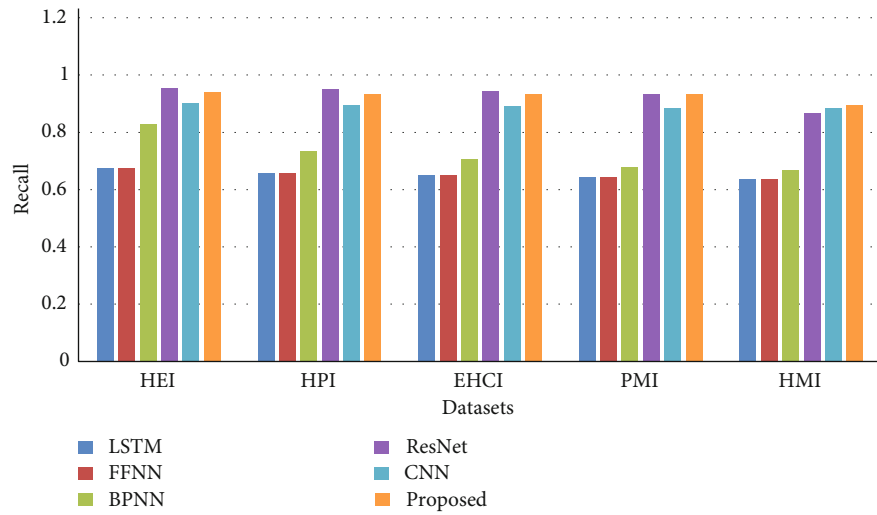


FIGURE 4: Recall.

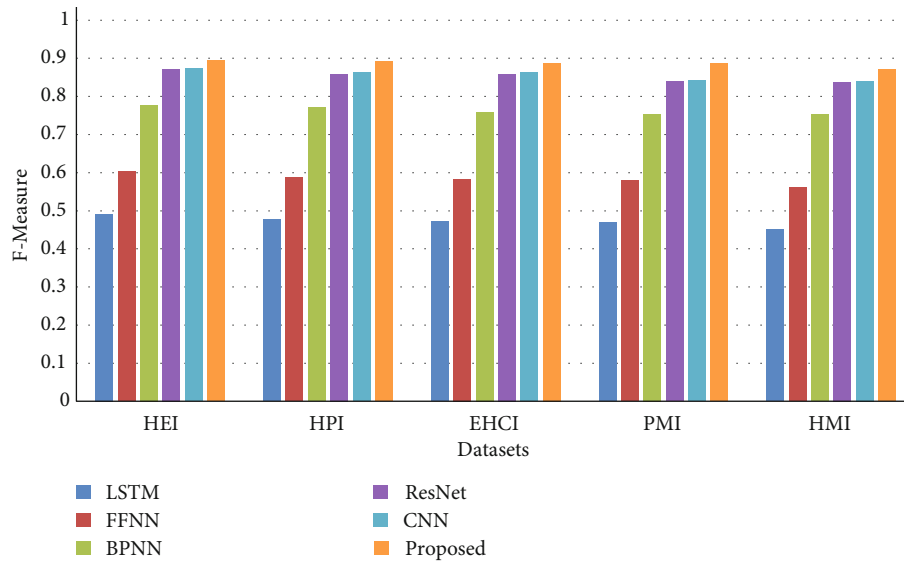


FIGURE 5: F-measure.

channel count at 32, resulting in an additional 128 channels for each dense block. The stride of 2 reduces the height and width of each module in ResNet by a residual block.

3.7.5. Training. Because of this, the input height and breadth will be reduced from 224×96 to facilitate computation because the study is employing a deeper network.

3.8. Fitness Function. A DenseNet model was developed that uses a dataset subset for training and testing. Nine input variables (HMs) and the resulting indices of subset are normalised using the (0–1) scale in order to avoid the inverse effect of the changing scale of the input variables. The constant datasets convergence is achieved through data normalisation. The following equation was

used to normalise the data before it was preprocessed for analysis:

$$r = (r - r_{\min}) / (r_{\max} - r_{\min}), \quad (4)$$

where,

r *: input data (of normalised one),

r_{\min} : minimum input value,

r_{\max} : maximum input value.

The training dataset allocation is another crucial component of this study. A total of 226 datasets were used, of which 184 datasets were used to train the model. Additional groundwater samples with As and Mn concentrations below detection limits were detected and removed from the training sets.

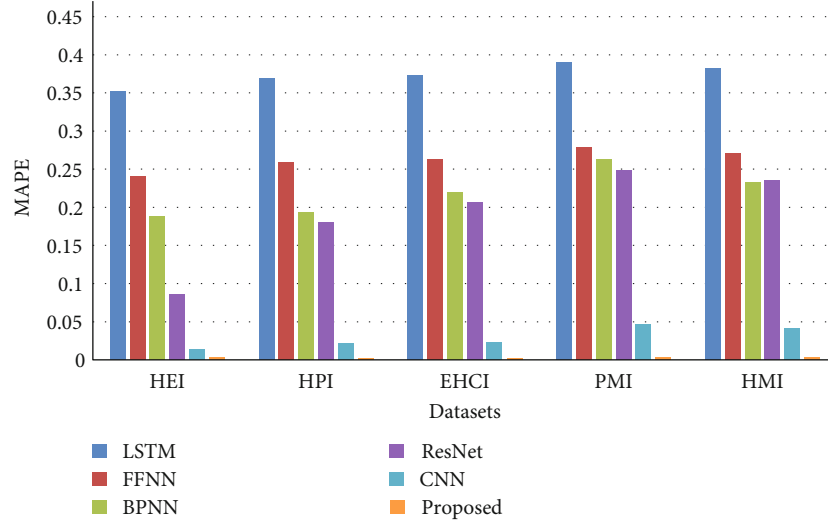


FIGURE 6: Percentage error.

In addition, applying L2 regularisation to the DL algorithm minimises the model complexity by computing the sum of weighted parameters and it is given as follows:

$$L_0 = \frac{1}{n} \sum_{i=1}^n (O - P)^2, \quad (5)$$

where,

- L_0 : loss function,
- n : training datasets,
- O : observed output,
- P : predicted output.

4. Results and Discussions

Different indices were used to evaluate groundwater HM pollution, as well as the performance and the accuracy of computed indices. Groundwater HM contamination indices for a groundwater are analysed in this section to determine the model correctness.

The evolution of different indices is assessed by the validation metrics that includes accuracy, precision, recall, F-measure, and error.

Figure 2 shows the accuracy of validating the prediction of how well the pollution indices find the pollution level in ground water. The results are assessed in terms of HEI, HPI, EHCI, CI, PMI, and HMI. The results of the simulation show that DenseNets achieves higher rate of accuracy using these quality protocols than other AI models.

Figure 3 shows the precision of validating the prediction of how well the pollution indices find the pollution level in ground water. The results are assessed in terms of HEI, HPI, EHCI, CI, PMI, and HMI. The results of the simulation show that DenseNets achieves higher rate of precision using these quality protocols than other AI models.

Figure 4 shows the recall of validating the prediction of how well the pollution indices finds the pollution level in ground water. The results are assessed in terms of HEI, HPI, EHCI, CI, PMI, and HMI. The results of the simulation show that DenseNets achieves higher rate of recall using these quality protocols than other AI models.

Figure 5 shows the F-measure of validating the prediction of how well the pollution indices find the pollution level in ground water. The results are assessed in terms of HEI, HPI, EHCI, CI, PMI, and HMI. The results of the simulation show that DenseNets achieves higher rate of F-measure using these quality protocols than other AI models.

Figure 6 shows the percentage error of validating the prediction of how well the pollution indices find the pollution level in ground water. The results are assessed in terms of HEI, HPI, EHCI, CI, PMI, and HMI. The results of the simulation show that DenseNets achieves reduced error rate using these quality protocols than other AI models.

5. Conclusions

In this paper, prediction of presence of HMs using various quality protocols on the drinking water is analysed using the adsorbents from residuals using DenseNet. DenseNet analyzes the microscopic images of the residual adsorbents. The study initially preprocesses and extracts features using standardised procedure. The DenseNets are used finally for detection purpose, and it is trained and tested with standard set of microscopic images.

The experimental results are conducted to test the efficacy of the deep learning model on detecting the HM composition. The results of simulation show that the proposed deep learning model achieves higher rate of detecting the HM composition from the adsorption residuals than other methods. In the future, the proposed modelling can be improved with the several utilization of machine learning or deep learning methods.

Data Availability

The datasets used and/or analyzed during the current study are available from the corresponding author on reasonable request.

Conflicts of Interest

There is no conflict of interest.

References

- [1] T. Zhang, W. Wang, Y. Zhao et al., "Removal of heavy metals and dyes by clay-based adsorbents: from natural clays to 1D and 2D nano-composites," *Chemical Engineering Journal*, vol. 420, article 127574, 2021.
- [2] C. Duan, T. Ma, J. Wang, and Y. Zhou, "Removal of heavy metals from aqueous solution using carbon-based adsorbents: a review," *Journal of Water Process Engineering*, vol. 37, p. 101339, 2020.
- [3] F. S. Abdulraheem, Z. S. Al-Khafaji, K. S. Hashim, M. Muradov, P. Kot, and A. A. Shubbar, "Natural filtration unit for removal of HMs from water," *IOP Conference Series: Materials Science and Engineering*, vol. 888, no. 1, article 012034, 2020.
- [4] Y. Zhang, M. Zhao, Q. Cheng et al., "Research progress of adsorption and removal of heavy metals by chitosan and its derivatives: a review," *Chemosphere*, vol. 279, article 130927, 2021.
- [5] K. G. Pavithra, P. S. Kumar, V. Jaikumar, K. H. Vardhan, and P. Sundar Rajan, "Microalgae for biofuel production and removal of HMs: a review," *Environmental Chemistry Letters*, pp. 1–19, 2020.
- [6] R. Shahrokhi-Shahraki, C. Benally, M. G. El-Din, and J. Park, "High efficiency removal of heavy metals using tire-derived activated carbon vs commercial activated carbon: insights into the adsorption mechanisms," *Chemosphere*, vol. 264, article 128455, 2021.
- [7] M. Bilal, I. Ihsanullah, M. Younas, and M. U. H. Shah, "Recent advances in applications of low-cost adsorbents for the removal of heavy metals from water: a critical review," *Separation and Purification Technology*, vol. 278, article 119510, 2021.
- [8] L. M. Pandey, "Surface engineering of nano-sorbents for the removal of heavy metals: interfacial aspects," *Journal of Environmental Chemical Engineering*, vol. 9, no. 1, p. 104586, 2021.
- [9] A. Y. Li, H. Deng, Y. H. Jiang et al., "Superefficient removal of Heavy Metals from wastewater by Mg-loaded biochars: adsorption characteristics and removal mechanisms," *Langmuir*, vol. 36, no. 31, pp. 9160–9174, 2020.
- [10] S. H. Awa and T. Hadibarata, "Removal of Heavy Metals in contaminated soil by phytoremediation mechanism: a review," *Water, Air, & Soil Pollution*, vol. 231, no. 2, pp. 1–15, 2020.
- [11] O. A. R. Calderón, O. M. Abdeldayem, A. Pugazhendhi, and E. R. Rene, "Current updates and perspectives of biosorption technology: an alternative for the removal of Heavy Metals from wastewater," *Current Pollution Reports*, vol. 6, no. 1, pp. 8–27, 2020.
- [12] S. S. Dhaliwal, J. Singh, P. K. Taneja, and A. Mandal, "Remediation techniques for removal of heavy metals from the soil contaminated through different sources: a review," *Environmental Science and Pollution Research*, vol. 27, no. 2, pp. 1319–1333, 2020.
- [13] A. M. Al Ketife, F. Al Momani, and S. Judd, "A bioassimilation and bioaccumulation model for the removal of heavy metals from wastewater using algae: new strategy," *Process Safety and Environmental Protection*, vol. 144, pp. 52–64, 2020.
- [14] Y. Na, J. Lee, S. H. Lee, P. Kumar, J. H. Kim, and R. Patel, "Removal of heavy metals by polysaccharide: a review," *Polymer-Plastics Technology and Materials*, vol. 59, no. 16, pp. 1770–1790, 2020.
- [15] R. Sun, Y. Li, N. Lin et al., "Removal of heavy metals using a novel sulfidogenic AMD treatment system with sulfur reduction: configuration, performance, critical parameters and economic analysis," *Environment International*, vol. 136, article 105457, 2020.
- [16] G. K. R. Angaru, Y. L. Choi, L. P. Lingamdinne et al., "Facile synthesis of economical feasible fly ash-based zeolite-supported nano zerovalent iron and nickel bimetallic composite for the potential removal of heavy metals from industrial effluents," *Chemosphere*, vol. 267, article 128889, 2021.
- [17] D. Huang, B. Li, J. Ou et al., "Megamerger of biosorbents and catalytic technologies for the removal of heavy metals from wastewater: preparation, final disposal, mechanism and influencing factors," *Journal of Environmental Management*, vol. 261, p. 109879, 2020.
- [18] A. Baimenov, D. A. Berillo, S. G. Pouloupoulos, and V. J. Inglezakis, "A review of cryogels synthesis, characterization and applications on the removal of heavy metals from aqueous solutions," *Advances in Colloid and Interface Science*, vol. 276, article 102088, 2020.
- [19] A. Jawed, V. Saxena, and L. M. Pandey, "Engineered nanomaterials and their surface functionalization for the removal of heavy metals: a review," *Journal of Water Process Engineering*, vol. 33, article 101009, 2020.

DATA POISON DETECTION USING ASSOCIATIVE SUPPORT-VECTOR MACHINE (ASVM) ALGORITHM

¹Satheesh Kumar D, ²Divya R, ³Sampath Kumar S, ⁴Dr.Charanya R, ⁵Adaikkalaraj R, ⁶Naveenkumar E

¹Assistant Professor, Department of Computer Science and Engineering, Hindusthan College of Engineering and Technology, Coimbatore, India, dsatheeshme@gmail.com

²Assistant Professor, Department of Computer Science and Engineering, JCT College of Engineering and Technology, Coimbatore, India, divya.ap.2090@gmail.com

³Assistant Professor, Department of Computer Science and Engineering, Sri Eshwar College of Engineering, Coimbatore, India, sampathkumar.s@sece.ac.in

⁴Assistant Professor, School of Information Technology and Engineering, Vellore Institute of Technology, Chennai, India, charanyame@gmail.com

⁵PG Scholar, Hindusthan College of Engineering and Technology, Coimbatore, India, abishravi101@gmail.com

⁶PG Scholar, Hindusthan College of Engineering and Technology, Coimbatore, India, naveenkr211292@gmail.com

Abstract

Behaviour-based data Poisoning detection and data Poisoning detection techniques are widely used. It can easily detect malicious programs on your computer, but problems arise when data virus detection is unknown. Unknown data Poison diagnoses cannot be detected using available Poison detection behaviours. For data Poison detection, using well-known techniques such as graph-based techniques. Detecting data about the unknown family of poison attacks is a challenging task. Data poison detection uses graph-based mining. The classification process improves the detection process for data poisonousness detection. A graph-based approach to the classification and detection of data addiction detection. Diagnosis of various data poisons is a graph-based technique for collecting features from data. The proposed algorithm is very efficient at compressing previous methods. Associative Support Vector Machine (ASVM) algorithms for analyzing software behaviour. The ASVM algorithm learns the detection model from an adequate malware database. Signature-based detection technology detects unknown data toxins. It can be detected using available known data poison detection signatures. A method is needed to classify data toxin detection efficiently and detect confusing, unknown and different data toxins. We have highlighted the behaviours, characteristics and properties of data Poisoning detection extracted by various analytical techniques and decided to include them in the development of signature-based data Poisoning identifies.

Keywords: Data Poison Detection, Behavior-based Data, Associative Support-Vector Machine (ASVM), malicious software, signature-based Data Poison.

I. INTRODUCTION

With the rapid advances in technology, the use of computers and the data generated by these systems has increased significantly. As the rate of data generated increases, the computer gains

direct access to the data and can use this generated data without further programming. The computer can give meaningful results by learning from its data. They are provided by machine learning techniques, which are artificial

intelligence applications currently used in cyber security.

In addition, with the rise of cybercrime, machine learning techniques are being used to detect malicious behaviour of computers, malware, and malicious traffic on the network. Two opposite mechanistic learning methods depend on the time of the attack.

Pre-sample training data poisoning: An attacker changes the label of the training dataset before the sample is trained.

Data preparation based on the trained model: After training the model, the attacker forces the model to create an interaction with the actual output data. Both attacks are very dangerous with consequences and impacts.

Examining off-the-shelf machine learning products reveals that data addition attacks pose an even bigger threat. Almost all commercial products require training datasets from the installation company. Attackers can easily poison this database.

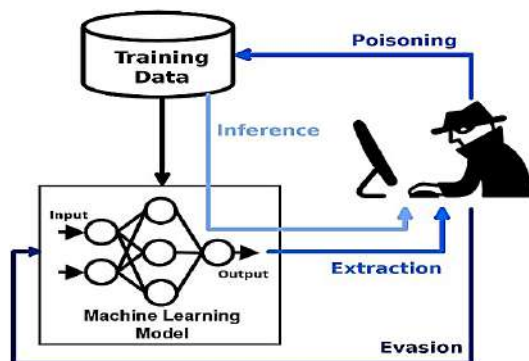


Figure 1.1 *Data poisoning attack*

Figure 1.1 shows the malware can be placed in a company where the malware determines the attack time and what the best attack vector is. These attacks vary by design, making the detection very difficult and lengthy.

Based on its credibility and other factors, the ASVM Foundation was subject to credible attacks. No matter how reliable the system is, ASVM can go unreliable. In many cases, both the trust and the trustee are people. However, for our purposes, the end-user or other person is the trustee or machine learning system, trustee. Details may vary, but there is not much difference between a reliable person and a reliable machine learning method. During the

training phase, the attackers can mask the laser pulse signals, and the deployed ASVMs detect incorrect interference distances during the test phase, creating dangerous driving conditions for passengers. Recent advances in infrastructure have further increased the likelihood of new addition attacks in machine learning in network systems.

2. Related work

P. Zhao et al. (2021) described location data as often consolidated in favour of applications such as mobility management, location recommendation, and map rationality. However, if the attacker deliberately sends the contaminated area to the accumulator, these overall results can target oxidative attacks inside and outside the piece. Therefore, we will focus on data acquisition input and introduce the behaviour of the first Poisoning Attacks on Location Data Aggregation (PALDA) attack.

L. Zhao et al. (2021) described Collaborative learning allows multiple clients to practice a collaborative model without sharing data. Each client trains locally and sends sample updates to a central server for collection. Collective learning can be subject to toxic attacks because the server does not know how to create the update. In this case, a malicious client may create poison-laden updates and introduce a backdoor functionality on the federation model.

J. Chen et al. (2021) described Deep Poison as an innovative hostile network with one generator and two distinctions to solve this problem. In particular, the generator automatically extracts hidden features of the target class and embeds them in harmless training models. A discriminator controls the rate of addiction harassment. Another discriminator acts as a target model to demonstrate the effects of the drug. The novelty of Deep Poison is that the toxic training models developed cannot be distinguished from harmless ones by defensive methods or human visual inspection, and even harmless test models can be attacked.

Y. Jin et al. (2019) described that DNS cache poisoning is also a serious threat in the online world. In addition to the Kaminski attacks, fake data from compromised trusted domain name

system (DNS) servers is a threat today. Some solutions have been proposed in the previous case, such as DNSSEC (DNS Security Extensions), to prevent DNS cache toxic attacks. Still, no effective solution has been proposed in the latter case.

A. Takiddin et al. (2021) described as, Data-driven power theft detectors rely on customer-report energy consumption measurements to detect malicious activity. One of such inventors' most common indirect hypotheses is that labelling training data is accurate. Unfortunately, these detectors are vulnerable to data addiction attacks with incorrect labels during training.

C. Li et al. (2021) described, Machine Learning (ML) is widely used to detect malware on various platforms, including Android. Detection models must be retested following the data collected (e.g., monthly) to continue the evolution of malware. However, it can also lead to toxic attacks, especially backdoor attacks, which disrupt the learning process and create evasion tunnels for manipulated malware models. No previous research has examined this critical issue with the Android Malware Detector.

Z. Xiang et al. (2019) described; Recently, there has been a lot of interest in taxonomies, such as backdoor data poisoning attacks. Whenever a backdoor system (such as a watermark or harmless system) is added to another class instance, the classifier learns to classify it as a target class.

K. Liu et al. (2020) described that Deep Neural Networks (DNNs) are susceptible to various hostile attacks, such as data toxicity that interferes with backdoor insertion training. Sensitivity to the integrity of training data creates protective vulnerabilities, especially if malicious insiders wish to disable the target neural network.

G. Lovisotto et al. (2020) described, Poisonous attacks on biometric systems using template adapters and allowing attackers to impersonate users will remain highly secretive for a long time. Demonstrates that attackers can carry out such attacks with physical limitations (no digital access to sensors) and knowledge of training data (no end ranges or user templates). Based on the attacker's template, they create some intermediate models that gradually reduce the

distance between their template and legitimate users.

K. Liu et al. (2021) described as Machine learning (ML) based technologies are gaining popularity to improve computer-aided design (CAD) processes. However, despite sophisticated performance in many domains, techniques such as deep learning (DL) can be subject to various hostile attacks. As part of the CAD process, explore the threat of malicious intruders training data poisoning attacks that attempt to insert a backdoor into deep neural networks (DNNs).

J. Zhang et al. (2021) described Federal learning structures provide specific vulnerabilities to active attacks. Poison attacks are one of the most powerful long-range attacks in which the local update created by the attacker can compromise the functionality of the global model.

J. Wen et al. (2021) described as, The security community demonstrates that when data and models are opaque, there are many potential security risks, and new risks are constantly being discovered.

J. Chen et al. (2021) described, Advanced attackers may be vulnerable to data poisoning attacks and may interfere with the learning process by inserting some malicious samples into the training database. Existing defences against drug attacks are primarily target-specific attacks. Designed for a specific type of attack. However, due to the explicit principles of the Master, it does not work for other types. However, some common safety strategies have been developed.

M. Li et al. (2019) described as, These individuals are often referred to as workers completing tasks posted by the crowd detection organization. Due to the relatively poor control of labour IDs, crowded identification systems are vulnerable to data poisoning attacks that interfere with data analysis results.

X. Liu et al. (2021) described, Distributed malicious users can send specially designed gradients to compromise sample integrity and usability during training. Also, solving two problems at once is paradoxical. While privacy-protection FL solutions attempt to stabilize the gradients of identity, defences against addiction attacks tend to eliminate outsiders based on their similarity.

3. Materials and Method

Classify meaningless samples with high accuracy to detect data toxicity. Related signatures provide greater accuracy in data toxicology detection. In addition, we classify data addiction diagnoses according to their family and check the accuracy of each data addiction detection behaviour. Signature-based detection is the traditional method of detecting data toxicity in the PC environment. Fixed and dynamic methods are used to define the signature. The standard analysis targets the source and object code and verifies the code without starting the program.

To detect commands, reports, and vulnerabilities in multiple programs, distort the source code for data toxicity detection. The dynamic analysis searches for data on specific types of memory leaks, traffic, and actual running code. However, using this method in a mobile environment requires a large amount of storage, and the system fit has a high-performance overlay.

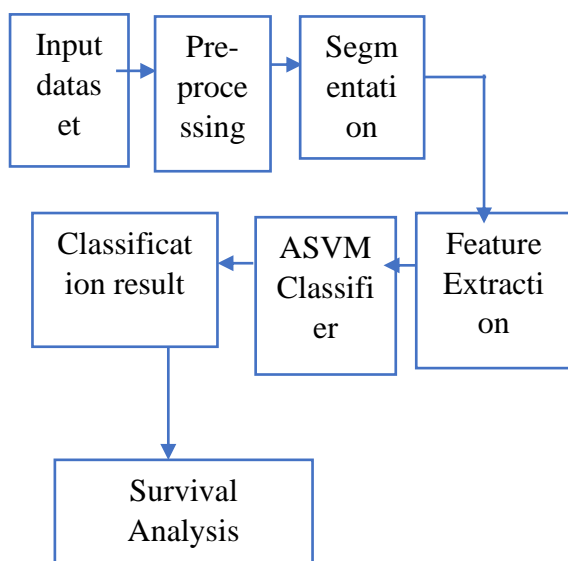


Figure 3.1: *Proposed Method block diagram*

Figure 3.1 describes a proposed block diagram for Data poisoning detection attack analysis using the preprocessing, feature extraction, and segmentation used for classification. The result shows a better performance than previous methods.

3.1 Data poisoning preprocessing

The proposed model has several steps to implement. Data preset, first step. The

prerequisite requires sequential operations. This data cleaning stage involves removing missing values, copying records, and checking outliers for data. It removes data that conflicts with noise, extracts information from the database and converts it into a form that intelligent classification algorithms can use. Collected files are executable source files stored as binary code in the file system. They were pre-treated to suit the task. First, it opens the executable in restricted environments, and the packaged executable opens automatically.

Missing data

In most methods, at the point of extraction of the predictive model feature, the predicted display distance does not indicate that the value attack data is missing. Missing values refer to most missing data, which is excluded directly from the data toxic data set.

Data Normalization

Measuring up to Min and Max-MinMaxScaling. Minimum and maximum scaling compress values between 0 and 1. Subtract the minimum value from all observations and divide by a range of values.

The above change is a distribution of values ranging from 0 to 1. However, the mean is not centred on zero and varies between constant deviation variables. The format of the minimum-maximum ratio distribution will be the same as the original variable, but the variation may change. This measurement technique is subject to externalization.

3.2 Data segmentation

Frequency model and imbalance model of attack data streams. Next, perform data processing such as digital automation, normalization, and missing value processing. Finally, get the input from the point of view of attack frequency. If the length of the data stream segment L is determined, there are situations where stream L interrupts T-1 to T at a given time. This means the L stream has offensive traffic and is harmless. Specify Attack Traffic, Attack Traffic Only, And Harmless Traffic Only, Data Flow Segment.

3.3 Data feature extraction

Feature extraction is a dimension reduction technique that reduces the number of

random variables considered. Toxic attacks focus primarily on clustering algorithms, and some consider feature selection methods. In some applications, especially high-dimensional data systems, feature selection techniques can detect low-dimensional representations of training data and retain as much information as possible about the original data. Toxic attacks are implemented in several embedded feature selections, using feature extraction techniques to enhance attackers' targets, the focus of which is the interruption of potential attack points.

In this task, the attacker is assumed to know the unreliable system thoroughly. This method can be very robust if you can find better starting points than randomly selecting data. The characteristics of the horn were evaluated using observations of the most effective venom points near the horn. Finally, select the value of the response variable (0 or 1) at the boundary to maximize the loss.

3.3 Classification using ASVM

Data poisoning with one generator and two discriminators can solve this problem. In particular, the generator automatically extracts hidden features of the target class and embeds them in a harmless training model. The discriminator controls the confusing rate of the drug. Another distinction is used as a target model to show the drug's effect. The toxicity training samples developed are indistinguishable from safety methods or manual visual inspection, and the data toxicity lies in the fact that even harmless test specimens can be attacked.

Algorithm steps

Input: Preprocessing data (P), features (F), Poisoning fraction ϵ , burn in $\llbracket \text{burn} \rrbracket_n$

Initialize the $\theta \in \mathbb{R}^{d \times m}$, $P_i \leftarrow \emptyset$

For $T=1 \dots \llbracket n \rrbracket_burn + \epsilon n$ do

Select $(\square(\rightarrow T^a), \square(\rightarrow T^b)) \in \arg\max(a, b) \in F, L(\theta, \square(\rightarrow T^a), \square(\rightarrow T^b))$ // Find highest loss point in F

If $T > \llbracket n \rrbracket_burn$ then

ASVM $\square(P)$
 $U\{\square(\rightarrow T^a), \square(\rightarrow T^b)\}$

End if

End for

End

To avoid detection as well. Since this optimization involves costly problem solving, all three attacks deal with different ways of approximating the problem according to the impact process.

4. Result and discussion

The proposed implementation results and performance were tested in the Mathematical Health Record process using the Trained Addiction Attack Database features. Trial case measurements are calculated based on the true and false locations of the error rates performed during the process. The test results have been compared to the Associative Support-Vector Machine (ASVM) Method. The analysis is done based on the Analysis of Sensitivity, specificity, accuracy, Error Rate and Time complexity in the proposed system.

Table 4.1: Simulation parameters for the proposed system

Simulation Parameters used	Simulation processed	Values
Name of the dataset	Poisoning Dataset	Attacks
Language	Python	
Tool	Anaconda	
No. of data	500	
Trained Data	300	
Test data	200	

Table 1 describes the proposed method based on the attack dataset. The proposed method provides improved results compared to the previous method results.

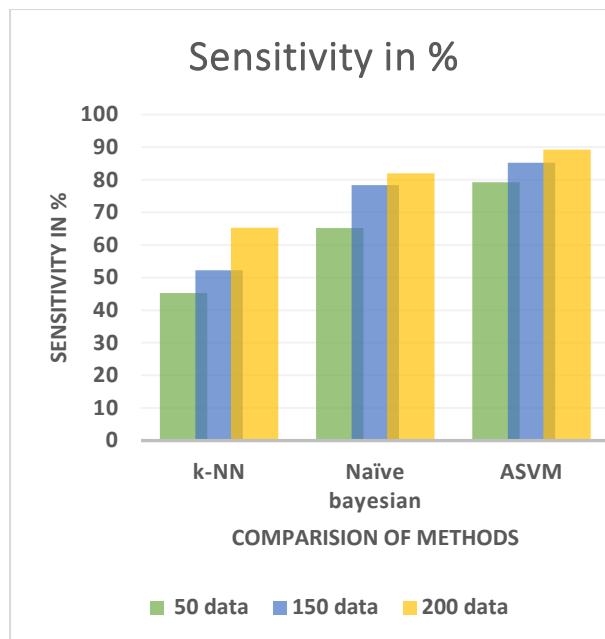


Figure 4.1: Analysis of the sensitivity

Figure 4.1 describes the Sensitivity performance of the proposed and existing methods. The proposed Associative Support-Vector Machine (ASVM) improves the sensitivity up to 89.2%, which is better than the previous method of K-Nearest Neighbor (k-NN) 65.3%, and Naïve Bayesian is 82%



Figure 4.2: Analysis of the Specificity

Figure 4.2 describes the Specificity performance of the proposed and existing methods; the proposed Associative Support-Vector Machine (ASVM) improves the specificity up to 88.2%, which is better than the previous method of K-Nearest Neighbor (k-NN) 51.2%, and Naïve Bayesian is 66.2%

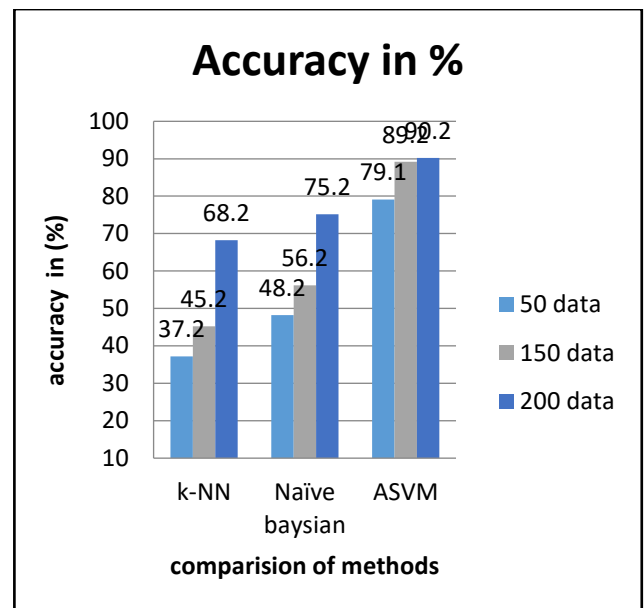


Figure 4.3: Analysis of the Accuracy

Figure 4.3 describes the Accuracy performance of the proposed and existing methods. The proposed Associative Support-Vector Machine (ASVM) improves the accuracy up to 90.2%, which is better than the previous method of K-Nearest Neighbor (k-NN) 68.2%, and Naïve Bayesian is 75.2%

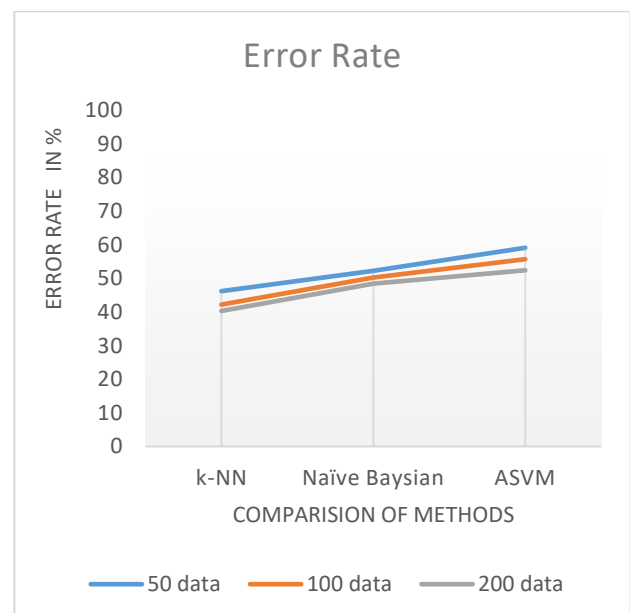


Figure 4.4: Analysis of the Error Rate

Figure 4.4 describes the Error Rate performance of the proposed and existing methods. The proposed Associative Support-Vector Machine (ASVM) improves the sensitivity up to 52.4%, which is better than the previous method of K-

Nearest Neighbor (k-NN) at 40.3%, and Naïve Bayesian is 48.4%

5. Conclusion

The impact of detecting computer files and mobile data poisoning in everyday life cannot be underestimated. To design an efficient solution, the computational limitations of mobile devices must be carefully considered. It is recommended to use quantitative data flow properties to extract height properties. ASVM (Associative support vector machine) patterns from known Data Poison Detection collections. The simulation results prove the sensitivity is 89.2 %, specificity is 88.2%, accuracy is 90.2%, and error rate 52.4%. You can also combine feature-based mining techniques with machine learning programs to add noise and test data. It is reflected in the standard diagnostic effect and the good diagnostic effect in the evaluation test. It is 10 times longer than the training time. It creates a hostile environment that leads to user dissatisfaction and can create false positives for some normal operations if the behaviour pattern of the software is not effectively developed. Above all, we can conclude that profile-based monitoring methods are most effective because they are signature-based methods, providing adequate security and a better user experience.




Reference

- [1] P. Zhao et al., "Garbage In, Garbage Out: Poisoning Attacks Disguised With Plausible Mobility in Data Aggregation," in *IEEE Transactions on Network Science and Engineering*, vol. 8, no. 3, pp. 2679-2693, 1 July-Sept. 2021, DOI: 10.1109/TNSE.2021.3103919.
- [2] L. Zhao et al., "Shielding Collaborative Learning: Mitigating Poisoning Attacks Through Client-Side Detection," in *IEEE Transactions on Dependable and Secure Computing*, vol. 18, no. 5, pp. 2029-2041, 1 Sept.-Oct. 2021, DOI: 10.1109/TDSC.2020.2986205.
- [3] J. Chen, L. Zhang, H. Zheng, X. Wang and Z. Ming, "DeepPoison: Feature Transfer Based Stealthy Poisoning Attack for DNNs," in *IEEE Transactions on Circuits and Systems II: Express Briefs*, vol. 68, no. 7, pp. 2618-2622, July 2021, DOI: 10.1109/TCSII.2021.3060896.
- [4] Y. Jin, M. Tomoishi and S. Matsuura, "A Detection Method Against DNS Cache Poisoning Attacks Using Machine Learning Techniques: Work in Progress," 2019 IEEE 18th International Symposium on Network Computing and Applications (NCA), 2019, pp. 1-3, DOI: 10.1109/NCA.2019.8935025.
- [5] Takiddin, M. Ismail, U. Zafar and E. Serpedin, "Robust Electricity Theft Detection Against Data Poisoning Attacks in Smart Grids," in *IEEE Transactions on Smart Grid*, vol. 12, no. 3, pp. 2675-2684, May 2021, DOI: 10.1109/TSG.2020.3047864.
- [6] Li et al., "Backdoor Attack on Machine Learning Based Android Malware Detectors," in *IEEE Transactions on Dependable and Secure Computing*, DOI: 10.1109/TDSC.2021.3094824.
- [7] Z. Xiang, D. J. Miller and G. Kesidis, "A Benchmark Study Of Backdoor Data Poisoning Defenses For Deep Neural Network Classifiers And A Novel Defense," 2019 IEEE 29th International Workshop on Machine Learning for Signal Processing (MLSP), 2019, pp. 1-6, DOI: 10.1109/MLSP.2019.8918908.
- [8] K. Liu, B. Tan, R. Karri and S. Garg, "Poisoning the (Data) Well in ML-Based CAD: A Case Study of Hiding Lithographic Hotspots," 2020 Design, Automation & Test in Europe Conference & Exhibition (DATE), 2020, pp. 306-309, DOI: 10.23919/DATE48585.2020.9116489.
- [9] G. Lovisotto, S. Eberz and I. Martinovic, "Biometric Backdoors: A Poisoning Attack Against Unsupervised Template Updating," 2020 IEEE European Symposium on Security and Privacy (EuroS&P), 2020, pp. 184-197, DOI: 10.1109/EuroSP48549.2020.00020.
- [10] K. Liu, B. Tan, R. Karri and S. Garg, "Training Data Poisoning in ML-CAD: Backdooring DL-Based Lithographic Hotspot Detectors," in *IEEE Transactions on Computer-Aided Design of Integrated Circuits and Systems*, vol. 40, no. 6, pp. 1244-1257, June 2021, DOI: 10.1109/TCAD.2020.3024780.
- [11] J. Zhang, B. Chen, X. Cheng, H. T. T. Binh and S. Yu, "PoisonGAN: Generative

- Poisoning Attacks Against Federated Learning in Edge Computing Systems," in *IEEE Internet of Things Journal*, vol. 8, no. 5, pp. 3310-3322, 1 March 1, 2021, DOI: 10.1109/JIOT.2020.3023126.
- [12] J. Wen, B. Z. H. Zhao, M. Xue, A. Oprea and H. Qian, "With Great Dispersion Comes Greater Resilience: Efficient Poisoning Attacks and Defenses for Linear Regression Models," in *IEEE Transactions on Information Forensics and Security*, vol. 16, pp. 3709-3723, 2021, DOI: 10.1109/TIFS.2021.3087332.
- [13] J. Chen, X. Zhang, R. Zhang, C. Wang and L. Liu, "De-Pois: An Attack-Agnostic Defense against Data Poisoning Attacks," in *IEEE Transactions on Information Forensics and Security*, vol. 16, pp. 3412-3425, 2021, DOI: 10.1109/TIFS.2021.3080522.
- [14] M. Li, Y. Sun, H. Lu, S. Maharjan and Z. Tian, "Deep Reinforcement Learning for Partially Observable Data Poisoning Attack in Crowdsensing Systems," in *IEEE Internet of Things Journal*, vol. 7, no. 7, pp. 6266-6278, July 2020, DOI: 10.1109/JIOT.2019.2962914.
- [15] X. Liu, H. Li, G. Xu, Z. Chen, X. Huang and R. Lu, "Privacy-Enhanced Federated Learning Against Poisoning Adversaries," in *IEEE Transactions on Information Forensics and Security*, vol. 16, pp. 4574-4588, 2021, DOI: 10.1109/TIFS.2021.3108434.
- [16] Kumar, D.S., Sundaram, S.S. Associative Zone Based Energy Balancing Routing for Expanding Energy Efficient and Routing Optimization Over the Sensor Network. *Wireless Pers Commun* (2022). <https://doi.org/10.1007/s11277-021-09443-7>.

Research Article

An Energy Efficient Architecture for Furnace Monitor and Control in Foundry Based on Industry 4.0 Using IoT

M. Dinesh ¹, **C Arvind** ², **S.S Sreeja Mole**,³ **C.S. Subash Kumar**,⁴ **P. Chandra Sekar**,⁵ **K. Somasundaram** ⁶, **K. Srihari**,⁷ **S. Chandragandhi**,⁸ **and Venkatesa Prabhu Sundramurthy** ⁹

¹Department of Electronics and Communication Engineering, Shri Angalamman College of Engineering and Technology, Trichy, India

²Department of Electronics and Communication Engineering, Karpagam College of Engineering, Coimbatore 641032, India

³Department of Electronics and Communication Engineering, Christu Jyothi Institute of Technology and Science, Yeswanthapur, Janagon 506167, India

⁴Department of Electrical and Electronics Engineering, PSG Institute of Technology and Applied Research, Coimbatore 641032, India

⁵Department of ECE, Siddhartha Institute of Science and Technology, Puttur, Andhra Pradesh, India

⁶Institute of Information Technology, Saveetha School of Engineering, SIMATS, Chennai, India

⁷Department of Computer Science and Engineering, SNS College of Technology, Coimbatore, India

⁸Department of Computer Science and Engineering, JCT College of Engineering and Technology, Coimbatore, India

⁹Center of Excellence for Bioprocess and Biotechnology, Department of Chemical Engineering, College of Biological and Chemical Engineering, Addis Ababa Science and Technology University, Addis Ababa, Ethiopia

Correspondence should be addressed to Venkatesa Prabhu Sundramurthy; venkatesa.prabhu@aastu.edu.et

Received 13 October 2021; Revised 22 November 2021; Accepted 8 December 2021; Published 22 January 2022

Academic Editor: M Pallikonda Rajasekaran

Copyright © 2022 M. Dinesh et al. This is an open access article distributed under the Creative Commons Attribution License, which permits unrestricted use, distribution, and reproduction in any medium, provided the original work is properly cited.

The global standards in the field of industrial automation are maintained in industries by completely digitizing their manufacturing process with industry 4.0 standard. Internet of Things (IoT) enables the conservation of cultural heritage with proper assistance on data management on the data collected from the sensors. However, energy efficient conservation is required to monitor the IoT sensors in order to deal with building a better infrastructure. In this paper, we develop a bio-inspired algorithm which can automate the entire furnace monitoring and controlling system in order to eliminate the human intervention involved in the physical process. The algorithm is blended as a web-based remote application for the better control of the tasks involved, energy utilized, and its subsequent log-report maintenance. The entire system employs Wi-Fi communication for data transfer from device to cloud where the stored data including temperature log, forth coming schedule, and process graphic are maintained by the proposed algorithm to predict the machine failure at an earlier stage. The real-time prototype system is supported by a heat treatment process that is completely automated using IoT to monitor and maintain the temperature during the production of metal casting process.

1. Introduction

In automobile sector, the quality and quantity production of vehicle accessories including gears, bearings, brake disk, piston, and brake lever and cam shaft should meet the everlasting demand in the market. Considering its

contribution to the economic growth, the intricacy involved in the manufacturing and its assembling process has a set of prescribed particulars and guidelines to be strictly followed based on Industry 4.0 [1]. The vehicle organizations will progressively focus on quality building in the manufacturing process by employing an optimized architecture [2] in order

to meet the industry standards and to provide quality product to its customers. The automation of the entire process with perfection is desired in order to avoid manual intervention [3].

In order to make the manufactured product more durable and light weight, the heat treat process (HTP) is used. The HTP is applicable for molding metals such as SG iron, aluminum, and steel. The resulting model is initially maintained at a very high temperature for a fixed duration. Later the metal casting is allowed to cool at a sufficiently low temperature in order to vary the meteorology structure without changing its shape. The entire process makes the metal parts harder, stronger, and more resistant to any undesired external impact. The heating process is carried out such that the temperature is maintained uniform at the top, bottom, left, and right side of the metal casting in order to make it stronger.

The steps involved in HTP are annealing, stress relieving, and normalizing. The temperature at which the heat treatment should be performed depends on the mechanical properties of the metal used for molding process. Ahead of the heat treatment, the casting part called cementite and pearlite have a gap, as shown in Figure 1. After the HTP, the cementite and pearlite molecular structure are joined together making the metal more durable. IoT sensors play a major role in finding the temperature during this process. Energy efficient conservation is required to monitor the IoT sensors in order to deal with building a better infrastructure.

The main contribution of the paper involves the following.

A bio-inspired algorithm can automate the furnace monitoring and controlling to eliminate the human intervention in the physical process.

The algorithm is combined with a web-based remote application for the better control of the tasks involved, energy utilized, and its subsequent log-report maintenance.

2. Automation of Heat Treatment Process

In underdeveloped or developing countries, manual labor is employed to perform heat treatment of metal casting. The furnace used for casting causes a pungent smoke and the hot ambience is hazardous to human beings. In some cases, the HTP is carried out continuously for two to three days during which the furnace will maintain an ambient temperature of 160°C. The major limitation of HTP is the health hazard; it directs to the human operators involved in the process. However, the overall hazardous procedure has to be followed to produce high-quality accessories for automobiles [4]. A decade back the furnace automation was supported by PLC-based systems, but they could hardly work after a year or so due to its feeble resistance to the high-temperature environment. In the literature, various optimization algorithms are suggested for industrial engineering and automation problems.

2.1. Importance of Heat Treatment in Automobile Industry. Any ambiguity of the internal properties of a metal during melting such as disorientation of microstructure shown in

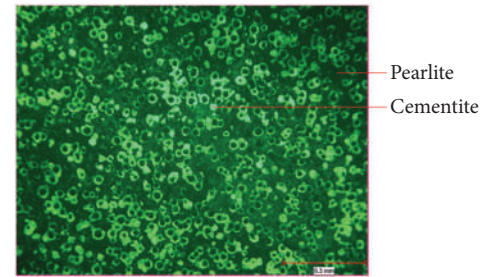


FIGURE 1: Before heat treatment microstructure.

Figure 1 can be rectified by the heat treatment process. The molecules in a metal are oriented for proper bonding by maintaining it at a constant temperature during the HTP. An appropriate heat treatment can form covalent bond among the molecules (pearlite and cementite) to improve the hardness and strength of the metal. The microstructure bonding after heat treatment is shown in Figure 2. The undesired temperature variation in metal casting (difference in upper and lower section) is shown in Figure 3.

3. Background: Major Issue in Heat Treatment Process

3.1. Pollution Area and People Management. To check the regular workflow of heat treatment, there is a particular time and temperature to maintain every casting part based on this instruction. This is given by the manager, the operator has to work on, and the supervisor needs to verify the process. At each interval, the operator has to monitor and record the temperature. Moreover, the operator should be trained; the temperature and time setting will be handled by the heat-treatment operator. The furnace operation runs nearly 1 to 2 days; the operator will be changing at shift bases. At the change over time and break time, the operator will not be there at field area if the temperature and time setting should be done right. If any problem occurs at the temperature and time setting, the product will be affected; the affected product will complicate to find it. Manual instruction process flow is shown in Figure 4.

3.2. Quality Checking Process. Over all the companies and organization with respect to quality, the quality inspection system will be checked under customer specification requirement (CSR); CSR will vary for every product. In the quality system, each and every product quantity is not included for quality check. The quality standard is 1 to 10 pieces which will be going for quality inspection in a bundle or batch. Some of the quality-checking inspectors find shortcuts to go fast. Visual inspection and dimension inspections are automobiles major parts.

3.3. Manual Controls. The furnace operator sets the particular time and temperature, and he/she needs to check the top, bottom, left, and right temperature levels. This process takes a minimum of 6 hours to maximum of 2 days to

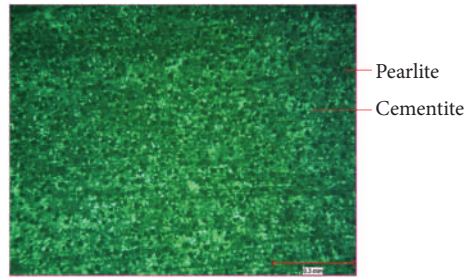


FIGURE 2: After heat treatment microstructure.

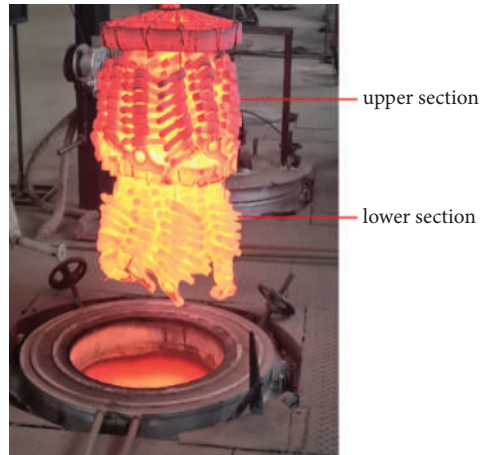


FIGURE 3: The undesired temperature variation in metal casting (difference in upper and lower section).

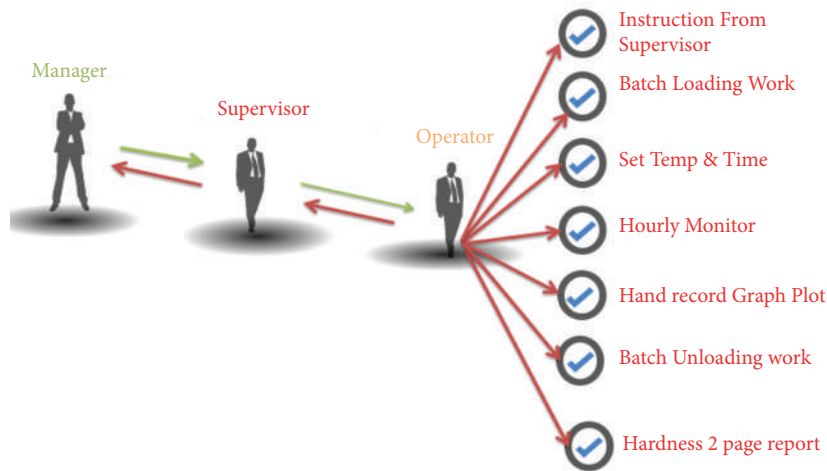


FIGURE 4: Manual instruction process flow.

complete. If any mistakes occur in this process, it consumes 250 units to 500 units per day; also, currently running parts of microstructure get uneven.

3.4. Analogy Measurement. In the previous method, the graph recorder of the heat treatment is in an analog format; the analog graph recorder automatically reads the four temperatures and plots the graph. For this method,

the graph record uses more paper to plot and the hot environment damage; moreover, the recorder gets struck; if any mistake occurs in the previous completed record, we cannot analyze or check that in the paper form; the operator will be able to create the fake record if he has made any mistake in the process [5]. At the yearly, once auditing time the heat treatment area audit is more complicated, it contains a whole one-year graph record in the paper format.

4. Hardware Stability Analysis

In order to design a reliable industrial automation system, the evaluation process at two stage architecture is used. The study required a simple microcontroller to carry out this operation. Hence, in this paper, at the first stage, we used the PIC16f877A controller shown in Figure 5, and at the second stage, we had an ARM-based 32 bit lpc2148 Philips microcontroller shown in Figure 6. The architecture used for evaluation performed well for three weeks, after which the system stopped functioning due its inability to withstand the high-temperature foundry environment [6–8]. Hence, it is inferred that, for HTP, a reliable microcontroller which can handle high temperature has to be used.

The furnace located in different parts of the unit has to be interconnected using local area network (LAN) so that a stable network is established for intermachine communication.

The above requirement is satisfied by an IoT-based Xmc4700 ARM Cortex M4 industry standard microcontroller which is resistant to high temperature and enables to safeguard the furnace from hazards due to explosion and fire. With the support of interfacing with automatic burner control and gas fired controlled dryer, the controller can operate in the furnace ambient temperature range upto 125°C. Any compromise in maintaining a constant temperature during HTP can lead to severe consequence including wastage of all the preliminary casting process and the power consumed. The undesired variation in temperature during HTP is presented by the temperature-monitoring graph, as shown in Figure 7. The respective real-time metal casting in a foundry is given in Figure 7. Hence, maintaining constant temperature is very primary for manufacturing durable accessories for automobile.

5. Experimental Setup for Data Communication Using IoT

5.1. Device and Furnace. The temperature measurement at the top, bottom, left, and right of the furnace is measured using four different temperature controllers interfaced with IoT-based Xmc4700 [9]. The PCB architecture which is based on IoT for the heat treatment process is shown in Figure 8. While the flowchart for heat treatment process is shown in Figure 9.

The data are collected from Xmc4700 using RS485 Modbus communication to monitor the holding time of temperature and its set point [10]. The Modbus protocol reads temperature from Xmc IoT board at a baud rate of 9600 such that the temperatures from four corners of the furnace are collected within 800 millisecond. The study records the threshold temperature limit as 125°C and upon which if the temperature increases, the time gets restarted and the process is iterated in similar manner until the decision is made. The RS485 serial communication employs balanced data transmission and performs good noise rejection so that it can drive for long communication lines at relatively high data rates [11, 8].



FIGURE 5: Hardware of PIC16f877a with Zigbee.

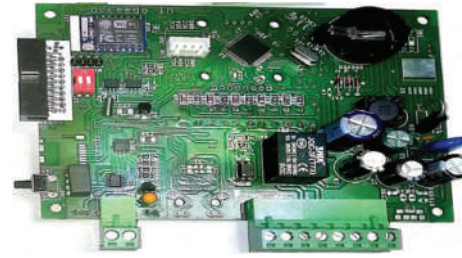


FIGURE 6: Hardware of lpc2148 with Wi-Fi.

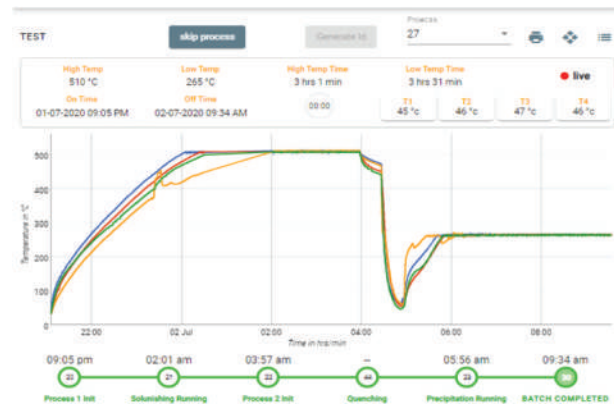


FIGURE 7: Temperature-monitoring graph.

5.2. Device and Server System. The XMC board collects the temperature information and transfers it through ESP8266 Wi-Fi using hypertext transfer protocol (HTTP). It is a request/response protocol based on client/server-based architecture. The XMC collects the temperature data every 7 seconds and transfers it to the server through ESP8266 Wi-Fi. The block diagram for machine monitoring and controlling is shown in Figure 10. The server collects the furnace temperature data to store it in a database. It gives an acknowledgment with temperature setpoint and performs data analysis to predict warnings and intimates the same through an e-mail notification.

Digital Application virtual Engineering (DAvE) is a C/C++ code development platform which can generate code for microcontroller and software driver applications [12]. It is a free and unlicensed application environment that can automatically create user-defined functions using C-level templates. DAvE generates code to read temperature using RS485 from the temperature controller and store the data in EPROM AT24C64 ATMEL. The microcontroller collects the

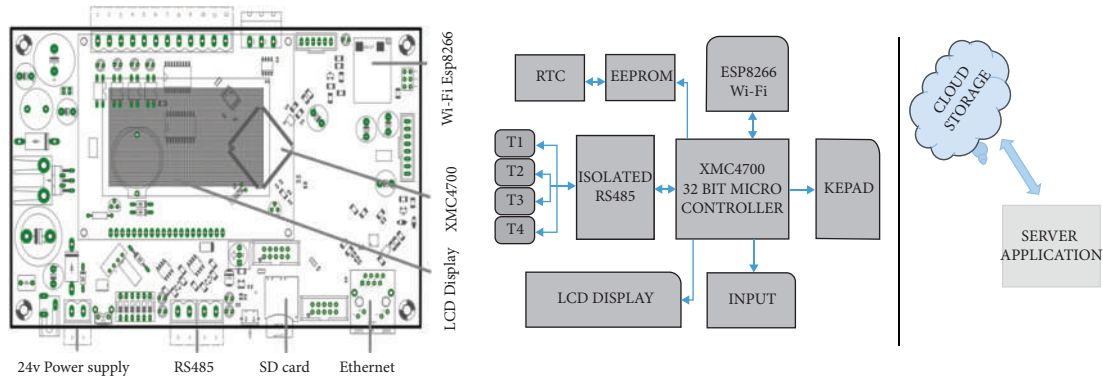


FIGURE 8: IoT-based PCB architecture for the heat treatment process.

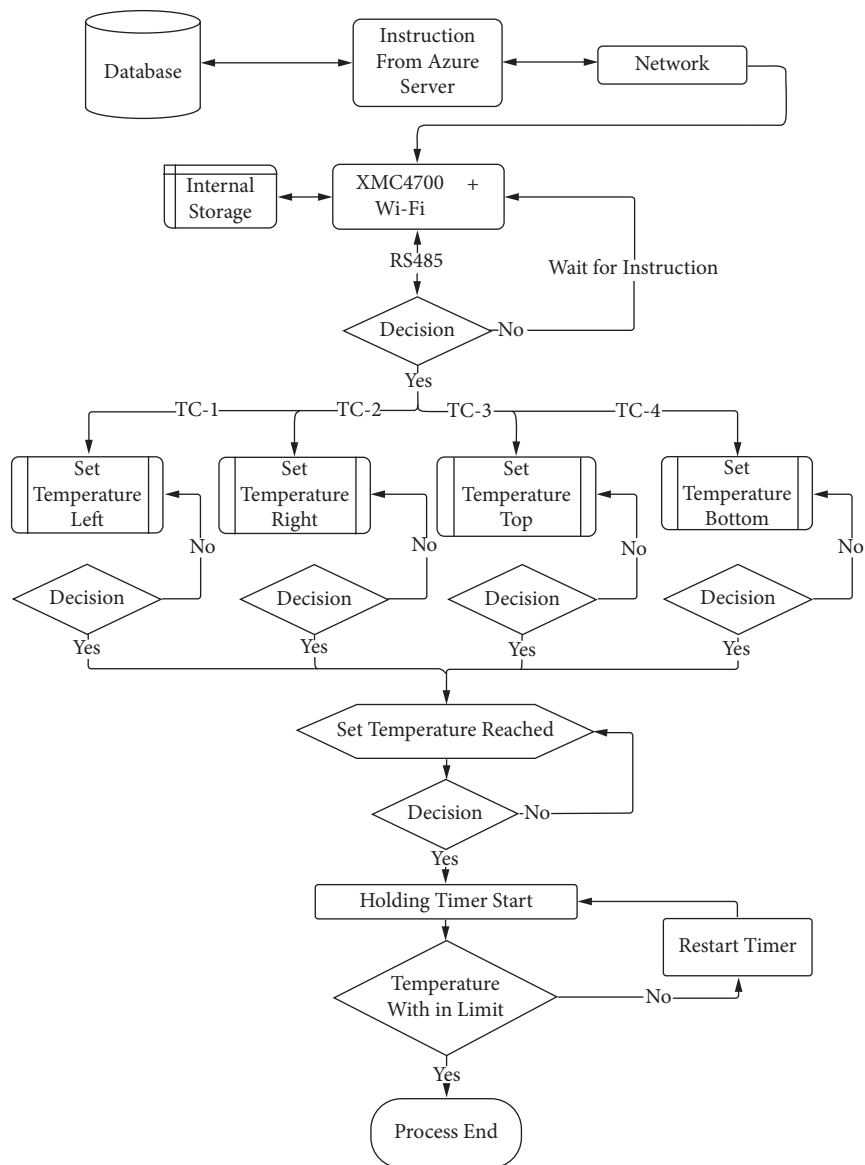


FIGURE 9: Flow diagram for heat treatment process.

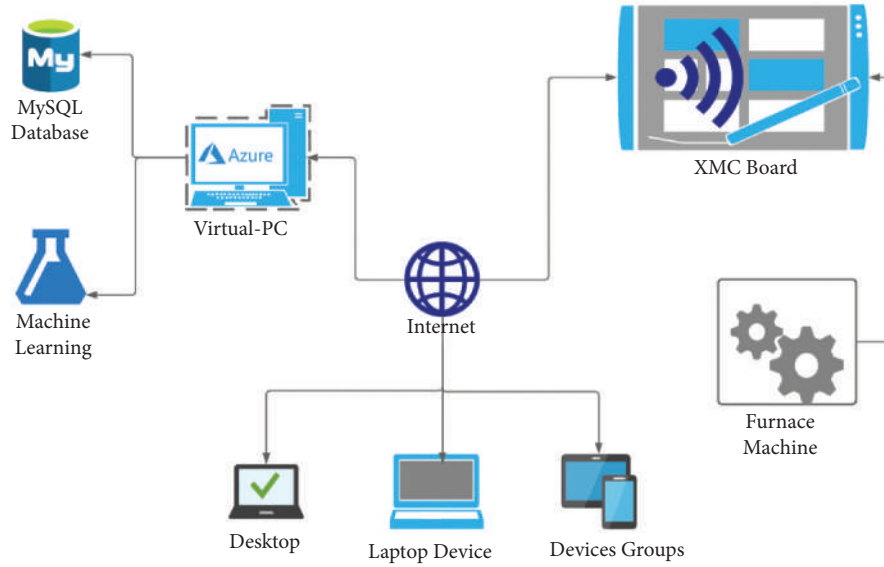


FIGURE 10: Block diagram for machine monitoring and control.

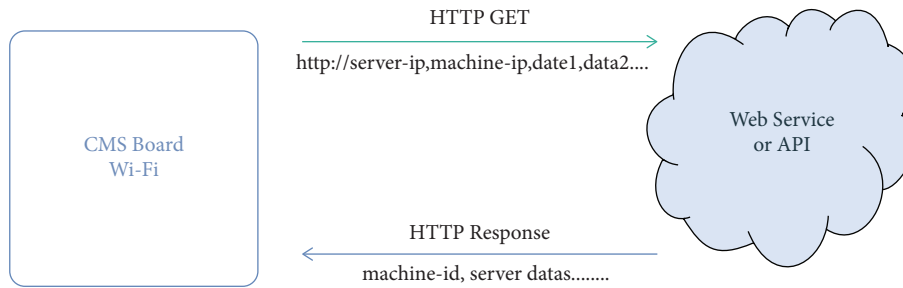


FIGURE 11: Data communication by HTTP request and response.

The steps and flow of proposed are summarized below.

Step 1: initialize temperature (160°C) and time setting instruction from Azure Server

Step 2: XMC board receive initial parameter through and save in internal memory

Step 3: temperature set point received through XMC board and assigning to four temperature controller (TC-1, TC-2, TC-3, and TC-4) through RS485 communication

Step 4: wait until temperature reaches set point

Step 5: once set temperature reached the XMC board, start the holding temperature time

Step 6: XMC board monitor and communicate the temperature to azure cloud

Step 7: if temperature deviation on hold time, the control restarts the time and timer will start again

ALGORITHM 1: Heat treatment process flow.

temperature data from EPROM and transfers it to Microsoft Azure cloud using Wi-Fi module ESP8266, as shown in Figure 11. (Algorithm 1)

6. Result and Discussion

This proposed IoT-based heat treatment prototype is an alternative for analog graph recorder and manual control

process [13, 14]. Figure 12 shows how the industrial automation model works in heat treatment process. This system designs with high industrial standard which can withstand in a high-temperature area. This system used Wi-Fi to transfer the temperature data to the system application, and moreover, this system can monitor the furnace temperature continually as reported in Figure 13.



FIGURE 12: Industrial automation model of the heat treatment process.



FIGURE 13: Browser http request and response chart.

7. Conclusion

To verify the accuracy of the proposed system, we conducted experiments in three cases. In the first case, we examined the microcontroller stability working in the foundry environment. In the second case, we examined the communication between the board and the furnace temperature controller. In the third case, we examined communication between board to cloud server application that controls and monitors the entire furnace; finally, we merge the three experiments; this proposed system helps to plot the live furnace temperature graph, deduct the furnace temperature failure at an earlier stage, reduce the power consumption, increase the product quality, and finally proved industrial 4.0 can be applied for foundry. The study focuses entirely on the temperature sensing, monitoring, and controlling it; however, the other parameters defining the manufacturing process are not taken into account. From the above results, it can be seen that the proposed method can be effectively utilized in maintaining the furnace temperature based on the requirements. It can hence be utilized on other temperature sensing applications to maintain the optimal temperature in sensor applications.

Data Availability

The datasets used and/or analyzed during the current study are available from the corresponding author on reasonable request.

Conflicts of Interest

The authors declare that there are no conflicts of interest.

References

- [1] J. Wan, H. Cai, and K. Zhou, "Industrie 4.0: enabling-technologies," in *Proceedings of the Intelligent Computing and Internet of Things (ICIT), 2014 International Conference on. IEEE*, pp. 135–140, Harbin, China, January 2015.
- [2] T. M. ZeeshanKaleem and C. Lee, "Energy efficient outdoor light monitoring and control architecture using embedded system," *IEEE Embedded systems letters*, vol. 8, no. No.1, 2016.
- [3] T. Andreas and F. O. luis, "Voltage control in PV-rich LV networks without remote monitoring," *IEEE Transaction on Power systems*, vol. 32, no. .2, 2017.
- [4] M. Fazio and A. Puliafito, "Cloud4sens: a cloud-based architecture for sensor controlling and monitoring," *IEEE Communications Magazine*, vol. 53, no. 3, pp. 41–47, 2015.
- [5] W. Dai, "Redesign distributed PLC control system using IEC 61499 function blocks," *IEEE Transactions on Automation Science and Engineering*, vol. 9, no. 2, 2012.
- [6] C.-H. Lu and C. C. Tsai, "Adaptive decoupling predictive temperature control for an extrusion barrel in a plastic injection molding process," *IEEE Transactions on Industrial Electronics*, vol. 48, no. 5, pp. 968–975, 2001.
- [7] E. Vuerich, F. Malaspina, M. Barazutti, T. Georgiadis, T. Georgiadis, and M. Nardino, "Indoor measurements of microclimate variables and ozone in the church of San Vincenzo (Monastery of Bassano Romano - Italy): a pilot study," *Microchemical Journal*, vol. 88, no. 2, pp. 218–223, 2008.
- [8] G. Visco, S. H. Plattner, P. Fortini, and M. Sammartino, "A multivariate approach for a comparison of big data matrices. Case study: thermo-hygrometric monitoring inside the CarcerTullianum (Rome) in the absence and in the presence of visitors," *Environmental Science and Pollution Research*, vol. 24, pp. 1–15, 2017.
- [9] T. Liu, K. Yao, and F. Gao, "Identification and autotuning of temperature-control system with application to injection molding," *IEEE Transactions on Control Systems Technology*, vol. 17, no. 6, pp. 1282–1294, 2009.
- [10] C.-C. Tsai and C.-H. Lu, "Multivariable self-tuning temperature control for plastic injection molding process," *IEEE Transactions on Industry Applications*, vol. 34, no. 2, pp. 310–318, 1998.
- [11] G.-Y. Liao, Y.-J. Chen, W.-C. Lu, and T.-C. Cheng, "Toward authenticating the master in the Modbus protocol," *IEEE Transactions on Power Delivery*, vol. 23, no. 4, pp. 2628–2629, 2008.
- [12] T. Cucinotta, A. Mancina, G. F. Anastasi et al., "A real-time service-oriented architecture for industrial automation," *IEEE*

Transactions on Industrial Informatics, vol. 5, no. 3, pp. 267–277, 2009.

- [13] Y. Tabunschikov and M. Brodatch, “Indoor air climate requirements for Russian churches and cathedrals,” *Indoor Air*, vol. 14, no. s7, pp. 168–174, 2004.
- [14] F.-J. Garca-Diego and M. Zarzo, “Microclimate monitoring by multivariate statistical control: the renaissance frescoes of the Cathedral of Valencia (Spain),” *Journal of Cultural Heritage*, vol. 11, pp. 339–344, 2010.



RESUME SCREENING USING TF-IDF

Chandraghandi S¹, Shilpa S², Anamika P³, Kamalakkannan R⁴, Santhoshsivan N⁵

Assistant Professor, Department of Computer Science And Engineering, JCT College Of Engineering And Technology¹

Computer Science And Engineering, JCT College Of Engineering And Technology, Coimbatore, India²⁻⁵

Abstract: The goal of resume screening is to find the best candidates for a position. In order to match and rate candidates in real-time, the software must employ natural language processing and machine learning. Our system is a resume ranking software that uses natural language processing (NLP) and machine learning. Input would be resumes and job descriptions, output would be a highly ranked candidate's resume. Output results are acquired instantly in real-time. We will be using Mong for string matching, Cosine Similarity, TF-IDF. The existing systems are simple and effective but are not robust in terms of accuracy, efficiency, and processing. Through the analysis of the works of literature on existing methods, it can be found that these are traditional systems that could lead to inaccurate assumptions and loss of human potential. We propose a web application that aims to order the resumes, by intelligently reading job descriptions as input and comparing the resumes which fall into the category of given Job Descriptions. In order to match and rate candidates in real-time, the software employs natural language processing. It provides a ranking after filtering and recommends the better resume for a given textual job description. The Advantages of the proposed system are Secured, Interpretability, High accuracy, Lightweight model & fast processing. Real-time use cases. It could be used in MNC's where multiple resumes must be screened every single day for multiple jobs, government, and administrative offices.

INTRODUCTION

Recruitment is a 200-billion-dollar business. It deals with hiring the best-fit candidates having the relevant skills for a given job profile from an immensely large pool of candidates. If a company has any job opening for a position, scores of candidates mail their resumes to the company to apply for that opening. In the hiring process, the first task for any recruiter is to screen the resumes of all the job applicants. Any company having a job opening for a particular position will have their mail inboxes bombarded with thousands of emails from aspiring job applicants every single day. Selecting the prospective candidates for that job position from a large pool of candidates for any recruiter is very tedious. It is an extremely daunting task for the recruiters of a company to manually go through thousands of resumes and select the most appropriate candidates for the job. Out of those thousands of resumes submitted to the company for the given job posting, about 75% of them do not showcase the relevant skills that are required for the job profile.

Due to this, the recruiters quite often find it really arduous to narrow down the most appropriate candidates from a large applicant pool. In recent years, there have been more than 50,000 e-recruitment sites have been developed. The developers of these online recruitment sites have used various approaches to identify the prospective candidates for a given job profile of a company. Some of these, have managed to employ classification techniques that will classify the candidate resumes into various categories for every job posting given by every company. In these approaches, every candidate's resume is tried to match with every given job posting on the recruitment site. The aim of these recruitment sites is to throw up the results to the candidate to which they are the best fit. The techniques used by these sites have resulted in high accuracy and precision, but one of the major disadvantages is the factor of time complexity. If every candidate's resume is matched with every other job posting given on the online recruitment site, the time complexity for acquiring the results is very high.

The world of Artificial Intelligence [AI] and Machine Learning [ML] has grown significantly in recent times. The availability of large amounts of data brought about by advancements in technology which has made the internet cheap and accessible to previously inaccessible regions of the world has contributed to a great increase in the performance of the ML models in recent times. Software companies around the world exploit the advances in ML to drive automation and increase their productivity in areas that relied mostly on manual human labor. The approach discussed in this project is by using machine learning to train the dataset for a particular type of job position. It is also proposed to use section-based segmentation for data extraction using Natural language Processing (NLP). In order to improve the time efficiency of the web application, the candidate's resume will only be matched to those job openings where they are interested in and have applied to which will, in turn, reduce the time complexity. Besides, the results of the resume matching of all the candidates who have applied for the job opening will be visible only to the recruiter of that particular company. This is



done with the aim to aid the recruiters of any company from the long and tedious task of viewing and analyzing thousands of candidates' resumes. In this intelligent-based approach, they will be given the option to view the candidate's resume as well as they will get the results of the best candidates suitable for the required job position.

NLP

Natural Language Processing, or NLP for short, is broadly defined as the automatic manipulation of natural language, like speech and text, by software.

Step #1: Sentence Segmentation

Breaking the piece of text in various sentences.

Step #2: Word Tokenization

Breaking the sentence into individual words known as tokens. We can tokenize them whenever we encounter a space, we can train a model in that way. Even punctuations are considered as individual tokens as they have some meaning.

Step #3: Predicting Parts of Speech for each token

Predicting whether the word is a noun, verb, adjective, adverb, pronoun, etc. This will help to understand what the sentence is talking about. This can be achieved by feeding the tokens(and the words around it) to a pre-trained part-of-speech classification model. This model was fed a lot of English words with various parts of speech tagged to them so that it classifies the similar words it encounters in future in various parts of speech. Again, the models don't really understand the 'sense' of the words, it just classifies them on the basis of its previous experience. It's pure statistics.

Step #4: Lemmatization Feeding the model with the root word.

For example – There's a Buffalo grazing in the field. There are Buffaloes grazing in the field. Here, both Buffalo and Buffaloes mean the same. But, the computer can confuse it as two different terms as it doesn't know anything. So we have to teach the computer that both terms mean the same. We have to tell a computer that both sentences are talking about the same concept. So we need to find out the most basic form or root form or lemma of the word and feed it to the model accordingly. In a similar fashion, we can use it for verbs too. 'Play' and 'Playing' should be considered as same.

Step #5: Identifying stop words

There are various words in the English language that are used very frequently like 'a', 'and', 'the' etc. These words make a lot of noise while doing statistical analysis. We can take these words out. Some NLP pipelines will categorize these words as stop words, they will be filtered out while doing some statistical analysis. Definitely, they are needed to understand the dependency between various tokens to get the exact sense of the sentence. The list of stop words varies and depends on what kind of output are you expecting.

Step 6.1: Dependency Parsing

This means finding out the relationship between the words in the sentence and how they are related to each other. We create a parse tree in dependency parsing, with root as the main verb in the sentence. If we talk about the first sentence in our example, then 'is' is the main verb and it will be the root of the parse tree. We can construct a parse tree of every sentence with one root word(main verb) associated with it. We can also identify the kind of relationship that exists between the two words. In our example, 'San Pedro' is the subject and 'island' is the attribute. Thus, the relationship between 'San Pedro' and 'is', and 'island' and 'is' can be established. Just like we trained a Machine Learning model to identify various parts of speech, we can train a model to identify the dependency between words by feeding many words. It's a complex task though. In 2016, Google released a new dependency parser Parsey McParseface which used a deep learning approach.

Step 6.2: Finding Noun Phrases

We can group the words that represent the same idea. For example – It is the second-largest town in the Belize District and largest in the Belize Rural South constituency. Here, tokens 'second', 'largest' and 'town' can be grouped together as they together represent the same thing 'Belize'. We can use the output of dependency parsing to combine such words.



Whether to do this step or not completely depends on the end goal, but it's always quick to do this if we don't want much information about which words are adjectives, rather focus on other important details.

Step #7: Named Entity Recognition(NER)

San Pedro is a town on the southern part of the island of Ambergris Caye in the 2. Belize District of the nation of Belize, in Central America. Here, the NER maps the words with the real-world places. The places that actually exist in the physical world. We can automatically extract the real-world places present in the document using NLP. If the above sentence is the input, NER will map it like this way: San Pedro - Geographic Entity Ambergris Caye - Geographic Entity Belize - Geographic Entity Central America - Geographic Entity NER systems look for how a word is placed in a sentence and make use of other statistical models to identify what kind of word actually it is. For example – 'Washington' can be a geographical location as well as the last name of any person. A good NER system can identify this. Kinds of objects that a typical NER system can tag: People's names. Company names. Geographical locations Product names. Date and time. Amount of money.

Step #8: Coreference Resolution

San Pedro is a town on the southern part of the island of Ambergris Caye in the Belize District of the nation of Belize, in Central America. According to 2015 mid-year estimates, the town has a population of about 16, 444. It is the second-largest town in the Belize District and largest in the Belize Rural South constituency. Here, we know that 'it' in sentence 6 stands for San Pedro, but for a computer, it isn't possible to understand that both the tokens are the same because it treats both the sentences as two different things while it's processing them. Pronouns are used with a high frequency in English literature and it becomes difficult for a computer to understand that both things are the same.

Exploratory Data Analysis (EDA)

Exploratory Data Analysis (EDA) is an approach to analyze the data using visual techniques. It is used to discover trends, patterns, or to check assumptions with the help of statistical summary and graphical representations. EDA is the process of investigating the dataset to discover patterns, and anomalies (outliers), and form hypotheses based on our understanding of the dataset. EDA involves generating summary statistics for numerical data in the dataset and creating various graphical representations to understand the data better. EDA assists Data science professionals in various ways: -

- 1 Getting a better understanding of data
- 2 Identifying various data patterns
- 3 Getting a better understanding of the problem statement

EDA is primarily used to see what data can reveal beyond the formal modeling or hypothesis testing task and provides a better understanding of data set variables and the relationships between them. It can also help determine if the statistical techniques you are considering for data analysis are appropriate. The main purpose of EDA is to help look at data before making any assumptions. It can help identify obvious errors, as well as better understand patterns within the data, detect outliers or anomalous events, find interesting relations among the variables.

Data cleaning

This is the most important step in EDA involving removing duplicate rows/columns, filling the void entries with values like mean/median of the data, dropping various values, removing null entries

Data visualization

Data Visualization is the process of analyzing data in the form of graphs or maps, making it a lot easier to understand the trends or patterns in the data. There are various types of visualizations

- Univariate analysis: This type of data consists of only one variable. The analysis of univariate data is thus the simplest form of analysis since the information deals with only one quantity that changes. It does not deal with causes or relationships and the main purpose of the analysis is to describe the data and find patterns that exist within it.
- Bi-Variate analysis: This type of data involves two different variables. The analysis of this type of data deals with causes and relationships and the analysis is done to find out the relationship among the two variables.



- Multi-Variate analysis: When the data involves three or more variables, it is categorized under multivariate.

Some of the most common data science tools used to create an EDA include:

- **Python:** An interpreted, object-oriented programming language with dynamic semantics. Its high-level, built-in data structures, combined with dynamic typing and dynamic binding, make it very attractive for rapid application development, as well as for use as a scripting or glue language to connect existing components together. Python and EDA can be used together to identify missing values in a data set, which is important so you can decide how to handle missing values for machine learning.
- **R:** An open-source programming language and free software environment for statistical computing and graphics supported by the R Foundation for Statistical Computing. The R language is widely used among statisticians in data science in developing statistical observations and data analysis.

TF-IDF

It is a numerical statistic that is intended to reflect how important a word is to a document in a collection or corpus. It is often used as a weighting factor in searches of information retrieval, text mining, and user modeling. The tf-idf value increases proportionally to the number of times a word appears in the document and is offset by the number of documents in the corpus that contain the word, which helps to adjust for the fact that some words appear more frequently in general. tf-idf is one of the most popular term-weighting schemes today.

TF-IDF (term frequency-inverse document frequency) is a statistical measure that evaluates how relevant a word is to a document in a collection of documents.

This is done by multiplying two metrics: how many times a word appears in a document, and the inverse document frequency of the word across a set of documents.

It has many uses, most importantly in automated text analysis, and is very useful for scoring words in machine learning algorithms for Natural Language Processing (NLP).

TF-IDF was invented for document search and information retrieval. It works by increasing proportionally to the number of times a word appears in a document but is offset by the number of documents that contain the word. So, words that are common in every document, such as this, what, and if, rank low even though they may appear many times since they don't mean much to that document in particular.

However, if the word *Bug* appears many times in a document, while not appearing many times in others, it probably means that it's very relevant. For example, if what we're doing is trying to find out which topics some NPS responses belong to, the word *Bug* would probably end up being tied to the topic Reliability, since most responses containing that word would be about that topic.

How is TF-IDF calculated?

TF-IDF for a word in a document is calculated by multiplying two different metrics:

- The **term frequency** of a word in a document. There are several ways of calculating this frequency, with the simplest being a raw count of instances a word appears in a document. Then, there are ways to adjust the frequency, by the length of a document, or by the raw frequency of the most frequent word in a document.
- The **inverse document frequency** of the word across a set of documents. This means, how common or rare a word is in the entire document set. The closer it is to 0, the more common a word is. This metric can be calculated by taking the total number of documents, dividing it by the number of documents that contain a word, and calculating the logarithm.
- So, if the word is very common and appears in many documents, this number will approach 0. Otherwise, it will approach 1.

Multiplying these two numbers results in the TF-IDF score of a word in a document. The higher the score, the more relevant that word is in that particular document.



Why is TF-IDF used in Machine Learning?

Machine learning with natural language is faced with one major hurdle – its algorithms usually deal with numbers, and natural language is, well, text. So, we need to transform that text into numbers, otherwise known as text vectorization. It's a fundamental step in the process of machine learning for analyzing data, and different vectorization algorithms will drastically affect end results, so you need to choose one that will deliver the results you're hoping for.

Once you've transformed words into numbers, in a way that's machine learning algorithms can understand, the TF-IDF score can be fed to algorithms such as Naive Bayes and Support Vector Machines, greatly improving the results of more basic methods like word counts.

Why does this work? Simply put, a word vector represents a document as a list of numbers, with one for each possible word of the corpus. Vectorizing a document is taking the text and creating one of these vectors, and the numbers of the vectors somehow represent the content of the text. TF-IDF enables us to give us a way to associate each word in a document with a number that represents how relevant each word is in that document. Then, documents with similar, relevant words will have similar vectors, which is what we are looking for in a machine learning algorithm.

Applications of TF-IDF

Determining how relevant a word is to a document, or TD-IDF, is useful in many ways, for example:

- **Information retrieval**

TF-IDF was invented for document search and can be used to deliver results that are most relevant to what you're searching for. Imagine you have a search engine and somebody looks for LeBron. The results will be displayed in order of relevance. That's to say the most relevant sports articles will be ranked higher because TF-IDF gives the word LeBron a higher score. It's likely that every search engine you have ever encountered uses TF-IDF scores in its algorithm.

- **Keyword Extraction**

TF-IDF is also useful for extracting keywords from the text. How? The highest scoring words of a document are the most relevant to that document, and therefore they can be considered *keywords* for that document. Pretty straightforward.

Cosine Similarity

Cosine similarity measures the similarity between two vectors of an inner product space. It is measured by the cosine of the angle between two vectors and determines whether two vectors are pointing in roughly the same direction. It is often used to measure document similarity in text analysis. A document can be represented by thousands of attributes, each recording the frequency of a particular word (such as a keyword) or phrase in the document. Thus, each document is an object represented by what is called a *term-frequency vector*. Term-frequency vectors are typically very long and sparse (i.e., they have many 0 values). Applications using such structures include information retrieval, text document clustering, biological taxonomy, and gene feature mapping. The traditional distance measures that we have studied in this chapter do not work well for such sparse numeric data. For example, two term-frequency vectors may have many 0 values in common, meaning that the corresponding documents do not share many words, but this does not make them similar. We need a measure that will focus on the words that the two documents do have in common, and the occurrence frequency of such words. In other words, we need a measure for numeric data that ignores zero matches.

Cosine similarity is a measure of similarity that can be used to compare documents or, say, give a ranking of documents with respect to a given vector of query words. We've chosen the Cosine Similarity Algorithm, in which the employer's Job Description is matched against the content of resumes in the space, and the topmost similar resumes are suggested to the recruiter.

Overlap coefficient

The overlap coefficient is a similarity measure that measures the overlap between two finite sets. It is related to the Jaccard index and is defined as the size of the intersection divided by the smaller of the size of the two sets:

$$O(A,B) = \frac{|A \cap B|}{\min(|A|, |B|)}$$



If set A is a subset of B or the converse then the overlap coefficient is equal to 1.

LITERATURE SURVEY

Recruitment of appropriate people for certain positions is critical for any company or organization. Manually screening to select appropriate candidates from large amounts of resumes can be exhausted and time-consuming. The traditional methods normally entail a time-consuming process of manually looking through all of the individuals who have applied, examining their resumes, and then establishing a shortlist of prospects who should be interviewed. The authors in [1] created an automated machine learning-based algorithm that recommends acceptable applicant resumes to HR based on the job description provided. The suggested methodology had two stages: first, it classified resumes into various groups. Second, it suggests resumes based on their resemblance to the job description. If an industry produces a high number of resumes, the proposed approach can be used to create an industry-specific model.

In [2], the objective was to create a résumé shortlisting system using natural language processing. In [4], The proposed system, JARO accelerates the interview process towards an unbiased decision-making process by proposing a chatbot that would conduct interviews by analyzing the candidate's Curriculum Vitae (CV), based on which, it then prepares a set of questions to be asked to the candidate. The system will consist of features like resume analysis and automatic interview processes.

The manual process of screening resumes could stymie the team's efforts to locate the right individual at the right moment. The laborious screening may be greatly aided by an automated technique for screening and ranking applicants. In [5], the top applicants might be rated using content-based suggestion, which uses cosine similarity to find the curriculum vitae that are the most comparable to the job description supplied and KNN algorithm is used to pick and rank Curriculum Vitae (CV) based on job descriptions in huge quantities. Experimental results indicate the performance of the proposed system as an average text parsing accuracy of 85% and a ranking accuracy of 92%. Pradeep Kumar Roy and Sarabhjit Singh [6] suggested that an automated way of "Resume Classification and Matching" could really ease the tedious process of fair screening and shortlisting, it would certainly expedite the candidate selection and decisionmaking process. This system could work with a large number of resumes for first classifying the right categories using different classifier, once classification has been done then as per the job description, top candidates could be ranked using Content-based Recommendation, using cosine similarity and by using k-NN to identify the CVs that are nearest to the provided job description.

The research work of authors in [7] presented a hybrid approach that employs conceptual-based classification of resumes and job postings and automatically ranks candidate resumes (that fall under each category) to their corresponding job offers. In this context, the exploit an integrated knowledge base for carrying out the classification task and experimentally demonstrate - using a real-world recruitment dataset- achieving promising precision results compared to conventional machine learning-based resume classification approaches. To address the issues associated with the previously highlighted techniques, what has been presented is a hybrid approach that employs conceptual-based classification of resumes and job postings and automatically ranks candidate resumes (that fall under each occupational category) to their corresponding job postings. The study work in [8] was conducted among 115 HR professionals at various IT sectors in Delhi/NCR region. A multiple regression method was used to test the hypothesis and confirmed a positive relationship between these two factors establishing about the increased use of AI at work results in better HR functional performance. However, AI has a significant relationship with innovativeness and also with the ease of use which reflects AI affects HR with innovations and ease of use.

The research work in [9] focuses on extracting data from resumes and performing the required analysis on the data to convert it into useful information for the recruiters. Thus, the Resume Parser would help the recruiters to select the best relevant candidates in a minimal amount of time, consequently saving their time and effort. The authors in [10] developed a method for automatic RQA. Since there is also no public dataset for model training and evaluation, we build a dataset for RQA by collecting around 10K resumes, which are provided by a private resume management company. By investigating the dataset, we identify some factors or features that could be useful to discriminate good resumes from bad ones, e.g., the consistency between different parts of a resume. Then a neural-network model is designed to predict the quality of each resume, where some text processing techniques are incorporated. To deal with the label deficiency issue in the dataset, they proposed several variants of the model by either utilizing the pair/triplet-based loss or introducing some semi-supervised learning technique to make use of the abundant unlabeled data.



[11] presents an overview of fairness definitions, methods, and tools as they relate to recruitment and establishes ethical considerations in the use of machine learning in the hiring space. Considering Deep Learning (DL) method recognize artificial Neural Network (NN) to nonlinear process, NLP tools become increasingly accurate and efficient that begin a debacle. Multi-Layer Neural Network obtaining the importance of the NLP for its capability including standard speed and resolute output. Hierarchical designs of data operate recurring processing layers to learn and with this arrangement of DL methods manage several practices. In [12], this resumed striving to reach a review of the tools and the necessary methodology to present a clear understanding of the association of NLP and DL for truly understanding in the training. Efficiency and execution both are improved in NLP by Part of speech tagging (POST), Morphological Analysis, Named Entity Recognition (NER), Semantic Role Labeling (SRL), Syntactic Parsing, and Coreference resolution. Artificial Neural Networks (ANN), Time Delay Neural Networks (TDNN), Recurrent Neural Network (RNN), Convolution Neural Networks (CNN), and Long-Short-Term-Memory (LSTM) dealings among Dense Vector (DV), Windows Approach (WA), and Multitask learning (MTL) as a characteristic of Deep Learning.

[13] proposes a system for resume parsing using deep learning models such as the convolutional neural network (CNN), Bi-LSTM (Bidirectional Long Short-Term Memory), and Conditional Random Field (CRF). CNN Model is used for classifying different segments in a resume. CRF and Bi-LSTM-CNN models were used for sequence labeling in order to tag different entities. The pre-trained Glove model is used for word embedding. The proposed system could classify a resume into three segments and extract 23 fields. At an industry sector level such as Information Technology or across such different industry sectors (such as retail, insurance, health care), mining and recommending the most relevant career paths for a user is still an unsolved research challenge. Towards addressing this problem, [14] proposes a system that leverages the notion of skills to construct skill graphs that can form the basis for career path recommendations. Skills are more amenable for career path standardizations across the organizations. This system ingests a user's profile (in a pdf, word format, or other public and shared data sources) and leverages an Open IE pipeline to extract education and experiences. Subsequently, the extracted entities are mapped as specific skills that are expressed in the form of a novel unified skill graph.

[16] presents a survey of e-recruiting process and existing recommendation approaches for building personalized recommender systems for candidates/job matching.

Every job advertisement receives a significant number of applications, many of which are related to the listed position. Because they must identify the most qualified profile/resume from a broad pool of prospects, job recruiters encounter substantial challenges. Because it is the profile of the applicant recommended for a specific role, the method of matching the candidate CV with the job description is similar to a recommender system. Otaibi et al. [16] investigated the utilization of employment referral services in-depth and discussed the measures that must be taken during the hiring process for any organization and also described how the organization benefits from the e-recruitment portal, what candidate criteria might lead to the selection, and a variety of other essential recruiting approaches. To produce employment suggestions, Malinowski et al. used an Expectation-Maximization (EM) algorithm that took into account both the candidate's resume and the employer's job description. Golec et al. [17] suggested a fuzzy-based method for determining candidate relevance to the job description

One of more useful and efficient retrieval model [19] is the vector space model. It uses term weighting tf-idf for assigning a score to a query/document pair, in order to rank the documents. This method in [19] is based on the bag-of-words model and does not capture position of terms in document and semantics. Keeping this approach, here we propose a new ranking measure that combines the vector space measure denoted tf-idf and new factor deducted from association rules technique based on dominance relations. This approach will help the user to get the most relevant documents at the beginning. The experiments on TREC collection show that the proposed method is giving better results compared to the baselines and the semantic ranking ESA.

Using NLP(Natural Language Processing) and ML(Machine Learning) to rank the resumes according to the given constraint, this intelligent system ranks the resume of any format according to the given constraints or the following requirement provided by the client company. We will basically take the bulk of input resume from the client company and that client company will also provide the requirement and the constraints according to which the resume should be ranked by our system. Besides the information provided by the resume, we are going to read the candidate's social profiles (like LinkedIn, GitHub, etc.) which will give us more genuine information about that candidate.

**METHODOLOGY AND SYSTEM DESIGN**

Recruitment in the IT sector has been on the rise in recent times. Software companies are on the hunt to recruit raw talent right from the colleges through job fairs. The process of allotment of projects to the new recruits is a manual affair, usually carried out by the Human Resources department of the organization. This process of project allotment to the new recruits is a costly affair for the organization as it relies mostly on human effort. In recent times, software companies around the world are leveraging the advances in machine learning and Artificial intelligence, in general, to automate routine tasks in the enterprise to increase productivity. The existing system is a traditional Machine Learning based system that gives lower rates of accuracy. It has lower efficiency and gives lower inaccurate results. This system may lead to loss of human potential.

The major objective of our system is to take the current resume ranking system to another level and makes it more flexible for both the entity.

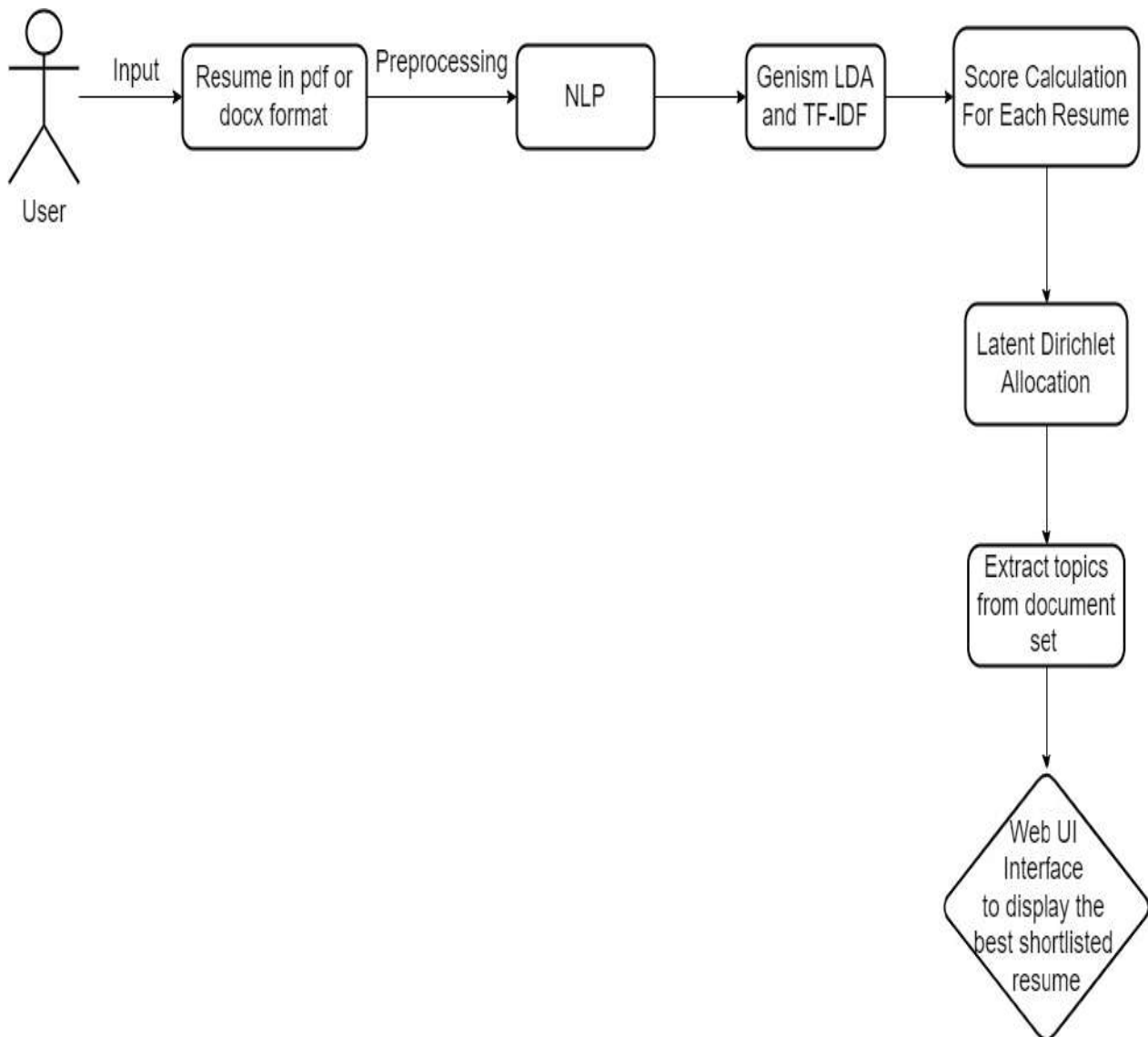
- 1) Candidates, who have been hired.
- 2) Client company, who is hiring the candidates

The report also aims to propose an algorithm that provides a list of applicants with appropriate experience and then presents the high points of each selected resume, unlike the conventional way of applying filters and manually scanning resumes to identify the most qualified candidates for a certain vacancy. The model is also designed with an aim to automate tasks that the human resources can do and recognize and identify human faces

We propose a web application that aims to order the resumes, by intelligently reading job descriptions as input and comparing the resumes which fall into the category of given Job Descriptions. It provides a ranking after filtering and recommends the better resume for a given textual job description. Our system is a resume ranking software that uses natural language processing (NLP) and machine learning. This AI-powered resume screening program goes beyond keywords to contextually screen resumes. Following resume screening, the software rates prospects in real-time depending on the recruiter's job needs. In order to match and rate candidates in real-time, the software employs natural language processing. Unlike generic processes, this app utilizes Mong for string matching, Cosine Similarity, Overlapping coefficient Natural Language.

Our work takes a different approach as it focuses mainly on the content of the resumes where we perform the extraction of skills and related parameters to match candidates with the job descriptions. The interactive web application will allow the job applicants to submit their resumes and apply for job postings they may still be interested in. The resumes submitted by the candidates are then compared with the job profile requirement posted by the company recruiter by using techniques like machine learning and Natural Language Processing (NLP). Scores can then be given to the resumes and they can be ranked from highest match to lowest match. This ranking is made visible only to the company recruiter who is interested to select the best candidates from a large pool of candidates. This is done with the aim to aid the recruiters of any company from the long and tedious task of viewing and analyzing thousands of candidates' resumes. The calculated ranking scores can then be utilized to determine best-fitting candidates for that particular job opening. Since the dynamic model leverages NLP, it gives the output instantly. While going through all these pipelines, it will score each resume and give out accurate output with higher efficiency, precision, and accuracy.

Input is the job applicant's resume which will be further preprocessed to remove any special or garbage characters from the resumes. All unique characters, numerals, and words with only single letters are eliminated during cleaning. After these processes, we'll have a clean dataset with no unique characters, numerals, or single letter words. The web application returns a highly ranked candidate's resume that is most similar to the job description. The approach would aid the recruiter in expediting profile shortlisting while also ensuring the shortlisting process's authenticity, since they would be able to examine a large number of resumes in a short period of time, also with the proper fit, which a human would not be able to perform in near real-time. This application makes use of Natural Language Processing (NLP) which helps in data training and feature extraction of the text data. NLP is an analysis of natural languages so that computers can understand them. Natural language, whether spoken, written, or typed, is the most natural means of communication between humans, and the mode of expression of choice for most of the documents they produce. Using NLP methods, semi-structured text data is converted to a structured format with required extracted features. We've chosen the Cosine Similarity Algorithm, in which the employer's Job Description is matched against the content of resumes in the space, and the topmost similar resumes are suggested to the recruiter.



SYSTEM ARCHITECTURE

Natural Language Processing [NLP] and EDA

This application makes use of Natural Language Processing (NLP) which helps in data training and feature extraction of the text data. NLP is an analysis of natural languages so that computers can understand them. Natural language, whether spoken, written, or typed, is the most natural means of communication between humans, and the mode of expression of choice for most of the documents they produce. Using NLP methods, semi-structured text data is converted to a structured format with required extracted features. The profiles of the new recruits are fed as input to the NLPP by the HR team of the organization. The module is responsible for eliminating the unnecessary information from the resume and providing only the required data in the form of tokens which could aid in the process of allotment of projects to the classification module. Resume collection is being performed and folder Structure creation is being done. Data Cleaning such as removing clutter and unnecessary punctuation would be taken off, Feature Engineering would be performed for enhancement. This includes removing stop words, punctuation, and stemming. This process will construct a graph with sentences as the vertices. Importing necessary libraries is performed. This library creates a summary of the supplied information within the word limit. With the help of Natural language processing techniques, the application which extracts the names of people, places, and other entities from text, the main goal is to get a reduced version of it that retains the most important information.



There are several different methods of statistical analysis and data visualization techniques in the dataset that can be used to explore the data to identify the appropriate data cleaning operations to be conducted. Also known as E.D.A, exploratory data analysis is a very important phase in researching and investigating various data sets and summarizing their significant characteristics. The application of EDA can assist in uncovering hidden patterns in datasets and how important is it in data science. Exploratory data analysis (EDA) is often a necessary task in uncovering hidden patterns, detecting outliers, and identifying important variables and any anomalies in data. The data is cleaned and pre-processed at this stage, where missing and null value records are dropped. The main purpose of preprocessing is to identify and drop or substitute the missing values in the dataset which occupy a very small part of the whole data, to ensure an accurate result.

Term frequency-inverse document frequency (TF-IDF)

The TF-IDF method is the most frequently used method for determining word frequencies. This is an abbreviation for "Term Frequency – Inverse Document" Frequency, one of the criteria used to determine the final score for each word. TF-IDF is word frequency scores that aim to emphasize phrases that are more interesting, e.g., common in a text but not across texts, without delving into the arithmetic. The TF-IDF Vectorizer tokenizes texts, learns vocabulary, inverts frequency weightings, and allows encoding new ones. At this stage, a dynamic Script for the Tf-Idf approach is written. Term frequency-inverse document frequency is a numerical statistic that is intended to reflect how important a word is to a document in a collection. TF-IDF is word frequency scores that aim to emphasize phrases that are more interesting, e.g., common in a text but not across texts, without delving into the arithmetic. The TF-IDF Vectorizer tokenizes texts, learns vocabulary, inverts frequency weightings, and allows encoding new ones.

$$TF - IDF(t, d) = TF(t, d) * IDF(t, d) \quad (1)$$

$$TF(t, d) = \frac{\text{freq}(t, d)}{\sum \text{freq}(t_i, d)} \quad (2)$$

$$IDF(t) = \log\left(\frac{N}{\text{count}(t)}\right) \quad (3)$$

Where $\text{freq}(t, d)$ is the count of the instances of the term t in document d .

$TF(t, d)$ is the proportion of the count of term t in document d

N is the number of distinct terms in document d .

It provides information on a word frequency in the documents. Higher the TF- IDF score of a term which is computed using the above equations represents more relevance in a document. It provides information on a word frequency in the documents.

Higher the TF- IDF score of a term which is computed using the above equations represents more relevance in a document. In our system, we modeled the CVs and JD into a vector space. This is accomplished by compiling a glossary of terms found in the papers and converting them. Each phrase corresponds to a vector space dimension. Using the Count Vectorizer and the TF- IDF matrix, we generated the TF- IDF matrix for the CVs and the job query.

Latent Dirichlet Allocation (LDA)

A tool and technique for Topic Modeling, Latent Dirichlet Allocation (LDA) classifies or categorizes the text into a document and the words per topic, these are modeled based on the Dirichlet distributions and processes. Latent Dirichlet Allocation has been used in the application for the following functions-

- Discovering the hidden themes in the data.
- Classifying the data into the discovered themes.
- Using the classification to organize/summarize/search the documents.

The application then deals with the calculation of the score for a candidate's resume according to the job posting they have applied for. According to the score each candidate's resume receives, a rank list will be made with the candidate receiving a higher score placed higher as compared to the candidate receiving a lower score. By displaying a resume list in order of relevance to the position, the technique ranks CVs according to their match with the job description, making it easy for recruiters. Customized options for job description in our web application is shown. Slider options are present



in our app for a better user experience. The web application would also have a Bar Chart that shows the stats. The Resume Screening System replaces ineffective manual screening, ensuring that no candidate is overlooked

CONCLUSION

The results from the model are encouraging. The resume classifier application is successful in automating the manual task of project allocation to the new recruits of the organization based on the interests, work experience, and expertise mentioned by the candidate in the profile. The Resume Screening System replaces ineffective manual screening, ensuring that no candidate is overlooked. The need for efficient and effective resume screening is at the heart of every excellent recruitment strategy. The system will be able to accept or reject a job applicant based on two factors: the company's requirements must match the skills listed in the applicant's resume, and the test evaluation will be based on the applicant's skills, ensuring that the resumes uploaded by the applicant are genuine and the applicant is truly knowledgeable about the skills. Using NLP(Natural Language Processing) and ML(Machine Learning) to rank the resumes according to the given constraint, this intelligent system ranks the resume of any format according to the given constraints or the following requirement provided by the client company. We will basically take the bulk of input resume from the client company and that client company will also provide the requirement and the constraints according to which the resume should be ranked by our system. Besides the information provided by the resume, we are going to read the candidate's social profiles (like LinkedIn, GitHub, etc.) which will give us more genuine information about that candidate. The application automates the task of project allocation, thereby eliminating the tedious and redundant affair of opening and analyzing the resumes manually by the HR team of the organization.

REFERENCES

- [1] Rajath V; Riza Tanaz Fareed; Sharadadevi Kaganurmah," Resume Classification And Ranking Using KNN And Cosine Similarity",international JOURNAL OF ENGINEERING RESEARCH & TECHNOLOGY, Volume 10, Issue 08, AUGUST 2021
- [2] Akshay Kulkarni; Adarsha Shivananda; Anoosh Kulkarni," Creating a Résumé Parsing, Screening and Shortlisting System", Natural Language Processing Projects pp 125-155, December 2021
- [3] Sujit Amin; Nikita Jayakar; Sonia Sunny; Pheba Babu; M. Kiruthika; Ambarish Gurjar, "Web Application for Screening Resume", 2019 International Conference on Nascent Technologies in Engineering (ICNTE), January 2020
- [4] Jitendra Purohit; Aditya Bagwe; Rishabh Mehta; Ojaswini Mangaonkar; Elizabeth George, "Natural Language Processing based Jaro-The Interviewing Chatbot", 2019 3rd International Conference on Computing Methodologies and Communication (ICCMC), August 2019
- [5] Tejaswini K; Umadevi V; Shashank M Kadiwal; Sanjay Revanna," Design and Development of Machine Learning based Resume Ranking System", Global Transitions Proceedings, October 2021
- [6] Pradeep Kumar Roy; Sarabjeet Singh Chowdhary; Rocky Bhatia," A Machine Learning approach for automation of Resume Recommendation system", Procedia Computer Science Volume 167, Pages 2318-2327, 2020
- [7] Abeer Zaroor; Mohammed Maree; Muath Sabha," A Hybrid Approach to Conceptual Classification and Ranking of Resumes and Their Corresponding Job Post", Smart Innovation, Systems and Technologies book series (SIST, volume 72), 2017
- [8] Garima Bhardwaj; S. Vikram Singh; Vinay Kumar," An Empirical Study of Artificial Intelligence and its Impact on Human Resource Functions", International Conference on Computation, Automation and Knowledge Management (ICCAKM), 2020
- [9] Anushka Sharma; Smiti Singhal; Dhara Ajudia," Intelligent Recruitment System Using NLP", International Conference on Artificial Intelligence and Machine Vision (AIMV), 2021
- [10] Yong Luo; Huaizheng Zhang; Yongjie Wang; Yonggang Wen; Xinwen Zhang," ResumeNet: A Learning-Based Framework for Automatic Resume Quality Assessment", 2018 IEEE International Conference on Data Mining (ICDM), December 2018
- [11] Mujtaba, Dena F., and Nihar R. Mahapatra. "Ethical Considerations in AI-Based Recruitment." 2019 IEEE International Symposium on Technology and Society (ISTAS). IEEE, 2019.
- [12] Fahad, SK Ahmed, and Abdul Samad Ebrahim Yahya. "Inflectional review of deep learning on natural language processing." 2018 International Conference on Smart Computing and Electronic Enterprise (ICSEE). IEEE, 2018
- [13] Ayisha Thahir, C. H., C. Sreejith, and C. Rasik. "Combination of Neural Networks and Conditional Random Fields for Efficient Resume Parsing." 2018 International CET Conference on Control, Communication, and Computing (IC4). IEEE, 2018.



- [14] Gugnani, Akshay, Vinay Kumar Reddy Kasireddy, and Karthikeyan Ponnalagu. "Generating unified candidate skill graph for career path recommendation." 2018 IEEE International Conference on Data Mining Workshops (ICDMW). IEEE, 2018.
- [15] Naim, M.I. Tanveer, D. Gildea and E. Hoque, "Automated analysis and prediction of sjob interview performance", IEEE Transactions on Affective Computing, 2016.
- [16] Shaha T. Al-Otaibi, Mourad Ykhlef , "A survey of job recommender systems", International Journal of Physical Sciences, 7 (29) (2012), pp. 5127-5142
- [17] Adem Golec, Esra Kahya , "A fuzzy model for competency-based employee evaluation and selection", Computers & Industrial Engineering, 52 (1) (2007), pp. 143-161
- [18] Siham Jabri, Azzeddine Dahbi, Taoufiq Gadi, Abdelhak Bassir , "Ranking of text documents using TF-IDF weighting and association rules mining", 2018 4th international conference on optimization and applications (ICOA), IEEE (2018), pp. 1-6
- [19] Jyothis Joseph, Jaimy Sunny, R Raveena, BlessyElzaByju, KC Laya, , "Resume Analyser: Automated Resume Ranking Software", International Journal for Research in Applied Science & Engineering Technology (IJRASET), 8 (7) (2020), pp. 896-899



Location Based Alarm System Using Android Development

Dr. Rajiv Suresh Kumar¹, Anirudh M², Manuvel Victor J³, Rakesh R⁴

¹Head of the Department, JCT college of Engineering & Technology

^{2,3,4}BE Computer Science And Engineering JCT college of Engineering & Technology

Abstract: Location based alarm using GPS is an attempt to add an alarm facility for mobiles, based on the location of the device and to find the nearest places from the current location of the mobile device. The location based alarm will give you alert when you reach your desired destination. Location based alarm is a GPS based alarm, If you set an alarm, it will make a sound and notification once it's detected you are within the user defined range from the destination. The user needs to save the current location using longitude and latitude, the alarm will ring when the user is near to the location. This location based alarm is useful for the traveling sales persons and persons who are traveling in a train. The traveling sales person needs to do different kind of works in different places. It is difficult to remember all the places for him. So by using this application he can set an alarm to the places, where he need to go. The GPRS settings must be enabled on a mobile device to use this application. we are using a SHA1 signature to generate a key google map API key and google play service API for displaying the map in mobile device. The generation of SHA1 signature will be discussed in the methodology.

Objective

The main objective of the project is to develop a GPS (Global Positioning System) based application to handle the following requirements: To alert the users through an alarm when the user reaches near a preset location, to retrieve the users current location coordinates (latitudes and longitudes), to allows users to set their target location and save that target to the list, allows user to delete and edit the alarms, to allow user to the put the reminder text along with the alarm.

Keywords: GPS (Global Positioning System), GPRS (General Packet Radio Service), Android.

I. INTRODUCTION

The location based alarm system is an android application. The use of android mobile devices vastly increases in the present generation because Android is an open source operating system and there are more than 4,00,000 apps available in the Android market. Android is a Linux based operating system for mobile devices such as Smartphone's and tablet computers. The android can run multiple applications at the same time. There are different versions in android i.e. Android 1.0, Android 1.1, Android 1.5 (Cupcake), Android 1.6 (Donut), Android 2.0 (Éclair), Android 2.2 (Froyo), Android 2.3 (Gingerbread), Android 3.0 (Honeycomb), Android 4.0 (Ice cream sandwich), Android 4.1 (Jelly Bean). Our application can run only above the version 2.3. The location based service allows software to obtain the phone's current location. This includes location obtained from the Global Positioning System (GPS) satellite constellation. In this application, we will try to get the user current location using the longitude latitude.

II. MAIN TITLE

- With the location based alarm system depending on latitude and longitude, a user gets reminder of what to do, when to do and thus work depending upon the location.
- Application side has the Google Map which contains list of locations of any particular city.
- Stores the database in the form of table which contains message of place and work for location based on alarm system.
- While moving every time the location changes will be observed by the mobile through the GSM connection.
- Application checks the database if it matches through the mobile connected via serial port the alarm is raised in the form of message.

III. RELATED WORK

There exists a lot of location/proximity-based systems that can automate the simple tasks such as locking/unlocking your mobile devices, computers and launching various applications by using Bluetooth enabled computer and mobile



phone. There are even many home automation area that allows users to control just about every piece of electronics, including security and surveillance system. However, most of these systems are not location based. Nor Alarm has developed in a mobile application that enables users to control an alarm system through a Android devices based on the Location. This application allows the user to manually place an alarm and then the alarm will trigger when the location is arrived, it includes automatic activation of the alarm and deactivation based on the location of the user.

IV.PROPOSED METHOD

To set an alarm user need to enter the location. The alarm will raise when the user is near to the location. (the default radius is 500meters, user can also change the radius according to his desire). The mobile device is a hardware equipment which enables the usage of the location based alarm system. The GPS is a space-based satellite navigation system that provides longitude and latitude of location in all weather conditions, anywhere on or near the Earth where there is an unobstructed line of sight to four or more GPS satellites. It will also enable the user to view the nearby places and place the alarm at any of the desire location which be tracked by the GPS. The main aim of this system is to provide an alarm facility in the mobile devices based purely upon the Location.



IMPLEMENTATION

This application includes two modules

1. Set Alarm
2. Find Nearest Place

Set Alarm: User needs to enter the desired location, where he wants to get an alert. The alarm will monitor the mobile screen. The alarm will raise When the user is within the radius of 500meters. By default, the radius will be 500meters, user can also change the radius according to his desire. Along with the alarm, alarm description and route map to the destination location is also provided.

Finding a nearest place: In this application we can find nearby ATMs, Restaurants, Movie theaters, Shopping malls, Schools/ Colleges, Police Stations, Hospitals, Railway stations/ Bus stations/Airports and few other modules. First user needs to enter the current location by using the Google map which we will provided in our application. If user click on “find a nearer place” all the nearest places within the user specified radius will be displayed. Here we will use the concept of clustering. Clustering means grouping of similar objects. By using this concept, all the nearest ATMs will be displayed as one cluster and all the nearest restaurants will be displayed in another cluster, like this each nearest place is displayed in separate clusters. So user can select any one of the clusters according to his requirement. Suppose, if user selects ATM near to his current location, then our application will provide the longitude and latitude and also the address of that particular ATM and route to reach the ATM, the distance between the current location and desired location and the time taken to reach the particular location, all the related



information will be displayed. To implement this we need different API's and Google map API key. Process to generate Google map API key is shown in methodology section. To implement Login we are using parse web service, in this we are storing user details in server. To fetch Location results we are using Places API, it will give places information. For maps we are using Google maps.

METHODOLOGY:

Locate "Keytool.exe" in your java\jdk\bin folder.
With the help of this keytool.exe SHA1 certificate is generated.

For Example:

```
"C:\Program Files\Java\jdk1.6.0_18\bin\keytool.exe" -list -v -alias androiddebugkey -keystore  
"C:\Users\LINDI\android\debug.keystore" -storepass android -keypass android
```

This command will generate a SHA1 certificate signature like this
HA1:E4:DE:65:56:5F:1F:39:D0:58:D2:BF:71:AB:2A:48:8 9:EC:AF:32:2B. Now we need to paste this signature in android developer's website, we will get a Google map API key.

SYSTEM REQUIREMENTS

4.1 HARDWARE REQUIREMENTS

- System: Intel i5 2.4 GHz.
- Hard Disk: 40 GB.
- Floppy Drive: 1.44 Mb.
- Monitor: 15 VGA Colour.
- Mouse: Zebronic Vega 1211
- RAM: 8 GB.

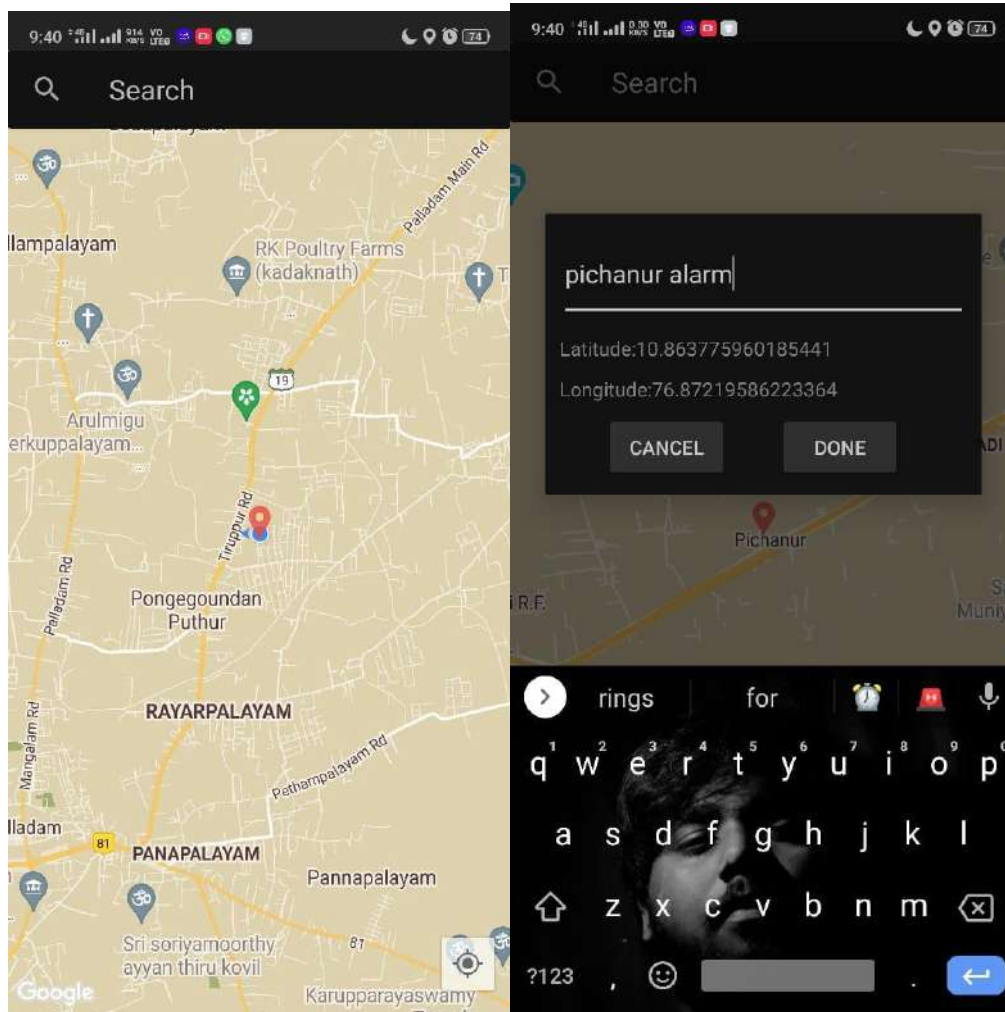
4.2 SOFTWARE REQUIREMENTS

- Coding Language: Java 1.6
- Tool Kit: Android 2.2
- IDE: Eclipse 3.6.2 (Helios) or greater
- Back End: SQL

4.3 OPERATING SYSTEMS

- Windows 10 (32 or 64-bit)
- Vista (32- or 64-bit)
- Windows 7 (32- or 64-bit)

Google-play-service API: Google play service is a proprietary software development kit and application programming interface set for Android devices. The layer provides APIs that allow apps for Android to provide functionality that directly integrates with Google services, such as account syncing, Google+, Google Maps and many more services.



CONCLUSION

The overall purpose of this application is to remind the works which we are having in our daily life based on the work location to which we are going. In this location based alarm system based on the location of the mobile devices user will automatically retrieves the notification in relevant situations allowing them easily to activate or deactivate the alarm system. Till now there were so many applications for reminding the work schedule which are working based on the time. But in our application we have introduced a new thought for reminding the daily works by using the GPS location system for placing alarm based on the location and by using clustering concept, we are able to place the alarm to the nearby places according to the user's desire. For the future enhancement of our application we are planning to add the Data Mining concepts for better understanding of the user.

REFERENCES

1. Deepika Garg, Dr. Anupam Shukla, faculty of Jayoti Vidyapeeth Women's University, Jaipur, India, ABV-IIITM, Gwalior, India
2. Jacob Christensen, Jai Modi, Computer Science and Engineering, University of Washington, Seattle, WA
3. PHP(preprocessor hyper text) programming language <<http://phpjava-bridge.sourceforge.net/pjb/installation.php>>
4. Android developers <<http://developer.android.com>>
5. Dr.Biju Balakrishnan, Asst. Dean, Department of Computer Science and Engineering, JCT college of Engineering & Technology, Coimbatore



Diabetes Disease Prediction using Machine Learning Technique

**Dr. G RAJIV SURESH KUMAR¹, Shubham Kumar Mishra², Merwin Prabhu³,
Vishnu Priya MK⁴, Sruthi S⁵**

¹PROFESSOR & HOD (CSE), JCT College of Engineering and Technology

²⁻⁵BE Computer Science Engineering, JCT College of Engineering and Technology

Abstract: we aim to develop a prediction system using machine learning to detect and classify the presence of diabetes in e-healthcare environment using Ensemble Decision Tree Algorithms for high feature selection. A significant attention has been made to the accurate detection of diabetes which is a big challenge for the research community to develop a diagnosis system to detect diabetes in a successful way in the e-healthcare environment. The existing diagnosis systems have some drawbacks, such as high computation time, and low prediction accuracy. To handle these issues, we have proposed diagnosis system using machine learning methods, such as preprocessing of data, feature selection, and classification for the detection of diabetes disease in e- healthcare environment. Model validation and performance evaluation metrics have been used to check the validity of the proposed system. We have proposed a filter method based on the Decision Tree algorithm for highly important feature selection. Two ensemble learning Decision Tree algorithms, such as Ada Boost and Random Forest are also used for feature selection and compared the classifier performance with Wrapper based feature selection algorithms also. Machine learning classifier Decision Tree has been used for the classification of healthy and diabetic subjects. The experimental results show that the Decision Tree algorithm based on selected features improves the classification performance of the predictive model and achieved optimal accuracy. Additionally, the proposed system performance is high as compared to the previous state-of-the-art methods. High performance of the proposed method is due to the different combinations of selected features set. Furthermore, the experimental results statistical analysis demonstrated that the proposed method would be effectively detected diabetes disease.

Index Terms: Machine Learning , Random Forest, PIMA Dataset, IDT-3, ADA Boost, e-Health Care.

I.INTRODUCTION

Machine Learning is a system of computer algorithms that can learn from example through self-improvement without being explicitly coded by a programmer. Machine learning is a part of artificial Intelligence which combines data with statistical tools to predict an output which can be used to make actionable insights. The breakthrough comes with the idea that a machine can singularly learn from the data (i.e., example) to produce accurate results. Machine learning is closely related to data mining and Bayesian predictive modeling. The machine receives data as input and uses an algorithm to formulate answers. A typical machine learning tasks are to provide a recommendation. For those who have a Netflix account, all recommendations of movies or series are based on the user's historical data. Tech companies are using unsupervised learning to improve the user experience with personalizing recommendation. Machine learning is also used for a variety of tasks like fraud detection, predictive maintenance, portfolio optimization, automatize task and so on.

A. Problem Definition

The current systems working on diabetes disease prediction works on a small dataset. The aim of our system is to work on a larger dataset to increase the efficiency of the overall system. The number of medical tests also affects the performance of the system; thus, our aim is to reduce the number of medical tests to increase the efficiency of the system.

II.LITERATURE REVIEW

Following is some of the search which has been reviewed for the proposed system: -

1) Intelligible support vector machines for diagnosis of diabetes mellitus

N. H. Barakat, et al [1]Diabetes mellitus is a chronic disease and a major public health challenge worldwide. According to the International Diabetes Federation, there are currently 246 million diabetic people worldwide, and this number is expected to rise to 380 million by 2025. Furthermore, 3.8 million deaths are attributable to diabetes



complications each year. It has been shown that 80% of type 2 diabetes complications can be prevented or delayed by early identification of people at risk. In this context, several data mining and machine learning methods have been used for the diagnosis, prognosis, and management of diabetes. In this paper, we propose utilizing support vector machines (SVMs) for the diagnosis of diabetes. In particular, we use an additional explanation module, which turns the “black box” model of an SVM into an intelligible representation of the SVM's diagnostic (classification) decision. Results on a real-life diabetes dataset show that intelligible SVMs provide a promising tool for the prediction of diabetes, where a comprehensible ruleset have been generated, with prediction accuracy of 94%, sensitivity of 93%, and specificity of 94%. Furthermore, the extracted rules are medically sound and agree with the outcome of relevant medical studies.

2) Medical diagnosis on Pima Indian diabetes using general regression neural networks

K. Kayaer and T. Yildirim [2] The performance of recently developed neural network structure, general regression neural network (GRNN), is examined on the medical data. Pima Indian Diabetes (PID) data set is chosen to study on that had been examined by more complex neural network structures in the past. The results of early studies and of the GRNN structure presented in this paper is compared. Close classification accuracy to the reference work using ARTMAP-IC structured model, which is the best result obtained since now, is achieved by using GRNN, which has a simpler structure. The performance of the standard multilayer perceptron (MLP) and radial basis function (RBF) feed forward neural networks are also examined for the comparison as they are the most general and commonly used neural network structures. The performance of the MLP was tested for different types of backpropagation training algorithms.

I. PROPOSED SYSTEM

In this system we design e-health care diagnosis system for diabetes detection.

In this system we propose Filter based DT-(ID3) algorithm for features selection and the proposed algorithm select more appropriate features from the dataset. Also, two DT ensembles algorithms, such as Ada Boost and Random Forest are used for feature selection and compared the performance of DT on the proposed feature selection algorithm with these two FS algorithms and Wrapper based feature selection methods.

In this system we use the classifier DT and the performance have been checked on original features set and on selected features set along with cross validation methods, such as Training/testing set, K-fold, and LOSO. The LOSO is more suitable than train/test and k-folds validations.

In this system we recommend that the proposed method can be used to effectively detect the diabetes disease and the system can be easily incorporated in healthcare.

2. ALGORITHMS

Random Forest:

Random forest is a Supervised Machine Learning Algorithm that is used widely in Classification and Regression problems.

It builds decision trees on different samples and takes their majority vote for classification and average in case of regression.

One of the most important features of the Random Forest Algorithm is that it can handle the data set containing continuous variables as in the case of regression and categorical variables as in the case of classification.

It performs better results for classification problems.

TABLE I. Random Forest EXAMPLE



Problem: In Random forest n number of random records are taken from the data set having k number of records.

Step 2: Individual decision trees are constructed for each sample.

Step 3: Each decision tree will generate an output.



TABLE II. FREQUENCY TABLE

Frequency Table		
Weather	No	Yes
Overcast		4
Rainy	1	2
Sunny	2	3
Grand total	5	9

TABLE III. LIKELIHOOD TABLE

Likelihood Table				
Weather	No	Yes		
Overcast		4	$=4/14$	0.29
Rainy	3	2	$=5/14$	0.36
Sunny	2	3	$=5/14$	0.36
All	5	9		
	$= 5/14$	$= 9/14$		
	0.36	0.64		

$$P(\text{Yes in Sunny}) = P(\text{of Sunny in Yes}) * P(\text{Yes}) / P(\text{Sunny})$$

Now that we possess $P(\text{Sunny in Yes}) = 3/9 = 0.33$, $P(\text{Sunny}) = 5/14 = 0.36$, $P(\text{Yes}) = 9/14 = 0.64$

Also, there is $P(\text{Yes in Sunny}) = 0.33 * 0.64 / 0.36 = 0.60$, so this has probability.

AdaBoost:

AdaBoost also called Adaptive Boosting is a technique in Machine Learning used as an Ensemble Method.

The most common algorithm used with AdaBoost is decision trees with one level that means with Decision trees with only 1 split.

These trees are also called Decision Stumps.

A. Working of Ada Boost:

Steps For Ada Boost: -

The example is in below Fig. 2 to acknowledge this algorithm. Following is a wide spread of red circles (RC) and green squares (GS):

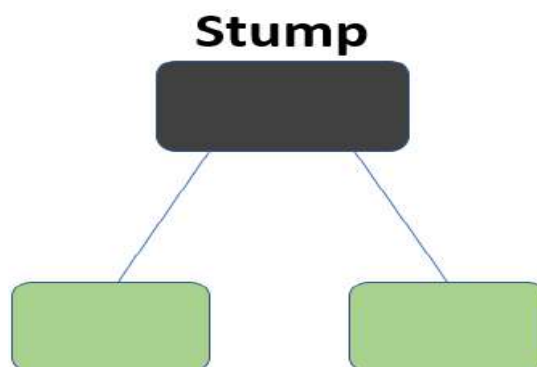


Fig 2. Ada Boost Example



The formula to calculate the sample weights is:

$$w(x_i, y_i) = \frac{1}{N}, \quad i = 1, 2, \dots, n$$

Where N is the total number of datapoints Here since we have 5 data points so the sample weights assigned will be 1/5.

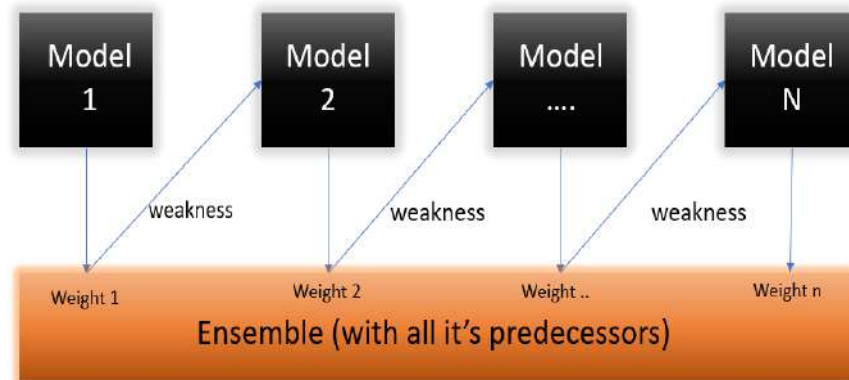


Fig 3. K-NN Example

$$\text{Performance of the stump} = \frac{1}{2} \log_e \left(\frac{1 - \text{Total Error}}{\text{Total Error}} \right)$$

$$\alpha = \frac{1}{2} \log_e \left(\frac{1 - \frac{1}{5}}{\frac{1}{5}} \right)$$

$$\alpha = \frac{1}{2} \log_e \left(\frac{0.8}{0.2} \right)$$

$$\alpha = \frac{1}{2} \log_e(4) = \frac{1}{2} * (1.38)$$

$$\alpha = 0.69$$

1. Assign **equal weights** to all the datapoints
2. Find the stump that does the **best job classifying** the new collection of samples by finding their Gini Index and selecting the one with the lowest Gini index
3. Calculate the “**Amount of Say**” and “**Total error**” to update the previous sample weights.
4. Normalize the new sample weights.

III. EXPECTED RESULT

The goal of our project is to know whether patient is diabetic or not, patient will be diagnosed and it will be depending on the attributes that we are going to take, such as age, pregnancy, pg concentration, tri fold thick, serum ins, body mass index (bmi), dp function, diastolic bp i.e. the factors which are majorly responsible for diabetes.

So, to reduce the correctly know whether the patient is diabetic or not, we are developing a system which will be a prediction system for the diabetes patients. Another best thing about the system is it is will give accurate results whether the patient is diabetic or not with the help of the knowledge base of the larger dataset that we are going to use added the recommendations we are going to provide based on the diabetic levels of the patients. Also, the prediction of the disease will be done with the help of Random Forest Algorithm algorithm and Ada Boost algorithm.

CONCLUSIONS

By our in-depth analysis of literature survey, we acknowledged that the prediction done earlier did not use a large dataset [12]. A large dataset ensures better prediction. Also what it lacks is recommendation system. When we predict we will give some recommendation to the patient on how to control or prevent diabetes in case of minor signs of diabetes.

The recommendations would be such, that when followed it will help the patient. Thus we will build up a system which will anticipate diabetic patient with the assistance of the Knowledge base which we have of dataset of around 2000 diabetes



patients and furthermore to give suggestions on the premise of the nearness of levels of diabetes patients. Prediction will be done with the help of two algorithms Random Forest and Ada Boost Neighbor and also we will compare which algorithm gives better accuracy on the basis of their performance factors. This system which will be developed can be used in HealthCare Industry for Medical Check of diabetes patients.

FUTURE SCOPE

The proposed system can be developed in many different directions which have vast scope for improvements in the system. These includes:

1. Increase the accuracy of the algorithms.
2. Improving the algorithms to add more efficiency of the system and enhance its working.
3. Working on some more attributes so to tackle diabetes even more.
4. To make it as a complete healthcare diagnosis system to be used in hospitals.

REFERENCES

- [1] Y. Cai, D. Ji, D. Cai, "A KNN Research Paper Classification Method Based on Shared Nearest Neighbor", Proceedings of NTCIR-8 Workshop Meeting, 2010.
- [2] I. Rish, "An empirical study of the naive Bayes classifier", T.J. Watson Research Center, 2001.
- [3] M.Elkourdi, A.Bensaid, T.Rachidi, "Automatic Arabic Document Categorization Based on the Naïve Bayes Algorithm", Alakhawayn University, 2001.
- [4] L.Wang, L.Khan and B.Thuraisingham, "An Effective Evidence Theory based on nearest Neighbor (KNN) classification", IEEE International Conference, 2008.
- [5] M.Muja, David G.Lowe, "Fast Approximate Nearest Neighbors
- [6] B. Gallwitz, "Implications of postprandial glucose and weight control in people with type 2 diabetes: Understanding and implementing the inter-national diabetes federation guidelines," Nov. 2009
- [7] Ramezani, Rohollah, Mansoureh Maadi, and Seyedeh Malihe Khatami. "A novel hybrid intelligent system with missing value imputation for diabetes diagnosis." Alexandria engineering journal 57.3 (2018): 1883-1891
- [8] Amin Ul Haq et.al, Comparative Analysis of the Classification Performance of Machine Learning Classifiers and Deep Neural Network Classifier for Prediction of Parkinson Disease, 2018 15th International computer Conference on Wavelet Active Media Technology and Information Processing (ICCWAMTIP), IEEE, 14- 16 Dec 2018.
- [9] Y. Liu et al., "Detecting Diseases by Human-Physiological-Parameter-Based Deep Learning," in IEEE Access, vol. 7, pp. 22002-22010, 2019. doi: 10.1109/ACCESS.2019.2893877
- [10] A. Tsanas, et al., "Novel speech signal processing algorithms for high-accuracy classification of Parkinson's disease," IEEE Transactions on biomedical engineering, vol. 59, pp. 1264-1271, January 2020.



REAL TIME PEDESTRIAN DETECTION

Prof. Karthikeyini¹, Adarsh AV², Akhilesh A³, Aswin N L⁴, Prathin Pratheesh⁵

¹ASP-CSE, JCT College of Engineering & Technology

²⁻⁵BE Computer Engineering, JCT College of Engineering & Technology

Abstract: Object detection is the process of determining the presence, location, and type or class of at least one object using a bounding box. The person detection process produces a bounding box and allot a class label as a person based on YOLOv3. In YOLO v3 the features are learned, divides the image cells and each cell says a bounding box and entity classification directly. There could be more than one bounding box per person, but the system makes use of non-maximum suppression to reduce the number of bounding boxes to one per person. Finally, the number of persons in the image and video are calculated using the count of the bounding boxes. The dataset used for static pedestrian detection is the INRIA dataset and ShanghaiTech dataset. Yolo_Mark is used for marking bounding boxes of persons and gets its annotation files using 243 images from the INRIA dataset. Darknet is used as the framework for implementing YOLOv3. From INRIA Dataset 120 images are used for testing purposes. Testing on the INRIA dataset resulted in an accuracy of 96.1%. From the Shanghai tech-B, dataset 56 images are used for testing. Testing resulted in an accuracy of 87.3%.

Keywords: Yolo, CNN, CUDA.

I. INTRODUCTION

Computer vision is the region of study that expects to build up a technique that upholds computers to watch and comprehend the substance of advanced pictures, for example, photos and recordings. Computer vision has a number of multidisciplinary applications like military human-computer interaction, mobile robot navigation, industrial inspection, and medical image analysis. Many popular computer vision applications like object classification, object identification, object verification, object detection [3], and object recognition recognize objects in images or videos.

Object detection has two levels; Object tracking and Object localization. Object tracking is the process to detect and track individual objects and grouped objects. Object Detection is made easy with the introduction of Neural Network. Neural networks are used to simulate the human cerebrum framework to take care of general learning issues. Neural networks use numerous algorithms that help to identify patterns. Deep learning [1] is the group of machine learning networks. Deep learning has become a popular implementation of speech recognition [2]. Deep learning is the field of computer vision, which contains better performing models that may require more data but less digital signal processing expertise to train and operate.

A CNN, or ConvNet [4] is gaining much popularity in the area of deep learning. A CNN has an input, multiple hidden and an output layer. The pooling layer in the form of non-linear down-sampling and the most commonly used one is max pooling function. Finally, the fully connected layers done high-level reasoning. YOLO is the second group of strategies object recognition focused on real-time processing. YOLO represents You Only Look Once, introduced in 2015.

Outdoor pedestrian counting techniques help to monitor parks, recreational facilities, and trails help to recognize and count the number of individuals visiting public spots. The system assists in designing traffic infrastructure according to the peak traffic experienced in an area and finding out the bottlenecks in the existing traffic system. It also helps in calculating the capacity ratings for the traffic infrastructure like bridges while designing the infrastructure projects. During pedestrian detection, there might be many bounding boxes representing different entities of regard within the image, and it is difficult to know how many beforehand.

ILSVRC is a strategy including classification and recognition of several object classes and images. Image classification process algorithms generate a catalogue of entity classes there in the image, with a bounding box representing the location [5]. The R-CNN, Regions with CNN Features was presented by Ross Girshick et al. in the year of 2014. Selective search [6] choosing a vast number of regions using this method to get only 2000 regions.

The R-CNN model [7], comprises three modules: Region Proposal, Feature Extractor, and Classifier. AlexNet deep



CNN [8] is the feature extractor used here. Linear SVM is the classifier that takes the output of the CNN layer.

To solve the speed issue of R-CNN, Ross Girshick, introduced an extension to create a faster object detection method, Fast R-CNN [9] in 2015. This technique is similar to the R-CNN process. This model took the image and a group of region recommendations. For feature extraction, a pre-trained CNN using VGG-1 is employed. To improve the speed of training, detection techniques, Faster R-CNN [10] in the year 2016.

A. Motivation

All the advanced methods use locales to detect the object within the image. Those methods only consider the image pieces that have peak probabilities of acquiring the object. YOLO applies a single neural network trained process that takes an input image and plots bounding boxes for entities with corresponding class labels. YOLO looks at the image once and makes predictions with a single network evaluation model, which makes YOLO fast. YOLO is trained on full images and directly optimized detection performance. For improving the accuracy, YOLO reached out to variants YOLO v2 and YOLO v3.

B. Contributions

The proposed method contributes an efficient pedestrian detection and counting using the YOLO v3 model. The proposed method detects the person on both images and videos. It handles images of different lighting conditions, varying viewing angles, and scales. Estimate the count of detected persons in the images, using the Inria dataset and Shanghaitech-B dataset. Estimate the peak count of persons in the videos.

II. RELATED TECHNIQUES

In [11], Zhang et al. introduced a technique that can calculate the crowd count by using the MCNN system influenced by the multi-column deep neural networks [12]. The system holds three columns of CNN with filters sizes, large, medium, and small. The arrangement of MCNN consists of Max pooling for every region. Features maps transform to the density map, they use filters with dimensions 1×1 [13]. The system calculates the final prediction by averaging the unique predictions of every deep neural network. They evaluate the design on four distinct datasets; three existing datasets and their dataset. The performances of MCNN on Shanghai tech dataset obtain values 110.2, 173.2, 26.4, 41.3 for MAE and MSE respectively.

In [14], Siyu Huang, Xi Li et al., developed the person counting method from the view of semantic modelling. Existing methods [11,15] mostly focused on modelling using the properties of full body or the heads, disregarding the semantic structure data. The pedestrian semantic model consists of three elements: peoples, heads, and their context structure. They formulate three elements and design them as two models: a first-named body map and context structure of body parts [16].

Existing methods like conventional density maps [17], ignored the shapes of individual pedestrians, structured density maps focus on both density distributions and shapes of humans and to model semantic structure information. They evaluate the method using four datasets, the WorldExpo'10 dataset [18], the Shanghai tech-B dataset [11], the UCSD dataset [19], and the UCF_CC_50 dataset [20].

In [21], Boominathan et al. developed a framework for calculating the density of crowd from dense crowds. Focusing on the obstacle of scale variation, the model concurrently performs at high and low-level patterns generated using deep and shallow cnn. The deep network concentrates on the desired high-level semantics required architectural design similar to the VGG-16 model [22]. Adding the total predicted density maps gives the total count. By using a Gaussian kernel, They also perform two types of augmentation for scale variations in crowd images and improves CNN's performance.

In [23], Lingke Zeng et al. introduced MSCNN for static crowd counting. In prior systems [11] [21], that overcomes the problem of scale variations, but it has two weaknesses; needs a pre-trained model and requires more parameters to added computing resources. Multi-Scale Blob (MSB) is the scale feature, contains various filters with various kernel sizes. ReLU [24], which performs as the activation function of preceding convolutional layers. The ShanghaiTech and UCF CC 50 datasets. Using the ShanghaiTech dataset MCNN attains MAE and MSE values 83.8, 127.4, 17.7, and 30.2 respectively. Using UCF CC 50 dataset achieves MAE and MSE values 363.7 and 468.4.

In [25], Jianing Qiu et al. proposed a Two-Column CNN (TCCNN) to calculate highly dense crowds. The design is derived from VGG-16 and Alexnet. They joined two networks to output the density map. Before being fed into the



network, the system creates crowd image patches with a resolution of 224 x 224 pixels. The number of people within each patch can be obtained by finding the integral density map, and the sum of people in each patch can add up to find the total number of people. The combination of adjusted VGG-16 and Alex net gave an excellent performance. The method achieves high accuracy on the above datasets.

In [26], Youmei Zhang et al. proposed a model to focus on head positions used for crowd counting. AM-CNN contains 3 shallow layers, attention models. The system evaluates using the above 3 datasets. They use Gaussian kernels for density maps. For ShanghaiTech and UCF CC 50 datasets, the MAE values for Large, Medium, Small are 112.0, 121.1, 129.1.1 respectively, and MSE values obtained are 166.1, 200.8, 198. The performance of this model is 29.2/40.7 (L), 39.4/39.1 (M), and 32.6/29.4 (S).

In [27], Hailong Li et al. proposed method Alex Net [28] with multi-layers and edge boxes. For extracting training data edge boxes were used. The INRIA pedestrian dataset, including 614 samples used for training and 218 samples for testing. Boxes algorithm achieves good results. The false rate is 10%, missing range is 23%. In [29], Joseph Redmon proposes that YOLO is swift for object detection in images. Existing methods repurpose classifiers to perform detection. Data sets from PASCAL VOC 2007 [30] and 2012. The VOC 2012 test set achieves a mAP of 57.9%.

In [32], Jiahuan Zhou et al. developed a detection system the model consists of 9 convolutional layers. The YOLO bounding boxes coordinates data contains (xcentre, ycentre, w, h) with a confidence value [0, 1]. The pre-trained method trained on VOC2007. The system obtained a MAP of 44.3% in their dataset. In [33], Igor R. de Almeida et al. developed a computer vision technique to find the dynamic changes in crowds.

In [34], Qiming proposed a discriminative weighted sparse partial least model for feature selection. This method is used for human detection. This applies sparse PLS for feature selection. To create a latent matrix, formulate a discriminative regularized weighted least square problem. The training phase extracts different channel features, including LUV colour channels, gradient magnitude, and histograms to generate a large number of channel features.

The discriminative features can be selected based on the weight matrix. Evaluated the performance of the DW SPLS approach on three challenging human datasets, including INRIA [35], Caltech [36], and TUD-Brussels [37] pedestrian data sets.

In [40], Athanasios Tsitsoulis et al. presented a method for the extraction of the person in an image. For person detection, this system uses the location, dimensions, and colour of the face. The primary contribution of the method joins information from several kinds of image segmentation. First, the algorithm can assign firm edges in the image. This system combines the global detection technique with an appearance model. Evaluated the algorithm using INRIA person dataset.

In [42], Kuan-Hui Lee et al. proposed a system which detects persons from video and finds the persons. The system uses the ETH Mobile Scene (ETHMS) dataset. The detection rate of the model is 75%. In [43], Shen Li et al. developed a CD-CNN, for visual tracking. The method evaluated on OTB 2015 benchmark and the OTB 2013 Benchmark. The method has 0.600 AUC value for OTB2015 and 0.627 on OTB 2013. In [44], Zheng Tang et al. proposed a video scene framework that tracks multiple human objects and estimates their 3D poses.

c). The (x, y) coordinates signify the centre of the box, comparative with the matrix cell area. The (x, y) values are normalized to [0, 1]. The (w, h) coordinates denote width and height also normalized to [0, 1]. Here, c denotes the class of the corresponding object (1 denotes a person). The system obtains the objectness score using logistic regression.

YOLO v3 makes predictions over scales; YOLO v3 applies three various scales. The most powerful feature of YOLO v3 is prediction across three distinct scales for all positions of the input image. YOLO v3 makes predictions identical to the feature pyramid network, FPN. Every prediction is made of a boundary box, objectness, and class score. In Darknet-53 the convolutional layers are added for feature extraction. The earlier version YOLO v2 utilized Darknet-19. YOLO is a fully convolutional network.



III. METHODOLOGY

A. Overview

Object detection is the process of recognizing the presence, area, and class of at least one object within an image. The person detection process draws a bounding box around every person in the image and allots them with a 'person' label. YOLO is an object detection strategy with a deep convolutional neural network to detect the object. YOLO was proposed by Redmon et al.[29], in the year of 2016. It looks at the full image only once then it passes through the network and detects objects.

YOLO takes an input image and divides it into $S \times S$ matrices. The centre of an object drops into a matrix region, that region is responsible for distinguishing an object. The confidence value represents how likely the box contains an object and how exact is the bounding box. YOLO has an organization structure of 24 convolutional layers, a max-pooling layer, and two completely connected layers towards the end.

YOLO v2 is a version of the YOLO, proposed in the year 2017 to improve the accuracy. But, in the case of small-sized object detections YOLOv2 struggles. YOLO v3 has few incremental improvements compared to YOLO v2 [46]. YOLO v3 was introduced in April 2018 [47].

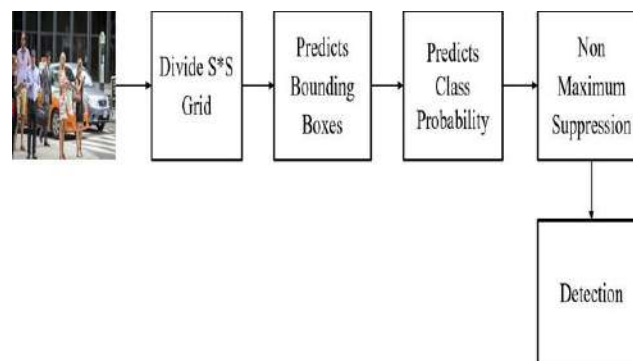


Fig.1. YOLO Person Detection flow

The proposed method begins with the dataset collection step. From the dataset images are divided into two, train dataset, and test dataset. Using 243 images from the train dataset, Yolo_mark labelling tool marks the bounding boxes for persons and obtains the corresponding annotation files. The darknet YOLO v3 framework gets trained using the weight values obtained from annotation files. After pedestrian detection, the system determines the count of people in that image. Figure.2 shows the procedure for pedestrian detection and counting.

The proposed system is designed for pedestrian detection in images and videos using YOLO v3. YOLO v3 first takes an input image then divides it into grids, that grid region is liable for recognizing an object. YOLO v3 then figures the bounding boxes, their corresponding probabilities for person objects.

Bounding Box Prediction is the process to draw the bounding

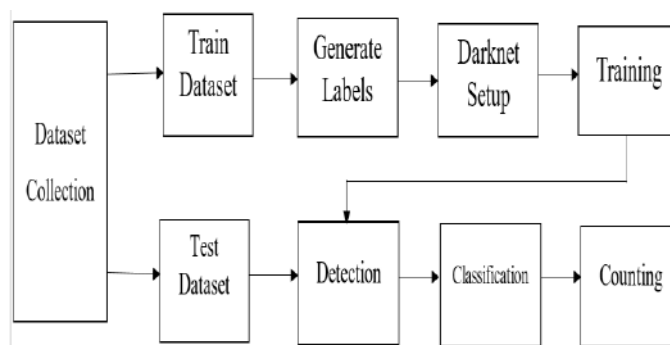


Fig.2.Represents proposed system working

boxes for each recognized object and predict confidence value, which has five components; x-coordinate, y -coordinate, width, height and class of the object (x, y, w, h, DATASET

Pedestrian detection and counting process uses an extensive collection of images and videos. The image datasets used



are the INRIA dataset and Shanghai tech-B Dataset. INRIA used a static pedestrian detection data set. The INRIA dataset is categorized into two, for training, testing purposes. From the INRIA dataset, 243 positive samples which contain a total of 1416 persons are used for training YOLO v3. The test set has 122 positive samples which contain a total of 309 persons and include 58 negative samples. The negative samples do not contain pedestrians. The ground truth of the images is not available, and thus, the total count is estimated via visual inspection. Shanghai tech-B Dataset contains comments on images that were taken using various cameras in the busy streets in Shanghai. In the Shanghai tech-B dataset, for testing purposes the ground truth of the given images is given. For the testing, the system uses 56 images containing persons.

For pedestrian detection in videos, the system randomly selected 15 videos from the internet. The system aims to detect the highest traffic experienced in different locations in a city over different periods of time. For identifying the highest density of traffic experienced in an area in a specified period, the peak count is calculated rather than the total count. The ground truth of the videos is not available, and thus the peak count is estimated via visual inspection.

B. GENERATE LABELS

Annotation tools are used for annotating the image for training YOLO. First, each person is marked in the images, from the INRIA dataset, using visual GUI-software, and then label each of them for generating annotation files. The system uses Yolo_Mark labeling tool [48] for marking each person in that image. Yolo_Mark creates a .txt file for each .jpg image in the same folder with the same name. The .txt record contains the following values: <object-class> <x_center> <y_center> <width> and <height>.

The object-class denotes the class of the object using integer numbers starting from 0. This system focuses only on one class, which is a person so it is set to 0. The x_center and y_center are the x and y coordinates of the center of the bounding box, it can range from 0.0 to 1.0. Width and height denote the width, height of the bounding box also it can range from 0.0 to 1.0.

Normally annotation tools follow two steps, first draw the bounding box in an image and then store top-left and bottom-right points in the corresponding text file. Then convert the points into YOLO input format. Yolo_Mark labeling tool combines these two steps. It draws the bounding boxes on image and creates a .txt-file for each .jpg image-file that contains points in the YOLO input format. Yolo_Mark calculate the annotation values using equations 3.1, 3.2, 3.3, 3.4 as follows:

$$\text{Center-x} = x / W \quad (3.1)$$

$$\text{Center-y} = y / H \quad (3.2)$$

$$\text{Width} = w / W \quad (3.3)$$

$$\text{Height} = h / H \quad (3.4)$$

Here x denotes the x-coordinate of the center of bounding box, y denotes y-coordinate of the center of bounding box, w denotes the width of the bounding box, h denotes the height of the bounding box, W denotes the width of the whole image and H denotes the height of the whole image. For the labeling process, the system loads images from the Inria dataset to the Yolo_Mark image directory and sets the number of classes to zero and object name as a person. Then run Yolo_Mark using the command, yolo_mark.exe data/img data/train.txt data/obj.names. Then open all the images from the dataset, mark bounding boxes for each pedestrian, and finally the corresponding .txt file containing the coordinates are obtained. The .txt file contains values as follows:

```
0 0.508594 0.516667 0.367188 0.755556
```

```
0 0.458984 0.433333 0.280469 0.636111
```

```
0 0.499609 0.531944 0.308594 0.561111
```

In the first line 0 represents the value for the object class person, 0.508594 denotes the x-center value, 0.516667 denotes the y-center value, 0.367188 denotes the width and 0.755556 denotes the height.

C. TRAINING

The training process method makes use of three files .data, .names and .cfg. After creating the files of the above-mentioned extensions copy the dataset images and annotations to the corresponding directory. Using pre-trained weights YOLO starts training [51]. Darknet [49] [50], is an open-source framework to train neural networks, which is written in C or CUDA (Compute Unified Device Architecture), and serves as the basis for implementing YOLO. It supports CPU and GPU computation and installation is simple. Darknet is easy to install as it only requires two optional dependencies, OpenCV and CUDA. OpenCV is used to increase the variety of supported image types and CUDA is used for enabling GPU computation. Clone the Darknet git repository and run make- file to compile it.



1. YOLO v3 Configuration Parameters

Firstly, create the configuration files to train YOLO v3 for person detection. Download the yolov3.cfg file and copy the same contents to the Yolo-person.cfg file. The configuration file contains the training parameters like batch size, subdivision, etc. Here set the batch=64, the batch parameter represents the batch size. For one iteration 64 images were used to update the parameters. Then set subdivisions = 8, darknet provides a variable called subdivisions to define the part of the batch size to be used for one time on our GPU. The GPU process batch/subdivision number of pictures at any time. The Complete iteration would be finished only after processing all the 64 images.

The parameters determine the input size and the number of channels. Assign the values for width = 416 and height = 416. If the design expands the size, it will produce good results but the training takes more time. Then set the channels = 3, it denotes the 3 channels for processing RGB input. The momentum and decay parameters manage the weight is updated. Here momentum equal to 0.9 and decay equal to 0.0005, which controls the penalty term.

The learning parameter rate regulates aggressive methods should learn based on the current batch of data. Generally, the value ranges from 0.01 to 0.0001. In training, it starts with zero learning. The learning rate should decrease over time. The method has a below learning rate for a small period of time frame at the origin.

Data augmentation is a process to create new training data from our training data artificially. For the data augmentation process, the angle parameter in the config file will provide a random rotate to the given image by \pm angle. The process transforms the colors of the whole image using saturation, exposure, and hue, it is yet an image containing the person. For training, the model system wants to determine the number of iterations. It contains only one object class, person, so change the max_batches to (classes*2000), so set max_batches=2000.

The training process wants to specify the number of classes used for detection. Here having only one object class, people so set classes = 1 in every YOLO layer. The process wants to determine the number of filters, set filters = (classes + 5) * 3 in all the YOLO layers. So in our model value of classes=1 and value of filters=18.

2. Creating Data File

For training, the process wants to create a '.data' file. Person.data file contains the number of classes, names of the object classes, t path to train and validation files, and the path to a backup file for storing the weights file. The Person.data file contains the following values:

classes equal to 1

train equal to data/train.txt valid equal to data/test.txt

names equal to data/person. namesbackup equal to backup/

3. Creating Name File

In the data file, the line names represent the way the file consists of the name of the classes. For that, we create a file Person.names that contains the name of the objects with a newline. The named file contains only one object name, person.

4. Image and Annotation File

Copy the set of .jpg images from the INRIA dataset, used for training, and corresponding .txt files created by Yolo_Mark to the object directory of the darknet, build\darknet\x64\data\obj\ . Then create a train.txt file in the data directory of the darknet. The train.txt file consists of filenames of the images. Add each filename with a new line, for example;

data\person\crop_000010.png data\person\crop_000011.png data\person\crop_000012.png

5. Download Pre-trained Weight

For training purposes, the model needs the convolutional weight file. The pre-trained weights are downloaded to the darknet directory. The convolutional weights are trained on ImageNet. Finally, start training the darknet YOLO v3. The weight file will be saved in the backup file after completing the 100 iterations. The best weight used for person detection.

D. DETECTION

Person detection using YOLO-v3 requires four input arguments; Input image, YOLO-v3 configuration file, trained YOLO-v3 weights, and the text file containing class name person. Firstly, the width and the height of the input image are obtained. Then the colors for the label and the bounding boxes are applied. The function cv2.read From Darknet, creates a network using weight and configuration files. Finally, the input image passes through the deep neural network [52][53].

YOLO-v3 uses multiple output layers to obtain the prediction. The detected person region is marked by the bounding boxes. The function draw-bounding-box for draw the bounding boxes. The class label value is assigned over the bounding boxes. The confidence value obtained indicates how confident that the bounding box contains a person. Higher confidence value indicates the network trust the bounding box contains the object, lower confidence value indicates that



the network distrusts the objects in the bounding box. For that reason, the model considers only the objects with a confidence value greater than 0.5. Filtered out all the weak detections using the confidence value.

The same object can be detected more than one time. The model wants only one detection for one object with bounding boxes and confidence value. This is obtained using Non-max suppression. Non-max suppression is the process to ignore the weak detection for the same objects. There could be more than one bounding box per person. First check the value of pc, which is the confidence of an object to be in the image, for each box then discard all boxes with $pc \leq 0.6$. Then if there are any remaining boxes left, select the box with the largest pc value. Example, if the YOLO-v3 detects the single person with three bounding boxes. The confidence value for three bounding boxes 0.6, 0.7, and 0.9 respectively. Here the model selects the bounding box with the greatest value, 0.9 for that person.

E. GROUND TRUTH

After detecting the persons, the total count of people in that image is calculated and the model wants the actual count in the image to assess the accuracy. This actual value is named as ground truth. The ground truth of the images is not available and thus, the total count is estimated via visual inspection in the case of the INRIA dataset, video files. In the case of the Shanghai tech-B dataset, which was used for testing purposes, the ground truth of the given images is available. ShanghaiTech B-Dataset consists of 120 images and its corresponding ground-truth value as .mat files.

Filename :	GT_IMG_1.mat	Total count :	23
Filename :	GT_IMG_10.mat	Total count :	181
Filename :	GT_IMG_100.mat	Total count :	157
Filename :	GT_IMG_101.mat	Total count :	37
Filename :	GT_IMG_102.mat	Total count :	70
Filename :	GT_IMG_103.mat	Total count :	57
Filename :	GT_IMG_104.mat	Total count :	44
Filename :	GT_IMG_105.mat	Total count :	227
Filename :	GT_IMG_106.mat	Total count :	165
Filename :	GT_IMG_107.mat	Total count :	476
Filename :	GT_IMG_108.mat	Total count :	139
Filename :	GT_IMG_109.mat	Total count :	316
Filename :	GT_IMG_11.mat	Total count :	164
Filename :	GT_IMG_110.mat	Total count :	110
Filename :	GT_IMG_111.mat	Total count :	20
Filename :	GT_IMG_112.mat	Total count :	131
Filename :	GT_IMG_113.mat	Total count :	40
Filename :	GT_IMG_114.mat	Total count :	183
Filename :	GT_IMG_115.mat	Total count :	101
Filename :	GT_IMG_116.mat	Total count :	204
Filename :	GT_IMG_117.mat	Total count :	40
Filename :	GT_IMG_118.mat	Total count :	143
Filename :	GT_IMG_119.mat	Total count :	146
Filename :	GT_IMG_12.mat	Total count :	513
Filename :	GT_IMG_120.mat	Total count :	70
Filename :	GT_IMG_121.mat	Total count :	175
Filename :	GT_IMG_122.mat	Total count :	51
Filename :	GT_IMG_123.mat	Total count :	55
Filename :	GT_IMG_124.mat	Total count :	67
Filename :	GT_IMG_125.mat	Total count :	72
Filename :	GT_IMG_126.mat	Total count :	56
Filename :	GT_IMG_127.mat	Total count :	165
Filename :	GT_IMG_128.mat	Total count :	32
Filename :	GT_IMG_129.mat	Total count :	149
Filename :	GT_IMG_13.mat	Total count :	40
Filename :	GT_IMG_130.mat	Total count :	80
Filename :	GT_IMG_131.mat	Total count :	117
Filename :	GT_IMG_132.mat	Total count :	162
Filename :	GT_IMG_133.mat	Total count :	137
Filename :	GT_IMG_134.mat	Total count :	120

Fig.3.Ground Truth values for ShanghaiTech B-Dataset

IV. EXPERIMENTAL RESULT

A. REQUIREMENTS

Pedestrian detection and counting uses the software and hardware platform listed as follows;

- CMake 3.8
- CUDA 10.0
- OpenCV 3.7.1
- cuDNN 7.4 for CUDA 10.0
- MSVS 2017 (v15)
- NVIDIA GeForce 920MX

B. DATASET:

From the INRIA dataset, 243 positive samples which contain a total of 1416 persons are used for training YOLO v3. The test set has 122 positive samples which contain a total of 309 persons and also include 58 negative samples. The negative samples don't contain pedestrians. The negative samples contain images of the road, desert, etc.

From ShanghaiTech-B dataset 56 images containing persons used for the testing purpose, the ground truth of the given images is available. For the testing process using video is conducted over a sample of 15 videos, containing people collected randomly from the internet. The ground truth of the videos is not available and thus the peak count is estimated via visual inspection.

Yolo_Mark is used for drawing bounding boxes of persons, gets its annotation files using 243 images from the INRIA dataset. Yolo_Mark creates a .txt-file for each .jpg image-file in the same directory with the same name. Figure 3 shows the labeling process of the Yolo mark Labelling Tool using the Inria dataset images.



The pedestrian detection using YOLO v3 draws a bounding box around every person in the picture, and allot with a person label, and the confidence scores each person. The detection process uses the images from the Inria dataset and ShanghaiTech B-Dataset. Detection results both Inria and ShanghaiTech B-Dataset images shown in the figures, Fig.4 and Fig.5. Each person detected with the bounding boxes labeled as a person and corresponding class confidence values greater than 0.6.



Fig.4..Generating Label Using Yolo_mark Labelling Tool



Fig.5.Using Inria dataset image persons detected with their confidence values

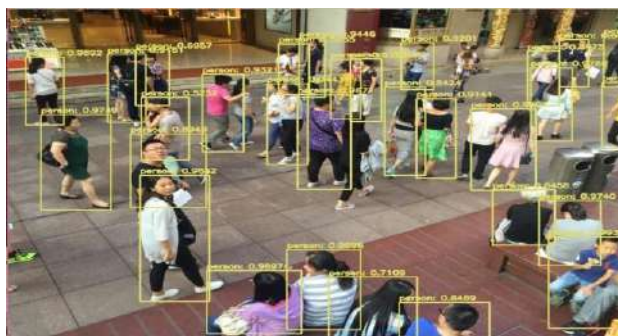


Fig.6 Using ShanghaiTech-B Dataset image persons detected

After detecting the pedestrians, the total count of people in that image is calculated. In the case of videos, the peak count is calculated rather than the total count for identifying the highest density of traffic experienced in an area in a specified time period. The ground truth of the videos is not available and thus the peak count is estimated via visual inspection. Count the total number of pedestrians present in images using the Inria dataset shown in the figures Fig: 6 & Fig: 7. Calculate the total number of pedestrians present in picture using ShanghaiTech B-dataset shown in the figures, Fig: 8 & Fig: 9. Fig: 10 & Fig:11 shows the total count of pedestrians obtained using video samples.

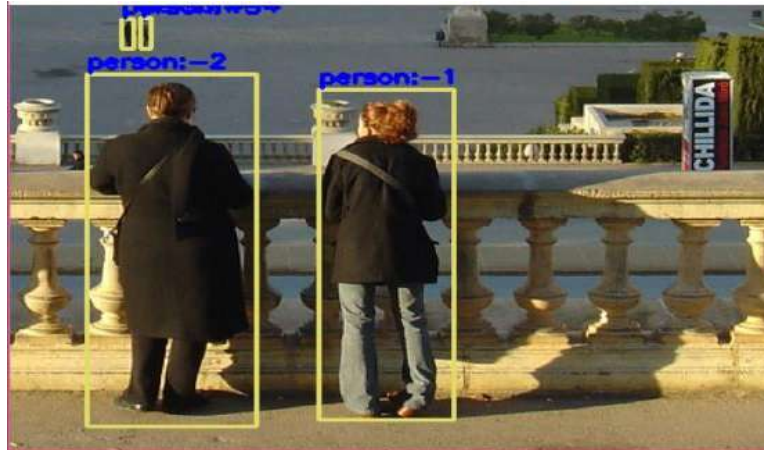


Fig: 7. Detection and counting using Inria dataset image

```
D:\project aishwarya\yoloV3-final>python yolo.py --image images/crop_000005.png --yolo yolo-person
[INFO] loading YOLO from disk...
[INFO] YOLO took 1.793490 seconds
Total Count = 4
```

Fig:8.Total count of detected pedestrians using Inria dataset

```
D:\project aishwarya\yoloV3-final>python yolo.py --image images/IMG_32.jpg --yolo yolo-person
[INFO] loading YOLO from disk...
[INFO] YOLO took 1.803654 seconds
Total Count = 43
```

Fig:9.Total count of detected pedestrians using ShanghaiTech B-Dataset

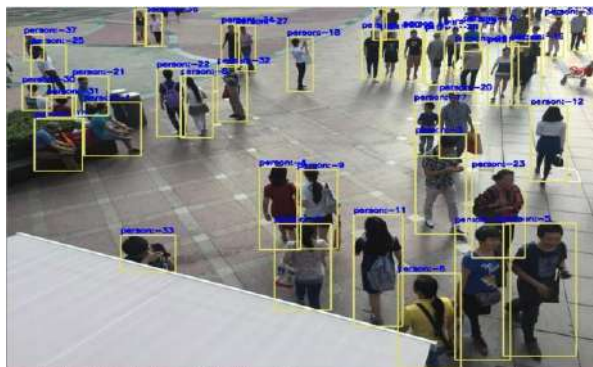


Fig.10.Detection and counting using ShanghaiTech B-Dataset image

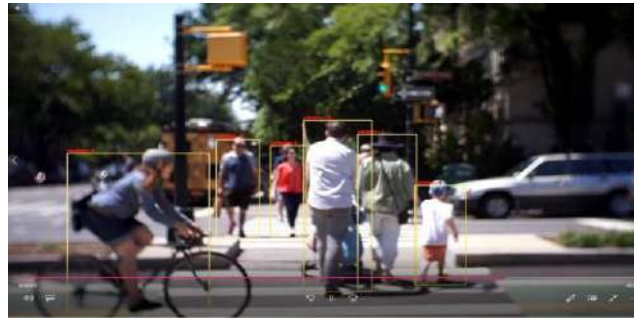


Fig.11.Detection and counting using Video samples

```
D:\project aishwarya\yoloV3-final>python yolo_video.py --input videos/family_crossing.mp4
put output/family_crossing.avi --yolo yolo-person
[INFO] loading YOLO from disk...
[INFO] 300 total frames in video
[INFO] single frame took 3.0960 seconds
[INFO] estimated total time to finish: 928.8105
Total count = 10
[INFO] cleaning up...
```

Fig:12.Total count of detected pedestrians in video

V. CONCLUSION

Object detection decreases human endeavors in numerous fields. YOLO-based Convolutional Neural Network group of models for object detection and the most recent version is called YOLOv3. Pedestrian detection and counting using YOLO v3 fastest, and one of the most accurate algorithms. The efficiencies of the yolov3 system are the greatest advantage of it, as the system only needs to go over the input only once. The results obtained in person detection using yolov3 is one of the best among the existing systems. The time taken by the system to produce the output is much less than the existing ones. Detections at 3 layers helps to address the issue of detecting very small objects compared to the previous versions of YOLO. The testing on the Inria dataset resulted in an accuracy of 96.1% whereas that on the ShanghaiTech dataset is comparatively less at 82.1% as the images are crowded.

VI. FUTURE SCOPE

The algorithm detects the persons whose full body is included in the frame, which degrades the accuracy in crowded scenes, which could be improved in the future. It can't detect duplicates when someone re-enters into the frame the person has counted again as a new person. The algorithm could be extended to overcome this problem. The training could be extended to detect persons using the head for better handling of crowded inputs. Slightest improvements in these algorithms can improve accuracy.

REFERENCES

- [1] Gozde Karatas, Onder Demir and Ozgur Koray Sahingoz "Deep Learning in Intrusion Detection Systems" International Congress on Big Data, Deep Learning and Fighting Cyber Terrorism (IBIGDELFT) 2006 vol 4, Pages: 113 - 116.
- [2] G. Hinton, L. Deng, D. Yu, G. E. Dahl, A.-r. Mohamed, N. Jaitly, A. Senior, V. Vanhoucke, P. Nguyen, T. N. Sainath et al, "Deep neural networks for acoustic modeling in speech recognition: "The shared views of four research groups, IEEE Signal Process. Mag 2012, vol. 29, no. 6, pp. 82–97.
- [3] P. F. Felzenszwalb, R. B. Girshick, D. Mcallester, and D. Ramana "Object detection with discriminatively trained part-based models" IEEE Trans. Pattern Anal. Mach. Intell., 2010, vol. 32, no. 9, p. 1627.
- [4] Zhong-Qiu Zhao, and Shou-tao Xu, "Object Detection with Deep Learning: A Review" IEEE TRANSACTIONS ON NEURAL NETWORKS AND LEARNING SYSTEMS FOR PUBLICATION, arXiv:1807.05511v2 [cs.CV] 16 Apr 2019,.
- [5] Olga Russakovsky, Jia Deng, Hao Su Jonathan Krause et al. "ImageNet Large Scale Visual Recognition Challenge" arXiv:1409.0575v3 [cs.CV] 2015.
- [6] J. R. R. Uijlings, K. E. A. van de Sande T. Gevers, A. W. M. Smeulders "Selective Search for Object Recognition" International Journal of Computer Vision September 2013 Volume 104, Issue 2, pp 154–171.
- [7] Ross Girshick Jeff Donahue Trevor Darrell Jitendra Malik UC Berkeley "Rich Feature Hierarchies For Accurate



- ObjectDetection And Semantic Segmentation”, arXiv:1311.2524v5 [cs.CV] 22 Oct 2014.
- [8] A. Krizhevsky, I. Sutskever, and G. E. Hinton, “Imagenet classification with deep convolutional neural networks”, 2012 in NIPS.
- [9] Ross Girshick, Microsoft Research “Fast R-CNN” arXiv:1504.08083v2 [cs.CV] 27 Sep 2015.
- [10] Shaoqing Ren, Kaiming He, Ross Girshick, and Jian Sun, “Faster R-CNN: Towards Real-Time Object Detection with Region Proposal Networks” arXiv:1506.01497v3 [cs.CV] 6 Jan 2016.
- [11] Y. Zhang, D. Zhou, S. Chen, S. Gao, and Y. Ma, “Single-image crowd counting via multi-column convolutional neural network” in Proc. IEEE Conf. CVPR, June 2016, pp. 589–597.
- [12] D. Ciresan, U. Meier, and J. Schmidhuber “Multi-column deep neural networks for image classification” IEEE 2012, In CVPR, pages 3642–3649.
- [13] J. Long, E. Shelhamer, and T. Darrell, “Fully convolutional networks for semantic segmentation”, arXiv:1411.4038, 2014.
- [14] Siyu Huang, Xi Li, Zhongfei Zhang, Fei Wu, Shenghua Gao, Rongrong Ji, and Junwei Han “Body Structure Aware Deep Crowd Counting” IEEE Transactions On Image Processing, Vol.27, No. 3, March 2018.
- [15] C. Zhang, H. Li, X. Wang, and X. Yang “Cross-scene crowd counting via deep convolutional neural networks” in Proc. IEEE Conf. CVPR, June 2015, pp. 833–841.
- [16] P. Luo, X. Wang, and X. Tang “Pedestrian parsing via deep compositional network” in Proc. IEEE ICCV, Dec. 2013, pp. 2648–2655.
- [17] V. Lempitsky and A. Zisserman “Learning to count objects in images”, in Proc. Adv. NIPS, pp. 1324–1332, 2010.
- [18] C. Zhang, H. Li, X. Wang, and X. Yang, “Cross-scene crowd counting via deep convolutional neural networks” in Proc. IEEE Conf. CVPR, June 2015, pp. 833–841.
- [19] H. Idrees, I. Saleemi, C. Seibert, and M. Shah “Multi-source multi-scale counting in extremely dense crowd images” in Proc. IEEE Conf. CVPR, June 2013, pp. 2547–2554.
- [20] A. B. Chan, Z.-S. J. Liang, and N. Vasconcelos “Privacy- preserving crowd monitoring: Counting people without people models or tracking” in Proc. IEEE Conf. CVPR, Jun 2008. pp. 1–7.
- [21] L. Boominathan, S. S. Kruthiventi, and R. V. Babu “Crowdnet: a deep convolutional network for dense crowd counting” in Proceedings of the 2016 ACM on Multimedia Conference, pp. 640–644, ACM. K. Simonyan and A. Zisserman “Very deep convolutional networks for large-scale image recognition” arXiv:1409.1556, 3.1.1 2014.
- [22] Lingke Zeng, Xiangmin Xu, Bolun Cai, Suo Qiu, Tong Zhang “Multi-Scale Convolutional Neural Networks For Crowd Counting” arXiv:1702.02359v1 [cs.CV] 8 Feb 2017.
- [23] Vinod Nair and Geoffrey E Hinton (2010), “Rectified linear units improve restricted Boltzmann machines,” in Proceedings of the 27th international conference on machine learning (ICML-10), pp. 807–814.
- [24] Jianing Qiu, Wanggen Wan, Haiyan Yao, Kang Han “Crowd counting and density estimation via two-column convolutional neural network” 4th International Conference on Smart and Sustainable City ICSSC 2017.
- [25] Youmei Zhang, Chunlin Zhou, Faliang Chang, and Alex C. Kot, “Attention to Head Locations for Crowd Counting” arXiv:1806.10287v1 [cs.CV] 27 June 2018.
- [26] Hailong Li, Zhendong Wu, Jianwu Zhang “Pedestrian Detection Based on Deep Learning Model” 9th International Congress on Image and Signal Processing, BioMedical Engineering and Informatics (CISP-BMEI 2016).
- [27] A. Krizhevsky, I. Sutskever, G. E. Hinton “Imagenet classification with deep convolutional neural networks”, Advances in neural information processing systems, 2012 1097–1105.
- [28] Joseph Redmon, Santosh Divvala, Ross Girshick, Ali Farhadi “You Only Look Once: Unified, Real-Time Object Detection” arXiv:1506.02640v5 [cs.CV] May 2016.
- [29] M. Everingham, S. M. A. Eslami, L. Van Gool, C. K. I. Williams, J. Winn, and A. Zisserman, “The pascal visual object classes challenge: A retrospective” International Journal of Computer Vision, 111(1):98–136, Jan 2015.
- [30] Wenbo Lan, Jianwu Dang, Yangping Wang and Song Wang “Pedestrian Detection Based on YOLO Network Model” Proceedings of IEEE International Conference on Mechatronics and Automation August 2018 5 - 8, Changchun, China.
- [31] Jiahuan Zhou, Lihang Feng, Ryad Chellali, and Haonan Zhu, “Detecting and tracking objects in HRI: YOLO networks for the NAO I See You function” 27th IEEE International Symposium on Robot and Human Interactive Communication, Nanjing, China, August 27-31 2018.
- [32] Igor R. de Almeida, Vinicius J. Cassol, Norman I. Badler, Soraia R. Musse, Claudio R. Jung “Detection of Global and Local Motion Changes in Human Crowd” IEEE Transactions On Circuits And Systems For Video Technology, 2016.
- [33] Qiming Li, Yan Yan, Hanzi Wang “Discriminative Weighted Sparse Partial Least Squares for Human Detection” IEEE Transactions On Intelligent Transportation Systems, Vol. 17, No.4, April 2016.
- [34] N. Dalal and B. Triggs “Histograms of oriented gradients for human detection” in Proc. IEEE Conf. Comput. Vis. Pattern Recog., San Diego, CA, USA, 2005, pp. 886–893.



- [35] P. Dollr, C. Wojek, B. Schiele, and P. Perona "Pedestrian detection: An evaluation of the state of the art" IEEE Trans. Pattern Anal. Mach. Intell, vol. 34, no. 4, pp. 743–761, Apr 2002.
- [36] C. Wojek, S. Walk, and B. Schiele "Multi-cue onboard pedestrian detection" in Proc. IEEE Conf. Comput. Vis. Pattern Recog, Miami Beach, FL, USA, 2009, pp. 794–801.
- [37] Hyeok-June Jeong, Kyeong-Sik Park, Young-Guk Ha "Image Preprocessing for Efficient Training of YOLO Deep Learning Networks" IEEE International Conference on Big Data and Smart Computing, 2018.
- [38] Zihan Ni¹, Jia Chen¹, Nong Sang¹, Changxin Gao¹, Leyuan Liu² "Light Yolo For High-speed Gesture Recognition" 25th IEEE International Conference on Image Processing (ICIP), 2018.
- [39] Athanasios Tsitsoulis, Nikolaos G. Bourbakis "A Methodology for Extracting Standing Human Bodies From Single Images, IEEE Transactions On Human-Machine Systems, Vol. 45, No. 3, June 2015.
- [40] Pengpeng Liang, Yu Pang, Chunyuan Liao, Xue Mei, and Haibin Ling "Adaptive Objectness for Object Tracking" IEEE Signal Processing Letters, Vol. 23, No. 7, July 2016.
- [41] Kuan-Hui Lee, Jenq-Neng Hwang, Fellow "Ground-Moving- Platform-Based Human Tracking Using Visual SLAM and Constrained Multiple Kernels" IEEE Transactions On Intelligent Transportation Systems, Vol. 17, No. 12, December 2016.
- [42] Shen Li, Bingpeng Ma, Hong Chang Shiguang Shan, Xilin Chen "Continuity-discrimination Convolutional Neural Network For Visual Object Tracking" IEEE International Conference on Multimedia and Expo (ICME), 2018.
- [43] Zheng Tang, Renshu Gu, Jenq-Neng Hwang "Joint Multi-view People Tracking And Pose Estimation For 3d Scene Reconstruction" IEEE International Conference on Multimedia and Expo (ICME), 2018.
- [44] Jing Tao, Hongbo Wang, Xinyu Zhang, Xiaoyu Li, Huawei Yang "An object Detection System Based on YOLO in Traffic Scene" 6th International Conference On Computer Science And Network Technology (ICCSNT), 2017.
- [45] Joseph Redmon, Ali Farhadi, University of Washington and Allen Institute for AI "YOLO9000: Better, Faster, Stronger" arXiv:1612.08242v1 [cs.CV] 25 Dec 2016.
- [46] Joseph Redmon, Ali Farhadi, University of Washington "YOLO v3: An Incremental Improvement" arXiv:1804.02767v1 [cs.CV] 8 Apr 2018
- [47] For generating labels using Yolo mark available on https://github.com/AlexeyAB/Yolo_mark
- [48] Darknet framework available on <https://pjreddie.com/darknet/yolo/>
- [49] Darknet framework available on <https://pjreddie.com/darknet/>
- [50] For training YOLO v3 under darknet framework available on <https://github.com/AlexeyAB/darknet#how-to-train-to-detect-your-custom-objects>.
- [51] For pedestrian detection using YOLO v3 available on <https://www.arunponnusamy.com/yolo-object-detection-opencv-python.html>.
- [52] For object detection using YOLO v3 available on <https://www.pyimagesearch.com/2018/11/12/yolo-object-detection-with-opencv/>.



Detection Of Cyberbullying On Social Media Using Machine Learning

Athira S¹, Joel Saji², Abin Biju³, Shon Alex Chacko⁴

Assistant Professor, Department of Computer Science and Engineering, JCT College Of Engineering and Technology¹

Computer Science And Engineering, JCT College Of Engineering And Technology, Coimbatore, India^{2,3,4}

Abstract: Cyberbullying is a major problem encountered on internet that affects teenagers and also adults. It has lead to mishappenings like suicide and depression. Regulation of content on Social media platforms has become a growing need. The following study uses data from two different forms of cyberbullying, hate speech tweets from Twitter and comments based on personal attacks from Wikipedia forums to build a model based on detection of Cyberbullying in text data using Natural Language Processing and Machine learning. Three methods for Feature extraction and four classifiers are studied to outline the best approach. For Tweet data the model provides accuracies above 90% and for Wikipedia data it gives accuracies above 80%.

INTRODUCTION

Machine Learning is a system of computer algorithms that can learn from example through self-improvement without being explicitly coded by a programmer. Machine learning is a part of artificial Intelligence which combines data with statistical tools to predict an output which can be used to make actionable insights.

The breakthrough comes with the idea that a machine can singularly learn from the data (i.e., example) to produce accurate results. Machine learning is closely related to data mining and Bayesian predictive modeling. The machine receives data as input and uses an algorithm to formulate answers. A typical machine learning tasks are to provide a recommendation. For those who have a Netflix account, all recommendations of movies or series are based on the user's historical data. Tech companies are using unsupervised learning to improve the user experience with personalizing recommendation.

Machine learning is also used for a variety of tasks like fraud detection, predictive maintenance, portfolio optimization, automatize task and so on. Machine learning involves computers discovering how they can perform tasks without being explicitly programmed to do so. It involves computers learning from data provided so that they carry out certain tasks. For simple tasks assigned to computers, it is possible to program algorithms telling the machine how to execute all steps required to solve the problem at hand; on the computer's part, no learning is needed. For more advanced tasks, it can be challenging for a human to manually create the needed algorithms. In practice, it can turn out to be more effective to help the machine develop its own algorithm, rather than having human programmers specify every needed step. The discipline of machine learning employs various approaches to teach computers to accomplish tasks where no fully satisfactory algorithm is available. In cases where vast numbers of potential answers exist, one approach is to label some of the correct answers as valid. This can then be used as training data for the computer to improve the algorithm(s) it uses to determine correct answers. For example, to train a system for the task of digital character recognition, the MNIST dataset of handwritten digits has often been used.

PROBLEM DEFINITION

The current system working on cyberbullying on social media prediction works on a small dataset. The aim of our system is to work on a larger dataset to increase the efficiency of the overall system. The number of comments also affects the performance of the system, thus our aim is to detect the cyberbullying and to increase the efficiency of the prediction.

LITERATURE REVIEW

Following is some of the search which has been reviewed for the proposed system.

1) Towards the detection of cyberbullying based on social network mining techniques

AUTHORS: I. H. Ting, W. S. Liou, D. Liberona, S. L. Wang, and G. M. T. Bermudez

In recent years, users are widely intend to express and share their opinions over the Internet. However, due to the characters of social media, it appears negative use of social media. Cyberbullying is one of the abuse behavior in the Internet as well as a very serious social problem. Under this background and motivation, it can help to prevent the happen of cyberbullying if we can develop relevant techniques to discover cyberbullying in social media. Thus, in this paper we propose an approach based on social networks analysis and data mining for cyberbullying detection. In the approach, there are three main techniques for cyberbullying discovery will be studied, including keyword matching technique,



opinion mining and social network analysis. In addition to the approach, we will also discuss the experimental design for the evaluation of the performance.

2) Supervised machine learning for the detection of troll profiles in twitter social network: Application to a real case of cyberbullying

AUTHORS: P. Galán-García, J. G. de la Puerta, C. L. Gómez, I. Santos, and P. G. Bringas

The use of new technologies along with the popularity of social networks has given the power of anonymity to the users. The ability to create an alter-ego with no relation to the actual user, creates a situation in which no one can certify the match between a profile and a real person. This problem generates situations, repeated daily, in which users with fake accounts, or at least not related to their real identity, publish news, reviews or multimedia material trying to discredit or attack other people who may or may not be aware of the attack. These acts can have great impact on the affected victims' environment generating situations in which virtual attacks escalate into fatal consequences in real life. In this paper, we present a methodology to detect and associate fake profiles on Twitter social network which are employed for defamatory activities to a real profile within the same network by analysing the content of comments generated by both profiles. Accompanying this approach we also present a successful real life use case in which this methodology was applied to detect and stop a cyberbullying situation in a real elementary school.

PROPOSED SYSTEM

SVM is basically used to plot a hyperplane that creates a boundry between data points in number of features (N)-dimensional space. To optimize the margin value hinge function is one of best loss function for this. Linear SVM is used in the following case which is optimum for linearly seperable data. In case of 0 misclassification, i.e. the class of data point is accurately predicted by our model, we only have to change the gradient from the regularisation arguments. A random forest consists of many individual decision trees which individually predict a class for given query points and the class with maximum votes is the final result. Decision Tree is a building block for random forest which provides a prediction by decision rules learned from feature vectors. An ensemble of these uncorrelated trees provide a more accurate decision for classification or regression.

ALGORITHMS

Support Vector Machine

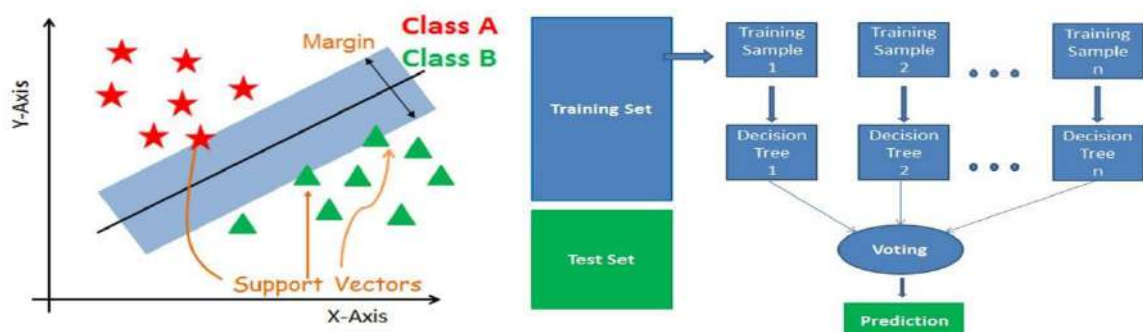
SVM is basically used to plot a hyperplane that creates a boundry between data points in number of features (N)-dimensional space.

To optimize the margin value hinge function is one of best loss function for this. Linear SVM is used in the following case which is optimum for linearly seperable data.

Random Forest Classifier

A random forest consists of many individual decision trees which individually predict a class for given query points and the class with maximum votes is the final result.

Decision Tree is a building block for random forest which provides a prediction by decision rules learned from feature vectors. An ensemble of these uncorrelated trees provide a more accurate decision for classification or regression.



EXPECTED RESULT

The goal of our project is to predict whether the comment is offensive or non offensive and it is personal or non personal attack. We mainly looking forward for the celebrities who cannot look all the comments in there post by our invention we can check many comments at the same time so that we provide more time and energy. We implement two algorithms to work efficient and more accurate than the existing system. Our proposed system algorithms are 1. Support Vector



Machine 2. Random Forest Classifier these two algorithms are more efficient and more accurate than the other systems. **Linear Kernel** A linear kernel can be used as normal dot product any two given observations. The product between two vectors is the sum of the multiplication of each pair of input values.

$$K(x, x_i) = \sum(x * x_i)$$

Polynomial Kernel A polynomial kernel is a more generalized form of the linear kernel. The polynomial kernel can distinguish curved or nonlinear input space.

$$K(x, x_i) = 1 + \sum(x * x_i)^d$$

Where d is the degree of the polynomial. d=1 is similar to the linear transformation. The degree needs to be manually specified in the learning algorithm.

Radial Basis Function Kernel The Radial basis function kernel is a popular kernel function commonly used in support vector machine classification. RBF can map an input space in infinite dimensional space.

$$K(x, x_i) = \exp(-\gamma * \sum((x - x_i)^2))$$

CONCLUSION

Cyber bullying across internet is dangerous and leads to mishappenings like suicides, depression etc and therefore there is a need to control its spread. Therefore cyber bullying detection is vital on social media platforms. With availability of more data and better classified user information for various other forms of cyber attacks Cyberbullying detection can be used on social media websites to ban users trying to take part in such activity In this paper we proposed an architecture for detection of cyber bullying to combat the situation. We discussed the architecture for two types of data: Hate speech Data on Twitter and Personal attacks on Wikipedia.

FUTURE SCOPE

The scope of the project is reduce the cyberbullying on the social media using SVM and Random forest classifier algorithms and it also provide more efficient than the existing algorithms

REFERENCES

- [1] I. H. Ting, W. S. Liou, D. Liberona, S. L. Wang, and G. M. T. Bermudez, "Towards the detection of cyberbullying based on social network mining techniques," in Proceedings of 4th International Conference on Behavioral, Economic, and Socio Cultural Computing, BESC 2017, 2017, vol. 2018-January, doi: 10.1109/BESC.2017.8256403.
- [2] P. Galán-García, J. G. de la Puerta, C. L. Gómez, I. Santos, and P. G. Bringas, "Supervised machine learning for the detection of troll profiles in twitter social network: Application to a real case of cyberbullying," 2014, doi: 10.1007/978-3319-01854-6_43.
- [3] A. Mangaonkar, A. Hayrapetian, and R. Raje, "Collaborative detection of cyberbullying behavior in Twitter data," 2015, doi: 10.1109/EIT.2015.7293405.
- [4] R. Zhao, A. Zhou, and K. Mao, "Automatic detection of cyberbullying on social networks based on bullying features," 2016, doi: 10.1145/2833312.2849567.



INTEGRATED PARKING SYSTEM FOR REAL-TIME PARKING

Greeshma K¹, Shibin K², Nabeel Kallan³, Amal E R⁴, Mohammed Musthafa A P⁵

Assistant Professor, JCT College of engineering and technology, Coimbatore¹

BE Computer Engineering, JCT College of Engineering & Technology, Coimbatore²⁻⁵

ABSTRACT: The world is aware of the current scenario, the population is increasing day by day hence number of vehicles are also increasing. Thus, everyone is facing the problem of parking, as there are less options available for legitimate parking. This problem leads to congestion, accidents, lack of space availability etc. Annual survey which is carried out has figured out that there is consistent growth in the ratio of traffic jam and accidents. Illegal parking plays a vital role in increasing the chances of traffic jams for hours. Due to increase in the number of vehicles. Moreover, it is much more time consuming as well. In this world of fast growing technologies, we should be able to save our time for the thing which is essential rather than searching space to park our vehicle. A car user must be able to book car before starting the journey and heading to the destination. The main objective behind developing such applications is to overcome such problems. An application will be developed according to the user point of view, which will be user friendly, so that a user can easily make use of it and could be able to book their parking space. The user will be able to book parking space in advance.

Keyword: - Android Application, Smart Parking, Reservation of Parking, and Parking Guidance.

1. INTRODUCTION

As the name "online parking booking" reflects that the proposed research will help in booking a parking space for vehicle. The problem with the traditional method is that it is more time consuming hence less efficient. The proposed research will provide an ease to such problems. Practically conventional methods that are available for booking a vehicle are not more efficient. A large number of human support is required to maintain the data of the user who had booked parking space. The whole concept is hectic as car drivers park their car on roadside. This results in a large traffic jam or congestion. Therefore, there is a need of a smart parking application. The main objective of the application is to resolve all such problems which we are faced by all in our day to day life. The application need to be designed in a simple way so the user can make use of it. The user is not restricted for parking their vehicles which makes this manual technique inefficient. A smart parking is one which allows user to perform the task such as:

1. Space availability for parking.
2. Parking places available near destination.
3. Cost for parking space allotted.
4. Legalized approval of booking.
5. Parking facility in advance should also be available.

During the application development phase developers should keep these points in mind. Application should also be a user-friendly application, so that a user can conveniently book a place for parking. According to user point of view, here we are trying to develop an application by keeping the needs of user in mind. The smart parking application will help user to book a parking space in advance, so that user should be able to make their plan accordingly. Our application will make the parking process much more simple and efficient as well as time saving. This will also help in saving fuel as we all know most of the today's population are living in cities, so the urban areas have reached full of its occupancy as people use their personal vehicles for transportation as per their convenience. Most of the time it is an agony for people to find parking space spend to park their vehicles. Most traffic occurs only because of vehicle congestion in the urban areas thus people are wasting time in searching the parking area abnormally to park their vehicles.

1.1. MODULES:

There are two modules: -1. Admin login

2. User login



Admin login will manage all the booking which will be made by the user. Admin can check how many bookings are made by the user. Admin will also be notified about the space availability as the updates will be made after each booking.

Users have to first register themselves to login into the system. After logging in application, the user can book their parking place in advance. Along with advance booking the user can also check the availability of parking place near their current location.

2. LITERATURE SURVEY:

Parking lots have become inessential and requires lot of manual work to handle and maintain it. These types of parking lot do not provide data regarding availability of free spaces. Many researchers have contributed to this issue and gave shape with various methods to better optimize the parking lot to fulfill the need. The project proposed smart parking reservation system using mobile application [2]. The system provides direction towards the allocated slots, thus making it simple to use. This system is used to designate parking space. The system checks the unique registration number stored in the database to check if the new vehicle needs to be parked. This system is a perpendicular parking positioning for the vehicles [4]. The user can find various parking places available at sole spot, find the suitable according to them and book a place.

A. Parking Management: -

Searching for comparison between different transport parking guidance policy. Many parking guidance systems has been developed in the last decade. This sub-section we have studied the methods of guidance for many of the existing parking and explain their limitations. Moreover, we simulate realistic traffic and parking in various parking management policy or situation.

B. Traffic volume: -

In our proposed model, the traffic volume is defined as the amount of traffic generated especially for parking. This component is not negligible and traffic congestion and related pollution.

3. PROPOSED SYSTEM

In this proposed system, we are implementing a real time parking reservation system combines with smart payment method. this system consists a web based application for parking slot reservation and payment. here we might have 2 types of booking:

- Pre-booking
- Spot-booking

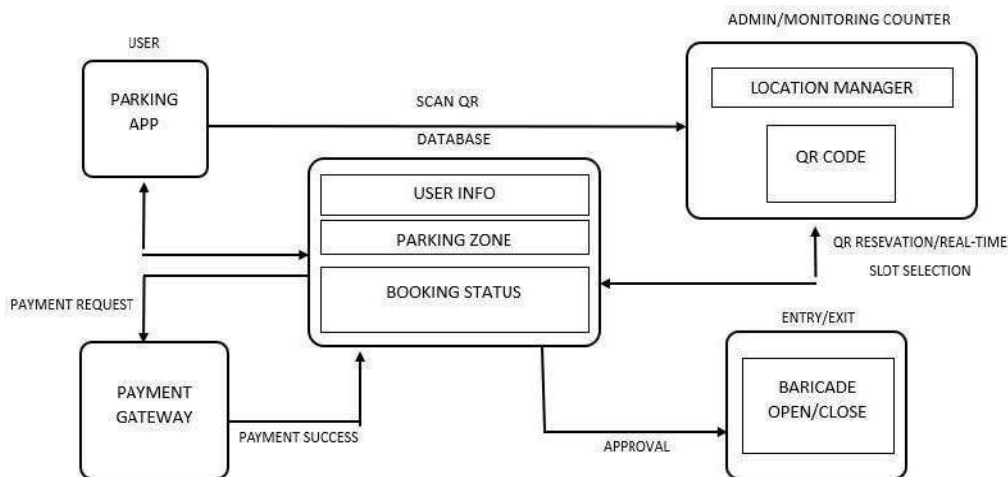


FIGURE 4.1: BLOCK DIAGRAM



Using the application, user can reserve their convenient slots and pay the charges in advance. and we are also providing spot-booking facility on the non-reservation counter using the app. the users can enter the parking area by scanning their qr code on the entry gate. the barricade will automatically open for those who reserved and those who completed the payment. after the completion of their reserved time, they can exit through the exit gate by scanning the same qr code.

Integrated parking system for real time parking system design consist of web based application, android application, payment gateway, qr scanner, automatic barrier-ade. it has 3 modules:

- Admin module
- User module
- Location manager module

Here admin and manager modules are developed as web applications and user modules as android applications.

4. DATA FLOW DIAGRAM

4.1.1 Level 0

Base dfd contains 3 modules admin module, user module and location manager module.

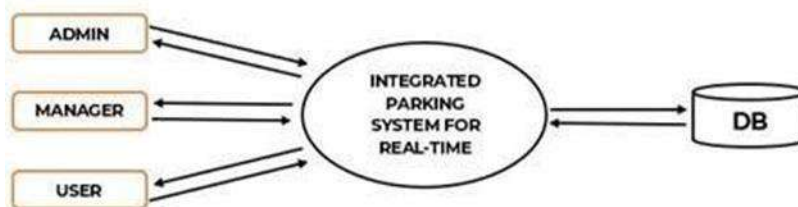


FIGURE 5.1: Base Dfd

4.1.2 Level 1

Admin has a unique Id(username) and password, if both entries are valid then the admin can view the registered users. Then admin can approve the registered locations and also can view the rejected and blocked locations. The admin can also view the complaints of the users and can send replies to them.

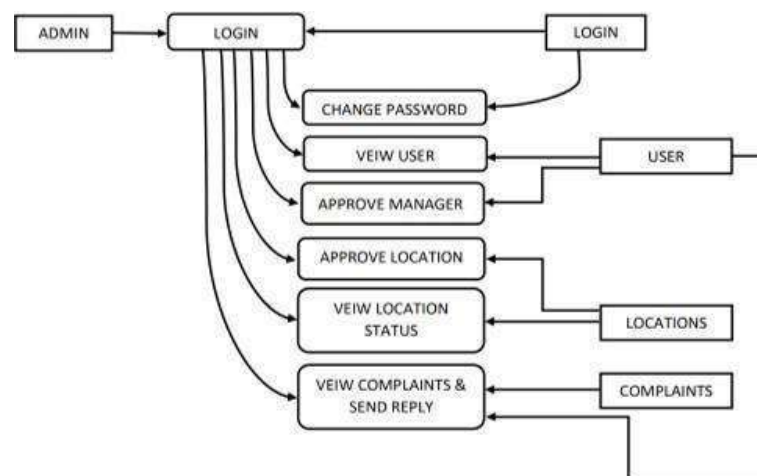


FIGURE 5.2: Admin

4.1.3 Level 2

Location manager has a unique id(username) and password, if both entries are valid then the admin can view the registered users. They can add parking slots, view parking slot status, approve booking, and view booking status. They can also send complaints about customers and can view replies like users.

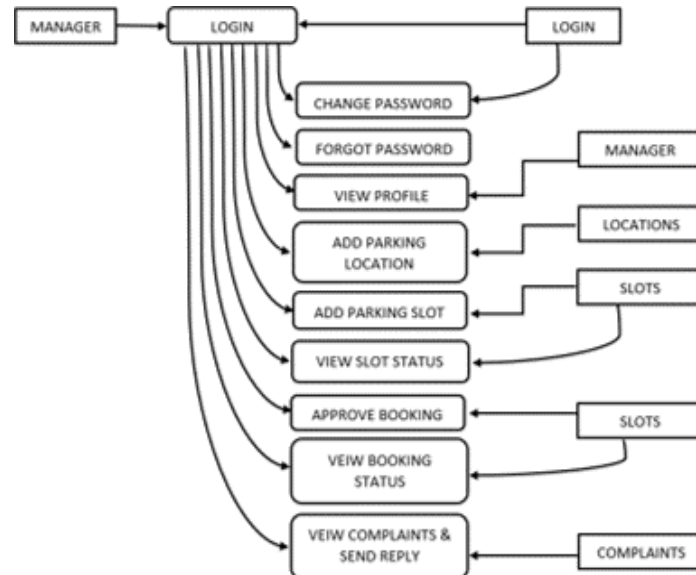


FIGURE 5.3: Manager

4.1.4 Level 3

In this system when the user enters his user id and password the software goes to the database and validates the user login details if it is correct the system fetches all details of the user towards the global variable. Then the customer can select their parking slot and confirm it through the payment. They can also do complaints if any and can view the replies from the admin.

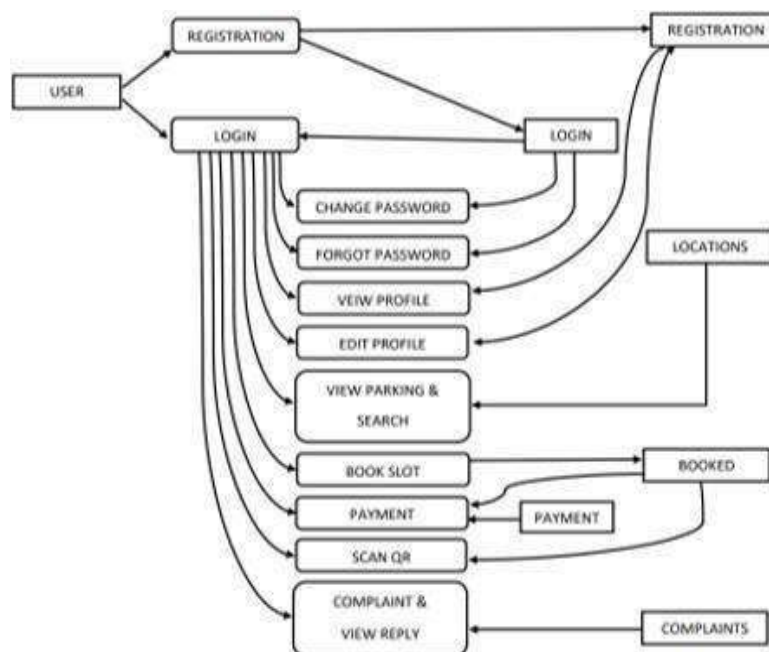
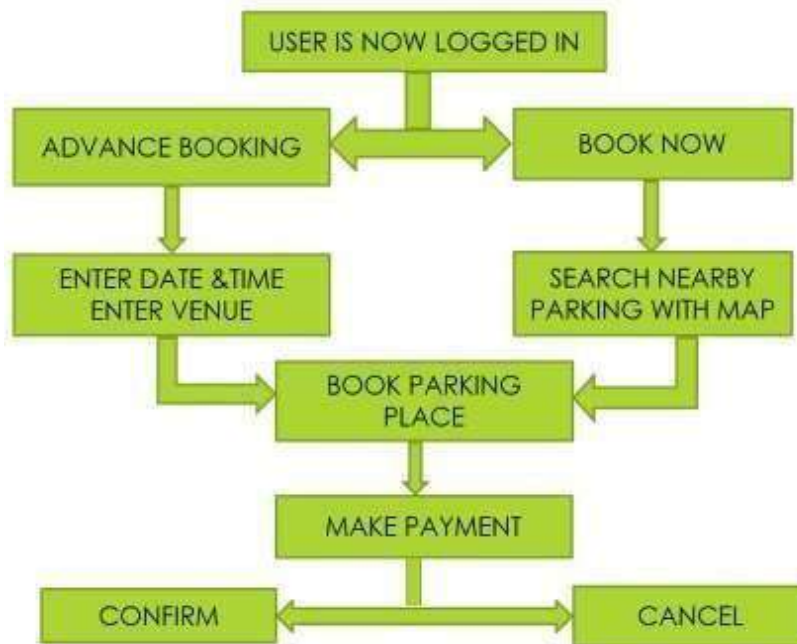


FIGURE 5.4 User



5. SYSTEM ARCHITECTURE:



6. CONCLUSION

This work presents the prototype of an integrated parking system that provides a novel parking management solution for various parking facility areas like a shopping malls, theaters, etc throughout the city. The system enables the drivers to obtain information on the availability of parking spaces and to reserve the parking lot via a web-based application.

It also enables the automatic collection of parking charges by providing smart payment options to the driver. This can save the user's time and fuel and also can relieve traffic in cities like Mumbai. In contrast to the existing parking strategies, this system limits the exertion of the driver in the parking areas, and also it could reduce the manual intervention in parking areas. By using this application, people can tackle the major issues while parking.

REFERENCES:

1. A. N.M.R Abhinav Kumar, Ankur Raj, "Smart Parking System (S-Park) – A Novel Application to provide Real-Time Parking Solution", in IEEE 2020.
2. F.M.Y. Rahayu, "A Secure Parking System Using GSM Technology", In International Journal of Future Computer and Communication, Vol 3, pp.337 – 395, 2014.
3. V.K.A.S.H, Singh, C. Anand, "Automated Parking System With Bluetooth Access", in international Journal of Engineering and computer science, vol 5, pp, 275-315, 2012.
4. Anuja Deokar, Ruchita Bhoje, Shristi Nayak, Nidhi Sharma, Online Parking Booking System, April 4, 2020.
5. G.K.Jakir Hussain, O.S.Dharshini, G.U.Kavipriya, G.Jeevanandhini, E-Parking Reservation System based on IoT for Smart cities, March, 2019.
6. Shubham Harde, Lalitkumar Khade, Shantanu Kale "A Review On Online Parking Booking System Via Android Application", 2018.
7. Arkadepta Roy, Pratik Bhuwalka, Prabhu.s, Chirag Kedia "Online Parking Booking Systems", April 2, 2018.
8. Lakkiya. S. N, Nevetha. R, Deepa. R, Online Booking System For Car Parking, February 2020.
9. Ali Ziat, Bertrand Leroy Nicolas Baskiotis and Ludovic denoyer "Joint Prediction of Road-Traffic and Parking Occupancy Over a City With Representation Learning" 2016 IEEE 19th International Conference on Intelligent Transportation Systems (ITSC) Windsor Oceanico Hotel, Rio De Janeiro, Brazil, November 1-4, 2016.
10. Chinmay Pawar, Ajay Wavhal, Akash Sigal, Anikat Patil, Randeep Kaloon "Online Parking Slot Booking" International Research Journal Of Engineering and Technology. Volume-05, Issue-03, Mar 2018.



ANDROID GAME DEVELOPMENT USING VCROSS – PLATFORM APPLICATION IN UNITY GAME ENGINE WITH C# LANGUAGE ZOMBIE SHOOTER

Prof. M. Ravi Kumar, Praveen Kumar J, Sivahari S, Bavan Kumar V, Sivasankar A

Department of Computer Science and Engineering , JCT College of Engineering and Technology Coimbatore,
Tamil Nadu, India

Abstract: In this paper, we present the design and implementation of the Cross Platform game called ZOMBIE SHOOTER. This game get vary from other Zombies game, because the idea of our game is different form others. It is a shooting game and was developed keeping the Android, Windows, and Windows Phone Operating System in mind. The aim of our project is to connect player with more than four guns and hundred percent of health and consumables are provided. The players should rescue two members from the zombie world. It's like an one man army game. This game can be played in the Android, Windows, and Windows Phone Operating System, it depend upon the game conversion. The game has been designed and implemented and soon will be available on the Google Play Market and Windows Store. The game has been tested on Windows 10 for PC, running Android Lollipop and Redmi Note 7S running Android KitKat. So, it should run on other compatible devices as well.

Keywords: Cross-Platform Plugins, Unity Game Engine, ZOMBIE SHOOTER, Software Development, Android Development, Windows Development.

I. INTRODUCTION

Unity3D Game Engine is an integrated development tool used to develop interactive contents like video games, architectural visualization and real-time 3D animations. Its editor runs on Windows and Mac OS X platforms. Though it runs on only two platforms, it has the ability of developing applications for multiple platforms which are mentioned as follows – Windows, Windows Phone, Mac OS X, iOS, Wii, Linux, Android, Web Player, etc. All we need for it to develop the application on respective platforms is the software development kit (SDK) for it. There are various plugins to export the application to different players like Flash Player, etc.

The functions that are supported by Unity3D are very abundant. All type of game developments are possible with Unity3d such as shaders, physics engine, network, terrain manipulation, audio, video and animation. Unity3D produces the applications based on JavaScript and/or C#. These are used to assign the animation or real-time transition of the Game-Objects defined in the application. GUI of Unity3D helps a new developer to approach easily, and script and program the transition of the GameObject.

This study aims to design and develop applications on multiple platforms using Unity3D Game Engine and with the help of scripting and programming get enable between one or two devices. So, the users can play either in a single or same/different devices running same/different platforms can play against each other. For the efficiency of the game development process, this study aims to plan, design, develop and test a smart game based on multi-platform game

II. RELATED STUDIES

Introduction to Unity3D:

Now-a-days the devices like Smartphones, tablets, iPad, iPhones have taken the application development to a whole another level. The cameras on these devices can be used to recognize business card and decrypt encrypted codes like



barcodes, QR-codes, etc. by simply scanning them. Here in this era, networking is also a major factor, as many or mostly all applications running no-a-days require a proper network connectivity. So, we have come up with an idea of using this network connectivity to next level by using this cross-platform connectivity in the gaming applications. Usually, we have heard about handheld-tohandheld connectivity (i.e. Android - Android, iOS - iOS, Windows Phone - Windows Phone, Android-iOS, Android - Windows Phone, iOS - Windows Phone), but our aim is to enable all-to-all device connectivity so there can be Handheld – PC along with above connections.

Unity3D is a cross-platform game creation system developed by Unity Technologies containing game engine and an integrated development environment (IDE). It is used to develop games for websites, desktops, handheld devices and consoles. Previously released on Mac OS in 2005, it was then expanded to target more than fifteen platforms. It can be run on Windows or Mac OS X system. Supported Platforms include BlackBerry 10, Windows Phone 8, Windows, OS X, Linux(mainly Ubuntu), Android, iOS, Unity Web Player (including Facebook), Adobe Flash, PlayStation 3, PlayStation 4, PlayStation Vita, Xbox 360, Xbox One, Wii U, and Wii. It includes an asset server and Nvidia PhysX physics engine.

The latest version is the Unity released on June 4th 2021. It supports the real-time global illumination based on the Geometries Enlighten technology. Other major changes include physically-based shaders, HDR sky-boxes, reflection probes, a new audio mixer with effects and enhanced animator workflows. Unity 5 brings support for Windows, Mac, Linux/Steam OS, Unity Web player, Android, iOS, Blackberry 10, Windows Phone 8, Tizen, Windows Store apps, WebGL, PlayStation 3, PlayStation 4, PlayStation Vita, Wii U. Xbox One, Xbox 360, Android TV, Samsung Smart TV, Oculus Rift, and Gear VR and AR for a total of 25 supported platforms. The Unity3D game engine is downloadable from their website in two different versions – Unity and Unity Pro.

Rendering:

The graphics engine uses Direct3D (Windows), OpenGL (Mac, Windows, Linux), OpenGL ES (Android, iOS), and proprietary APIs (Wii). There is support for bump mapping, reflection mapping, parallax mapping, screen space ambient occlusion (SSAO), dynamic shadows using shadow maps, render-to-texture and full-screen post-processing effects.[4] Unity supports art assets and file formats from 3ds Max, Maya, Softimage, Blender, Modo, ZBrush, Cinema 4D, Cheetah3D, Adobe Photoshop, Adobe Fireworks and Algorithmic Substance. These assets can be added to the game project, and managed through Unity's graphical user interface.

The ShaderLab language is used for shaders, supporting both declarative "programming" of the fixed-function pipeline and shader programs written in GLSL or Cg. A shader can include multiple variants and a declarative fallback specification, allowing Unity to detect the best variant for the current video card, and if none are compatible, fall back to an alternative shader that may sacrifice features for performance.[6] Unity also has built-in support for Nvidia's (formerly Ageia's) PhysX physics engine, (as of Unity 3.0) with added support for real-time cloth simulation on arbitrary and skinned meshes, thick ray casts, and collision layers.

Scripting:

The game engine is based upon the JavaScript and C#. Unity's scripting is built on Mono, an open-source implementation of .NET Framework.[8] MonoDevelop is an open-source IDE for Linux, Mac OS X and Windows. It supports Boo, C, C++, C#, CIL, D, F#, Java, Oxygene, Python, Vala and VB .NET.

Graphics:

Physics: Unity utilizes the NVIDIA PhysX physics engine, which supports:

1. Cloth
2. Soft and rigid-body interactions
3. Ragdolls



4. Joint systems
5. Wheel collision system

Terrain:

1. Terrain Painting
2. Detail Texture Painting
3. Tree Creator

Networking:

Unity has a number of built-in features to facilitate creation of standard multiplayer games. Some of the features State Synchronization, Real-time Networking, Remote Procedure Calls, Backend Connectivity. Web integration allows the game to communicate with container web pages and services. Massive Multiplayer Online: Development requires additional work by the developer or the addition of one of several third-party software packages designed for that purpose.

Asset Tracking:

Unity also includes the Unity Asset Server - a version control solution for the developer's game assets and scripts. It uses PostgreSQL as a backend, an audio system built on the FMOD library (with ability to playback Ogg Vorbis compressed audio), video playback using the Theora codec, a terrain and vegetation engine (which supports tree bill boarding, Occlusion Culling with Umbra), built-in light mapping and global illumination with Beast, multiplayer networking using RakNet, and built-in pathfinding navigation meshes.

Platforms:

Unity supports deployment to multiple platforms. Within a project, developers have control over delivery to mobile devices, web browsers, desktops, and consoles. Unity also allows specification of texture compression and resolution settings for each platform the game supports.[13] Currently supported platforms include for Windows, Mac, Linux/Steam OS, Unity Web player, Android, iOS, Blackberry 10, Windows Phone 8, Tizen, Windows Store apps, WebGL, PlayStation 3, PlayStation 4, PlayStation Vita, Wii U. Xbox One, Xbox 360, Android TV, Samsung Smart TV, Oculus Rift, and Gear VR.

Unity Asset Store:

Launched in November 2010, the Unity Asset Store is a resource available within Unity Editor. Store consists of over 7000 asset packages, including 3D models, textures and materials, particle systems, music and sound effects, tutorials and projects, scripting packages, editor extensions and online services. The store also contains many extensions, tools and asset packages such as the package NGUI: Next-Gen UI by Tasharen Entertainment,[14] and the visual scripting extension uScript by Detox Studios, Tidy Tile Mapper, a 2D/3D tile-based game design extension by Doppler Interactive and the input scripting package FingerGestures.

Invector third person controller:

Invector's Third Person Templates can help bring your game to life with a high quality Character Controller that takes minutes to set up, we have a solid and highly customizable template so you can focus on making your game unique.

Beginners will have a great learning curve with our several [Tutorials] and [Documentation], no scripting skills are necessary to create something cool. Advanced users will enjoy the thousands of features we included and continue to include over the past 4 years of development and support of our assets.



Investor's [Community] get's bigger every day with thousands of registered users and hundreds of daily visitations posting questions, helping each other or sharing their creations, integrations, and add-ons developed by users.

Importing investor third person controller to unity:

Our Templates are a **COMPLETE PROJECT** which means it comes with a custom **Project Setting**, so when you import the package from the AssetStore this warning will show up and that's why we recommend to **import the package on a New and Empty Project**.

There are basically 3 files that are **extremely necessary** for the correct functioning of this template:

- **InputManager.asset** - We have a custom input mapped to support the Xbox360 controller, without it you will receive errors about missing input.
- **TagManager.asset** - Includes all the necessary Tags and Layers for the project to work correctly.
- **DynamicsManager asset** - We use a Layers Collision Matrix, for example, we need the layer "Triggers" to not collide with the layer "Player".

Not every version of Unity will import those Project Settings by default, you can manually import those files by going to the tab **Investor** > **Import ProjectSettings** or **in the Welcome Window**.

Now that you have imported the necessary files, you can explore the several demo scenes and figure it out what kind of Third Person Game you want to create.

INVECTOR THIRD PERSON SHOOTER TEMPLATES FEATURES:

- Shooter Behavior & Animations (Basic & Melee features already included).
- Projectile bullets with trail renderer.
- Throwing objects with Trajectory system (granade, bottles, etc..).
- Optional Melee attacks for Shooter Weapons.
- Advanced damage based on distance & velocity.
- Decal for projectiles based on tags (different materials).
- Advanced Scope View.
- Aiming System with dispersion, range, shot frequency, recoil, etc...
- Particles, Sounds, Custom Bullets to emitt on attack.
- Archery System included.
- Advanced IK Adjustment System based on Weapon/Stance.
- Large number of customization to create different types of weapon.
- Secondary Shot to create powerful weapons.
- Hipfire.

Vcross-Platform Input Plugins:

Plugins supports all the software inputs such as Android (Mobile Plugins), Windows (PC Plugins) ect., With the input system, you can quickly setup controls for multiple Platforms, from Mobile to VR. The input system package is available from the package manager and verified for Unity latest version(LTS). The Input..GetAxis function is convenient in desktop platform to consolidate Keyboard and Joy stick input. By this Vcross platform input plugins the input for all the controllers are get accessed by the cross platform plugins. Where in cross platform all the mobile control input functions are get Inbuilt in the plugins. This plugins supports on all character controller in FPS and TPS shooting game, by this plugins writing of scripts get reduced.

III. BODY

Summary of the Game Development:-

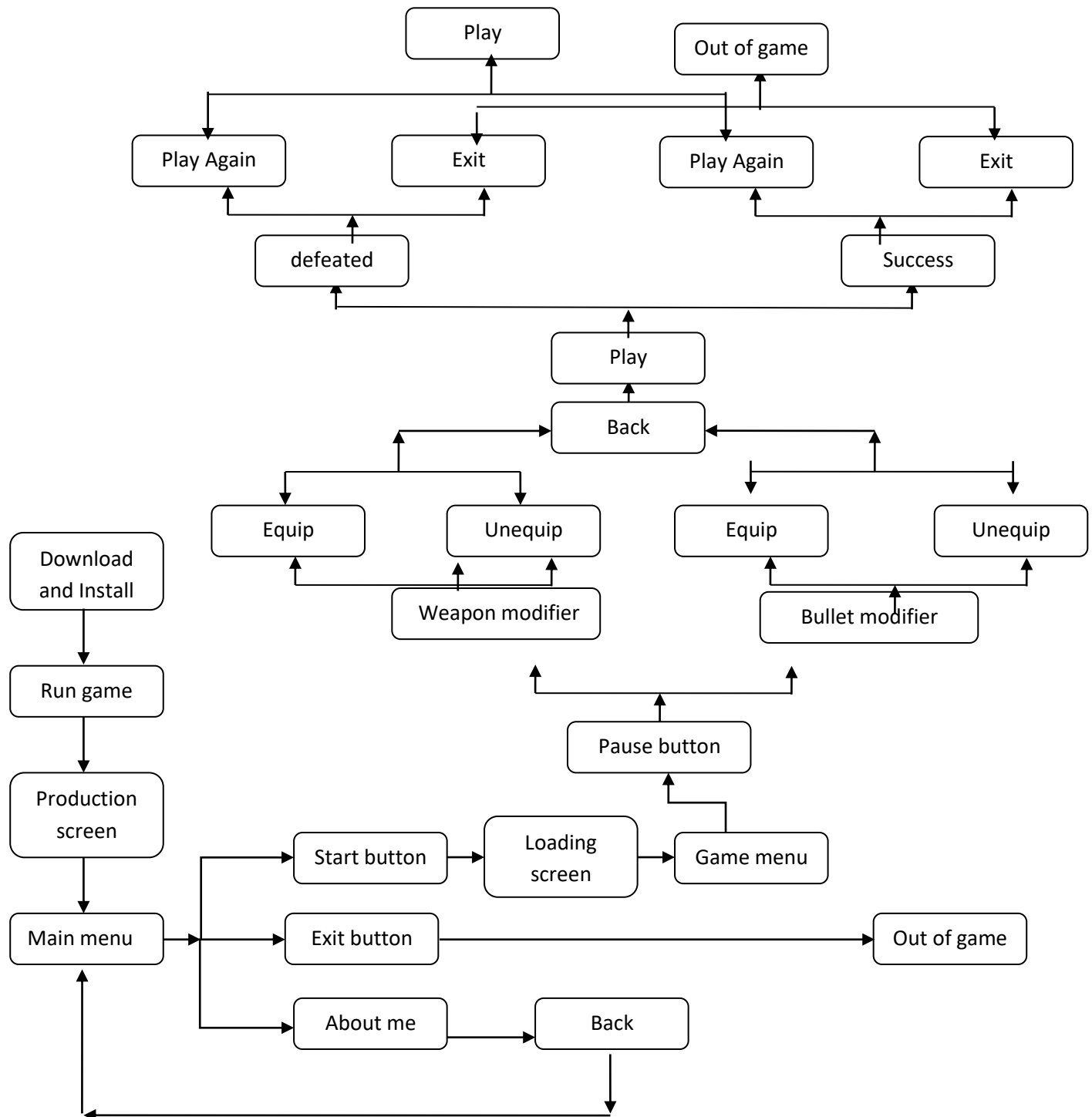
In this research paper

1. Game Name: Zombie Shooter.
2. Game Genre: Classic, terrain (land).



3. Platform: Supports Android-platform by switch platform it can convert Multi- platform (Windows pc, Linux etc.,).

The game working can be seen from following chart:



Game Characteristics:

In this zombie game there are four character plays a role.

1. Player (Hero):

In this game, player has a more amount of consumables then the enemy ,because more amount of enemies are follow. He has a four set of weapons with scope.

**2. Enemies (Zombies):**

Here, enemies are like a zombie character with ugly face. They are provided with more amount of health than the player and other consumables except weapons. But, the player health gets reduced by attacking by their hands.

3. Boss Enemy (Zombies leader):

The boss enemy has a high consumable than all other characters in this game.


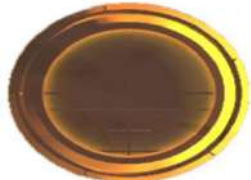

4. People to rescue (still humans):

There are two persons who are still human in this city. They should be rescued by the player. These humans are provided with minimum amount of health like a player, no attackable weapons are provided.







Core Idea of the Game:

The main idea of our game is to rescue the people who are still humans in the zombies world. So, the player should kill all the enemies by the consumables provided to the player and then he should rescue the people and get back to the helicopter, where he has started his journey of rescue.

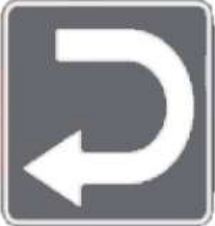
Graphic Concept Art:-**Character Designing and Modelling**

SL. No	Description	Image
1.	<p>Joy stick button is used to control and move the player all over the city. He can move in such direction they are :</p> <ul style="list-style-type: none"> • Forward, • Backward, • Left, • Right. 	 <p>JOY STICK</p>
2.	<p>Fire button is used to fire enemies (Zombies) And its designed using the unity epic icon.</p>	
3.	<p>Aim button is to make ready the player at position and aim on enemies.</p>	 <p>Aim</p>











4.	<p>Scope is used to zoom and get attack an enemy. There are variant scope over there.,</p> <ul style="list-style-type: none"> ✓ 3x ✓ 6x ✓ Rocket scope 	 <p>Scope</p>
5.	<p>Reload button is used to reload the gun ,when the bullet get finished in the gun. It takes over 2 to 3 minutes to reload it.</p>	
6.	<p>Crouch is the means of sitting at some position by bending the legs and get shoot an enemy, by doing this the player can hide from the enemy.</p>	
7.	<p>Jump button is used to jump over a thing ,which is slightly half of higher then the player.</p>	 <p>Jump</p>
8.	<p>Weapon change button is used to change the weapon ,depend upon the player selection. The weapons are..</p> <ul style="list-style-type: none"> ○ M416 gun ○ Shot gun ○ AWM sniper ○ Rocket launcher ○ pistol 	 <p>Weapon Changer</p>
9.	<p>Pause button is used to pause the game and take some rest to modify the game, how to make it solve. It provide some of the option to select the weapon and drop like he think.</p>	 <p>Pause</p>







10.	Back button is used to get back to the game when the weapon and bullets are selected .	 Back
-----	--	---

Game Development:




Sketch architecture

SL. No	Description	Image
1.	This is our production screen to start up our game by using the production name of ours "POPINZS DREAMS PRESENTS" the game "ZOMBIE SHOOTER". Some of pictured images are placed over there.	 Production screen
2.	<p>This is the menu screen of our game. Here there are some button to start up our game.</p> <p>  Start  Exit  About me </p>	 Menu screen
3.	<p>This is the about me screen of our game. Here there are some button to go back after knowing about us.</p> <p>  About me  Back </p>	 About Me screen



4.	<p>This is the game UI screen ,here contain all the button used by the player. The buttons are...,</p> <ul style="list-style-type: none"> ➤ Shoot ➤ Joystick ➤ Aim ➤ Crouch ➤ Jump ➤ Scope ➤ Reload ➤ pause. 	
5.	<p>This attacking screen shows the game situation while the player get attacked by the zombies. and the energy of the player getting reduced</p>	 <p style="text-align: center;">Attacking Screen</p>
6.	<p>The rescue screen shows ,how many people he have to rescue from the zombie. and get back to the helicopter after getting rescued.</p>	 <p style="text-align: center;">Rescue Screen</p>
7.	<p>If the player rescued the people ,who are in the zombies hand. After rescued he should move back to helicopter, when the rescued people hits the helicopter ,the win scene get visible.</p>	 <p style="text-align: center;">Win screen</p>



8.	If the player unable to rescue the people or he died in the middle of the game , then the loss scene will be produced.	 <p>Loss screen</p>
9.	In the bullet modifier scene ,the player can choose the bullet ,what he like to shoot an enemy.	 <p>Bullet Modifier screen</p>
10.	In the weapon modifier scene ,the player can choose the weapon ,what he like to shoot an enemy. in here the player can equip and unequip the weapon.	 <p>Weapon Modifier screen</p>

IV. FUTURE SCOPE

By using the cross platform application for creating the game in unity, it help the user to create the game quick. It has a great future ahead. By this application the user work get reduced. In some ways they are;

- The input script get lesser.
- For the player movement and action The plugins help much better.

So in the future, this cross platform application Plays a vital role.

V. CONCLUSION

This study aims to design and develop a cross-platform gaming application using Unity Game Engine. The functions that Unity3D supports autonomously are very abundant. All game developments are possible such as shader, physics engine, network, terrain manipulation, audio, video, and animation, and it is enabled so that it is possible to revise, meeting demand of user according to the need. For the efficiency of game development process, this study aims to plan, design, and develop a game based on multi-platform game engine using V-cross platform input plugin.

**REFERENCES**

1. "Is Unity Engine written in Mono/C# or C++?" <http://answers.unity3d.com/questions/2187/is-unity-engine-written-in-mono-c-or-c>. Retrieved 2011-04- 26..
2. "Unity - Fast Facts". <http://unity3d.com/company/public-relations/>. Retrieved 5 February 2013
3. "Unity - Multiplatform". Unity Technologies. <http://unity3d.com/unity/multiplatform/>. Retrieved 5 February 2013.
4. "Using DirectX11 in Unity 4". Unity Technologies. <http://docs.unity3d.com/Documentation/Manual/DirectX11.html>. Retrieved 19 February 2013..
5. "How do I import objects from my 3D app?" Unity Technologies. <http://docs.unity3d.com/Documentation/Manual/HOWTO-importObject.html>. Retrieved 19 February 2013.
6. "Shaders". Unity Technologies. Retrieved 19 February 2013.. <http://docs.unity3d.com/Documentation/Manual/Shaders.html>.
7. "Physics". Unity Technologies. Retrieved 19 February 2013. <http://docs.unity3d.com/Documentation/Manual/Physics.html>.
8. "Using Scripts". Unity Technologies. <http://docs.unity3d.com/Documentation/Manual/Scripting.html>. Retrieved 19 February 2013
9. "MonoDevelop". Mono Technologies <http://www.monodevelop.com/documentation/>
10. "Getting started with Mono Develop". Unity Technologies. <http://docs.unity3d.com/Documentation/Manual/HOWTO-MonoDevelop.html>. Retrieved 19 February 2013.
11. "Unity Features", GameIndustry.com <http://gameindustry.about.com/od/game-development/a/Unity-Engine-Feature-Guide.htm>
12. "Asset Server (Pro Only)". Unity Technologies. <http://docs.unity3d.com/Documentation/Manual/AssetServer.html>. Retrieved 19 February 2013.
13. "Unleash your game with effortless deployment to 10 global platforms". Unity Technologies. <http://unity3d.com/unity/multiplatform/>. Retrieved 19 February 2013.
14. "NGUI: Next-Gen UI kit". Tasharen. http://www.tasharen.com/?page_id=140.
15. "Autodesk 3ds Max — Detailed Features", 25 March 2008 <http://usa.autodesk.com/adsk/servlet/pc/index?siteID=123112&id=13567426>
16. "Unity Networking with Photon", Exit Games <http://doc.exitgames.com/en/pun/current/getting-started/pun-intro>



HUMAN COMPUTER INTERACTION (HCI) THROUGH EYE-GAZE TECHNOLOGIES BASED ON IMAGE PROCESSING

Rupa M¹, Srinivasan S², Harish V³, Raja S⁴

Assistant Professor, Department of Computer Science And Engineering JCT College Of Engineering And Technology,
Coimbatore, India¹

Computer Science And Engineering, JCT College Of Engineering And Technology, Coimbatore, India^{2,3,4}

Abstract: Eye movement can be regarded as a pivotal real-time input medium for human-computer communication, which is especially important for people with physical disability. In order to improve the reliability, mobility, and usability of eyetracking technique in user-computer dialogue, a novel eye control system with integrating both mouse and keyboard functions is proposed in this paper. The proposed system focuses on providing a simple and convenient interactive mode by only using user's eye. The usage flow of the proposed system is designed to perfectly follow human natural habits. Additionally, a magnifier module is proposed to allow the accurate operation. In the experiment, two interactive tasks with different difficulty (searching article and browsing multimedia web) were done to compare the proposed eye control tool with an existing system. The Technology Acceptance Model (TAM) measures are used to evaluate the perceived effectiveness of our system. It is demonstrated that the proposed system is very effective with regard to usability and interface design.

Objective

The main objective of the project is to develop a software that useful to all peoples including physical disabilities to access system through eye commands and files (multimedia). and some peoples affected by diseases like Cerebral palsy or Amyotrophic lateral sclerosis (losing control of hands) also can access system through eye gaze actions and pointer access.

Keywords: Eye Gaze, TAM (Technology Acceptance Model), Mouse Functions, Eye Tracking.

I. INTRODUCTION

Eye trackers have existed for a number of years but, early in the development of the field decade ago, it was too expensive to consider use in real user computer interfaces. In recent years, with the development of better and cheaper components for gaze interaction, low-cost eye trackers have been produced by several high-profile companies, such as Tobii's eye tracker gaze point's GP3 tracker, and the eye tracker. As eye tracking gear gets cheaper, new applications with the concept of using eye tracking in HCI are clearly beginning to blossom. Various methods have been developed based on tracking Contact lenses. disabled people usually type on the computer keyboard with long sticks that they hold in their mouth, but the technique being presented is a benefaction for handicaps to help them be independent in their lives. Giving them a chance to work, socialize, and entertain in their lives. The remainder of this paper is structured as follows

1. The proposed system realizes all of the functions of regular input sources, including mouse and keyboard. User can efficiently interact with computer by only using their eyes.
2. The proposed system provides more natural and more convenient communication mechanism for user computer dialogue and could also avoid annoying user with unwanted responses to their actions..

II. HCI TRACKING

- Accessing system through nose track moments and eye gaze is our primary work.
- The applications, outcomes, and possibilities of facial landmarks are immense and intriguing. Dlib's prebuilt model, which is essentially an implementation and not only does a fast face-detection but also allows us to accurately predict 68 2D facial landmarks
- It sends the view point of user to the mouse function module; it receives information from modules and executes the corresponding mouse events for users



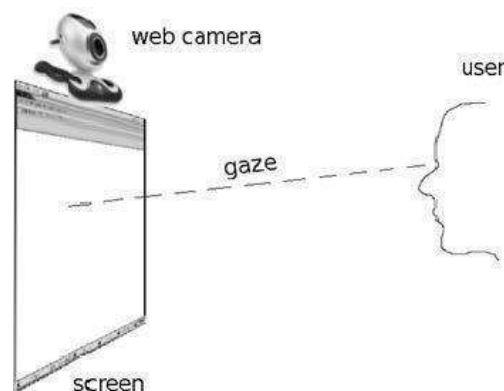
III. RELATED WORK

There exists a lot of HCI systems that can automate the simple tasks such as speech recognition, touch sensitive on different devices, computers and launching various applications by using HCI enabled computer.

The research issue in designing improved eye gaze based human computer interaction (HCI) for argumentative and alternative communication (AAC). Argumentative and alternative communication is the domain of communicating methods or techniques that provide improved human-human or human-system interaction. AAC technique help user with certain communication disability to perform everyday conversation without helper. The paper of this author gives main idea of Augmentative and alternative communication (AAC) for developing main AAC.

PROPOSED METHOD

The proposed system is based on existing system. The most important part in our system is that the system can be able to use by both the persons whether they are normal persons or handicapped. The current system is not able to do this so we are developing a new system which will help a lot to disable peoples and also illiterate peoples. Current system focuses more on normal users but our system is friendly to all types of users whether they are normal, visually impaired or else illiterate. When using this system, the computer will guide the user for performing the operation which he/she wants to perform. The most important advantage of this system is that the user doesn't have to worry about how to use keyboard because all the operations are based on voice recognition and eye tracking in this user use their eye movement and voice command to operate computers and laptops.



IMPLEMENTATION

This application includes modules

1. Eye Gaze Tracking
2. Main Interface
3. Mouse function module
4. Algorithms
5. User action detection module
6. Halt (sleep) module
7. Mouse simulation engine

Eye Gaze Tracking: An illustration of setup is given in fig.13. A user is looking at computer screen and at the same time webcam is capturing live stream. The idea is to enable computer system to manipulate eye gaze by detecting important feature points and combining those features in a way which can result in useful information to calculate user's point of interest. Basic concept of eye gaze tracking and framework implemented in this project is being explained using following points:

- Determine facial features which are necessary and sufficient for eye gaze tracking.
- Detecting and tracking these features points in live feed coming web-cam.
- Using these features in a way to extract user's point of interest.
- Track user's point of interest.

Main Interface:

It sets and manages the startup dialogue, provides user access to user action detection module, halt (sleep) module, mouse function module, and keyboard function module. In our system we use various packages of python which are



discussed below.

1. NumPy
2. Scipy
3. OpenCV
4. PyautoGUI

Mouse Function Module:

it receives the view point of user from simulation engine and transfers the coordinate to the fixation function within user action detection module, which allows the system to perform directly at the view point after the function is selected. If a second view point is required to finish the action, the view coordinate is transferred to the simulation engine to execute the event. Besides, the module provides various virtual mouse functions for users to operate computers with eye movement. There are totally six mouse functions in this module, namely, left-click (LEFT), continuous left-click (LEFT), double left-click (DOUBLE), right-click (RIGHT), drag (IDRAG), and scroll (SCROLL).

Algorithms:

1. Harr-cascade Algorithm:

Har-cascade is a protest detection algorithm used to find faces, people on foot, items, outward appearances in a picture and primarily utilized for face detection. In Har-course, the framework is given a few quantities of constructive pictures (like appearances of changed people at various foundations) and pessimistic (pictures that do not face but rather can be whatever else like the seat, table and divider and so forth).

2. Hough Transform Algorithm:

The Hough transform [28], algorithm is a worldwide strategy for discovering straight lines, picture examination, computer vision, and advanced imaging preparing. The reason for this method is to discover flawed occurrences of courses classified, a specific lesson of figures through a polling technique. The Hough transforms are connected for the inquiry of a typical focus of round or mostly roundabout segments exhibit in a picture.

Halt (sleep) module:

it determines whether to stop eye tracking and enter the sleep mode and determines whether to jump out of the sleep mode and restart the eye tracking.

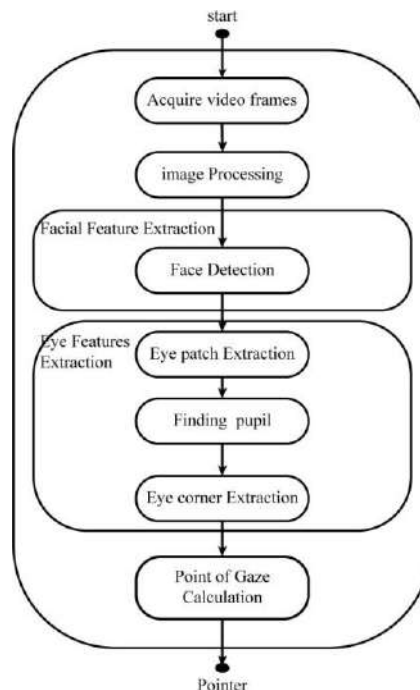
Mouse simulation engine:

- 1) RIGHT CLICK: When Right Eye is blinked then it performs Right click operation of mouse.
- 2) LEFT CLICK: As same as that of the left Click, when left eye is blinked left click will be performed.
- 3) CURSOR MOVEMENT: Whenever the eye gaze is relocated from one point to the another, position of cursor will move according to the gaze.
- 4) DOUBLE CLICK: When both eyes are blinked twice with a very short delay then double click operation can be performed. To avoid collisions and for better performance there is no operation for simultaneous single blink of both eyes

Action	Function
 Opening Mouth	Activate / Deactivate Mouse Control
 Right Eye Wink	Right Click
 Left Eye Wink	Left Click
 Squinting Eyes	Activate / Deactivate Scrolling
 Head Movements (Pitch and Yaw)	Scrolling / Cursor Movement

- 5) ACTIVATE SCROLLING: When squeezing the both eyes, scrolling enable, the same way to disable scrolling cursor.
- 6) SCROLLING: When head look upwards screening scrolling up, when head look downwards scrolling down, right and left side look decides landscape scrolling both right and left side.

METHODOLOGY:



SYSTEM REQUIREMENTS

Software Requirements:

- ☐ FRONT END - PYTHON 3
- ☐ IDE - PYCHARM

Hardware Requirements

- ☐ OPERATING SYSTEM - WINDOWS 11
- ☐ PROCESSOR - INTEL ® CORE I5
- ☐ RAM - 8 GB
- ☐ CAMERA - ASUS ® INBUILD WEBCAM

CONCLUSION

In order to make user interact with computer naturally and conveniently by only using their eye, we provide an eye trackingbased control system. The system combines both the mouse functions and keyboard functions, so that users can use our system to achieve almost all of the inputs to the computer without traditional input equipment. The system not only enablesthe disabled users to operate the computer the same as the normal users do but also provides normal users with a novel choice to operate computer. According to our TAM questionnaire analysis, the participants considered our eye movement system to be easy to learn. Meanwhile, participants show their interest in using the proposed eye control system to search and browse information. They are looking forward to see more of our research results on the use of eye tracking technique to interact with the computer. In future, we will try to add new operation functions for more usage situations for users to communicate with media and adjust our system on new platform, such as tablet or phone. We will also develop series operation modules in order to achieve a complete operating experience for users from turning on to turning off the computer.

REFERENCES

- 1.)Q. Sun, J. Xia, N. Nadarajah, T. Falkmer, J. Foster, and H. Lee, "Assessing drivers' visual- motor coordination using eyetracking, GNSS and GIS: a spatial turn in driving psychology," Journal of Spatial Science, vol. 61, no. 2, pp. 299–316, 2016. View at: Publisher Site | Google Scholar
- 2.)N. Scott, C. Green, and S. Fairley, "Investigation of the use of eye tracking to examine tourism advertising effectiveness," Current Issues in Tourism, vol. 19, no. 7, pp. 634–642, 2016. View at: Publisher Site | Google Scholar
- 3.)K. Takemura, K. Takahashi, J. Takamatsu, and T. Ogasawara, "Estimating 3-D point-of- regard in a real environment using a head-mounted eye-tracking system," IEEE Transactions on Human-Machine Systems, vol. 44, no. 4, pp. 531–536, 2014. View at: Publisher Site | Google Scholar



- 4.)R. J. K. Jacob and K. S. Karn, "Eye Tracking in human-computer interaction and usability research: ready to deliver the promises," Minds Eye, vol. 2, no. 3, pp. 573–605, 2003. View at: Google Scholar
- 5.)O. Ferhat and F. Vilarino, "Low cost eye tracking: the current panorama," Computational Intelligence and Neuroscience, vol. 2016, Article ID 8680541, pp. 1–14, 2016. View at: Publisher Site | Google Scholar
- 6.)Tobii EyeX, "EyeX," 2014, <http://www.tobii.com/eyex>. View at: Google Scholar
- 7.)GazePoint, "Gazept," 2013, <http://www.gazept.com/category/gp3-eye-tracker>. View at: Google Scholar
- 8.)The eyeTribe, "EyeTribe," 2014, <http://www.theeyetribe.com>. View at: Google Scholar
- 9.)M. A. Eid, N. Giakoumidis, and A. El Saddik, "A novel eye-gaze-controlled wheelchair system for navigating unknown environments: case study with a person with ALS," IEEE Access, vol. 4, pp. 558–573, 2016. View at: Publisher Site | Google Scholar
- 10.)L. Sun, Z. Liu, and M.-T. Sun, "Real time gaze estimation with a consumer depth camera," Information Sciences, vol. 320, pp. 346–360, 2015. View at: Publisher Site | Google Scholar | MathSciNet



ONLINE BUSPASS ISSUE AND RENEWAL USING SELENIUM

DIVYA R¹, Arunabishek A², Joy prasanna S³, Sridharan R⁴, Vinoth K⁵

¹Assistant Professor, Department of Computer Science and Engineering, JCT College Of Engineering and Technology, Coimbatore, India

²⁻⁵Computer Science and Engineering, JCT College Of Engineering and Technology, Coimbatore, India

Abstract: The world today is largely dependent on computers; therefore, not being aware of the tricks of this trade is bound to make a person feel left out. Computers changed the world a lot. It helped man step forward into the future. Thanks to computer, exploration came true, new designs of vehicles and other transportation were made; entertainment became more entertaining, medical science made more cures for diseases, etc. the computers impacted our lives in many ways. They did make life a lot easier. Without computers, world would be a harder place to live in. Thanks to the computer, everyday life is easier for us. This project is proposed for people those who are using public transport for daily commuters in Tamil Nadu. Even though the automobile industry has been developed in India still may of the commuters are depend on public transport which is the budget friendly way in metropolitan cities and college students. But in morning time it is difficult to get a ticket in the crowd. Daily we need a proper chance for our transport. Even bus pass renewal also in manual process. This manual process requires man power and consumes more time. Also, user needs to go bus depot on the particular date and time to apply with required details with in due-date. If they fail to appear with in due-date they can't apply .to avoid such difficulties, this service rectifies those problems. It will help to save their time without standing in a line for hours in counters.

INTRODUCTION

A real-time webserver system of online bus pass application and renewal service has been proposed using web service which helps the students and employees to apply or renewal bus pass through online from anywhere anytime. The bus pass will be differing for different types of users. In this bus pass, all the required details such as candidate name, address, DOB, mail ID, photo identity of the candidate and payment details are provided. In of working organization details will be provided in employees bus pass. The renewal process can be done monthly as per user wish and based on that renewal period amount will be detected.

In all place websites online mode of process has been evolved but even our daily basis of need, is not been yet. This make the people easier and their ticket form of travel has going to be changed. People can make their ticket (Bus Pass) on monthly basis not even going for depot the get pass through online using websites. This website method of project will be helpful for people those using regular public transport.

The bus pass registration and renewal are still a manual process in Tamil Nadu. On monthly basis the commuters should go to the depot and stand in a queue for long time and get their pass for a month. On that renewal date some people may not be available on that particular time and in getting more complication. To overcome these kinds of difficulties we developed a website.

OBJECTIVE:

Simple system allows the offline bus commuters. this website is then generated as HTML files and graphics that can be uploaded to a web-space. These systems do not use an online database. A high-end solution can be bought or rented as a standalone program

This site gets the user (applicant of bus pass) "name, date of birth, mobile number image

Source and destination information from the applicant of bus pass and those who are renewing the bus pass. Then the admin will receive the information form the applying candidate and verify the given details is correct and valid or not. If all the given details is satisfied then the admin will approve for the pass for the particular candidate. By using a frame work already existing, software modules for different functionalities required by a web site can be adapted and combined. The end user of this is a bus pass depot counter where the website is hosted on the web and administrator maintains the database. The website which is arranged at the candidate database, the details of the candidate forward from the database for the candidate view based on the selection through citizen, admin and head officer login and amount is created using online transaction.

Data entry into the application can be done through various screens designed for various level of candidate.



Database column user Id-name-password-date of birth-mobile number-email- gender-pass type-image-region-district-depot-source-destination 1-destination 2destination-3-renewal month-money.

SYSTEM ANALYSIS

1.EXISTING SYSTEM

The existing system is intended to overcome the major drawbacks of the currently existing manual system. The features are as follows 1. This online bus pass software system will help students and commuters get bus passes and eliminate the need of standing in queues for passes. Research Article Volume 7 Issue No.5 International Journal of Engineering Science and Computing, May 2017 12571 <http://ijesc.org/> 2. Public can find all the bus pass related information along with timetable without going to the bus station. 3. Minimum time is required to process the details submitted and to generate the bus pass. 4. Renewal can be done online with the reference identification that is provided during the registration of the pass

The passengers will apply the bus pass, going to depot counter apply the form manually. Every month will go to depot then renew the pass. So, Passengers time is consuming for this process at every month.

Disadvantages:

- > Consumes more time and Tedious process.
- > User have to wait for a long time in queue to renewal.

2.PROPOSED SYSTEM

The proposed system is intended to overcome the major drawbacks of the currently existing manual system. The features are as follows 1. This online bus pass software system will help students and commuters get bus passes and eliminate the need of standing in queues for passes. Research Article Volume 7 Issue No.5 International Journal of Engineering Science and Computing, May 2017 12571 <http://ijesc.org/> 2. Public can find all the bus pass related information along with timetable without going to the bus station. 3. Minimum time is required to process the details submitted and to generate the bus pass. 4. Renewal can be done online with the reference identification that is provided during the registration of the pass.

User can register the application. Then login the application using username and password. User can apply the pass and renew the pass through the login. User will enter details, and then Admin will check and verify the user details. If all details are satisfied then admin will confirm pass, then user will download the report. These are main propose of this project.

Advantage:

- > In this proposed method can rectify all disadvantages of manual work.
- > It will reduce the passenger time at every month renewal.
- > Data Process is Easy to manage.
- > In manual method can renew the document at specific time. But in this system can renew document as anywhere any time.

LITERATURE SURVEY

1.COMMUTERS FULFILLMENT

This chapter will mainly discuss on the study that are done by previous research of other authors in the similar area of the present study. Throughout practical views of previous studies done in online bus pass issues and renewal in offline in a tedious process. This study combines factors that other studies have done that will make this is such easier way but not the random commuters. Includes the both students and employees.

All of these factors will contribute to the study of other state bus commuters where travelling mode of transport have been verified and find an exact solution for that bus pass issue. In Tamil Nadu the online mode form can get and we need to fill the and handover to the depot

2.PRIVACY AND SECURITY

In some other business websites, there may be issue to cyber-attack but in this case no profit or unreason for cyber-attack. Only we can pay for our commutes and getting the pass for that. This is daily public dependent passenger issues for

Their way of travelling even-though in western country has been developed a lot in paying their travel charge using but in Tamil Nadu is not have to pay for bus pass in online

**PROJECT DESCRIPTION****1.OVERVIEW OF THE PROJECT**

Bus pass can be applied only through our manual mode for both students and working profession. At first can register their details in our web services, after registration. So that they can able to access the online bus pass facility. For students and they must login with password and mail Id, after verification they are allowed to send the student's required details (mobile number, photo, source and destination) to make bus pass. Received information are stored in MY SQL database. The generated bus pass will send through post and finally an acknowledgement will get from college or office to make sure of receive.

STUDENTS

An Institution which are allowed 30% travel concession they should submit some required documents to avail the Buss pass. Candidates who came under this category are need to pay amount to our government based on their travel. Transactions are made via reliable way such as credit cards, debit cards or net banking. After completing the transaction process, they will receive their applied bis pass through email (soft copy).

EMPLOYEES

For employees to get their pass, they must provide photocopy of Employee's Id or appointment order of working organization.

OTHERS

If the employee or student applying the pass they need to start applying before month of 25th. After applying, particular candidate can get report monthly once within from 1st day of the month to the 10th day of month. All the data in the database are cleared yearly once and stored in excel sheets.

Lost or stolen bus pass will not be refunded or replaced. Every Bus pass will have unique Id.

SOFTWARE DESCRIPTION**1.HTML:**

HTML stands for Hypertext Markup Language. It is used to design web pages using a markup language. HTML is the combination of Hypertext and Markup language. Hypertext defines the link between the web pages. A markup language is used to define the text document within tag which defines the structure of web pages. This language is used to annotate (make notes for the computer) text so that a machine can understand it and manipulate text accordingly. Most markup languages (e.g., HTML) are human-readable. The language uses tags to define what manipulation has to be done on the text. HTML is a markup language used by the browser to manipulate text, images, and other content, in order to display it in the required format. HTML was created by Tim Berners-Lee in 1991. The first ever version of HTML was HTML 1.0, but the first standard version was HTML 2.0, published in 1999.

2.CSS:

CSS stands for Cascading Style Sheets. It is the language for describing the presentation of Web pages, including colours, layout, and fonts, thus making our web pages presentable to the users. CSS is designed to make style sheets for the web. It is independent of HTML and can be used with any XML-based markup language. Now let's try to break the acronym:

Cascading: Falling of Styles

Style: Adding designs/Styling our HTML tags

Sheets: Writing our style in different documents

1994: First Proposed by Hakon Wium Lie on 10th October 1996: CSS was published on 17th November with influencer Bert Bos Later he became co-author of CSS

1996: CSS became official with CSS was published in December

1997: Created CSS level 2 on 4th November

1998: Published on 12th May

3.JAVASCRIPT

JavaScript is a cross-platform, object-oriented scripting language used to make webpages interactive (e.g., having complex animations, clickable buttons, popup menus, etc.). There are also more advanced server-side versions of JavaScript such as Node.js, which allow you to add more functionality to a website than downloading files (such as Realtime collaboration between multiple computers). Inside a host environment (for example, a web browser), JavaScript can be connected to the objects of its environment to provide programmatic control over them. JavaScript contains a standard library of objects, such as Array, Date, and Math, and a core set of language elements such as operators, control structures, and statements. Core JavaScript can be extended for a variety of purposes by supplementing it with additional objects; for example:



Client-side JavaScript extends the core language by supplying objects to control a browser and its Document Object Model (DOM). For example, client-side extensions allow an application to place elements on an HTML form and respond to user events such as mouse clicks, form input, and page navigation.

Server-side JavaScript extends the core language by supplying objects relevant to running JavaScript on a server. For example, server-side extensions allow an application to communicate with a database, provide continuity of information from one invocation to another of the application, or perform file manipulations on a server.

4.Bootstrap:

Bootstrap is a free and open-source tool collection for creating responsive websites and web applications. It is the most popular HTML, CSS, and JavaScript framework for developing responsive, mobile-first websites. It solves many problems which we had once, one of which is the cross-browser compatibility issue. Nowadays, the websites are perfect for all the browsers (IE, Firefox, and Chrome) and for all sizes of screens (Desktop, Tablets, Phablets, and Phones). All thanks to Bootstrap developers -Mark Otto and Jacob Thornton of Twitter, though it was later declared to be an open-source project.

5.Php:

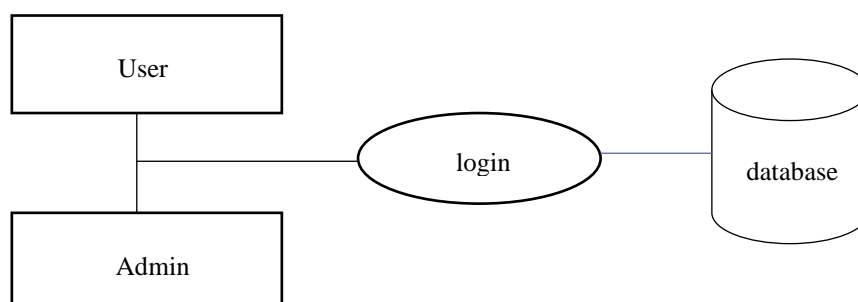
The term PHP is an acronym for PHP: Hypertext Pre-processor. PHP is a server-side scripting language designed specifically for web development. It is opensource which means it is free to download and use. It is very simple to learn and use. The files have the extension “Php”. Rasmus Leadoff inspired the first version of PHP and participating in the later versions. It is an interpreted language and it does not require a compiler. PHP code is executed in the server. It can be integrated with many databases such as Oracle, Microsoft SQL Server, MySQL, PostgreSQL, Sybase, Informix. It is powerful to hold a content management system like WordPress and can be used to control user access. It supports main protocols like HTTP Basic, HTTP Digest, IMAP, FTP, and others. Websites like www.facebook.com, www.yahoo.com are also built on PHP. One of the main reasons behind this is that PHP can be easily embedded in HTML files and HTML codes can also be written in a PHP file. The thing that differentiates PHP from the client-side language like HTML is, PHP codes are executed on the server whereas HTML codes are directly rendered on the browser. PHP codes are first executed on the server and then the result is returned to the browser. The only information that the client or browser knows is the result returned after executing the PHP script on the server and not the actual PHP codes present in the PHP file. Also, PHP files can support other client-side scripting languages like CSS and JavaScript.

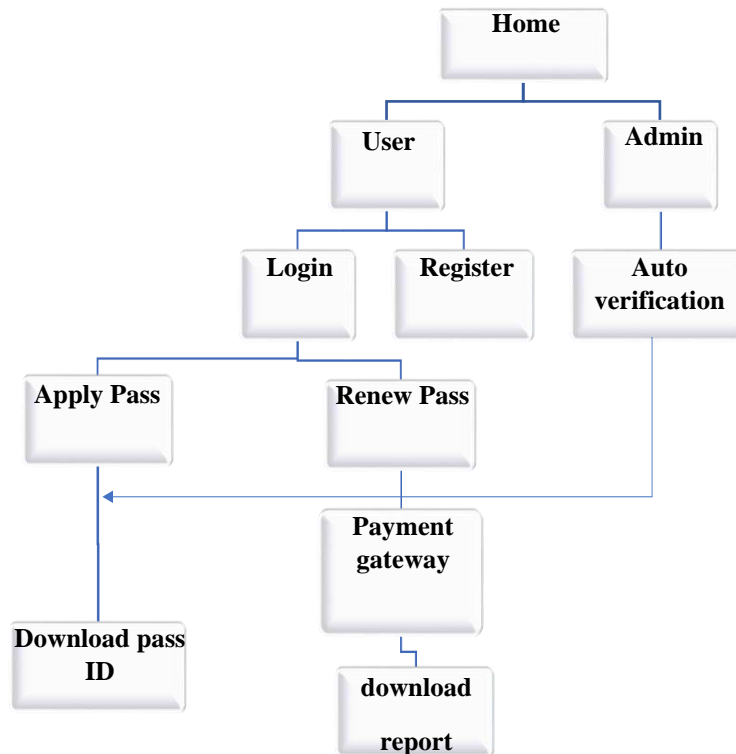
6.MySQL:

MySQL is an open-source relational database management system (RDBMS). It is the most popular database system used with PHP. MySQL is developed, distributed, and supported by Oracle Corporation. The data in a MySQL database are stored in tables which consists of columns and rows. MySQL is a database system that runs on a server. MySQL is ideal for both small and large applications. MySQL is very fast, reliable, and easy to use database system. It uses standard SQL MySQL compiles on a number of platforms. PHP 5 and later can work with a MySQL database using: MySQL extension, PDO (PHP Data Objects).

SYSTEM DESING

1.BLOCK DIAGRAM



**2.Data Flow diagram:****DATABASE DESING****TABLE 1: USER**

Usr001	NAME
Usr002	ID
Usr003	PASSWORD
Usr004	DATE OF BIRTH
Usr005	MOBILE.NO
Usr006	EMAIL
Usr007	GENDER
Usr008	PASSTYPE
Usr009	PHOTO
Usr0010	REGION
Usr0011	DISTRICT
Usr0012	DEPOT
Usr0013	SOURCE
Usr0014	DECINATION1
Usr0015	REQUEST
Usr0016	RENEWAL MONTH
Usr0017	MONEY

TABLE 2: ADMIN

Amn001	USER NAME
Amn002	PASSWORD

**CONCLUSION**

This project is useful for the students who are facing problems with the current manual process of bus pass registration and renewal. It will send an email for the students before completion of his validity period. We provide two kinds of bus pass instead of earlier service in manual system and employees. One is 30 days bus pass and other is 45 days bus pass. This project has highly secured payment gateway. It is user friendly and very easy to handle with simple implementation. This project stores all the activity of the users in a database and also works in light-weight process. In future we are going to implement QR code service and provide high security with user friendly. Also provide fully automated system like after done the payment bus pass generated automatically and send to the required user mail ID.

REFERENCES

- 1.K. Ganesh, M. Thirvikraman, J. Kuri, H. Dagale, G. Sudhakar and S. Sanyal, "Implementation of a Real Time Passenger Information System", CoRR abs/1206.0447 (2012).
- 2.B. Caulfield and M. O'Mahony, "An examination of the public transport information requirements of users", IEEE Transactions on Intelligent Transportation Systems, vol. 8, no. 1, (2007), pp. 21–30. International Conference on Explorations and Innovations in Engineering & Technology (ICEIET - 2016) ISSN: 2348 – 8387 <http://www.internationaljournalssrg.org> Page 151
- 3.Development of an Effective Online Bus Pass Generation System for Transportation System for Transportation Service in Karnataka State.
- 4.Online Bus Pass Generation System for Transportation System for Transportation Service in Andhra Pradesh State. <http://online.apsrtpass.in/> <https://pmmodiyojana.in/apsrtc-student-bus-pass/>
- 5.Online Bus Pass Generation System for Transportation System for Transportation Service in Telungana State. <https://online.tsrtcpass.in/>
- 6.Baid.A, Rae.I, Li.J, Doan.A, and Naughton.J,(2010) "Toward Scalable Keyword Search over Relational Data," Proc. VLDB Endowment, vol. 3, no. 1, pp. 140-149.
- 7.Hristidis.V and Papakonstantinou.Y,(2002) "DISCOVER: Keyword Search in Relational Databases," Proc. 28th Int'l Conf. Very Large Data Base (VLDB'02), pp. 670-681.
- 8.Qin.L, Yu.J.X, and Chang.L, (2009) "Keyword Search in Databases: The Power of RDBMS," Proc. ACM SIGMOD Int'l Conf. Management of Data (SIGMOD '09), pp. 681-694.
- 9.K. G. Zografos, K. N. Androutsopoulos and V. Spitadakis, "Design and assessment of an online passenger information system for integrated multimodal trip planning", Trans. Intell. Transport. Syst. vol. 10, (2009), pp. 311–323.
- 10.Kasha K, Abhisek Chowdhury, Keerthana D,A "Survey on Online BusPass Generation System using Aztec code", International Journal ofInnovative Research in Computer and Communication Engineering (An ISO 3297: 2007 Certified Or- ganization) Vol. 4, Issue 2, February 2016

Research Article

Machine Learning Empowered Accurate CSI Prediction for Large-Scale 5G Networks

**R. Uma Mageswari,¹ Gousebaigmohammad¹,¹ Devesh siva prasad Dulam,¹ S. Shitharth²,
G. Surya Narayana,³ A. Suresh,⁴ JaikumarR,⁵ Leena Bojaraj,⁵ S. Chandragandhi,⁶
and Amsalu GosuAdigo⁷**

¹Department of Computer Science and Engineering, Vardhaman College of Engineering, Hyderabad, Telangana, India

²Department of Computer Science Engineering, Kebri Dehar University, Kebri Dehar-250, Ethiopia

³Department of Computer Science & Engineering, Sreyas Institute of Engineering and Technology, Hyderabad, Telangana, India

⁴Department of Computer Science and Engineering, Veltech Rangarajan Dr. Sagunthala R&D Institute of Science and Technology, Chennai, India

⁵Department of Electronics and Communication Engineering, KGiSL Institute of Technology, Coimbatore, India

⁶Department of Computer Science Engineering, JCT College of Engineering and Technology, India

⁷Center of Excellence for Bioprocess and Biotechnology, Department of Chemical Engineering, College of Biological and Chemical Engineering, Addis Ababa Science and Technology University, Ethiopia

Correspondence should be addressed to Gousebaigmohammad; gousebaig@vardhaman.org
and Amsalu GosuAdigo; amsalu.gosu@aastu.edu.et

Received 24 December 2021; Revised 9 February 2022; Accepted 19 February 2022; Published 31 March 2022

Academic Editor: Mohammad Farukh Hashmi

Copyright © 2022 R. Uma Mageswari et al. This is an open access article distributed under the Creative Commons Attribution License, which permits unrestricted use, distribution, and reproduction in any medium, provided the original work is properly cited.

Wi-Fi networks rely on channel estimation to ensure their performance. The computational complexity and dependability of fifth generation telecommunication networks have significantly improved using supervised learning. In this paper, we develop a channel estimation model that uses a machine learning approach and the study uses multipath channel simulations for the estimation of channel state information (CSI) over arbitrary transceiver antennas. The simulation is conducted to test the efficacy of the model against various machine learning channel estimation models. The results of simulation show that the proposed model obtains increased channel estimation quality than other methods. Further, the bit error rate is recorded low among other methods using the machine learning model. Thus, it is seen that the proposed method achieves a reduced mismatch rate of $1.26 \times 10^{-1.5}$ than other methods on Doppler frequency during channel estimation, where the mismatch rate is higher in existing methods.

1. Introduction

In the current mobile communication systems, more devices are connected at the base stations, and the volume of data traffic is predicted to grow rapidly as well [1]. Because of the large number of devices and applications, infrastructure management has become increasingly challenging [2].

Low-power connectivity is necessary for the Internet of Things (IoT), whereas higher speeds of mobile communication are required for trains travelling at speeds of up to 300

kilometres per hour, and fiber-like broadband access is required for users at home [3]. A number of technologies are presented to support the aforementioned goals [4]. In antenna beamforming, MIMO, use of custom-tailored, and virtualized network functions (VNFs), adequately provisioned network slices are only a few examples of these technologies [5].

It is feasible to use some data-based technologies to manage 5G networks, which would be advantageous. Dynamic mobile traffic analysis, for example, can be used to forecast

the position of the user when it comes to handover procedures [4, 5]. Another example is the allocation of network slices, which takes into account the state of the network and the availability of resources [6]. Each of these scenarios is built on the foundation of data analysis. Depending on the source, some predictions regarding future behaviour are based on historical data, while others are based on present conditions and are designed to assist in decision-making. It is possible to overcome these types of challenges with the use of machine learning techniques [7–9].

The algorithms are only capable of handling raw natural data in their current form. Building a machine learning or pattern recognition system requires substantial domain expertise and rigorous engineering across many decades, which is why the design of a feature extractor is so important. The data can then be translated into a suitable representation for the learning system when this stage has been completed [7].

The use of two alternative sparsifying basis in a hybrid feedback compression approach for a slowly variable propagation environment can help to achieve a better balance between the feedback load and the CSI recovery performance. CSI recovery performance because massive MIMO is likely to be deployed in mmWave frequency ranges in cellular networks; the use of a compressive sensing-based approach may not be feasible, because the occurrence of strong spatial correlation is not likely to occur at high carrier frequencies. The beamforming-based solution, on the other hand, is probably more practical due to the restricted number of propagation channels available, which allows the user to concentrate on only a few angular beams for CSI measurements and reporting, which is probably more practical. This study discusses the downlink estimation that utilizes a machine learning approach to maintain the trade-off between the resource and energy consumption. This does not require CSI feedback from the users, which is extremely efficient in terms of resource and power savings on the user end.

In this paper, we develop a novel channel estimation model that uses machine learning approach, namely, back propagation neural network (BPNN), and the study uses multipath channel simulations for the estimation of channel state information (CSI) over arbitrary transceiver antennas.

2. Background

The problem of estimation of CSI is considered persistent in wireless systems. The next section [4] discusses the quality of communications links. This brief explanation will use these characteristics to determine how a signal travels from its source to its intended destination. Transmissions can be tailored to the current channel conditions depending on the CSI in order to improve overall communication performance. The CSI has an impact on a variety of things, including radio resources, modulation, and coding schemes.

Traditional CSI estimation methods [10] sometimes necessitate the use of high-performance computation [11]. As a result, machine learning models are now being used by numerous writers in their CSI estimation work, which is

a significant advancement. Five papers on machine learning-based CSI estimation were identified as a result of our thorough review.

Three models in [11–13] proposed a machine learning-based technique for MIMO systems, each of which was based on machine learning. MIMO systems employ an array of antennas for both the transmitter and the receiver, resulting in more efficient transmission and reception. If we compare it to LTE, this is an extremely important 5G technology because of the huge reductions in spectral and energy consumption it delivers [14]. It should be noted that while MIMO is utilized in LTE, massive MIMO is employed in 5G, which makes use of extremely large antenna configurations.

In [11], they use MIMO system which helps to avoid Doppler rate estimation and thereby avoid Doppler rate estimation. Carrier channels, in which the estimation of Doppler rate varies between the packets, make the computation difficult to perform the optimal operations. The MIMO fading channels with varying Doppler rates were learned and estimated using machine learning models, which were applied to the problem.

Using a combination of machine learning and overlay coding techniques, the authors of [12] demonstrated channel state CSI feedback. CSI estimation at the downlink and identification of user data in base stations are the key goals of this research project. The authors in [13] describe an evaluation of the employment of machine learning models to estimate CSI in three different use cases. Xu et al. [13] also reported on this research. The first scenario involved the use of machine learning models to estimate the angular power spectrum; the other two scenarios involved static estimates based on machine learning and its version, which took into account temporal variation, i.e., the machine learning model is recommended for estimating in-band CSI across time. According to Albataineh et al. [4], one method of predicting the quality of an Internet radiolink transmission is to take into account elements. A machine learning model is used to replace the traditional methods of CSI estimation, equalization, and demapping [15, 16].

3. Proposed Method

A transmitter and receiver are depicted in Figure 1 as part of a MIMO-OFDM system in this section. Since the 5G channel profile is modeled after the NTN MIMO channel model.

3.1. 5G Channel Model. The 3GPP standard defines the 5G model, where the Doppler shifting induces time-selective and frequency fading. The TDL-C model with Rayleigh fading distribution is used in frequency range between 0.25 and 100 GHz.

The MATLAB 5G toolbox is used to simulate the instantaneous channels in this propagation channel models. The TDL-C profile shown is used for 5G and beyond channels showing the gain of channel. The gain changes from 12 to 47 dB in more detail. Because the mobile communication

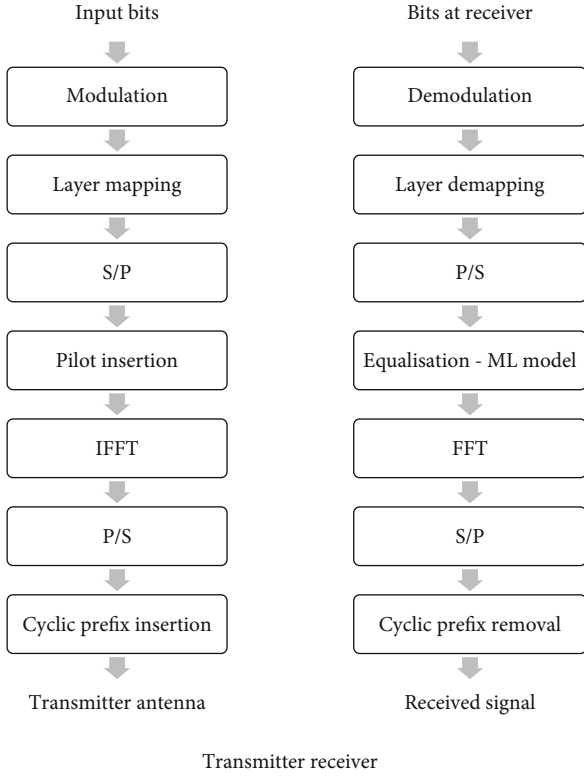


FIGURE 1: MIMO-OFDM with the BPNN Model.

frequency is of 4 GHz in this case, where the channel profile is not sparse.

3.2. Transmitter. The modulation block as in Figure 1 (transmitter block) is used to encode and map binary data on the transmitter side using quadrature amplitude modulation (QAM). There are T time slots, and the symbols (QAM) are concatenated to $x(t) \in C^N$ at time t :

$$x(t) = [x_1(t), x_2(t), \dots, x_N(t)], \quad (1)$$

where N is the symbols of modulation. Data is decoded as vectors N_T that correspond to the antennas N_T and it is given as below:

$$x_i(t) = [x_i(t), x_i + N_T(t), x_i + 2N_T(t), \dots]. \quad (2)$$

This is accomplished by first converting the data from the transmitter and reception antennas in a parallel form, and finally, the pilot signals are inserted with the data into each layer for use in channel estimation. To translate signals from frequency domain, we use what we call an IFFT to transform

$$X_a(t) = \text{IFFT}\{x_a(t)\}. \quad (3)$$

The signal vector $x_a(t)$ contains a pilot embedded in the data $x_i(t)$. By inserting the CP insertion block, a cyclic prefix (CP) of length N_G is then used to alleviate intersymbol interference (ISI). The transmitted signal, indicated by $x_{ga}(t)$, is

expressed in the time domain by adding the cyclic prefix:

$$[X_{ga}(t)]_n = \begin{cases} |X_a(t)|_{N_{\text{FFT}}+n} & n = -N_G, \dots, -1, \\ |X_a(t)|_n & n = 0, 1, \dots, N_{\text{FFT}}, \end{cases} \quad (4)$$

where N_{FFT} is the size of FFT.

That is, in order to make the signal in this symbol longer, the cyclic prefix at the end of each $X_{ga}(t)$ sample is utilized to prefix the beginning of this symbol.

3.3. Receiver. It is initially eliminated from each antenna received signal using the removal of cyclic prefix in order to obtain vectors of length N_{FFT} from each antenna (Figure 1 receiver block). For channel estimation, the pilot signal from frequency domain is extracted. In addition to calculating the channel, a layer demapping module equalizes and concatenates incoming signals from all receiver antennas. A specific demodulation strategy, based on the transmitter approach, is utilized to decode the signal. At this stage, the complete binary data sequence from the MIMO-OFDM model is acquired.

The mapping of pilot signals in accordance with the pilot structure. Pilots in 5G networks are organized in a comb-like pattern across the antennae. Symbols in the time and frequency domains, Dt and Df , respectively, are evenly spaced. Different use scenarios for a 5G system specify the values of Dt and Df . Pilot signals are organized into an alternating pattern among transmission antennas.

4. Machine Learning Channel Estimation

Traditional estimation approaches can be used to estimate the propagation channels between transmitters and receivers in wireless communication systems that need coherent detection. Using machine learning frameworks to improve channel estimation mistakes is motivated in this part by presenting two widely used channel estimation approaches.

Error convergence is a critical issue in supervised learning, i.e., the reduction of the difference between the intended and computed unit values. We determine a set of weights that are as accurate as possible. Less mean square (LMS) convergence has been used in many different learning paradigms.

$$E(\mathbf{w}) = E\{\mathbf{x}^\alpha, \mathbf{y}^\alpha, \mathbf{y}(\mathbf{x}^\alpha, \mathbf{w})\}. \quad (5)$$

Both the transfer function and weights for the units influence the behaviour of a BPNN.

$$f(a) = \frac{1}{(1 + \exp(-a))}. \quad (6)$$

Signals are generated constantly but not linearly for sigmoid devices. Sigmoid units have a closer similarity to neurons than threshold units but should be taken as approximations.

It is necessary to change the unit weights in a neural network so that the difference between the expected output is

minimized. An erroneous derivative of the weights is calculated by the neural network (EW). The error must be calculated in the following manner: as weight is increased or decreased, the error must be calculated in the following manner. The EW can be determined using the back propagation methodology.

In order to comprehend the back propagation algorithm, it is best if all network units are linear. For each EW, the process begins by calculating a unit EA (changing error rate). It is the difference between what you actually get and what you want to get. The weights connect one hidden unit with other hidden units and output units must be identified in order to construct an EA.

The study then multiplies weights by EAs by output units and sum of the products. There is a total equal to this value for each concealed unit that was selected. When all the EAs in one layer have been computed, we can proceed to calculate the EAs for next neural layers, where the progressing from layer takes place in opposite direction of activity propagation. Back propagation is the name given to this process. Once the EA has been computed, EA and EW can be computed for each incoming connection of a unit. It is the result of a combination of the EA and incoming activity.

5. Results and Discussions

Here, we compare our proposed machine learning-based channel predictions to existing approaches to the 5G channel profile and evaluate their effectiveness. This was a simulation of a MIMO-OFDM system that included the characteristics necessary to model the 5G network.

All of the proposed estimation are implemented on an Intel i5 CPU running at 2.90 GHz with 16 GB of memory. It is used for Monte Carlo simulations in MATLAB 2021a. BER and MSE vs. SNR were used as a comparison tool to evaluate the performance, and the results were compared to conventional estimation.

Figure 2 shows the BER performance of the scenarios under consideration using the various channel estimation approaches. There is a strong correlation between the BER performance and the MSE performance of the estimators under study. In both instances, DBN performance of BER is marginally lower than MLP. As a result of this, the loss function is designed to decrease channel estimation errors rather than the bit error rate.

Tables 1 and 2 illustrates the effect of pilot density on the robustness of BPNN estimators as shown. The performance of the three machine learning estimators remained constant when the pilot density fell, regardless of the SNR. As a result, we may conclude that the BPNN models are resistant to variable pilot densities.

The proposed machine learning models are tested for the impact of the maximum Doppler frequency. As the maximum Doppler frequency grew, the machine learning model performance degraded. As the Doppler frequency grew, the channel changed more frequently. We can also see from the figure that the BPNN model performance fell more severely than the other models. However, it still outper-

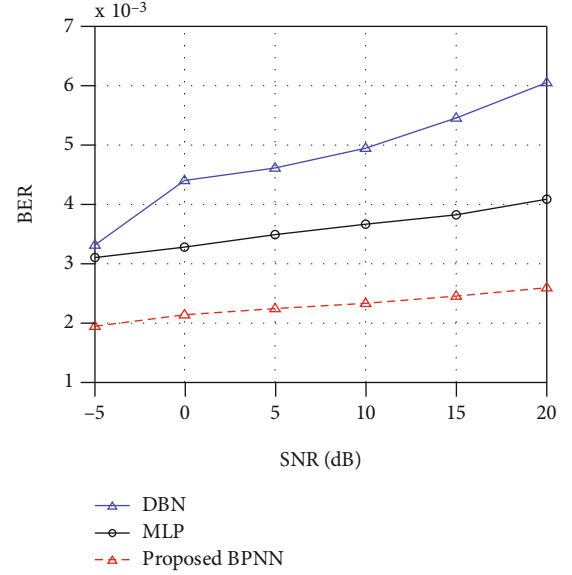


FIGURE 2: BER vs. SNR.

TABLE 1: Influence of pilot density in terms of the minimum mean square error during channel estimation by machine learning.

SNR (dB)	MMSE (dB)		
	DBN	MLP	Proposed BPNN
-5	$1.32 \times 10^{-0.5}$	$1.24 \times 10^{-0.75}$	$0.78 \times 10^{-1.8}$
0	$1.76 \times 10^{-0.74}$	$1.31 \times 10^{-0.98}$	$0.85 \times 10^{-2.28}$
5	$1.84 \times 10^{-0.9}$	$1.39 \times 10^{-1.12}$	$0.89 \times 10^{-2.78}$
10	$1.98 \times 10^{-1.15}$	$1.47 \times 10^{-1.51}$	$0.93 \times 10^{-3.11}$
15	$2.18 \times 10^{-1.24}$	$1.53 \times 10^{-1.92}$	$0.98 \times 10^{-3.29}$
20	$2.41 \times 10^{-1.32}$	$1.63 \times 10^{-2.02}$	$1.03 \times 10^{-3.5}$

TABLE 2: Influence of pilot density in terms of mean square error during channel estimation by machine learning.

SNR (dB)	MMSE (dB)		
	DBN	MLP	Proposed BPNN
-5	$5.28 \times 10^{-0.5}$	$4.93 \times 10^{-0.75}$	$3.09 \times 10^{-1.8}$
0	$6.99 \times 10^{-0.74}$	$5.20 \times 10^{-0.98}$	$3.39 \times 10^{-2.3}$
5	$7.34 \times 10^{-0.9}$	$5.55 \times 10^{-1.12}$	$3.56 \times 10^{-2.8}$
10	$7.88 \times 10^{-1.15}$	$5.84 \times 10^{-1.51}$	$3.70 \times 10^{-3.12}$
15	$8.69 \times 10^{-1.24}$	$6.08 \times 10^{-2.00}$	$3.90 \times 10^{-3.32}$
20	$9.62 \times 10^{-1.32}$	$6.50 \times 10^{-2.69}$	$4.12 \times 10^{-3.51}$

formed the DBN and MLP models in terms of performance which is discussed in Table 3.

On the ground, we used Doppler frequency variation as a way to test the neural network sensitivity to changes in the receiver velocity. The proposed models were also examined for accuracy in prediction when the Doppler frequency between training and testing was out of whack. In this simulation, a uniform distribution was used to randomly

TABLE 3: Influence of minimum mean square error during channel estimation by machine learning.

SNR (dB)	DBN	MMSE (dB) MLP	Proposed BPNN
-5	$2.10 \times 10^{-0.6}$	$1.96 \times 10^{-0.8}$	$1.23 \times 10^{-1.6}$
0	$2.79 \times 10^{-0.85}$	$2.07 \times 10^{-1.0}$	$1.35 \times 10^{-2.1}$
5	2.92×10^{-1}	$2.21 \times 10^{-1.2}$	$1.42 \times 10^{-2.5}$
10	$3.14 \times 10^{-1.24}$	$2.33 \times 10^{-1.6}$	$1.48 \times 10^{-2.9}$
15	$3.46 \times 10^{-1.32}$	$2.42 \times 10^{-2.1}$	$1.55 \times 10^{-2.95}$
20	$3.83 \times 10^{-1.39}$	$2.59 \times 10^{-2.8}$	1.64×10^{-3}

TABLE 4: Influence of mismatch on Doppler frequency during channel estimation by machine learning.

SNR (dB)	DBN	MSE (dB) MLP	Proposed BPNN
-5	$2.15 \times 10^{-1.5}$	$2.01 \times 10^{-1.5}$	$1.26 \times 10^{-1.5}$
0	2.85×10^{-2}	2.12×10^{-2}	1.38×10^{-2}
5	$2.99 \times 10^{-2.5}$	$2.26 \times 10^{-2.5}$	$1.45 \times 10^{-2.5}$
10	$3.21 \times 10^{-2.8}$	$2.38 \times 10^{-2.8}$	$1.51 \times 10^{-2.8}$
15	3.54×10^{-3}	2.48×10^{-3}	1.59×10^{-3}
20	$3.92 \times 10^{-3.1}$	$2.65 \times 10^{-3.1}$	$1.68 \times 10^{-3.1}$

disperse values in the testing stage, while we preserved them in the training stage. Table 4 shows the results.

In spite of the mismatch in Doppler frequency, all of the machine learning channel estimate models performed well, as shown in Table 4. When SNR is set to 20 dB, only the BPNN model performance suffers marginally. Even with channel mismatching, all of the BPNN model than DBN and MLP. Based on the results, BPNN is sensitive on Doppler frequency than DBN and MLP.

Due to the time-varying channel features, BPNN has greater impact on Doppler frequency than on MLP and DBN. However, the three presented models are still more efficient than conventional approaches because they are more resistant to variations in the Doppler frequency.

6. Conclusions

In this paper, a channel estimation model is conducted using BPNN and the study uses multipath channel simulations for the estimation of CSI over arbitrary transceiver antennas. The simulation is conducted to test the efficacy of the model against various machine learning channel estimation models. The results of simulation show that the proposed model obtains increased channel estimation quality than other methods. Further, the bit error rate is recorded low among other methods using the machine learning model. Because of its capacity to utilize the temporal and frequency correlation across channels, BPNN showed the biggest reduction in channel estimation error among the proposed channel estimation. Furthermore, the BPNN channel esti-

mation algorithms showed excellent resilience to changes in pilot density and Doppler frequency. In future, the application of noise modeling can be varied to check the efficacy of the model under different rugged scenarios.

Data Availability

The datasets used and/or analyzed during the current study are available from the corresponding author on reasonable request.

Conflicts of Interest

There authours declare that they have no conflict of interest.



References

- [1] T. Karthikeyan, K. Praghash, and K. H. Reddy, "Binary flower pollination (BFP) approach to handle the dynamic networking conditions to deliver uninterrupted connectivity," *Wireless Personal Communications*, vol. 121, no. 4, pp. 3383–3402, 2021.
- [2] A. S. Kumar, L. T. Jule, K. Ramaswamy, S. Sountharajan, and A. H. Gandomi, "Analysis of false data detection rate in generative adversarial networks using recurrent neural network," in *Generative Adversarial Networks for Image-to-Image Translation*, pp. 289–312, Academic Press, 2021.
- [3] K. Praghash, R. A. Raja, and T. Karthikeyan, "An investigation of garbage disposal electric vehicles (GDEVs) integrated with deep neural networking (DNN) and intelligent transportation system (ITS) in smart city management system (SCMS)," *Wireless Personal Communications*, pp. 1–20, 2021.
- [4] Z. Albataineh, K. Hayajneh, H. B. Salameh, C. Dang, and A. Dagmeh, "Robust massive MIMO channel estimation for 5G networks using compressive sensing technique," *AEU-International Journal of Electronics and Communications*, vol. 120, p. 153197, 2020.
- [5] M. Mehrabi, M. Mohammadkarimi, M. Ardakani, and Y. Jing, "Decision directed channel estimation based on deep neural network k-step predictor for MIMO communications in 5G," *IEEE Journal on Selected Areas in Communications*, vol. 37, no. 11, pp. 2443–2456, 2019.
- [6] R. A. Raja, T. Karthikeyan, and K. Praghash, "Improved authentication in secured multicast wireless sensor network (MWSN) using opposition frog leaping algorithm to resist man-in-middle attack," *Wireless Personal Communications*, pp. 1–17, 2021.
- [7] L. Ge, Y. Zhang, G. Chen, and J. Tong, "Compression-based LMMSE channel estimation with adaptive sparsity for massive MIMO in 5G systems," *IEEE Systems Journal*, vol. 13, no. 4, pp. 3847–3857, 2019.
- [8] X. Shen, Y. Liao, X. Dai, M. Zhao, K. Liu, and D. Wang, "Joint channel estimation and decoding design for 5G-enabled V2V channel," *China Communications*, vol. 15, no. 7, pp. 39–46, 2018.
- [9] A. Riadi, M. Boulouird, and M. M. R. Hassani, "Least squares channel estimation of an OFDM massive MIMO system for 5G wireless communications," in *International conference on the Sciences of Electronics, Technologies of Information and Telecommunications*, pp. 440–450, Springer, Cham, 2020.

- [10] M. Robaei and R. Akl, "Examining spatial consistency for millimeter-wave massive MIMO channel estimation in 5G-NR," in *2020 IEEE International Conference on Consumer Electronics (ICCE)*, pp. 1–6, IEEE, Taiwan, 2020.
- [11] M. Saideh, M. Berbineau, and I. Dayoub, "On the performance of sliding window TD-LMMSE channel estimation for 5G waveforms in high mobility scenario," *IEEE Transactions on Vehicular Technology*, vol. 67, no. 9, pp. 8974–8977, 2018.
- [12] J. T. Dias, R. C. de Lamare, and Y. V. Zakharov, "BEM-based channel estimation for 5G multicarrier systems," in *WSA 2018; 22nd International ITG Workshop on Smart Antennas*, pp. 1–5, VDE, 2018.
- [13] C. Xu, N. Ishikawa, R. Rajashekar et al., "Sixty years of coherent versus non-coherent tradeoffs and the road from 5G to wireless futures," *IEEE Access*, vol. 7, pp. 178246–178299, 2019.
- [14] Z. Na, Z. Pan, M. Xiong, J. Xia, and W. Lu, "Soft decision control iterative channel estimation for the internet of things in 5G networks," *IEEE Internet of Things Journal*, vol. 6, no. 4, pp. 5990–5998, 2019.
- [15] N. Shaik and P. K. Malik, "A comprehensive survey 5G wireless communication systems: open issues, research challenges, channel estimation, multi carrier modulation and 5G applications," *Multimedia Tools and Applications*, vol. 80, no. 19, pp. 28789–28827, 2021.
- [16] G. Kiruthiga, G. U. Devi, and N. V. Kousik, "Analysis of hybrid deep neural networks with mobile agents for traffic management in vehicular adhoc networks," in *Distributed Artificial Intelligence*, pp. 277–290, CRC Press, 2020.

Research Article

Public Auditing Scheme for Integrity Verification in Distributed Cloud Storage System

K. Mahalakshmi,¹ K. Kousalya,² Himanshu Shekhar,³ Aby K. Thomas,⁴ L. Bhagyalakshmi,⁵ Sanjay Kumar Suman,⁶ S. Chandragandhi,⁷ Prashant Bachanna,⁸ K. Srihari ,⁹ and Venkatesa Prabhu Sundramurthy ¹⁰

¹Department of Computer Science Engineering, SSM College of Engineering, Namakkal, India

²Department of Computer Science Engineering, Kongu Engineering College, Erode, India

³Department of Electronics and Communications Engineering, Hindustan Institute of Technology and Science, Kelambakkam, Chennai 603103, India

⁴Department of Electronics and Communications Engineering, Alliance College of Engineering and Design, Alliance University, Bengaluru-562106, Karnataka, India

⁵Department of Electronics and Communications Engineering, Rajalakshmi Engineering College, Chennai, India

⁶Department of Electronics and Communications Engineering, Bharat Institute of Engineering and Technology, Hyderabad, India

⁷Department of Computer Science Engineering, Jct College of Engineering and Technology, Coimbatore, India

⁸Department of Computer Science Engineering, SNS College of Technology, Coimbatore, India

⁹Department of Electronics and Communications Engineering, Bharat Institute of Engineering and Technology, Hyderabad, Telangana 501510, India

¹⁰Department of Chemical Engineering, Addis Ababa Science and Technology University, Addis Ababa, Ethiopia

Correspondence should be addressed to Venkatesa Prabhu Sundramurthy; venkatesa.prabhu@aastu.edu.et

Received 25 October 2021; Revised 8 November 2021; Accepted 6 December 2021; Published 22 December 2021

Academic Editor: M Pallikonda Rajasekaran

Copyright © 2021 K. Mahalakshmi et al. This is an open access article distributed under the Creative Commons Attribution License, which permits unrestricted use, distribution, and reproduction in any medium, provided the original work is properly cited.

Cloud storage provides a potential solution replacing physical disk drives in terms of prominent outsourcing services. A threaten from an untrusted server affects the security and integrity of the data. However, the major problem between the data integrity and cost of communication and computation is directly proportional to each other. It is hence necessary to develop a model that provides the trade-off between the data integrity and cost metrics in cloud environment. In this paper, we develop an integrity verification mechanism that enables the utilisation of cryptographic solution with algebraic signature. The model utilises elliptic curve digital signature algorithm (ECDSA) to verify the data outsources. The study further resists the malicious attacks including forgery attacks, replacing attacks and replay attacks. The symmetric encryption guarantees the privacy of the data. The simulation is conducted to test the efficacy of the algorithm in maintaining the data integrity with reduced cost. The performance of the entire model is tested against the existing methods in terms of their communication cost, computation cost, and overhead cost. The results of simulation show that the proposed method obtains reduced computational of 0.25% and communication cost of 0.21% than other public auditing schemes.

1. Introduction

The cloud storage behaves as a modern paradigm in cloud computing services that is considered proven to deliver extraordinary services to the management and data storage capabilities. The individuals and cloud enterprises tend to

outsource their personal or official data to the cloud server via a pay-as-you-go model. The storage services developed to collect the outsourced data reduce their services greatly that affects the local storage essentialities of users. The integrity of data while verifying it is considered as a significant challenge in case of cloud computing [1, 2].

The data offloading and downloading, on the contrary, are often considered as a major consideration for testing the integrity of outsourced data, and this will increase dramatically the processing and connection overhead. The cloud devices used for storage, on the contrary, are often attacked by the hackers, where the data might get stolen while it is been outsourced. Hence, it is essential for the cloud service provider (CSP) to conceal the outsourced data against loss or corruption in order to maintain the trust of the users. The CSP further may reserve more storage spaces by proper removal of redundant information or the data that are accessed less [3] in order to avoid data leaks or leak of private confidential information. It is hence necessary for the CSP to develop an effective protocol that should validate the data integrity in cloud storage environment.

Various methods are developed in conventional literatures that support the verification of private and public information in handling large data. The verification of data allows the cloud users to validate the integrity of their outsourced data. However, such substantial computing poses a serious burden to the CSP, where the cloud resources are of constrained one. The publication verification of outsourced data reduces the computing cost of the client with the optimal usage of third-party authority (TPA) that helps in checking the data integrity. With such optimal processing and reduced user of resources, the public verification in recent past gained an increased attention [4–14].

In order to support the update of dynamic data, the researchers developed several models [3, 15–18] to update the outsourced data without affecting the completion of download. Certain techniques allow the data to be update dynamically using the cryptographic encryption model, and this requires optimal usage of cloud resources. This would increase the computational and communication cost in significant manner.

There exist various pitfalls that still need to be identified. There exist multiple storage spaces that are explicitly required for the storage of the outsourced data. The storage activities involve the deletion and insertion of the data that may result in increased cost of computation and communication since the movement of data in dynamical way cannot be forfeited. Furthermore, the lack of communication links poses a serious challenge in locating the required outsourced data. This system poses increased severity over forgery attack, replay attack, and replacement attack. In order to mitigate such challenges, an integrity verification is suitably designed in the proposed method that uses cryptographic algorithm to verify the sources.

In this paper, an integrity verification mechanism is formed that enables the utilisation of cryptographic solution with algebraic signature. The model utilises elliptic curve digital signature algorithm (ECDSA) to verify the data outsources. The study further resists the malicious attacks including forgery attacks, replacing attacks, and replay attacks. The symmetric encryption guarantees the privacy of the data.

The outline of paper is as follows. Section 2 provides the related works. Section 3 discusses the proposed method. Section 4 evaluates the entire works, and Section 5 concludes the work with possible direction of future work.

2. Related Works

Wang et al. [6] developed an auditing model combining privacy-preserving approach. The model is developed with a homomorphic random mask in order of preventing the TPA from obtaining the data collection without the outsourced data.

Shacham et al. [12] develop an integrity model using public verification scheme that consists of a BLS signature. The BLS [13] tends to use limited resources for its communication and processing requirements.

Chen et al. [14] developed an algebraic solution that is developed to check the integrity of the model. This model improves the efficiency of verification without a public key.

Sookhak et al. [18], on the contrary, develop a limitless verification model, but it suffers mostly from the security flaws. This model computes the secret key based on the signature with the tags and data blocks even if the tags gets attacked.

Juels et al. [19] proposed an identity verification model that helps in preserving the data privacy, where the cloud leverages the user identity to validate the integrity.

Ateniese et al. [20] developed a model that checks the data integrity in the cloud with a technique that combines the block tags with the homomorphic encryption.

3. Proposed Method

We begin by illustrating the system model with ECDLP algorithm.

3.1. System Model. The suggested public verification approach uses a three-party model, as depicted in Figure 1. The following are the roles in this model:

- (i) Users who rely on the cloud to store the data
- (ii) A CSP is a company that sells users a lot of storage and computing power
- (iii) TPA checks the data integrity in response to user requests

In Figure 1, the proposed verification scheme shows the communication between the third-party administrator and cloud service provide in terms of proof information and challenge information between them. The user and TPA process between the version information and verification request and result. The data are only transmitted to CSP after a confirmation is obtained from the TP to CSP.

We present each user ability to implement the proposed paradigm. To begin with, the TPA is thought to be trustworthy yet suspicious. The TPA is truthful in its data integrity checks. Furthermore, the CSP is untrustworthy since it has the option of concealing data loss or corruption in order to maintain the user trust. As a result, the CSP can carry out the following attacks: forgery attack, replay attack, and replacing attack.

A data structure is designed in this part to facilitate dynamic data updating. It combines the benefits of a linked list and hash table in TPA. The ECC is made up of a hash

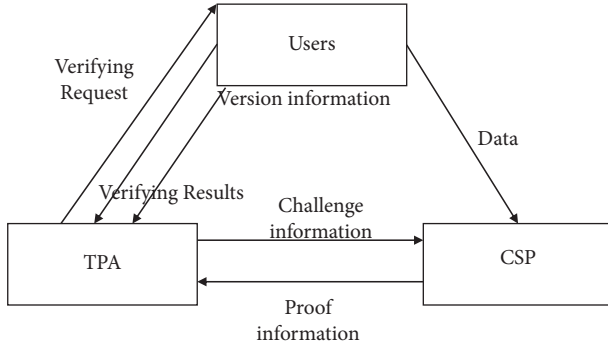


FIGURE 1: Proposed verification scheme.

table and several linked lists. The user organises the data into groups that compute the group based on its length. Each group index and length are saved in the hash table. Pointers are linked to data version information.

3.2. Verification Scheme. To begin, the TPA merely has to change the list pointer when inserting and deleting items. Second, the group index may be stored and managed using only a continuous space, which is very practical in practise. Third, if operations such as insertion or deletion are considered frequent, the TPA can change the ECDSA flexibly. As a result, the data format can lower the computational and communication costs of updating procedures dramatically.

3.2.1. Key Initiation. For encrypting data blocks, the user first produces a symmetric key dk . He then chooses $x \in \mathbb{Z}_q$ at random and calculates

$$GA = xG, \quad (1)$$

where G is an element that is known by TPA and user.

The public key is computed as follows:

$$Q(x, y) = d \times G(x, y), \quad (2)$$

where d is the scalar.

A two different integers, namely, s and r , are used to compute the signature with proper computation of integer r from a base point $G(x, y)$ and random number k :

$$\begin{aligned} (x_1, y_1) &= k \times G(x, y) \bmod p, \\ r &= x_1 \bmod n. \end{aligned} \quad (3)$$

Meanwhile, with an algebraic signature, the user selects a secure element. The secret key is (dk, x) and the public key is GA in this case.

In order the signature to be a valid one, the integer r should be treated as null. This helps in the generation of a random number (k) , and after this, the integer r is computed again. Once the successful completion of integer r , the integer s is computed as below:

$$s = (k - 1(h(m) + d * r) \bmod n, \quad (4)$$

where $h(m)$ is the message digest, d and r are the private key, and k is the random number.

3.2.2. Data Blocks' Encryption. To encrypt each data block M_i , the user uses the symmetric encryption method $Enc()$ with the key dk to acquire the encrypted M_i .

3.2.3. Tag Initiation. For each encrypted data block, the user computes the data block tag i :

$$Mi\sigma_i = \text{Sig}_\alpha(x(Mi + H(vi kti))). \quad (5)$$

The user then deletes the information that was previously saved locally. The TPA is in charge of launching a verification challenge to ensure that the outsourced data are accurate. It is worth to note that the technique uses dk for data protection and tag initiation using x which is used for public verification. It is difficult for attackers to extract x and the public key GA by exploiting an ECDSA characteristic:

$$x(Mi + H(vi kti)). \quad (6)$$

3.2.4. Challenge. The user tends to forward the verification request to TPA. The TPA selects the data from the pool of data blocks. The TPA further forwards the challenge information to CSP, which initiates a challenge.

3.2.5. Proof Generation. Once receiving the information on challenge, the CSP estimates the following:

$$M0 = \sum Mi \text{ and } \sigma = \sum \sigma_i. \quad (7)$$

3.2.6. Proof Verification. The TPA is used to estimate the hash value sum.

3.2.7. Signature Verification. The verification of signature is considered as a counterpart while computing the signature. This verifies the authenticity of the message after proof verification using the public key of the authenticator. A secure has algorithm in the formation of signature and helps in computation of authenticator's signed message digest. This is essentially computed using the components of digital signature r and s and public key $Q(x, y)$.

4. Results and Discussion

In this section, the simulation is conducted in a CloudSim software tool on a high-end computing engine that consists i9 processor with 8 GB RAM. The study transferred image files from the user module to CSP module after getting a verification from TPA. The CSP consists of 10 Virtual Machine (VM) running with 24 cores. The simulation has taken place to assess the communication and computation cost at various ends.

Figure 2 shows the storage computational cost between the proposed public auditing scheme and other methods. The results of simulation show that the proposed method achieves reduced storage cost than other methods. The use of ECDSA helps in reducing the computation cost than other methods.

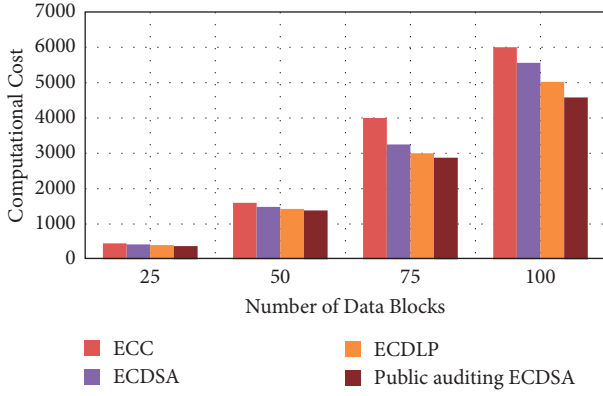


FIGURE 2: Storage computational cost.

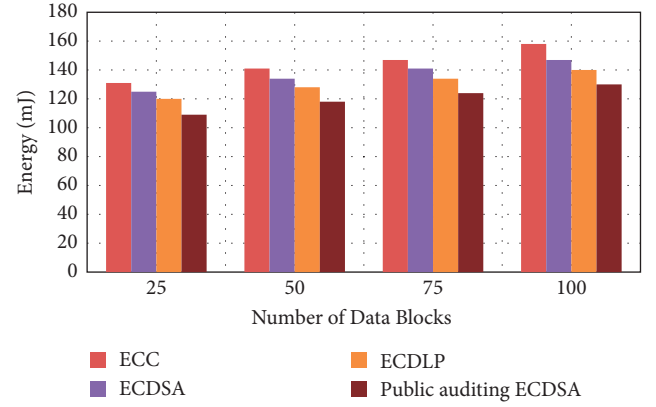


FIGURE 5: Data computation cost.

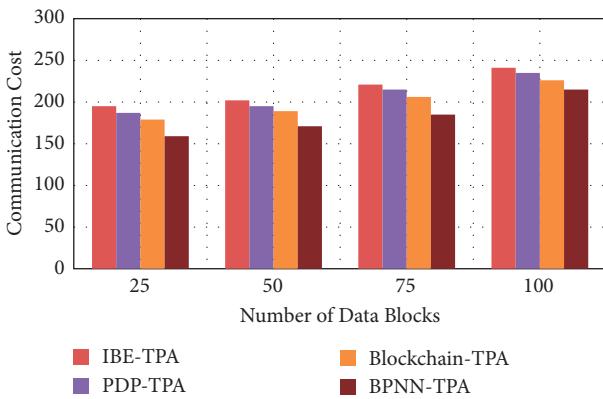


FIGURE 3: Storage communication cost.

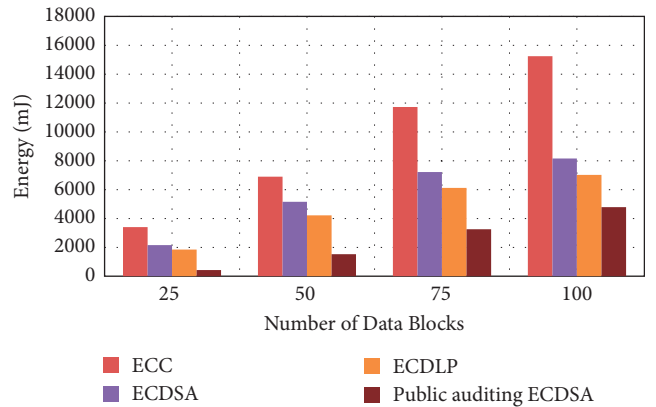


FIGURE 6: Control overhead cost.

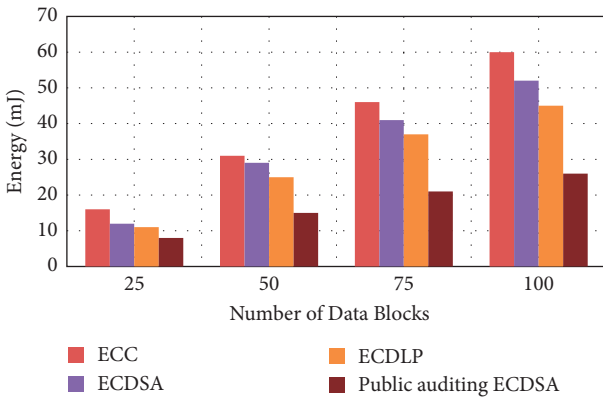


FIGURE 4: Data communication cost.

Figure 3 shows the storage communication cost between the proposed public auditing scheme and other methods. The results of simulation show that the proposed method achieves reduced storage communication cost than other methods. The use of ECDSA helps in reducing the computation cost than other methods.

Figure 4 shows the data communication cost between the proposed public auditing scheme and other methods. The results of simulation show that the proposed method achieves reduced data communication cost than other methods.

The use of ECDSA helps in reducing the communication cost than other methods.

Figure 5 shows the data computation cost between the proposed public auditing scheme and other methods. The results of simulation show that the proposed method achieves reduced data computation cost than other methods. The use of ECDSA helps in reducing the computation cost than other methods.

Figure 6 shows the control overhead cost between the proposed public auditing scheme and other methods. The results of simulation show that the proposed method achieves reduced control overhead cost than other methods. The use of ECDSA helps in reducing the overhead cost than other methods.

5. Conclusions

In this paper, we develop an integrity verification mechanism that enables the utilisation of cryptographic solution with algebraic signature. The model utilises elliptic curve digital signature algorithm (ECDSA) to verify the data outsources. The study further resists the malicious attacks including forgery attacks, replacing attacks, and replay attacks. The symmetric encryption guarantees the privacy of the data. The simulation is conducted to test the efficacy of the algorithm in maintaining the data integrity with reduced

cost. The results of simulation show that the proposed method obtains reduced computational and communication cost than other public auditing schemes. In future, the utilisation of advanced cryptographic encryption models is deployed to improve the rate of reducing the computational and communication cost in cloud systems.

Data Availability

The datasets used and/or analyzed during the current study are available from the corresponding author on reasonable request.

Ethical Approval

No participation of humans has taken place in this implementation process.

Disclosure

No violation of human and animal rights is involved.

Conflicts of Interest

The authors declare that they have no conflicts of interest.

References

- [1] B. Grobauer, T. Walloschek, and E. Stocker, "Understanding cloud computing vulnerabilities," *IEEE Security & privacy*, vol. 9, no. 2, pp. 50–57, 2010.
- [2] T. Wu, G. Yang, Y. Mu, R. Chen, and S. Xu, "Privacy-enhanced remote data integrity checking with updatable timestamp," *Information Sciences*, vol. 527, pp. 210–226, 2020.
- [3] Q. Wang, C. Wang, K. Ren, W. Lou, and J. Li, "Enabling public auditability and data dynamics for storage security in cloud computing," *IEEE Transactions on Parallel and Distributed Systems*, vol. 22, no. 5, pp. 847–859, 2010.
- [4] G. Ateniese, R. Burns, R. Curtmola et al., "Provable data possession at untrusted stores," in *Proceedings of the 14th ACM Conference on Computer and Communications Security*, pp. 598–609, Virginia, VA, USA, October 2007.
- [5] C. C. Erway, A. K  p  , C. Papamanthou, and R. Tamassia, "Dynamic provable data possession," *ACM Transactions on Information and System Security*, vol. 17, no. 4, pp. 1–29, 2015.
- [6] C. Wang, S. S. Chow, Q. Wang, K. Ren, and W. Lou, "Privacy-preserving public auditing for secure cloud storage," *IEEE Transactions on Computers*, vol. 62, no. 2, pp. 362–375, 2011.
- [7] S. S. Abdul-Jabbar, A. Aldujaili, S. G. Mohammed, and H. S. Saeed, "Integrity and security in cloud computing environment: a review," *Journal of Southwest Jiaotong University*, vol. 55, no. 1, 2020.
- [8] K. Yang and X. Jia, "An efficient and secure dynamic auditing protocol for data storage in cloud computing," *IEEE Transactions on Parallel and Distributed Systems*, vol. 24, no. 9, pp. 1717–1726, 2012.
- [9] K. Yang and X. Jia, "Data storage auditing service in cloud computing: challenges, methods and opportunities," *World Wide Web*, vol. 15, no. 4, pp. 409–428, 2012.
- [10] Y. Zhu, G. J. Ahn, H. Hu, S. S. Yau, H. G. An, and C. J. Hu, "Dynamic audit services for outsourced storages in clouds," *IEEE transactions on services computing*, vol. 6, no. 2, pp. 227–238, 2011.
- [11] Y. Zhu, H. Hu, G.-J. Ahn, and M. Yu, "Cooperative provable data possession for integrity verification in multicloud storage," *IEEE Transactions on Parallel and Distributed Systems*, vol. 23, no. 12, pp. 2231–2244, 2012.
- [12] H. Shacham and B. Waters, "Compact proofs of retrievability," in *Proceedings of the Advances in Cryptology-ASIA-CRYPT 2008. In International Conference on the Theory and Application of Cryptology and Information Security*, pp. 90–107, Springer, Melbourne, Australia, December 2008.
- [13] D. Boneh, B. Lynn, and H. Shacham, "Short signatures from the Weil pairing," *Journal of Cryptology*, vol. 17, no. 4, pp. 297–319, 2004.
- [14] L. Chen, "Using algebraic signatures to check data possession in cloud storage," *Future Generation Computer Systems*, vol. 29, no. 7, pp. 1709–1715, 2013.
- [15] H. Tian, Y. Chen, C. C. Chang et al., "Dynamic-hash-table based public auditing for secure cloud storage," *IEEE Transactions on Services Computing*, vol. 10, no. 5, pp. 701–714, 2015.
- [16] J. Shen, J. Shen, X. Chen, X. Huang, and W. Susilo, "An efficient public auditing protocol with novel dynamic structure for cloud data," *IEEE Transactions on Information Forensics and Security*, vol. 12, no. 10, pp. 2402–2415, 2017.
- [17] M. Sookhak, "Dynamic Remote Data Auditing for Securing Big Data Storage in Cloud Computing," *Information Sciences*, vol. 380, pp. 101–116, 2015.
- [18] M. Sookhak, A. Akhunzada, A. Gani, M. Khurram Khan, and N. B. Anuar, "Towards Dynamic Remote Data Auditing in Computational Clouds," *The Scientific World Journal*, vol. 2014, Article ID 269357, 12 pages, 2014.
- [19] G. Ateniese, R. Di Pietro, L. V. Mancini, and G. Tsudik, "Scalable and efficient provable data possession," in *Proceedings of the 4th International Conference on Security and Privacy in Communication Networks*, pp. 1–10, Istanbul, Turkey, September 2008.
- [20] A. Juels and B. S. Kaliski, "PORs: proofs of retrievability for large files," in *Proceedings of the 14th ACM Conference on Computer and Communications Security*, pp. 584–597, New York, NY, USA, October 2007.